MAY 2026
VOLUME 85
ISSUE
5

ANNALS OF THE RHEUMATIC DISEASES

THE EULAR JOURNAL

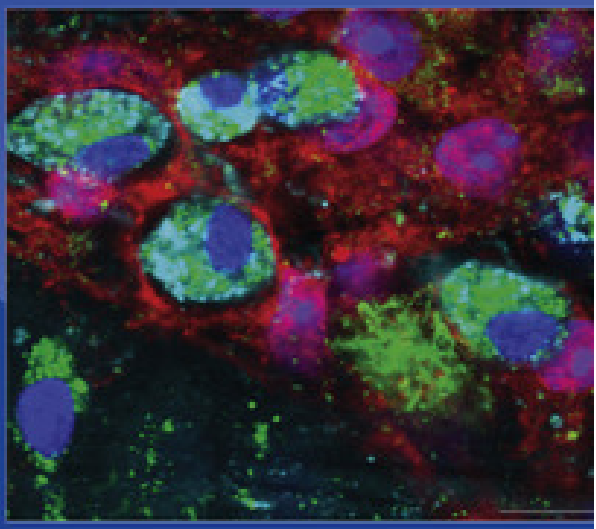

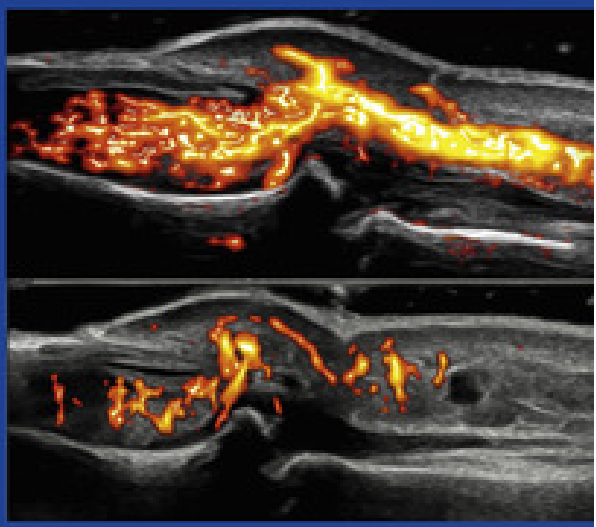

ELSEVIER

eular
EUROPEAN ALLIANCE OF ASSOCIATIONS FOR RHEUMATOLOGY

The home of innovative rheumatology research

Ann Rheum Dis 85 (2026) 781–786

Contents lists available at ScienceDirect

Annals of the Rheumatic Diseases

journal homepage: https://www.sciencedirect.com/journal/annals-of-the-rheumatic-diseases

Viewpoint

From the grey area of pre-systemic sclerosis to very early disease and irreversible tissue damage: the challenge of defining at-risk patients for future preventive trials in systemic sclerosis

Alain Lescoat[1,2,*], Yannick Allanore[3], Francesco Del Galdo[4], Masataka Kuwana[5], Silvia Bellando-Randone[6,7], Christopher P. Denton[8], Dinesh Khanna[2], Marco Matucci-Cerinic[9,10,11]

[1] *Inserm, EHESP, Irset-Institut de Recherche en Sante, Environnement et Travail-UMRS, University of Rennes CHU Rennes, Rennes, France*
[2] *Scleroderma Program, Division of Rheumatology, Department of Internal Medicine, University of Michigan, Ann Arbor, MI, USA*
[3] *Department of Rheumatology, INSERM U1016 UMR 8104, Université Paris Cité, Hôpital Cochin, Paris, France*
[4] *Department of Rheumatology, Leeds Institute of Rheumatic and Musculoskeletal Medicine, University of Leeds, Leeds, UK*
[5] *Department of Allergy and Rheumatology, Graduate School of Medicine, Nippon Medical School, Tokyo, Japan*
[6] *Department of Experimental and Clinical Medicine, University of Florence, Florence, Italy*
[7] *Scleroderma Unit and Division of Rheumatology, AOUC, Florence, Italy*
[8] *Centre for Rheumatology, Division of Medicine, Royal Free Campus, University College London, London, UK*
[9] *Unit of Immunology, Rheumatology, Allergy and Rare Diseases (UnIRAR), Scleroderma Unit, IRCCS San Raffaele Hospital, Milan, Italy*
[10] *Vita-Salute San Raffaele University, Milan, Italy*
[11] *Inflammation Fibrosis and Ageing Initiative (INFLAGE), Division of Genetics and Cell Biology, IRCCS San Raffaele Scientific Institute, Milan, Italy*

ARTICLE INFO

Article history:
Received 18 March 2025
Received in revised form 23 November 2025
Accepted 25 November 2025

ABSTRACT

This viewpoint aims to explore whether precondition trials could be applied in systemic sclerosis (SSc)—the systemic autoimmune rheumatic disease (SARD) associated with the highest mortality and substantial morbidity. In contrast to type 1 diabetes and rheumatoid arthritis (RA), where predisease states have been more clearly defined, a consensus definition for pre-SSc is still lacking. A consensus framework for patients with signs and symptoms also common to other SARDs/connective tissue diseases, but that potentially identify a patient at a pre-SSc stage, needs to be collectively drafted. Such a framework would provide the basis for earlier recognition, risk stratification, and ultimately, timely intervention in pre-SSc. Considering the paradigm shift already achieved in type 1 diabetes and RA, a similar strategy targeting patients at risk of SSc could foster the development of innovative approaches to SSc management—preventing the onset of key SSc-related signs and symptoms, promoting long-term remission, and reducing SSc-related morbidity and mortality.

*Correspondence to Dr Alain Lescoat, Internal Medicine, CHU Rennes, CHU South Hospital, Rennes, France.
E-mail address: alain.lescoat@chu-rennes.fr (A. Lescoat).
Handling editor Josef S. Smolen.

https://doi.org/10.1016/j.ard.2025.11.021

INTRODUCTION: RECENT ADVANCE IN THE MANAGEMENT OF AUTOIMMUNE DISEASES AT A PREDISEASE STAGE

The management of autoimmune diseases is undergoing a major paradigm shift. Although rescue therapies have been traditionally introduced in symptomatic patients, the focus is now gradually shifting towards preventive strategies aimed at blocking the onset of clinically meaningful damage in at-risk populations [1–3]. In the field of type I diabetes, Teplizumab, an anti-CD3 antibody, successfully slowed the progression to clinical onset of type I diabetes in at-risk patients, ie, nondiabetic relatives of patients with diabetes who had at least 2 autoantibodies and abnormal results of an oral glucose-tolerance test at trial entry [1]. These findings were recently confirmed in newly diagnosed type I diabetes [2], and teplizumab is now Food and Drug Administration approved to prevent the onset of clinical disease [4]. This marks a turning point in the management of the world's most common autoimmune disease. In the field of rheumatic diseases, the APIPPRA (arthritis prevention in the preclinical phase of rheumatoid arthritis) trial assessed abatacept in patients at high risk of rheumatoid arthritis (RA), defined by a positivity for anticyclic citrullinated peptide antibody and rheumatoid factor with inflammatory joint pain [5]. The primary endpoint was the time to development of clinical synovitis in 3 or more joints or to development of RA according to the American College of Rheumatology (ACR) and European Alliance of Associations for Rheumatology (EULAR) 2010 criteria. This was a positive trial where the estimated proportion of participants remaining arthritis-free at 12 months was 93% in the abatacept group and 69% in the placebo group. The success of teplizumab for type I diabetes and the results from the APPIPRA trial in RA support the use of immunomodulators at predisease states.

This viewpoint aims to explore whether precondition trials could be applied in systemic sclerosis (SSc)—the systemic autoimmune rheumatic disease (SARD) with the highest mortality and substantial morbidity. Moreover, we discuss what candidate items defining a clinical condition in the area of 'pre-CTD (connective tissue diseases)' might be, with a specific focus on patients at risk of progression to SSc. Therefore, the purpose of this viewpoint is not to propose a definitive definition of pre-SSc, but rather to stimulate the development of a collectively endorsed framework, highlighting that the predisease area is pivotal to design further preventive treatments for SSc in the future.

NOSOLOGY OF SSC: FROM EARLY LIMITED SCLERODERMA TO VERY EARLY DISEASE AND PRE-SSC

Implementing therapeutics in the predisease stage of SSc—ie, pre-SSc, defined by patients at risk of developing overt SSc—could mark a turning point. However, a consensus definition of pre-SSc is still to be framed. Several important milestones have participated in defining SSc nosology, from the initial ACR 1980 classification criteria to the proposed definition for early limited SSc (early lSSc) by LeRoy and Medsger [6] in 2001, and to the 2013 ACR/EULAR classification criteria. More recently, the Very Early Diagnostic criteria Of Systemic Sclerosis (VEDOSS) were validated: these diagnostic criteria allowed a very early diagnosis of SSc, and also predicted the progression to definite SSc defined by the 2013 classification criteria [7–9]. The VEDOSS criteria have opened a new area of investigation and also of intervention trials that might support the use of therapies in this very early context to halt disease progression [7]. However, this endorsed definition of VEDOSS may be considered too narrow for the inclusion criteria of future prevention trials, supporting the notion that the definition of an 'at-risk population' should be broader to capture a wider spectrum of patients, potential clinical manifestations, and surrogate markers (Table). Looking at the abovementioned experiences in type I diabetes and RA, identifying patients in a disease stage preceding the VEDOSS phase—ie, a pre-SSc phase—could open a new window of opportunity to be investigated in the future [3,10]. SARDs and CTDs may share several signs and symptoms before they differentiate into a precise clinical picture, allowing the diagnosis of a specific disease. Raynaud's phenomenon (RP) is found in several SARDs, and other clinical features or biomarkers are mandatory to definitively identify a disease, and SSc in particular. The natural history of SSc evolution could thus include a pre-SSc phase—ie, at-risk patients—which might then be followed by the VEDOSS phase, and by SSc defined by the 2013 ACR/EULAR classification criteria. Such a nosological framework for the natural history of SSc could enable the design and selection of tailored interventions, outcome measures, and surrogate markers appropriate to each disease phase. This proposed framework for pre-SSc would not represent a disease state entirely devoid of clinical manifestations or reversible organ involvement, but would describe a stage in which patients who do not yet meet the VEDOSS or ACR/EULAR criteria can be identified and considered 'at risk' of developing established SSc. However, the question of how pre-SSc should be defined in the current era has not yet been adequately addressed, in contrast to the more clearly proposed definitions in type I diabetes and RA.

CANDIDATE ITEMS TO BE DEBATED, WEIGHED, AND REFINED IN FUTURE DISCUSSIONS FOR A CONSENSUS DEFINITION OF PRE-SSC

Considering that RP is among the hallmarks of many CTDs and SSc, it should be considered among the key candidate entry criteria for pre-CTDs—including pre-SSc—mirroring what was already thought in early lSSc [6] and in the VEDOSS strategy [11]. Items to be debated, weighed, and refined in future discussions to specifically define pre-SSc are suggested in the Table. The cons of several candidate items, regarding availability, feasibility, and reliability, will likely lead to the exclusion of many candidates. In addition to the early manifestations, key biomarkers of interest, either diagnostic biomarkers or surrogate markers of early reversible organ involvement or damage, should be addressed. In RA and type I diabetes, autoantibodies were the cornerstones of the definition of the 'at-risk population'. Similarly, SSc-related autoantibodies are also among the earliest SSc-related features of interest [12,13]. The 2013 ACR/EULAR SSc classification only considers anticentromere, antitopoisomerase I, and anti-RNA polymerase III antibodies in its scoring strategy [14]. Such an approach was conducted to favour specificity as expected for classification criteria. On the contrary, a pre-SSc framework might prioritise sensitivity, encouraging the inclusion of other SSc-related autoantibodies at a significant titre (>1:80) in the pre-SSc definition, as proposed by LeRoy and Medsger [6] in 2001. Antinucleolar fluorescence pattern, NOR-90, U1-RNP, U3-RNP (anti-fibrillarin), Th/To, PM-Scl, and anti-Ku antibodies should be discussed as candidate items [15]. However, the optimal methods of determination of each of these candidates are still on the research agenda, and robust validation assays are mandatory before any dissemination to practice. Moreover, a strategy relying solely on autoantibodies may not be successful due to low progression rate in some cases, as suggested by previous unsuccessful studies such as StopRA [16]. Established risk factors (Table) should

complement autoantibodies in a future definition of pre-SSc [17,18]. To date, a clinical scenario limited to known risk factors (Table), RP, and autoantibodies is not encompassed by any of the collectively endorsed definitions of SSc (neither VEDOSS nor the 2013 ACR-EULAR criteria), underscoring the need for a consensus definition of an 'at-risk population'. Emerging biomarkers such as type I interferon signature and assessment of early microvascular damage using largely validated nailfold capillaroscopy [19] should also be considered for a new framework of pre-SSc. To improve sensitivity to change and to select an at-risk population, the use of novel surrogate markers, assessing key domains of SSc at a potentially reversible state, could include magnetic resonance imaging (MRI), and/or Doppler ultrasound for vasculopathy [20,21], and/or skin ultrasound for cutaneous involvement, and/or molecular skin genotyping (Table) [22]. MRI was indeed included in the definition of pre-RA on the ARIAA trial [23], and similar surrogate markers should also be considered for pre-SSc.

PRIMARY OBJECTIVE AND RELATED OUTCOME MEASURES FOR FUTURE PRE-SSC TRIALS

Beyond selecting the target population, the choice of the primary objective for future intervention in at-risk patients will be crucial. In the RA TREAT EARLIER trial, the primary objective was to prevent the development of clinical arthritis defined as the involvement of 2 or more joints or the fulfilment of the 2010 classification criteria [10]. In SSc, the ACR/EULAR classification criteria for SSc were not designed to define the transition from pre-SSc to definite SSc, so their use in this setting warrants careful consideration. Likely, a pragmatic approach pairing fulfilment of some SSc classification (ACR/EULAR) or diagnostic criteria (VEDOSS) and the prevention of the onset of SSc-related clinical signs and irreversible complications, mirroring what was proposed in APIPPRA, could be a stimulating approach [5]. The damage to be prevented would include ischaemic/vascular complications (digital ulcers with pitting scars, pulmonary arterial hypertension or scleroderma renal crisis), inflammatory (myocarditis, arthritis or myositis) or functional complications (oesophageal dysmotility), or ultimately fibrotic manifestations (ie, ILD, heart and skin fibrosis) (Table). This scenario could mirror the onset of clinical arthritis in the RA TREAT EARLIER trial or the use of surrogate markers like in the ARIAA trial [23]. The inclusion of patient-reported outcome measures [24], and the careful assessment of how patients feel (ie, fatigue) and function will also be an assessment of utmost importance because it may also reflect the impact of early damage onset on patients' lives [25,26]. Robust surrogates of damage will have to be validated in pre-SSc patients to empower future trials by potentially reducing trial duration, thanks to the choice of measures with a high sensitivity to change (Table 1), because a preventive study with a duration of 12 months may not be sufficient to observe a

Table 1
. Candidate parameters to be included in the research agenda to shape a discussion on a multistage framewor for patients at risk of SSc

Risk factors	Potential red flags to be considered for a definition of pre-SSc: imaging, biological or clinical signs, and symptoms[a]	Surrogates of reversible tissue and organ involvement or damages[a]	Clinically meaningful SSc-related fibrotic or ischaemic features to be prevented
Established risk factors: • Crystalline silica exposure • Cancers in patients with anti-RNA polymerase III • Genetic variants In HLA and non-HLA variants.	Clinical signs and symptoms[b]: • Raynaud's phenomenon • Puffy fingers • Arthralgia • Gastro-oesophageal reflux	Vasculopathy: • Vascular MRI (DAVIX) • Blood flow determination: power Doppler, colour Doppler, laser Doppler or thermography	Vasculopathy: • Digital ulcers/gangrene • Scleroderma renal crisis • Pulmonary arterial hypertension (PAH)
Suspected risk factors: • Past viral infections • Solvent exposures • History of familial autoimmunity	Imaging and biological parameters: • Acute phase reactants • High interferon signature • Specific SSc-related autoantibodies at a significant titre (>1:80) (anticentromere antibodies, antitopoisomerase I antibodies, anti-RNA polymerase III antibodies). • Candidate nonspecific SSc-related antibodies (NOR-90, U1-RNP, U3-RNP, Th/To, PM-Scl, and anti-Ku antibodies) at a significant titre (>1:80). • Capillaroscopic findings	Synovial, tenosynovial, and bone involvement: • Joint ultrasound (synovitis and tenosynovitis) • Hand X-rays (acro-osteolysis/calcinosis) Skin involvement: • Skin ultrasound Interstitial lung disease: • Pulmonary functional tests • Lung imaging: HRCT, nuclear medicine/PET-CT, MRI Cardiopulmonary disease: - Cardiac imaging: echocardiography and MRI - Muscle/cardiac enzymes - ECG Gastrointestinal involvement: Oesophageal and rectal manometry GI ultrasound	Synovial, tenosynovial, and bone involvement: - Joint contractures - Arthritis - Tendon friction rub Skin involvement: • Skin fibrosis and atrophy Pulmonary disease: - ILD (PPF, Honey combing, OP) with an impact on functional capacities and QoL - PAH Cardiac disease attributable to SSc: • Myocarditis • Arrhythmias • Myocardial failure • Sudden death Gastrointestinal involvement: • Upper digestive complications • (oesophageal stricture, GAVE) • Malabsorption • Chronic pseudo-occlusion • Faecal incontinence • Small intestinal bacterial overgrowth (SIBO)

ECG, electrocardiogram; GI, gastrointestinal; GAVE, gastric antral vascular ectasia; HLA, human leukocyte antigen; HRCT, high-resolution computed tomography; ILD, interstitial lung disease; MRI, magnetic resonance imaging; NOR, nucleolar organizing region; OP, organizing pneumonia; PPF, progressive pulmonary fibrosis; PET-CT, positron emission tomography–computed tomography; PM, polymyositis; PAH, pulmonary arterial hypertension; QoL, quality of life; RNP, ribonucleoprotein; SSc, systemic sclerosis. For several candidate parameters, cut-offs will need to be established to ensure optimal sensitivity and specificity in this pre-SSc population/at-risk population.

[a] The majority of these candidate parameters or surrogate markers have not been evaluated in very early or pre-SSc/at-risk populations and require further investigation in these groups.

[b] Some of these clinical symptoms may represent manifestations at an 'early or very early' clinical stage of SSc. Some of these features may not strictly fall within a predisease definition, although this assumption should be discussed collectively for each item.

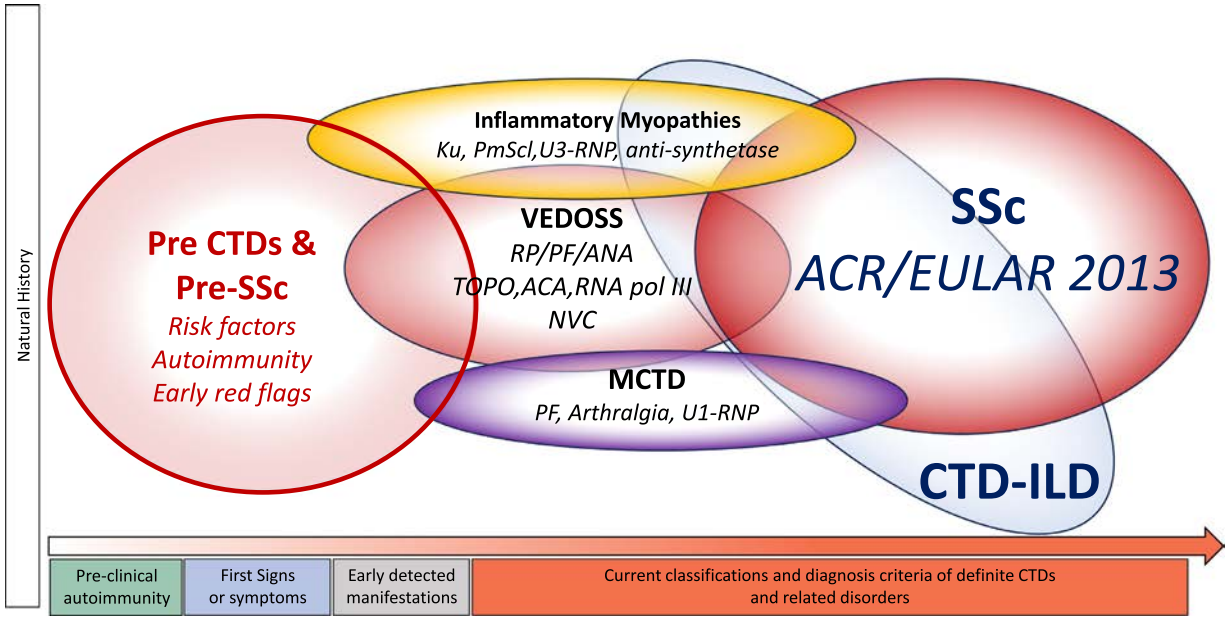

Figure 1. Nosological framework of scleroderma-like disorders, positioning pre-SSc as the earliest concept. The interplays between pre-SSc and the other nosological entities within the SSc landscape are also still to be determined. ACA, anti-centromere antibodies; ACR, American College of Rheumatology; ANA, anti-nuclear antibodies; CTD, connective tissue disease; EULAR, European Alliance of Associations for Rheumatology; ILD, interstitial lung disease; MCTD, mixed connective tissue disease; NVC, Nailfold Videao capillaroscopy; PF, puffy fingers; RP, Raynaud's phenomenon; RNP, ribonucleoprotein; SSc, systemic sclerosis; TOPO, anti-topoIsomerase I antibodies; VEDOSS, Very Early Diagnostic criteria of Systemic Sclerosis.

beneficial impact of treatment on disease progression. Candidate surrogate markers of future irreversible damage for such combined approaches could include ultrasound for skin or joint involvement, or Doppler and MRI for vascular damage. It remains to be determined whether priority should be given to the completion of a combined outcome or a time-to-event approach.

INTERVENTIONS AT A PREDISEASE STAGE IN SSC: A CAREFUL WEIGHING OF THE BENEFIT-RISK RATIO WILL BE WARRANTED

Another important challenge will be the choice of intervention. Our current understanding of SSc pathogenesis would encourage the use of immunosuppressants to prevent fibrosis. In VEDOSS, an initial attempt to demonstrate the impact of early anti-inflammatory intervention with glucocorticoids failed to differentiate the active drug from placebo when using capillaroscopic pattern change as the primary outcome [27,28]. In SSc, Mycophenolate Mofetil (MMF) is among the drugs with the highest level of evidence for interstitial lung disease (ILD) and skin disease [29–31], and could represent an option, while vasoactive drugs, lower intensity immunosuppression, or immunomodulators could also be options to be discussed. At-risk patients with high interferon signature may also benefit from interferon-targeting strategies, although the lack of current evidence may not support the use of such therapeutic as a first approach at a predisease stage [32–34]. There is burgeoning interest in innovative cellular therapies, but CD19-targeted chimeric antigen receptor T-cell are unlikely to be appropriate for a predisease stage considering the substantial burden associated with the procedure [35].

CONCLUSION: DEVELOPING A COLLECTIVELY ENDORSED FRAMEWORK FOR PRE-SSC

In contrast to type I diabetes and RA, where predisease states have been more clearly defined, a consensus definition for pre-SSc is still lacking. A consensus framework for patients with signs and symptoms also common to other SARDs/CTDs, but that potentially identify a patient at a pre-SSc stage, needs to be collectively drafted. Such a framework would provide the basis for earlier recognition, risk stratification, and ultimately, timely intervention. This may be achieved—as wisely proposed by LeRoy and Medsger [6] in 2001—by thinking outside the 'scleroderma' box (literally skin fibrosis) on which several classifications have crystallised their main interest. This effort is fundamental to reshape the nosology of the earliest stages of SSc (Fig. 1) [36]. Identifying genetic variants [37] or environmental factors [17], determining the earliest course of the disease, and shaping clinical trajectories will likely allow a personalised approach to improve the specificity of the definition and to enrich for populations at risk of cumulative damage in preventive trials. Considering the shift of paradigm in type I diabetes or RA, a similar strategy for patients at risk of SSc could foster the development of an innovative approach to SSc management, preventing key SSc-related signs and symptoms [28], leading to long-term remission and decreasing SSc-related individual morbidity and mortality.

FUNDING

This work was supported by a grant from the World Scleroderma Foundation: ad-hoc committee for Establishing a consensus definition for pre-systemic sclerosis (ECOPRESS ad-hoc committee).

COMPETING INTERESTS

AL and SB-R declared no conflicts of interest. YA reports a relationship with Corbus, Alpine ImmunoScience, and Merck that includes: funding grants. YA reports a relationship with Boehringer Ingelheim, BMS, GSK, Amgen, AbbVie, Topadur, Horizon, AstraZeneca, and Novartis that includes: consulting or advisory. FDG reports a relationship with AbbVie, Argenx,

AstraZeneca, Boehringer Ingelheim, Calluna, DeepCure, and Ergomed that includes: funding grants. FDG reports a relationship with Calluna, DeepCure, Ergomed, GSK, Janssen, Merck, Mitsubishi-Tanabe, Novartis, Serono, and Ventus that includes: funding grants. CPD reports a relationship with GSK, Horizon, Servier, and Arxx Therapeutics that includes: funding grants. CPD reports a relationship with Boehringer Ingelheim, Roche, CSL Behring, Acceleron, Horizon, Arxx Therapeutics, Centessa, AstraZeneca, Lilly, and Novartis that includes: consulting or advisory. CPD reports a relationship with Boehringer Ingelheim and Janssen that includes: speaking and lecture fees. DK reports a relationship with BMS, Bayer, Pfizer, and consulting fees from AbbVie, Genentech, GSK, Boehringer Ingelheim, AstraZeneca, Horizon, UCB, and Prometheus that includes: funding grants. DK reports a relationship with AbbVie Ltd. that includes: board membership. MK reports a relationship with Boehringer Ingelheim Canada Ltd that includes: funding grants and paid expert testimony. MK reports a relationship with Boehringer Ingelheim, AstraZeneca, GSK, and Novartis that includes: consulting or advisory. MK reports a relationship with Boehringer Ingelheim, Chugai that includes: speaking and lecture fees. MK reports a relationship with Agrenx that includes: board membership. MM-C reports a relationship with Boehringer Ingelheim, MSD, Lilly, Novartis, and Argenx that includes: speaking and lecture fees.

PATIENT CONSENT FOR PUBLICATION

Not applicable.

ETHICS APPROVAL

Not applicable.

PROVENANCE AND PEER REVIEW

Not commissioned; externally peer reviewed.

DECLARATION OF GENERATIVE AI AND AI-ASSISTED TECHNOLOGIES IN THE WRITING PROCESS

During the preparation of this work the authors used ChatGPT (OpenAI, San Francisco, CA, USA) was used solely for grammar and spelling editing in order to improve the readability and language. After using this tool/service, the authors reviewed and edited the content as needed and take full responsibility for the content of the published article.

CRediT authorship contribution statement

Alain Lescoat: Writing – review & editing, Writing – original draft, Validation, Conceptualization. **Yannick Allanore:** Writing – review & editing, Writing – original draft, Investigation, Conceptualization. **Francesco Del Galdo:** Writing – review & editing. **Masataka Kuwana:** Writing – review & editing. **Silvia Bellando-Randone:** Writing – review & editing. **Christopher P. Denton:** Writing – review & editing. **Dinesh Khanna:** Writing – review & editing. **Marco Matucci-Cerinic:** Writing – review & editing, Writing – original draft, Conceptualization.

REFERENCES

[1] Herold KC, Bundy BN, Long SA, Bluestone JA, DiMeglio LA, Dufort MJ, et al. An anti-CD3 antibody, teplizumab, in relatives at risk for type 1 diabetes. N Engl J Med 2019;381:603–13.

[2] Ramos EL, Dayan CM, Chatenoud L, Sumnik Z, Simmons KM, Szypowska A, et al. Teplizumab and β-Cell function in newly diagnosed type 1 diabetes. N Engl J Med 2023;389:2151–61.

[3] Lescoat A, Bellando-Randone S, Campochiaro C, Del Galdo F, Denton CP, Farrington S, et al. Beyond very early systemic sclerosis: deciphering pre-scleroderma and its trajectories to open new avenues for preventive medicine. Lancet Rheumatol 2023;5:e683–94.

[4] Keam SJ. Teplizumab: first approval. Drugs 2023;83:439–45.

[5] Cope AP, Jasenecova M, Vasconcelos JC, Filer A, Raza K, Qureshi S, et al. Abatacept in individuals at high risk of rheumatoid arthritis (APIPPRA): a randomised, double-blind, multicentre, parallel, placebo-controlled, phase 2b clinical trial. Lancet 2024;403:838–49.

[6] LeRoy EC, Medsger TA. Criteria for the classification of early systemic sclerosis. J Rheumatol 2001;28:1573–6.

[7] Bellando-Randone S, Del Galdo F, Lepri G, Minier T, Huscher D, Furst DE, et al. Progression of patients with Raynaud's phenomenon to systemic sclerosis: a five-year analysis of the European Scleroderma Trial and Research group multicentre, longitudinal registry study for Very Early Diagnosis of Systemic Sclerosis (VEDOSS). Lancet Rheumatol 2021;3:e834–43.

[8] Siqueira VS, Helbingen MFS, Medeiros-Ribeiro AC, Carriço da Silva H, Miossi R, Luppino-Assad AP, et al. Predictors of progression to systemic sclerosis: analysis of very early diagnosis of systemic sclerosis in a large single-centre cohort. Rheumatology (Oxford) 2022;61:3686–92.

[9] Lescoat A, Cavalin C, Ehrlich R, Cazalets C, Ballerie A, Belhomme N, et al. The nosology of systemic sclerosis: how lessons from the past offer new challenges in reframing an idiopathic rheumatological disorder. Lancet Rheumatol 2019;1:e257–64.

[10] Krijbolder DI, Verstappen M, van Dijk BT, Dakkak YJ, Burgers LE, Boer AC, et al. Intervention with methotrexate in patients with arthralgia at risk of rheumatoid arthritis to reduce the development of persistent arthritis and its disease burden (TREAT EARLIER): a randomised, double-blind, placebo-controlled, proof-of-concept trial. Lancet 2022;400:283–94.

[11] Avouac J, Fransen J, Walker UA, Riccieri V, Smith V, Muller C, et al. Preliminary criteria for the very early diagnosis of systemic sclerosis: results of a Delphi Consensus Study from EULAR Scleroderma Trials and Research Group. Ann Rheum Dis 2011;70:476–81.

[12] Burbelo PD, Gordon SM, Waldman M, Edison JD, Little DJ, Stitt RS, et al. Autoantibodies are present before the clinical diagnosis of systemic sclerosis. PLoS One 2019;14:e0214202.

[13] Chepy A, Bourel L, Koether V, Launay D, Dubucquoi S, Sobanski V. Can antinuclear antibodies have a pathogenic role in systemic sclerosis? Front Immunol 2022;13:930970.

[14] van den Hoogen F, Khanna D, Fransen J, Johnson SR, Baron M, Tyndall A, et al. 2013 classification criteria for systemic sclerosis: an American College of Rheumatology/European League against Rheumatism collaborative initiative. Arthritis Rheum 2013;65:2737–47.

[15] Lazzaroni MG, Marasco E, Campochiaro C, DeVries-Bouwstra J, Gonzalez-Perez MI, Rojas-Serrano J, et al. The clinical phenotype of systemic sclerosis patients with anti-PM/Scl antibodies: results from the EUSTAR cohort. Rheumatology (Oxford) 2021;60:5028–41.

[16] Haville S, Deane KD. Pre-RA: can early diagnosis lead to prevention? Best Pract Res Clin Rheumatol 2022;36:101737.

[17] Tomic D, Hoy RF, Sin J, Jimenez Martin J, Gwini SM, Barnes H, et al. Autoimmune diseases, autoantibody status and silicosis in a cohort of 1238 workers from the artificial stone benchtop industry. Occup Environ Med 2024;81:388–94.

[18] Smith V, Vanthuyne M, Vander Cruyssen B, Van Praet J, Vermeiren F, Smets H, et al. Over-representation of construction-related occupations in male patients with systemic sclerosis. Ann Rheum Dis 2008;67:1448–50.

[19] Smith V, Herrick AL, Ingegnoli F, Damjanov N, De Angelis R, Denton CP, et al. Standardisation of nailfold capillaroscopy for the assessment of patients with Raynaud's phenomenon and systemic sclerosis. Autoimmun Rev 2020;19:102458.

[20] Hughes M, Di Donato S, Gjeloshi K, Abignano G, Danzo F, Lettieri G, et al. MRI Digital Artery Volume Index (DAVIX) as a surrogate outcome measure of digital ulcer disease in patients with systemic sclerosis: a prospective cohort study. Lancet Rheumatol 2023;5:e611–21.

[21] Lescoat A, Robin F, Belhomme N, Ballerie A, de Saint, Riquier M, Sebillot M, et al. Ultrasound classification of finger pulp blood flow in patients with systemic sclerosis: a pilot study. Arthritis Care Res (Hoboken) 2023;75:299–306.

[22] Santiago T, Santiago M, Ruaro B, Salvador MJ, Cutolo M, da Silva JAP. Ultrasonography for the assessment of skin in systemic sclerosis: a systematic review. Arthritis Care Res (Hoboken) 2019;71:563–74.

[23] Rech J, Tascilar K, Hagen M, Kleyer A, Manger B, Schoenau V, et al. Abatacept inhibits inflammation and onset of rheumatoid arthritis in individuals at high risk (ARIAA): a randomised, international, multicentre, double-blind, placebo-controlled trial. Lancet 2024;403:850–9.
[24] Pauling JD, Caetano J, Campochiaro C, De Luca G, Gheorghiu AM, Lazzaroni MG, et al. Patient-reported outcome instruments in clinical trials of systemic sclerosis. J Scleroderma Relat Disord 2020;5:90–102.
[25] Murphy SL, Whibley D, Kratz AL, Poole JL, Khanna D. Fatigue predicts future reduced social participation, not reduced physical function or quality of life in people with systemic sclerosis. J Scleroderma Relat Disord 2021;6:187–93.
[26] Stamm T, Mosor E, Omara M, Ritschl V, Murphy SL. How can fatigue be addressed in individuals with systemic sclerosis? Lancet Rheumatol 2020;2:e128–9.
[27] Kersten BE, Lemmers JMJ, Vanhaecke A, Velauthapillai A, van den Hombergh WMT, van den Hoogen FHJ, et al. Efficacy of methylprednisolone in very early systemic sclerosis: results of the "Hit hard and early" randomized controlled trial. Rheumatology (Oxford) 2025;64:1261–9.
[28] Denton CP, De Lorenzis E, Roblin E, Goldman N, Alcacer-Pitarch B, Blamont E, et al. The 2024 British Society for Rheumatology guideline for management of systemic sclerosis. Rheumatology (Oxford) 2024;63:2956–75.
[29] Del Galdo F, Lescoat A, Conaghan PG, Bertoldo E, Čolić J, Santiago T, et al. EULAR recommendations for the treatment of systemic sclerosis: 2023 update. Ann Rheum Dis 2025;84:29–40.
[30] Lescoat A, Bertoldo E, Čolić J, Santiago T, Suliman YA, Emmel J, et al. Results from the international collaborative systematic literature review informing the 2023 EULAR recommendations for the treatment of systemic sclerosis. Ann Rheum Dis 2025;84:77–92.
[31] Tashkin DP, Roth MD, Clements PJ, Furst DE, Khanna D, Kleerup EC, et al. Mycophenolate mofetil versus oral cyclophosphamide in scleroderma-related interstitial lung disease (SLS II): a randomised controlled, double-blind, parallel group trial. Lancet Respir Med 2016;4:708–19.
[32] Brkic Z, van Bon L, Cossu M, van Helden-Meeuwsen CG, Vonk MC, Knaapen H, et al. The interferon type I signature is present in systemic sclerosis before overt fibrosis and might contribute to its pathogenesis through high BAFF gene expression and high collagen synthesis. Ann Rheum Dis 2016;75:1567–73.
[33] Di Donato S, Ross R, Karanth R, Kakkar V, De Lorenzis E, Bissell LA, et al. Serum type I interferon score for prediction of clinically meaningful disease progression in limited cutaneous systemic sclerosis. Arthritis Rheumatol 2025;77:929–41.
[34] Ross RL, Caballero-Ruiz B, Clarke EL, Kakkar V, Wasson CW, Mulipa P, et al. Biological hallmarks of systemic sclerosis are present in the skin and serum of patients with Very Early Diagnosis of Systemic Sclerosis (VEDOSS). Rheumatology (Oxford) 2025;64:3606–17.
[35] Lescoat A, Ghosh M, Kadauke S, Khanna D. Innovative cell therapies for systemic sclerosis: available evidence and new perspectives. Expert Rev Clin Immunol 2025;21:29–43.
[36] LeRoy EC, Black C, Fleischmajer R, Jablonska S, Krieg T, Medsger TA, et al. Scleroderma (systemic sclerosis): classification, subsets and pathogenesis. J. Rheumatol. 1988;15:202–5.
[37] Orvain C, Assassi S, Avouac J, Allanore Y. Systemic sclerosis pathogenesis: contribution of recent advances in genetics. Curr Opin Rheumatol 2020;32:505–14.

Ann Rheum Dis 85 (2026) 787–796

Contents lists available at ScienceDirect

Annals of the Rheumatic Diseases

journal homepage: https://www.sciencedirect.com/journal/annals-of-the-rheumatic-diseases

Rheumatoid arthritis

Safety and immunogenicity of the recombinant zoster vaccine in patients with rheumatoid arthritis using abatacept: a pilot multicentre, double-blind, randomised controlled trial

Jeremy A Hawkins[1], Jeffrey R Curtis[2], Adriana Weinberg[3], Sarah A R Siegel[1], Joseph E Huffstutter[4], James Loveless[5], Suzanne Gharib[6], Shanmugapriya Reddy[7], Jayashree Sinha[8], David Ridley[9], Ilhem Messaoudi[10], Jin Kyun Park[11], Eun Bong Lee[11], Kevin L Winthrop[1,12,*]

[1] *Oregon Health & Science University, School of Public Health, Portland, OR, USA*
[2] *Division of Clinical Immunology & Rheumatology, University of Alabama at Birmingham, Birmingham, AL, USA*
[3] *Departments of Pediatrics, Medicine, and Pathology, University of Colorado, University of Colorado School of Medicine, Aurora, CO, USA*
[4] *Arthritis Associates, Hixson, TN, USA*
[5] *St. Luke's Health System, Rheumatology, Boise, ID, USA*
[6] *Charleston Area Medical Center, Charleston, WV, USA*
[7] *Southwest Florida Rheumatology, Riverview, FL, USA*
[8] *Arthritis & Medical Center, Clovis, NM, USA*
[9] *St. Paul Rheumatology, Eagan, MN, USA*
[10] *University of Kentucky Microbiology, Immunology, and Molecular Genetics, Lexington, KY, USA*
[11] *Division of Rheumatology, Department of Internal Medicine, Seoul National University College of Medicine, Seoul, South Korea*
[12] *Oregon Health & Science University, School of Medicine, Portland, OR, USA*

ARTICLE INFO

Article history:
Received 30 September 2025
Received in revised form 31 December 2025
Accepted 2 January 2026

ABSTRACT

Objectives: The objective of the study is to evaluate the safety and immunogenicity of the recombinant zoster vaccine (RZV) in patients with rheumatoid arthritis (RA) using abatacept.
Methods: We randomised 70 participants to receive 2 doses of RZV or placebo 8 weeks apart. The primary immunologic endpoint was the proportion of participants developing a ≥4-fold increase in anti-glycoprotein E (gE) immunoglobulin (Ig)G antibodies (humoral responders) and those developing a ≥2-fold increase in interferon gamma (IFN-γ)$^+$ or interleukin-2 (IL-2)$^+$ gE-specific spot-forming cells (cellular responders), at week 12 (ie, 4 weeks post-second RZV dose). The secondary immunologic endpoint was the geometric mean fold rise (GMFR) in cellular and humoral vaccine responses. For safety, we solicited adverse events following each dose, serious adverse events (SAEs) during the 52-week study period, and evaluated the potential for RA flares by assessing pre- and postvaccination Disease activity score-28 for rheumatoid arthritis with erythrocyte sedimentation rate, Clinical Disease Activity Index (CDAI), and Outcome Measures in Rheumatology (OMERACT) rheumatoid arthritis flare questionnaire (RA-FQ) scores.
Results: Fifty-six (75%) participants received RZV, and 14 (25%) received a placebo. Among those receiving RZV, only 22 (42.3%) of participants surpassed the 4-fold threshold for humoral

*Correspondence to Dr Kevin L Winthrop, Oregon Health & Science University, Portland, OR, USA.
E-mail address: winthrop@ohsu.edu (K.L. Winthrop).
Handling editor Josef S Smolen

https://doi.org/10.1016/j.ard.2026.01.002

response, and anti-gE IgG GMFR at week 12 was 4.55 (3.16, 6.47). Only 5 (10.2%) patients with RZV mounted cellular responses. Six SAEs were noted, and the proportion of patients with RA flare was similar between RZV and placebo groups (38 [68%] vs 9 [64%]).
Conclusions: Our data suggest that RZV is safe in patients with RA using abatacept, but that the vaccine response is attenuated in such patients. Further studies should be undertaken to evaluate whether holding abatacept around the time of vaccination would improve vaccine response.

WHAT IS ALREADY KNOWN ON THIS TOPIC

- Patients with immune-mediated inflammatory diseases are at increased risk for herpes zoster (shingles), and its prevention remains an important unmet need in this setting.
- The recombinant zoster vaccine (RZV) is recommended to be used in such patients, but little experimental data exist in this setting, evaluating its immunogenicity, efficacy, or safety.
- Real-world data suggest reduced effectiveness of the vaccine among patients with immune-mediated inflammatory diseases.
- Abatacept is frequently used to treat rheumatoid arthritis (RA), and given its mechanism of action, it is likely to reduce vaccine immunogenicity. However, the immunogenicity, safety, and efficacy of RZV are unknown in those using abatacept.

WHAT THIS STUDY ADDS

- Our data suggest that patients with RA using abatacept, who are vaccinated with RZV, mount little humoral or cell-mediated responses to the vaccine.
- Patients with RA using abatacept were no more likely to suffer RA flares after RZV vaccination than were those receiving placebo vaccine.

HOW THIS STUDY MIGHT AFFECT RESEARCH, PRACTICE OR POLICY

- Our study suggests that vaccinating patients with RA against RZV while they are using abatacept is unlikely to produce robust immune responses. Future studies should evaluate whether alternative vaccination strategies for patients in this population may improve vaccine immunogenicity (eg, holding abatacept for some time period before or after vaccination).

BACKGROUND

Prevention of herpes zoster (HZ), or shingles, remains an important unmet need in the field of rheumatology. Patients with rheumatoid arthritis (RA), systemic lupus erythematous, and other autoimmune inflammatory rheumatic diseases (AIIRDs) are at several fold higher risk of HZ than individuals of similar ages without these underlying diseases [1]. This increased risk is not only due to the immune dysregulation of their disease but also in part to the disease-modifying antirheumatic drugs (DMARDs) used to treat these conditions, particularly Janus kinase inhibitors (JAKi) and corticosteroids [1,2]. Prevention of HZ is possible with the recombinant subunit vaccine—recombinant zoster vaccine (RZV) (aka Shingrix). RZV provided robust humoral and cell-mediated immune (CMI) responses in phase 3 trials of healthy individuals aged 50 years and greater and included clinical efficacy of over 90% [3,4]. More recently, long-term data from these participants showed continued high vaccine efficacy 10 years postvaccination [5]. Although AIIRD populations are advised to be immunised with RZV by the United States (U.S.) Center for Disease Control (CDC) and Specialty societies such as the American College of Rheumatology [6,7], there is little information regarding the immunogenicity, efficacy, or safety of this vaccine among such patients.

Clinically, recent evidence has found RZV to be immunogenic in patients with AIIRD with systemic lupus erythematosus [8]. Real-world data suggest effectiveness of RZV among these and other immunosuppressed patients, however, is somewhat reduced [9,10]. A recent population-based study of those with inflammatory arthritis found RZV to have 50% effectiveness [11]. It is likely that DMARD usage partially explains the observed decrease in RZV efficacy, as some immunomodulatory therapies used in RA have been shown to attenuate responses to influenza and other vaccinations [12,13]. Abatacept (ABA), a costimulatory CD80/86 antagonist that decreases T cell proliferation, is one such DMARD. It has been shown to attenuate humoral and cell-mediated response to some vaccines in patients with RA, but to date, RZV has not formerly been studied [14–17]. In this study, we sought to evaluate the immunogenicity and safety of RZV in patients with RA using abatacept.

METHODS

The study was approved by Oregon Health & Science University's (OHSU) Institutional Review Board (IRB), with subsites either waiving oversight to OHSU's IRB or opting for local IRB oversight. This trial is registered with ClinicalTrials.gov, NCT03604406, and was first registered on May 7, 2021. The first participant was enrolled in the trial on May 25, 2021.

Study design

Participating rheumatology sites screened prospective patients with RA aged 18 or older actively using intravenous (IV) or subcutaneous (SQ) abatacept with stable dosing for ≥30 days at the time of enrolment. ABA use was defined as receipt of an IV dose within the last 1 month, or SQ use within the previous week. Patients with a history of shingles in the last 12 months, or prior shingles vaccination with RZV, or receipt of the live zoster vaccine (ie, Zostavax) in the previous 6 months were not eligible. Concomitant methotrexate (MTX) use (≤25 mg/wk) or other traditional synthetic DMARDs was allowable if dosing was stable for at least 30 days prior to enrolment. Prednisone-equivalent glucocorticoids were permitted up to doses of 10 mg/d. Concomitant use of other biologics was not permitted; prior B-cell depleting therapy was permitted if the most recent dose was >6 m before randomisation. Participants were randomised in a double-blind fashion to receive RZV (Shingrix) or placebo (saline) at a 4:1 ratio, respectively (Fig 1). The placebo vaccine comparator was chosen to evaluate whether the occurrence of flares of underlying RA disease was more common in participants with RA using ABA after being vaccinated with RZV. After consent, patients were vaccinated on day 1 and again at 8 weeks to complete the 2-dose series. We collected blood 4 weeks after vaccine completion (week 12) for our primary immunogenicity outcome. We evaluated long-term maintenance of response at week 60 (ie, 52 weeks after completion of the series). We actively solicited adverse event (AE) and reactogenicity information using daily diaries and phone calls once

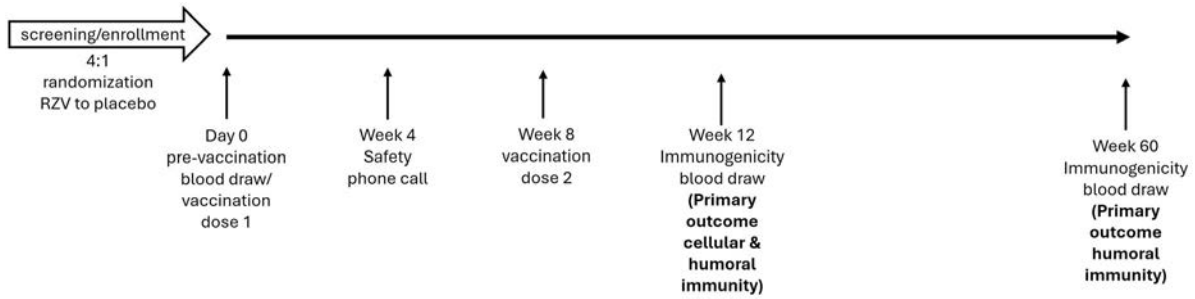

Figure 1. Study design. RZV, recombinant zoster vaccine.

weekly in the 4 weeks after each vaccination. We collected serious AE (SAE) information from day 1 through the end of week 60. We sought evidence of RA flares once weekly using the Outcome Measures in Rheumatology (OMERACT) RA flare questionnaire (RA-FQ) [18], and at weeks 8 and 12 at clinical visits using the Disease activity score-28 for rheumatoid arthritis with erythrocyte sedimentation rate (DAS28-ESR) [19] and the Clinical Disease Activity Index (CDAI) [20].

Laboratory methods

Humoral response

Varicella zoster virus (VZV) glycoprotein E (gE) enzyme-linked immunosorbent assay (ELISA) was performed in Dr Weinberg's laboratory at the University of Colorado using recombinant VZV-gE (VZV-rgE) courtesy of Glaxo-Smith-Kline. The assay was developed and validated in Dr Schmid's at the CDC National VZV Laboratory [21] and subsequently validated in Dr Weinberg's laboratory using 20 plasma samples from pre-vaccination and 30 days after the second dose of vaccine previously tested at the CDC. The assay has intra- and interassay coefficient of variation of 12%. The mean (SD) at 30 days after the second dose of RZV in older adults without known immunocompromising conditions is 94 (88) EU/mL. Ninety-six-well Immulon microtiter ELISA plates (Dynex Technologies, Inc) are coated with 100 µL/well VZV-rgE in phosphate-buffered saline (PBS) at 1 µg/mL. After 18- to 20-hour incubation at 4°C plates are washed, blocked with 5% skim milk in wash buffer (0.1% PBS/Tween 20). Test plasma samples at 1:20 in blocking solution are added to antigen-coated duplicate wells at 100 µL/well and incubated at room temperature for 35 minutes. Plates are washed and goat antihuman immunoglobulin (Ig)G-alkaline phosphatase conjugate (SouthernBiotech, Cat. no 2040-04) diluted 1:1000 in blocking solution is added at 100 µL/well and incubated for 30 minutes. Plates are washed, and p-nitrophenyl phosphate substrate (ImmunoChemistry Tech, SKU: 6279) is added for 10 minutes, after which the reaction is stopped with 3N NaOH as per the manufacturer's instructions. Plates are read on a spectrophotometer at 405 nm. Adjusted optical density (OD) is calculated as: mean test OD minus blank. Serial dilutions of the same control sample are included on every plate. Test samples OD are interpolated onto the control standard curve as above.

Cell-mediated immune (CMI) response

Fluorescence-Linked ImmunoSpot (FLUOROSPOT) assays to assess CMI response to RZV were performed in Dr Weinberg's laboratory at the University of Colorado. Dr Weinberg's laboratory participated in multiple zoster vaccine studies, including the pivotal zoster vaccine live (ZVL) clinical trial that led to the vaccine licensure and a subsequent trial that led to the U.S. Food and Drug Administration (FDA) approval of a booster dose of ZVL ≥10 years after the initial dose. Most recently, the laboratory performed studies comparing the immunogenicity of RZV and ZVL in older adults and immunocompromised hosts that used the same FLUOROSPOT assays that were used in this study [22–24]. The performance characteristics of the assay were extensively studied. For gE, the assay was validated using 30 paired peripheral blood mononuclear cell (PBMC) samples from prevaccination and 30 days after the second dose of vaccine kindly provided by GSK from their phase 2 studies. The FLUOROSPOT assay is highly reproducible with intra-assay and inter-assay mean coefficient of variations of 14% and 24% for interferon gamma (IFN-γ) and 25% and 33% for interleukin-2 (IL-2). These cytokines characterise effector and memory T helper type 1 (Th1) responses, respectively, that are deemed to be critical for protection against HZ. The gE-specific lower limit of detection of 20 spot-forming cells (SFCs)/10^6 PBMC was defined by the mean ± 2 SD SFC/10^6 PBMC in VZV-seronegative individuals. Mean (SD) responses in older adults without known immunocompromising conditions at 30 days after the second dose of RZV are 268.4 (216.2) SFC/10^6 PBMC for IFN-γ and 475.1 (297.8) SFC/10^6 PBMC for IL-2. PBMCs are separated from heparinised blood on Ficoll-Hypaque gradients (Sigma) and cryopreserved for viability [25]. Cryopreserved PBMCs are thawed and rested overnight at 37°C and 5% CO_2 humidified atmosphere at 10^6 PBMC/mL in growth medium consisting of Roswell Park Memorial Institute (RPMI) 1640 (Mediatech) with L-glutamine (Gemini BioProducts), 10% human AB serum (Gemini BioProducts), 2% 4-(2-hydroxyethyl)-1-piperazineethanesulfonic acid (HEPES) (Mediatech), and 1% penicillin-streptomycin (Gemini BioProducts). PBMCs are stimulated with VZV-gE overlapping peptides at 2.5 µg/mL final concentration (Millipore) or inactivated VZV cell lysate at the equivalent of 50,000 plaque-forming units/mL and incubated at 37°C and 5% CO_2 humidified atmosphere for 48 h in 96-well dual-colour IFN-γ and IL-2 FLUOROSPOT plates (Mabtech) in duplicate wells at 250,000 cells/well. Unstimulated and phytohemagglutinin (PHA) controls are included. SFCs are revealed as per the manufacturer's instructions. Results were reported as the mean number of SFC/10^6 PBMC in VZV-gE- or VZV lysate-stimulated wells after subtraction of the SFC in mock-stimulated controls. Test samples were considered positive if antigen-stimulated wells had SFC ≥2-fold higher than mock control and the results were ≥20 SFC/10^6 PBMC after subtraction of SFC in mock control, which is the threshold that differentiates VZV-seropositive from seronegative individuals [21] in this Clinical Laboratory Improvement Ammendments (CLIA)-certified assay. An assay control of PBMC from a single leukopack with known performance characteristics was included in each run for reproducibility and validation. Note that all CMI result data presented within the results section of this manuscript are those using

VZV-gE-stimulated assays. The results using VZV-lysate-stimulated wells were similar and are presented in Supplementary Tables S1 and S2.

Safety

Safety was assessed by tabulating AE frequencies by treatment group, and by evaluating rheumatologic disease activity at pre- and postvaccination study visits and phone calls as described in the study design section. We calculated proportions of participants experiencing RA flares as measured by participant self-report as well as by assessing the change in DAS28-ESR, CDAI, and RA-FQ scores over time and comparing them against a threshold above which was considered evidence of RA flare. DAS28-ESR categories were used in the descriptive analyses to better characterise prevaccination disease. The categories were defined by the following cut-offs: <2.6: remission, >2.6 and ≤3.1: low activity, ≥3.2 and ≤5.0: moderate disease activity, and ≥5.1: high disease activity [26]. At the postvaccination assessments, our primary method for detecting RA disease flare was the DAS28-ESR, with score increase >1.2, or >0.6 if the follow-up score was >3.2, indicating flare [27]. We considered a score increase >2 by CDAI as evidence of a flare. We used a change threshold of >10 in RA-FQ score in weeks 1 to 4 or weeks 9 to 12 as evidence of a flare as measured by RA-FQ. Participants with evidence of a flare at multiple follow-up assessments were only counted in the earliest study week in which a flare was identified.

Statistical analyses

Given the pilot nature of this study, formal sample size calculations were not performed, and a sample size of 70 participants was considered sufficient to provide enough information to assess whether a future study was warranted. Primary and secondary immunogenicity outcomes were evaluated in the per-protocol population, defined as both having received the study intervention and having paired valid blood samples for pre- and postvaccination measurements. Descriptive and safety analyses were conducted in the intention-to-treat population, defined as all randomised participants.

For humoral evaluation, we used pre- and postvaccine anti-gE IgG levels to calculate individual fold rises and group-level geometric mean fold rises (GMFRs) at each postvaccination time point. We used a ≥4-fold increase threshold to define humoral responders, and also conducted a sensitivity analysis using a ≥2-fold increase for response. GMFR was calculated by computing the fold changes between pre-and postvaccination measurements, log transforming these values, calculating the mean, and exponentiating the results to transform them back to their original units.

For evaluation of CMI, IFN-γ^+ and IL-2$^+$ gE-specific SFC measurements that were negative or zero were replaced with 10 for the purpose of statistical analyses, which was equivalent to one-half of the positive signal threshold of 20 established for the FLUOROSPOT assay. Response was defined as a ≥2-fold increase in SFCs for participants who had a prevaccination measurement ≥20, or seroconversion to any value above the positive signal threshold for participants whose prevaccination CMI measurements were <20. GMFR and 95% CIs were calculated using pre- and postvaccine SFC levels. Participants were included in each calculation that they had a paired measurement for by time and immunological marker, unless they experienced a HZ event, in which case they were censored from immunological analyses at subsequent weeks.

Any participants missing prevaccination measurement for a specific marker were excluded from immunological analyses for that marker. Participants who did not receive both doses of RZV/placebo, or who withdrew before reaching week 12, were excluded from immunologic analyses but included in descriptive and safety analyses. We conducted a prespecified subgroup stratified analysis of our immunogenicity endpoints according to concomitant MTX use (yes/no) at the time of enrolment.

Proportions of immune response and RA flare detection were compared between treatment groups using Fisher's exact test at $\alpha = 0.05$ significance level. We evaluated the correlation between the fold change in humoral and CMI measures using Kendall's tau. Pairwise comparisons between DAS28-ESR and our secondary flare measures were made using Cohen's kappa to assess the agreement between measures.

RESULTS

We enrolled a total of 70 participants (vaccine: 56, placebo: 14) in the study (Table 1). Participant retention throughout the study is presented in Supplementary Figure. Median ages of participants at enrolment were 66 and 64 years in the vaccine and placebo groups, respectively. Most participants were using IV

Table 1
Summary statistics at enrolment by treatment group

Characteristic	Vaccine (n = 56)[a]	Placebo (n = 14)[a]
Age (y)[b]	66 (41, 88)	64 (31, 80)
Sex		
Female	47 (84%)	11 (79%)
Race		
American Indian/Alaska Native	1 (1.8%)	0 (0%)
Black or African American	1 (1.8%)	0 (0%)
White	53 (95%)	14 (100%)
Other	1 (1.8%)	0 (0%)
Hispanic or Latino ethnicity	12 (21%)	3 (21%)
Duration of rheumatoid arthritis disease (y)[b]	10 (1, 67)	12.5 (5, 47)
Duration of abatacept therapy at enrolment (y)[b]	2 (<1, 11)	2 (<1, 8)
Abatacept route of administration		
Intravenous	37 (66%)	8 (57%)
Subcutaneous	13 (23%)	5 (36%)
Not reported	6 (11%)	1 (7%)
Time between previous dose of abatacept and first dose of vaccine/placebo (days)[b]		
Intravenous	0 (0, 34)	0 (0, 35)
Subcutaneous	3 (1, 6)	5 (2, 11)
Not reported	0 (0, 2)	0 (0, 0)
Ever received anti-TNF therapy	50 (89%)	10 (71%)
Ever received rituximab therapy	8 (14%)	0 (0%)
Ever received tocilizumab therapy	13 (23%)	3 (21%)
Methotrexate use at time of first vaccination	18 (32%)	7 (50%)
Corticosteroid use in last 30 d	10 (18%)	3 (21%)
Dose per day (mg)[b]	5 (2.5, 10)	5 (5, 5)
DAS28-ESR score[c]	3.3 (1.5)	2.8 (1.9)
DAS28-ESR category		
In remission (<2.6)	21 (37.5%)	8 (57.1%)
Low activity (2.6-3.1)	8 (14.3%)	0
Moderate activity (3.2-5.0)	16 (28.6%)	3 (21.4%)
High activity (≥5.1)	10 (17.9%)	3 (21.4%)
CDAI score[c]	20.0 (15.7)	19.2 (19.2)

Anti-TNF, antitumour necrosis factor; CDAI, Clinical Disease Activity Index; DAS28-ESR, Disease Activity Score for rheumatoid arthritis with erythrocyte sedimentation rate.
[a] n (%) unless otherwise indicated.
[b] Median (range).
[c] Mean (SD).

abatacept, with 37 (66%) and 8 (57%) in the vaccine and placebo groups, respectively. Most participants in each group received their next dose of abatacept on the same day as the first vaccination with RZV or placebo. Moreover, all but 2 participants received their most recent dose of abatacept within the required dosing window (4 weeks for IV abatacept and 1 week for SQ abatacept), but 2 participants (1 vaccine, 1 placebo) were enrolled despite being >1 month since their last IV abatacept dose at 34 and 35 days for each and were considered protocol violators, but were included in the primary analyses. Most participants reported previously receiving antitumour necrosis factor therapy (Table 1). Concomitant MTX was used by 18 (32%) participants in the RZV group and 7 (50%) in the placebo group. Roughly half of participants in each treatment group were in remission or had low disease activity at enrolment (Table 1).

Immunogenicity results

Humoral response

Among those receiving RZV, 22 (42.3%) exhibited a ≥4-fold change in anti-gE IgG concentration at week 12, and 9 (18.4%) at week 60 (Table 2, Supplementary Table S3). The anti-gE IgG GMFR (95% CI) at week 12 was 4.55 (3.16, 6.47) and 2.24 (1.65, 2.94) at week 60 (Fig 2). No participants in the placebo group had humoral responses at any timepoint. In a sensitivity analysis using a 2-fold increase in anti-gE IgG antibodies threshold, the proportion of humoral responders in the RZV group increased to 36 (69.2%) at week 12 and 19 (38.8%) at week 60.

Among RZV participants using concomitant MTX with valid paired blood samples (n = 17), 5 (29.4%) were humoral responders. In participants lacking MTX, 17 (48.6%) were responders. At week 60, 2 (12.5%) MTX users and 7 (21.2%) nonusers were humoral responders. An additional subgroup analysis of the vaccine group found that participants with or without concomitant corticosteroid use had similar proportions of humoral responders as was seen in MTX/no MTX subgroups, respectively (Table 2).

CMI response

Among patients with RZV with a week 12 measurement, 9 (18.4%) were CMI responders and 6 (13.0%) were responders at week 60, compared to 1 (7.1%) and 2 (15.4%) in the placebo group at weeks 12 and 60, respectively (Table 2). IFN-γ^+ and IL-2^+ SFC/10^6 PBMC GMFRs at week 12 were negligible in those receiving RZV (1.13 [0.94, 1.35] and 1.23 [1.00, 1.48], respectively) and similar to those receiving placebo (1.07 [0.89, 1.20] and 1.05 [0.90, 1.21], respectively).

MTX did not appear to influence CMI responses. Among participants in the RZV group using MTX at entry, 3 (17.6%) were CMI responders at week 12, compared to 6 (18.8%) among those not taking MTX. When stratified by concomitant corticosteroid use, the proportion of responders was also similar among steroid users and nonusers.

We evaluated whether age was associated with responses and stratified the vaccine group by age ≥50 (n = 9) and <50 (n = 43). At week 12, the younger group had a greater humoral response, with 7 (78%) responders compared to 15 (35%) (P = .027). While humoral responses were diminished at week 60, the difference remained with 4 (44%) in the younger group compared to 5 (12.5%) in the older group (P = .046). CMI responses were similarly poor across age groups, with 2 (25%) week 12 responders in the younger group compared to 7 (17%) in the older group. We stratified the vaccine group by whether they experienced an injection site reaction or not to seek

Table 2
Proportion of participants with immune response within strata

Week	By treatment group[a]			By concomitant methotrexate use (vaccine group only)[a]			By concomitant corticosteroid use (vaccine group only)[a,b]		
Humoral immunity	Vaccine n[c] % (95% CI)	Placebo n[c] % (95% CI)	*P* value[d]	MTX n[c] % (95% CI)	No MTX n[c] % (95% CI)	*P* value[d]	CS n[c] % (95% CI)	No CS n[c] % (95% CI)	*P* value[d]
Week 12	22/52	0/14	.003	5/17	17/35	.24	3/10	19/42	.49
	42.3 (28.7, 56.8)	0		29.4 (10.3, 56.0)	48.6 (31.4, 66.0)		30.0 (6.7, 65.2)	45.2 (29.8, 61.3)	
Week 60	9/49	0/13	.18	2/16	7/33	.70	0/10	9/39	.17
	18.4 (8.8, 32.0)	0		12.5 (1.6, 38.3)	21.2 (9.0, 38.9)		0	23.1 (11.1, 39.3)	
Cellular immunity									
Week 12	9/49	1/14	.43	3/17	6/32	1	2/10	7/39	1
	18.4 (8.8, 32.0)	7.1 (0.18, 33.9)		17.6 (3.8, 43.4)	18.8 (7.2, 36.4)		20.0 (2.5, 55.6)	17.9 (7.5, 33.5)	
Week 60	6/46	2/13	1	3/16	3/30	.41	0/10	6/36	.31
	13.0 (4.9, 26.3)	15.4 (1.9, 45.4)		18.8 (4.0, 45.6)	10.0 (2.1, 26.5)		0	16.7 (6.4, 32.8)	

CS, corticosteroid; MTX, methotrexate.
Cellular response was defined as ≥2-fold increase in either IFN-γ+ or IL-2+ gE-specific spot-forming cells. Humoral response was defined as ≥4-fold increase in anti-gE IgG antibodies. IFN-γ, interferon gamma; IL-2, interleukin-2; gE, glycoprotein E; IgG, immunoglobulin G.
[a] Participants included in immunological analyses by group: vaccine: 54, placebo 14; MTX: 17; no MTX = 37; CS: 10, No CS: 44.
[b] The proportions of participants in the MTX/No MTX groups that were also using CS were: MTX + CS: 3 (18%), CS only: 7 (19%). Responder proportions are further broken down by these measures in Supplementary Table S3.
[c] Each results cell includes the count of participants that mounted a response out of the total participants in that group with evaluable samples for the specified timepoint and immunity marker in addition to the proportion with 95% CI calculated using the Clopper-Pearson method.
[d] Fisher's exact test, α = 0.05.

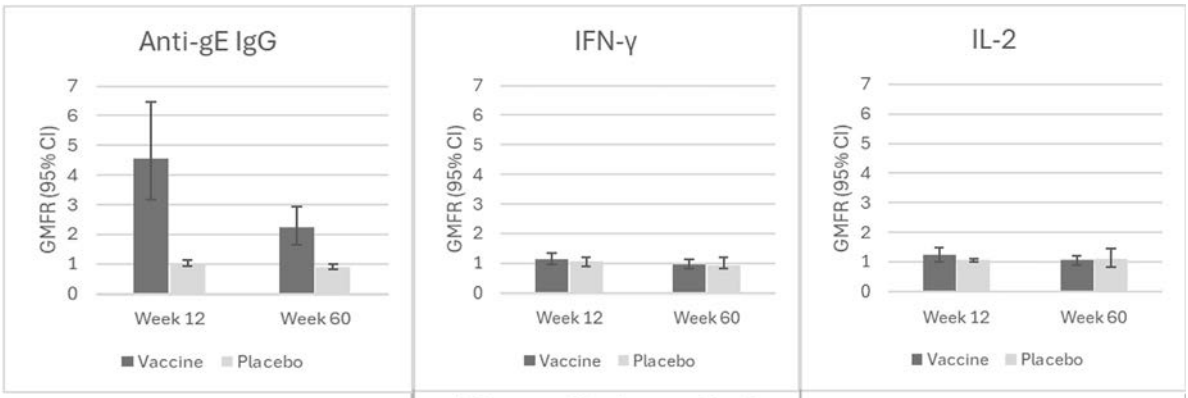

Anti-gE IgG	Vaccine	Placebo
Week 12	4.55 (3.16, 6.47)	1.02 (0.91, 1.13)
Week 60	2.24 (1.65, 2.94)	0.89 (0.80, 0.99)

IFN-γ	Vaccine	Placebo
Week 12	1.13 (0.94, 1.35)	1.07 (0.89, 1.20)
Week 60	0.97 (0.82, 1.12)	0.91 (0.81, 1.19)

IL-2	Vaccine	Placebo
Week 12	1.23 (1.00, 1.48)	1.05 (0.98, 1.10)
Week 60	1.05 (0.90, 1.21)	1.11 (0.83, 1.44)

Figure 2. Geometric mean fold rise (GMFR) (95% Confidence interval) in humoral (anti-gE IgG) and cell-mediated (IFN-γ^+ and IL-2^+ gE-specific spot-forming cells) immune responses from prevaccination measurements. Cellular response was defined as ≥2-fold increase in either CMI activation marker; humoral response was defined as ≥4-fold increase in anti-gE IgG antibodies. gE, glycoprotein E; IgG: immunoglobulin G; IFN-γ, interferon gamma; IL-2, interleukin-2; CMI, cell-mediated immune.

evidence of a reactogenicity-immunogenicity link. While there were small differences in proportions of responders, they were not statistically significant. When comparing immune responses in the vaccine group between participants who were receiving ABA IV vs SQ, we found statistically significant differences, with SQ having a greater proportion of participants achieving immune response. At week 12, 8 (62%) SQ participants had humoral response compared to 12 (35%) IV participants (P = .19), whereas at week 60, 5 (50%) SQ participants achieved humoral response compared to 4 (12%) in the IV group (P = .02). CMI response at week 12 was also greater in the SQ group, at 5 (42%) vs 2 (6%) in the IV group (P = .01). We also evaluated whether those with humoral responses were more likely to have CMI responses (and vice versa). While small numbers of CMI responders hindered this comparison, we found no suggestion of concordance or discordance between humoral response and the 2 measures of CMI response using Kendall's tau, with τ values ranging from -0.06 to 0.07 when comparing the change in week 12/week 60 humoral responses to that of the IFN-γ and IL-2 responses.

Table 3
Proportion of participants experiencing the most commonly reported AEs, and all AESIs and SAEs by treatment group

AE term	Vaccine (n = 56)	Placebo (n = 14)
Reactogenicity		
Injection site reaction	45 (80%)	2 (14%)
Other AEs		
COVID-19	4 (7%)	1 (7%)
Myalgia	3 (5%)	2 (14%)
Diarrhoea	3 (5%)	0
Allergic reaction	2 (4%)	0
Chills	2 (4%)	0
Fatigue	2 (4%)	0
Fever	2 (4%)	0
Nausea	2 (4%)	0
Abdominal pain	1 (2%)	1 (7%)
Headache	1 (2%)	1 (7%)
AESIs		
Herpes zoster event	0	1 (7%)
SAEs		
High-grade urothelial carcinoma in situ	0	1 (7%)
Gastroesophageal reflux disease	1 (2%)	0
Lung infection	1 (2%)	0
Myocardial infarction	1 (2%)	0
Breast carcinoma	1 (2%)	0
Hepatocellular carcinoma	1 (2%)	0

AE, adverse event; AESI, adverse event of special interest; SAE, serious adverse event.

Safety results

Vaccine reactogenicity was common, with injection site reactions reported in 45 (80%) of RZV participants (Table 3). Most AEs were nonserious and more frequently reported among the RZV group vs placebo. Of the 45 participants who had injection site reaction AEs, 40 (89%) had them after the first injection, 35 (78%) after the second injection, and 30 (66%) after both injections. Six SAEs were reported (5 in the RZV group), and all were judged to be unrelated to the study. Three SAEs in the RZV group resulted in death and occurred 8 to 12 months after RZV receipt. The deaths were attributed to myocardial infarction, lung infection resulting in acute renal failure, and hepatocellular carcinoma in the setting of alcoholic cirrhosis. One HZ event was detected in a participant (age <40 years old) in the placebo group, with symptom onset occurring 16 weeks after receipt of the second placebo dose.

RA flare detection varied by tool but did not differ between treatment groups. At week 8, among the RZV group, 10 (17.9%) RA flares were detected using the DAS28-ESR and 16 (28.6%) by the CDAI (Table 4). In the placebo group, 3 (21.4%) flares were detected by CDAI and 3 (21.4%) by DAS28-ESR. Few flares were detected by a change in the RA-FQ score. One patient participant with RZV had evidence of a flare after dose 1, and only 5 (13%) and 3 (38%) of participants in the RZV and placebo groups, respectively, had RA-FQ score change >10 in the 4 weeks following dose 2 of RZV (Table 4). Unlike the DAS28-ESR and CDAI, most of the flares detected by RA-FQ were found after dose 2. Self-reported flares were higher than what was detected by the other 3 methods, with 24 (63%) and 5 (63%) of participants in the vaccine and placebo groups, respectively, self-reporting a RA flare after dose 1.

Table 4
Proportion of participants experiencing a new rheumatoid arthritis flare as defined by changes from prevaccination scores in DAS28-ESR, CDAI, or RA-FQ, or by self-report

	DAS28-ESR[a] n (%)			CDAI[b] n (%)		
Week	Vaccine	Placebo	*P* value[c]	Vaccine	Placebo	*P* value[c]
Week 8	10 (17.9%)	3 (21.4%)	.71	16 (28.6%)	3 (21.4%)	.74
Week 12	1 (1.8%)	0	1	5 (8.9%)	1 (7.1%)	1

	RA-FQ[d] n (%)			Self-report n (%)		
Week	Vaccine	Placebo	*P* value[c]	Vaccine	Placebo	*P* value[c]
Weeks 1-4 (post-first dose)	1 (1.8%)	0	1	24 (42.9%)	5 (35.7%)	.77
Weeks 9-12 (post-second dose)	5 (8.9%)	3 (21.4%)	.19	4 (7.1%)	3 (21.4%)	.14

Within each measure, participants were only counted at the earliest time point at which a flare was identified.
[a] DAS28-ESR: Disease Activity Score-28 for rheumatoid arthritis with erythrocyte sedimentation rate; flare defined as score increase >1.2 or >0.6 if the follow-up score is >3.2.
[b] CDAI: Clinical Disease Activity Index; flare defined as score increase >2.
[c] Fisher's exact test, $\alpha = 0.05$.
[d] RA-FQ: Outcome Measures in Rheumatology (OMERACT) rheumatoid arthritis flare questionnaire; flare defined as score increase >10.

When comparing self-reported flares with DAS28-ESR using Cohen's kappa, raw agreement between the 2 measures was 55% ($\kappa = 0.11$), indicating only slight agreement. Overall, 38 (68%) and 9 (64%) in the RZV and placebo arms respectively had flares detected by any method at any timepoint.

DISCUSSION

We evaluated the immunogenicity and safety of RZV in patients using abatacept. Our findings suggest that such patients mount attenuated responses to RZV and may lack clinical protection after vaccination.

RZV is the only shingles vaccine commercially available in the United States and in many countries around the world. It has shown robust immunogenicity and efficacy in clinical trials of nonimmunosuppressed people, including high levels of long-term humoral and CMI responses up to 10 years after vaccination. Clinical efficacy, while above 90% among healthy people in phase 3 trials, diminished in the 10 years postvaccination, but still was observed to be above 70% [28] at that timepoint. The phase 3 Zoster Efficacy (ZOE) study reported ≥2-fold increase in CMI response in 93.3% of participants, and ≥4-fold increase in humoral response in 97.8% of participants 1 month after the second dose [3]. The immunogenicity results in healthy individuals in the ZOE study put our study's relative lack of immunogenicity in perspective and highlight the need for conducting studies in immunosuppressed populations. Several such trials have been conducted, including in autologous stem-cell transplant patients, which found that 67% of participants had a ≥4-fold response at 1 month after the second dose, which was reduced to 45% at 24 months after vaccination. In contrast to our results, this study observed a robust CMI response to RZV in their trial with 93% of participants in the vaccine group having a 2-fold or greater response to RZV at 1 month after the second dose [29]. A retrospective study by Camargo et al [30] in a more immunosuppressed transplant group, allogeneic haematopoietic stem-cell transplant recipients, evaluated only humoral responses and found that 37% had ≥4-fold increase in VZV IgG titres after vaccination. A study conducted in adults with HIV (mostly treated with antiretroviral therapy (ART) or with CD4 >500) by Berkowitz et al [31] found that 98.1% had ≥4 fold increase in anti-gE antibody and 85.7% of participants had ≥2 fold increase in CMI responses 1 month after the second dose of RZV.

Within rheumatology, few studies have evaluated DMARD effects on RZV immunogenicity or efficacy. Källmark et al [32] evaluated responses in patients with RA using JAKi with or without MTX. Among JAKi users, 80.5% in the vaccine group achieved ≥4-fold increase in antibody levels, but concomitant use of MTX was associated with markedly reduced humoral response. Kojima et al [33] evaluated RZV response in patients with RA across several DMARDs and found that while CMI and humoral responses were diminished in participants using biologic DMARDs compared to non-RA controls, the differences were not statistically significant. Although they stratified their analyses by type of DMARD used, they did not break it out by specific drugs, and only 4/23 biologic—using participants were using abatacept. Venerito et al [34] found that patients using JAKi or biologic DMARDs had similar humoral responses (anti-VZV IgG) to RZV compared to healthy controls at 1 month post-second dose, although titres only increased 2 to 3 fold on average. More recently, Winthrop et al [35] evaluated RZV responses among patients with RA using upadacitinib, the majority of whom were using background MTX. Although limited by the lack of a control group, over 80% of patients mounted satisfactory humoral and nearly two-thirds of the patients mounted adequate cell-mediated responses.

Our data suggest that abatacept greatly interfered with RZV immune-building responses. Interestingly, although not reported in this manuscript, we performed a similar study using live zoster vaccine (Zostavax), where we similarly observed little CMI response and diminished humoral response in those using abatacept (findings reported in Supplementary Tables S4 and S5). Although the reason for these poor responses deserves further investigation, it is likely due to abatacept's mechanism of action: ABA binds to CD80 and CD86 molecules on antigen presenting cells, which mitigates binding to CD28 on T cells [36], and disrupts differentiation of B cells into memory B and plasma cells, as well as T cells into T_H1 and T_{FH} [37,38]. Though IFN-γ and IL-2 are validated markers for evaluating cellular response to RZV, abatacept may also inhibit cytokine production, which could impact our evaluation of immunogenicity [39,40]. These are all downstream effects of the CD28 blockade caused by abatacept, and the combination of these factors may explain the attenuated RZV responses that we saw in our study.

All participant samples in our study had acceptable PHA responses, indicating that their T cells were functional. PHA directly stimulates T cells, including memory and naive,

bypassing antigen recognition. This observation suggests that the absence of VZV-gE-specific T cell responses postvaccination in the study was due to insufficient development of T cell memory to RZV-containing antigens. Diminished humoral responses have been reported with other vaccines in those using abatacept, but few have evaluated cellular responses [14,15,17]. Of note, at least 1 study of a SARS-CoV-2 mRNA vaccine had participants temporarily hold ABA for 1 week before and after each vaccine dose, and found that humoral responses were still diminished in comparison to controls [16]. Lastly, it should be noted that MTX and corticosteroid use both alone and in conjunction with one another appeared to interfere modestly in humoral responses within our trial. Other studies with influenza and COVID-19 vaccines highlight MTX's ability to diminish humoral responses [41,42]. It is possible that CMI responses to RZV are also diminished with MTX, although given the low numbers of individuals with CMI responses in our study, we could not evaluate that question.

While RZV immunogenicity was poor, RZV appeared safe and did not cause flares of RA more often than placebo. Though mild injection site and systemic reactions were common, our data show that the vaccine was well tolerated and no SAEs appeared to be related to vaccination. Though RA flare rates after vaccination differed depending on the method used to identify them, the occurrence of flares was similar across treatment groups. Although participants self-reported flares in higher numbers than what we detected using DAS28-ESR, CDAI, and RA-FQ, it is possible some of the self-reported flares could be attributed to reactogenicity as opposed to true RA disease flare.

Strengths of this study include its novelty (ie, the first randomised clinical trial to formerly evaluate RZV immunogenicity among patients with RA using abatacept) and the use of robust laboratory methods consistent with prior clinical trial evaluations of RZV immunogenicity. Although our study suggests such patients have lesser immune responses than expected, we were limited by a small sample size and the lack of a direct RA comparator group not using abatacept. We chose, rather, to enrol a control group consisting of similar patients with RA using abatacept who were given a placebo vaccine. Although our sample was small, this comparison suggested that no substantial increase in RA flare occurred after RZV was given. Lastly, we were underpowered to fully evaluate the influence of MTX, particularly with regard to cell-mediated vaccine responses, where few responders were observed.

In summary, our study suggests that RZV is safe and well tolerated by patients with RA using abatacept with or without MTX. However, our immunogenicity results suggest poor vaccine responses, and future studies should evaluate if the attenuated immunogenicity we observed in this population correlates with reduced efficacy. Alternative strategies to administering this vaccine to those using abatacept should be sought. Further studies should evaluate whether increasing the vaccine dose or quantity of doses given, or holding abatacept before or after vaccination, would maximise the immunogenicity of RZV.

Competing interests

JRC reports a relationship with AstraZeneca Pharmaceuticals LP that includes: consulting or advisory and funding grants. JRC reports a relationship with AbbVie Inc that includes: consulting or advisory and funding grants. JRC reports a relationship with Amgen Inc that includes: consulting or advisory and funding grants. JRC reports a relationship with Aqtual that includes: consulting or advisory and funding grants. JRC reports a relationship with Bristol Myers Squibb Co that includes: consulting or advisory and funding grants. JRC reports a relationship with Immunovant Inc that includes: consulting or advisory and funding grants. JRC reports a relationship with EBL and Company that includes: consulting or advisory and funding grants. JRC reports a relationship with GlaxoSmithKline LLC that includes: consulting or advisory and funding grants. JRC reports a relationship with Janssen Pharmaceuticals Inc that includes: consulting or advisory and funding grants. JRC reports a relationship with Novartis that includes: consulting or advisory and funding grants. JRC reports a relationship with Pfizer that includes: consulting or advisory and funding grants. JRC reports a relationship with Sanofi that includes: consulting or advisory and funding grants. JRC reports a relationship with SetPoint Medical Corporation that includes: consulting or advisory and funding grants. JRC reports a relationship with Scipher Medicine Corp that includes: consulting or advisory and funding grants. JRC reports a relationship with UCB Pharma SA that includes: consulting or advisory and funding grants. AW reports a relationship with GlaxoSmithKline LLC that includes: consulting or advisory and funding grants. AW reports a relationship with Seqirus that includes: consulting or advisory and speaking and lecture fees. AW reports a relationship with Curevo Vaccine that includes: consulting or advisory. SR reports a relationship with UCB Pharma SA that includes: consulting or advisory, speaking and lecture fees, and travel reimbursement. SR reports a relationship with Amgen Inc that includes: consulting or advisory, speaking and lecture fees, and travel reimbursement. SR reports a relationship with AbbVie Inc that includes: consulting or advisory, speaking and lecture fees, and travel reimbursement. SR reports a relationship with Novartis that includes: consulting or advisory, speaking and lecture fees, and travel reimbursement. SR reports a relationship with Sanofi that includes: consulting or advisory, speaking and lecture fees, and travel reimbursement. SR reports a relationship with Swedish Orphan Biovitrum AB that includes: consulting or advisory, speaking and lecture fees, and travel reimbursement. SR reports a relationship with Bristol Myers Squibb Co that includes: consulting or advisory, speaking and lecture fees, and travel reimbursement. Coauthor current president of the West Virginia Rheumatology Society—SG coauthor immediate past president of the West Virginia State Medical Society—SG coauthor with leadership or fiduciary role in the Association of Women in Rheumatology—SR coauthor with leadership or fiduciary role in the Florida Society of Rheumatology—SR. KLW reports financial support was provided by Bristol Myers Squibb Co. IM reports financial support was provided by National Institute of Allergy and Infectious Diseases. KLW reports a relationship with AbbVie Inc that includes: consulting or advisory. KLW reports a relationship with AstraZeneca Pharmaceuticals LP that includes: consulting or advisory. KLW reports a relationship with Bristol Myers Squibb Co that includes: consulting or advisory. KLW reports a relationship with EBL and Company that includes: consulting or advisory. KLW reports a relationship with Galapagos that includes: consulting or advisory. KLW reports a relationship with Gilead Sciences Inc that includes: consulting or advisory. KLW reports a relationship with GlaxoSmithKline LLC that includes: consulting or advisory. KLW reports a relationship with Moderna Inc that includes: consulting or advisory. KLW reports a relationship with Novartis that includes: consulting or advisory. KLW reports a relationship with Roche that includes: consulting or advisory. KLW reports a relationship with Sanofi that includes: consulting or advisory. KLW reports a relationship with UCB Pharma SA that includes: consulting or advisory. KLW

reports a relationship with Zura Bio that includes: consulting or advisory. KLW reports a relationship with Takeda Pharmaceutical Company Limited that includes: consulting or advisory. KLW reports a relationship with Ouro Medicines that includes: consulting or advisory. KLW reports a relationship with Otsuka Pharmaceutical Co Ltd that includes: consulting or advisory. All authors declare they have no competing interests.

CRediT authorship contribution statement

Jeremy A Hawkins: Writing – review & editing, Writing – original draft, Visualization, Software, Project administration, Methodology, Formal analysis, Data curation. **Jeffrey R Curtis:** Writing – review & editing, Writing – original draft, Visualization, Validation, Methodology, Investigation, Funding acquisition, Formal analysis, Conceptualization. **Adriana Weinberg:** Writing – review & editing, Writing – original draft, Visualization, Validation, Methodology, Investigation, Formal analysis, Data curation, Conceptualization. **Sarah A R Siegel:** Writing – review & editing, Supervision, Resources, Project administration, Methodology, Funding acquisition, Conceptualization. **Joseph E Huffstutter:** Writing – review & editing, Investigation. **James Loveless:** Writing – review & editing, Investigation. **Suzanne Gharib:** Writing – review & editing, Investigation. **Shanmugapriya Reddy:** Writing – review & editing, Investigation. **Jayashree Sinha:** Writing – review & editing, Investigation. **David Ridley:** Writing – review & editing, Investigation. **Ilhem Messaoudi:** Writing – review & editing, Writing – original draft, Methodology, Investigation, Formal analysis, Conceptualization. **Jin Kyun Park:** Writing – review & editing, Writing – original draft, Visualization, Validation. **Eun Bong Lee:** Writing – review & editing, Writing – original draft, Visualization, Validation. **Kevin L Winthrop:** Writing – review & editing, Writing – original draft, Visualization, Validation, Supervision, Project administration, Methodology, Investigation, Funding acquisition, Formal analysis, Data curation, Conceptualization.

Acknowledgements

We thank Ms Jessica Baxter and Krystle Garth for technical support. We also thank Amanda Brunton, Peter Sullivan, and Noah Lininger for their support in coordinating the trial.

Funding

This study was supported through an investigator-initiated research grant from Bristol Myers Squibb. The project described was supported by the National Center for Advancing Translational Sciences, National Institutes of Health, United States, through grant award No. UL1TR002369 and NIAMS P30AR072583. The content is solely the responsibility of the authors and does not necessarily represent the official view of the National Institutes of Health.

Patient consent for publication

Not applicable.

Ethics approval

The study was approved by Oregon Health & Science University's (OHSU) Institutional Review Board (IRB), with the following subsites waiving oversight to OHSU's IRB under IRB #00010433: Arthritis Associates, Jayashree Sinha, MD, St. Paul Rheumatology, SW Florida Rheumatology, and West Virginia Research Institute. Oversight of St. Luke's Rheumatology was conducted by their local IRB. All study procedures were performed in compliance with relevant laws and institutional guidelines.

Provenance and peer review

Not commissioned; externally peer reviewed.

Supplementary materials

Supplementary material associated with this article can be found in the online version at doi:10.1016/j.ard.2026.01.002.

Orcid

Jeremy A Hawkins: http://orcid.org/0009-0003-1108-019X
Kevin L Winthrop: http://orcid.org/0000-0002-3892-6947

REFERENCES

[1] Singer D, Thompson-Leduc P, Poston S, Gupta D, Cheng WY, Ma S, et al. Incidence of herpes zoster in patients with rheumatoid arthritis in the United States: a retrospective cohort study. J Rheumatol 2023;50(7):873–80. doi: 10.3899/jrheum.220986.

[2] Winthrop KL, Nash P, Yamaoka K, Mysler E, Khan N, Camp HS, et al. Incidence and risk factors for herpes zoster in patients with rheumatoid arthritis receiving upadacitinib: a pooled analysis of six phase III clinical trials. Ann Rheum Dis 2022;81(2):206–13. doi: 10.1136/annrheumdis-2021-220822.

[3] Cunningham AL, Heineman TC, Lal H, Godeaux O, Chlibek R, Hwang SJ, et al. Immune responses to a recombinant glycoprotein E herpes zoster vaccine in adults aged 50 years or older. J Infect Dis 2018;217(11):1750–60. doi: 10.1093/infdis/jiy095.

[4] Lal H, Cunningham AL, Godeaux O, Chlibek R, Diez-Domingo J, Hwang SJ, et al. Efficacy of an adjuvanted herpes zoster subunit vaccine in older adults. N Engl J Med 2015;372(22):2087–96. doi: 10.1056/NEJMoa1501184.

[5] Boutry C, Hastie A, Diez-Domingo J, Tinoco JC, Yu CJ, Andrews C, et al. The adjuvanted recombinant zoster vaccine confers long-term protection against herpes zoster: interim results of an extension study of the pivotal phase 3 clinical trials ZOE-50 and ZOE-70. Clin Infect Dis 2022;74(8):1459–67. doi: 10.1093/cid/ciab629.

[6] Bass AR, Chakravarty E, Akl EA, Bingham CO, Calabrese L, Cappelli LC, et al. 2022 American College of Rheumatology Guideline for vaccinations in patients with rheumatic and musculoskeletal diseases. Arthritis Care Res (Hoboken) 2023;75(3):449–64. doi: 10.1002/acr.25045.

[7] Dooling KL, Guo A, Patel M, Lee GM, Moore K, Belongia EA, et al. Recommendations of the advisory committee on immunization practices for use of herpes zoster vaccines. MMWR Morb Mortal Wkly Rep 2018;67:103–8. doi: 10.15585/mmwr.mm6703a5.

[8] Park JK, Kim M, Jung JI, Kim JY, Jeong H, Park JW, et al. Immunogenicity, reactogenicity, and safety of two-dose adjuvanted herpes zoster subunit vaccine in patients with systemic lupus erythematosus in South Korea: a single-centre, randomised, double-blind, placebo-controlled trial. Lancet Rheumatol 2024;6(6):e352–60. doi: 10.1016/S2665-9913(24)00084-5.

[9] Izurieta HS, Wu X, Forshee R, Lu Y, Sung HM, Agger PE, et al. Recombinant zoster vaccine (Shingrix): real-world effectiveness in the first 2 years post-licensure. Clin Infect Dis 2021;73(6):941–8. doi: 10.1093/cid/ciab125.

[10] Rayens E, Sy LS, Qian L, Wu J, Ackerson BK, Luo Y, et al. Effectiveness and safety of the recombinant zoster vaccine in individuals ≥50 years of age with rheumatoid arthritis: a matched cohort and self-controlled case series study. Ann Rheum Dis 2025;84(6):960–9. doi: 10.1016/j.ard.2025.01.045.

[11] Curtis JR, Conrad DM, Krueger WS, Gara AP, Winthrop KL. Real-world data on the use of the Shingrix vaccine among patients with inflammatory arthritis and risk of cardiovascular events following herpes zoster. Arthritis Res Ther 2025;27(1):108. doi: 10.1186/s13075-025-03565-0.

[12] Friedman MA, Curtis JR, Winthrop KL. Impact of disease-modifying antirheumatic drugs on vaccine immunogenicity in patients with inflammatory

rheumatic and musculoskeletal diseases. Ann Rheum Dis 2021;80(10):1255–65. doi: 10.1136/annrheumdis-2021-221244.
[13] Weinberg A, Boulware D, Dighero B, Orban T, Type 1 Diabetes TrialNet Abatacept Study Group. Effect of abatacept on immunogenicity of vaccines in individuals with type 1 diabetes. Vaccine 2013;31(42):4791–4. doi: 10.1016/j.vaccine.2013.07.086.
[14] Crnkic Kapetanovic M, Saxne T, Jönsson G, Truedsson L, Geborek P. Rituximab and abatacept but not tocilizumab impair antibody response to pneumococcal conjugate vaccine in patients with rheumatoid arthritis. Arthritis Res Ther 2013;15(5):R171. doi: 10.1186/ar4358.
[15] Klebanoff SD, Rodda LB, Morishima C, Wener MH, Yuzefpolskiy Y, Bettelli E, et al. Diminished responses to mRNA-based SARS-CoV-2 vaccines in individuals with rheumatoid arthritis on immune-modifying therapies. JCI Insight 2023;8(15):e168663. doi: 10.1172/jci.insight.168663.
[16] Picchianti-Diamanti A, Aiello A, Laganà B, Agrati C, Castilletti C, Meschi S, et al. ImmunosuppressiveTherapies differently modulate humoral- and T-cell-Specific responses to COVID-19 mRNA vaccine in rheumatoid arthritis patients. Front Immunol 2021;12:740249. doi: 10.3389/fimmu.2021.740249.
[17] Tay L, Leon F, Vratsanos G, Raymond R, Corbo M. Vaccination response to tetanus toxoid and 23-valent pneumococcal vaccines following administration of a single dose of abatacept: a randomized, open-label, parallel group study in healthy subjects. Arthritis Res Ther 2007;9(2):R38. doi: 10.1186/ar2174.
[18] Bartlett SJ, Barbic SP, Bykerk VP, Choy EH, Alten R, Christensen R, et al. Content and construct validity, reliability, and responsiveness of the rheumatoid arthritis flare questionnaire: OMERACT 2016 workshop report. J Rheumatol 2017;44(10):1536–43. doi: 10.3899/jrheum.161145.
[19] Prevoo ML, van 't Hof MA, Kuper HH, van Leeuwen MA, van de Putte LB, van Riel PL. Modified disease activity scores that include twenty-eight-joint counts. Development and validation in a prospective longitudinal study of patients with rheumatoid arthritis. Arthritis Rheum 1995;38(1):44–8. doi: 10.1002/art.1780380107.
[20] Aletaha D, Nell VP, Stamm T, Uffmann M, Pflugbeil S, Machold K, et al. Acute phase reactants add little to composite disease activity indices for rheumatoid arthritis: validation of a clinical activity score. Arthritis Res Ther 2005;7(4):R796–806. doi: 10.1186/ar1740.
[21] Schmid DS, Miao C, Leung J, Johnson M, Weinberg A, Levin MJ. Comparative antibody responses to the live-attenuated and recombinant herpes zoster vaccines. J Virol 2021;95(12) e00240-21. doi: 10.1128/jvi.00240-21.
[22] Levin MJ, Kroehl ME, Johnson MJ, Hammes A, Reinhold D, Lang N, et al. Th1 memory differentiates recombinant from live herpes zoster vaccines. J Clin Invest 2018;128(10):4429–40. doi: 10.1172/JCI121484.
[23] Johnson MJ, Liu C, Ghosh D, Lang N, Levin MJ, Weinberg A. Cell-mediated immune responses after administration of the live or the recombinant zoster vaccine: 5-year persistence. J Infect Dis 2022;225(8):1477–81. doi: 10.1093/infdis/jiab580.
[24] Weinberg A, Kroehl ME, Johnson MJ, Hammes A, Reinhold D, Lang N, et al. Comparative immune responses to licensed herpes zoster vaccines. J Infect Dis 2018;218(Suppl 2):S81–7. doi: 10.1093/infdis/jiy383.
[25] Weinberg A, Song LY, Wilkening C, Sevin A, Blais B, Louzao R, et al. Optimization and limitations of use of cryopreserved peripheral blood mononuclear cells for functional and phenotypic T-cell characterization. Clin Vaccine Immunol 2009;16(8):1176–86. doi: 10.1128/CVI.00342-08.
[26] van Gestel AM, Haagsma CJ, van Riel PL. Validation of rheumatoid arthritis improvement criteria that include simplified joint counts. Arthritis Rheum 1998;41(10):1845–50. doi: 10.1002/1529-0131(199810)41:10<1845::AID-ART17>3.0.CO;2-K.
[27] van der Maas A, Lie E, Christensen R, Choy E, de Man YA, van Riel P, et al. Construct and criterion validity of several proposed DAS28-based rheumatoid arthritis flare criteria: an OMERACT cohort validation study. Ann Rheum Dis 2013;72(11):1800–5. doi: 10.1136/annrheumdis-2012-202281.
[28] Strezova A, Diez-Domingo J, Al Shawafi K, Tinoco JC, Shi M, Pirrotta P, et al. Long-term protection against herpes zoster by the adjuvanted recombinant zoster vaccine: interim efficacy, immunogenicity, and safety results up to 10 years after initial vaccination. Open Forum Infect Dis 2022;9(10):ofac485. doi: 10.1093/ofid/ofac485.
[29] Bastidas A, de la Serna J, El Idrissi M, Oostvogels L, Quittet P, López-Jiménez J, et al. Effect of recombinant zoster vaccine on incidence of herpes zoster after autologous stem cell transplantation: a randomized clinical trial. JAMA 2019;322(2):123–33. doi: 10.1001/jama.2019.9053.
[30] Camargo JF, Lin RY, Natori Y, Anderson AD, Alencar MC, Wang TP, et al. Reduced immunogenicity of the adjuvanted recombinant zoster vaccine after hematopoietic cell transplant: a pilot study. Blood Adv 2020;4(19):4618–22. doi: 10.1182/bloodadvances.2020002269.
[31] Berkowitz EM, Moyle G, Stellbrink HJ, Schürmann D, Kegg S, Stoll M, et al. Safety and immunogenicity of an adjuvanted herpes zoster subunit candidate vaccine in hiv-infected adults: a phase 1/2a randomized, placebo-controlled study. J Infect Dis 2014;211(8):1279–87. doi: 10.1093/infdis/jiu606.
[32] Källmark H, Bergström T, Nagel J, Gullstrand B, Einarsson JT, Bengtsson AA, et al. Serologic immunogenicity and safety of herpes zoster subunit vaccine in patients with rheumatoid arthritis receiving Janus kinase inhibitors. Rheumatology (Oxford) 2024;63(7):2024–33. doi: 10.1093/rheumatology/kead552.
[33] Kojima S, Iwamoto T, Kobayashi Y, Kato M, Takizawa F, Ida T, et al. Immunogenicity and influence on disease activity of recombinant zoster vaccine in patients with rheumatoid arthritis treated with DMARDs. RMD Open 2024;10(1):e003902. doi: 10.1136/rmdopen-2023-003902.
[34] Venerito V, Stefanizzi P, Cantarini L, Lavista M, Galeone MG, Di Lorenzo A, et al. Immunogenicity and safety of adjuvanted recombinant zoster vaccine in rheumatoid arthritis patients on anti-cellular biologic agents or JAK inhibitors: a prospective observational study. Int J Mol Sci 2023;24(8):6967.
[35] Winthrop KL, Klaff J, Penn SK, Liu Y, García C, Mysler E, et al. Immunogenicity of adjuvanted recombinant zoster vaccine in patients with rheumatoid arthritis treated with upadacitinib: 60-week results from a randomised controlled trial substudy. RMD Open 2025;11(3):e005521. doi: 10.1136/rmdopen-2025-005521.
[36] Bonelli M, Scheinecker C. How does abatacept really work in rheumatoid arthritis? Curr Opin Rheumatol 2018;30(3):295–300. doi: 10.1097/bor.0000000000000491.
[37] Haacke EA, van der Vegt B, Meiners PM, Vissink A, Spijkervet FK, Bootsma H, et al. Abatacept treatment of patients with primary Sjögren's syndrome results in a decrease of germinal centres in salivary gland tissue. Clin Exp Rheumatol 2017;35(2):317–20.
[38] Aldridge J, Andersson K, Gjertsson I, Hultgård Ekwall AK, Hallström M, van Vollenhoven R, et al. Blood PD-1 + TFh and CTLA-4 + CD4 + T cells predict remission after CTLA-4Ig treatment in early rheumatoid arthritis. Rheumatology (Oxford) 2022;61(3):1233–42. doi: 10.1093/rheumatology/keab454.
[39] Scarsi M, Zanotti C, Chiarini M, Imberti L, Piantoni S, Frassi M, et al. Reduction of peripheral blood T cells producing IFN-γ and IL-17 after therapy with abatacept for rheumatoid arthritis. Clin Exp Rheumatol 2014;32(2):204–10.
[40] Carreno BM, Bennett F, Chau TA, Ling V, Luxenberg D, Jussif J, et al. CTLA-4 (CD152) can inhibit T cell activation by two different mechanisms depending on its level of cell surface expression. J Immunol 2000;165(3):1352–6. doi: 10.4049/jimmunol.165.3.1352.
[41] Haberman RH, Herati R, Simon D, Samanovic M, Blank RB, Tuen M, et al. Methotrexate hampers immunogenicity to BNT162b2 mRNA COVID-19 vaccine in immune-mediated inflammatory disease. Ann Rheum Dis 2021;80(10):1339–44. doi: 10.1136/annrheumdis-2021-220597.
[42] Park JK, Lee YJ, Shin K, Ha YJ, Lee EY, Song YW, et al. Impact of temporary methotrexate discontinuation for 2 weeks on immunogenicity of seasonal influenza vaccination in patients with rheumatoid arthritis: a randomised clinical trial. Ann Rheum Dis 2018;77(6):898–904. doi: 10.1136/annrheumdis-2018-213222.

Ann Rheum Dis 85 (2026) 797–805

Contents lists available at ScienceDirect

Annals of the Rheumatic Diseases

journal homepage: https://www.sciencedirect.com/journal/annals-of-the-rheumatic-diseases

Rheumatoid arthritis

Dimerization as a key feature of autoreactive IgA antibody responses

Anouk G. van Mourik[1], Jim B.D. Keijser[2,3,4], Myrthe A.M. van Delft[3,4], Sanne Reijm[5], Alice Bacon[1], Theo Rispens[2,3,4], Nivine E.W. Levarht[1], Rayman T.N. Tjokrodirijo[6], Peter A. van Veelen[6], Leendert A. Trouw[7], René E.M. Toes[1], Karin A. van Schie[1], Nienke Oskam[2,3,4], Diane van der Woude[1,*], T2B! immunity against SARS-CoV-2 study group

[1] *Department of Rheumatology, Leiden University Medical Center, Leiden, The Netherlands*
[2] *Sanquin Research Amsterdam, Amsterdam, The Netherlands*
[3] *Department of Molecular Cell Biology and Immunology, Amsterdam UMC location Vrije Universiteit Amsterdam, Amsterdam, The Netherlands*
[4] *Amsterdam Institute for Immunology and Infectious Diseases, Immunology, Amsterdam, The Netherlands*
[5] *Department of Immunology, MS Center ErasMS, Erasmus MC, University Medical Center, Rotterdam, The Netherlands*
[6] *Center for Proteomics and Metabolomics, Leiden University Medical Center, Leiden, The Netherlands*
[7] *Department of Immunology, Leiden University Medical Center, Leiden, The Netherlands*

ARTICLE INFO

Article history:
Received 14 August 2025
Received in revised form 13 October 2025
Accepted 3 November 2025

ABSTRACT

Objectives: The presence of immunoglobulin A (IgA) autoantibodies has been described in many autoimmune diseases, and some of its characteristics, such as IgA dimerization, are considered a sign of a mucosal origin. However, limited information is available about the (patho)physiological conditions leading to the development of monomeric vs dimeric (autoreactive) IgA in humans. Therefore, we investigated IgA dimerization in rheumatic autoimmune diseases with a possible mucosal origin, as well as after vaccination.

Methods: Plasma of patients with rheumatic disease (rheumatoid arthritis [RA], systemic sclerosis [SSc], anti-neutrophil cytoplasmic antibody associated vasculitis [AAV], systemic lupus erythematosus [SLE]), SARS-CoV-2 vaccinated healthy individuals, and healthy controls was used for size exclusion chromatography (SEC). Enzyme-linked immunosorbent assays were performed on SEC fractions to determine the size of IgA. Results were confirmed using western blot and tandem mass spectrometry.

Results: The proportion of dimeric IgA was increased for autoantibodies compared to total IgA. This was most evident in RA, AAV, and SLE (dimeric autoreactive IgA ≈ 60%-80% vs total IgA ≈ 20%, SLE ≈ 60% total IgA), but not in SSc. Intramuscular vaccination against SARS-CoV-2 also led to an increased proportion of dimeric anti-spike IgA shortly after vaccination, irrespective of previous mucosal exposure.

Conclusions: These findings indicate that dimeric (autoreactive) IgA responses are associated with newly emerging antigen-specific immune activation, where production temporarily shifts to dimeric IgA. Mucosal triggering is not necessarily always involved in these IgA immune responses. These findings provide key insights into the circumstances for IgA dimerization and suggest that dimeric IgA could serve as a marker for immunological disease activity in autoimmunity.

*Correspondence to Dr. Diane van der Woude, Department of Rheumatology, Leiden University Medical Center, Leiden, The Netherlands.
E-mail address: dvanderwoude@lumc.nl (D. van der Woude).

Handling editor Josef S. Smolen.

T2B! immunity against SARS-CoV-2 study group members are listed in Supplementary Material.

https://doi.org/10.1016/j.ard.2025.11.003

WHAT IS ALREADY KNOWN ON THIS TOPIC

- Immunoglobulin A (IgA) and especially dimeric IgA play a crucial role in mucosal and vaccine responses.
- Mucosal triggers have been hypothesized to underlie the emergence of autoreactivity in various rheumatic diseases.

WHAT THIS STUDY ADDS

- In several rheumatic diseases, autoantibody IgA is predominantly present in a dimeric state.
- Mucosal triggering is not necessarily always involved in the generation of dimeric IgA.
- Dimerization of IgA can be regulated by recent immune activation, shifting the IgA production temporarily to dimeric IgA.

HOW THIS STUDY MIGHT AFFECT RESEARCH, PRACTICE OR POLICY

- Dimeric IgA could serve as a marker for immunological disease activity in rheumatic autoimmune diseases such as rheumatoid arthritis.

INTRODUCTION

Immunoglobulin A (IgA) is a key mediator in immune protection, and especially plays an important role in neutralizing antigens. Recently, it became apparent that IgA is important in COVID-19 vaccine responses, where it is superior in neutralizing antigens compared to IgG, and where the size of IgA determines the efficiency of neutralization [1,2]. Previously, a similar mechanism has been described in influenza [3,4]. In addition to its neutralizing function in vaccine responses, IgA helps maintain homeostasis with foreign commensal microbes at mucosal sites. The size of IgA is key in the functions it exhibits, and differences can be observed between the composition of IgA in circulation and in mucosal secretions. In circulation, IgA is mainly found in the monomeric form, while a small amount is dimeric, composed of two IgA molecules and a joining (J) chain [5–7]. Dimeric IgA can be translocated across the epithelium from the basolateral surface to the apical surface via the polymeric immunoglobulin receptor (pIgR). At the apical side, the pIgR is cleaved, resulting in secretory IgA, which contains the secretory component (SC, a polypeptide derived from the pIgR) and the J chain. Since high amounts of dimeric IgA are encountered at mucosal sites, dimeric IgA has long been linked to local mucosal antibody production [8].

Mucosal triggers and local mucosal immune responses are believed to play a role in certain autoimmune responses [9]. These diseases, including rheumatoid arthritis (RA), systemic sclerosis (SSc), anti-neutrophil cytoplasmic antibody (ANCA) associated vasculitis (AAV), and systemic lupus erythematosus (SLE), are characterised by autoantibodies. These autoantibodies have provided important insights into the underlying immunological mechanisms, as evidenced by their association with key genetic risk factors [10,11]. This applies to autoantibodies in RA directed against post-translational modifications (PTMs), mainly anti-citrullinated protein antibodies (ACPA), as well as to ANCA in AAV [12–14]. While it is unknown if there is a pathogenic role for these autoantibodies, they serve as prominent markers for the underlying disease [15,16].

IgA autoantibodies are present in many rheumatic diseases [17–20]. In RA, ACPA of the IgA isotype can be detected years before disease onset [17]. This is in line with the concept that the induction of autoantibody responses occurs after mucosal triggering, by, e.g. a bacterial protein harbouring a PTM, that elicits an immune response cross-reactive to modified self-proteins, ultimately leading to the development of RA [9]. There are several other indications that a mucosal site might be associated with the development of RA. For example, ACPA and rheumatoid factor (RF) IgA have not only been detected in blood but also in mucosal secretions such as sputum [21,22]. Furthermore, citrullinated bacterial antigens can be detected at mucosal sites and bound by human ACPA *in vitro* [23].

As limited information is available about the circumstances leading to the formation of dimeric IgA antibodies, and as insights into this aspect could indicate that the mucosa may be the site for breach of tolerance in rheumatic autoimmune diseases, we set out to characterise the IgA response in RA, AAV, SLE, and SSc. To investigate the occurrence of dimer formation, we also explored the dynamics of a *de novo* IgA response to SARS-CoV-2 induced after intramuscular vaccination or after infection.

METHODS

Patient and control samples

Peripheral blood samples of 12 patients with ACPA+ RA, 11 anti-topoisomerase (ATA) positive SSc, and 12 anti-myeloperoxidase (MPO) positive patients with AAV and 6 patients with anti-double-stranded(ds)-DNA-positive SLE visiting the outpatient clinic of the rheumatology department at the Leiden University Medical Center (LUMC) were included in this study. Additionally, 3 healthy control (HC) samples and 3 patients with ACPA- RA were also included. The patient characteristics are reported in Supplementary Material (disease, year of sampling, age, sex (male (M) & female (F)), disease duration at the point of sampling in years, disease activity [for RA and SLE], organ involvement [for SSc], diagnosis [for AAV], treatment and B cell-depleting therapies [only reported here for AAV]). All other participants had no B cell-depleting therapies before sampling. For SARS-CoV-2 vaccinated individuals, peripheral blood samples of 9 HC participants were obtained from the previously described Target-2-B! cohort study, including 3 participants who were SARS-CoV-2-naïve before vaccination and 6 who were experienced as a result of previous infection (Supplementary Material).

Study approval

Written informed consent was obtained from all individuals with RA, ANCA, SSc, SLE, and HC, and all protocols were approved by the ethical committee of the LUMC, the Netherlands. Regarding the samples from the T2B! immunity against SARS-CoV-2 study group, this was approved by the medical ethical committee (NL74974.018.20 and EudraCT 2021-001102-30). All participants provided written informed consent. Patients or the public were not involved in the design of the study.

Antibody measurement by ELISA

In-house enzyme-linked immunosorbent assays (ELISAs) were performed to screen for the presence of autoantibodies. For the RA samples, ELISAs were carried out to measure RF IgA, anti-modified protein antibodies (AMPA) (ACPA, anti-carbamylated protein antibodies [anti-CarP], and anti-acetylated protein antibodies [AAPA]) IgA as described before with minor changes

reported in Supplementary Material [21]. For the AAV samples, the presence of anti-MPO IgA in serum was measured as described previously [24]. In short, Corning 384-well microplates (3700, Sigma Aldrich) were coated with human MPO (MY862, Elastin Products Company). Samples were tested at a 1:200 dilution for screening and a 1:2 dilution for size exclusion chromatography (SEC). Antibody binding was detected using goat anti-human IgA (1:500, 2050-04, Southern Biotech) followed by visualisation with p-nitrophenyl phosphate (34047 and 36064, Sigma) at 405 nm. For SSc, an ATA IgA ELISA was performed as described before with minor changes (adapted from [18]). Lastly, for SLE, an anti-dsDNA IgA ELISA was performed. Corning 384-well microplates (3700, Sigma Aldrich) were coated with ultraPure Salmon Sperm DNA Solution (15632011, Thermofisher). Samples were tested in a titration starting at 1:10 for sera (screening) and 1:2 dilution after SEC. Antibody binding was detected using goat anti-human IgA horseradish peroxidase (HRP) (A80-102P, Bethyl). SEC fractions of rheumatic diseases and HC were also utilised in total Ig ELISAs for IgM (1:250 or 1:500), IgA (1:3000 or 1:5000), and IgG (1:5000) (A80-100, 102, and 104, Bethyl Laboratories) according to the manufacturer's protocols. All ELISAs were developed using ABTS (2,2′-azino-bis 3-ethylbenzothiazoline-6-sulphonic acid, in-house) and measured at 415 nm.

For the detection of SARS-CoV-2-specific antibodies, 96-well maxisorp plates (ThermoFisher) were coated overnight with recombinant Wuhan-Hu-1 (WH1) full spike (1 μg/mL). Fractionated sera were tested at 1:50 and 1:500 dilutions in phosphate-buffered saline (PBS) with 0.1% v/v Tween-20 and 0.2% w/v gelatin (PTG buffer) and bound IgA was detected with mouse anti-human IgA HRP (0.5 μg/mL, MH-14-1-HRP, Sanquin) in PTG buffer. A serum pool with a known concentration of IgA was used as a reference. Total IgA was measured similarly, using mouse anti-human IgA (1 μg/mL, MH14-1, Sanquin) as coating instead, and samples were tested at 1:1000 and 1:5000 dilution. Binding was visualised using tetramethylbenzidine, and the absorbance was read at 450 nm and 540 nm for background correction.

Size exclusion chromatography

Plasma of participants was diluted 1:1 in PBS, 1:3 for SARS-CoV-2 vaccinated participants, and subsequently filtered (0.2 μM filters, Millipore). SEC of the plasma of rheumatic diseases and HC was performed using the ÄKTA Pure equipped with a Hiload 16/600 Superdex 200 column (GE Healthcare, 28-9893-35) and analyzed with Unicorn software (version 7.1) according to the manufacturer. The SARS-CoV-2 sera were run on a Superdex 200 10/300 GL column (GE Healthcare) using an ÄKTA Go system.

Western blot

For SDS-PAGE, plasma from a patient with RA (1:2000 diluted), purified human IgA (20 ng) and purified AMPA (800-1000 ng; containing AMPA IgG, IgM and IgA, purified according to [25]), dimeric human IgA (666x diluted, Nordic), and plasma of an IgA-deficient donor (20 μL) were mixed with Laemmli buffer (Bio-Rad) and incubated for 5 min at 95°C. Samples were loaded on a 4% to 15% mini TGX precast protein gel (Bio-Rad), and the PageRulerTM Plus Prestained Protein Ladder (Thermo Fisher) was used as reference. Proteins were blotted on a mini 0.2 μm polyvinylidene fluoride (PVDF) membrane using the Trans-blot Turbo system (Bio-Rad). Blots were blocked with PTS (PBS/0.05% Tween-20/3% skim milk powder [Sigma]) at 4°C overnight. The next day, primary staining was performed at RT with polyclonal rabbit anti-human IgA (1:10,000 in PTS, DAKO, A0262) and afterwards at RT with polyclonal goat anti-rabbit-Ig HRP (1:5000 in PTS, DAKO, P0448) in PTS. Blots were developed using Pierce ECL Western Blotting Substrate (GE Healthcare), the readout was performed on a Bio-Rad Chemidoc Touch Imaging system, and the images were analyzed using Image Lab (Version 6.1).

Tandem mass spectrometry (MS/MS)

In short, tandem mass spectrometry (MS/MS) was performed on 3 size exclusion fractions (A, B, and C) of 3 patients to analyse the presence of J chain and SC. Approximately 1 μg of IgA was purified from these fractions by a 2-hour incubation with CaptureSelect IgA Affinity Matrix beads (Thermo Scientific, 1942880250) on RT. IgA was released from the beads by incubating them in Laemmli buffer at 95°C for 5 minutes. Sodium dodecyl-sulfate polyacrylamide gel electrophoresis (SDS-PAGE) was performed as previously described and stained with Coomassie blue (Abcam) for 15 minutes. For MS analysis, gel bands of interest (ie, monomeric [A], dimeric [B], and polymeric [C] IgA) were cut out and processed as described in Supplementary Material.

Statistical analysis

For ELISA, arbitrary units (AUs) were calculated from the standards that were added to all ELISAs. For graphs, AUs were normalized to a percentage whereby the highest AU in each participant for a particular ELISA was set to 100%. To calculate the percentage of high molecular weight (HMW) IgA, we defined a cut-off distinguishing monomeric from HMW IgA for each individual participant, using the area under the curve of each respective ELISA. As illustrated in Figure 1E, the cut-off was set 2 fractions to the left based on the highest monomeric peak of the total IgA. Statistical analysis was performed using GraphPad Prism 7.02. Kruskal-Wallis tests were performed to investigate differences in the percentage of HMW IgA. A Pearson correlation was performed to investigate the differences between clinical parameters and the proportion of HMW IgA. P values below .05 were considered statistically significant. Significant differences are noted as follows: not significant (ns; $P > .05$), $*P < .05$, $**P < .01$, $***P < .001$, or $****P < .0001$.

RESULTS

Characterization of IgA autoantibodies in RA

To investigate the size distribution of IgA autoantibodies in patients with RA, plasma was fractionated using SEC. Fractions were collected and analyzed for the presence of antibodies by total Ig ELISAs in patients with ACPA+ RA, ACPA− RA, and HC (Fig 1A, Supplementary Material). No difference was detected between the size profiles of total IgM, IgA, or IgG in the patients with ACPA+ RA compared to the patients with HC or ACPA− RA (Fig 1B, Supplementary Material). As expected, antibodies eluted according to size, with IgM eluting first, followed by IgA and lastly IgG. IgA eluted in a broad range of fractions, suggesting the presence of both monomeric and HMW IgA, although monomeric IgA dominated the SEC spectrum. Next, the size distribution of AMPA IgA and RF IgA in the fractions was investigated. All AMPA IgA, as well as RF IgA, were found to have a

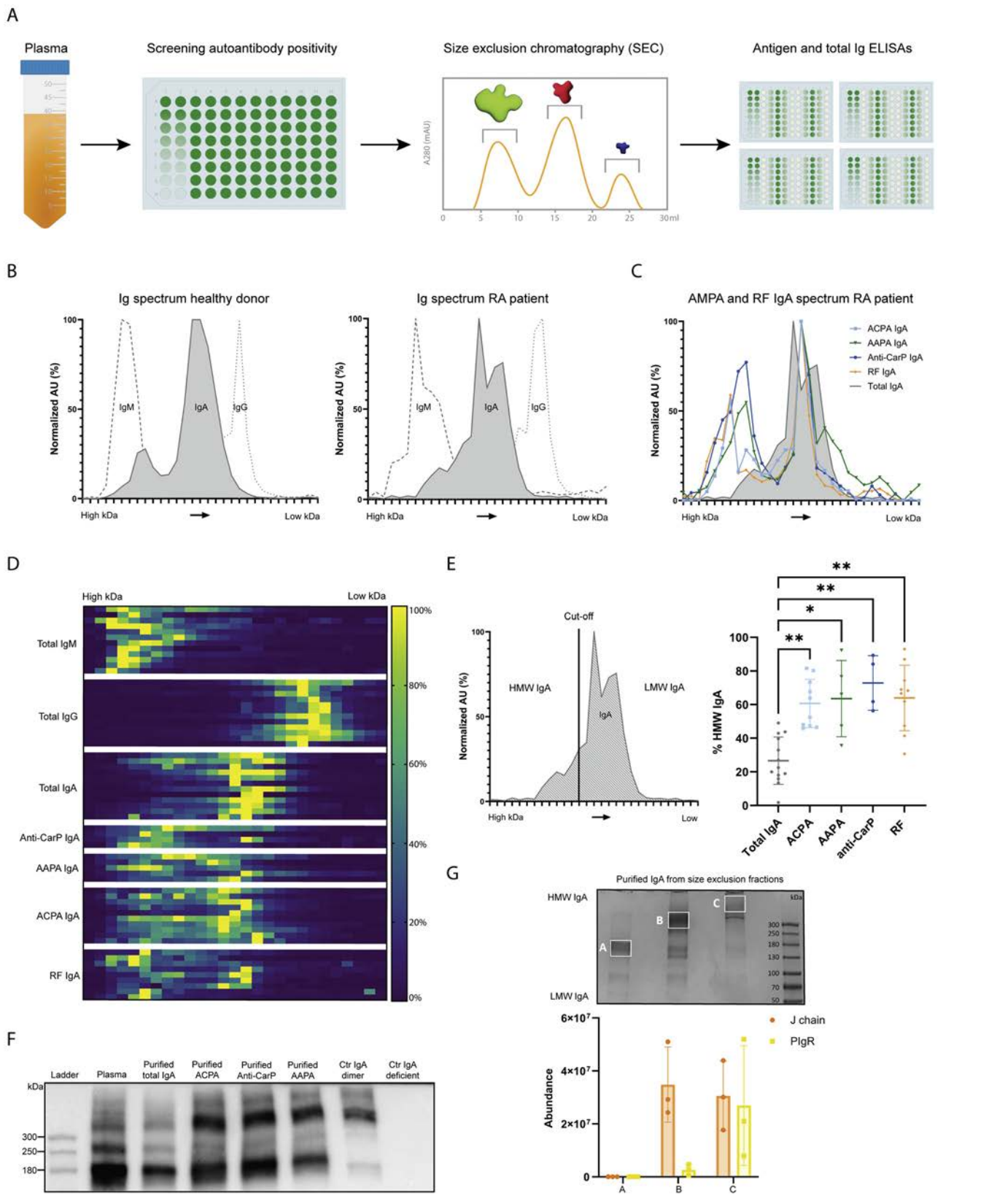

Figure 1. Characterization of IgA autoantibodies in RA. (A) Method for the determination of HMW IgA. Plasma samples of patients with RA were screened for AMPA positivity, and SEC followed by ELISA was conducted with positive samples. (B) Normalized AUs of total Ig patterns of a HC and a patient with RA (representative of N = 3). (C) AMPA and RF IgA compared to total IgA in a patient with RA positive for all AMPA (ACPA = light blue = square, AAPA = green = triangle, anti-CarP = dark blue = circle) and RF (RF = orange = diamond) IgA. (D) Heatmap of the ELISA data of SEC fractions of 12 patients with RA (anti-CarP N = 4, AAPA N = 5, ACPA N = 10, RF N = 9). (E) Cut-off for HMW IgA and LMW IgA based on the total IgA peak of each participant. The percentages of HMW IgA are depicted in the graph for all the participants with RA. A nonparametric test, Kruskal-Wallis test, was performed to compare total IgA to ACPA IgA ($P < .01$), AAPA IgA ($P < .05$), anti-CarP IgA ($P < .01$), and RF IgA ($P < .01$). (F) IgA western blot of plasma, purified plasma IgA, purified AMPA of a patient with RA, commercial dimeric IgA antibody (control), and IgA-deficient serum (control). (G) SDS-Page of 3 different fractions from the SEC of a patient with RA (representative of N = 3). The respective bands visible in the SDS-Page were subjected to MS/MS. The summed abundance of 3 peptides in, respectively, J chain (J chain = orange = circle and 3 peptides in SC (SC = yellow = square) is depicted in the graph for 3 patients with RA for each band

larger proportion of HMW species compared to total IgA (Fig 1C). We confirmed this change in size distribution towards HMW of autoreactive IgA in other patients with ACPA+ RA for all the AMPA and RF IgA (Fig 1D). The proportion of HMW autoantibody IgA was different for each patient, in some cases resulting in a complete shift of the peak from monomeric autoantibody IgA towards the HMW protein side. The percentage of HMW IgA was significantly higher in ACPA IgA ($P < .01$), AAPA IgA ($P < .05$), anti-CarP IgA ($P < .01$), and RF IgA ($P < .01$) compared to total IgA (Fig 1E). The increased proportion of dimeric ACPA IgA also demonstrated a correlation ($R = 0.47$) with the disease activity score, although not significant. An inverse correlation was seen between the symptom duration and the proportion of dimeric ACPA IgA ($R = -0.50$, NS) (Supplementary Material). These data complement each other since disease activity generally decreases with a longer disease duration. Age did not show any association with the proportion of dimeric autoantibody IgA.

To confirm whether this change in size distribution could be attributed to the presence of HMW IgA, we subsequently isolated AMPA and total IgA. Isolated supernatant was next submitted to SDS-PAGE, and the molecular weight of purified AMPA and total purified IgA from the same ACPA+ participant was assessed by IgA-specific western blot (Fig 1F). Total plasma as well as purified IgA from plasma demonstrated a band at the expected height of monomeric IgA. For AMPA IgA, a second band, with the same intensity as the monomer band, was visible at the height of a control IgA dimer. This band can only be explained by interactions via disulfide bridges, such as J chain binding to IgA, indicating the abundant presence of HMW IgA in the isolated IgA AMPA fractions. To further investigate whether the difference in IgA distribution, detected after SEC, was indeed due to the formation of HMW IgA, we utilized MS/MS. The abundance of J chain and SC was analyzed in 3 purified IgA SEC fractions (A, B, and C) of participants with ACPA+ RA by MS/MS (Fig 1G). No sequences derived from J chain or SC were detected in the monomeric fractions (band A). In contrast, in band B at the height of dimeric IgA, J chain-derived sequences were detected, indicating the presence of J chain. In the polymeric fraction, band C, sequences derived from J chain as well as SC were present. Although we also detected the presence of IgM, this was at a considerably lower abundance as compared to IgA, indicating that the J chain and SC were mainly associated with IgA. Together, these data indicate that AMPA IgA are present in a dimeric form, as shown by the increased size and the presence of J chain and SC.

The size of IgA autoantibodies in rheumatic autoimmune diseases

To address the question of whether the increase in the proportion of dimeric autoreactive IgA is specific for RA, we next investigated IgA autoantibodies in other autoimmune rheumatic diseases. To this end, SEC was performed on plasma samples from patients with AAV, SSc, and SLE followed by the measurement of total Ig and the respective autoantibody IgA by ELISA. The analysis of sera from patients with AAV revealed changes in the distribution of anti-MPO IgA compared to total IgA, in line with the results of patients with RA ($P < .0001$) (Fig 2A). Participants with SLE also demonstrated an increased proportion of dimeric anti-dsDNA IgA compared to total IgA ($P < .01$). Surprisingly, total IgA also had an increased proportion of dimeric IgA in SLE compared to other rheumatic diseases (Fig 2C). Lastly, a more diffuse pattern was obtained by investigating the ATA response present in patients with SSc where in some cases a small proportion of dimeric ATA IgA was observed, whereas in other cases almost no dimeric ATA IgA was detectable (Fig 2B). Together, these data indicate that an increase in dimeric autoantibody IgA is found in some but not all autoimmune diseases.

HMW IgA formation upon vaccination

As dimeric IgA responses in rheumatic diseases are hypothesized to be related to a mucosal trigger, we aimed to investigate the dynamics of mucosal and non-mucosal immune response by taking primary (intramuscular vaccination) and recall (respiratory infection) responses in SARS-CoV-2 as a model [9]. To this end, we examined serum samples from individuals who developed an immune response to SARS-CoV-2 through infection before vaccination and from individuals without such exposure before vaccination ('Naïve'). Samples were included from 4 different timepoints: directly before the first vaccination (Pre-Vac 1), 10 days after the first vaccination (Post-Vac 1), directly before the second vaccination (Pre-Vac 2), and 10 days after the second vaccination (Post-Vac 2) (Fig 3A). As shown in Figure 3B, the vaccinations elicited a SARS-CoV-2-specific immune response with detectable anti-spike IgA levels. Samples before vaccination 1 were negative for anti-spike IgA in all naïve individuals and 3 out of 6 previously infected individuals ('Nondetectable Pre-Vac 1'). The other 3 previously infected individuals had positive anti-spike IgA levels at this timepoint and had reported positive SARS-CoV-2 polymerase chain reaction (PCR) tests 22, 38, and 55 days before their first vaccine dose and were therefore analyzed as a separate subset ('Detectable Pre-Vac 1'). The other 3 individuals, 'Nondetectable Pre-Vac 1', were positive for anti-nucleocapsid antibodies or had a positive PCR test more than half a year before the study.

We then investigated the dynamics of dimeric anti-spike IgA after primary or recall responses by SEC. Unsurprisingly, the 'Detectable Pre-Vac 1' group showed dimeric anti-spike IgA in all the sampled timepoints, with the largest proportion of dimeric IgA at Post-Vac 1 (Fig 3C, Supplementary Material). In the 'Nondetectable Pre-Vac 1' group, the anti-spike IgA response after Post-Vac 1 also clearly demonstrated a highly dimeric nature. Later timepoints showed less dimeric IgA, indicating that repeated vaccination in a short time period did not lead to, or sustain, a markedly dimeric anti-spike IgA response. Surprisingly, in the naïve group, the intramuscular COVID vaccination also led to an anti-spike IgA response with dimeric IgA. An increase in dimeric IgA was visible compared to total IgA for the 2 timepoints at which anti-spike IgA could be detected.

DISCUSSION

In this study, we characterised the dimerization of the IgA autoantibody response in rheumatic autoimmune diseases. The

separately (A, B, and C). AAPA, anti-acetylated protein antibody; ACPA, anti-citrullinated antibody; AMPA, anti-modified protein antibodies; anti-CarP, anti-carbamylated protein antibodies; AU, arbitrary unit; ELISA, enzyme-linked immunosorbent assay; HC, healthy control; HMW, high molecular weight; Ig, immunoglobulin; LMW, low molecular weight; MS/MS, tandem mass spectrometry; SC, secretory component; SDS-Page, sodium dodecyl-sulfate polyacrylamide gel electrophoresis; PIgR, polymeric immunoglobulin receptor; RA, rheumatoid arthritis; RF, rheumatoid factor; SEC, size exclusion chromatography.

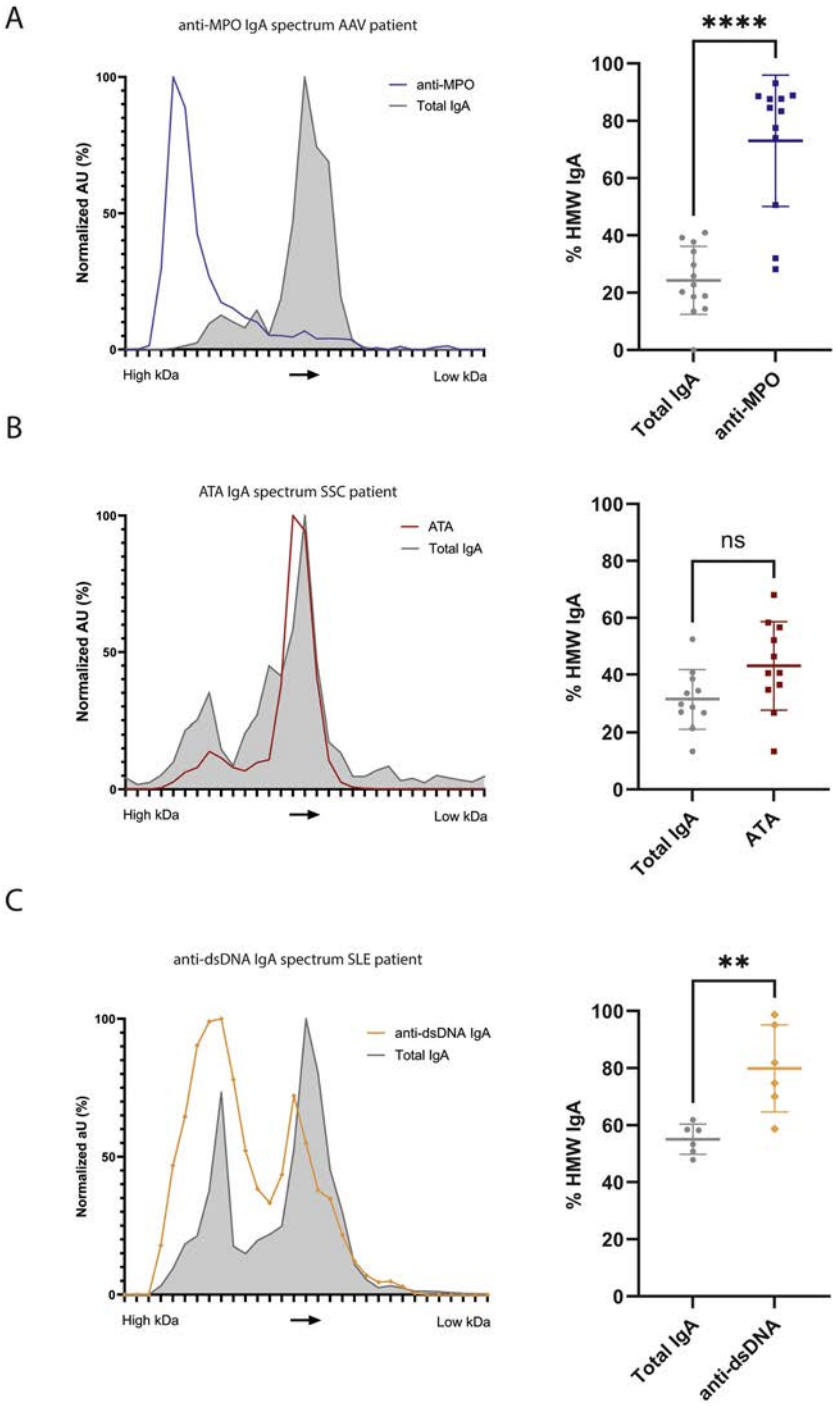

Figure 2. The size of IgA autoantibodies in AAV, SSc, and SLE. (A) Left is the SEC profile for a patient with AAV (representative of N = 12). The normalized AU values are shown for the respective autoantibody (anti-MPO IgA = purple square) as well as for total IgA. Right is the percentage HMW IgA for the autoantibody and total IgA. A nonparametric test, Kruskal-Wallis test, was performed (anti-MPO [$P < .0001$]). (B) Left is the SEC profile for a patient with SSc (representative of N = 11). The normalized AU values are shown for the respective autoantibody (ATA IgA = red square) as well as for total IgA. Right is the percentage HMW IgA for the autoantibody and total IgA. A nonparametric test, Kruskal-Wallis test, was performed (ATA = ns). (C) Left is the SEC profile for a patient with SLE (representative of N = 6). The normalized AU values are shown for the respective autoantibody (anti-dsDNA IgA = orange diamond) as well as for total IgA. Right is the percentage HMW IgA for the autoantibody and total IgA. A nonparametric test, Kruskal-Wallis test, was performed (anti-dsDNA IgA [$P < .01$]). AAV, ANCA-associated vasculitis; ATA, antitopoisomerase; AU, arbitrary unit; dsDNA, anti-double stranded DNA; HMW, high molecular weight; Ig, immunoglobulin; MPO, myeloperoxidase; ns, not significant; SEC, size exclusion chromatography; SLE, systemic lupus erythematosus; SSc, systemic sclerosis.

results revealed that the RA-associated AMPA and RF IgA responses had an increase in dimeric IgA compared to total IgA, which consisted of approximately 20% dimeric IgA, while AMPA and RF consisted of 60% to 80% dimeric IgA. This was not exclusive to RA autoantibodies as the AAV-associated anti-MPO response as well as the anti-dsDNA response in SLE displayed similar features, indicating that increased dimeric IgA responses are present in other, although not all, autoimmune diseases. Surprisingly, the proportion of dimeric total IgA in SLE was increased compared to other autoimmune diseases. A possible explanation could be that the multitude of different autoantibodies known to be present in SLE, this could affect the total proportion of dimeric total IgA if they make up a significant amount of the total IgA [20,26]. Furthermore, to shed light on the origin of this dimeric autoimmune response, analysis of plasma from healthy individuals vaccinated against SARS-CoV-2 revealed that anti-spike IgA displayed a similar predominance of dimeric IgA. As this was also observed in non-infected, but intramuscularly vaccinated individuals, these data reveal a crucial finding that mucosal immune activation is not required for the formation of a dimeric IgA response.

These outcomes are in line with previous studies indicating that elevated SC binding is observed to ACPA IgA, RF IgA, and total IgA in RA [27–29]. Likewise, our findings are in line with studies into post-vaccination IgA responses in patients with IgA nephropathy, where dimeric antigen-specific IgA increased shortly after vaccination [30,31]. Together with our new data on the presence of dimeric autoantibodies in relationship to clinical data and the dynamics of the IgA response after vaccination, a clear picture emerges indicating that dimeric IgA could be a

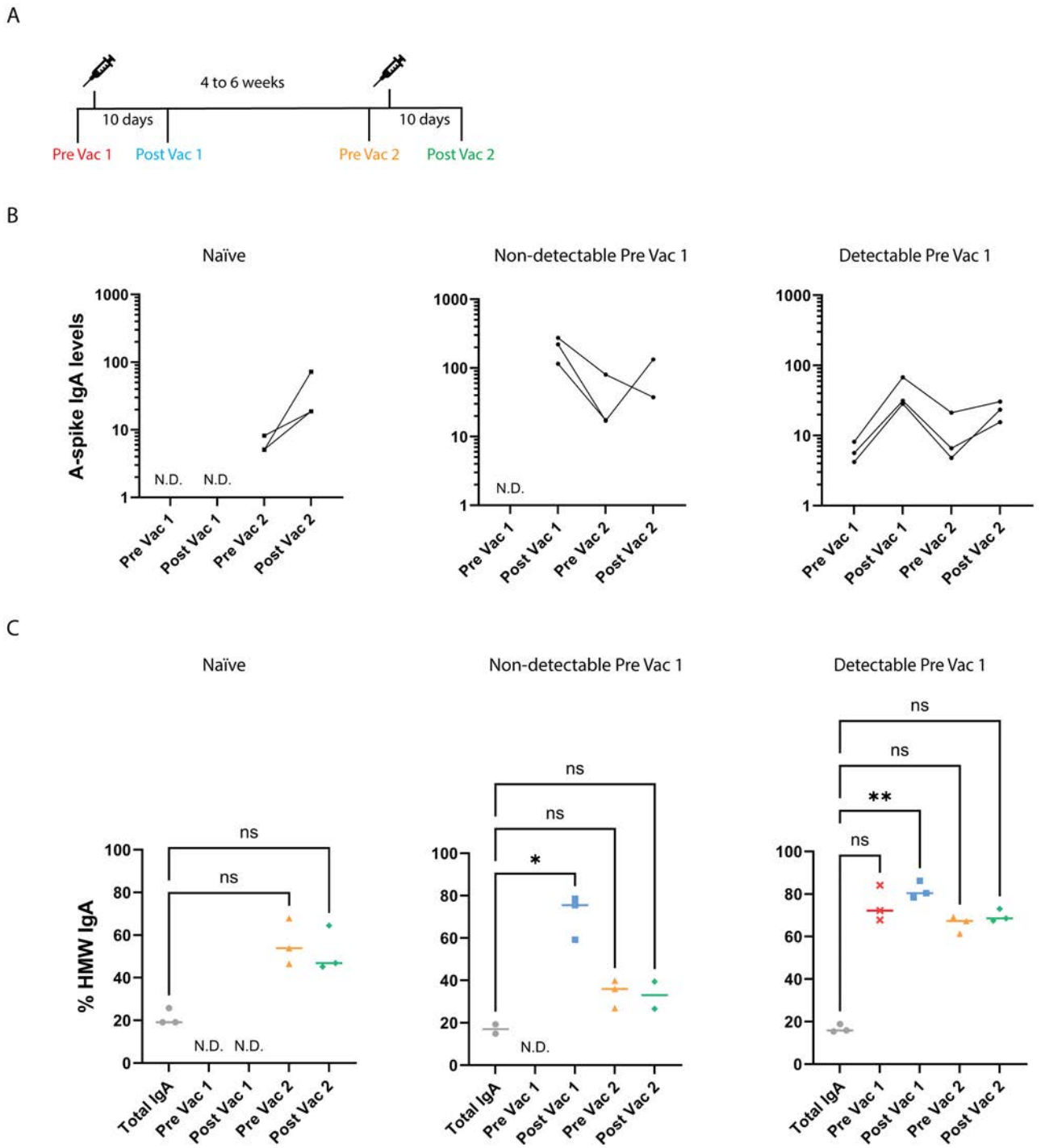

Figure 3. The dimeric IgA response after SARS-CoV-2 vaccination. (A) Scheme of the vaccination study. Samples were taken at 4 different timepoints (before vaccination 1 = Pre-Vac 1 = red/cross, 10 days after vaccination 1 = Post-Vac 1 = blue/square, before vaccination 2 = Pre-Vac 2 = orange/triangle, 10 days after vaccination 2 = Post-Vac 2 = green/diamond). Not all timepoints were available for all patients. Post-Vac 1 samples were not available for naïve participants, and Pre-Vac 1 samples were precluded from further analysis if seronegative in the screening anti-RBD IgA ELISA, which was the case in all 3 naïve participants and 3 of the previously infected individuals ('Nondetectable Pre-Vac 1'). (B) Anti-spike IgA levels at the different sample timepoints for the Naïve, Nondetectable Pre-Vac 1, and Detectable Pre-Vac 1 participants. N.D. = not determined. (C) Percentage of HMW IgA at different timepoints in SARS-CoV-2-vaccinated individuals. A nonparametric Kruskal-Wallis test was performed. Nondetectable Pre-Vac 1: Post-Vac 1 ($P < .05$). Detectable Pre-Vac 1: Post-Vac 1 ($P < .01$). Other timepoints were ns (not significant). ELISA, enzyme-linked immunosorbent assay; HMW, high molecular weight; Ig, immunoglobulin; anti-RBD, anti-receptor binding domain.

hallmark of recent immune activation. This can occur at mucosal surfaces, as evidenced by our data obtained following SARS-CoV-2 infection, but also at non-mucosal surfaces, as indicated by the observations made after intramuscular vaccination only. Nonetheless, it is still highly conceivable that the presence of dimeric autoreactive IgA results from immune activation at mucosal sites as several lines of evidence implicate a mucosal contribution to the induction of autoreactive B cell-mediated immune responses [21,32,33]. Through the persistent presence of autoantigens, autoimmune responses could stay active for prolonged periods. This is in line with data regarding ACPA-producing B cells which are characterised by the expression of

activation and proliferation markers, like Ki-67, indicating their continuous activation [34,35]. These previous observations therefore parallel the findings in this study, as they also point to continuous immunological disease activity even in subjects receiving adequate treatment for RA.

An important question that remains is which signals lead to the development of this dimeric IgA response in B cells, which seems to be temporary. Different lineages of B cells might be responsible for the production of monomeric or dimeric IgA as there are differences in clonality between monomeric and dimeric IgA [6]. The amount of J chain, needed for the production of polymeric IgA, could also be a determining factor, although this seems less likely, considering that J-chain expression is known to be widespread in all B cells and even present in IgG-producing B cells, despite the fact that IgG only exists in monomeric form [36]. Whether J-chain chaperone-proteins, cytokine/chemokine mix, or B cell location influence dimeric IgA antibody production currently remains unclear [37]. Therefore, further research is needed to elucidate the underlying mechanism. The function of dimeric IgA in plasma is almost as elusive as the formation, although in SARS-CoV-2 and influenza, it has been suggested that dimeric IgA displays an increased neutralizing activity [1–4]. Hence, it is also interesting to further investigate the effects of dimeric IgA since it could also very well be hypothesized that the effector functions are proinflammatory, through, e.g. receptor binding and neutrophil activation [38]. Simultaneously, it would be important to perform more in-depth studies into a possible relationship between the occurrence of dimeric IgA autoantibody responses and disease activity and remission. In light of the findings, it appears plausible that there could be a relationship between disease duration as well as disease activity and dimeric autoantibody IgA formation. This would indicate that dimeric IgA could serve as a marker for immunological disease activity.

Our study has some limitations, as the sample size in some of the groups is relatively small. Likewise, our data do not allow definitive conclusions about the origin of dimeric autoreactive IgA or the exact mechanism regulating the production of dimeric IgA. However, the strength of this study is that we present a new concept regarding the dynamics of IgA responses. We have investigated this in 4 autoimmune diseases and a vaccination study of an infectious disease, whereby we confirmed our findings in ELISA with multiple different methods (ie, western blot and MS/MS) and gained valuable insight into the development of the dimeric IgA response.

In summary, we propose that dimeric IgA is a key feature of newly emerging and autoreactive immune responses. The size of IgA plays an important role in neutralization, making our findings very relevant for the development of efficient vaccines. Besides, dimeric IgA could also serve as a marker for immunological disease activity in autoimmunity. Consequently, our findings are key to understanding the dynamics of dimeric IgA responses in autoimmunity as well as in fundamental immunology.

Acknowledgements

Renee van de Wetering, Corrie Wortel, Sam Neppelenbroek, Levi Coenen, Ella Huizen, Amber-Sarai Stalman, Sofie Keijzer, and Ninotska Derksen are gratefully acknowledged for their experimental contributions.

Contributors

AGvM designed the research studies, conducted experiments, acquired data, analyzed data, and wrote the manuscript. JBDK, SR, and AB conducted experiments, acquired data, and analyzed data. NEWL conducted experiments. RT and PV acquired and analyzed data. MAMvD, LAT, and TR designed the study. REMT, KvS, NO, and DvdW designed the study and supervised the project. REMT, DvdW, and AGvM drafted the manuscript. T2B! immunity against SARS-CoV-2 study group provided samples. All authors provided critical feedback, reviewed the results, and approved the final version of the manuscript.

Funding

DvdW was supported by a Vidi-grant from the NWO (Dutch research council, 09150172110053) for this work. TR was supported by a ZonMw grant (10430072010007).

Competing interests

REMT has a patent on anti-CarP in rheumatic diseases. TR is an inventor on a patent application based on the use of bioengineered IgG targets for the characterisation of rheumatoid factor reactivity patterns. The other authors declare they have no competing interests.

Patient consent for publication

Patients gave their written informed consent prior to their participation.

Ethics approval

The use of samples from the T2B! immunity against SARS-CoV-2 study group were approved by the medical ethical committee (NL74974.018.20 and EudraCT 2021-001102-30).

Provenance and peer review

Not commissioned; externally peer reviewed.

Supplementary materials

Supplementary material associated with this article can be found in the online version at doi:10.1016/j.ard.2025.11.003.

Orcid

Anouk G. van Mourik: http://orcid.org/0000-0002-3811-7373

Diane van der Woude: http://orcid.org/0000-0001-8121-5879

REFERENCES

[1] Wang Z, Lorenzi JCC, Muecksch F, Finkin S, Viant C, Gaebler C, et al. Enhanced SARS-CoV-2 neutralization by dimeric IgA. Sci Transl Med 2021;13(577):eabf1555.

[2] Zuo F, Cao Y, Sun R, Wang Q, Simonelli L, Du L, et al. Ultrapotent IgA dimeric antibodies neutralize emerging Omicron variants. J Virol 2025;99(1):e0174024.

[3] Suzuki T, Kawaguchi A, Ainai A, Tamura S, Ito R, Multihartina P, et al. Relationship of the quaternary structure of human secretory IgA to neutralization of influenza virus. Proc Natl Acad Sci U S A. 2015;112(25):7809–14.

[4] Taylor HP, Dimmock NJ. Mechanism of neutralization of influenza virus by secretory IgA is different from that of monomeric IgA or IgG. J Exp Med 1985;161(1):198–209.

[5] Brandtzaeg P. Molecular and cellular aspects of the secretory immunoglobulin system. APMIS 1995;103(1):1–19.

[6] Dingess KA, Hoek M, van Rijswijk DMH, Tamara S, den Boer MA, Veth T, et al. Identification of common and distinct origins of human serum and breastmilk IgA1 by mass spectrometry-based clonal profiling. Cell Mol Immunol 2023;20(1):26–37.
[7] Matsumoto ML. Molecular mechanisms of multimeric assembly of IgM and IgA. Annu Rev Immunol 2022;40:221–47.
[8] Macpherson AJ, McCoy KD, Johansen FE, Brandtzaeg P. The immune geography of IgA induction and function. Mucosal Immunol 2008;1 (1):11–22.
[9] Holers VM, Demoruelle MK, Kuhn KA, Buckner JH, Robinson WH, Okamoto Y, et al. Rheumatoid arthritis and the mucosal origins hypothesis: protection turns to destruction. Nat Rev Rheumatol 2018;14(9):542–57.
[10] Scott DL, Wolfe F, Huizinga TW. Rheumatoid arthritis. Lancet 2010;376 (9746):1094–108.
[11] Lyons PA, Rayner TF, Trivedi S, Holle JU, Watts RA, Jayne DR, et al. Genetically distinct subsets within ANCA-associated vasculitis. N Engl J Med 2012;367(3):214–23.
[12] Kroot EJ, de Jong BA, van Leeuwen MA, Swinkels H, van den Hoogen FH, van't Hof M, et al. The prognostic value of anti-cyclic citrullinated peptide antibody in patients with recent-onset rheumatoid arthritis. Arthritis Rheum 2000;43(8):1831–5.
[13] Ten Brinck RM, van Steenbergen HW, van Delft MAM, Verheul MK, Toes REM, Trouw LA, et al. The risk of individual autoantibodies, autoantibody combinations and levels for arthritis development in clinically suspect arthralgia. Rheumatology (Oxford) 2017;56(12):2145–53.
[14] Kitching AR, Anders HJ, Basu N, Brouwer E, Gordon J, Jayne DR, et al. ANCA-associated vasculitis. Nat Rev Dis Primers 2020;6(1):71.
[15] Aletaha D, Neogi T, Silman AJ, Funovits J, Felson DT. Bingham CO 3rd, et al. 2010 rheumatoid arthritis classification criteria: an American College of Rheumatology/European League Against Rheumatism collaborative initiative. Ann Rheum Dis 2010;69(9):1580–8.
[16] Cornec D, Cornec-Le Gall E, Fervenza FC, Specks U. ANCA-associated vasculitis - clinical utility of using ANCA specificity to classify patients. Nat Rev Rheumatol 2016;12(10):570–9.
[17] Verpoort KN, Jol-van der Zijde CM, Papendrecht-van der Voort EA, Ioan-Facsinay A, Drijfhout JW, van Tol MJ, et al. Isotype distribution of anti-cyclic citrullinated peptide antibodies in undifferentiated arthritis and rheumatoid arthritis reflects an ongoing immune response. Arthritis Rheum 2006;54 (12):3799–808.
[18] Wortel CM, Liem SI, van Leeuwen NM, Boonstra M, Fehres CM, Stöger L, et al. Anti-topoisomerase, but not anti-centromere B cell responses in systemic sclerosis display active, Ig-secreting cells associated with lung fibrosis. RMD Open 2023;9(3):e003148.
[19] Sandin C, Eriksson P, Segelmark M, Skogh T, Kastbom A. IgA- and SIgA anti-PR3 antibodies in serum versus organ involvement and disease activity in PR3-ANCA-associated vasculitis. Clin Exp Immunol 2016;184(2):208–15.
[20] Dema B, Charles N. Autoantibodies in SLE: specificities, isotypes and receptors. Antibodies (Basel) 2016;5(1):2.
[21] Derksen VFAM, Martinsson K, van Mourik AG, Wagenaar CA, Toes REM, Walrabenstein W, et al. Evidence of site-specific mucosal autoantibody secretion in rheumatoid arthritis. Arthritis Rheumatol 2025;77(3):272–82.
[22] Ottèn HG, Daha MR, van Laar JM, de Rooy HH, Breedveld FC. Subclass distribution and size of human IgA rheumatoid factor at mucosal and nonmucosal sites. Arthritis Rheum 1991;34(7):831–9.
[23] Brewer RC, Lanz TV, Hale CR, Sepich-Poore GD, Martino C, Swafford AD, et al. Oral mucosal breaks trigger anti-citrullinated bacterial and human protein antibody responses in rheumatoid arthritis. Sci Transl Med 2023;15 (684):eabq8476.
[24] Wortel CM, van de Wetering R, Stork EM, Kissel T, Reijm S, van der Woude D, et al. Anti-myeloperoxidase IgM B cells in anti-neutrophil cytoplasmic antibody-associated vasculitis. Nat Commun 2025;16(1):1582.
[25] Kampstra ASB, Dekkers JS, Volkov M, Dorjée AL, Hafkenscheid L, Kempers AC, et al. Different classes of anti-modified protein antibodies are induced on exposure to antigens expressing only one type of modification. Ann Rheum Dis 2019;78(7):908–16.
[26] Parodis I, Lagutkin D, Lindblom J, Idborg H, Beretta L, Borghi MO, et al. New IgG and IgA autoantibody specificities against DNA-binding and RNA-binding proteins discriminate systemic lupus erythematosus from health and non-lupus autoimmunity-could anti-LIN28A enhance precision in diagnostics? Ann Rheum Dis 2025;84(7):1180–94.
[27] Martinsson K, Kling LL, Roos-Ljungberg K, Griazeva I, Samoylovich M, Paul S, et al. Extramucosal formation and prognostic value of secretory antibodies in rheumatoid arthritis. Arthritis Rheumatol 2022;74(5):801–9.
[28] Martinsson K, Roos Ljungberg K, Ziegelasch M, Cedergren J, Eriksson P, Klimovich V, et al. Elevated free secretory component in early rheumatoid arthritis and prior to arthritis development in patients at increased risk. Rheumatology (Oxford) 2020;59(5):979–87.
[29] Jorgensen C, Moynier M, Bologna C, Youinou P, Sany J. Rheumatoid factor associated with a secretory component in rheumatoid arthritis. Br J Rheumatol 1995;34(3):236–40.
[30] Layward L, Allen AC, Harper SJ, Hattersley JM, Feehally J. Increased and prolonged production of specific polymeric IgA after systemic immunization with tetanus toxoid in IgA nephropathy. Clin Exp Immunol 1992;88(3):394–8.
[31] Eijgenraam JW, Oortwijn BD, Kamerling SW, de Fijter JW, van den Wall Bake AW, Daha MR, et al. Secretory immunoglobulin A (IgA) responses in IgA nephropathy patients after mucosal immunization, as part of a polymeric IgA response. Clin Exp Immunol 2008;152(2):227–32.
[32] Stegeman CA, Tervaert JW, Sluiter WJ, Manson WL, de Jong PE, Kallenberg CG. Association of chronic nasal carriage of Staphylococcus aureus and higher relapse rates in Wegener granulomatosis. Ann Intern Med 1994;120(1):12–7.
[33] Koning F, Thomas R, Rossjohn J, Toes RE. Coeliac disease and rheumatoid arthritis: similar mechanisms, different antigens. Nat Rev Rheumatol 2015;11(8):450–61.
[34] Neppelenbroek S, Blomberg NJ, Kampstra ASB, van der Hem JGK, Huizinga TWJ, Toes REM, et al. Autoreactive B cells remain active despite clinical disease control in rheumatoid arthritis. J Autoimmun 2024;149:103320.
[35] Kristyanto H, Blomberg NJ, Slot LM, van der Voort EIH, Kerkman PF, Bakker A, et al. Persistently activated, proliferative memory autoreactive B cells promote inflammation in rheumatoid arthritis. Sci Transl Med 2020;12(570): eaaz5327.
[36] Castro CD, Flajnik MF. Putting J chain back on the map: how might its expression define plasma cell development? J Immunol 2014;193(7):3248–55.
[37] Xiong E, Li Y, Min Q, Cui C, Liu J, Hong R, et al. MZB1 promotes the secretion of J-chain-containing dimeric IgA and is critical for the suppression of gut inflammation. Proc Natl Acad Sci U S A 2019;116(27):13480–9.
[38] Aleyd E, Al M, Tuk CW, van der Laken CJ, van Egmond M. IgA complexes in plasma and synovial fluid of patients with rheumatoid arthritis induce neutrophil extracellular traps via FcαRI. J Immunol 2016;197(12):4552–9.

Ann Rheum Dis 85 (2026) 806–817

Contents lists available at ScienceDirect

Annals of the Rheumatic Diseases

journal homepage: https://www.sciencedirect.com/journal/annals-of-the-rheumatic-diseases

Psoriatic arthritis

Microbial signatures in psoriatic arthritis distinguish disease phenotypes and newly diagnosed inflammatory bowel disease independent of faecal calprotectin

Alba Boix-Amorós[1], Kevin Bu[1], Rebecca B. Blank[2], Adam Cantor[1], Ana Gutiérrez-Casbas[3], Iago Rodríguez-Lago[4], Ignacio Marin-Jimenez[5], Jesus Sanz[6], Jordi Gratacos Masmitja[7], Elisa Trujillo[8], María Carmen Muñoz[9], María Luz García Vivar[10], Marta Carrillo[11], María Vanesa Hernández Hernández[8], Xavier Calvet[12], Marta Arévalo Salaet[7], Marta Izquierdo Romero[13], Anahy Brandy García[14], Sandra Pérez[15], Jose Francisco García Llorente[16], Yago Gonzalez-Lama[17], Carolina Merino Argumánez[6], Zulema Plaza[18], Marta Domínguez[18], Juan D. Cañete[19], Jose Federico Diaz-Gonzalez[8,20], Jose U. Scher[2,21], Jose C. Clemente[1,*]

[1] *Department of Genetics and Genomic Sciences, Icahn School of Medicine at Mount Sinai, New York, NY, USA*
[2] *Department of Medicine, Division of Rheumatology, New York University School of Medicine, New York, NY, USA*
[3] *Departamento de Gastroenterología, Hospital General Universitario Dr. Balmis, ISABIAL y CIBERehd, Alicante, Spain*
[4] *Departamento de Gastroenterología, Hospital Universitario Galdakao-Usansolo, Instituto de Investigación Sanitaria Biobizkaia, Galdakao Bizkaia, Spain*
[5] *Servicio Aparato Digestivo, Hospital General Universitario Gregorio Marañón, Instituto de Investigación Sanitaria Gregorio Marañón (IiSGM), Madrid, Spain*
[6] *Departamento de Reumatología, Hospital Universitario Puerta de Hierro, Majadahonda, Madrid, Spain*
[7] *Servicio de Reumatología, Parc Taulí, Hospital Universitari, Institut d'Investigació i Innovació Parc Taulí (I3PT-CERCA), Universitat Autònoma de Barcelona, Sabadell, Spain*
[8] *Departamento de Reumatología, Hospital Universitario Canarias, La Laguna, Spain*
[9] *Departamento de Gastroenterología, Hospital Universitario Basurto Hospital Universitario, Basurto Bilbao, Spain*
[10] *Departamento de Reumatología, Hospital Universitario Basurto, Bilbao, Spain*
[11] *Departamento de Gastroenterología, Hospital Universitario Canarias, La Laguna, Spain*
[12] *Servei d'Aparell Digestiu, Parc Taulí, Hospital Universitari, Institut d'Investigació i Innovació Parc Taulí (I3PT-CERCA), Universitat Autònoma de Barcelona, Sabadell, Spain*
[13] *Aparato Digestivo, Hospital Universitario Central de Asturias, Oviedo, Spain*
[14] *Servicio de Reumatología, Hospital Universitario Central de Asturias, Oviedo, Spain*
[15] *Bone and Joint Research Unit, Rheumatology Department, IIS-Fundación Jiménez Díaz UAM, Madrid, Spain*
[16] *Rheumatology Department, Hospital de Galdacano, Galdakao, Bilbao, Spain*

*Correspondence to Dr. Jose C. Clemente, Department of Genetics and Genomic Sciences, Icahn School of Medicine at Mount Sinai, New York, NY, USA.
E-mail address: jose.clemente@mssm.edu (J.C. Clemente).
Alba Boix-Amorós, Kevin Bu, and Rebecca B. Blank contributed equally.
Juan D. Cañete, Jose Federico Diaz-Gonzalez, Jose U. Scher, and Jose C. Clemente are joint senior authors, on behalf of the EISER Collaborative Group.
Handling editor Josef S. Smolen.

https://doi.org/10.1016/j.ard.2026.01.018

[17] *Unidad de Enfermedad Inflamatoria Intestinal, Servicio de Gastroenterología y Hepatología, Hospital Universitario Puerta de Hierro, Majadahonda, Madrid, Spain*
[18] *Unidad de Investigación, Sociedad Española de Reumatología, Madrid, Spain*
[19] *Hospital Clinic, FCRB-IIDIBAPS, Barcelona, Spain*
[20] *Departamento de Medicina Interna, Dermatología y Psiquiatría, Universidad de La Laguna, La Laguna, Spain*
[21] *NYU Colton Center for Autoimmunity, NYU School of Medicine, New York, NY, USA*

ARTICLE INFO

Article history:
Received 29 June 2025
Received in revised form 24 January 2026
Accepted 25 January 2026

ABSTRACT

Objectives: There is growing evidence of microbial involvement in immune-mediated inflammatory diseases, including psoriatic arthritis (PsA) and inflammatory bowel disease (IBD). However, it remains unclear whether different PsA phenotypes exhibit distinct microbial profiles. Furthermore, up to 4% of patients with PsA have comorbid IBD, which often remains undiagnosed. We hypothesised that the gut microbiome distinguishes PsA subphenotypes and serves as a biomarker of IBD in patients with PsA independent of faecal calprotectin (fCAL).
Methods: We obtained samples from 192 patients with axial or peripheral PsA and no prior diagnosis of IBD enrolled in the EISER study. Patients with elevated fCAL and subclinical IBD symptoms underwent colonoscopy with intestinal biopsy. Stool samples were used to measure fCAL, and gut microbiome was characterised using shotgun metagenomics. Serum samples were used for cytokine profiling.
Results: Axial PsA had lower alpha diversity and loss of several commensals compared with peripheral PsA, as well as a depletion of microbial biotin and arginine metabolism and higher levels of IL-23, IL-17F, and IL-8. Five subjects had newly diagnosed IBD which was characterised by a depletion of tryptophan and vitamin B6 metabolism. They also showed significant enrichment of several taxa compared to non-IBD and with a larger effect size than fCAL.
Conclusions: Our results identify a distinct microbiome and immune profile in axial PsA, with lower microbiome diversity, a depletion of commensals and protective microbial mechanisms, and higher levels of some proinflammatory cytokines. In patients with newly diagnosed IBD, we identified microbial taxa associated with the condition yet independent of fCAL, the current clinical standard.

INTRODUCTION

An accumulating body of evidence has revealed associations between the microbiome and immune-mediated inflammatory diseases. Among them, previous studies have shown that psoriatic arthritis (PsA) often exhibits a distinct microbial profile compared to healthy subjects [1,2]. PsA is one of the most prevalent spondyloarthritis (SpA) and develops in approximately 30% of patients with psoriasis [3]. Most patients with PsA present with peripheral involvement, typically affecting small and medium joints of the hands and feet [4]. Axial PsA is less frequent, typically occurring in the presence of peripheral synovioentheseal disease [5], and is associated with more severe clinical manifestations, including greater pain and impaired physical function [6]. Furthermore, the immune pathways involved are different from those in peripheral, which is reflected in the lack of efficacy of conventional, synthetic disease-modifying antirheumatic drugs (csDMARDs) and interleukin (IL)-23 inhibitors in axial SpA [7,8]. Therefore, biomarkers for axial PsA are needed for early diagnosis and to improve the treatment of this subphenotype. Importantly, the microbiome across PsA phenotypes has not yet been previously characterised.

In addition, up to 4% of patients with PsA also have concurrent inflammatory bowel disease (IBD) but often go undiagnosed [9]. Patients with PsA and comorbid IBD exhibit higher health resource utilisation, including more inpatient and emergency room visits, more IBD-related procedures, and increased use of medications [9]. Furthermore, several drugs prescribed for the treatment of PsA are either ineffective (etanercept) or can worsen IBD (IL-17i) [10,11]. Early and accurate diagnosis of comorbid IBD in patients with PsA is thus key for the deployment of tailored treatments that target both diseases, and that provide the best possible care for patients. Although faecal calprotectin (fCAL) is routinely used in the clinic to aid in the screening and diagnosis of IBD in the general population, its variability and broad range of values limit its predictive power [12,13]. Additional biomarkers are therefore critical, particularly to identify patients who might be at higher risk.

Here, we hypothesise that the gut microbiome might serve as a biomarker of disease phenotypes in patients with PsA and IBD. Leveraging samples collected from patients in the EISER cohort, a multicentre, cross-sectional study aimed at estimating the prevalence of undiagnosed IBD in patients with SpA (including PsA), we characterised the gut microbiome and serum proteomics of all patients with PsA. We evaluated the capacity of bacterial and serum biomarkers to differentiate patients with axial or peripheral PsA manifestations, and to identify patients with PsA who were newly diagnosed with IBD by comparing these biomarkers against levels of fCAL.

METHODS

Study design

The EISER study is a multicentre, cross-sectional study of patients with SpA, including both PsA and axial SpA. The study is a collaborative effort between the Spanish Society of Rheumatology and the Spanish Working Group on Crohn's Disease and Ulcerative Colitis. EISER was conducted in rheumatology and gastroenterology clinics in 13 Hospitals from the Spanish

WHAT IS ALREADY KNOWN ON THIS TOPIC

- Immune diseases such as psoriatic arthritis (PsA) and inflammatory bowel disease (IBD) exhibit unique gut microbiome signatures.
- Up to 4% of PsA patients have undiagnosed IBD. While biomarkers such as fecal calprotectin (fCal) are commonly used for IBD diagnosis, there is a lack of robust, accurate methods for early detection, particularly in patients with comorbidities such as PsA.

WHAT THIS STUDY ADDS

- Patients with axial and peripheral PsA had distinctive microbiome features, including lower alpha diversity, loss of commensals and a depletion of microbial biotin and arginine metabolism in axial PsA.
- Subjects with newly diagnosed IBD had a depletion of tryptophan and vitamin B6 metabolism and were characterized by an enrichment of several taxa that had a larger effect size than fCAL. Importantly, these taxa were not correlated with fCAL levels, suggesting they could potentially serve as orthogonal markers of IBD.
- Despite notable differences in study design and clinical characteristics of patients, we validated our findings of microbial features distinguishing SpA phenotypes and IBD in external cohorts.

HOW THIS STUDY MIGHT AFFECT RESEARCH, PRACTICE OR POLICY

- PsA presentation had a significant effect on gut microbiome, suggesting that future studies should explicitly consider whether patients have peripheral, axial phenotype or both.
- PsA patients with newly diagnosed IBD were also characterized by unique microbiome signatures that were independent of fCAL.
- Microbial signatures are partially conserved across cohorts, suggesting that future work on larger populations could identify additional microbial biomarkers for PsA phenotype and IBD.

National Public Health System. The study was approved by the Medical Research Ethics Committee of the Hospital Puerta de Hierro Majadahonda (Madrid, Spain, ref. FER-PRE-2020-01-H. U.P.H: 108/20), and all participants provided written consent before enrolment.

A subset of patients participating in the EISER study who had been previously diagnosed with PsA (n = 246) were invited to participate in a substudy to assess their gut microbiome and blood biomarkers. One hundred and ninety-four patients consented to participate, of which 192 provided a stool sample and were included in the study (Fig 1). Blood samples from 125 of the patients were available for proteomic analysis. Patients who had no available colonoscopy for IBD diagnosis (n = 13, 6.7%) were excluded from analyses related to IBD.

Patients aged over 18 years who had been diagnosed with PsA in accordance with the ClASsification for Psoriatic Arthritis criteria [14] were eligible to participate in the substudy. Patients older than 50 years were included if they had not undergone a complete colonoscopy within the previous 3 years or, if performed, was considered of inadequate quality. Patients were excluded if they had a previous IBD diagnosis or other known chronic gastrointestinal disease, if they were receiving biologics or systemic steroids within the 30 days prior to inclusion, or if they were participating in another clinical research study.

Demographic and clinical information and variables related to PsA disease activity and medications were collected at the rheumatologist's office. Patients were classified into 2 groups based on their symptomatology: peripheral PsA alone (n = 143), or axial PsA (n = 49), which included patients with pure axial PsA (n = 9, 18%) and those with both axial and peripheral symptoms (mixed PsA, n = 40, 82%) (Fig 1, Table). PsA disease activity in the axial group was measured using the Ankylosing Spondylitis Disease Activity Score (ASDAS), and in the peripheral group using the Disease Activity in PsA (DAPSA). Patients were classified into 4 PsA disease activity groups based on their respective disease activity scores: inactive (ASDAS: <1.3; DAPSA: <4), low (ASDAS: 1.3-2.1; DAPSA: 4-14), moderate/high (ASDAS: 2.1-3.5; DAPSA: 14-28), and high (ASDAS: >3.5; DAPSA: >28).

Patient and public involvement

Patients or the public were not involved in the study design.

Assessment of IBD symptoms and diagnosis

Assessment of symptoms compatible with IBD was performed by the rheumatologist using the screening criteria described by the Inflammatory Bowel and Joint Pathology working group (PIIASER) [15]. To measure fCAL, a stool sample was collected in a BÜHLMANN CALEX tube the day before the visit to the gastroenterologist, and levels were measured using the Quantum Blue fCAL rapid test technology (BÜHLMANN Laboratories AG) following the manufacturer's instructions. A gastroenterologist

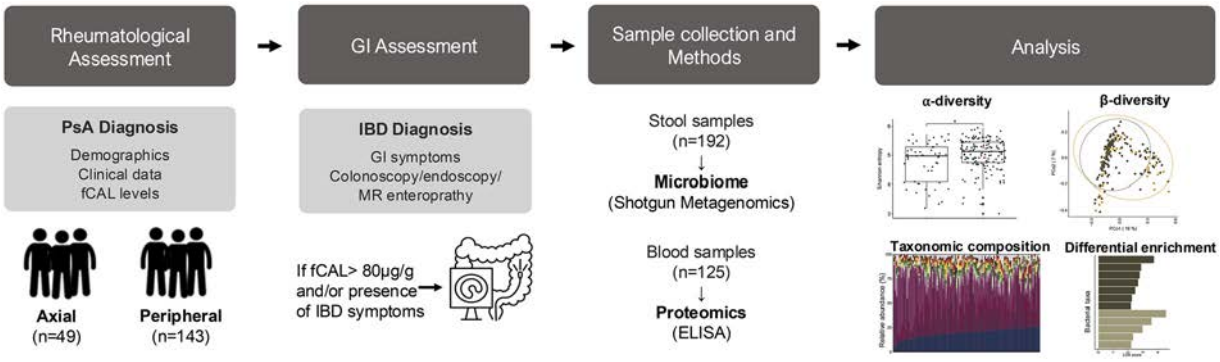

Figure 1. EISER study design. Overall study design, sample collection and analysis on gut microbiome, serum proteomics, and faecal calprotectin (fCAL). EISER, Enfermedad Inflamatoria Intestinal Sociedad Española de Reumatología; GI, gastrointestinal; IBD, inflammatory bowel disease; MR, magnetic resonance; PsA, psoriatic arthritis.

Table
Cohort summary

	Axial PsA	Peripheral PsA	P value
Subjects, n	49	143	NA
Sex (female), n (%)	28 (57.14)	65 (45.5)	.249
Age (y)	55.2 ± 13	55.7 ± 12.5	.844
Age at diagnosis (y)	45.1 ± 14.1	46.6 ± 12.2	.516
Disease duration (y)	10.1 ± 9.95	9.22 ± 9.81	.574
HLA-B27, positive/evaluable (%)	13/40 (32.5)	6/77 (7.8)	**9.92×10^{-05}**
PsA disease activity			
DAPSA	10.1 ± 8.15	10.8 ± 8.53	.663
ASDAS-CRP	2.25 ± 1.09	NA	NA
CRP (mg/L)	4.71 ± 4.96	4.50 ± 5.53	.809
Patient global assessment	4.22 ± 2.88	3.76 ± 2.53	.321
Medications			
NSAIDs, n (%)	24 (49)	43 (30.1)	**.033**
DMARDs, n (%)	32 (65.3)	108 (75.5)	.389
Methotrexate	19 (38.8)	84 (58.7)	.008
Leflunomide	3 (6.12)	15 (10.5)	.570
Sulfasalazine	7 (14.3)	3 (2.1)	.003
Apremilast	7 (14.3)	2 (1.4)	.001
PPIs, n (%)	20 (40.8)	43 (30.1)	.202
Smoking habits			
Never smoker	13 (26.5)	72 (50.3)	**.007**
Former smoker	19 (38.8)	52 (36.4)	.781
Current smoker	17 (34.7)	19 (13.3)	**.002**
Alcohol use (yes), n (%)	22 (44.9)	58 (40.6)	.639
Faecal calprotectin (fCAL)	140 ± 187	151 ± 216	.744
IBD symptoms, n (%)	10 (20.4)	15 (10.5)	.074
IBD diagnosis, n (%)	2/46 (4.35)	3/133 (2.26)	.415

ASDAS, Ankylosing Spondylitis Disease Activity Score; CRP, C-reactive protein; DMARD, disease-modifying antirheumatic drug; DAPSA, Disease Activity in Psoriatic Arthritis; IBD, inflammatory bowel disease; NA, Not available; NSAID, nonsteroidal anti-inflammatory drug; PPI, proton-pump inhibitor; PsA, psoriatic arthritis.
Demographics and clinical data for patients with peripheral vs axial PsA.
Significance of bold values $p < 0.05$.

evaluated the use of the fCAL test, clinical data, and symptoms collected by the rheumatologist. Patients underwent a colonoscopy if their fCAL levels were equal or greater than 80 μg/g of stool, or if levels were equal or greater than 160 μg/g if they were receiving nonsteroidal anti-inflammatory drugs (NSAIDs). If the patient was on NSAIDs and the fCAL was 80 to 160 μg/g, NSAIDs were discontinued and fCAL was reassessed 2 weeks later. If the fCAL levels were <80 μg/g after 2 weeks, the colonoscopy was not performed. However, colonoscopies were performed in patients with fCAL <80 μg/g if considered clinically indicated by the gastroenterologist (n = 7). Quantitative endoscopic results were measured using the Simple Endoscopic Score for evaluating Crohn's disease (CD), and the Ulcerative Colitis Endoscopic Index of Severity for the assessment of ulcerative colitis (UC). IBD diagnosis was confirmed through histological analysis of mucosal biopsies obtained during the colonoscopy. In case of a negative colonoscopy, an endoscopy with capsule was performed using a Patency Agile capsule (Given Imaging Ltd) (n = 35), and endoscopic findings were evaluated using the Lewis index. If capsule endoscopy was contraindicated, the patient underwent a magnetic resonance enterography (MRE, n = 3). Final determination of IBD diagnosis was performed by the gastroenterologist in every case and based on colonoscopy, histological analysis of biopsies, capsule endoscopy, and/or MRE findings. Patients with IBD were classified as having either CD or UC, or as unclassified IBD when clinical, endoscopic, and histological findings did not clearly support a definitive diagnosis of either [16].

Microbiome and serum biomarker characterisation

Stool samples were collected for microbiome analysis using OMNIGEN-gut OM-200 tubes and following the manufacturer's instructions. DNA was isolated from stool aliquots using the QIAGEN DNeasy PowerSoil Pro Kit according to the manufacturer's protocol. Extracted DNA was quantified in a GloMax Plate Reader System (Promega) using the QuantiFluor dsDNA System (Promega) chemistry. DNA libraries were prepared using the Nextera XT DNA Library Preparation Kit (Illumina) and IDT Unique Dual Indexes with a total DNA input of 1 ng. Genomic DNA was fragmented using a proportional amount of Illumina Nextera XT fragmentation enzyme. Unique dual indexes were added to each sample, followed by 12 cycles of PCR to construct libraries. DNA libraries were then purified using AMpure magnetic Beads (Beckman Coulter) and eluted in QIAGEN EB buffer. DNA libraries were quantified using a Qubit 4 fluorometer with the Qubit dsDNA HS Assay Kit. Libraries were then sequenced on an Illumina HiSeq platform (2 × 150 bp). Sequenced data were processed using MetaPhlAn 4 [17] and HUMANn 3.9 [18]. Bacterial load was predicted from shotgun metagenomics as previously described [19].

Blood samples were collected at the rheumatologist's office, using Acutainers BD SST II Advance Plus Tubes with BD Hemogard caps. Tubes were inverted 6 times for correct clot retraction and incubated for 30 minutes. Samples were centrifuged at 1300 −2000 × *g* for 10 minutes or at 3000 × *g* for 5 minutes at a temperature between 18 and 25°C. Serum was collected and transferred to a cryotube and frozen at -20°C until its subsequent analysis. Serum cytokines were analysed as follows: IL-23 and IL-17F were measured using Millipore SMC assays; IL-17A was measured using MSD S-Plex assay; other cytokines were measured using MSD V-Plex Plus Human Proinflammatory 10-Plex Panel 1: IFN-γ, IL-1β, IL-2, IL-4, IL-6, IL-8, IL-10, IL-12p70, IL-13, and TNF-α. Assays were performed according to manufacturer's instructions.

Statistical analyses

Microbiome data were processed using standard approaches as we have previously described [1] (see additional details in Supplementary Materials); alpha diversity was calculated using the Shannon entropy index, and beta diversity was calculated based on Bray-Curtis dissimilarity index. Differential enrichment analysis (LEfSe, MaAsLin2, ANCOM-BC, LinDA, and ALDEx2) was applied to identify enrichment/depletion of specific bacterial features/metabolic pathways between PsA types and patients with vs without IBD [20–24]. Statistical analysis was performed using R software v4.4.0. Statistical significance was calculated using the $\chi 2$ test for binary variables. Categorical variables were analysed using either the Wilcoxon or Kruskal-Wallis test, depending on the number of groups being compared. Correlations between continuous variables were analysed using CUTIE [25]. For multiple hypothesis testing, we used the false discovery rate-Benjamini Hochberg correction with $q < 0.1$. Multivariate models were conducted using generalised linear models in R and MaAsLin2 for microbial features.

RESULTS

Cohort summary

There were no significant differences in age, sex (biological sex), PsA disease duration, or age of diagnosis between patients with axial and peripheral PsA (Table). Of 117 patients for which

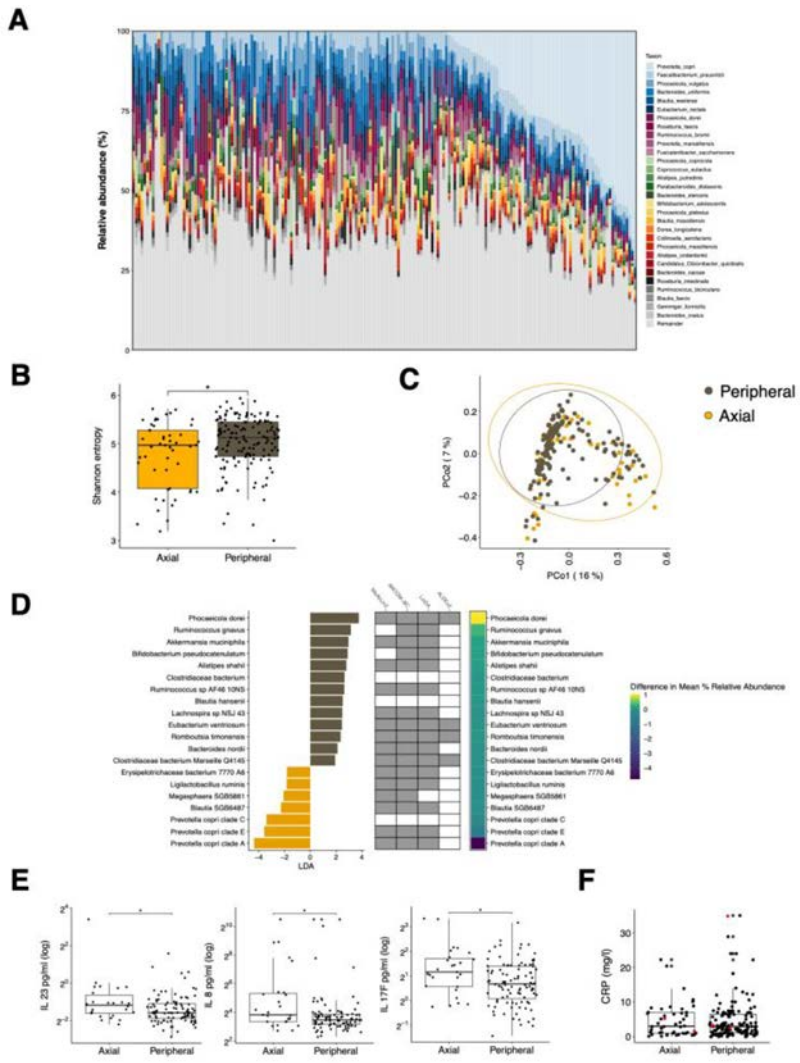

Figure 2. Microbiome and blood biomarkers across PsA disease phenotypes. (A) Species-level taxonomic composition across all samples. (B) Alpha diversity in axial vs peripheral PsA, measured by Shannon diversity. (C) PCoA plot representing beta diversity based on Bray-Curtis dissimilarity, samples coloured by PsA phenotype. (D) Differentially enriched taxa in axial (yellow) vs peripheral (dark brown) PsA. (Left) Taxa ranked according to linear discriminant analysis effect size (LEfSe). (Middle) Taxa identified as differential (grey boxes) according to MaAsLin2, ANCOM-BC, LinDA, and ALDEx2. (Right) Difference in mean relative abundance between axial and peripheral PsA. (E) Serum proinflammatory cytokines significantly elevated in axial compared to peripheral PsA. (F) Serum C-reactive protein (CRP) in axial and peripheral PsA. * $P < .05$. LDA, linear discriminant analysis; PCoA, principal coordinates analysis; PsA, psoriatic arthritis.

HLA-B27 information was available, 13 of 40 (32.5%) were positive in axial PsA, whereas only 6 of 77 (8%) were peripheral PsA ($P = 9.92 \times 10^{-05}$). On average, the mean disease activity was moderate in patients with axial PsA (ASDAS-C-reactive protein [CRP]: 2.25 ± 1.09) and low in peripheral PsA (DAPSA: 10.8 ± 8.53) (Table). As expected, patients with axial PsA received NSAIDs more frequently than patients with peripheral PsA (49% vs 30%, $P = .033$), but there were no significant differences in the overall use of csDMARDs and proton-pump inhibitors (PPIs) ($P = .389$ and $P = .202$, respectively).

We identified symptoms compatible with IBD in 20.4% of axial PsA and 10.5% of patients with peripheral PsA. Seventy-five patients had fCAL levels greater than 80 µg/g, with similar mean levels in axial and peripheral PsA ($P = .744$). Five of the 179 patients who were evaluated were ultimately diagnosed with IBD (2.8%; axial n = 2, peripheral n = 3) (Supplementary Table S1). Two of the patients with IBD had inactive PsA disease, 1 had low disease activity, and 2 had moderate/high disease activity. Four of the diagnosed patients had fCAL levels >80 µg/g and 1 lower levels (72 µg/g).

PsA phenotypes exhibit distinct gut microbiome and serum proinflammatory cytokines profiles

The gut microbiome of patients in this study was patient-specific and dominated by *Prevotella copri* (9.95% ± 16.65%), *Faecalibacterium prausnitzii* (5.07% ± 2.9%), *Phocaeicola vulgatus* (4.19% ± 5.29%), and *Bacteroides uniformis* (4.21% ± 4.55%) (Fig 2A). As expected and previously reported, we found that the microbiome composition of 23 healthy controls [26] was significantly different from that of patients with PsA in EISER ($P = .001$), with numerous differential features, including a notable enrichment of *P. copri* clade A in patients with PsA ($P = .019$). In EISER patients, DMARDs and NSAIDs did not have a significant effect on either microbial alpha ($P = .92$, $P = .12$, respectively) or beta diversity ($P = .45$, $P = .07$) (Supplementary Fig S1, Supplementary Table S2). PPIs did not have a significant effect on alpha diversity ($P = .45$) but did in beta diversity ($P = .03$) (Supplementary Table S2), while PPI usage was not significantly distinct between patients with axial and peripheral PsA ($P = .202$, Table). We found significantly lower levels of alpha diversity in patients with axial PsA compared to peripheral PsA ($P = .038$) (Fig 2B). Bacterial load was not significantly different between PsA phenotypes ($P = .615$). Although we did not observe significant differences in beta diversity between the 2 disease phenotypes (PERMANOVA, $P = .112$) (Fig 2C), several taxa were differentially abundant between the groups: 3 different *Prevotella copri* clades were enriched in patients with axial PsA, while *Phocaeicola dorei, Ruminococcus gnavus, Akkermansia muciniphila, Alistipes shahii*, and *Bifidobacterium pseudocatenulatum* among others, were enriched in peripheral PsA (Fig 2D, left). Enrichment of *P. copri* clades A and E in axial PsA and of *P. dorei* in peripheral PsA was further confirmed

using alternative methods for differential analysis (Fig 2D, middle; see Supplementary Fig S2 for specific results with each method). Of 13 cytokines measured (Supplementary Fig S3, Supplementary Table S3), 3 proinflammatory cytokines were significantly different between patients with axial and peripheral PsA: IL-23, IL-17F, and IL-8 all exhibited higher levels in axial PsA (P = .028, P = .018, P = .013, respectively) (Fig 2E). IL-13, a cytokine with both proinflammatory and anti-inflammatory effects, was also differential (higher in axial PsA, P = .028, Supplementary Fig. S3). We did not observe significant differences in CRP levels between axial and peripheral PsA (P = .354, Fig 2F), although patients with high or very high disease activity levels had, as expected, significantly higher levels of CRP compared to those with inactive or low disease activity (P = .001, P = .012, respectively). No differences in alpha or beta diversity were observed across PsA disease activity levels (P = .486 and .071, respectively).

Microbial biomarkers in patients with PsA with newly diagnosed IBD

Among patients with PsA with newly diagnosed IBD (axial n = 2; peripheral n = 3, Supplementary Table S3), we did not observe significant differences in alpha or beta diversity based on IBD diagnosis (Fig 3A,B). Furthermore, bacterial load was not significantly different between IBD and non-IBD subjects (P = .885). However, we identified several bacterial taxa differentially abundant in patients with IBD: *Prevotella copri* clade A, *P. stercorea, P. distasonis, Mitsuokella multacida, Eubacterium siraeum, Blautia stercoris*, and *Clostridium fessum*, among others, were significantly enriched in patients with IBD, whereas *Streptococcus lutetiensis* was depleted (Fig 3C, left). *P. copri* clade A was confirmed to be enriched in IBD based on all differential analysis methods tested, and *P. stercorea* was also enriched in IBD according to 4 of 5 methods (Fig 3C, middle; see Supplementary Fig S4 for specific results with each method). Patients diagnosed with IBD had higher fCAL levels (P = .016) (Fig 3D), although we found no significant differences in the levels of CRP (P = .377) or serum cytokines between patients with and without IBD (Supplementary Table S4). Importantly, several of the differentially abundant bacterial taxa had a larger effect size for IBD diagnosis compared with fCAL (Cohen's D; *P. stercorea*: 1.268, *P. copri* clade A: 1.23, *B. stercoris*: 1.107, *C. fessum*: 0.750; fCAL: 0.629) (Fig 3E). Differential taxa uniquely identified by other methods also had comparable effect sizes to fCAL (Supplementary Fig S5). The abundance of *P. stercorea, Blautia stercoris, and P. copri* clade A was not significantly correlated with the levels of fCAL (Spearman; P = .58, P = .36, P = .51, P = .42, respectively), whereas the levels of *C. fessum* were significantly correlated with fCAL (P = .029) although with low strength

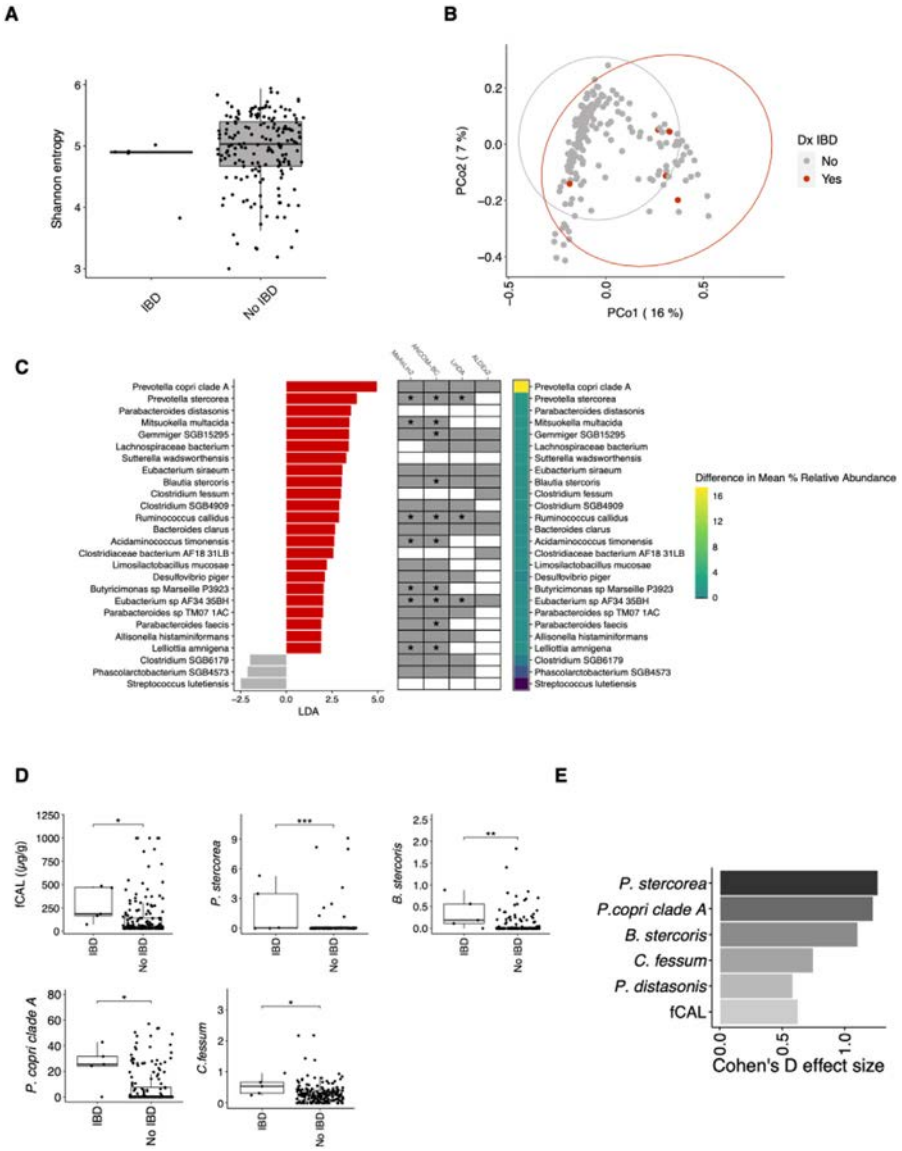

Figure 3. Microbiome and biomarkers of IBD in patients with PsA. (A) Alpha diversity in patients with PsA with and without IBD. (B) PCoA plot based on beta diversity in patients with and without IBD. (C) Taxa differentially enriched in patients with and without IBD. (Left) Taxa ranked according to linear discriminant analysis effect size (LEfSe). (Middle) Taxa identified as differential (grey boxes) according to MaAsLin2, ANCOM-BC, LinDA, and ALDEx2. Stars indicate a significant difference after FDR correction. (Right) Difference in mean relative abundance between IBD and no IBD. (D) fCAL and bacterial biomarkers significantly elevated in patients with IBD compared to without IBD. (E) Cohen's D effect size of bacterial taxa and fCAL in IBD diagnosis. Significance levels: *, $P < .05$; **, $P < .01$; ***, $P < .001$. FDR, false discovery rate; fCAL, faecal calprotectin; IBD, inflammatory bowel disease; LDA, linear discriminant analysis; PsA, psoriatic arthritis; PCoA, principal coordinates analysis.

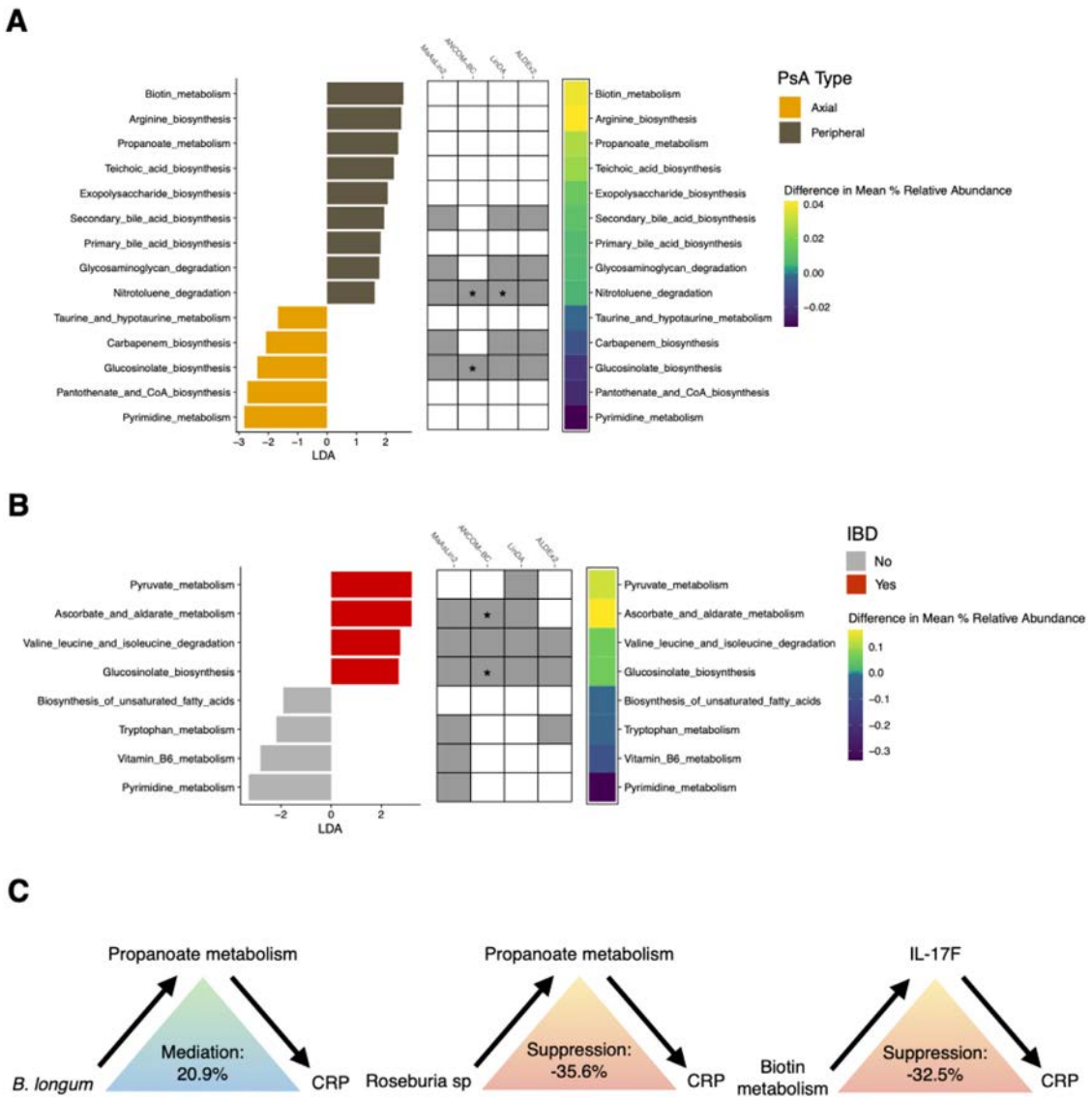

Figure 4. Bacterial metabolic pathways across subjects and differentially enriched. (A) Differentially enriched pathways in axial vs peripheral PsA. (Left) Pathways ranked according to linear discriminant analysis effect size (LEfSe). (Middle) Taxa identified as differential (grey boxes) according to MaAsLin2, ANCOM-BC, LinDA, and ALDEx2. Stars indicate significant difference after FDR correction. (Right) Difference in mean relative abundance between axial and peripheral PsA. (B) Differentially enriched pathways in patients with IBD vs without IBD. (Left) Pathways ranked according to linear discriminant analysis effect size (LEfSe). (Middle) Taxa identified as differential (grey boxes) according to MaAsLin2, ANCOM-BC, LinDA, and ALDEx2. Stars indicate significant difference after FDR correction. (Right) Difference in mean relative abundance between patients with IBD and without IBD. (C) Pathways and cytokines mediating the effect of microbial features in CRP. CRP, C-reactive protein; CoA, Coenzyme A; FDR, false discovery rate; IBD, inflammatory bowel disease; IL, interleukin; LDA, linear discriminant analysis; MR, magnetic resonance; PsA, psoriatic arthritis.

(rho = 0.16). Importantly, none of these taxonomic biomarkers were impacted by medication usage ($P > .05$ for DMARDs, NSAIDs, and PPI, Supplementary Fig S6). Overall, these results suggest that these taxa are not correlated with fCAL and are therefore associated with newly diagnosed IBD in patients with PsA independent of calprotectin levels.

Bacterial functions associated with PsA disease phenotypes and IBD

Abundance of microbial metabolism pathways in our cohort was heterogeneous across patients but generally more conserved than taxonomic composition (Supplementary Fig S7). In patients with peripheral PsA, we found that metabolic pathways encoding genes related to biotin metabolism, arginine, secondary bile acids, and glycan biosynthesis, among others, were significantly enriched, whereas pyrimidine metabolism, pantothenate and CoA biosynthesis, and glucosinolate biosynthesis, among others, were enriched in patients with axial PsA (Fig 4A). In patients without IBD, we found a significant enrichment of pathways encoding genes involved in pyrimidine, vitamin B6, and tryptophan metabolism. Pathways encoding genes related to metabolism of ascorbate, aldarate, and pyruvate, degradation of valine, leucine, and isoleucine, and biosynthesis of glucosinolate were enriched in patients with IBD (Fig 4B). Alternative methods for differential analysis of pathways were also performed in both axial vs peripheral PsA and IBD vs non-IBD (Supplementary Fig S8A,B). The contribution of bacterial species to pathways was generally dominated by *Bacteroides vulgatus, Faecalibacterium prausnitzii, Bacteroides dorei*, and *Eubacterium rectale* (Supplementary Fig S9). Depending on PsA phenotype, different bacteria contributed to specific pathways, with *B. vulgatus* and *Acidaminococcus intestini* primarily contributing in axial PsA, and *Roseburia intestinalis* and *B. dorei* primarily contributing in peripheral PsA. When comparing IBD and non-IBD, *B. vulgatus* and *E. siraeum* contributed primarily in IBD, whereas *B. dorei*

and *Coprococcus eutactus* contributed more in non-IBD (Supplementary Fig S10, S11). Lastly, we performed mediation analysis to investigate microbial contributions to CRP levels through specific pathways or proinflammatory cytokines. Using taxa and pathways differential in PsA phenotypes or IBD diagnosis, we identified 3 significant associations: propanoate metabolism mediates the effect of *B. longum* in CRP while suppressing (ie, negative mediation) the effect of *Roseburia* sp., and suppression through IL-17F of biotin metabolism effects (Fig 4C).

Predictive power of microbial features in PsA phenotypes and IBD across populations

We next investigated whether findings from the EISER study were generalisable across populations. We identified 3 studies that included patients with different forms of SpA and IBD with available microbiome data: a study by Maldarelli et al, of patients with peripheral (N = 38) and axial (N = 13) SpA who also had concomitant CD [27], a study by Berlinberg et al, of patients with SpA with (N = 13) and without (N = 23) CD [26], and a study by Sternes et al, of patients with ankylosing spondylitis with (N = 5) and without (N = 18) IBD [28]. Of note, none of these studies had a design comparable to EISER and IBD was already established in all patients and not newly diagnosed.

In the Maldarelli study, alpha diversity was higher in patients with axial SpA than those with peripheral presentation, although not significantly (P = .07) (Supplementary Fig S12A), whereas beta diversity was significantly different between the groups (P = .003) (Supplementary Fig S12B). In line with findings in the EISER cohort, we found that Phocaeicola was enriched in peripheral SpA, whereas *P. copri* was more abundant in axial presentation (Supplementary Fig S12C). Furthermore, and also consistent with results in EISER, biotin metabolism and teichoic acid biosynthesis were enriched in patients with peripheral SpA (Supplementary Fig S12D).

In the Berlinberg study, there were no significant differences between patients with SpA CD and without CD in alpha (P = .76) nor beta diversity (P = .32) (Supplementary Fig S13A,B). *E. coli, Enterocloster clostridioformis*, and *Anaerotignum lactatifermentans* were enriched in CD and *Finegoldia magna* in those without CD (Supplementary Fig S13D,E). In the study by Sternes et al of patients with ankylosing spondylitis with and without IBD, we found no significant differences in alpha diversity (P = .55) but significant differences in beta diversity (P = .002) with respect to IBD (Supplementary Fig S14A,B). *B fragilis, Eubacterium spp*., and *Ruthenibacterium lactatiformans* were enriched in IBD and *Bacteroides merdae* in patients without IBD (Supplementary Fig S14C). The valine, leucine, and isoleucine degradation pathway was also enriched in patients with IBD (Supplementary Fig S14D), in line with results in the EISER cohort. In this study, which included fCAL data, we found that, similar to EISER, microbial biomarkers of IBD were also not significantly correlated with fCAL (*B. fragilis,* r = 0.02, P = .87; *Eubacterium spp.* r = 0.03, P = .84; *R. lactatiformans* r = 0.28, P = .06), with *B. fragilis* having an effect size comparable to fCAL in distinguishing patients with IBD and without IBD (Supplementary Fig S14E).

Overall, results across these cohorts suggest that, despite notable differences in study design, clinical characteristics of patients, and microbiome characterisation techniques, microbial features can distinguish SpA phenotypes. Importantly, our findings from the EISER study on the potential for specific bacteria to identify IBD independent of fCAL were substantiated by results in the Berlinberg et al cohort.

DISCUSSION

Our study is the first to comprehensively characterise the gut microbiome, cytokine profiles, and fCAL of patients with PsA, aimed at identifying changes associated with PsA phenotypes and with IBD. Importantly, because patients in our cohort were newly diagnosed with IBD, our results are not confounded by the known effects of medications on the microbiome [29]. The gut microbiome of patients in the EISER cohort was dominated by *Prevotella copri* (9.95% ± 16.65%), *Faecalibacterium prausnitzii* (5.07% ± 2.9%), *Phocaeicola vulgatus* (4.19% ± 5.29%), and *Bacteroides uniformis* (4.21% ± 4.55%). Patients with axial PsA had lower alpha diversity and were enriched in *Prevotella copri*, a species that has been previously associated with diseases involving immune dysregulation and inflammation, most notably with rheumatoid arthritis [30–33]. Patients with peripheral involvement, on the other hand, exhibited higher abundance of various gut commensals generally regarded as beneficial, including *A. muciniphila* or *B. pseudocatenulatum,* although they were also enriched in *Ruminococcus gnavus*, a species known for its proinflammatory roles and its association with IBD [34,35]. Interestingly, Breban et al identified, in 2 consecutive cross-sectional cohorts, a 2- to 3-fold increase in abundance of *R. gnavus* in patients with SpA, compared with rheumatoid arthritis patients and healthy controls [36].

Patients with axial PsA had a depletion of functions related to biotin metabolism and of arginine biosynthesis. Biotin is an essential micronutrient which plays critical roles in immunity, and its deficiency has been associated with inflammatory processes. Under biotin-deficient conditions, innate immune cells (dendritic cells) produce increased levels of proinflammatory cytokines, such as TNF-α and IL-23 [37]. Moreover, mice deficient in biotin display intestinal inflammation similar to that observed in UC [38,39], which is alleviated by oral supplementation with biotin via reduction of the activation of NF-κB, which prevents the production of inflammatory cytokines [40]. Importantly, biotin deficiency has been recently reported in patients with IBD [41]. Arginine is also an important protective factor, as it inhibits arthritis and prevents bone erosion through the blocking of TNF-α mechanisms [42]. Our results thus point to a perturbation in biotin and arginine metabolism in axial PsA that could be associated with the higher proinflammatory levels and more pathogenic outcomes observed in these patients in our cohort. In addition, pathways related to primary and secondary bile acid metabolism were also depleted in axial PsA. Bile acids are metabolised by gut bacteria, contributing to the bile acid pool in the host, and are involved in important signalling and metabolic pathways that are crucial in homeostasis [43]. Interestingly, a recent study found lower levels of serum bile acids in patients with psoriasis who progressed to PsA, suggesting a potential association between the dysregulation of bile acid metabolism and PsA aetiology [44].

Up to 4% of patients with PsA also manifest symptoms that are compatible with IBD [9]. Early and accurate diagnosis of comorbid IBD in patients with PsA is therefore an important clinical problem. Colonoscopy and histological analysis of intestinal biopsies are the gold standard methods of detecting subclinical gut inflammation in patients with PsA without gastrointestinal symptoms [45–47]. However, colonoscopy is an invasive procedure and is not routinely performed in asymptomatic individuals. While fCAL is commonly used in the clinic to help diagnose IBD in the general population, its predictive value is limited. In our study, we found higher levels of calprotectin in most, but not all, patients with IBD, although many

patients without IBD also had elevated calprotectin levels. Screening criteria for the assessment of symptoms compatible with IBD have also been proposed [15]. In our cohort, 25 patients presented with IBD-like symptoms, but only 5 were diagnosed with IBD. Furthermore, PsA disease activity was not a strong predictor of IBD, as 2 patients diagnosed with IBD had inactive PsA and 1 had low activity. These findings thus strongly suggest that existing methods for diagnosis of IBD lack accuracy in subjects with PsA, and alternative approaches are required. Here, we identified multiple bacteria significantly enriched in patients with newly diagnosed IBD. Importantly, none of these species were correlated with levels of calprotectin and had a higher effect size than fCAL alone, suggesting that these taxa might be orthogonal markers of IBD. A recent study found that the microbiome can be used to identify accurate biomarkers of IBD in the general population [48], suggesting that our results are potentially informative in patients who also have PsA. We speculate that additional analyses of the data presented by Zheng et al [48] restricted to patients who had both IBD and PsA could yield additional insights, although it is unclear whether any of the patients with IBD in that study also had concomitant PsA. Within the taxa identified in our cohort, species in the *Prevotella* genus are known to drive intestinal inflammation and have been previously associated with disease development in mouse models of colitis [30,49,50], indicating that they might contribute to proinflammatory processes characteristic of IBD.

In addition to specific taxa, microbial metabolism of pyrimidine, vitamin B6, and tryptophan metabolism was significantly depleted in patients with newly diagnosed IBD. Tryptophan is an essential amino acid acquired from dietary sources and metabolised through host and microbial pathways. Disruption of tryptophan metabolism is a well-established feature of mouse models of colitis and in patients with IBD [51–53], and administration of tryptophan or its metabolites ameliorates inflammation and modulates epithelial homeostasis [53–55]. In a study of healthy controls, patients with axial SpA and axial SpA with CD, tryptophan synthesis was also found to be more abundant in healthy participants compared to SpA and SpA with CD, further highlighting the relation between underlying inflammatory processes and tryptophan metabolism [26]. Serum levels of vitamin B6, or its active form, pyridoxal 5'-phosphate (PLP), exhibit a strong negative association with inflammation, although the underlying mechanisms are poorly understood [56,57]. Reduced levels of plasma PLP have been observed in patients with inflammatory conditions, including rheumatoid arthritis and IBD, and this reduction has been inversely related to inflammatory markers [58–60]. Dietary vitamin B6 can also modulate colonic inflammation in a mouse model of colitis [61]. Finally, degradation of the branched-chained amino acids (BCAAs), valine, leucine, and isoleucine was enriched in patients with IBD. Previous studies have shown that BCAAs levels are often altered in patients with IBD, although this relationship remains incompletely understood, with some reports suggesting beneficial effects while others associate elevated BCAAs or its metabolism with disease activity [62,63]. In mouse models of colitis, BCAA supplementation has been shown to exacerbate disease severity, potentially through alterations in gut microbiota composition and reductions in protective metabolites [64,65].

We additionally sought to understand the generalizability of findings in the EISER study by analysing previously characterised cohorts. In those for which microbiome data were available, sample sizes were lower (EISER: 192 vs Maldarelli: 51, Berlinberg: 36, Sternes: 23), microbial characterisation used lower resolution techniques such as 16S rRNA sequencing (Maldarelli, Sternes), or samples were collected using rectal swabs instead of stool (Berlinberg), which is potentially less reflective of the gut environment [66]. More importantly, none of the previous studies prospectively enrolled patients with PsA with newly diagnosed IBD. This is particularly relevant, since established IBD significantly impacts microbial communities due to the underlying inflammatory process [67], while the use of IBD-specific medications can also induce changes in microbiome [29,68]. Despite these differences and limitations in previous studies, we found 2 notable consistencies with the EISER cohort: first, *P. copri* is a robust feature in distinguishing axial from peripheral involvement in SpA. *P. copri* has been reported by previous groups as associated with rheumatic disease [33]. Second, microbial taxa could distinguish IBD from patients without IBD with effect sizes comparable to or greater than fCAL, the clinical gold standard. Furthermore, these bacteria did not correlate with fCAL, suggesting that they contribute orthogonal information in the identification of IBD and supporting the hypothesis that bacteria may provide information relevant for pathogenesis that is currently not captured with calprotectin.

Our study has certain limitations. While we had a large number of participants with PsA, there were only a limited number of patients with IBD, although in line with previous estimates of IBD prevalence in PsA. Conclusions drawn from such small sample sizes are necessarily speculative, and future studies with larger sample sizes and *in vivo* experiments will be needed to confirm these findings. Analysis of longitudinal data would also improve the robustness of results. Additionally, peripheral PsA is more prevalent than axial PsA in the general population, which constrained our ability to recruit a comparable number of patients in both groups. In addition, we did not have cytokine data for all subjects, which might limit our power to detect significant differences. Finally, disease activity was heterogeneous across patients, which could further decrease our ability to identify differences, although microbiome and cytokine levels were not significantly associated with disease activity. In future work, endoscopic samples, especially from inflamed areas, could be integrated with microbiome and cytokine data to develop integrative models combining histologic and multiomic predictors of IBD in PsA.

Overall, our results identify microbial and inflammatory factors associated with PsA phenotypes, such as lower diversity, an enrichment in *Prevotella copri* (including clade A) and higher levels of proinflammatory cytokines in axial PsA. We also observed a disruption of biotin, arginine, and bile acid metabolism in these patients, further highlighting the role of distinct inflammatory mechanisms in axial PsA. Importantly, we identified microbial features associated with newly diagnosed IBD in patients with PsA that were independent of fCAL, which could provide valuable insights to better identify asymptomatic patients with IBD in this at-risk population.

Competing interests

Jose Federico Diaz-Gonzalez reports financial support was provided by Janssen Pharmaceuticals Inc.

CRediT authorship contribution statement

Alba Boix-Amorós: Writing – review & editing, Writing – original draft, Validation, Software, Methodology, Investigation, Formal analysis, Data curation, Conceptualization. **Kevin Bu:** Writing – review & editing, Validation, Software, Methodology, Investigation, Formal analysis, Data curation. **Rebecca B. Blank:** Writing – review & editing, Investigation, Data curation. **Adam Cantor:** Writing – review & editing, Validation,

Software, Methodology, Investigation, Formal analysis, Data curation. **Ana Gutiérrez-Casbas:** Writing – review & editing, Project administration, Methodology, Investigation, Conceptualization. **Iago Rodríguez-Lago:** Writing – review & editing, Project administration, Methodology, Investigation, Conceptualization. **Ignacio Marin-Jimenez:** Writing – review & editing, Project administration, Methodology, Investigation, Conceptualization. **Jesus Sanz:** Writing – review & editing, Project administration, Methodology, Investigation, Conceptualization. **Jordi Gratacos Masmitja:** Writing – review & editing, Project administration, Methodology, Investigation, Conceptualization. **Elisa Trujillo:** Writing – review & editing, Project administration, Methodology, Investigation, Conceptualization. **María Carmen Muñoz:** Writing – review & editing, Project administration, Methodology, Investigation, Conceptualization. **María Luz García Vivar:** Writing – review & editing, Project administration, Methodology, Investigation, Conceptualization. **Marta Carrillo:** Writing – review & editing, Project administration, Methodology, Investigation, Conceptualization. **María Vanesa Hernández Hernández:** Writing – review & editing, Project administration, Methodology, Investigation, Conceptualization. **Xavier Calvet:** Writing – review & editing, Project administration, Methodology, Investigation, Conceptualization. **Marta Arévalo Salaet:** Writing – review & editing, Resources, Project administration, Investigation, Data curation. **Marta Izquierdo Romero:** Writing – review & editing, Project administration, Methodology, Investigation, Conceptualization. **Anahy Brandy García:** Writing – review & editing, Methodology, Investigation, Conceptualization. **Sandra Pérez:** Writing – review & editing, Methodology, Investigation, Conceptualization. **Jose Francisco García Llorente:** Writing – review & editing, Methodology, Investigation, Conceptualization. **Yago Gonzalez-Lama:** Writing – review & editing, Methodology, Investigation, Conceptualization. **Carolina Merino Argumánez:** Writing – review & editing, Methodology, Investigation, Conceptualization. **Zulema Plaza:** Writing – review & editing, Project administration, Methodology, Data curation. **Marta Domínguez:** Writing – review & editing, Project administration, Methodology, Data curation. **Juan D. Cañete:** Writing – review & editing, Writing – original draft, Supervision, Project administration, Methodology, Investigation, Funding acquisition, Conceptualization. **Jose Federico Diaz-Gonzalez:** Writing – review & editing, Writing – original draft, Supervision, Resources, Project administration, Methodology, Investigation, Funding acquisition, Conceptualization. **Jose U. Scher:** Writing – review & editing, Writing – original draft, Supervision, Project administration, Methodology, Investigation, Conceptualization. **Jose C. Clemente:** Writing – review & editing, Writing – original draft, Supervision, Project administration, Methodology, Investigation, Conceptualization.

Acknowledgements

We would like to acknowledge Drs Randy Longman, Kristi Kuhn, and Peter Sternes for facilitating access to data from their studies, which were used as validation sets in this work.

Funding

The EISER clinical study and data generation were funded by Janssen Pharmaceutical. JDC has received funding from the Innovative Medicines Initiative 2 Joint Undertaking (JU) under grant agreement no. 101007757 (HIPPOCRATES). The JU receives support from the European Union's Horizon 2020 research and innovation program and EFPI. The JU is not responsible for any use that may be made of the information it contains.

Patient consent for publication

Not applicable.

Ethics approval

The study was approved by the Medical Research Ethics Committee of the Hospital Puerta de Hierro Majadahonda (Madrid, Spain, ref. FER-PRE-2020-01-H.U.P.H: 108/20), and all patients provided written consent before enrollment.

Provenance and peer review

Not commissioned; externally peer reviewed.

Data availability statement

Microbiome shotgun sequencing data have been deposited in the Sequence Read Archive (SRA) with BioProject ID PRJNA1365870.

Supplementary materials

Supplementary material associated with this article can be found in the online version at doi:10.1016/j.ard.2026.01.018.

Orcid

Jose C. Clemente: http://orcid.org/0000-0002-3970-9856

REFERENCES

[1] Boix-Amorós A, Badri MH, Manasson J, Blank RB, Haberman RH, Neimann AL, et al. Alterations in the cutaneous microbiome of patients with psoriasis and psoriatic arthritis reveal similarities between non-lesional and lesional skin. Ann Rheum Dis 2023;82(4):507–14.
[2] Scher JU, Ubeda C, Artacho A, Attur M, Isaac S, Reddy SM, et al. Decreased bacterial diversity characterizes the altered gut microbiota in patients with psoriatic arthritis, resembling dysbiosis in inflammatory bowel disease. Arthritis Rheumatol 2015;67(1):128–39.
[3] Ritchlin CT, Colbert RA, Gladman DD. Psoriatic Arthritis. N Engl J Med 2017;376(10):957–70.
[4] López-Medina C, Molto A, Sieper J, Duruöz T, Kiltz U, Elzorkany B, et al. Prevalence and distribution of peripheral musculoskeletal manifestations in spondyloarthritis including psoriatic arthritis: results of the worldwide, cross-sectional ASAS-PerSpA study. RMD Open 2021;7(1):e001450.
[5] Chandran V, Barrett J, Schentag CT, Farewell VT, Gladman DD. Axial psoriatic arthritis: update on a longterm prospective study. J Rheumatol 2009;36(12):2744–50.
[6] Proft F, Lüders S, Hunter T, Luna G, Rios Rodriguez V, Protopopov M, et al. Early identification of axial psoriatic arthritis among patients with psoriasis: a prospective multicentre study. Ann Rheum Dis 2022;81(11):1534–40.
[7] Baeten D, Østergaard M, Wei JC, Sieper J, Järvinen P, Tam LS, et al. Risankizumab, an IL-23 inhibitor, for ankylosing spondylitis: results of a randomised, double-blind, placebo-controlled, proof-of-concept, dose-finding phase 2 study. Ann Rheum Dis 2018;77(9):1295–302.
[8] Lubrano E, Chan J, Queiro-Silva R, Cauli A, Goel N, Poddubnyy D, et al. Management of axial disease in patients with psoriatic arthritis: an updated literature review informing the 2021 GRAPPA treatment recommendations. J Rheumatol 2023;50(2):279–84.
[9] Bergman MJ, Zueger P, Song J, Pivneva I, Betts KA, Joshi AD. Inflammatory bowel disease is associated with a substantial economic burden in patients with psoriatic arthritis and in patients with ankylosing spondylitis. Arthritis Rheumatol 2018;70(Suppl 9).

[10] Iriarte A, Zaera C, Bachiller-Corral J, López-Sanromán A. Inflammatory bowel disease as a paradoxical effect of anti-TNF alpha therapy. Gastroenterol Hepatol 2017;40(2):117–21.
[11] Deng Z, Wang S, Wu C, Wang C. IL-17 inhibitor-associated inflammatory bowel disease: a study based on literature and database analysis. Front Pharmacol 2023;14:1124628.
[12] van Rheenen PF, Van de Vijver E, Fidler V. Faecal calprotectin for screening of patients with suspected inflammatory bowel disease: diagnostic meta-analysis. BMJ 2010;341:c3369.
[13] Kristensen V, Malmstrøm GH, Skar V, Røseth A, Moum B. Clinical importance of faecal calprotectin variability in inflammatory bowel disease: intra-individual variability and standardisation of sampling procedure. Scand J Gastroenterol 2016;51(5):548–55.
[14] Taylor W, Gladman D, Helliwell P, Marchesoni A, Mease P, Mielants H, et al. Classification criteria for psoriatic arthritis: development of new criteria from a large international study. Arthritis Rheum 2006;54(8):2665–73.
[15] Sanz J, Roura XJ, Seoane-Mato D, Montoro M, Gomollón F, Grupo de Trabajo del proyecto PIIASER. Screening of inflammatory bowel disease and spondyloarthritis for referring patients between rheumatology and gastroenterology. Gastroenterol Hepatol 2018;41(1):54–62.
[16] Burisch J, Pedersen N, Čuković-Čavka S, Brinar M, Kaimakliotis I, Duricova D, et al. East-West gradient in the incidence of inflammatory bowel disease in Europe: the ECCO-EpiCom inception cohort. Gut 2014;63(4):588–97.
[17] Blanco-Míguez A, Beghini F, Cumbo F, McIver LJ, Thompson KN, Zolfo M, et al. Extending and improving metagenomic taxonomic profiling with uncharacterized species using MetaPhlAn 4. Nat Biotechnol 2023;41(11):1633–44.
[18] Beghini F, McIver LJ, Blanco-Míguez A, Dubois L, Asnicar F, Maharjan S, et al. Integrating taxonomic, functional, and strain-level profiling of diverse microbial communities with bioBakery 3. Elife 2021;10:e65088.
[19] Nishijima S, Stankevic E, Aasmets O, Schmidt TSB, Nagata N, Keller MI, et al. Fecal microbial load is a major determinant of gut microbiome variation and a confounder for disease associations. Cell 2025;188(1) 222−36.e15.
[20] Segata N, Izard J, Waldron L, Gevers D, Miropolsky L, Garrett WS, et al. Metagenomic biomarker discovery and explanation. Genome Biol 2011;12(6):R60.
[21] Mallick H, Rahnavard A, McIver LJ, Ma S, Zhang Y, Nguyen LH, et al. Multivariable association discovery in population-scale meta-omics studies. PLoS Comput Biol 2021;17(11):e1009442.
[22] Zhou H, He K, Chen J, Zhang X. LinDA: linear models for differential abundance analysis of microbiome compositional data. Genome Biol 2022;23(1):95.
[23] Lin H, Peddada SD. Analysis of compositions of microbiomes with bias correction. Nat Commun 2020;11(1):3514.
[24] Fernandes AD, Reid JN, Macklaim JM, McMurrough TA, Edgell DR, Gloor GB. Unifying the analysis of high-throughput sequencing datasets: characterizing RNA-seq, 16S rRNA gene sequencing and selective growth experiments by compositional data analysis. Microbiome 2014;2:15.
[25] Bu K, Wallach DS, Wilson Z, Shen N, Segal LN, Bagiella E, et al. Identifying correlations driven by influential observations in large datasets. Brief Bioinform 2022;23(1):bbab482.
[26] Berlinberg AJ, Regner EH, Stahly A, Brar A, Reisz JA, Gerich ME, et al. Multi 'omics analysis of intestinal tissue in ankylosing spondylitis identifies alterations in the tryptophan metabolism pathway. Front Immunol 2021;12:587119.
[27] Maldarelli GA, Metz M, Oguntunmibi S, Tran N, Xiang G, Lukin D, et al. IgG-seq identifies immune-reactive enteric bacteria in Crohn's disease with spondyloarthritis. Gut Microbes 2025;17(1):2464221.
[28] Sternes PR, Brett L, Phipps J, Ciccia F, Kenna T, de Guzman E, et al. Distinctive gut microbiomes of ankylosing spondylitis and inflammatory bowel disease patients suggest differing roles in pathogenesis and correlate with disease activity. Arthritis Res Ther 2022;24(1):163.
[29] Maier L, Pruteanu M, Kuhn M, Zeller G, Telzerow A, Anderson EE, et al. Extensive impact of non-antibiotic drugs on human gut bacteria. Nature 2018;555(7698):623–8.
[30] Scher JU, Sczesnak A, Longman RS, Segata N, Ubeda C, Bielski C, et al. Expansion of intestinal *Prevotella copri* correlates with enhanced susceptibility to arthritis. Elife 2013;2:e01202.
[31] Zhang X, Zhang D, Jia H, Feng Q, Wang D, Liang D, et al. The oral and gut microbiomes are perturbed in rheumatoid arthritis and partly normalized after treatment. Nat Med 2015;21(8):895–905.
[32] Maeda Y, Kurakawa T, Umemoto E, Motooka D, Ito Y, Gotoh K, et al. Dysbiosis contributes to arthritis development via activation of autoreactive T cells in the intestine. Arthritis Rheumatol 2016;68(11):2646–61.
[33] Nii T, Maeda Y, Motooka D, Naito M, Matsumoto Y, Ogawa T, et al. Genomic repertoires linked with pathogenic potency of arthritogenic *Prevotella copri* isolated from the gut of patients with rheumatoid arthritis. Ann Rheum Dis 2023;82(5):621–9.
[34] Henke MT, Kenny DJ, Cassilly CD, Vlamakis H, Xavier RJ, Clardy J. *Ruminococcus gnavus*, a member of the human gut microbiome associated with Crohn's disease, produces an inflammatory polysaccharide. Proc Natl Acad Sci U S A 2019;116(26):12672–7.
[35] Hall AB, Yassour M, Sauk J, Garner A, Jiang X, Arthur T, et al. A novel *Ruminococcus gnavus* clade enriched in inflammatory bowel disease patients. Genome Med 2017;9(1):103.
[36] Breban M, Tap J, Leboime A, Said-Nahal R, Langella P, Chiocchia G, et al. Faecal microbiota study reveals specific dysbiosis in spondyloarthritis. Ann Rheum Dis 2017;76(9):1614–22.
[37] Agrawal S, Agrawal A, Said HM. Biotin deficiency enhances the inflammatory response of human dendritic cells. Am J Physiol Cell Physiol 2016;311(3):C386–91.
[38] Sabui S, Bohl JA, Kapadia R, Cogburn K, Ghosal A, Lambrecht NW, et al. Role of the sodium-dependent multivitamin transporter (SMVT) in the maintenance of intestinal mucosal integrity. Am J Physiol Gastrointest Liver Physiol 2016;311(3):G561–70.
[39] Ghosal A, Lambrecht N, Subramanya SB, Kapadia R, Said HM. Conditional knockout of the Slc5a6 gene in mouse intestine impairs biotin absorption. Am J Physiol Gastrointest Liver Physiol 2013;304(1):G64–71.
[40] Skupsky J, Sabui S, Hwang M, Nakasaki M, Cahalan MD, Said HM. Biotin supplementation ameliorates murine colitis by preventing NF-kappaB activation. Cell Mol Gastroenterol Hepatol 2020;9(4):557–67.
[41] Erbach J, Bonn F, Diesner M, Arnold A, Stein J, Schröder O, et al. Relevance of biotin deficiency in patients with inflammatory bowel disease and utility of serum 3 hydroxyisovaleryl carnitine as a practical everyday marker. J Clin Med 2022;11(4):1118.
[42] Cao S, Li Y, Song R, Meng X, Fuchs M, Liang C, et al. L-arginine metabolism inhibits arthritis and inflammatory bone loss. Ann Rheum Dis 2024;83(1):72–87.
[43] Fleishman JS, Kumar S. Bile acid metabolism and signaling in health and disease: molecular mechanisms and therapeutic targets. Signal Transduct Target Ther 2024;9(1):97.
[44] Paine A, Brookes PS, Bhattacharya S, Li D, De La Luz Garcia-Hernandez M, Tausk F, et al. Dysregulation of bile acids, lipids, and nucleotides in psoriatic arthritis revealed by unbiased profiling of serum metabolites. Arthritis Rheumatol 2023;75(1):53–63.
[45] Scarpa R, Manguso F, D'Arienzo A, D'Armiento FP, Astarita C, Mazzacca G, et al. Microscopic inflammatory changes in colon of patients with both active psoriasis and psoriatic arthritis without bowel symptoms. J Rheumatol 2000;27(5):1241–6.
[46] Schatteman L, Mielants H, Veys EM, Cuvelier C, De Vos M, Gyselbrecht L, et al. Gut inflammation in psoriatic arthritis: a prospective ileocolonoscopic study. J Rheumatol 1995;22(4):680–3.
[47] Mielants H, Veys EM, Cuvelier C, De Vos M, Goemaere S, De Clercq L, et al. The evolution of spondyloarthropathies in relation to gut histology. II. Histological aspects. J Rheumatol 1995;22(12):2273–8.
[48] Zheng J, Sun Q, Zhang M, Liu C, Su Q, Zhang L, et al. Noninvasive, microbiome-based diagnosis of inflammatory bowel disease. Nat Med 2024;30(12):3555–67.
[49] Palm NW, de Zoete MR, Cullen TW, Barry NA, Stefanowski J, Hao L, et al. Immunoglobulin A coating identifies colitogenic bacteria in inflammatory bowel disease. Cell 2014;158(5):1000–10.
[50] Elinav E, Strowig T, Kau AL, Henao-Mejia J, Thaiss CA, Booth CJ, et al. NLRP6 inflammasome regulates colonic microbial ecology and risk for colitis. Cell 2011;145(5):745–57.
[51] Sofia MA, Ciorba MA, Meckel K, Lim CK, Guillemin GJ, Weber CR, et al. Tryptophan metabolism through the kynurenine pathway is associated with endoscopic inflammation in ulcerative colitis. Inflamm Bowel Dis 2018;24(7):1471–80.
[52] Gupta NK, Thaker AI, Kanuri N, Riehl TE, Rowley CW, Stenson WF, et al. Serum analysis of tryptophan catabolism pathway: correlation with Crohn's disease activity. Inflamm Bowel Dis 2012;18(7):1214–20.
[53] Michaudel C, Danne C, Agus A, Magniez A, Aucouturier A, Spatz M, et al. Rewiring the altered tryptophan metabolism as a novel therapeutic strategy in inflammatory bowel diseases. Gut 2023;72(7):1296–307.
[54] Islam J, Sato S, Watanabe K, Watanabe T, Ardiansyah, Hirahara K, et al. Dietary tryptophan alleviates dextran sodium sulfate-induced colitis through aryl hydrocarbon receptor in mice. J Nutr Biochem 2017;42:43–50.
[55] Zelante T, Iannitti RG, Cunha C, De Luca A, Giovannini G, Pieraccini G, et al. Tryptophan catabolites from microbiota engage aryl hydrocarbon receptor and balance mucosal reactivity via interleukin-22. Immunity 2013;39(2):372–85.
[56] Morris MS, Sakakeeny L, Jacques PF, Picciano MF, Selhub J. Vitamin B-6 intake is inversely related to, and the requirement is affected by, inflammation status. J Nutr 2010;140(1):103–10.

[57] Sakakeeny L, Roubenoff R, Obin M, Fontes JD, Benjamin EJ, Bujanover Y, et al. Plasma pyridoxal-5-phosphate is inversely associated with systemic markers of inflammation in a population of U.S. adults. J Nutr 2012;142(7):1280–5.
[58] Roubenoff R, Roubenoff RA, Selhub J, Nadeau MR, Cannon JG, Freeman LM, et al. Abnormal vitamin B6 status in rheumatoid cachexia. Association with spontaneous tumor necrosis factor alpha production and markers of inflammation. Arthritis Rheum 1995;38(1):105–9.
[59] Saibeni S, Cattaneo M, Vecchi M, Zighetti ML, Lecchi A, Lombardi R, et al. Low vitamin B(6) plasma levels, a risk factor for thrombosis, in inflammatory bowel disease: role of inflammation and correlation with acute phase reactants. Am J Gastroenterol 2003;98(1):112–7.
[60] Farrag K, Woldeab J, Stein J, Aksan A. P642 crossroads of vitamin B6 deficiency and inflammation in inflammatory bowel disease: preliminary results of a cross-sectional study. J Crohns Colitis 2022;16(Suppl 1):i558–9.
[61] Selhub J, Byun A, Liu Z, Mason JB, Bronson RT, Crott JW. Dietary vitamin B6 intake modulates colonic inflammation in the IL10-/- model of inflammatory bowel disease. J Nutr Biochem 2013;24(12):2138–43.
[62] Zhou J, Zhu F, Sun L. Causal relationship between branched-chain amino acids and inflammatory bowel disease: a bidirectional and multivariable Mendelian randomization study. Br J Hosp Med (Lond) 2025;86(2):1–17.
[63] Verdugo-Meza A, Ye J, Dadlani H, Ghosh S, Gibson DL. Connecting the dots between inflammatory bowel disease and metabolic syndrome: a focus on gut-derived metabolites. Nutrients 2020;12(5):1434.
[64] Mendes-Frias A, Vieira MC, Araújo M, Duarte-Oliveira C, Feys S, Micheli C, et al. Branched-chain amino acids exacerbate colitis progression by lowering colonic fumarate levels. Inflamm Bowel Dis 2025;31(10):2840–52.
[65] Kan K, Rondeau LE, Muppidi P, da Luz BB, Dang R, Caminero A. A167 dietary branched-chain amino acids mediate the impact of high protein diet on colitis severity through Mtor activation. J Can Assoc Gastroenterol 2025;8(Suppl 1):i68.
[66] Sun S, Zhu X, Huang X, Murff HJ, Ness RM, Seidner DL, et al. On the robustness of inference of association with the gut microbiota in stool, rectal swab and mucosal tissue samples. Sci Rep 2021;11(1):14828.
[67] Gevers D, Kugathasan S, Denson LA, Vázquez-Baeza Y, Van Treuren W, Ren B, et al. The treatment-naive microbiome in new-onset Crohn's disease. Cell Host Microbe 2014;15(3):382–92.
[68] Shapiro JM, de Zoete MR, Palm NW, Laenen Y, Bright R, Mallette M, et al. Immunoglobulin A targets a unique subset of the microbiota in inflammatory bowel disease. Cell Host Microbe 2021;29(1):83–93.e3.

Ann Rheum Dis 85 (2026) 818–835

Contents lists available at ScienceDirect

Annals of the Rheumatic Diseases

journal homepage: https://www.sciencedirect.com/journal/annals-of-the-rheumatic-diseases

Psoriatic arthritis

Th9-arterial endothelial cell crosstalk promotes psoriatic atherosclerosis

Ishita Baral[1], Yvonne Baumer[2], Aarohan Mukerjhee Burma[3], McKella Sylvester[4], Kyle Jones[1], Moses Mwesigwa Kitakule[5], Amit Dey[6], Justin Rodante[7], Cristhian A. Gutierrez-Huerta[8], Bhavani Taramangalam[9], Julio Diaz Perez[10], Liang Guo[11], Alyssa Grogan[12], Tatsuya Shiraki[12], Aloke V. Finn[12,13], Aran Son[14], Kyoungin Cho[15], Jaspal S. Khillan[15], Marcus Y. Chen[16], Tiffany M. Powell-Wiley[2,17], Pamela A. Frischmeyer-Guerrerio[18], Joshua D. Milner[19], Nehal N. Mehta[20], Guido H. Falduto[1], Daniella M. Schwartz[1,*]

[1] *Departments of Medicine and Immunology, University of Pittsburgh, Pittsburgh, PA, USA*
[2] *Social Determinants of Obesity and Cardiovascular Risk Laboratory, National Heart, Lung, and Blood Institute, National Institutes of Health, Bethesda, MD, USA*
[3] *Graduate Division, Roswell Park Comprehensive Cancer Center, Buffalo, NY*
[4] *Department of Graduate Medical Education, Alabama College of Osteopathic Medicine, Dothan, AL, USA*
[5] *School of Medicine, Columbia University Irving Medical Center, New York, NY, USA*
[6] *Department of Internal Medicine, Icahn School of Medicine at Mount Sinai Hospital, New York, NY, USA*
[7] *Laboratory of Heart Disease Phenomics, National Heart, Lung, and Blood Institute, National Institutes of Health, Bethesda, MD, USA*
[8] *Cardiovascular Center, Medical College of Wisconsin, Milwaukee, WI, USA*
[9] *Department of Immunology, University of Pittsburgh, Pittsburgh, PA, USA*
[10] *Department of Pathology, Virginia Commonwealth University, Richmond, VA, USA*
[11] *Research and Early Development, Cardiovascular, Renal, and Metabolism, BioPharmaceuticals Research and Development, AstraZeneca, Gaithersburg, MD, USA*
[12] *CVPath Institute, Gaithersburg, MD, USA*
[13] *School of Medicine, University of Maryland, Baltimore, MD, USA*
[14] *Neuroscience Area, International School for Advanced Studies (SISSA), Trieste, Italy*
[15] *Mouse Genetics and Gene Modification Section, National Institutes of Allergy and Infectious Diseases, National Institutes of Health, Bethesda, MD, USA*
[16] *Cardiovascular Computed Tomography Program, National Heart, Lung, and Blood Institute, National Institutes of Health, Bethesda, MD, USA*
[17] *Intramural Research Program, National Institute on Minority Health and Health Disparities, NIH, Bethesda, MD, USA*
[18] *Laboratory of Allergic Diseases, National Institutes of Allergy and Infectious Diseases, National Institutes of Health, Bethesda, MD, USA.*
[19] *Department of Pediatrics, Columbia University Irving Medical Center, New York, NY, USA*
[20] *Departments of Medicine and Dermatology, The George Washington University School of Medicine and Health Sciences, Washington, DC, USA*

*Correspondence to Dr Daniella M. Schwartz, Division of Rheumatology and Clinical Immunology, Departments of Medicine and Immunology, Pittsburgh, PA, USA.
E-mail address: Daniella.Schwartz@pitt.edu (D.M. Schwartz).

Handling editor Josef S. Smolen.

Ishita Baral and Yvonne Baumer contributed equally.

https://doi.org/10.1016/j.ard.2025.11.008

ARTICLE INFO

Article history:
Received 24 September 2025
Received in revised form 6 November 2025
Accepted 8 November 2025

ABSTRACT

Objectives: Atherosclerotic cardiovascular disease (ASCVD) is a leading cause of death. Systemic autoimmune and inflammatory diseases are associated with increased ASCVD risk, severity, and mortality. The inflammatory cytokine interleukin 9 (IL-9) has been linked to murine atherogenesis, raising fundamental questions about the populations in which and the mechanisms by which IL-9 drives ASCVD.

Methods: Circulating T helper subsets and coronary computed tomography angiography data were analysed in patients with psoriasis. Murine models of psoriatic atherogenesis (imiquimod-ApoE$^{-/-}$, IL-23-ApoE$^{-/-}$, and Card14$^{\Delta E138}$-ApoE$^{-/-}$) were investigated using IL-9 blockade or global and endothelial-specific Il9r deletion. Primary human aortic endothelial cells were used to assess IL-9/STAT3-dependent endothelial responses.

Results: Here, we found that expansion of IL-9-producing T helper cells (Th9) was significantly associated with high-risk radiographic ASCVD in patients with the autoimmune disease psoriasis. Th9 cells were poised to migrate to coronary vessels and were identified in human atherosclerotic plaque from individuals with psoriasis. *In vivo*, murine inflammatory atherogenesis was prevented by IL-9 blockade and by IL-9 receptor (IL-9R) deletion in endothelial cells. In human arterial endothelial cells, IL-9R/STAT3 signalling promoted endothelial dysfunction via diverse mechanisms including adhesion, activation, angiogenesis, and release of leukocyte chemoattractants.

Conclusions: These findings suggest the Th9^{high} state may represent a novel psoriatic ASCVD endotype that could be targeted using precision approaches to prevent ASCVD in at-risk individuals.

WHAT IS ALREADY KNOWN ON THIS TOPIC

- Atherosclerotic cardiovascular disease (ASCVD) is more prevalent and severe in patients with systemic inflammatory diseases. Multiple inflammatory cells and cytokines are implicated in ASCVD, including preliminary associations with IL-9 and T helper 9 (Th9) cells. Psoriasis is associated with both Th9 expansion and increased ASCVD risk.

WHAT THIS STUDY ADDS

- In patients with psoriasis, a Th9^{high} state is linked to early, high-risk radiographic ASCVD. Th9 cells are poised to migrate to coronary vessels, infiltrate atherosclerotic plaque, and drive atherogenesis through IL-9 receptor (IL-9R) signalling in arterial endothelial cells. In murine models, psoriatic atherogenesis is prevented by IL-9 blockade or by germline or endothelial-specific *Il9r* deletion.

HOW THIS STUDY MIGHT AFFECT RESEARCH, PRACTICE OR POLICY

- These findings identify the Th9/IL-9 axis as a potential psoriatic disease endotype that stratifies patients at the highest ASCVD risk. Targeting IL-9 may offer a precision therapeutic strategy to prevent or treat ASCVD in psoriasis or other Th9-associated inflammatory diseases.

INTRODUCTION

Atherosclerotic cardiovascular disease (ASCVD) is a leading cause of death worldwide, accounting for more than 10 million deaths per year [1]. The contribution of inflammation to ASCVD has been recognised for decades [2] and is most evident in patients with inflammatory and autoimmune diseases, who face increased risk, earlier onset, a stronger inflammatory phenotype, and higher mortality [3,4]. Psoriasis stands out as a particularly useful "human model" of autoimmunity-related ASCVD [5]. In addition to causing skin and joint disease, psoriasis is also linked to ocular, gastrointestinal, and osseous inflammation [6]. Psoriasis is strongly associated with ASCVD in a dose-dependent manner, via proatherogenic pathways like immune activation, metabolic dysregulation, and endothelial dysfunction [5–9]. However, the key pathogenic drivers of psoriatic ASCVD remain unclear. While immunomodulatory treatments reduce psoriatic ASCVD risk in some patients, and ASCVD is more severe in patients with psoriasis who develop psoriatic arthritis (PsA), real-world data and clinical trial results have been inconsistent [10–12]. This could be related to patient heterogeneity or to protective roles for some cytokines [10,12]. One promising approach to address this problem is to define inflammatory endotypes, or subtypes driven by distinct mechanisms, for patient stratification and therapeutic target discovery [2,13].

ASCVD immunopathogenesis begins with endothelial cell dysfunction, leading to the recruitment of immune cells such as monocytes and T cells. These infiltrate lipid-rich plaque and react to local mediators by releasing proinflammatory cytokines that promote plaque core necrosis, recruit additional immune cells, and worsen endothelial dysfunction [2,13]. An emerging body of literature implicates interleukin 9 (IL-9) and T helper 9 (Th9) cells as potential drivers of ASCVD based on murine models [14,15]. However, the relevance of IL-9/Th9 to ASCVD remains unclear—especially in the context of immune diseases. Critically, no studies have identified specific patient populations in whom early high-risk plaque correlates with Th9/IL-9—and who could potentially benefit from IL-9/Th9-targeting therapies. Notably, many immune diseases, including psoriasis, are characterised by a Th9^{high} endotype, or peripheral Th9 expansion [16–20]. In patients with psoriasis, IL-9/Th9 have been linked to PsA, which is associated with worse ASCVD severity [11,21]. However, the connection between this Th9^{high} endotype and ASCVD has not been explored.

Herein, we found that, in a cohort of individuals with psoriasis, a Th9^{high} state was significantly associated with early, high-risk ASCVD. In murine models, *in vivo* generated Th9 cells were poised to migrate to the arterial plaque. Th9 cell differentiation was modulated by proatherogenic factors, and Th9 cells were

identified within atherosclerotic plaques from individuals with psoriasis. *In vivo*, murine psoriasis worsened atherogenesis. Germline and endothelial IL-9R deletion ameliorated translational models of psoriatic atherogenesis, as did IL-9 blockade. *In vitro*, IL-9 directly targeted arterial endothelial cells to induce dysfunction by inducing genes important for adhesion, angiogenesis, and chemotaxis. Our findings implicate the Th9^{high} endotype as an attractive target for psoriatic ASCVD prevention and treatment.

METHODS

Patient involvement, human samples, and data

Patients contributed samples via informed consent but were not involved in study design. Deidentified blood, coronary computed tomography scores, and demographics were collected from patients (untreated and on immunomodulatory therapy) at the NIH Clinical Center. Additional controls were obtained from healthy volunteers or the NIH Blood Bank. Atherosclerotic coronary arteries were obtained via the CVPath autopsy registry. All human studies were IRB-approved (NIH: 13H-0065, 10-H-0126; CVPath IRB), with informed consent obtained.

Mouse experiments

Age- and sex-matched 8- to 12-week-old C57BL/6 mice, including Apolipoprotein E *ApoE*$^{-/-}$,Caspase Recruitment Domain Containing Protein 14 *(Card14)*$^{\Delta E138}$, *Il9r*$^{-/-}$, and Interleukin Nine Fluorescent Reporter (INFER) mice, were housed in pathogen-free facilities. *Il9r*$^{f/f}$ mice were generated by CRISPR/Cas9 deletion of exons 2-5 and validated by PCR. Endothelial-specific *Il9r* deletion was achieved by crossing with *Cdh5*^{MliaCre}. All procedures were Institutional Animal Care and Use Committee (IACUC)-approved.

Psoriasis and atherosclerosis models

Three murine models (imiquimod [IMQ]-ApoE, IL-23-ApoE, Card14-ApoE) were exposed to a high-fat diet (HFD) to induce atherogenesis. Mice received anti-IL-9 or isotype antibodies twice weekly. Skin and aortas were digested for flow cytometry; aortic plaque was quantified by en face Oil-Red-O staining. Plasma low-density lipoprotein (LDL) was measured after fasting.

Th9 differentiation, restimulation, and analysis

Naïve human and murine CD4+ T cells were cultured under Th9-polarising conditions and treated with vehicle, Vascular endothelial growth factor A (VEGF-A), or oxidised LDL. Cells were restimulated with phorbol 12-myristate13-acetate (PMA), ionomycin, and cytokines for flow cytometry. Tissue-infiltrating cells and INFER-derived Th9 cells were also analysed.

Endothelial studies

Primary human aortic endothelial cells (HAoEC) were assayed for barrier function, angiogenesis, and leukocyte chemotaxis using immunofluorescence, Electric cell substrate impedance sensing (ECIS), and Fluorescein Isothiocyanate (FITC)-dextran flux.

Molecular analyses

RNA was extracted for RT-qPCR and mRNA-sequencing. Differential expression, gene set enrichment analysis (GSEA), and single-cell RNA-seq analyses were performed using standard pipelines.

Statistics

Data were analysed using parametric or nonparametric tests with Analysis of Variance (ANOVA) and multiple testing correction as appropriate.

Full experimental details are available in the Extended Methods.

RESULTS

Psoriasis is associated with expansion of circulating Th9 cells

Based on prior reports that psoriasis is an IL-9/Th9^{high} state [16,22,23], we phenotyped circulating T helper subsets from psoriatic (n = 36) and nonpsoriatic subjects (n = 47). As a positive comparator, we measured the percentage of memory (CD4$^+$CD45RO$^+$) Th cells that expressed IL-17A (Fig 1A,B). As expected, IL-17A$^+$ memory T cells were significantly expanded in subjects with psoriasis (Fig 1B). Most had mild-to-moderate disease; accordingly, the percentage of circulating Th17 cells was only modestly elevated. We did not find expansion of Th1 cells (IFN-γ^+), Th2 cells (IL-4$^+$, IL-13$^+$, or IL-5$^+$), or of memory CD4$^+$ T cells expressing IL-2, IL-10, IL-21, or TNF-α (Supplementary Fig S1a-h). Circulating IL-9$^+$ memory CD4+ T cells were also significantly expanded in psoriatic subjects (Fig 1C, D), indicating that psoriasis is a Th9^{high} state.

In allergic disease, Th9 cells have been described as an inflammatory Th2-related subset [23,24]. In most subjects with psoriasis, Th9 cells did not coexpress Th2 cytokines (IL-4, IL-13, IL-5) or IL-17A but were instead single-positive cells (Supplementary Fig S1i). To comprehensively investigate Th9 identity in the context of psoriatic disease, we exposed IL-9 reporter (INFER) mice [25] to repeated topical applications of the toll-like receptor (TLR)-7/9 agonist IMQ to induce chronic psoriasiform inflammation (Supplementary Fig S1j) [26]. IMQ induced circulating T cells that expressed GFP/IL-9, confirming this model could be used to study Th9 identity in the context of psoriasiform skin disease (Fig 1E,F). Transcriptomic analysis of circulating IL-9$^+$CD4$^+$ T cells revealed significant (adj $P < .05$, DESeq2) differential upregulation of *Il9* and of the Th9 lineage-defining transcription factor (TF) *Spi1* (Fig 1G). We had previously identified a cassette of Th9 lineage-defining genes [17], which was also significantly enriched (false discovery rate [FDR] < 0.05, GSEA) in circulating IL-9$^+$CD4$^+$ T cells from IMQ-treated mice (Fig 1H). Th9 cells from IMQ-treated mice did not differentially express other T helper lineage-defining cytokines but did have increased expression of the Th2 master TF *Gata3* and the regulatory T cell (Treg) TF *Foxp3* (Fig 1G). Analysis of lineage-specific cassettes for other T helper subsets [27] revealed weak enrichment for Treg-specific genes and no enrichment for other T helper subsets (Fig 1I). Together, these results confirmed that murine psoriasis models recapitulated the systemic Th9^{high} state seen in human psoriatic disease, and that psoriasis-associated Th9 cells express a Th9-definiing transcriptional program conserved with allergic Th9 cells.

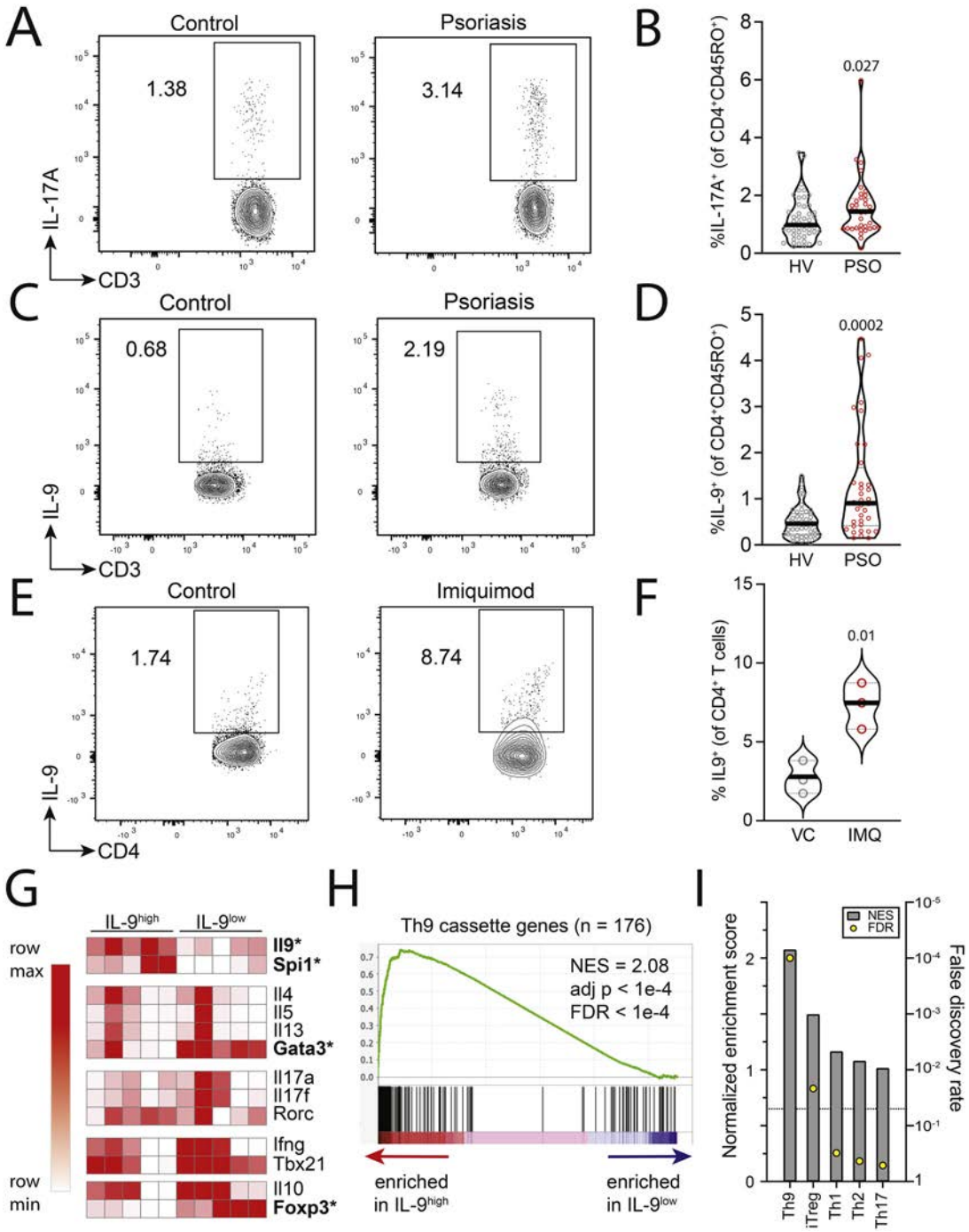

Figure 1. (A) Flow and (B) violin plot show circulating memory Th17 ($CD45^+/CD3^+/CD4^+/CD45RO^+/IL17A^+$) cells in nonpsoriatic healthy volunteers (HV, n = 47, grey) and patients with psoriasis (PSO, n = 36, red). (C) Flow and (D) violin plot show circulating memory Th9 (CD45 + /CD3 + /CD4 + /CD45RO + /IL9 +) cells in nonpsoriatic volunteers (HV, n = 47, grey) and patients with psoriasis (PSO, n = 36, red). *P* values, Mann-Whitney. (E) Flow and (F) violin plot show splenic Th9 (CD45 + /TCR-β + / CD4 + /IL9 +) cells in mice treated with 3 rounds of imiquimod (IMQ) or vehicle (Supplementary Fig S1j) *P* values, unpaired t-test, n = 3. For all violin plots, bars represent mean values for the group. (G) Heatmap shows expression (normalised across each row) of lineage-defining transcription factors and effector cytokines for Th9, Th2, Th17, Th1, and Treg (regulatory T cell). *Adjusted $P < .05$, DESeq2. (H) GSEA plot shows enrichment of "allergic Th9 cassette" in splenic green fluorescent protein GFP + (Th9) vs GFP− (non-Th9) cells from INFER mice treated with IMQ. (I) Bar graphs show normalised GSEA enrichment scores and false discovery rate for enrichment of lineage-defining cassettes for the Th9, Treg, Th1, Th2, and Th17 in splenic GFP + (Th9) and GFP− (non-Th9) cells from INFER mice treated with IMQ. INFER, Interleukin Nine Fluorescent Reporter; GFP, green fluorescent protein; HV, healthy volunteers; FDR, false discovery rate; GSEA, gene set enrichment analysis; IL, interleukin; Th9, T helper 9 cells; Th17, Th9, T helper 17 cells; VC, vanishing cream.

$Th9^{high}$ state is associated with coronary artery disease in psoriatic subjects

Th9/IL-9 have previously been linked to psoriatic skin inflammation [22]. We therefore hypothesised that $Th9^{high}$ state might correlate with psoriatic skin disease severity. Psoriasis Area Severity Scores had been calculated for a subset of patients (n = 20) but did not correlate with peripheral Th9 expansion (Supplementary Table S1), leading us to question whether Th9 cells might promote disease at other sites. Psoriasis is associated with arthritis, inflammatory bowel disease, and ASCVD, all of which have been associated with Th9 cells in other contexts [14,18,20,21,28]. A group of 19 patients with psoriasis had undergone cardiovascular disease screening with coronary artery computed tomography

Table 1
IL-9+ CD45RO+ CD4+ T cells and noncalcified burden adjusted regression analysis

Model	Standardised beta	*P* value[a]
Unadjusted	0.28	.039
Adjusted for BMI, FRS, and statin use	0.23	.002

BMI, body mass index; FRS, Framingham Risk Score; IL-9, interleukin 9.
[a] Multivariable regression analysis between noncalcified burden and %IL-9+ CD45RO+ CD4+ T cells unadjusted or adjusted for BMI, FRS, and statin use.

angiography (CCTA) (Supplementary Fig S1k). We analysed CCTA to calculate noncalcified coronary plaque burden, a high-risk type of plaque associated with increased mortality and myocardial infarction risk [29]. Th9^{high} state was significantly associated with total and noncalcified burden; this remained significant after adjusting for traditional ASCVD factors like BMI, Framingham risk score, and statin use (Table 1). Similar associations were not seen for other T helper subsets (Supplementary Table S2). There was no difference in BMI between Th9^{high} and Th9^{low} individuals; LDL cholesterol and total cholesterol were higher in Th9^{low} than in Th9^{high} patients (Supplementary Table S1). These data suggest that a Th9^{high} state is associated with the development of ASCVD in psoriasis, independent of traditional ASCVD risk factors.

Circulating Th9 cells express a proatherogenic program in psoriatic subjects

The strong association of Th9 expansion with noncalcified coronary burden led us to hypothesise that Th9 cells might be poised to infiltrate the vessel wall. Analysis of circulating Th9 cells from IMQ-treated mice revealed 1819 Th9-associated genes (FC > 2, Padj < .05, DESeq2, IL-9^{high} vs IL-9^{low}, Supplementary Fig S1l), 1330 of which were highly Th9-associated (FC > 4, Padj < .05, DESeq2, IL-9^{high} vs IL-9^{low}). Highly Th9-associated genes were enriched for multiple pathways associated with inflammatory atherogenesis including vascular adhesion, angiogenesis, and lipid metabolism (Fig 2A-C). Th9-associated genes associated with lymphocyte homing to the heart (Fig 2D) included *Met, Itgam, Itgb2,* and *Cxcr2* [30–32]. These findings suggested that circulating Th9 cells in psoriatic subjects are poised to traffic to the heart and undergo recruitment to coronary arteries.

Within coronary plaque, CD4$^+$ T cells are exposed to proatherogenic factors that modulate T helper subset expansion and cytokine production [33]. Among the pathways differentially upregulated in psoriatic Th9 cells, we identified VEGF-VEGFR signalling and lipid metabolism as potential proatherogenic factors that might affect plaque-resident Th9 differentiation and function (Fig 2A-C). Accordingly, the genes encoding VEGFR-1, VEGFR-2, and LDL receptor were significantly upregulated in Th9 cells (Fig 2D). We therefore differentiated naïve CD4$^+$ T cells under Th9-promoting conditions in the presence of VEGF-A and oxidised LDL. Oxidised LDL repressed Th9 differentiation, whereas VEGF-A enhanced Th9 differentiation, implicating VEGF-A as a proatherogenic factor that could enhance Th9 differentiation within arterial plaque (Fig 2E,F, Supplementary Fig S1m).

Th9 cells infiltrate the atherosclerotic plaque of psoriatic subjects

We next hypothesised that atherosclerotic plaques from psoriatic subjects would be characterised by Th9 infiltration. Because T-cell-driven atherogenesis is also a central driver of ASCVD in the general population [33], we first investigated Th9 infiltration in atherosclerotic plaque from nonpsoriatic subjects. Using CITE-seq data from the peripheral blood and carotid plaques of patients with ASCVD, we identified a population of CD4$^+$ T cells expressing the Th9 lineage-defining TF *SPI1* (Supplementary Fig S2a) [20,34]. Th9 lineage-defining genes [17] were significantly enriched (FDR < 0.05, GSEA) in plaque-infiltrating *SPI1*$^+$CD4$^+$ T cells, but not in circulating *SPI1*$^+$CD4$^+$ T cells (Fig 2G, H). Analysis of the 347 genes most closely correlated with *SPI1* expression (Pearson) revealed enrichment for canonical Th9-associated pathways like IL-2 induction, response to IL-4, and response to TGF-β (Supplementary Fig S2b). *SPI1*-associated genes were also enriched for PPAR signalling, which is important for Th9 differentiation, CD4$^+$ T cell activation, lipid metabolism, and cardiovascular function [23]. Other enriched pathways included cellular adhesion and responses to proatherogenic pathways downstream of hydrogen peroxide [35], NOD2 [36], oxidised phospholipids [37], and TLR2 [38]. Together, these data suggest that Th9 cells infiltrate atherosclerotic plaque and respond to plaque-resident inflammatory mediators. To specifically investigate Th9 infiltration in psoriatic coronary plaque, we obtained postmortem samples from subjects with psoriasis and coronary artery disease. Sampling 6 arteries from 3 deceased subjects with a history of psoriasis revealed multiple PU.1$^+$/CD3$^+$ and PU.1$^+$/CD4$^+$ cells within necrotic lipid-rich coronary artery plaque (Fig 2I,J).

To dissect the mechanisms by which Th9-derived IL-9 might promote inflammatory ASCVD, we next sought to develop a murine model in which inflammation was associated with accelerated atherogenesis. We exposed atherosclerosis-prone *ApoE*$^{-/-}$ mice to topical IMQ while giving them HFD to induce atherogenesis (IMQ-HFD, Fig 3A). Because the risk of psoriatic CVD is highest in young patients with severe skin disease [39], we used an early time point (6 weeks) and induced 3 cycles of inflammation over 7% to 10% body surface area to model moderate-severe psoriasis. IMQ significantly increased lipid-rich plaque in the aortic arch (Fig 3B,C), nonsignificantly induced CD4$^+$ T cell infiltration into skin, and significantly induced skin infiltration with IFN-γ^+, IL-13$^+$, IL-17A$^+$, and IL-9$^+$ CD4$^+$ T cells (Fig 3D, E, Supplementary Fig S2c). Counts of skin-resident IL-9$^+$ CD4$^+$ T cells correlated to aortic plaque area (Supplementary Fig S2d). IMQ also significantly induced IL-9$^+$ CD4$^+$ T cell infiltration into murine aortas but did not induce other T helper subsets or LDL; aortic Th9 percentages did not correlate to plaque area (Fig 3F,G, Supplementary Fig S2e-f).

IL-9 promotes atherogenesis in systemic inflammatory disease

To determine whether IL-9 directly promoted inflammatory atherogenesis, we next exposed *Il9r*$^{-/-}$*ApoE*$^{-/-}$ and *ApoE*$^{-/-}$ mice to IMQ-HFD for 6 weeks (Supplementary Fig S3a). Deletion of IL-9 receptor (IL-9R) reduced lipid-rich aortic plaque formation (Fig 4A,B) and aortic infiltration of neutrophils and inflammatory macrophages (Fig 4C,D). IL-9R deletion also reduced skin infiltration of neutrophils and inflammatory macrophages but had no significant effect on skin or aortic infiltration of other immune cell subsets or on LDL (S3b-d). Like IL-9R -deficient mice, *ApoE*$^{-/-}$ mice treated with IL-9-neutralising antibodies while exposed to IMQ-HFD (Supplementary Fig S3e) were protected from lipid-rich aortic plaque formation (Fig 4E,F). However, IL-9 blockade did not significantly reduce aorta-infiltrating immune cells (Fig 4G,H, Supplementary Fig S3f), skin-infiltrating immune cells (Supplementary Fig S3g), or LDL (Supplementary Fig S3h).

Because IMQ can induce severe systemic inflammation that may not fully recapitulate psoriatic disease [26], we tested our

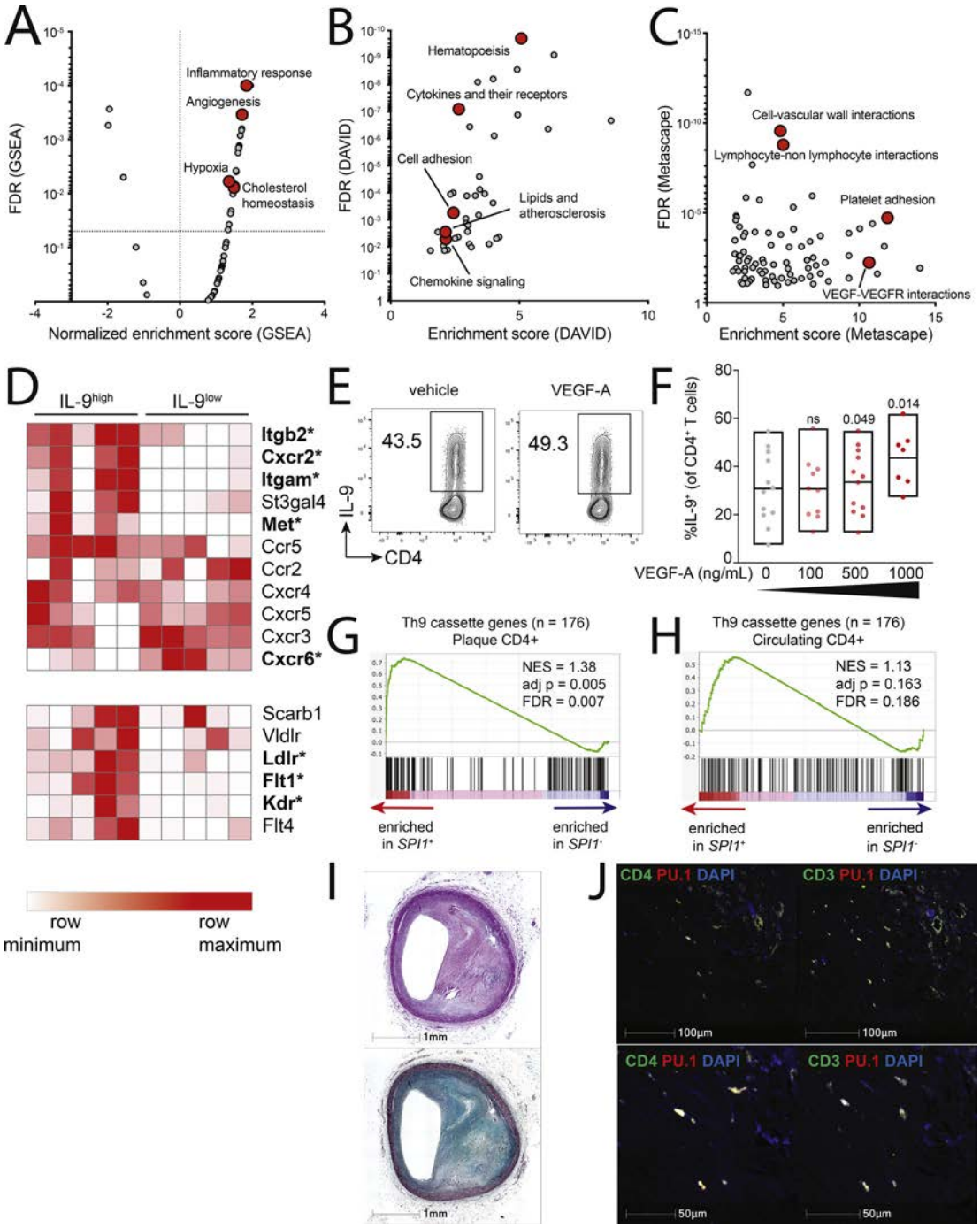

Figure 2. Scatter plots show enrichment scores vs false discovery rates (FDRs) from (A) GSEA, (B) DAVID, or (C) Metascape. All enrichments for splenic GFP+ (Th9) cells compared to GFP− (non-Th9) cells from IL-9 reporter (INFER) mice treated with imiquimod (IMQ) as in Supplementary Fig S1J. (D) Heatmap shows expression (normalised across each row) of genes important for trafficking to the blood vessel and/or heart (top) or encoding receptors of proangiogenic factors (bottom). *Adjusted $P < .05$, DESeq2. (E) Flow plot and (F) bar graph show percent murine Th9 cells (of CD4+ cells) differentiated in the presence of vehicle (grey) or escalating concentrations of VEGF-A (red). *P* values, ANOVA with multiple comparison adjustment. GSEA plots show enrichment of "allergic Th9 cassette" in carotid plaque-resident (G) and circulating (H) *SPI1*+ (Th9) vs *SPI1*- (non-Th9) cells from human carotid plaque-resident CD4+ T cells. Images of coronary artery plaque from subject with psoriasis show H&E and Movat staining (I), immunofluorescence staining (J) for the Th9 lineage-defining transcription factor PU.1 (red, encoded by *SPI1*) and CD4 (green, left panels), and immunofluorescence staining for PU.1 (red) and CD3 (green, right panels). Representative of 6 vessels. GSEA, gene set enrichment analysis; DAVID, Database for Annotation, Visualization, and Integrated Discovery; VEGF-A, vascular endothelial growth factor A; ANOVA, analysis of variance; DAPI, 4',6-diamidino-2-phenylindole; INFER, Interleukin Nine Fluorescent Reporter; GFP, green fluorescent protein, H&E, hematoxylin and eosin; NES, normalized enrichment score; Movat, Movat's pentachrome stain; IL, interleukin; Th9, T helper 9 cells.

findings in 2 other psoriasis models: *Card14*$^{\Delta E138}$ (Supplementary Fig S4a,d) and intradermal IL-23 (Supplementary Fig S4e). The gain-of-function (GOF) *Card14*$^{\Delta E138}$ mutation is orthologous to and phenocopies *CARD14*-GOF psoriasis, a monogenic form of psoriasis caused by germline mutations in human *CARD14* [26]. *Card14*$^{\Delta E138}$ worsened HFD-induced aortic plaque formation in *ApoE*$^{-/-}$ mice, confirming our findings in a more chronic and translational model of psoriatic atherogenesis (Supplementary Fig S4a-c). In both models, IL-9-neutralising antibodies reduced lipid-rich aortic plaque formation but not plaque-infiltrating or skin-infiltrating immune cell populations or LDL, recapitulating the phenotype of IMQ-*ApoE* mice (Fig 4I-

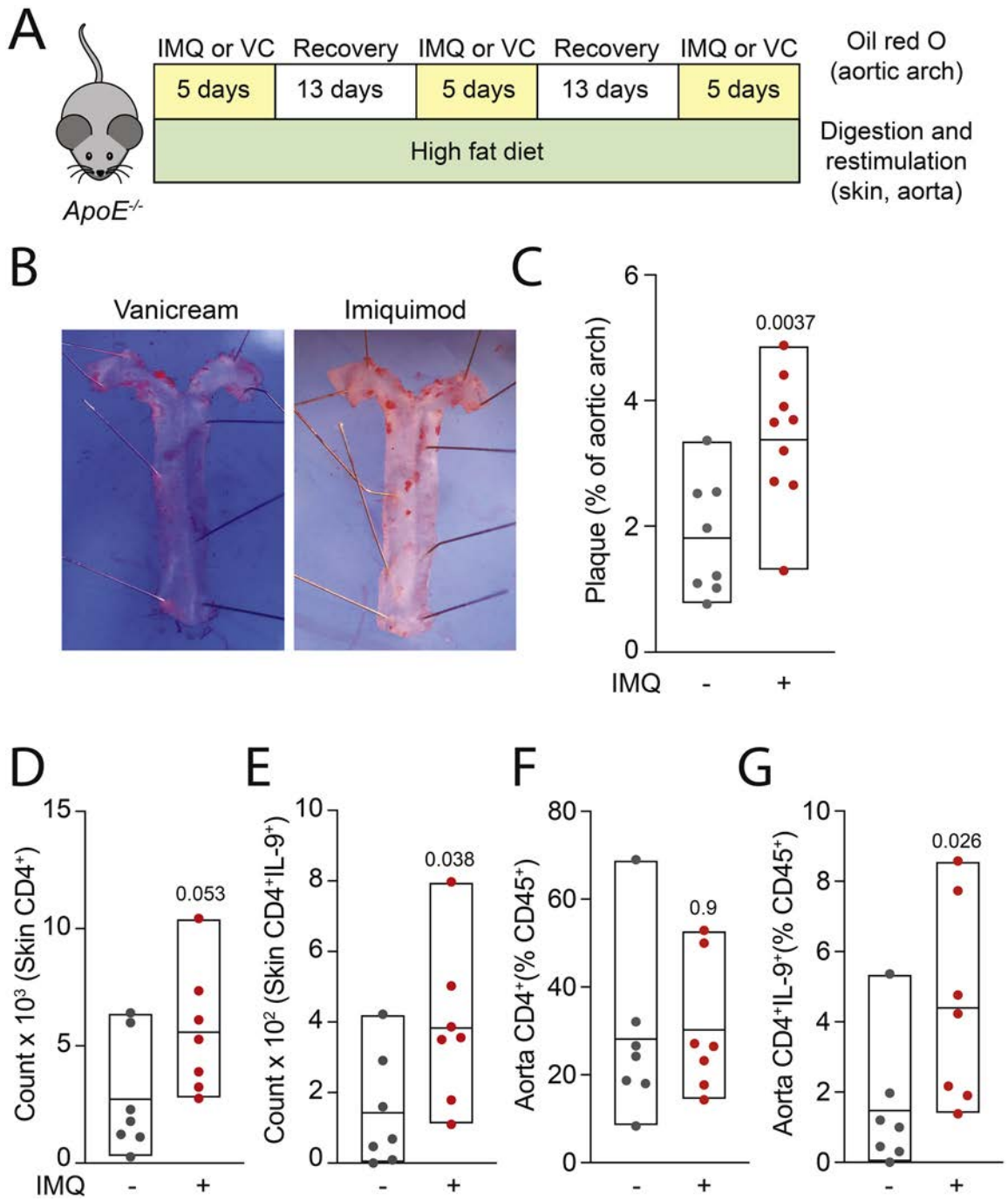

Figure 3. (A) Schematic of imiquimod (IMQ)-high-fat diet (HFD) model of psoriatic atherogenesis. *ApoE*$^{-/-}$ mice were exposed to 3 5-day rounds of IMQ or vanishing cream (VC) with 2 13-day recovery periods, while being fed HFD. After 6 weeks, mice were euthanised, thoracic aorta was stained for lipid-rich plaque (Oil-Red-O), and skin and abdominal aorta were digested for immune cell analysis (flow cytometry). (B) Representative images and (C) bar graph show pooled Oil-Red-O (+) lipid-rich plaque as percentage of aortic arch in *ApoE*$^{-/-}$ mice treated with HFD while being exposed to VC (grey) or IMQ (red). (D) Bar graphs show counts of total and (E) IL-9+ skin-infiltrating CD4+ T cells in mice treated with VC (grey) or IMQ (red). (F) Counts of total and (G) IL-9+ aorta-infiltrating CD4+ T cells in mice treated with VC (grey) or IMQ (red). For all experiments: *P* values, Mann-Whitney. ApoE, Apolipoprotein E.

P, Supplementary Fig S4e-g,i-k). These findings indicated that IL-9 promotes early inflammatory atherogenesis and aortic plaque formation, and that these effects might be independent of immune cell recruitment to atherosclerotic plaque.

IL9R signalling in endothelial cells promotes inflammatory atherogenesis

We next hypothesised that IL-9 might promote psoriatic atherogenesis through direct effects on endothelial cells. To test this, we generated mice with LoxP sites flanking exons 2-5 of *Il9r*, allowing conditional IL-9R deletion (Supplementary Fig S5a). To confirm that LoxP insertion did not disrupt endogenous IL-9R signalling, we differentiated memory B cells, which phosphorylate STAT3 and STAT5 in response to IL-9 [40], from *Il9r*$^{f/f}$ and WT mice (Supplementary Fig S5b). WT and *Il9*$^{f/f}$ derived B cells both responded to IL-9, confirming intact endogenous IL9R signalling (Supplementary Fig S5c). Treating B cells with Tat-Cre *in vitro* significantly reduced IL9R expression (Supplementary Fig S5d), confirming gene inactivation.

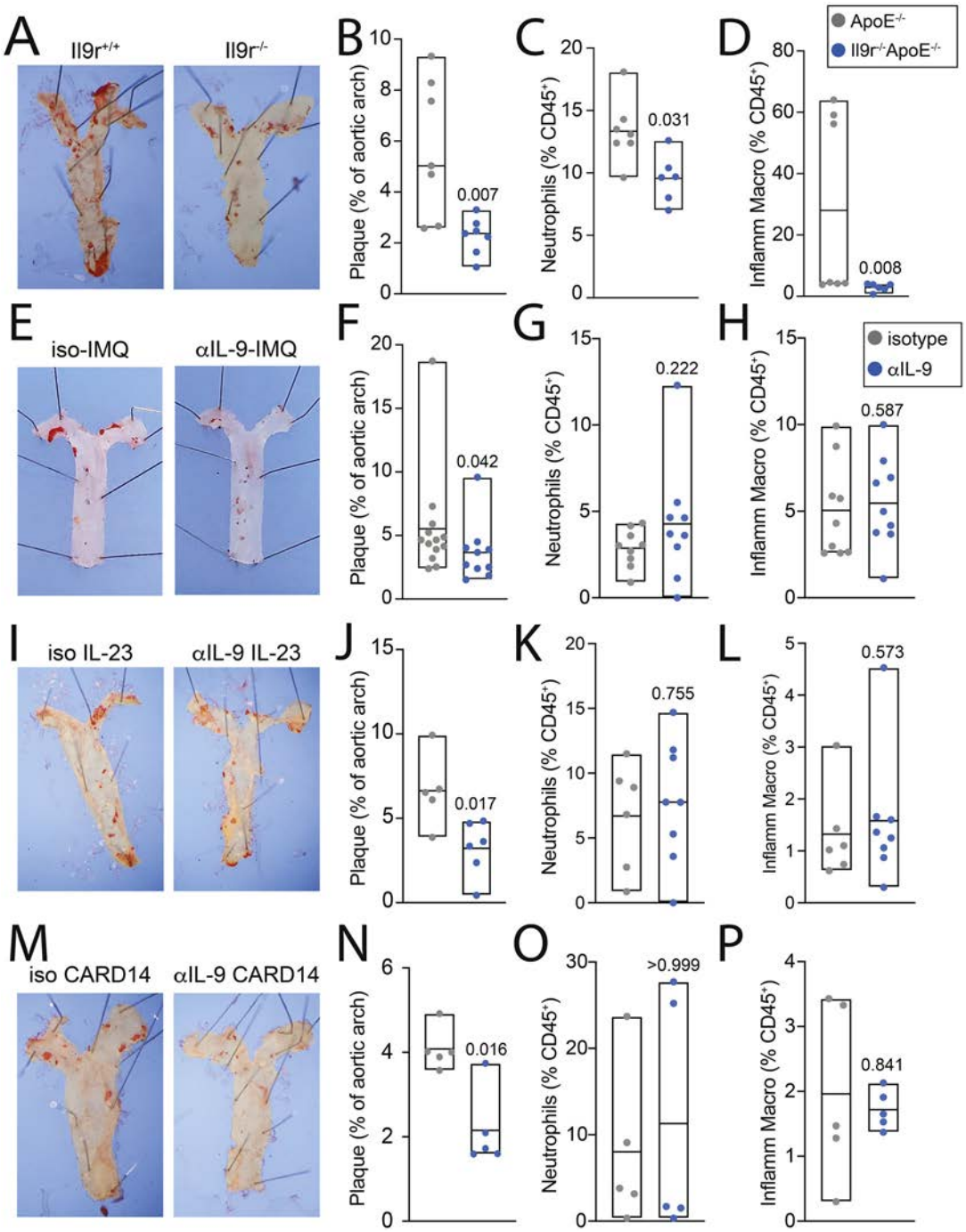

Figure 4. (A) Representative images and (B) bar graph show pooled Oil-Red-O (+) lipid-rich plaque as a percentage of aortic arch in *ApoE*$^{-/-}$ (grey) and *Il9r*$^{-/-}$*ApoE*$^{-/-}$ mice (blue) exposed to 3 rounds of imiquimod (IMQ, Fig 4A, Supplementary Fig S2j) while exposed to high-fat diet (HFD). Bar graphs show percent neutrophils (C) and Ly6C+ inflammatory macrophages (D) of aorta-infiltrating CD45^{+} cells in *ApoE*$^{-/-}$ (grey) and *Il9r*$^{-/-}$*ApoE*$^{-/-}$ mice (blue). (E) Representative images and (F) bar graph show lipid-rich plaque as a percentage of aortic arch in *ApoE*$^{-/-}$ mice exposed to IMQ-HFD while given isotype (grey) or αIL-9 (blue). Bar graphs show percent neutrophils (G) and Ly6C+ inflammatory macrophages (H) of aorta-infiltrating CD45^{+} cells. (E) Representative images and (F) bar graph show lipid-rich plaque as a percentage of aortic arch in *ApoE*$^{-/-}$ mice exposed to 3 rounds of intradermal IL-23 (Supplementary Fig S3a) while exposed to HFD and given isotype (grey) or αIL-9 (blue). Bar graphs show percent neutrophils (K) and Ly6C + inflammatory macrophages (L) of aorta-infiltrating CD45^{+} cells. (M) Representative images and (N) bar graph show lipid-rich plaque as a percentage of aortic arch in *Card14*$^{\Delta E138}$*ApoE*$^{-/-}$ mice (Supplementary Fig S3k) exposed to HFD and given isotype (grey) or αIL-9 (blue). Bar graphs show percent neutrophils (O) and Ly6C+ inflammatory macrophages (P) of aorta-infiltrating CD45^{+} cells. For all experiments: *P* values, Mann-Whitney. IL, interleukin. ApoE, Apolipoprotein E.

To delete IL-9R in endothelial cells, we crossed *Il9r*$^{f/f}$ mice to VE-Cre (*Cdh5*^{Mlia}-Cre) mice (Supplementary Fig S5a), which express Cre-recombinase in VE-Cadherin^{+} endothelial progenitor cells and show >95% efficiency in mature endothelial cells [41]. We confirmed specific deletion of *Il9r* in endothelial cells (Supplementary Fig S5e), then crossed *Il9r*$^{f/f}$ x VE-Cre (*Il9r*$^{\Delta VE}$) mice to *ApoE*$^{-/-}$ mice (*ApoE-Il9r*$^{\Delta VE}$). We exposed *ApoE-Il9r*^{DVE} mice and *ApoE-Il9r*$^{f/f}$ littermates to IMQ-HFD for 6 weeks. Compared with *ApoE-Il9r*$^{f/f}$ mice, *ApoE-Il9r*$^{\Delta VE}$ mice had significantly less lipid-rich aortic plaque (Fig 5A,B) but no significant difference in aorta-infiltrating leukocytes (Fig 5C,D, Supplementary Fig S5f), skin-infiltrating leukocytes (Supplementary Fig S5g), or LDL (Supplementary Fig S5h).

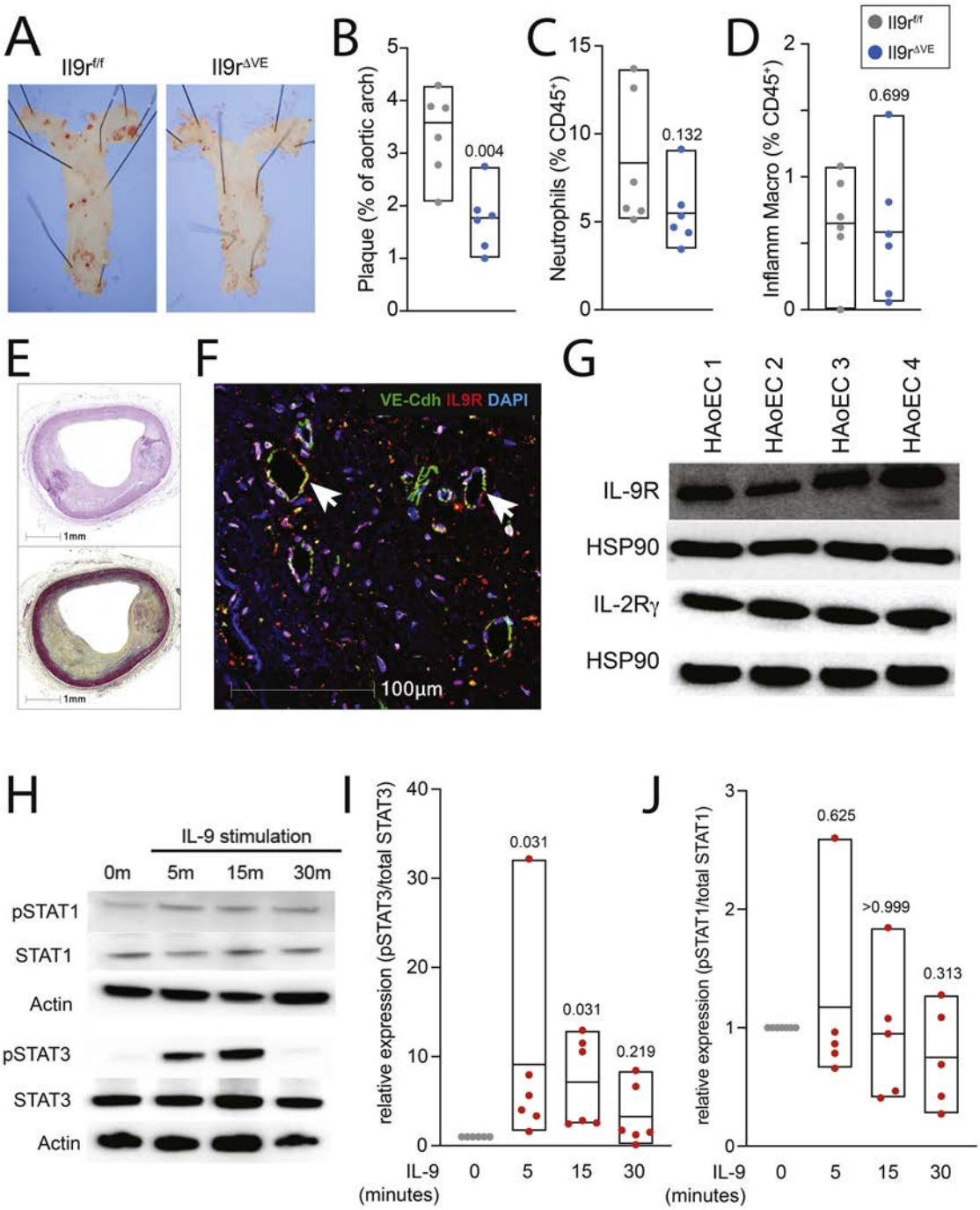

Figure 5. (A) Representative images and (B) bar graph show Oil-Red-O (+) lipid-rich plaque as percentage of aortic arch in *ApoE-Il9*$^{f/f}$ (grey) and *ApoE-Il9*^{DVE} mice (blue) exposed to 3 rounds of imiquimod (Fig 4A, Supplementary Fig S2j) and high-fat diet (IMQ-HFD). Bar graphs show (C) percent neutrophils and (D) Ly6C+ inflammatory macrophages. For all mouse experiments: *P* values, Mann-Whitney. Representative images of coronary artery plaque from subject with psoriasis show H&E and Movat staining (E) and immunofluorescence staining (F) for IL-9 receptor (red) and the endothelial marker VE-cadherin (green). Representative of 6 arteries. (G) Western blot shows expression of the IL-9 receptor subunits IL-9R and IL-2Rγ in primary human aortic endothelial cells (HAoEC) from 4 cadaveric donors. Representative Western blot (H) shows total and phosphorylated STAT1 and STAT3 expression at various time points in HAoEC treated with IL-9. Bar graphs show quantification of phosphorylated/total STAT3 (I) and STAT1 (J) from HAoEC (n = 5 for STAT1, n = 6 for STAT3). For all Western blots: *P* values, Wilcoxon. IL, interleukin; IMQ, imiquimod; ApoE, Apolipiprotein E; H&E, hematoxylin and eosin; Movat, Movat's pentachrome stain; STAT, signal transducer and activator of transcription; DAPI, 4',6-diamidino-2-phenylindole.

IL-9 directly regulates human arterial endothelial cells via STAT3

Our observation that deletion of IL-9R in endothelial cells prevented aortic plaque formation led us to hypothesise that IL-9 might directly target arterial endothelial cells to promote atherosclerotic disease. To test this, we first set out to investigate IL-9R expression in arterial endothelial cells. In 6 coronary arteries from 3 deceased subjects with a documented history of psoriasis, we found IL-9R+/VE-Cadherin+ cells surrounding lipid-rich plaque and at the arterial lumen (Fig 5E,F). IL-9 receptor is a heterodimeric molecule composed of the IL-9R and IL-2Rγ subunits [42]. Both subunits were highly expressed in HAoEC, suggesting the presence of a functional IL-9 receptor (Fig 5G). IL-9 can signal through STAT1, STAT3, and STAT5 [19]: HAoEC expressed STAT1 and STAT3, (Supplementary Fig S6a); IL-9 induced phosphorylation of STAT3 (Fig 5H,I) but not

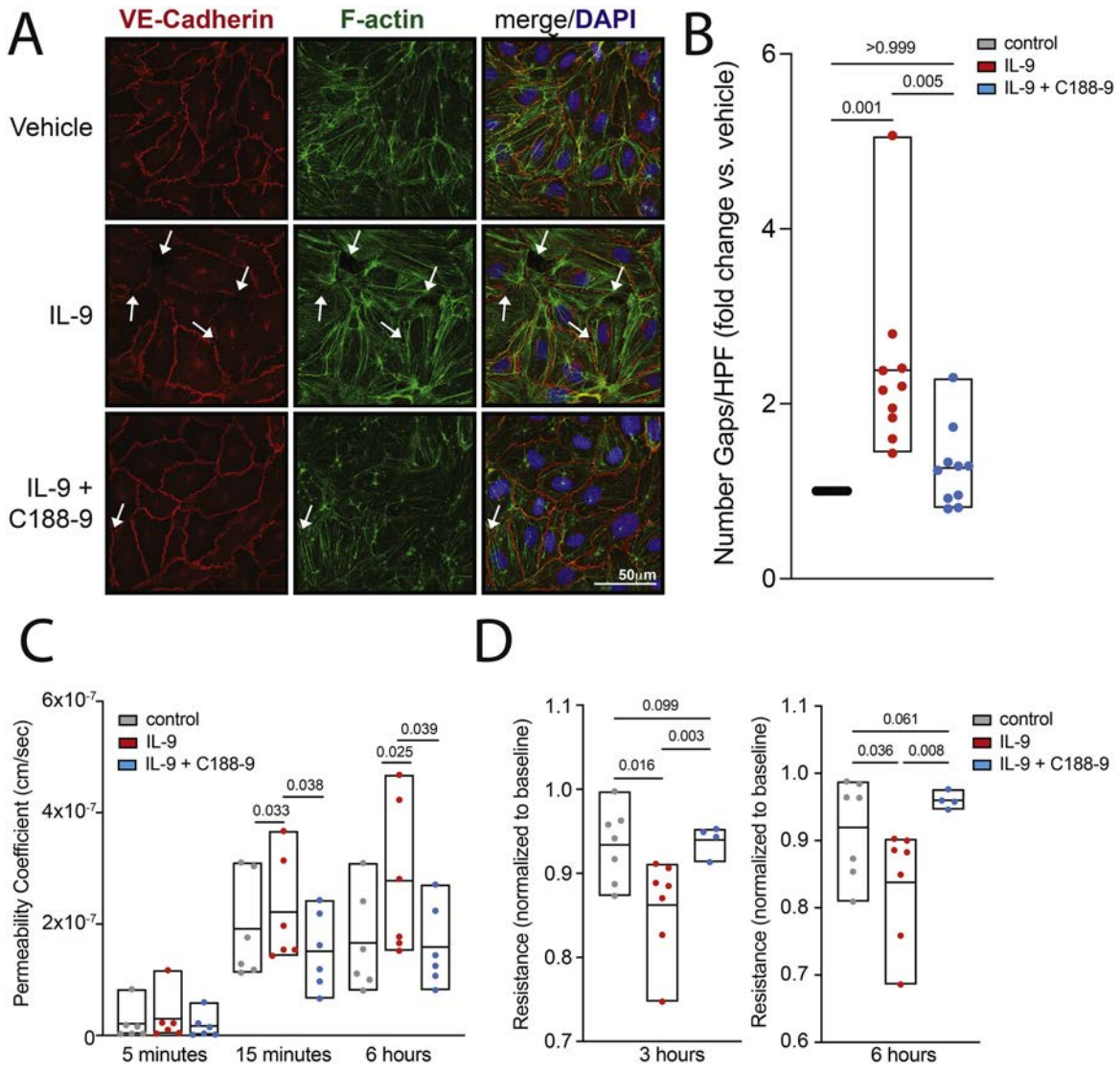

Figure 6. (A) Representative image shows immunofluorescence staining of primary human aortic endothelial cells (HAoEC) in monolayer, treated with vehicle vs IL-9 in the presence vs absence of STAT3-inhibitor C188-9 and stained for VE-Cadherin (red) and F-actin (green) to visualise monolayer integrity (nuclei in blue, DAPI). Bar graph shows pooled number of gaps between cells (B), FITC-dextran permeability coefficient (C), or impedance by ECIS (D) for HAoEC treated with vehicle vs IL-9 in the presence vs absence of C188-9. For all experiments: *P* values, ANOVA. IL, interleukin; STAT, signal transducer and activator of transcription; VE, vascular endothelial; DAPI, 4',6-diamidino-2-phenylindole; FITC, fluorescein isothiocyanate; ECIS, electric cell substrate impedance sensing; HPF, high powered field; ANOVA, analysis of variance.

STAT1 (Fig 5J). IL-9 also induced expression of the STAT3 target gene *SOCS3* (Supplementary Fig S6b)

IL-9 induces endothelial dysfunction through STAT3

Disruption of endothelial barrier integrity is a key step in the early pathogenesis of ASCVD [43], and STAT3 may play a role in endothelial barrier function [44,45]. We hypothesised that IL-9/STAT3 signalling might disrupt endothelial barrier integrity. To test this, we treated HAoEC with IL-9 alone or in the presence of the STAT3 inhibitor C188-9. IL-9 disrupted endothelial monolayer morphology, significantly increasing the number and size of gaps between cells (Fig 6A,B). IL-9 also increased endothelial monolayer permeability (Fig 6C,D). IL-9 significantly induced *VCAM1* and *SELE*, with a trend towards *ICAM1* induction (Supplementary Fig S6c-e). These genes are induced in proinflammatory states and are involved in leukocyte recruitment to lipid-rich plaque [9,43]. C188-9 prevented IL-9-mediated disruption of endothelial integrity (Fig 6A-D), suggesting that IL-9 promotes endothelial dysfunction via STAT3.

IL-9 regulates adhesion and barrier-promoting genes in endothelial cells

STAT3 primarily exerts its effects via transcriptional regulation, modulating large cassettes of target genes [42]. We therefore set out to determine the global targets of IL-9-STAT3 signalling by analysing the transcriptomes of IL-9-treated HAoEC. IL-9 induced 278 genes (FC ≥ 2, adj $P < .05$, DESeq2), and repressed 681 genes (FC ≤ -2, adj $P < .05$, DESeq2) in HAoEC (Fig 7A). Because IL-9/STAT3 signalling disrupted endothelial barrier integrity, we hypothesised that IL-9 might reduce the expression of intercellular junction proteins. Although IL-9 modestly repressed the junction protein *TJP2*, IL-9 induced other intercellular junction genes (Fig 7B). To identify other potential mechanisms promoting IL-9/STAT3-driven endothelial dysfunction, we analysed enriched pathways in IL-9-induced

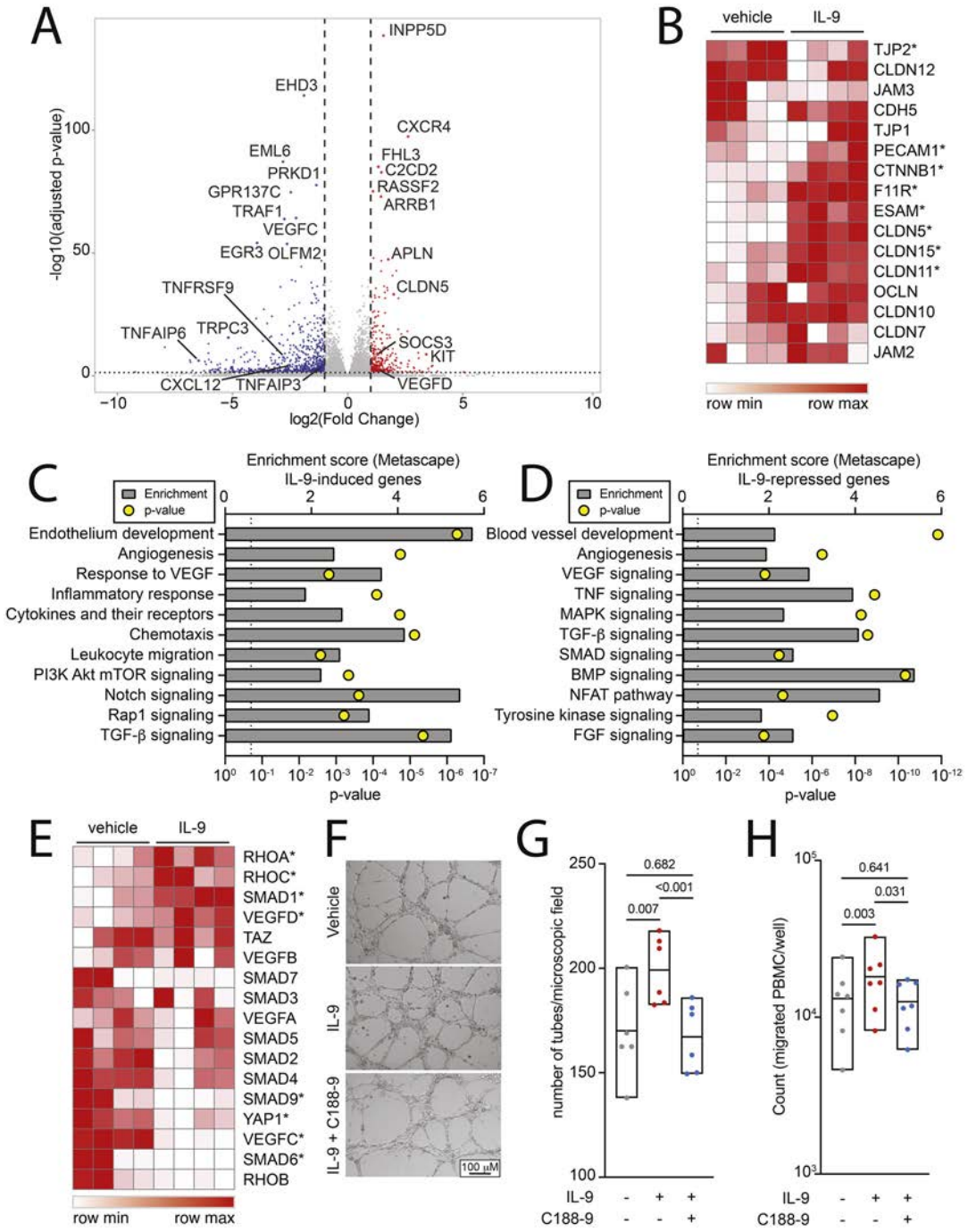

Figure 7. (A) Volcano plot shows $\log_2$ normalised fold-change in gene expression vs $-\log_{10}$ normalised Benjamini-Hochberg adjusted *P* value (DESeq2) for primary human aortic endothelial cells (HAoEC, n = 4) treated with IL-9 vs vehicle. Selected genes are marked. (B) Heatmap shows expression (normalised across rows) of genes encoding tight and adherens junction proteins in endothelial cells treated with IL-9 vs vehicle. Bar graphs show enrichment scores (grey) and *P* values (yellow) for selected enriched pathways (Metascape) in genes induced (C) or repressed (D) by IL-9 in HAoEC. (B) Heatmap shows expression (normalised across rows) of genes encoding proangiogenic pathways associated with STAT3-mediated endothelial dysfunction, in endothelial cells treated with IL-9 vs vehicle. *Adjusted *P* value < .05, DESeq2. IL, interleukin; STAT, signal transducer and activator of transcription; DESeq2, Differential Expression Sequencing quantification 2.

and IL-9-repressed gene cassettes. IL-9-induced and IL-9-repressed gene cassettes were both enriched for proangiogenic, proinflammatory, and TGF-β signalling pathways (Fig 7C,D). Multiple proangiogenic pathways are implicated in endothelial dysfunction downstream of STAT3, including Rho, VEGF, YAP-TAZ, and Smad signalling [44–46]. IL-9 modulated the expression of genes involved in all 4 pathways (Fig 7E). These findings suggest that IL-9/STAT3 signalling modulates a broad cassette of genes that combinatorially promote endothelial barrier disruption and atherogenesis.

Endothelial IL-9R/STAT3 signalling enhances angiogenesis and leukocyte chemotaxis

Our transcriptomic analysis suggested that, in addition to barrier disruption, endothelial IL-9R/STAT3 signalling might promote leukocyte chemotaxis and angiogenesis. We therefore treated primary HAoEC with IL-9 in the presence vs absence of C188-9, then investigated *in vitro* endothelial 2D tube formation, a measure of angiogenesis . IL-9-treated HAoEC formed more endothelial tubes (Fig 7F,G), confirming that IL-9 is

proangiogenic in arterial endothelial cells. Supernatants from IL-9-treated HAoEC also promoted recruitment of healthy donor-derived human peripheral blood mononuclear cells (PBMCs) through a transwell system (Fig 7H), suggesting that IL-9 stimulates release of leukocyte chemoattractant factors from HAoECs. Treatment with C188-9 reduced both PBMC migration and tube formation (Fig 7F-H). These data suggest that IL-9R/STAT3 signalling induces a prochemotactic and proangiogenic program in HAoEC, promoting endothelial dysfunction and inflammatory atherogenesis.

DISCUSSION

Inflammation is a major contributor to ASCVD, particularly in systemic immune diseases [2,3,5,7,13,47], and prior studies link the inflammatory cytokine IL-9 to murine atherogenesis and advanced, unstable plaque [14,15,48]. However, a critical prerequisite to preventing ASCVD development is identifying the individuals with early plaque, in whom intervention could prevent advanced ASCVD [29]. Key unanswered questions include the specific populations and diseases in which IL-9 promotes ASCVD, the cellular sources and targets of IL-9, and the mechanisms by which IL-9/IL-9R signalling promotes ASCVD. Addressing these questions could identify disease endotypes where IL-9 blockade might prevent ASCVD development.

To address these gaps, we studied psoriasis, a Th9-associated inflammatory disease, using transcriptomic, genetic, and functional approaches in translational murine models and primary human cells. We found that Th9 expansion is strongly linked to psoriatic ASCVD independent of traditional risk factors. Although psoriasis has been associated with Th9 expansion [16,18,20,49], our data show that only a subset of patients exhibits this Th9^{high} state. Previous studies, including work from our group, suggest the Th9^{high} state may represent a distinct endotype [17,19,24]. Our discovery that Th9-derived IL-9 directly promotes psoriatic ASCVD implicates a novel Th9^{high} endotype association. IL-9 promotes psoriatic atherogenesis in 3 distinct murine models, including a translational model developed based on human monogenic psoriasis. Several of these models have limitations: IMQ and IL-23 induce a more acute inflammatory state than that seen in human psoriasis, the *Card14* model is based on only one psoriasis-associated gene, and IMQ induces diverse inflammatory pathways. This last feature may be relevant to other immune diseases reported to include Th9^{high} patient endotypes like lupus, atopic dermatitis, and vasculitis [17,50]. Although Th9 cells are thought to be the major source of IL-9 in humans, IL-9 can also originate from other cell types including mast cells, CD8+ T cells, and innate lymphoid cells [51]. Future studies are needed to explore the links between IL-9-producing T cells, other IL-9-producing cells, and ASCVD pathogenesis in these populations.

Our findings also point to IL-9/Th9 blockade as a potential strategy to prevent or treat psoriatic ASCVD. Most trials using immunomodulation for ASCVD have targeted the IL-1/IL-6 pathway with colchicine, canakinumab, and tocilizumab [47,52,53]. While effective, these approaches carry major drawbacks including immunosuppression and off-target toxicities [47,52,53]. By contrast, IL-9 plays a limited role in host-pathogen defence: primarily defence against helminths [51], which rare in developed countries. Early IL-9-blocking trials in revealed no major safety concerns, and type 2 cytokine blockers generally well tolerated, even in combination with other biologics [51,54]. Moreover, the Th9^{high} endotype is associated with ASCVD independent of C-reactive protein, a biomarker of IL-1/IL-6 activation. The Th9^{high} state has previously been linked to arthritis in individuals with psoriasis [21]; however, our study design did not include comprehensive assessment for PsA. Because most patients with PsA also have psoriasis, and PsA has been linked to ASCVD severity [11], our findings may be highly relevant to patients with PsA-associated ASCVD.

Future studies will need to replicate these findings in larger cohorts of patients with moderate-to-severe disease, with PsA, and using longitudinal study designs. Nonetheless, these results highlight the novelty and potential utility of IL-9/IL-9R blockade as a safer, more effective strategy for ASCVD prevention in Th9^{high} endotypes.

Beyond identifying a novel ASCVD endotype, our results also clarify Th9 lineage identity across different tissues and disease states [25,27,34]. We previously identified a conserved "allergic Th9" transcriptional program [17], which we now find extends to psoriasis and ASCVD. Psoriatic Th9 cells are enriched for migratory markers that promote homing to atherosclerotic vessels, consistent with the presence of plaque-infiltrating Th9 cells. Prior studies suggest that Th9 cells in patients with psoriatic disease initially differentiate in barrier tissues such as the skin or small intestine before circulating to distal sites, which is partly supported by the specificity of some plaque-resident CD4+ T cells for viral epitopes [16,21,55]. Hyperlipidaemia may itself promote Th9 infiltration into skin: obesity worsens psoriasis, and HFD worsens IMQ-psoriasis [6,56]. Alternatively, plaque-resident Th9 cells may originate from visceral fat: both psoriasis and atherosclerosis involve visceral adipose inflammation [8,57], and some plaque-resident CD4+ T cells are specific for apolipoprotein B [55]. It is also possible that plaque-resident Th9 cells originate from the gut, as has been reported for joint-resident Th9 cells in PsA [21]. Defining the origin and migration of plaque-infiltrating Th9 cells, as well as the relationship to other psoriatic disease features like arthritis, will require fate-mapping and dynamic tracking approaches.

After migration into atherosclerotic plaque, local proatherogenic factors may sustain Th9 effector function, helping to explain persistent IL-9 production. Cytokines and mediators like IL-1β, hypoxia, nitric oxide, and intracellular fatty acids—all abundant in atherosclerotic lesions—modulate Th9 differentiation [34,49,51,58]. We now add VEGF-A and oxidised LDL to this network, underscoring the complex milieu that regulates Th9 effector function in psoriatic ASCVD. Sustained IL-9 production positions the endothelium as a key downstream target: IL-9/IL-9R/STAT3 directly regulates endothelial barrier function, activation, angiogenesis, and leukocyte recruitment. Because IL-9R can be broadly induced by inflammation across stromal and immune compartments [51], we used primary human arterial endothelial cells and conditional deletion models to establish endothelial IL-9R/STAT3 signalling as a critical pathway linking Th9/IL-9 to ASCVD. Endothelial-directed Cre recombinases can also affect haematopoietic lineages [51]. Although we confirmed endothelial-specific deletion relative to bulk leukocyte populations, we cannot entirely rule out a role for IL-9R signalling within the immune compartment in psoriatic atherogenesis, including in our endothelial-directed conditional deletion model. Nonetheless, our results highlight IL-9/IL-9R as a potent modulator of endothelial biology, with broad implications for vascular disease.

In summary, IL-9$^+$ Th9 cells are expanded in psoriasis, define a Th9^{high} endotypes associated with ASCVD, and express a conserved Th9 transcriptional program that directs them to atherosclerotic plaque. Within plaque, local factors modulate IL-9 production, which in turn directly promotes endothelial

dysfunction via IL-9R/STAT3 signalling. These findings uncover a novel mechanism of inflammatory atherogenesis that highlights IL-9 blockade a promising therapeutic strategy in patients with Th9^{high} diseases like psoriasis.

Acknowledgements

Results have been presented at the 2024 International Cytokine and Interferon Society meeting (oral abstract, unpublished). The authors would like to thank the NHLBI Microscopy core (Dr Christian Combs), the NHLBI Histology core (Dr Zu-Xi Yu), Dr Laurel G Mendelsohn, and Dr Abhinav Saurabh.

Contributors

IB and YB performed and supervised experiments, analysed data, and wrote the manuscript. AB, MS, MMK, GHF, CAG-H, BT, AS, KC, JK, and KJ performed experiments. AD, JR, and NNM provided patient samples and data, and performed statistical analysis. JDP performed histological analysis. MC provided representative coronary CT images. PAFG, JDM, TMP-W, and NNM developed study protocols, provided patient samples and data, and edited the manuscript. LG, AF, AG, and TS analysed data from human cadaveric coronary artery specimens. GHF designed the study, performed and supervised experiments, analysed data, and wrote the manuscript. DMS designed the study, performed and supervised experiments, analysed data, provided funding, supervised the study, and wrote the manuscript.

Funding

This research was supported in part by the Intramural Research Program of the National Institutes of Health (NIH). The contributions of the NIH author(s) were made as part of their official duties as NIH federal employees, are in compliance with agency policy requirements, and are considered Works of the United States Government. However, the findings and conclusions presented in this paper are those of the author(s) and do not necessarily reflect the views of the NIH or the U.S. Department of Health and Human Services.

Competing interests

DMS receives research funding from Eli Lilly and Sobi, consults for Sobi, and is on a speaker board for Sobi. NNM consults for Abcam, Caristo, Novartis, Celgene, Abbvie, and Janssen. LG is an AstraZeneca employee. AF consults for Amgen, Boston Scientific, CeloNova, Concept Medical, Cook, Cordis, Gore, Medtronic, and Recor. All disclosures are unrelated to this manuscript. The other authors report no conflicts. The contributions of the NIH author(s) were made as part of their official duties as NIH federal employees, are in compliance with agency policy requirements, and are considered Works of the United States Government. However, the findings and conclusions presented in this paper are those of the author(s) and do not necessarily reflect the views of the NIH or the U.S. Department of Health and Human Services.

Patient consent for publication

Not applicable.

Ethics approval

This study was conducted in accordance with the Declaration of Helsinki. All human studies were IRB-approved (NIH: 13H-0065, 10-H-0126; CVPath IRB), with written informed consent obtained from all participants. All mouse studies were approved by the Institutional Animal Care and Use Committee (IACUC) of the University of Pittsburgh and National Institutes of Health.

Provenance and peer review

Not commissioned; externally peer reviewed.

Data availability statement

All bulk sequencing data have been uploaded to the Gene Expression Omnibus (GSE312663). All single-cell data are publicly available (https://figshare.com/s/c00d88b1b25ef0c5c788). Representative plots of all gating strategies and unedited Western blots are available as an Extended Data Supplement. All other data are available on request.

Declaration of generative AI and AI-assisted technologies in the writing process

During the preparation of this work, the author(s) used PittGPT and Claude for Education software (the University of Pittsburgh's AI-assisted technology) to edit the text for conciseness. The author(s) reviewed and revised all content and take full responsibility for the final manuscript.

Supplementary materials

Supplementary material associated with this article can be found in the online version at doi:10.1016/j.ard.2025.11.008.

Extended Methods

Sex as a biological variable

Sex was considered as a variable in experimental design for all experiments. Both male and female subjects (mouse and human) were included; similar findings were seen for both sexes.

Human Samples and Data

Whole blood, coronary artery CT scores, and demographic data were collected from de-identified psoriasis patients at the NIH Clinical Center. Samples included untreated patients and those on immunomodulatory therapies. Additional details are described elsewhere [1]. De-identified blood samples from non-psoriatic controls were obtained from the NIH Blood Bank or de-identified healthy volunteers. Atherosclerotic coronary artery specimens from psoriasis patients were obtained via the CVPath autopsy registry.

Study approval, Patient and Public Involvement

Patients and members of the public were not directly involved in the design or conduct of this study. Study participation was limited to providing informed consent and contributing clinical samples or data. All procedures were conducted in accordance with institutional review board and ethical guidelines. Human studies were approved by the NIH Institutional Review Board (IRB) under protocol 13H-0065 (NCT01778569) or 10-H-0126 (NCT01143454). The CVPath autopsy registry was approved by the CVPath IRB. All mouse protocols were

approved by the NIAID (LAD12E) or University of Pittsburgh (22070649) IACUC

Mouse experiments

Experiments were performed on age- and sex-matched 8–12-week-old male and female mice, housed in specific-pathogen-free, AAALAC-accredited facilities. Mice were maintained on a 12-hour light–dark cycle with ad libitum food and water, except for a 24-hour fast before euthanasia in high-fat diet studies. Health was monitored regularly, with increased oversight in disease models. VE VE-Cre (*Cdh5-Mlia*), *Card14*^{DE138}, and *ApoE*$^{-/-}$ mice were purchased (Jackson); Il9r-/- and INFER mice were provided by M Kaplan and J-C Renauld. All mice were on a C57BL/6 background

Generation of *Il9r*$^{f/f}$ mice

Il9r$^{f/f}$ mice were generated by CRISPR/Cas9 at the Mouse Genetics and Gene Modification Section, Comparative Medicine Branch, NIH. Gene targeting was aimed to delete exon2-5 of *Il9r*. Flox insertion sites were carefully chosen not to disturb proper splicing of *Il9r*. A 3.5kb DNA cassette including 800bp homology arms at both sides was synthesized and inserted into pUC vector (Azenta). Guide RNAs were selected using CRISPOR (http://crispor.tefor.net/), and synthetic gRNA was manufactured (Synthego). C57BL/6Tac females were injected with 7.5IU of pregnant mare serum gonadotropin (Prospec) followed by 5IU of human chorionic gonadotropin (Sigma) after 47 hours, then mated with C57BL/6Tac males. The following morning, fertilized one-cell-stage embryos were collected, washed 6 times with EmbryoMax M2 media (Sigma), and then cultured in EmbryoMax KSOM media (Sigma) at 6% CO_2, 37°C for 3 hours or until the microinjection. The embryos were transferred to 50mm glass bottom dish in EmbryoMax M2 drop, overlaid with embryo-tested mineral oil (Sigma), and microinjected using an DMi8 inverted microscope (Leica) equipped with a set of TransferMan4 micromanipulator and FemtoJet4i (Eppendorf). Microinjection mixture was prepared fresh as following: 10ng/µl of HiFi Cas9 (IDTdna), 5ng/µl of sgRNA, 5ng/µl of plasmid in microinjection buffer (10mM Tris-HCL pH7.5 with 0.25mM EDTA), backfilled to microinjection needles for pronuclear injection. Injected embryos were implanted into the oviducts of pseudo-pregnant surrogate CD-1 females (Charles River) after 1h culture in EmbryoMax KSOM at 6% CO_2, 37°C. Offspring born to foster mothers were genotyped by PCR. Primer sequences for genotyping: il9r for, CACAAGTCCGAGTTGAGGTC; il9r 5flox rev, AATGTATGCTATACGAAGTTATGGTACC; il9r 3flox for, AGCATACATTATACGAAGTTATACGTG; il9r rev, GGATGCTGGCTGACCATT.

Generation and validation of *Il9r*^{DVE} mice

Cdh5^{Mlia} Cre mice were purchased (Jackson) and bred to *Il9r*$^{f/f}$ mice. Spleens were isolated from *Il9r*^{DVE} mice and pooled (n = 2) followed by red blood cell lysis and isolation of endothelial and leukocyte fractions as described previously [2]. Briefly, cells were sorted to CD45$^+$ (leukocytes) and CD45$^-$ fractions using magnetic depletion (Miltenyi). CD45$^-$ fractions were magnetically enriched for CD31$^+$ cells (Miltenyi) followed by flow cytometric sorting for CD45$^-$/CD31$^+$ endothelial cells. DNA was isolated from leukocytes and endothelial cells and genotyped by PCR using primers spanning a deleted intronic region: il9r for CCTCCTTAATGTCCCTCCAACAA, Il9r rev ACCCTGCAGGAGGTATGCTT. The resulting DNA amplicons were visualized on SYBR Gold agarose gel (ThermoFisher).

Psoriasis models

Three murine psoriasis models were used. In the IMQ-ApoE model, 9–11-week-old ApoE-/- mice received daily topical 5% Imiquimod (IMQ, Glenmark 60 mg) or Vanicream on shaved dorsal skin for three 5-day cycles with 13-day recovery periods (6 weeks total). In the IL-23-ApoE model, ApoE-/- mice received daily intradermal IL-23 (500 ng in 20 µL PBS, Thermo) on shaved flanks for two 5-day cycles with 59-day rest intervals (10 weeks total). *Card14*$^{\Delta E138}$ x *ApoE*$^{-/-}$ mice developed spontaneous psoriasis.

High-fat diet (HFD, 42% fat; Envigo TD.88137) was used to induce atherogenesis. IMQ and IL-23 model mice began HFD on day 1 of psoriasis induction, continuing for 6 or 10 weeks, respectively. *Card14-ApoE* mice began HFD at 8–12 weeks of age for 7 weeks. Mice received anti–IL-9 antibody (BioXCell BE0181) or IgG2a isotype control (BioXCell, BE0085) at 100 μg/200 μL twice weekly. In IMQ and IL-23 models, treatment began on day 1 of induction. In *Card14-ApoE* mice, treatment began on day 1 of HFD. Antibody dosing continued until euthanasia.

Skin digestion Mouse dorsal caudal/posterior skin (~3cm X 4cm) was digested as previously described [3]. Briefly, subcutaneous tissue was removed and samples placed in PBS. After trimming into small pieces, skin was minced on ice with 1 mL digestion buffer (10 μL of 25 mg/mL, 0.65 Wunsch units/mL Liberase TL in PBS), then combined with 4 mL additional buffer in a 6-well plate and incubated at 37 °C for 2 hours, with 1 mL Trypsin added for the final 10 minutes. Digestion was stopped with 4–5 mL 5% FACS buffer, filtered (100 μm), centrifuged (400g, 8 min, 4 °C), resuspended in FACS buffer, and filtered again (40 μm) prior to stimulation and/or staining.

Aorta digestion

Aortas were cut in 1mm rings and were collected in a 15ml Falcon tube containing 200μl aorta digestion buffer containing 10μl of 25mg/ml (0.65 Wunsch units/mL) Liberase TM in PBS. The tubes were incubated in a 37°C water-bath for 40 minutes, resuspending every 15 minutes. The reaction was stopped by adding 10ml PBS/2% FBS. The contents were passed through 40μm filters, then centrifuged (1400 rpm x 5 min) and resuspended.

Aortic plaque measurements (mice)

All aortic plaque measurements were performed according to AHA guidelines [4]. Vasculature was perfused with PBS, and the entire aorta was cleaned from adventitial fat under a dissection microscope. Subsequently, the thoracic part of the aorta was utilized for *en face* atherosclerotic lesion quantification while the abdominal aorta was used for flow cytometry. For *en face* atherosclerotic lesion analysis, the thoracic aorta was opened longitudinally, transferred to a wax-coated tray, and pinned under a dissection scope. The aorta was then fixed using 4% paraformaldehyde solution for 10 minutes. To visualize lipid-rich atherosclerotic plaque, Oil-Red-O staining was performed as described [5]. Briefly, after fixation aortas were washed with water and incubated with isopropanol (60%) for 5min. Subsequently, Oil-Red-O solution was added and incubated for 15 min under slow rotation. Excessive Oil-Red-O solution was washed away with 60% isopropanol, then the aorta was submerged in water and imaged. Photos taken at 10x magnification were analyzed for Oil-Red-O positive area (ImageJ) expressed as percentage of total aortic area. Quantification was performed by two independent investigators who were blinded to experimental groups and to each other's assessments.

Plasma LDL measurement

After 12-14h fasting, blood was collected into EDTA-coated tubes and plasma separated by centrifugation, then stored at −80°C. When all the samples were collected, LDL cholesterol levels were measured (Crystal Chemicals) according to the manufacturer's protocol.

In vitro human and murine Th9 differentiation

Naïve human and murine T cells (>90% purity, magnetic separation as previously described) [6]. were plated at 110^6 cells/mL. Human cells were cultured in 1 mL/well (48-well plate) in complete RPMI-1640 (10% FBS, glutamine, penicillin/streptomycin) with plate-bound αCD3 (OKT3, 1 μg/mL) and Th9-polarizing conditions: αCD28 (1 μg/mL), αIFN-γ (2.5 μg/mL), hTGF-β (5 ng/mL), hIL-2 (10 ng/mL), hIL-4 (30 ng/mL), and hIL-1β (10 ng/mL). Murine cells were cultured in 1 mL/well (24-well plate) in complete IMDM (10% FBS, penicillin/streptomycin, 55 μM β-mercaptoethanol) with plate-bound αCD3ε and αCD28 (10 μg/mL each), plus αIFN-γ (10 μg/mL), mIL-4 (20 ng/mL), hIL-2 (10 ng/mL), and hTGF-β (5 ng/mL). Where indicated, cells were treated with vehicle, VEGF-A (Peprotech), or oxidized LDL (oxLDL; Lee Biosolutions) in charcoal-stripped FBS (Gibco). Cells were analyzed after 3 days (mouse) or 5 days (human).

Restimulation

All cells were stimulated in 96-well plates. Human PBMCs were isolated by density centrifugation (Ficoll-Paque) and cryopreserved. For restimulation, cells were thawed and washed with complete RPMI-1640 with DNAse as previously described, then restimulated at 37°C with 10 ng/mL phorbol 12-myristate13-acetate (PMA), 1µg/mL ionomycin, 20 ng/mL hIL-2, and 60 ng/mL hIL-4. After 2 hours, 10 mg/mL brefeldin was added for 4h (total 6h stimulation).

Murine *in vitro* differentiated Th9 cells were stimulated with 100 ng/mL PMA, 1 µg/mL ionomycin; 20 ng/mL hIL-2; 40 ng/mL mIL-4. Human *in vitro* differentiated Th9 cells were stimulated with 20 ng/mL PMA; 1 µg/mL ionomycin; 20 ng/mL hIL-2; 60 ng/mL hIL-4. In both, 10 mg/mL brefeldin was added after 2h, and the incubation was continued for another 4h (total 6h stimulation). Murine *in vivo* differentiated Th9 cells (skin, spleen, aorta): organs were digested as above, then resuspended in cIMDM for 5 hours with PMA (100ng/mL), ionomycin (1 µg/mL), hIL-2 (20 ng/mL), and mIL-4 (40 ng/mL).

Flow cytometry

Human PBMC were stained for viability (Live-Dead BLUE, Invitrogen), then fixed and permeabilized (BD Cytofix/Cytoperm). Cells were then stained with: CD3/APC/Cy7, CD4-BUV395, CD8-v500, CD45RO-PE/Texas Red, IL-2-PerCp/Cy5.5, IL-4-BUV605, IL-13/BV711, IL-9-PE, IL-5-v450, IFN-γ-AF700, TNF-α-PE/Cy7, IL-17A-FITC, IL-21-AF647, IL-10-e655. Live, doublet-excluded (single) cells were used for all analyses.

In vitro differentiated murine Th9 cells were stained for viability (Zombie AQUA, BioLegend), then fixed and permeabilized (BD Cytofix/Cytoperm). Cells were then stained with CD4-PerCp/Cy5.5, IL-9-APC, IFN-γ-PE, Foxp3-v450, IL-4-AF488. Live, doublet-excluded (single) cells were used for all analyses.

Tissue-infiltrating murine cells: suspensions of digested organs were transferred to 96-well plates and centrifuged (400g x 3min, 4°C), then washed (1X PBS) and stained for viability (Zombie AQUA, Biolegend) in the presence of Fc block. After 10 minutes, the following antibodies were added for 30 minutes, 4°C: F4/80-SB600, CD11b-FITC, Siglec-F-PE, Ly6G-PerCP/Cy5.5, Ly6C-AF647. Cells were fixed and permeabilized (BD Cytofix/Cytoperm), followed by intracellular staining, 3 hours: CD3-BV421, TCRβ-APC/Cy7, CD45.2-PE/Cy7, CD4-PE/Dazzle 594, CD8a-AF700. In some cases, cells were stimulated for analysis of *in vivo* differentiated T cells and stimulated as above, then stained for viability (Zombie UV, Biolegend) in the presence of Fc block. After 10 minutes, the following antibodies were added for 30 minutes, 4°C: CD11b-FITC, Ly6C-Alexa Fluor 700, F4/80-SB 600, followed by intracellular staining for 2 hours: CD45-APC/Cy7, CD3-BV421, TCRβ-SB645, CD4-PerCP/Cy5.5, IL9-PE, IL13-PE-Cy7, IL17-APC, IFNγ-Pacific Blue. Live, doublet-excluded (single) cells were used for all analyses.

Th9 cells from INFER mice: organ suspensions were transferred to 96-well plates and stained with DAPI and cell surface antibodies in the presence of Fc block (20 mg/mL), heat-inactivated rat serum (1:50 dilution, ThermoFisher 10170C), and heat-inactivated hamster serum (Abcam ab7483). Cells were stained with: CD4-PerCpCy5.5, CD8-PE, TCR-b-APC-Cy7, CD45.2-PE-Cy7, and CD44-AF700. Live, doublet-excluded cells were sorted for CD45.2+/TCR-b+/CD4+/CD8-/CD44+ cells, then for GFP+ (Th9) and GFP- (non-Th9) cells.

Data were collected on a LSRFortessa (BD) or Cytek Aurora and analyzed with FlowJo (Treestar) and Prism (GraphPad).

For all experiments, gating strategies are available in the extended data.

For immunofluorescence, deparaffinized sections underwent heat-induced antigen retrieval and were incubated overnight at 4 °C with antibodies against CD3 (0.2 μg/mL) or CD4 (1.25 μg/mL) (Roche), co-labeled with PU.1 (1:400, CST). Secondary antibodies included Alexa Fluor 488 anti-mouse IgG and Alexa Fluor 555 anti-rabbit IgG (1:150, Thermo Fisher), followed by DAPI (1:500).

For VE-cadherin/IL-9R co-staining, sections were incubated with VE-cadherin (1:100, R&D) and IL-9R (1:400, BioLegend), followed by Alexa Fluor 488 anti-goat IgG and Alexa Fluor 555 anti-mouse IgG (1:150), and DAPI. Histological images were scanned at 10X (AxioScan Z1, Zeiss) and immunofluorescent images were acquired using a laser-scanning confocal microscope (LSM800, Carl Zeiss Microscopy, Jena, Germany) with optical sectioning along the z-axis at 20X.

Primary human aortic endothelial cells (HAoEC) from >9 donors (PromoCell) were cultured and passaged up to 9 times as described[5, 7]. Cells were treated with recombinant human IL-9 (Peprotech) 100 ng/mL vs. vehicle control; in some experiments the STAT3 inhibitor C188-9 (1mMol/L) vs. vehicle control was added. Assays were performed on confluent monolayers using >4 biological replicates to assess endothelial function. Immunofluorescence was used to visualize monolayers and quantify intercellular gaps as described [5]. After 6h of treatment, cells were fixed (2% paraformaldehyde), permeabilized (0.1% Triton X-100), blocked (5% goat serum in 2% BSA), and stained with anti−VE-cadherin (1:100), Phalloidin-AF488 (F-actin), and DAPI (nuclei). Images were captured using the EchoRevolve and Zeiss 780 microscopes, and gaps were quantified with ImageJ. Gaps were quantified by two investigators who were blinded to the groups and to each other's assessments. Endothelial barrier integrity was assessed using ECIS and FITC-dextran (70 kDa) flux across 0.4 μm transwells, as previously described [5] [8].

Angiogenesis

For MatrigelTM tube formation assay [8], HAoECs were treated overnight, supernatants were removed, and HAoECs removed from culture surfaces then maintained on the Matrigel matrix for 4 hours to allow tube formation. Images were taken (EchoRevolve), and tubes/microscopic field were quantified (ImageJ). Quantification was performed by two independent investigators who were blinded to experimental groups and to each other's assessments.

HAoEC-leukocyte chemotaxis assays

HAoECs were treated as indicated for 6h, and supernatants were collected. PBMCs (2×10^6 per condition) from healthy blood bank donors were seeded on a 5μm transwell filter in a 24-well plate. The lower chamber was filled with HAoEC supernatant (300μl), and PBMCs were allowed to transmigrate (4h).

Cells were suspended in Trizol LS (Invitrogen). Total RNA was extracted and treated with DNAse to remove genomic DNA, then 500 ng RNA was reverse transcribed using a cDNA synthesis kit (Applied Biosystems) and quantitative PCR (qPCR) was performed in triplicate using TaqMan master mix (Applied Biosystems). The following primers were used: TBP (qHsaCIP0036255), VEGFA (qHsaCEP0050716), VCAM1 (qHsaCIP0030799), ICAM1 (qHsaCEP0024986), SELE (qHsaCIP0028854), SOCS3 (qHsaCEP0024741). Expression was normalized to TBP.

Libraries for mRNA-sequencing were prepared using the NEBNext Ultra II Directional RNA-seq Library kit. Samples were sequenced on a NovaSeq 6000, paired end (PE), for 50 cycles and processed with bcl2fastq v.2.20.0.422. Reads of 50 bases were processed using the nextflow-core pipeline [9] (https://nf-co.re/rnaseq/2.0). Adaptor sequences were trimmed (Trim Galore) and mapped to mouse transcriptome mm10 or human transcriptome GRCh38 (STAR). Gene expression values (fragments per kilobase exon per million mapped reads; tags per million mapped reads; counts) were generated using RSEM. Differential gene expression was calculated using DESeq2. To calculate FC cutoffs, datasets were normalized based on FPKM and purged of micro-RNAs, sno-RNAs and sca-RNAs. When multiple transcripts were detected for one gene, only the most abundant (highest average RPKM across all replicates) was analyzed. Transcripts with FPKM < 1 were excluded. Downstream analyses were performed with R 4.3.2, Morpheus (https://software.broadinstitute.org/morpheus/), VolcanosER (https://huygens.science.uva.nl/VolcaNoseR/), DAVID (https://davidbioinformatics.nih.gov), and Metascape (https://metascape.org/gp/index.html#/main/step1). Metascape enrichment scores were calculated using nN/kM, where N = total genes in the study pool, i.e. human/mouse genome, k = genes in the pathway of interest, M = # genes in the input gene list, and n = overlap between k and M.

Geneset Enrichment Analysis (GSEA)

For GSEA (https://www.gsea-msigdb.org/gsea/index.jsp) analysis [10, 11], enrichment score curves and member ranks were generated by GSEA software (Broad Institute). The Th9 cassette was obtained using our previously published analysis of Th9 cells [6]. Other T helper subset cassettes were also obtained from datasets we previously generated [12]. Other pathways were analyzed based on Human Molecular Signatures Database (MSigDB) collections.

CITE-seq data were analyzed using Seurat 5.2.0 [13]. UMI files for plaque-resident and circulating (PBMC) T cells were obtained from https://figshare.com/s/c00d88b1b25ef0c5c788. CD4+ T cells were identified based on CITE-seq antibody labeling (CD4+CD8-), and UMI matrices for "CD4.Tcells.plaque" and "CD4.Tcells.pbmc" were used for downstream analysis. UMAPs and SPI1+ cell visualization followed standard pipelines [13]. GSEA was performed on SPI1+ vs. SPI1- cells using signal-to-noise ranking and phenotype permutation to assess "allergic Th9" enrichment. For pathway analysis, genes with Pearson correlation > 0.2 with SPI1 in plaque CD4+ T cells were selected.

Endothelial cells were treated with vehicle (PBS + 0.1% recombinant human serum albumin) or recombinant hIL-9 (PeproTech), then lysed at indicated time points in RIPA buffer with protease/phosphatase inhibitors (ThermoFisher). Lysates were centrifuged (4°C, 14,000g), and protein concentration was measured (Pierce BCA Kit). Equal protein amounts were run on Mini-Protean TGX gels (BioRad), transferred to nitrocellulose membranes, and blocked with 5% NFDM or 2% BSA (for phospho-antibodies) for 1 hour. Membranes were incubated overnight at 4°C with primary antibodies (1:1000), washed in TBS-T, then incubated with HRP-conjugated secondary antibodies (1:5000) for 1 hour. After washing, membranes were treated with substrate (SuperSignal West Pico Plus) and imaged using Fluor Chem E or Azure CCD systems. Antibody details are in Supplementary Table 3. Experiments used 3–6 biological replicates. Full (unedited) blots are available in the Extended Data.

For all non-transcriptomic analyses, statistics were performed in GraphPad Prism. Normality was assessed before testing. Parametric tests (paired/unpaired t-test) were used for normally distributed data; non-parametric tests (Wilcoxon or Mann-Whitney) for non-normal data. ANOVA was used for group comparisons, with Benjamini-Hochberg correction for multiple testing. All tests were two-sided.

References (Methods only)

1. Harrington CL, Dey AK, Yunus R, Joshi AA, Mehta NN. Psoriasis as a human model of disease to study inflammatory atherogenesis. Am J Physiol Heart Circ Physiol. 2017 May 1; 312 (5):H867-H873.

2. Dumas SJ, Meta E, Conchinha NV, Sokol L, Chen R, Borri M, et al. Protocols for endothelial cell isolation from mouse tissues: kidney, spleen, and testis. STAR Protoc. 2021 Sep 17; 2 (3):100523.

3. Sakamoto K, Goel S, Funakoshi A, Honda T, Nagao K. Flow cytometry analysis of the subpopulations of mouse keratinocytes and skin immune cells. STAR Protoc. 2022 Mar 18; 3(1):101052.

4. Daugherty A, Tall AR, Daemen M, Falk E, Fisher EA, Garcia-Cardena G, et al. Recommendation on Design, Execution, and Reporting of Animal Atherosclerosis Studies: A Scientific Statement From the American Heart Association. Arterioscler Thromb Vasc Biol. 2017 Sep; 37(9):e131-e157.

5. Baumer Y, McCurdy S, Weatherby TM, Mehta NN, Halbherr S, Halbherr P, et al. Hyperlipidemia-induced cholesterol crystal production by endothelial cells promotes atherogenesis. Nat Commun. 2017 Oct 24; 8(1):1129.

6. Son A, Meylan F, Gomez-Rodriguez J, Kaul Z, Sylvester M, Falduto GH, et al. Dynamic chromatin accessibility licenses STAT5- and STAT6-dependent innate-like function of T(H)9 cells to promote allergic inflammation. Nat Immunol. 2023 Jun; 24(6):1036-1048.

7. Baumer Y, Dey AK, Gutierrez-Huerta CA, Khalil NO, Sekine Y, Sanda GE, et al. Hyperlipidaemia and IFNgamma/TNFalpha Synergism are associated with cholesterol crystal formation in Endothelial cells partly through modulation of Lysosomal pH and Cholesterol homeostasis. EBioMedicine. 2020 Sep; 59:102876.

8. Baumer Y, Funk D, Schlosshauer B. Does telomerase reverse transcriptase induce functional de-differentiation of human endothelial cells? Cell Mol Life Sci. 2010 Jul; 67 (14):2451-2465.

9. Ewels PA, Peltzer A, Fillinger S, Patel H, Alneberg J, Wilm A, et al. The nf-core framework for community-curated bioinformatics pipelines. Nat Biotechnol. 2020 Mar; 38(3):276-278.

10. Subramanian A, Tamayo P, Mootha VK, Mukherjee S, Ebert BL, Gillette MA, et al. Gene set enrichment analysis: a knowledge-based approach for interpreting genome-wide expression profiles. Proc Natl Acad Sci U S A. 2005 Oct 25; 102 (43):15545-15550.

11. Mootha VK, Lindgren CM, Eriksson KF, Subramanian A, Sihag S, Lehar J, et al. PGC-1alpha-responsive genes involved in oxidative phosphorylation are coordinately downregulated in human diabetes. Nat Genet. 2003 Jul; 34(3):267-273.

12. Schwartz DM, Farley TK, Richoz N, Yao C, Shih HY, Petermann F, et al. Retinoic Acid Receptor Alpha Represses a Th9

Transcriptional and Epigenomic Program to Reduce Allergic Pathology. Immunity. 2019 Jan 15; 50(1):106-120 e110.

13. Satija R, Farrell JA, Gennert D, Schier AF, Regev A. Spatial reconstruction of single-cell gene expression data. Nat Biotechnol. 2015 May; 33(5):495-502.

Orcid

Daniella M. Schwartz: http://orcid.org/0000-0002-1660-8438

REFERENCES

[1] Vaduganathan M, Mensah GA, Turco JV, Fuster V, Roth GA. The Global burden of cardiovascular diseases and risk: a compass for future health. J Am Coll Cardiol 2022;80(25):2361–71.
[2] Libby P, Ridker PM, Maseri A. Inflammation and atherosclerosis. Circulation 2002;105(9):1135–43.
[3] Manning ES, Shroff GR, Jacobs Jr. DR, Duprez DA. Chronic inflammatory-related disease and cardiovascular disease in MESA. JACC Adv 2025;4(4):101640.
[4] Conrad N, Verbeke G, Molenberghs G, Goetschalckx L, Callender T, Cambridge G, et al. Autoimmune diseases and cardiovascular risk: a population-based study on 19 autoimmune diseases and 12 cardiovascular diseases in 22 million individuals in the UK. Lancet 2022;400(10354):733–43.
[5] Harrington CL, Dey AK, Yunus R, Joshi AA, Mehta NN. Psoriasis as a human model of disease to study inflammatory atherogenesis. Am J Physiol Heart Circ Physiol 2017;312(5):H867–73.
[6] Griffiths CEM, Armstrong AW, Gudjonsson JE, Barker J. Psoriasis. Lancet 2021;397(10281):1301–15.
[7] Eder L, Thavaneswaran A, Chandran V, Cook R, Gladman DD. Increased burden of inflammation over time is associated with the extent of atherosclerotic plaques in patients with psoriatic arthritis. Ann Rheum Dis 2015;74(10):1830–5.
[8] Schwartz DM, Parel P, Li H, Sorokin AV, Berg AR, Chen M, et al. PET/CT-Based characterization of 18F-FDG uptake in various tissues reveals novel potential contributions to coronary artery disease in psoriatic arthritis. Front Immunol 2022;13:909760.
[9] Baumer Y, McCurdy S, Weatherby TM, Mehta NN, Halbherr S, Halbherr P, et al. Hyperlipidemia-induced cholesterol crystal production by endothelial cells promotes atherogenesis. Nat Commun 2017;8(1):1129. 24.
[10] Chen TL, Huang JY, Lin HY, Chang YT, Li CY, Wei JC. Risk of major adverse cardiovascular events and venous thromboembolic events between patients with psoriasis or psoriatic arthritis on tumor necrosis factor inhibitors, interleukin 17 inhibitors, interleukin 12/23 inhibitors, and interleukin 23 inhibitors: an emulated target trial analysis. J Am Acad Dermatol 2025;92(5):1015–23.
[11] Eder L, Jayakar J, Shanmugarajah S, Thavaneswaran A, Pereira D, Chandran V, et al. The burden of carotid artery plaques is higher in patients with psoriatic arthritis compared with those with psoriasis alone. Ann Rheum Dis 2013 May;72(5):715–20.
[12] Ding L, Chen C, Yang Y, Zhang X. Major cardiovascular events under biologic psoriasis therapies: a 19-year real-world analysis of FAERS data. Front Immunol 2024;15:1349636.
[13] Wolf D, Ley K. Immunity and inflammation in atherosclerosis. Circ Res 2019;124(2):315–27.
[14] Zhang W, Tang T, Nie D, Wen S, Jia C, Zhu Z, et al. IL-9 aggravates the development of atherosclerosis in ApoE$^{-/-}$ mice. Cardiovasc Res 2015;106(3):453–64.
[15] Li Q, Ming T, Wang Y, Ding S, Hu C, Zhang C, et al. Increased Th9 cells and IL-9 levels accelerate disease progression in experimental atherosclerosis. Am J Transl Res 2017;9(3):1335–43.
[16] Schlapbach C, Gehad A, Yang C, Watanabe R, Guenova E, Teague JE, et al. Human TH9 cells are skin-tropic and have autocrine and paracrine proinflammatory capacity. Sci Transl Med 2014;6(219):219ra218.
[17] Son A, Meylan F, Gomez-Rodriguez J, Kaul Z, Sylvester M, Falduto GH, et al. Dynamic chromatin accessibility licenses STAT5- and STAT6-dependent innate-like function of T(H)9 cells to promote allergic inflammation. Nat Immunol 2023;24(6):1036–48.
[18] Rauber S, Luber M, Weber S, Maul L, Soare A, Wohlfahrt T, et al. Resolution of inflammation by interleukin-9-producing type 2 innate lymphoid cells. Nat Med 2017;23(8):938–44.
[19] Scharli S, Luther F, Di Domizio J, Hillig C, Radonjic-Hoesli S, Thormann K, et al. IL-9 sensitizes human T(H)2 cells to proinflammatory IL-18 signals in atopic dermatitis. J Allergy Clin Immunol 2025;155(2):491–504.e499.
[20] Gerlach K, Hwang Y, Nikolaev A, Atreya R, Dornhoff H, Steiner S, et al. TH9 cells that express the transcription factor PU.1 drive T cell-mediated colitis via IL-9 receptor signaling in intestinal epithelial cells. Nat Immunol 2014;15(7):676–86.
[21] Ciccia F, Guggino G, Ferrante A, Raimondo S, Bignone R, Rodolico V, et al. Interleukin-9 overexpression and Th9 polarization characterize the inflamed gut, the synovial tissue, and the peripheral blood of patients with psoriatic arthritis. Arthritis Rheumatol 2016;68(8):1922–31.
[22] Clark RA, Schlapbach C. TH9 cells in skin disorders. Semin Immunopathol 2017;39(1):47–54.
[23] Micosse C, von Meyenn L, Steck O, Kipfer E, Adam C, Simillion C, et al. Human "TH9" cells are a subpopulation of PPAR-gamma(+) TH2 cells. Sci Immunol 2019;4(31):eaat5943.
[24] Alladina J, Smith NP, Kooistra T, Slowikowski K, Kernin IJ, Deguine J, et al. A human model of asthma exacerbation reveals transcriptional programs and cell circuits specific to allergic asthma. Sci Immunol 2023;8(83):eabq6352.
[25] Licona-Limon P, Henao-Mejia J, Temann AU, Gagliani N, Licona-Limon I, Ishigame H, et al. Th9 cells drive host immunity against gastrointestinal worm infection. Immunity 2013;39(4):744–57.
[26] Gangwar RS, Gudjonsson JE, Ward NL. Mouse models of psoriasis: a comprehensive review. J Invest Dermatol 2022;142(3 Pt B):884–97.
[27] Schwartz DM, Farley TK, Richoz N, Yao C, Shih HY, Petermann F, et al. Retinoic acid receptor alpha represses a Th9 transcriptional and epigenomic program to reduce allergic pathology. Immunity 2019;50(1):106–120.e110.
[28] Son A, Baral I, Falduto GH, Schwartz DM. Locus of (IL-9) control: IL9 epigenetic regulation in cellular function and human disease. Exp Mol Med 2024;56(6):1331–9.
[29] Abdelrahman KM, Chen MY, Dey AK, Virmani R, Finn AV, Khamis RY, et al. Coronary computed tomography angiography from clinical uses to emerging technologies: JACC state-of-the-art review. J Am Coll Cardiol 2020;76(10):1226–43.
[30] Komarowska I, Coe D, Wang G, Haas R, Mauro C, Kishore M, et al. Hepatocyte growth factor receptor c-met instructs T cell cardiotropism and promotes T cell migration to the heart via autocrine chemokine release. Immunity 2015;42(6):1087–99.
[31] Marchini T, Mitre LS, Wolf D. Inflammatory cell recruitment in cardiovascular disease. Front Cell Dev Biol 2021;9:635527.
[32] Wang L, Zhao XC, Cui W, Ma YQ, Ren HL, Zhou X, et al. Genetic and pharmacologic inhibition of the chemokine receptor CXCR2 prevents experimental hypertension and vascular dysfunction. Circulation 2016;134(18):1353–68.
[33] Saigusa R, Winkels H, Ley K. T cell subsets and functions in atherosclerosis. Nat Rev Cardiol 2020;17(7):387–401.
[34] Kaplan MH. The transcription factor network in Th9 cells. Semin Immunopathol 2017;39(1):11–20.
[35] Batty M, Bennett MR, Yu E. The role of oxidative stress in atherosclerosis. Cells 2022;11(23):3843.
[36] Liu HQ, Zhang XY, Edfeldt K, Nijhuis MO, Idborg H, Back M, et al. NOD2-mediated innate immune signaling regulates the eicosanoids in atherosclerosis. Arterioscler Thromb Vasc Biol 2013;33(9):2193–201.
[37] Lee S, Birukov KG, Romanoski CE, Springstead JR, Lusis AJ, Berliner JA. Role of phospholipid oxidation products in atherosclerosis. Circ Res 2012;111(6):778–99.
[38] Mullick AE, Soldau K, Kiosses WB, Bell 3rd TA, Tobias PS, Curtiss LK. Increased endothelial expression of Toll-like receptor 2 at sites of disturbed blood flow exacerbates early atherogenic events. J Exp Med 2008;205(2):373–83.
[39] Samarasekera EJ, Neilson JM, Warren RB, Parnham J, Smith CH. Incidence of cardiovascular disease in individuals with psoriasis: a systematic review and meta-analysis. J Invest Dermatol 2013;133(10):2340–6.
[40] Takatsuka S, Yamada H, Haniuda K, Saruwatari H, Ichihashi M, Renauld JC, et al. IL-9 receptor signaling in memory B cells regulates humoral recall responses. Nat Immunol 2018;19(9):1025–34.
[41] Alva JA, Zovein AC, Monvoisin A, Murphy T, Salazar A, Harvey NL, et al. VE-Cadherin-Cre-recombinase transgenic mouse: a tool for lineage analysis and gene deletion in endothelial cells. Dev Dyn 2006;235(3):759–67.
[42] Schwartz DM, Bonelli M, Gadina M, O'Shea JJ. Type I/II cytokines, JAKs, and new strategies for treating autoimmune diseases. Nat Rev Rheumatol 2016;12(1):25–36.
[43] Pepin ME, Gupta RM. The role of endothelial cells in atherosclerosis: insights from genetic association studies. Am J Pathol 2024;194(4):499–509.
[44] Wang L, Astone M, Alam SK, Zhu Z, Pei W, Frank DA, et al. Suppressing STAT3 activity protects the endothelial barrier from VEGF-mediated vascular permeability. Dis Model Mech 2021;14(11):dmm049029.
[45] Shen Y, Wang X, Liu Y, Singhal M, Gurkaslar C, Valls AF, et al. STAT3-YAP/TAZ signaling in endothelial cells promotes tumor angiogenesis. Sci Signal 2021;14(712):eabj8393.
[46] Becerra A, Rojas M, Vallejos A, Villegas V, Perez L, Cabello-Verrugio C, et al. Endothelial fibrosis induced by suppressed STAT3 expression mediated by

signaling involving the TGF-beta1/ALK5/Smad pathway. Lab Invest 2017;97 (9):1033–46.
[47] Ridker PM, Everett BM, Thuren T, MacFadyen JG, Chang WH, Ballantyne C, et al. Antiinflammatory therapy with canakinumab for atherosclerotic disease. N Engl J Med 2017;377(12):1119–31.
[48] Gregersen I, Skjelland M, Holm S, Holven KB, Krogh-Sorensen K, Russell D, et al. Increased systemic and local interleukin 9 levels in patients with carotid and coronary atherosclerosis. PLOS ONE 2013;8(8):e72769.
[49] Xue G, Jin G, Fang J, Lu Y. IL-4 together with IL-1beta induces antitumor Th9 cell differentiation in the absence of TGF-beta signaling. Nat Commun 2019;10(1):1376.
[50] Ohtsuki S, Wang C, Watanabe R, Zhang H, Akiyama M, Bois MC, et al. Deficiency of the CD155-CD96 immune checkpoint controls IL-9 production in giant cell arteritis. Cell Rep Med 2023;4(4):101012.
[51] Pajulas A, Zhang J, Kaplan MH. The World according to IL-9. J Immunol 2023;211(1):7–14.
[52] Mitsis A, Kyriakou M, Sokratous S, Karmioti G, Drakomathioulakis M, Myrianthefs M, et al. Exploring the landscape of anti-inflammatory trials: a comprehensive review of strategies for targeting inflammation in acute myocardial infraction. Biomedicines 2024;12(3):701.
[53] Tardif JC, Kouz S, Waters DD, Bertrand OF, Diaz R, Maggioni AP, et al. Efficacy and safety of low-dose colchicine after myocardial infarction. N Engl J Med 2019;381(26):2497–505.
[54] Gisondi P, Maurelli M, Costanzo A, Esposito M, Girolomoni G. The combination of dupilumab with other monoclonal antibodies. Dermatol Ther (Heidelb) 2023;13(1):7–12.
[55] Saigusa R, Roy P, Freuchet A, Gulati R, Ghosheh Y, Suthahar SSA, et al. Single cell transcriptomics and TCR reconstruction reveal CD4 T cell response to MHC-II-restricted APOB epitope in human cardiovascular disease. Nat Cardiovasc Res 2022;1(5):462–75.
[56] Higashi Y, Yamakuchi M, Fukushige T, Ibusuki A, Hashiguchi T, Kanekura T. High-fat diet exacerbates imiquimod-induced psoriasis-like dermatitis in mice. Exp Dermatol 2018;27(2):178–84.
[57] Ohman MK, Shen Y, Obimba CI, Wright AP, Warnock M, Lawrence DA, et al. Visceral adipose tissue inflammation accelerates atherosclerosis in apolipoprotein E-deficient mice. Circulation 2008;117(6):798–805.
[58] Nakajima T, Kanno T, Ueda Y, Miyako K, Endo T, Yoshida S, et al. Fatty acid metabolism constrains Th9 cell differentiation and antitumor immunity via the modulation of retinoic acid receptor signaling. Cell Mol Immunol 2024;21(11):1266–81.

Ann Rheum Dis 85 (2026) 836–847

Contents lists available at ScienceDirect

Annals of the Rheumatic Diseases

journal homepage: https://www.sciencedirect.com/journal/annals-of-the-rheumatic-diseases

Systemic lupus erythematosus

Heterogeneous responses of IM19 anti-CD19 CAR T-cell therapy in refractory systemic lupus erythematosus: an open-label pilot study and a mini-review

Jinxia Zhao[1,2], Xiaoying Zhang[1,2], Yime Zhang[1], Xinyi Li[1], Hui Wei[1], Yinji Jin[1], Rui Liu[1], Zhaohua Li[1], Wei Guo[1], Zhenqing Wang[1], Yue Guo[1], Yunxia Xia[1], Yang Yu[3], Haijing Liu[4], Lin Zeng[5], Qiang Shu[6], Jinlian Sun[7], Yang Tian[7], Yanping Ding[7], Ting He[7], Xin'an Lu[7], Lin Sun[1,2], Rong Mu[1,2,*]

[1] *Department of Rheumatology and Immunology, Peking University Third Hospital, Beijing, China*
[2] *Beijing Key Laboratory of Clinical Evaluation of Cardiovascular-Kidney-Metabolic and Immuno-Inflammatory Innovative Drugs and Medical Devices, Peking University Third Hospital, Beijing, China*
[3] *Clinical Stem Cell Research Center, Peking University Third Hospital, Beijing, China*
[4] *Department of Pathology, Peking University Third Hospital, Beijing, China*
[5] *Research Center of Clinical Epidemiology, Peking University Third Hospital, Beijing, China*
[6] *Department of Rheumatology, Qilu Hospital of Shandong University, Jinan, China*
[7] *Imunopharm Technology Co., Beijing, China*

ARTICLE INFO

Article history:
Received 29 August 2025
Received in revised form 20 December 2025
Accepted 26 December 2025

ABSTRACT

Objectives: This study aims to evaluate the efficacy and safety of IM19, an autologous anti-CD19 chimeric antigen receptor (CAR) T cell, in patients with refractory systemic lupus erythematosus (SLE), with a particular focus on lupus nephritis (LN).
Methods: This is an open-label, single-arm clinical trial. IM19 was administered following lymphodepletion. Repeated renal biopsies were performed at day 180. Single-cell RNA sequencing on peripheral blood mononuclear cells was performed pre- and 180-day post-CAR-T infusion. A literature search on the efficacy of CAR T-cell therapy in LN in PubMed database was conducted.
Results: Six patients with refractory SLE and renal involvement were enrolled. IM19 therapy was well tolerant, with mild cytokine release syndrome occurring in 4 patients. The median Systemic Lupus Erythematosus Disease Activity Index-2000 score decreased from 12 (range, 10-24) to 4 (range, 2-8) at day 90, and remained stable at 5 (range, 2-6) at day 180. The renal responses were heterogeneous with 2 complete responders, 2 partial responders, and 2 nonresponders. Repeated renal biopsies showed no B-cell infiltration, but dominant chronic changes and podocytopathies post-CAR-T therapy. A mini-review demonstrated that the renal complete response rate of CAR-T therapy was 72.4%, and advanced age was associated with suboptimal response. Single-cell analysis confirmed B-cell reconstitution in 3/6 patients.
Conclusions: IM19 CAR T-cell therapy demonstrated a favourable safety profile and clinically meaningful systemic improvement. Responses to CAR-T therapy in LN were variable. Chronic renal manifestations, podocytopathy, and ageing were associated with suboptimal therapeutic outcome.

*Correspondence to Dr Rong Mu, Department of Rheumatology and Immunology, Peking University Third Hospital, Beijing, China.
E-mail address: murongster@163.com (R. Mu).

Handling editor Josef S. Smolen

Jinxia Zhao and Xiaoying Zhang contributed equally to this work.

https://doi.org/10.1016/j.ard.2025.12.014

WHAT IS ALREADY KNOWN ON THIS TOPIC

- Chimeric antigen receptor (CAR) T-cell therapy targeting CD19 or B-cell maturation antigen has emerged as a transformative intervention for refractory systemic lupus erythematosus, demonstrating potent depletion of B cell and long-lived plasma cells and induction of clinical remission in multiple pilot studies.

WHAT THIS STUDY ADDS

- The pilot investigator-initiated research showed that IM19, an autologous anti-CD19 CAR-T product, achieved significant reductions in systemic disease activity and effective depletion of CD19+ B cells in both peripheral blood and renal tissue.
- Despite robust systemic improvement, renal responses of IM19 were heterogeneous. A pooled mini-review of published CAR-T studies in lupus nephritis (LN) revealed an overall renal complete response rate of 72.4%.
- Chronic histological changes and podocytopathy are key determinants of poor renal outcomes of CAR T-cell therapy in our patients with LN. Advanced age might also predict suboptimal outcomes.
- The study demonstrated the feasibility of continuing immunosuppressive therapy during leukapheresis, which provided an evidence-based treatment protocol for optimising therapeutic frameworks in CAR T-cell therapy.

HOW THIS STUDY MIGHT AFFECT RESEARCH, PRACTICE OR POLICY

- This study advocates for the integration of routine renal biopsy into patient selection protocols for CAR T-cell therapy, promoting histopathology-guided stratification to refine clinical trial design and therapeutic precision.

INTRODUCTION

Chimeric antigen receptor (CAR) T-cell therapy has shown remarkable potential in systemic lupus erythematosus (SLE), given the central role of B cells in SLE pathogenesis [1]. Current CAR-T approaches, including autologous CAR T cells targeting CD19 [2–7], B-cell maturation antigen (BCMA) [8], or both CD19-BCMA [9], alongside allogeneic CD19-targeted CAR T cells [10], improved clinical outcomes in refractory patients with SLE. However, heterogeneity in the efficacy and safety profile has been found across different CAR-T products, attributable to multiple factors, such as designs and antigen targets [11]. IM19, an autologous 41BB-based CD19 targeting CAR-T, lacks established clinical experience in autoimmune diseases so far, and its efficacy and safety in SLE remain to be determined through careful investigation.

A key advantage of CAR-T therapy lies in its potent tissue infiltration capabilities [12], rendering it an ideal choice for lupus nephritis (LN) which is characterised by the infiltration of pathogenic autoreactive B cells within the renal parenchyma and interstitium [13]. Conventional B-cell depleting agents, such as rituximab and obinutuzumab, demonstrate limited efficacy in eliminating these tissue-resident B-cell populations and contribute to suboptimal clinical responses [14,15]. Although preliminary clinical data suggest that CAR T-cell therapy may overcome this limitation and induce renal improvement [2–4,6,8,9], its efficacy on LN requires further investigation. Moreover, factors influencing treatment response are not well understood, underscoring the urgent need for additional studies.

To elucidate the clinical efficacy of IM19 in refractory SLE, we conducted a pilot study. Beyond the observations reported in other CAR T-cell therapy studies, the exclusive enrolment of participants with active LN at baseline afforded a unique opportunity to conduct longitudinal analyses of renal outcomes—directly addressing a key unmet clinical need in the field. Because current evidence on CAR-T therapy for LN predominantly derives from case reports, small-scale case series, and pilot studies, we conducted a mini-review synthesising extant literature alongside our original data to better understand treatment efficacy and predictive factors. Additionally, this study pioneered a novel protocol retaining baseline immunosuppressants during leukapheresis.

METHODS

Study design

This open-label, single-arm investigator-initiated clinical study was conducted at Peking University Third Hospital, Beijing, People's Republic of China, to assess the safety and efficacy of IM19 therapy in refractory SLE (ClinicalTrials. gov number, NCT06513429), in accordance with the Declaration of Helsinki and Good Clinical Practice guidelines. The study was approved by the Cellular Clinical Research Scientific Review and Medical Science Research Ethics Committee Review (M2023469), and then by the National Health Commission of China, following the Interim Measures for the Clinical Research and Translational Application of Somatic Cell Therapies (People's Republic of China, 2023). All patients provided written informed consent.

Participants

Patients were recruited from the Department of Rheumatology and Immunology of Peking University Third Hospital between July 30, 2024 and November 16, 2024. Eligible patients were aged 18 to 65 years and fulfilled the 2019 American College of Rheumatology and the European Alliance of Associations for Rheumatology classifications of SLE [16]. Inclusion criteria required active disease with SLE disease activity score (Systemic Lupus Erythematosus Disease Activity Index-2000 [SLEDAI-2K]) with a score of 10 or above [17]. Active LN was defined as 24-hour urinary protein excretion >0.5 g daily. Refractory SLE was defined as persistent disease activity or relapse despite standard treatment, including steroids (adequate doses or pulse therapy), immunosuppressants (cyclophosphamide or mycophenolate mofetil), and biologics (belimumab or telitacicept). All the patients had maintained stable background therapy for at least 12 weeks preceding the screening. Detailed inclusion and exclusion criteria are provided in the protocol (see Supplementary Material).

Outcomes

The primary endpoint was the change from baseline in SLEDAI-2K score at 90 days post-IM19 CAR T-cell infusion, alongside safety assessments within 28 days postinfusion. Adverse events (AEs) and severe AEs were evaluated according to Common Terminology Criteria for AE version 5.0 [8]. Cytokine release syndrome (CRS) and immune effector cell–associated neurotoxicity syndrome (ICANS) were assessed according to the American Society for Transplantation and Cellular Therapy consensus criteria [18].

The secondary endpoints included: (1) the efficacy of SLE, as evaluated by the improvement of SLEDAI-2K score and

achieving lupus low disease activity (LLDAS) [19] at day 180 and day 360; (2) renal response at day 180 and day 360. Regarding LN, complete renal response was defined as 24-hour urine protein ≤0.5 g/d; partial renal response was defined as a ≥50% reduction in proteinuria from baseline with 24-hour proteinuria <3.5 g/d or protein-creatinine ratio <3.0 mg/g, along with stable or improved kidney function (±10%-15% of baseline) [20,21]; and (3) dynamics of IM19 CAR-T expansion *in vivo*.

CAR T-cell manufacturing, therapeutic procedure, and follow-ups

IM19, a 41BB-based CD19 CAR-T, was composed of FMC63 scFv, CD8a hinge and transmembrane region, 41BB costimulatory domains, and a CD3ζ T-cell activation domain (Imunopharm Technology Co., Ltd.) [22]. Briefly, T cells were purified from the apheresis and activated by CD3/CD28 Dynabeads (ThermoFisher) at a T cell/bead ratio of 1:1. One day later, T cells were transduced with IM19 lentiviral vector and cultured in X-VIVO 15 medium (Lonza Group) containing 500 IU/mL of Interleukin (IL)-2 at a density of 0.3×10^6 to 1.5×10^6/mL for 6 to 12 days. CAR T cells were formulated, cryopreserved, and sent for quality control in both Imunopharm Technology Co., Ltd. and the central lab of Stem Cell Center, Peking University Third Hospital.

Leukapheresis was performed without interrupting ongoing immunosuppressants and hydroxychloroquine. T-cell expansion during manufacturing was observed (Supplementary Fig S1). A median number of 1.5 (range, 0.4-2.1) $\times 10^9$ CD19 CAR T cells were manufactured per patient, with flow cytometric analysis confirming transduction efficiencies (CAR positivity) of 23.5% to 53.7% (Supplementary Fig S2).

Immunosuppressants and hydroxychloroquine were discontinued before lymphodepletion; steroid doses were maintained at ≤10 mg/d prednisone equivalent. Lymphodepleting chemotherapy comprised fludarabine (25 mg/m^2/d) and cyclophosphamide (300 mg/m^2/d) for 3 consecutive days (D-5 to D-3). IM19 CAR T cells were infused on day 0 at a dose of 1×10^6 CAR T cells/kg for patients 1, 3, and 4, and 1×10^8 cells per patient for patients 2, 5, and 6, following prophylactic antihistamine administration.

The follow-up schedule is summarised in the protocol (Supplementary material: Protocol). Patients were monitored daily for CRS and ICANS. Safety was evaluated by the frequency and severity of AEs for 180 days. Clinical efficacy was assessed via SLEDAI-2K score, and laboratory parameters including autoantibody titres, complement levels, and proteinuria measurements. Repeated renal biopsies were made in patients 1-3 at day 180. The follow-up schedule is detailed in the protocol (Supplementary material: Protocol).

Immunomonitoring

To monitor CAR T cells, peripheral blood mononuclear cells (PBMCs) from each patient were isolated by density centrifugation, stained with CD19 CAR detection reagent, washed twice, and stained with Biotin antibody, a standardised panel of antibodies against CD45, CD3, CD4, and CD8. To evaluate the change of B cells, PBMCs were stained with anti-CD3 AF488 (clone UCHT1), anti-CD45 BV510 (clone 2D1), anti-CD19 PE/Cy7 (clone HIB19), anti-CD20 BV650 (clone 2H7), anti-CD27 BV750 (clone O323), anti-CD38 PE/Dazzle594 (clone HIT2), anti-CD11c BV421 (clone 3.9), anti-immunoglobulin (Ig) D APC (clone IA6-2), and anti-CD21 PE (clone HB5). All antibodies were from BioLegend (USA), except anti-CD21 PE from Invitrogen (USA). Absolute cell counts were determined with Northern Lights (Cytek Biosciences) according to the manufacturer's instructions. Gating strategies are depicted in Supplementary Figure S3. Data were analysed using SpectroFlo software (Cytek). All measurements were taken from distinct samples.

Single-cell RNA sequencing

We conducted single-cell RNA sequencing (scRNA-Seq) on PBMCs in 3 patients pre- and 180-day post-CAR-T infusion. Libraries were generated using the Chromium Next GEM Single Cell 5′ Kit (10 × Genomics), simultaneously capturing 5′ gene expression and enriched V(D)J sequences for T-cell receptor (TCR) and B-cell receptor (BCR) immune profiling.

For quality control, cells were retained if they expressed at least 500 genes and had less than 5% mitochondrial RNA content. Erythrocytes and platelets in PBMC were excluded in downstream analysis. Doubletfinder (v2.0.3) was applied to eliminate potential doublets. Seurat (v5.3.0) R package was used for normalisation, dimension reduction, clustering and cell annotation, and Harmony (v1.2.3) algorithm was used for batch effect correction. Gene set enrichment was performed by 'AddModuleScore' function in Seurat, and gene sets were obtained from the MSigDB database. scRepertoire (v2.2.1) was used for single-cell immune profiling analysis.

Quantification of autoantibodies

Autoantibodies, including anti-double-stranded DNA (dsDNA), anti-Smith, anti-SSA/Ro60, anti-Ro52, and anti-U1-RNP antibodies, were measured using a Chemiluminescence Immunoassay analyser (Kangrun Biotech, China), which is widely used and validated in clinical practice for SLE management [23]. Antinuclear antibody (ANA) was assessed by Indirect Immunofluorescence (EUROIMMUN).

Detection of antibodies against pathogens

Antibodies against the hepatitis B virus (HBV) and cytomegalovirus (CMV) were analysed using Electrochemiluminescence (Roche Diagnostics GmbH). Antibodies against Epstein-Barr virus (EBV) were tested using Electrochemiluminescence (YHLO Biotech).

Measurement of cytokines

IL-6, IL-10, interferon (IFN)-γ and tumour necrosis factor (TNF)-α were quantified via flow cytometry fluorescence technology (CellGene Biotech) following the manufacturer's instructions.

Mini-review

As of July 31, 2025, the PubMed databases had been searched. The keywords used were 'systemic lupus erythematosus', 'lupus nephritis', and 'CAR T cell'. Case reports, case series, and pilot studies in English were included. Two reviewers (JZ, XZ) abstracted the patients, the interventions, and the outcomes. Baseline active disease, defined as proteinuria >0.5 g/d, was required in patients with LN for efficacy analysis. Given the high risk of bias inherent in case reports, we restricted our efficacy analysis to cohort studies and clinical trials, ensuring a

more reliable assessment of response rates and prognostic factors.

Statistical analysis

Due to the small sample size, individual values are presented. Descriptive statistics were used to illustrate parameter changes, and median (range) was used to describe disease duration, SLEDAI-2K scores, circulating T cells, peak time of CAR T-cell expansion, and time of B-cell reconstitution. Paired comparisons of laboratory indices, such as antibodies against pathogens and B-cell proportions between 2 different time points, were performed with the paired Wilcoxon rank-sum test. Statistical analyses for baseline demographic and disease characteristics were done using the Mann-Whitney U test for comparisons of continuous variables and Fisher's test for comparisons of categorical variables. The Kolmogorov-Smirnov test was performed to detect the difference in gene set. A nominal significance level of 0.05 (2-sided) was applied to all the analyses. Descriptive analyses and visualisation were carried out using GraphPad Prism V10.0 (GraphPad Software, LLC). Visualisation of individual SLEDAI-2K score and all statistical analyses were carried out with R 4.1.0 (R Foundation for Statistical Computing).

RESULTS

Patients

Baseline characteristics are summarised in Table 1. Six patients (3 women and 3 men) aged between 19 and 43 years, with a median disease duration of 9.5 (range, 3-14) years, were enrolled in the study. Although LN was not a mandatory inclusion criterion, all patients who were enrolled had active LN at baseline, enabling a focused analysis of renal outcomes. All 6 patients had active SLE with median SLEDAI-2K scores of 12 (range, 10-24). Four patients had biopsy-proven glomerulonephritis of World Health Organization grade IV or V, and the other 2 patients had clinical LN diagnosis with persistent proteinuria, 1.0 and 0.9 g/d, respectively. All the patients had an inadequate response to ≥2 immunosuppressants/biologics, including mycophenolate mofetil (6/6), cyclophosphamide (6/6), tacrolimus (5/6), azathioprine (1/6), leflunomide (2/6), belimumab (6/6), and telitacicept (1/6). None had been exposed to B-cell depleting therapies, including rituximab or obinutuzumab. Supplementary Table S1 summarises the therapies and duration before screening. At baseline, 1 patient discontinued glucocorticoids, whereas 5 patients received low-dose

Table 1
Characteristics of 6 patients with refractory SLE at baseline

Characteristics	Patient 1	Patient 2	Patient 3	Patient 4	Patient 5	Patient 6
Age (y)	43	41	39	19	35	32
Sex (female/male)	F	M	F	F	M	M
Weight (kg)	68	62	83	69	73	69
Disease duration (y)	7	6	14	3	13	12
Follow-up (mo)	9	6	7	7	6	6
PGA score	3	2	2	2	2	2
Disease activity SLEDAI-2K	24	12	10	20	10	17
Baseline laboratory value						
White blood cells (N/μL)	2.43	9.25	3.73	7.92	4.13	4.13
Haemoglobin (g/l)	74	108	112	108	121	112
Lymphocyte (N/μL)	0.78	1.89	0.4	0.91	1.23	1.13
Platelets (N/μL)	80	152	226	241	189	188
proteinuria (g/24 h)	2.9	3.3	8.0	1.0	0.6	0.9
eGFR (mL/min/1.73 m^2)	96.7	63.2	119.3	132.6	118.4	122.2
Baseline autoantibodies						
ANA (titre)	1:160	1:160	1:640	1:640	1:320	1:640
Anti-dsDNA (IU/mL)	329.9	247.9	56.0	177.4	127.3	2979.6
Anti-Sm (U/mL)	18.2	0	0.4	0	1.3	10.3
Other autoantibodies	U1-RNP	–	SSA, SSB, Ro52	–	SSA, Ro52	SSA, Ro52
Organ involvement (presence/absence)						
Mucocutaneous	–	+	–	+	–	+
Renal	+	+	+	+	+	+
Renal biopsy stage	IV	IV	V	NA	IV	NA
Serosal	+	–	–	–	–	–
Haematologic	+	–	–	–	–	+
Musculoskeletal	–	–	–	+	–	–
Treatments (yes/no)						
Glucocorticoids	+	+	+	+	+	+
Hydroxychloroquine	+	+	–	+	+	+
Cyclophosphomide	+	+	+	+	+	+
Mycophenolate	+	+	+	+	+	+
Tacrolimus	+	+	+	+	+	–
Leflunomide	–	–	+	+	–	–
Azathioprine	–	–	–	–	+	–
Belimumab	+	+	+	+	+	+
Telitacicept	–	–	–	–	+	–
ACE inhibitors	+	+	–	+	+	–

ACE, angiotensin converting enzyme; ANA, antinuclear antibody; dsDNA, double-stranded DNA; eGFR, estimated glomerular filtration rate; NA, not available; PGA, physician global assessment; SLE, systemic lupus erythematosus; SLEDAI-2K, Systemic Lupus Erythematosus Disease Activity Index-2000; Sm, Smith.

glucocorticoids (5-10 mg/d), and 2 of them subsequently tapered to 2.5 mg/d during follow-up. Immunosuppressants and hydroxychloroquine were withdrawn from all patients 5 days before lymphodepletion, whereas after CAR-T infusion, no additional immunosuppressants were administered (Supplementary Table S2). Regarding nephroprotective agents, angiotensin converting enzyme (ACE) inhibitors were administered in patients 1, 2, 4, and 5 at baseline. Patients 4 and 5 discontinued ACE inhibitors during follow-up.

Primary endpoint

Disease activity of SLE decreased significantly after IM19 infusion. Median SLEDAI-2K scores demonstrated a significant reduction from 12 (range, 10-24) at baseline to 4 (range, 2-8) at day 90. Key clinical manifestations resolved following therapy, including arthritis (patients 4 and 6), skin rash (patient 6), and pleural effusion (patient 1) (Fig 1A,B).

At baseline, all patients were anti-dsDNA antibody-positive. A consistent decline in antibody titres was observed in the cohort, with 3 patients (patients 1, 3, and 4) achieving seroconversion (Fig 1C). Hypocomplementemia occurred in 4 patients (patients 1, 3, 5, and 6), and normalised by 60 days for all patients (Fig 1D). The patient with low C4 level (patient 1) normalised by day 10 after IM19 CAR-T infusion (Fig 1E). During the 180-day follow-up period, ANA titres decreased in all patients except patient 5. Anti-SSA antibodies remained persistently positive in patients 3 and 5, with a mild decline in patient 6. Notably, 1 patient (patient 1) achieved complete seroconversion (ANA, anti-RNP, anti-SSA, and anti-dsDNA) by day 60, and sustained at day 270 (Supplementary Table S3).

IM19 therapy was well tolerated. Transient low fever (<38.5 °C, no more than 36 hours) occurred in patients 2, 4, and 6, managed with nonsteroidal anti-inflammatory drugs or physical cooling. Patient 3 with fever (38.0-39.0°C) persisting >48 hours received a single dose of tocilizumab (8 mg/kg), and the symptom resolved within 12 hours. No relevant hemodynamic changes, hypoxia, or ICANS occurred (Table 2).

Secondary endpoint

At day 180, the median score of SLEDAI-2K was 5 (range, 2-6) (Fig 1B). Two patients (patients 4 and 6) reached LLDAS, with complete renal remission at day 180. Patients 1 and 3 achieved partial renal remission. Proteinuria in patient 1 decreased to 1.2 g/d from 2.9 g/d. Patient 3 exhibited a significant short-term reduction in proteinuria to 1.0 g/d, whereas levels subsequently rebounded to 3.0 g/d (8.0 g/d at baseline). Patient 2 had persistent proteinuria (3.2 g at baseline, 5.6 g at day 90, and 3.7 g at day 180 of follow-up) and increasing estimated glomerular filtration rate from 36 to 51 mL/min/1.73 m^2 (Fig 1F,G). Patient 5 exhibited mildly elevated proteinuria at baseline (0.6 g/d), whereas no significant changes were observed postinfusion. In addition to proteinuria, active urinary sediment (defined as >5 Red Blood Cells (RBCs)/High-Power Field (HPF), >5 WBCs/HPF, and/or cellular casts) was present in patients 1-4 at baseline. Following CAR-T therapy, the urinary sediment improved in patients 2 and 4 (Supplementary Table S4).

Robust CAR T-cell expansion occurred in all patients, peaking at a median of 8.5 days (range, 7-11 days) postinfusion. Peak CAR T-cell percentages among circulating T cells ranged from 17.3% to 75.0% of total circulating T cells (median circulating count: 188 cells/μL; range, 45-440 cells/μL) (Fig 1H, Supplementary Table S5). This variation showed no significant correlation with the type or intensity of immunosuppressive therapy maintained during leukapheresis. CAR T-cell levels declined rapidly postpeak. Area under curve ranged from 627.3 to 2481 cells/μL.

Predictive factors for renal response

To elucidate the reasons for suboptimal renal response following CAR T therapy, we performed repeat renal biopsies in patients 1- 3 at day 180. Patient 5 did not consent to a renal biopsy because his urinary protein was <1 g/d. The pretreatment renal biopsies for patients 1- 3 were performed in 2023, 2021, and 2022, respectively.

Repeated biopsy findings for patient 1 (partial responder) indicated diffuse segmental proliferative (LN [Class IV-S {A/C}]) with an activity index (AI) of 7 and a chronicity index of 5, compared to pretreatment scores of 10 and 2, respectively (Fig 1I). The observed chronic damage manifested as segmental glomerulosclerosis, tubular atrophy, and interstitial fibrosis. Biopsy in patient 2 (nonresponder) showed diffuse global proliferative LN (Class IV-G [A/C]), accompanied by severe glomerulosclerosis and subacute tubulointerstitial nephropathy, with an AI of 9 and chronicity index of 8 (Fig 1J). Pretreatment renal pathology scores of patient 2 were an AI of 12 and a chronicity index of 3. Renal biopsy in patient 3 revealed proliferative LN with glomerular basement membrane thickening (Class III-A/C +V), with an AI of 3 and chronicity index of 2 (with an AI of 4 and chronicity index of 1 before the treatment) (Fig 1K). Podocytopathies were identified in all the patients, particularly patient 3. Immunohistochemistry analysis revealed no CD19+ B-cell deposits in any case.

To identify clinical correlates of renal response following IM19 CAR T-cell therapy, we compared demographic and serological characteristics among complete or partial responders and nonresponders (Supplementary Table S6). No significant differences were observed among the 3 groups regarding sex distribution, disease duration, or background therapy. In this very small preliminary sample, we observed that ages in partial responders and nonresponders (median 37; range, 35-43) were higher than those in complete responders (median: 25.5; range, 19-32), suggesting a positive trend. Complete and partial responders exhibited higher median baseline SLEDAI-2K scores 18.5 (range, 17-20) and 17 (range, 10-24), respectively, compared to nonresponders 11 (range, 10-12). Responders exhibited higher peak IL-6 levels (range, 12.27-285.74 ng/mL) compared to nonresponders (range, 6.41-17.29 ng/mL).

To further understand the potential influencing factors of CAR T-cell treatment efficacy on LN, we did a mini-review of previous reports (Table 3) [2–4,6,8–10,24,25]. A pooled analysis of 4 published studies (1 case series study [3] and 3 open-label pilot clinical trials [8–10]), and our cohort included a total of 35 patients. Among these patients, 5 with a history of pathologically confirmed LN had pretreatment urine protein <0.5 g/d, and they were considered to have inactive disease. One patient was excluded from the analysis due to receipt of a half-dose CAR T-cell infusion, which precluded a standard assessment of efficacy [9]. The remaining 29 patients were included in the statistical analysis and categorised according to complete response achievement (Table 4). The renal complete response rate of CAR-T therapy was 72.4% (21/29), with 17.2% (5/29) of patients achieving partial response and 3 (10.3%) patients failing to respond. Our mini-review indicated that advanced age was significantly associated with suboptimal

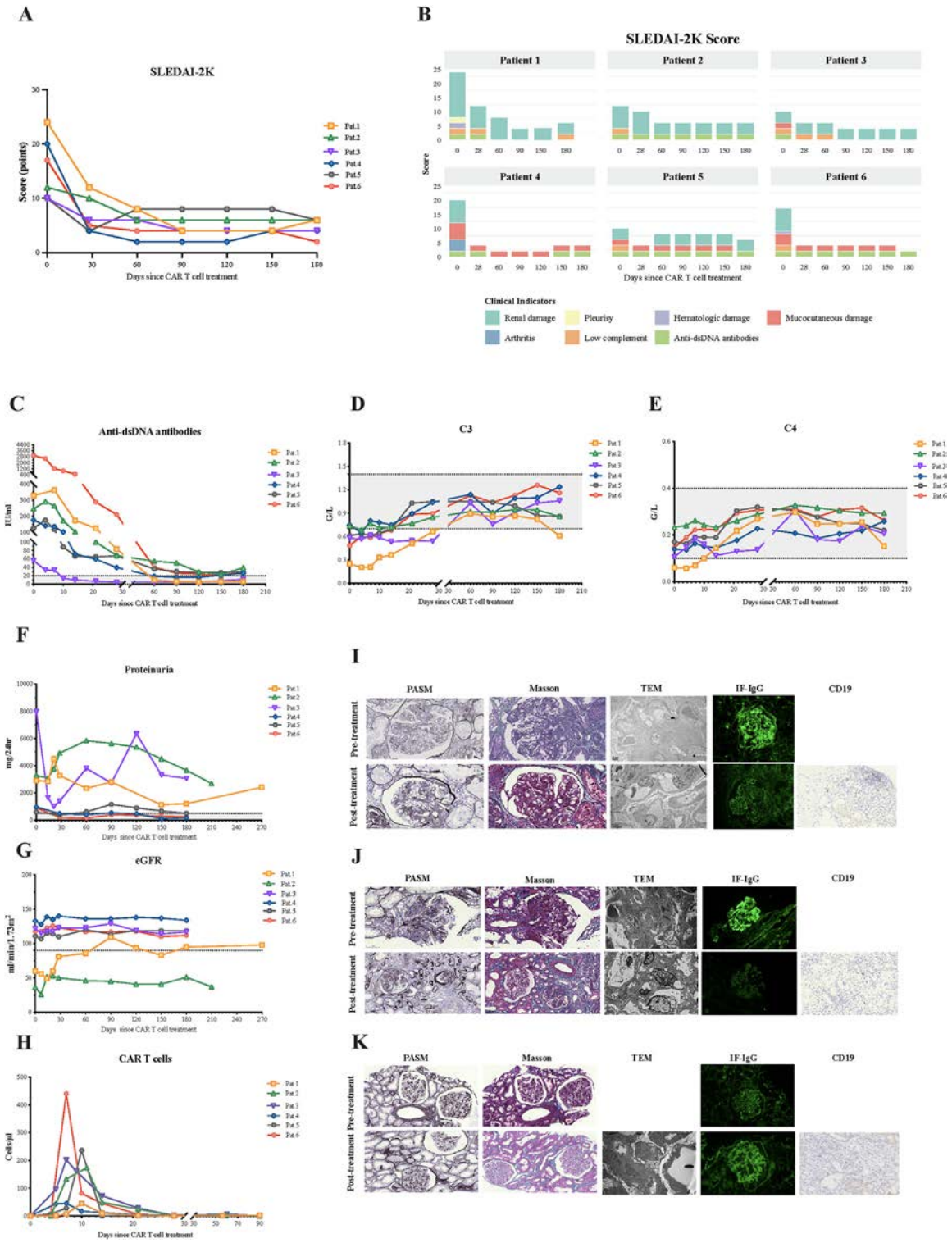

Figure 1. Effects of IM19 CAR T-cell treatment on systemic lupus erythematosus. (A) and (B) The change of SLEDAI-2K scores after IM19 administration (N = 6). At the day 120 follow-up, patient 1 was unable to undergo the scheduled urinalysis and 24-h urine protein measurement due to menstruation, which led to the missing SLEDAI-2K for that time point. (C) Anti-ds DNA antibodies assessed by radioimmunoassay after CAR T-cell administration (N = 6). (D) and (E) The change of complement factor C3 and C4 levels after IM19 administration (N = 6). (F) The change of proteinuria after CAR T-cell administration (N = 6). (G) The change of eGFR after CAR T-cell administration. (H) Circulating CAR T-cell number in the 6 patients grey within the 90 days after treatment (N = 6). (I-K) Representative histopathological images before and after CAR T-cell infusion of patient 1 (AI 7 and chronicity indexI 5 posttreatment; AI 10 and chronicity index 2 pretreatment), patient 2 (AI 9 and chronicity index 8 posttreatment; AI 12 and chronicity index 3 pretreatment), and patient 3 (AI 3 and chronicity index 2 posttreatment; AI 4 and chronicity index 1 pretreatment). TEM for the renal tissue specimen of patient 3 was not available. The shaded areas indicate the normal range in (C-F). AI, activity index; CAR, chimeric antigen receptor; C3, complement component 3; dsDNA, double-stranded DNA; eGFR, estimated glomerular filtration rate; IF, immunofluorescence; Ig, immunoglobulin; PASM, periodic acid-methenamine silver stain; SLEDAI-2K, Systemic Lupus Erythematosus Disease Activity Index-2K; TEM, transmission electron microscopy.

Table 2
Short-term safety of IM19 CAR T-cell therapy in SLE

Variables	Patient 1	Patient 2	Patient 3	Patient 4	Patient 5	Patient 6
CRS (grade)	0	1	1	1	0	1
ICANS (grade)	0	0	0	0	0	0
Bone marrow toxicity[a]	+	0	0	0	0	0
Tocilizumab treatment	0	0	+	0	0	0

CAR, chimeric antigen receptor; CRS, cytokine release syndrome; ICANS, immune effector cell–associated neurotoxicity syndrome; SLE, systemic lupus erythematosus.
[a] Bone marrow toxicity was defined as persisting grade 2 or higher thromocytopenia, leukopaenia, or granulocytopenia at or beyond day 28 post-CD19 CAR T-cell infusion.

response ($P = .001$). A trend towards higher baseline proteinuria levels was observed in patients with poor treatment response; however, this association was not statistically significant. The renal response rate was similar among CAR T-cell therapy with different targets, with 69.2% (9/13) for CD19 CAR T cells, 66.7% (4/6) for anti-BCMA-CD19 compound CAR T cells, and 71.4% (5/7) for anti-BCMA CAR T cells in LN. The incidences of CRS were also comparable among the 3 groups.

Effect on protective antibodies

The impact of IM19 on the levels of protective antibodies against viruses was assessed. The levels of antibodies against HBV, CMV, and EBV were not significantly altered after CAR T-cell therapy ($P = .999$, $P = .789$, $P = .419$, respectively, Supplementary Fig S4), suggesting preservation of humoral immunity from long-lived plasma cells.

Longitudinal B-cell reconstitution dynamics

Complete CD19+ B-cell aplasia (<5 cells/μL) was achieved in 5/6 patients by day 1 and all patients by day 4 postinfusion (Fig 2A). B-cell reconstitution occurred in 4/6 patients at a mean of 90 ± 42 days (median: 75 days; range, 60-150). Patient 2, who was a nonresponder to IM19 CAR T-cell therapy, remained in sustained B-cell aplasia at the last assessment.

Immunophenotyping revealed early B-cell reconstitution (≤180 days) dominated by naive B cells (CD20+CD27-) (Supplementary Fig S5A). CD20+CD27+ memory B cells, though markedly depleted postinfusion (Supplementary Fig S5B). Notably, CD20-CD27+ plasmablasts and CD20+CD27-CD21-CD11c+ activated memory B cells remained undetectable, suggesting profound impairment of antigen-experienced and antibody-producing capacities during early immune recovery (Supplementary Fig S5C,D).

To analyse the dynamics of the immune cell repertoire following IM19 CAR T-cell therapy, we conducted scRNA-seq to identify key transcriptional changes, along with sequencing of BCR to evaluate clonal remodelling posttreatment. In total, we profiled 77,614 PBMCs, including 6004 B cells (Fig 2B). Clustering and annotation revealed 13 distinct immune cell types identified based on canonical markers (Fig 2C, Supplementary Fig S5E). Proportions of B cells increased significantly at 180 days postinfusion (Supplementary Fig S5F). To demonstrate the landscape of B-cell reconstitution following IM19 CAR T-cell therapy, we categorised B cells into 3 subsets, namely naive B cells, activated B cells, and memory B cells, using canonical B-cell subset markers (Fig 2D,E). By day 180, the B-cell compartment consisted predominantly of naive B cells (Fig 2F). We have further investigated the interactions between B cells and other cell types (Supplementary Fig S5G). Additionally, analysis following CAR T-cell therapy revealed a significant reduction in type 1

Table 3
An overview of CAR-T therapy in patients with lupus nephritis

S.no.	Authors (year published)	No. of participants	CAR-T used	SLEDAI-2K at baseline	Proteinuria at baseline	Renal response
1	Mougiakakos et al [2] (2021)	1	Autologous anti-CD19 CAR T cell (1.1×10^6/kg)	16	2000 mg/g of creatinine	CR at 1-mo follow-up
2	Mackensen et al [4] (2022)	5	Autologous anti-CD19 CAR T cell (1.1×10^6/kg)	10 (8-16)[a]	3080 (88-8096) mg/g of creatinine[a]	CR for all patients at 3-mo follow-up
3	Müller et al [3] (2024)	8	Autologous anti-CD19 CAR T cell (1.1×10^6/kg)	13 (9.3-16)[b]	Not available	CR for 8 patients at 3-mo follow-up 1 patient had a rebound of proteinuria due to podocytopathy
4	Wang et al [9] (2024)	11	Autologous anti-BCMA-CD19 compound CAR T cells (3×10^6/kg)	10 (8-15)[b]	2143 (71-14417.2) mg/24 h[b]	CR for 9 patients at 6-mo follow-up 2 patients did not observe renal recovery
5	Taubmann et al [24] (2024)	1	Autologous anti-CD19 CAR T cell (1.1×10^6/kg)	10	3270 mg/g of creatinine	CR at 3-mo follow-up
6	Krickau et al [6] (2024)	1	Autologous anti-CD19 CAR T cell (1.1×10^6/kg)	23	10,717 mg/g of creatinine	PR at 6-mo follow-up
7	He et al [25]. (2024)	2	Autologous anti-CD19 CAR T cell (1×10^5/kg)	12	28 mg/kg/d; 64.7 mg/kg/d	CR for 1 patient and PR for 1 patient
8	Yang et al [10] (2025)	3	Allogeneic anti-CD19 CAR T cells (1×10^6/kg)	16 (14-26)[b]	0.87 (0.54-1.3) g/24 h[b]	CR for all patients at 6-mo follow-up
9	Hu et al [8] (2025)	7	Autologous BCMA CAR T cells (2.5×10^6/kg or 35×10^6)	18 (10-22)[b]	1.95 (1.10-12.22) g/24 h[b]	CR for 5 patients and PR for 2 patients at 6-mo follow-up

BCMA, B-cell maturation antigen; CAR, chimeric antigen receptor; CR, complete response; PR, partial response; SLEDAI-2K, systemic lupus erythematosus disease activity score 2000.
[a] Median (interquartile range).
[b] Median (range).

Table 4
A review of characteristics in patients with LN

Characteristics[a]	Complete responder (n = 21)	Partial + non-responders (n = 8)	p value
Age (years)	27 (23, 35)	40 (36.8, 43.2)	**0.001**[e]
Female sex, n (%)	15 (71.4)	5 (62.5)	0.999
Disease duration (years)	6 (3, 11)	8.5 (6, 13.2)	0.292
Disease activity SLEDAI-2K>12, n (%)	12 (57.1)	3 (37.5)	0.596
Proteinuria			
Proteinuria>3.5g/24 hours, n (%)	5 (23.8)	3 (37.5)	0.646
Proteinuria>1.0g/24 hours, n (%)	13 (61.9)	7 (87.5)	0.371
Renal biopsy stage			
III	3 (18.8)	0 (0.0)	0.122
III + V	2 (12.5)	0 (0.0)	
IV	7 (43.8)	5 (62.5)	
IV + V	4 (25.0)	1 (12.5)	
V	0 (0.0)	2 (25.0)	
NA	4 (30.4)	0 (0.0)	
Anti-dsDNA positive, n (%)	18 (85.7)	6 (75.0)	0.597
Anti-Sm positive, n (%)[b]	5 (27.8)	0 (0.0)	0.274
Anti-RNP positive, n (%)[b]	11 (61.1)	2 (20.0)	0.357
Anti-SSA positive, n (%)[b]	12 (66.7)	5 (71.4)	0.999
Anti-nucleosome positive, n (%)[b]	5 (27.8)	0 (0.0)	0.274
Decrease of C3, n (%)[c]	14 (77.8)	8 (100.0)	0.277
Seroconversion, n (%)	14 (66.7)	5 (62.5)	0.999
CAR-T antigen target			
Autologous CD19	9 (42.9)	4 (50.0)	0.874
Autologous BCMA	5 (23.8)	2 (25.0)	
Autologous BCMA/CD19	4 (19.0)	2 (25.0)	
Allogeneic CD19	3 (14.3)	0 (0.0)	
Adverse events[d]			
CRS, n (%)[d]	11 (64.7)	4 (66.7)	0.341
Low IgG, n (%)	13 (76.5)	6 (100.0)	0.539

BCMA, B cell maturation antigen; CAR, chimeric antigen receptor; C3, complement component 3; CRS, cytokine release syndrome; dsDNA, double-stranded DNA; Ig, immunoglubin; NA, not avalible; LN, lupus nephritis; SLEDAI-2K, systemic lupus erythematosus disease activity index-2000; Sm, Smith.
[a] Data are presented as median (interquartile, IQR) unless stated otherwise.
[b] Data are not avalible for 3 complete responsders and 1 partial + non-responders.
[c] Data are not avalible for 3 complete responsders.
[d] Data are not avalible for 4 complete responsders and 2 partial + non-responders.
[e] P value in bold indicate statistical significance (p<0.05).

interferon-stimulated gene (ISG) activity within B cells (Fig 2G, H). BCR diversity showed no significant difference before and after IM19 therapy (Fig 2I, Supplementary Fig S5H). The BCR repertoire at day 180 was substantially distinct from baseline, suggesting that the reconstituted B cells comprised mainly newly emergent clonotypes rather than pre-existing ones (Fig 2K, Supplementary Fig S5I). There was no significant difference in high-abundance TCR clones before and after treatment. Furthermore, these high-frequency TCRs were predominantly found in activated cytotoxic T cells (Fig 2J,L).

Cytokine change

Cytokine profiling showed transient IL-6 elevation in patients 2, 3, 4, and 6, peaking at 17.29, 285.74, 12.27, and 190.65 ng/mL, respectively, within 4 to 14 days postinfusion, correlating with CRS. Patient 1 exhibited elevated IL-6 levels ranging from 15.84 to 63.01 pg/mL postinfusion, yet remained asymptomatic throughout the monitoring period. IL-10 levels peaked (range, 10.2735.87 ng/mL) on day 7 postinfusion and returned to baseline within 14 days. IFN-γ and TNF-α remained within normal ranges throughout treatment (Supplementary Fig S6), indicating no pronounced T helper 1 cell (Th1)-driven cytokine storm, consistent with the mild toxicity profile.

Long-term safety

Upper respiratory tract infection constituted the most frequent AE postinfusion, occurring in 4 patients with 7 discrete episodes. A urinary tract infection occurred in patient 1 during B-cell aplasia. All patients, except patient 5, experienced low IgG and received intravenous immunoglobulin (Supplementary Table S7, Supplementary Fig S7).

DISCUSSION

This pilot study demonstrates IM19 consistently induced systemic disease improvement and B-cell depletion of both peripheral blood and kidney, and was well tolerated in patients with refractory SLE. Half of the patients achieved seroconversion. Despite improvement in the overall clinical symptoms, a notable disparity was observed in renal outcomes. The presence of chronic damage and podocytopathy, as well as older age, underlay suboptimal therapeutic outcomes. Higher baseline disease activity and elevated IL-6 peak levels were associated with a better treatment response. The mini-review confirmed that older age predicted suboptimal outcomes of CAR T-cell therapy in LN and revealed that renal response rate was similar among CAR T-cell therapies with different targets.

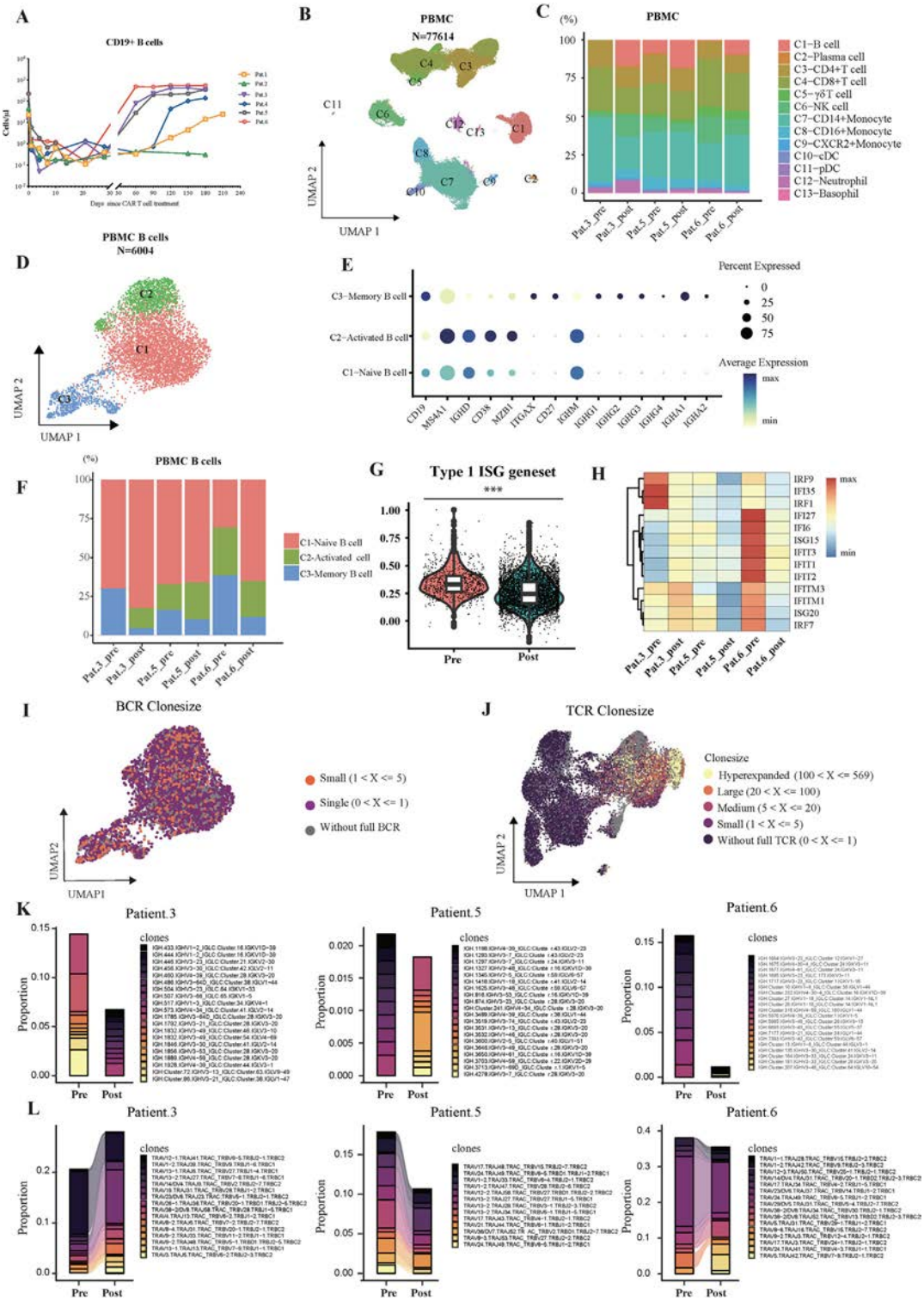

Figure 2. Longitudinal B-cell reconstitution dynamics with IM19 CAR T-cell therapy in patients with SLE. (A) Circulating B-cell numbers in the 6 patients since treatment (N = 6). (B) UMAP plot of PBMCs from patients at baseline and month 6, coloured by cell types (N = 3). (C) Proportions of major immune cell types in PBMCs. (D) UMAP plot of B cells from patients at baseline and month 6, coloured by subset (N = 3). (E) Dot plot of cell clusters annotated by expression of known marker genes of B cells. (F) Proportions of B-cell subsets before and postinfusion. (G) The violin plot shows a marked decrease in the expression of the Type 1 ISG gene set in B cells following treatment. The Kolmogorov-Smirnov test was performed. *** $P < .001$. (H) The heatmap shows the expression of type 1 ISGs in patients pre- and posttreatment. (I) and (J) UMAP plot of B cells coloured by BCR and TCR detection. (K) and (L) Bar plots show the changes in BCR and TCR repertoire postinfusion at month 6. BCR, B-cell receptor; CAR, chimeric antigen receptor; cDC, conventional dendritic cell; CXCR2, C-X-C chemokine receptor 2; ISG, interferon-stimulated gene; PBMC, peripheral blood mononuclear cell; pDC, plasmacytoid dendritic cell; SLE, systemic lupus erythematosus; TCR, T cell receptor; UMAP, Uniform Manifold Approximation and Projection.

Our study demonstrated that the new anti-CD19 CAR T product, IM19, effectively depleted peripheral B cells and enabled B-cell reconstitution. We observed that autoimmune inflammation-mediated manifestations, such as rash, arthralgia, and hypocomplementemia, were more readily alleviated following treatment, accompanied by a reduction in autoantibody levels. In contrast, one-third of the patients with LN showed suboptimal response. Responders tended to be younger and exhibited higher

baseline disease activity, as well as elevated IL-6 peak levels within 30 days postinfusion. Our results imply that patients with higher disease activity may often have a greater abundance of autoreactive B cells, and this higher antigenic burden provides a more robust stimulus for the administered CAR T cells, leading to a more potent response. The efficacy of CAR T-cell therapy is considered independent of prior treatments, as patients had maintained stable background therapy for at least 12 weeks preceding the infusion. Due to the extremely small sample size (n = 2-4/group), reliable statistical inference cannot be drawn. Based on the results of our study, a phase 1 clinical trial is now underway and will provide more definitive conclusions.

The cause of heterogeneous renal remission warrants further investigation. The study was fundamentally designed to investigate IM19 in refractory SLE. However, the fact that all enrolled patients had active LN provided a unique opportunity to perform a deep, longitudinal analysis of renal outcomes within this study. The similar response rates between CD19- and BCMA-directed CAR T therapy imply that targeting autoreactive B cells and plasma cells alone might not be sufficient for all LN subtypes. Repeated renal biopsies in our study identified chronic damage and podocytopathy as drivers of poor outcomes. Our findings underscore the need for therapies that also address the broader pathogenic environment [13]. Nonimmune mechanisms of tissue injury within the kidney, such as glomerulosclerosis, tubular atrophy, and interstitial fibrosis, may limit the effects of CAR T-cell therapy [26,27]. It is also important to note that podocytopathy may not respond to current CAR T-cell therapy. A combined approach, integrating agents that target podocyte-intrinsic pathways or fibrotic signalling, may therefore be necessary to induce complete remission in refractory LN patients [28]. Consequently, these findings underscore the necessity of histopathological stratification in patient selection for this high-cost intervention.

To better enable patient stratification based on clinical characteristics, we performed a mini-review to analyse the factors affecting renal outcomes. The result identified that the older patients with LN had lower remission rates following CAR T-cell therapy. The previous study demonstrated that age was 1 of the risk factors for damage accrual in patients with SLE [29]. Long-term comparisons showed significantly worse kidney outcomes in elderly patients than in younger adults, consistent with higher rates of advanced chronicity and systemic damage in older patients [30]. These results suggest that selecting younger patients for CAR T-cell therapy may lead to superior treatment outcomes.

Another management dilemma is the necessity of discontinuing baseline immunosuppressants during leukapheresis for autologous CAR T therapy in autoimmune patients. European Society for Blood and Marrow Transplantation (EBMT)/European Hematology Association (EHA) guidelines recommend suspending immunosuppressants at least 2 weeks before leukapheresis to avoid compromising the function and efficacy of CAR T cells [31,32], whereas this risks disease flare in the time window required for CAR T manufacturing. Most of the published studies on autologous CAR T-cell therapy have adopted this drug withdrawal regimen [33,34], whereas Schett et al [32] previously reported successful CAR T-cell generation in a patient with severe LN receiving treatment of glucocorticoid pulse and cyclophosphamide [3]. In this study, we confirmed that CAR T cells could be successfully generated without functional impairment despite ongoing immunosuppressive therapy. Data analysis showed no correlation between CAR T-cell expansion *in vivo* and immunosuppressant use at leukapheresis. Our study provided an evidence-based treatment protocol for optimising therapeutic frameworks in CAR T-cell therapy.

The analysis of the single-cell data revealed that the anti-CD19 CAR T therapy enabled B-cell reconstitution. Further analysis revealed a decrease in Type 1 ISG activity within B cells posttreatment. This suggests that CAR T-cell therapy may exert its therapeutic effects through modulation of the interferon gene expression pathway—a mechanism not previously reported in prior studies.

This study has several limitations. First, the limited follow-up duration precludes robust assessment of long-term efficacy, relapse risks post-B-cell reconstitution, and late-onset toxicities. In response, we are currently extending follow-up to 36 months for all enrolled patients. Second, the restricted cohort size limits subgroup analysis. Multicentre phase I study is now ongoing. Based on the result of this study, prospective validation through universal baseline renal biopsies is now implemented in our ongoing trial. Third, our study did not strictly require a renal biopsy within 1 year before CAR T-cell infusion. Given the prolonged disease duration, chronic kidney changes may have already developed in these patients. This complicates the interpretation of the results—including the repeat biopsy data—and may have limited the potential for complete proteinuria reversal. Comparative renal pathology, before and after treatment, offers valuable insights for patients with LN, irrespective of whether clinical response is good or poor.

Conclusion

IM19 CAR T-cell therapy achieved rapid and clinically meaningful improvements in patients with refractory SLE with a favourable safety profile. Divergent renal responses highlight the critical influence of renal pathology phenotypes on therapeutic efficacy in LN. Additionally, advanced age may predict diminished clinical benefit from CAR T therapy. These findings urge stratification based on baseline clinical and histopathological characteristics in future trials. Definitive evidence for integrating this approach into SLE treatment paradigms will require large-scale multicentre trials using renal histopathology-guided stratification.

Competing interests

All authors declare they have no competing interests.

CRediT authorship contribution statement

Jinxia Zhao: Writing – original draft, Project administration, Methodology, Investigation, Formal analysis. **Xiaoying Zhang:** Writing – original draft, Resources, Project administration, Methodology, Investigation, Formal analysis. **Yime Zhang:** Software, Methodology, Formal analysis. **Xinyi Li:** Project administration, Investigation, Data curation. **Hui Wei:** Resources, Investigation, Data curation. **Yinji Jin:** Resources, Investigation, Data curation. **Rui Liu:** Resources, Investigation. **Zhaohua Li:** Resources, Investigation. **Wei Guo:** Resources, Investigation. **Zhenqing Wang:** Project administration, Investigation. **Yue Guo:** Project administration, Investigation. **Yunxia Xia:** Resources, Investigation. **Yang Yu:** Supervision. **Haijing Liu:** Visualization, Investigation. **Lin Zeng:** Methodology, Formal analysis. **Qiang Shu:** Resources, Investigation. **Jinlian Sun:** Supervision, Methodology. **Yang Tian:** Resources,

Methodology. **Yanping Ding:** Resources, Methodology. **Ting He:** Resources, Methodology. **Xin'an Lu:** Supervision, Resources. **Lin Sun:** Project administration, Investigation. **Rong Mu:** Writing – review & editing, Visualization, Validation, Resources, Project administration, Methodology, Investigation, Funding acquisition, Conceptualization.

Acknowledgements

The authors would like to thank all the participants. The authors thank Jiansuo Zhou and Yan Qiao for their assistance with laboratory methods. The authors also thank Guanlin Li, Hui Liu, and Haifang Wang for their assistance with CAR T-cell product quality control.

Contributors

RM designed the study, and supervised the study and the writing. JZ conceived the project, recruited patients, and wrote the original draft. XZ contributed to data analysis, interpretation, and visualisation, and wrote the original draft. XL, HW, YJ, RL, YG, YX, ZW, and QS recruited and took care of patients. YZ contributed to bioinformatics analysis. ZL, WG, and LS collected samples and extracted clinical data. HL interpreted the renal biopsy results. LZ contributed to the statistical analysis. YY supervised the study and contributed to product quality control. JS, YT, YD, TH, and XL managed cell product manufacturing and quality control. All authors contributed to drafting the manuscript or revising it critically for important intellectual content, provided final approval of the final manuscript, and agreed to be accountable for all aspects of the work.

Funding

This work was supported by a grant from the National Natural Science Foundation of China (32288102). The study was partially supported by Imunopharm Technology Co, Ltd.

Patient consent for publication

Consent obtained directly from patients.

Ethics approval

The study was approved by the Ethics Committee of Peking University Third Hospital (M2023469). All patients provided written informed consent.

Provenance and peer review

Externally peer reviewed.

Supplementary materials

Supplementary material associated with this article can be found in the online version at doi:10.1016/j.ard.2025.12.014.

REFERENCES

[1] Scherlinger M, Nocturne G, Radic M, Launay D, Richez C, Bousso P, et al. CAR T-cell therapy in autoimmune diseases: where are we and where are we going? Lancet Rheumatol 2025 Jun;7(6):e434–47. doi: 10.1016/s2665-9913(24)00377-1.

[2] Mougiakakos D, Krönke G, Völkl S, Kretschmann S, Aigner M, Kharboutli S, et al. CD19-Targeted CAR T cells in refractory systemic lupus erythematosus. N Engl J Med 2021 Aug 5;385(6):567–9. doi: 10.1056/NEJMc2107725.

[3] Müller F, Taubmann J, Bucci L, Wilhelm A, Bergmann C, Völkl S, et al. CD19 CAR T-cell therapy in autoimmune disease - a case series with follow-up. N Engl J Med 2024 Feb 22;390(8):687–700. doi: 10.1056/NEJMoa2308917.

[4] Mackensen A, Müller F, Mougiakakos D, Böltz S, Wilhelm A, Aigner M, et al. Anti-CD19 CAR T cell therapy for refractory systemic lupus erythematosus. Nat Med 2022 Oct;28(10):2124–32. doi: 10.1038/s41591-022-02017-5.

[5] Li M, Zhang Y, Jiang N, Ning C, Wang Q, Xu D, et al. Anti-CD19 CAR T cells in refractory immune thrombocytopenia of SLE. N Engl J Med 2024 Jul 25;391(4):376–8. doi: 10.1056/NEJMc2403743.

[6] Krickau T, Naumann-Bartsch N, Aigner M, Kharboutli S, Kretschmann S, Spoerl S, et al. CAR T-cell therapy rescues adolescent with rapidly progressive lupus nephritis from haemodialysis. Lancet 2024 Apr 27;403(10437):1627–30. doi: 10.1016/s0140-6736(24)00424-0.

[7] Hagen M, Müller F, Wirsching A, Kharboutli S, Spörl S, Aigner M, et al. Treatment of CNS systemic lupus erythematosus with CD19 CAR T cells. Lancet 2024 Nov 30;404(10468):2158–60. doi: 10.1016/s0140-6736(24)02265-7.

[8] Hu Z, Cai S, Yu Y, Chen Y, Wang B, Wang D, et al. BCMA-targeted CAR T cell therapy can effectively induce disease remission in refractory lupus nephritis. Ann Rheum Dis 2025 Jul 17;84:1675–83. doi: 10.1016/j.ard.2025.06.2128.

[9] Wang W, He S, Zhang W, Zhang H, DeStefano VM, Wada M, et al. BCMA-CD19 compound CAR T cells for systemic lupus erythematosus: a phase 1 open-label clinical trial. Ann Rheum Dis 2024 Sep 30;83(10):1304–14. doi: 10.1136/ard-2024-225785.

[10] Yang C, Sun C, Tan B, Hu C, Wan L, Wang C, et al. Allogeneic anti-CD19 CAR-T cells induce remission in refractory systemic lupus erythematosus. Cell Res 2025 May 8;35:607–9. doi: 10.1038/s41422-025-01128-1.

[11] Mc Laughlin AM, Milligan PA, Yee C, Bergstrand M. Model-informed drug development of autologous CAR-T cell therapy: strategies to optimize CAR-T cell exposure leveraging cell kinetic/dynamic modeling. CPT Pharmacometrics Syst Pharmacol 2023 Nov;12(11):1577–90. doi: 10.1002/psp4.13011.

[12] June CH, Sadelain M. Chimeric antigen receptor therapy. N Engl J Med 2018 Jul 5;379(1):64–73. doi: 10.1056/NEJMra1706169.

[13] Mohan C, Zhang T, Putterman C. Pathogenic cellular and molecular mediators in lupus nephritis. Nat Rev Nephrol 2023 Aug;19(8):491–508. doi: 10.1038/s41581-023-00722-z.

[14] Rovin BH, Furie R, Latinis K, Looney RJ, Fervenza FC, Sanchez-Guerrero J, et al. Efficacy and safety of rituximab in patients with active proliferative lupus nephritis: the lupus nephritis assessment with rituximab study. Arthritis Rheum 2012 Apr;64(4):1215–26. doi: 10.1002/art.34359.

[15] Furie RA, Rovin BH, Garg JP, Santiago MB, Aroca-Martínez G, Zuta Santillán AE, et al. Efficacy and safety of obinutuzumab in active lupus nephritis. N Engl J Med 2025 Apr 17;392(15):1471–83. doi: 10.1056/NEJMoa2410965.

[16] Aringer M, Costenbader K, Daikh D, Brinks R, Mosca M, Ramsey-Goldman R, et al. 2019 European League Against Rheumatism/American College of Rheumatology classification criteria for systemic lupus erythematosus. Ann Rheum Dis 2019 Sep;78(9):1151–9. doi: 10.1136/annrheumdis-2018-214819.

[17] Gladman DD, Ibañez D, Urowitz MB. Systemic lupus erythematosus disease activity index 2000. J Rheumatol 2002 Feb;29(2):288–91.

[18] Lee DW, Santomasso BD, Locke FL, Ghobadi A, Turtle CJ, Brudno JN, et al. ASTCT consensus grading for cytokine release syndrome and neurologic toxicity associated with immune effector cells. Biol Blood Marrow Transplant 2019 Apr;25(4):625–38. doi: 10.1016/j.bbmt.2018.12.758.

[19] Franklyn K, Lau CS, Navarra SV, Louthrenoo W, Lateef A, Hamijoyo L, et al. Definition and initial validation of a Lupus Low Disease Activity State (LLDAS). Ann Rheum Dis 2016 Sep;75(9):1615–21. doi: 10.1136/annrheumdis-2015-207726.

[20] Kidney Disease: Improving Global Outcomes (KDIGO) Lupus Nephritis Work Group. KDIGO 2024 clinical practice guideline for the management of LUPUS NEPHRITIS. Kidney Int 2024 Jan;105(1s):S1–69. doi: 10.1016/j.kint.2023.09.002.

[21] Hagen M, Müller F, Wirsching A, Kharboutli S, Spoerl S, Düsing C, et al. Local immune effector cell-associated toxicity syndrome in CAR T-cell treated patients with autoimmune disease: an observational study. Lancet Rheumatol 2025 Apr 30;7:e424–33. doi: 10.1016/s2665-9913(25)00091-8.

[22] Ying Z, He T, Jin S, Wang X, Zheng W, Lin N, et al. A durable 4-1BB-based CD19 CAR-T cell for treatment of relapsed or refractory non-Hodgkin lymphoma. Chin J Cancer Res 2022 Feb 28;34(1):53–62. doi: 10.21147/j.issn.1000-9604.2022.01.05.

[23] Rojo R, Calvo Alén J, Prada Á, Valor S, Roy G, López-Hoyos M, et al. Recommendations for the use of anti-dsDNA autoantibodies in the diagnosis and follow-up of systemic lupus erythematosus - a proposal from an expert panel.

Autoimmun Rev 2023 Dec;22(12):103479. doi: 10.1016/j.autrev.2023.103479.
[24] Taubmann J, Müller F, Yalcin Mutlu M, Völkl S, Aigner M, Bozec A, et al. CD19 Chimeric antigen receptor T cell treatment: unraveling the role of B cells in systemic lupus erythematosus. Arthritis Rheumatol Apr 2024;76(4):497–504. doi: 10.1002/art.42784.
[25] He X, Hu B, Zhang Y, Liu F, Li Q, Zheng C, et al. Treatment of two pediatric patients with refractory systemic lupus erythematosus using CD19-targeted CAR T-cells. Autoimmun Rev 2024;24(1):103692 Nov 17. doi: 10.1016/j.autrev.2024.103692.
[26] Davidson A. What is damaging the kidney in lupus nephritis? Nat Rev Rheumatol 2016 Mar;12(3):143–53. doi: 10.1038/nrrheum.2015.159.
[27] Remuzzi G, Benigni A, Remuzzi A. Mechanisms of progression and regression of renal lesions of chronic nephropathies and diabetes. J Clin Invest 2006 Feb;116(2):288–96. doi: 10.1172/jci27699.
[28] Ahmadian E, Eftekhari A, Atakishizada S, Valiyeva M, Ardalan M, Khalilov R, et al. Podocytopathy: the role of actin cytoskeleton. Biomed Pharmacother 2022 Dec;156:113920. doi: 10.1016/j.biopha.2022.113920.
[29] Bruce IN, O'Keeffe AG, Farewell V, Hanly JG, Manzi S, Su L, et al. Factors associated with damage accrual in patients with systemic lupus erythematosus: results from the Systemic Lupus International Collaborating Clinics (SLICC) Inception Cohort. Ann Rheum Dis 2015 Sep;74(9):1706–13. doi: 10.1136/annrheumdis-2013-205171.
[30] Calatroni M, Andrulli S, Doti F, Bello F, De Vivo G, Mastrangelo A, et al. Long-term prognosis of lupus nephritis: comparison between pediatric, adult, and advanced age onset. Front Immunol 2025;16:1531675. doi: 10.3389/fimmu.2025.1531675.
[31] Greco R, Alexander T, Del Papa N, Müller F, Saccardi R, Sanchez-Guijo F, et al. Innovative cellular therapies for autoimmune diseases: expert-based position statement and clinical practice recommendations from the EBMT practice harmonization and guidelines committee. EClinicalMedicine 2024 Mar;69:102476. doi: 10.1016/j.eclinm.2024.102476.
[32] Schett G, Mackensen A, Mougiakakos D. CAR T-cell therapy in autoimmune diseases. Lancet 2023 Nov 25;402(10416):2034–44. doi: 10.1016/s0140-6736(23)01126-1.
[33] Auth J, Müller F, Völkl S, Bayerl N, Distler JHW, Tur C, et al. CD19-targeting CAR T-cell therapy in patients with diffuse systemic sclerosis: a case series. Lancet Rheumatol 2025 Feb;7(2):e83–93. doi: 10.1016/S2665-9913(24)00282-0.
[34] Pecher AC, Hensen L, Klein R, Schairer R, Lutz K, Atar D, et al. CD19-Targeting CAR T cells for myositis and interstitial lung disease associated with antisynthetase syndrome. JAMA 2023 Jun 27;329(24):2154–62. doi: 10.1001/jama.2023.8753.

Ann Rheum Dis 85 (2026) 848–857

Contents lists available at ScienceDirect

Annals of the Rheumatic Diseases

journal homepage: https://www.sciencedirect.com/journal/annals-of-the-rheumatic-diseases

Systemic lupus erythematosus

Untargeted breathomics identifies metabolic signatures of immune activity, intestinal integrity, and fatigue in systemic lupus erythematosus

Ioannis Parodis[1,2,*], Martina Iacubino[3], Lorenzo Rocco[3], Dionysis Nikolopoulos[1], Leonardo Palazzo[1], Liam Grimmett[4], Matt Kerr[4], Chiara Bellocchi[3,5], Barbara Vigone[3], Alessandro Santaniello[3], Guillermo Barturen[6,7], Alexandre E. Voskuyl[8], Marta E. Alarcón-Riquelme[6,9], Lorenzo Beretta[3,**]

[1] *Division of Rheumatology, Department of Medicine Solna, Karolinska Institutet, Karolinska University Hospital, and Center for Molecular Medicine (CMM), Stockholm, Sweden*
[2] *Department of Rheumatology, Faculty of Medicine and Health, Örebro University, Örebro, Sweden*
[3] *Fondazione IRCCS Ca' Granda Ospedale Maggiore Policlinico di Milano, Referral Center for Systemic Autoimmune Diseases, Milan, Italy*
[4] *Owlstone Medical Ltd, Cambridge, UK*
[5] *Department of Clinical Sciences and Community Health, Department of Excellence 2023–2027, University of Milan, Milan, Italy*
[6] *GENyO, Center for Genomics and Oncological Research Pfizer/University of Granada, Department of Medical Genomics, Granada, Spain*
[7] *Department of Genetics, Faculty of Sciences, University of Granada, Granada, Spain*
[8] *Department of Rheumatology and Clinical Immunology, Amsterdam Rheumatology and Immunology Center, Amsterdam UMC, Amsterdam, the Netherlands*
[9] *Department of Environmental Medicine, Karolinska Institutet, Stockholm, Sweden*

ARTICLE INFO

Article history:
Received 8 July 2025
Received in revised form 7 December 2025
Accepted 9 December 2025

ABSTRACT

Objectives: Systemic lupus erythematosus (SLE) is a complex autoimmune disease with pronounced clinical heterogeneity and symptom burden. Despite growing knowledge of SLE biology, sensitive noninvasive biomarkers for monitoring disease activity remain lacking. This study aimed to characterise the breath metabolome in SLE and to explore associations between volatile organic compounds (VOCs) and clinical features, including disease activity and fatigue.

Methods: Exhaled breath was collected from 30 SLE patients and 30 matched healthy controls using the ReCIVA Breath Sampler and analysed by thermal desorption gas chromatography-mass spectrometry. VOCs were identified using high-resolution libraries and classified by confidence levels. Associations with clinical and patient-reported outcomes were evaluated, including disease activity indices, fatigue scores, Definition Of Remission In SLE remission, and Lupus Low Disease Activity State.

Results: Of 1433 detected VOCs, 539 exhibited levels over background and were considered breath-derived. Distinct breathomic signatures discriminated patients from controls and stratified patients by SLE activity and fatigue burden. Five VOC clusters were identified. Methyl acetate was inversely associated with disease activity and fatigue, suggesting a role in immune homeostasis. A cluster of branched alkenes and alcohols was associated with active disease and greater fatigue,

*Correspondence to Dr. Ioannis Parodis, Division of Rheumatology, Department of Medicine Solna, Karolinska Institutet and Karolinska University Hospital, Stockholm, Sweden.

**Correspondence to Dr. Lorenzo Beretta, Referral Center for Systemic Autoimmune Diseases, Fondazione IRCCS Ca' Granda, Ospedale Maggiore Policlinico di Milano, Milan, Italy.

E-mail addresses: ioannis.parodis@ki.se (I. Parodis), lorenzo.beretta@policlinico.mi.it (L. Beretta).

Handling editor Josef S. Smolen.

https://doi.org/10.1016/j.ard.2025.12.005

aligning with oxidative stress and lipid peroxidation. Nitrogen-containing heterocycles displayed U-shaped patterns across disease states, potentially reflecting varying intestinal permeability.
Conclusions: This is the first study to characterise the breath metabolome in SLE. VOC signatures reflected immunometabolic perturbations, oxidative stress, and gut barrier integrity. Breathomics may provide a noninvasive means to monitor disease activity and symptom burden in SLE.

WHAT IS ALREADY KNOWN ON THIS TOPIC

- Metabolomic alterations in systemic lupus erythematosus (SLE) have been identified in urine, blood, and stool.
- Fatigue in SLE is common, multifactorial, and not fully explained by disease activity.
- Breathomics has shown promise in other systemic and inflammatory diseases.

WHAT THIS STUDY ADDS

- This is the first study to explore breathomics in SLE using high-resolution untargeted volatile organic compound (VOC) profiling.
- Distinct breath signatures associated with disease activity, immune regulation, gut permeability, and fatigue were identified.
- Methyl acetate emerged as a potential marker of immune homeostasis, and branched alkenes as markers of lipid peroxidation and fatigue.

HOW THIS STUDY MIGHT AFFECT RESEARCH, PRACTICE OR POLICY

- Breathomics may serve as a noninvasive tool for monitoring disease activity and symptom burden in SLE.
- The study findings support further exploration of VOCs as biomarkers for patient stratification and treatment response in future SLE studies.

INTRODUCTION

Systemic lupus erythematosus (SLE) is a complex, multifactorial autoimmune disease characterised by clinical manifestations involving multiple organs and systems, along with biochemical alterations indicative of immune system activation [1]. Despite recent advances in the understanding of SLE pathogenesis, its aetiology remains elusive, and treatment outcomes are still largely unsatisfactory, with patients experiencing alternating phases of remission and flare. The approval of novel targeted therapies has broadened therapeutic options for clinicians [2], yet treatment failure rates remain disappointingly high. A key barrier to effective patient stratification and treatment allocation is the lack of sufficiently sensitive and specific biomarkers beyond standard clinical and laboratory measures [3], likely contributing to heterogeneous and incomplete therapeutic responses. Addressing this limitation is essential for improving diagnostic precision and treatment efficacy. In this context, omics technologies provide powerful tools to elucidate disease mechanisms and enhance patient classification, potentially improving clinical outcomes [4].

Metabolomics, the comprehensive analysis of metabolites in biological samples such as saliva, faeces, urine, and breath, offers a holistic overview of physiological and pathological processes [5]. By capturing the dynamic interplay between endogenous physiology and environmental exposures, metabolomics enables the identification of disease-associated metabolic perturbations. Metabolomic markers may be rapidly translated into assays for patient stratification and serve as pharmacodynamic indicators of therapeutic response, thereby supporting personalised medicine [6]. In SLE, diverse metabolomic approaches have been applied to study lipid, amino acid, gut microbiota, and urinary profiles, aiming to elucidate pathogenesis, refine diagnostic criteria, and inform pharmacometabolomics [7].

Breathomics, a subfield of metabolomics, investigates volatile organic compounds (VOCs) in exhaled breath and has recently emerged as a promising research avenue. The lung acts as a dynamic interface for VOC exchange, reflecting systemic pathological processes. Breath analysis offers a noninvasive, repeatable sampling method with considerable clinical appeal [8]. While most breathomic studies to date have focused on respiratory disorders, VOC perturbations have been reported in malignancies, infections, gastrointestinal and hepatic conditions [9], cardiovascular diseases [10], and autoimmune disorders [11,12]. Nonetheless, breathomics is challenged by issues of standardisation and consistency in breath collection and analysis. Environmental contaminants and dietary-derived compounds may influence VOC profiles [13]. To mitigate these issues, standardised collection protocols and analytical methods have been developed. Interpretation of biologically meaningful VOCs is aided by reference libraries of chemically confirmed endogenous and exogenous compounds, such as the Breath Biopsy VOC Atlas [14] and other established databases.

In the present study, we aimed to identify, for the first time, breathomic signatures in a well-characterised cohort of SLE patients using state-of-the-art methodologies [15]. Our focus was on the discovery of putative noninvasive biomarkers of disease activity, inflammation, dysbiosis, and fatigue, the latter being a highly prevalent and debilitating symptom in patients with SLE, which often shows a weak correlation with disease activity [16].

METHODS

Patients

This monocentric case–control study included 30 patients fulfilling the 2019 European Alliance of Associations for Rheumatology/American College of Rheumatology Classification Criteria for SLE [17], and 30 healthy controls, matched for age and biological sex with the patients. None of the study participants were current smokers, a restriction imposed to minimise exogenous VOC contamination, and none had a documented history of interstitial lung disease or chronic respiratory disease requiring inhaled corticosteroids. Participants were recruited at the Policlinico Hospital, Milan, Italy, within the framework of the European Taxonomy, Treatment, Targets and Remission (3TR) initiative (https://www.3tr-imi.eu). The study protocol was approved by the local ethics review board, and all participants provided written informed consent for recruitment in the study.

Relevant clinical data were extracted from the 3TR electronic case report form hosted at Karolinska Institutet, including Systemic Lupus Erythematosus Disease Activity Index 2000 (SLEDAI-2K) scores [18], British Isles Lupus Assessment Group (BILAG)-2004 index scores [19], current medications, as well as physician's global assessment (PhGA) and patient's global assessment (PtGA) using visual analogue scales (VAS).

Laboratory assessments included anti-double-stranded DNA (dsDNA) antibodies and complement component 3 (C3) and complement component 4 (C4) levels, analysed according to local laboratory standards. Disease state was further classified according to the Lupus Low Disease Activity State (LLDAS) criteria [20] and the Definition Of Remission In SLE (DORIS) criteria [21]. Transformation of BILAG-2004 evaluations into scores was conducted according to standardised recommendations by the index developers [22].

All participants completed the Functional Assessment of Chronic Illness Therapy-Fatigue (FACIT-F) questionnaire [23], which ranges from 0 to 52, with higher scores reflecting lower levels of fatigue. Fatigue was also assessed using a 0 to 100 VAS, where higher scores indicate greater fatigue over the preceding week, and the fatigue subscale of the Lupus Quality of Life (LupusQoL) questionnaire [24], where higher scores reflect a greater impact of fatigue over a short timeframe of 4 days.

Analytical procedures

Sample collection and analysis

A detailed methodologic description is available in the online Supplementary Methods. In brief, exhaled breath was collected using the ReCIVA Breath Sampler with a mouthpiece (Owlstone Medical Ltd), while participants inhaled clean air provided by the CASPER Portable Air Supply. Exhaled air was captured onto Breath Biopsy Cartridges comprising 4 Tenax TA/Carbograph 5TD sorbent tubes (Markes International). Background blank samples were collected using the same cartridges and workflow to enable discrimination of environmental/background VOCs from breath-derived signals. To optimise sample integrity and selectively capture the VOC-rich alveolar fraction, only the latter half of the exhalation—representing alveolar gas from the lower airways—was collected, excluding the initial dead space air. Samples were subsequently dry purged to remove excess water and stored at 4°C pending analysis.

Breath samples were analysed via thermal desorption gas chromatography/mass spectrometry, following a prespecified protocol to minimise analytical bias. Samples were randomised across 4 analytical sequences, each comprising up to 30 samples, with breath samples interspersed with purpose-collected background blank samples to monitor analytical performance and minimise batch effects.

Data preparation

Breath analysis produced an untargeted feature table, where each molecular feature was defined by a deconvoluted mass spectrum. Peak areas of quantifier ions, representing relative concentrations, were used for statistical analysis.

To enhance data quality, a 2-step filtering and imputation process was applied. VOCs present in fewer than 80% of breath samples were excluded. For retained features, remaining missing values (assumed to be below the limit of detection) were imputed at 80% of the minimum observed intensity for that feature across all groups. An in-house normalisation method, using internal standards to adjust for instrumental variability and analytical drift, was employed to ensure comparability across analytical sequences.

Feature identification was carried out using the Owlstone Medical high-resolution accurate mass (HRAM) spectral library. Features not found in the HRAM library were matched against the National Institute of Standards and Technology electron impact reference libraries. VOC identifications were assigned confidence levels based on the Metabolomics Standards Initiative (MSI) criteria (see Supplementary Table S1 in the Supplementary Methods).

Statistical analysis

To identify VOCs genuinely present in exhaled breath and minimise type II error, analysis was limited to VOCs classified as 'on-breath' by at least one of the following criteria: (i) VOC levels in ≥50% of samples in either group exceeding the blank mean + 3 SDs; (ii) statistically significant sample-to-blank differences (one-sided test, $P < .05$) and exceeding a 2-fold change; (iii) VOCs demonstrating an area under the receiver operating characteristic curve >0.8 compared to blanks.

All concentrations were $\log_{10}$-transformed prior to analysis. Outliers were handled using a double mean absolute deviation method [25], incorporating the Harrell-Davis quantile estimator.

Linear regression models tested associations between VOCs and disease status, with covariates for adjustment including age, sex, collection date, time since the last meal (hours), time since the last drink (hours), body mass index (BMI), and time since tooth brushing (hours). In these models, β coefficients represent expected $\log_{10}$ fold-changes per unit change in the predictor. Partial correlations adjusted for the aforementioned covariates were estimated using robust Pearson's correlation (rw) [26], which is resilient to deviations from normality, small sample sizes, and outliers. Effect sizes were quantified using covariate-adjusted robust Cohen's d (dr) [27].

Principal component analysis (PCA) on covariate-adjusted residuals was used as an exploratory tool to summarise shared variance among VOCs. PCA was first applied to the group of VOCs forming cluster 2 (branched alkenes and alcohols), which showed the broadest set of clinical associations, to visualise their multidimensional structure. A global PCA of all breath-derived VOCs indicated that the orthogonal reduction provided a poor explanation of the data, with principal component (PC)1 and PC2 together accounting for only about 30% of the variance and the first 5 components accounting for <50%.

For descriptive analyses, pairwise t-tests were used for normally distributed variables; otherwise, the nonparametric Mann–Whitney U test was applied. Results are expressed as mean ± SD or median with IQR, as appropriate. Only VOCs identified at MSI Tier 1 (validated) or Tier 2 (putative) levels with $P < .1$ are presented and discussed in detail.

RESULTS

Patient characteristics

Of the total collected samples, 30 from SLE patients and 29 from healthy controls passed the quality control. There were no significant differences between the 2 groups in key demographic characteristics (Table).

Most patients exhibited quiescent disease, as reflected by low SLEDAI-2K and BILAG-2004 scores, low PhGA and PtGA values, and a low requirement for glucocorticoids. Accordingly, two-thirds of the patients (n = 20; 66.6%) fulfilled the criteria for LLDAS. However, only 6 of these 20 patients (30%) also had negative serologies (normal complement levels and absence of anti-dsDNA antibodies).

Patients in LLDAS had significantly higher FACIT-F scores compared to those not in LLDAS (median = 43.5, IQR = 38.5 to 40.25 vs median = 32, IQR = 19.5 to 39.5; $P = .022$), suggesting less fatigue. Compared to healthy controls, SLE patients

Table
Demographic and clinical characteristics

Variable	SLE (n = 30)	Controls (n = 29)	*P* value
Age, mean ± SD	46.3 ± 13.8	46.7 ± 14.7	NS
Women, n (%)	25 (83.3%)	24 (82.8%)	NS
BMI, mean ± SD	23.5 ± 4.7	23.9 ± 3.6	NS
Time since last meal (h), mean ± SD	7.1 ± 5.6	7.7 ± 5.3	NS
Time since last drink (h), mean ± SD	4.3 ± 4.4	3.7 ± 4.2	NS
Time since brushing teeth (h), mean ± SD	3.8 ± 2.1	4.1 ± 2.5	NS
Disease duration (y), mean ± SD	14 ± 10.4	-	-
SLEDAI-2K, median (IQR)	2.5 (1.3-5.8)	-	-
BILAG-2004, median (IQR)	5 (1-10)	-	-
PhGA (0-3), median (IQR)	0.3 (0.2-0.8)	-	-
PtGA (0-100), median (IQR)	40 (2.5-70.0)	-	-
Low C3 and/or low C4, n (%)	18 (60.0%)	-	-
Increased anti-dsDNA binding, n (%)	14 (46.7%)	-	-
Steroid use, n (%)	18 (60.0%)	-	-
Steroid dose (mg/day), mean ± SD	2.6 ± 2.7	-	-
Hydroxychloroquine use, n (%)	21 (70.0%)	-	-
Immunosuppressant use, n (%)	13 (43.3%)	-	-
LLDAS, n (%)	20 (66.6%)	-	-
DORIS remission, n (%)	13 (43.3%)	-	-
FACIT-F, median (IQR)	41.5 (31.5-47.5)	48.0 (44.0-51.0)	$<2.2 \times 10^{-16}$
VAS fatigue (0-100), median (IQR)	50 (0-80)	0 (0-10)	3.2×10^{-4}
LupusQoL fatigue (0-100), median (IQR)	81.3 (51.6-93.7)	-	-

Anti-dsDNA, anti-double stranded DNA antibodies; BILAG, British Isles Lupus Assessment Group; BMI, body mass index; C4, complement component 4; C3, complement component 3; DORIS, Definition Of Remission In Systemic lupus erythematosus; FACIT-F, Functional Assessment of Chronic Illness Therapy-Fatigue; LLDAS, Lupus Low Disease Activity State; LupusQoL, Lupus Quality of Life; NS, nonsignificant; PhGA, physician's global assessment; PtGA, patient's global assessment; SLE, systemic lupus erythematosus; SLEDAI-2K, Systemic Lupus Erythematosus Disease Activity Index 2000; VAS, visual analogue scale.
Values are expressed as the mean ± SD, except for non-normally distributed data, where the median and IQR are indicated. For FACIT-F and LupusQoL fatigue, higher values indicate lower levels of fatigue.

showed significantly lower FACIT-F scores (median = 41.5, IQR = 31.5 to 47.5 vs median = 48, IQR = 45 to 51; $P < 2.2 \times 10^{-16}$), indicating a higher fatigue burden.

VOC analysis

Total VOC peak areas did not significantly differ between SLE patients (9151 ± 32.9) and healthy controls (9080 ± 35.5), suggesting no systematic bias in the sample collection. Of 1433 molecular features retained after quality control, 539 VOCs (37.6%) fulfilled at least one predefined criterion for being 'on-breath' and were included in statistical analyses. The distribution of these VOCs across healthy controls and SLE subgroups (LLDAS vs non-LLDAS; DORIS remission vs nonremission) is shown in Supplementary Figure.

Significant differences in VOC profiles were observed between SLE patients and healthy controls, between patients in LLDAS vs non-LLDAS, and between patients in DORIS remission vs. nonremission. Additionally, multiple VOCs correlated with clinical indices of disease activity (LLDAS, DORIS remission, SLEDAI-2K, BILAG-2004, PhGA, PtGA), as well as patient-reported fatigue assessed with the FACIT-F, VAS fatigue, and LupusQoL fatigue scores (see online Supplementary Tables S1 to S9).

Associations meeting either the exploratory threshold ($P < .1$) or the canonical significance threshold ($P < .05$), and with effect size $|dr| > 0.5$ and either $|\log_{10}FC| > \log_{10}(1.5)$ for categorical variables or $|rw| > 0.3$ for continuous variables, are summarised in online Supplementary Tables S10 to S14.

VOC clusters associated with disease activity and fatigue

The heatmap in Figure 1 displays the effect sizes (dr) for selected VOCs that were significantly associated with both SLEDAI-2K and LLDAS ($P < .05$). Among those VOCs, none was associated with levels of anti-dsDNA antibodies or C3 levels, while levels of glycerol and 3-pentanol were inversely correlated with C4 levels (rw = −0.373; $P = .042$ and rw = −0.451; $P = .014$, respectively). Five distinct VOC clusters were identified, as detailed below.

Cluster 1: Methyl acetate

Methyl acetate formed a unique cluster, standing apart from all other compounds. It showed positive associations with LLDAS and DORIS remission, and inverse associations with SLEDAI-2K, BILAG-2004, PhGA, and PtGA scores. Moreover, methyl acetate was inversely associated with fatigue, as measured by LupusQoL fatigue scores. Its levels were significantly lower in SLE patients compared to healthy controls (dr = −1.21, $\log_{10}FC = -0.3$, $P = .003$). Individual concentrations stratified by LLDAS status are shown in Figure 2.

Cluster 2: Branched alkenes and alcohols

This cluster included 4 VOCs, ie, 3-methyl-2-pentene, 2-methyl-1-butene, dipropenyl, and 3-pentanol, all of which were associated with increased disease activity, absence of LLDAS or DORIS remission, and increased fatigue. PCA on covariate-adjusted residuals (post outlier removal) revealed a latent component (PC1) that was significantly associated with clinical indices: absence of LLDAS ($P = .007$), absence of DORIS remission ($P = .048$), higher SLEDAI-2K scores ($P = .001$), higher BILAG-2004 scores ($P = .002$), higher PhGA scores ($P = .02$), higher PtGA scores ($P = .003$), and worse fatigue (FACIT-F, $P = 0.014$; VAS fatigue, $P = .04$). No significant association with LupusQoL fatigue was observed (Fig 3).

All 4 VOCs in this cluster loaded positively on PC1, which explained 78% of the within-cluster variance, confirming that PC1 captured their shared increase in patients with higher

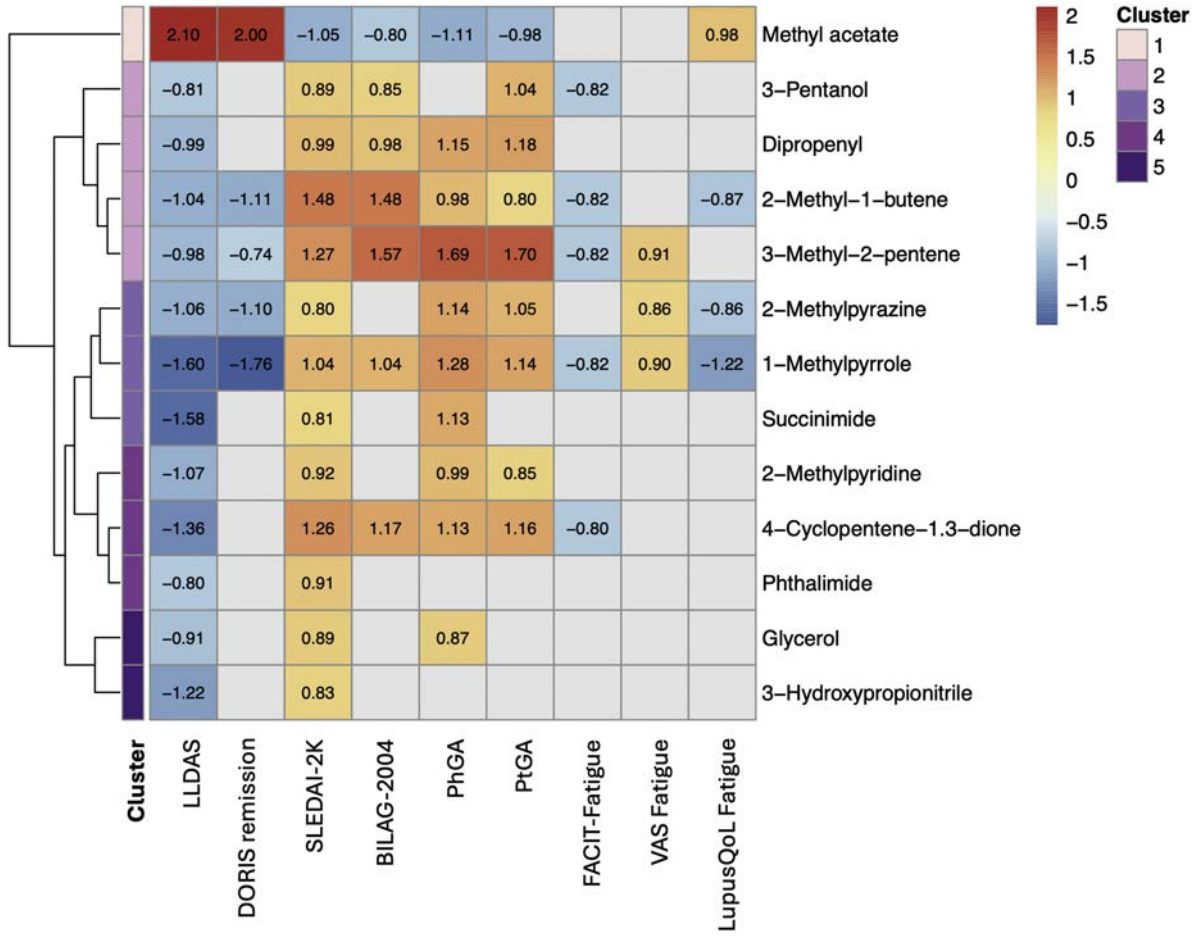

Figure 1. Strength of associations with selected compounds. Heatmap showing the strength of association between selected volatile organic compounds (VOCs) and clinical outcomes, as measured by the robust Cohen's d (dr). Compounds included were significantly associated with both SLEDAI-2K scores and LLDAS ($P < .05$). Rows and columns were clustered using robust Pearson's correlation (rw) to visualise similarity patterns. Effect sizes are interpreted as follows: $|dr| > 0.5$ indicates a moderate effect; $|dr| > 0.8$ indicates a strong effect. Negative values for LLDAS and DORIS remission reflect lower VOC levels in patients meeting the outcome. Positive values for SLEDAI-2K, BILAG-2004, PhGA, and PtGA indicate increased disease activity with higher VOC levels. For FACIT-F and LupusQoL fatigue, negative values indicate greater fatigue associated with elevated VOCs; for VAS fatigue, positive values reflect greater perceived fatigue. BILAG-2004, British Isles Lupus Assessment Group 2004; DORIS, Definition Of Remission In Systemic lupus erythematosus; FACIT-F, Functional Assessment of Chronic Illness Therapy-Fatigue; LLDAS, Lupus Low Disease Activity State; LupusQoL, Lupus Quality of Life; PhGA, physician's global assessment; PtGA, patient's global assessment; SLEDAI-2K, Systemic Lupus Erythematosus Disease Activity Index 2000; VAS, visual analogue scale.

disease activity and fatigue. By contrast, a global PCA of all breath-derived VOCs provided limited separation across groups, with PC1 and PC2 together explaining only ~30% of the variance and the first 5 components <50%.

Cluster 3: Nitrogen-containing heterocycles

This cluster comprised 1-methylpyrrole, 2-methylpyrazine, and succinimide, compounds of predominantly exogenous origin. 1-Methylpyrrole and 2-methylpyrazine showed U-shaped trajectories across disease states, with lower levels in patients in remission and higher levels in both active disease and healthy controls. These patterns suggest a link to intestinal barrier integrity and absorption mechanisms.

Cluster 4: Phthalimide and oxidative stress-related VOCs

This chemically heterogeneous cluster included phthalimide, 4-cyclopentene-1,3-dione, and 2-methylpyridine. These VOCs, whose shared characteristics suggest contributions from environmental exposure or altered microbial or host metabolism, were positively correlated with disease activity and inversely with LLDAS.

Cluster 5: Small polar molecules

The final cluster comprised glycerol and 3-hydroxypropionitrile. While these VOCs showed associations with SLEDAI-2K scores and inverse associations with LLDAS, the lack of consistent correlations across multiple disease activity measures suggests a limited or nonspecific role in broader pathophysiologic mechanisms.

Adjustment for disease activity

To assess whether the observed associations between VOCs and fatigue were entirely explained by disease activity, we fitted additional linear models including SLEDAI-2K as a covariate. Several VOCs, particularly oxidative stress-related species described in cluster 4, remained significantly associated with fatigue scores after adjustment, indicating a component of fatigue-related breath alteration that is not fully dependent on disease activity (Supplementary Table S15).

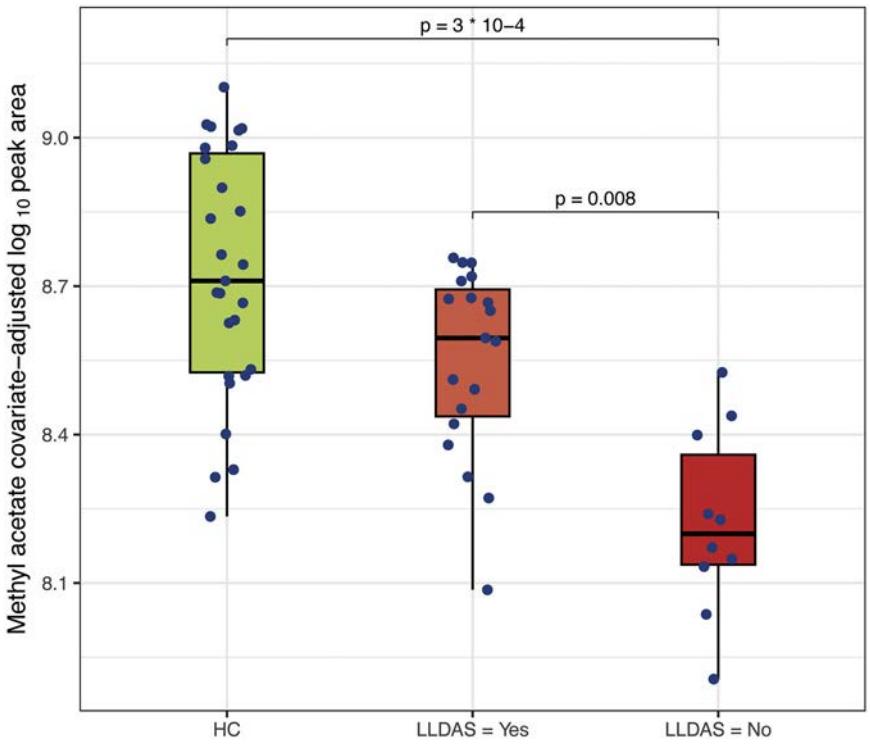

Figure 2. Methyl acetate concentrations in healthy controls and in relation to LLDAS. Boxplots illustrating methyl acetate concentrations in healthy controls (HCs) and SLE patients, stratified by fulfilment of LLDAS criteria (yes/no). Values shown are adjusted for covariates and presented after outlier removal. Reduced methyl acetate levels were observed in patients not fulfilling LLDAS. LLDAS, Lupus Low Disease Activity State.

DISCUSSION

This is the first study to investigate breathomics in SLE, exploring VOCs as potential noninvasive biomarkers of disease activity, immune dysregulation, intestinal integrity, and fatigue. Our findings provide novel insights into the breath metabolome in SLE and highlight key metabolic perturbations associated with disease states and symptom burden.

Among the most compelling findings, methyl acetate emerged as a candidate marker of immune homeostasis. Its levels were significantly reduced in SLE patients, particularly those who did not meet criteria for LLDAS or DORIS remission. Reduced exhaled methyl acetate in active SLE may reflect increased consumption or impaired production of acetate-derived anti-inflammatory mediators in the context of chronic immune activation. This is consistent with experimental data showing that methyl acetate modulates interleukin (IL)-6 and IL-10 production and alleviates inflammatory responses, suggesting that lower levels in our patients may be a surrogate of insufficient endogenous regulatory activity [28]. In addition, reduced availability may arise upstream from gut dysbiosis, whereby altered microbial ecology impairs the intestinal generation of acetate-derived metabolites, including esters such as methyl acetate [29]. In our setting, methyl acetate was inversely associated with multiple indices of disease activity and, to a lesser extent, with fatigue. Taken together, its depletion in active SLE may reflect a failure of endogenous regulatory mechanisms and impaired resolution of inflammation, which are central features in the chronic immune activation characterising SLE.

Supporting this notion of unresolved inflammation, the second cluster, comprising branched alkenes (3-methyl-2-pentene, 2-methyl-1-butene, dipropenyl) and the branched alcohol 3-pentanol, was associated with higher disease activity and fatigue. These alkenes are likely derived from lipid peroxidation, specifically from branched-chain prenols, which undergo oxidative degradation [30]. Prior studies have linked altered lipid metabolism and increased lipid peroxidation with SLE pathophysiology [31,32], as well as correlations with SLEDAI-2K scores [33,34]. Beyond serving as markers of oxidative stress, branched alkenes may have pathogenic roles by inducing epigenetic changes, such as DNA hypomethylation, that promote proinflammatory gene expression [35].

Importantly, this same cluster was linked to multiple measures of fatigue. Previous literature has associated fatigue in chronic inflammatory conditions with lipid peroxidation [36,37] and oxidative stress more broadly [38,39]. Our findings support the hypothesis that persistent oxidative stress not only contributes to immune dysregulation but also to self-reported symptom burden affecting patients' health-related quality of life. These results emphasise the entwinement of inflammation, disease control, and fatigue.

The third cluster, composed of nitrogen-containing heterocycles, ie, 2-methylpyrazine, 1-methylpyrrole, and succinimide, was of particular interest for its potential link to gastrointestinal function. 2-Methylpyrazine and 1-methylpyrrole are generally of exogenous origin and showed a U-shaped distribution across disease states: reduced in remission and elevated in both healthy controls and patients with active disease. This may reflect a shift from impaired gastrointestinal absorption during quiescent disease to increased intestinal permeability, or 'leaky gut', in active SLE, allowing re-entry of these exogenous compounds into the systemic circulation. As BMI and hepatic or renal function were not associated with these fluctuations in prior literature [40,41], impaired barrier function appears to be the most plausible explanation. Previous evidence supports increased intestinal permeability in SLE and its association with disease severity [42–45]. Thus, changes in VOC levels may offer indirect markers of gut integrity in SLE.

The fourth cluster, comprising phthalimide, 4-cyclopentene-1,3-dione, and 2-methylpyridine, showed consistent associations with disease activity and may point to a combination of environmental exposures and host or microbial metabolism. 4-Cyclopentene-1,3-dione, a base compound of the cyclopentenedione family [46], is of particular interest due to its structural similarity with the cyclopentenone core of prostaglandin J_2, a reactive lipid mediator generated during inflammation and oxidative stress [47]. Its accumulation in active SLE may therefore

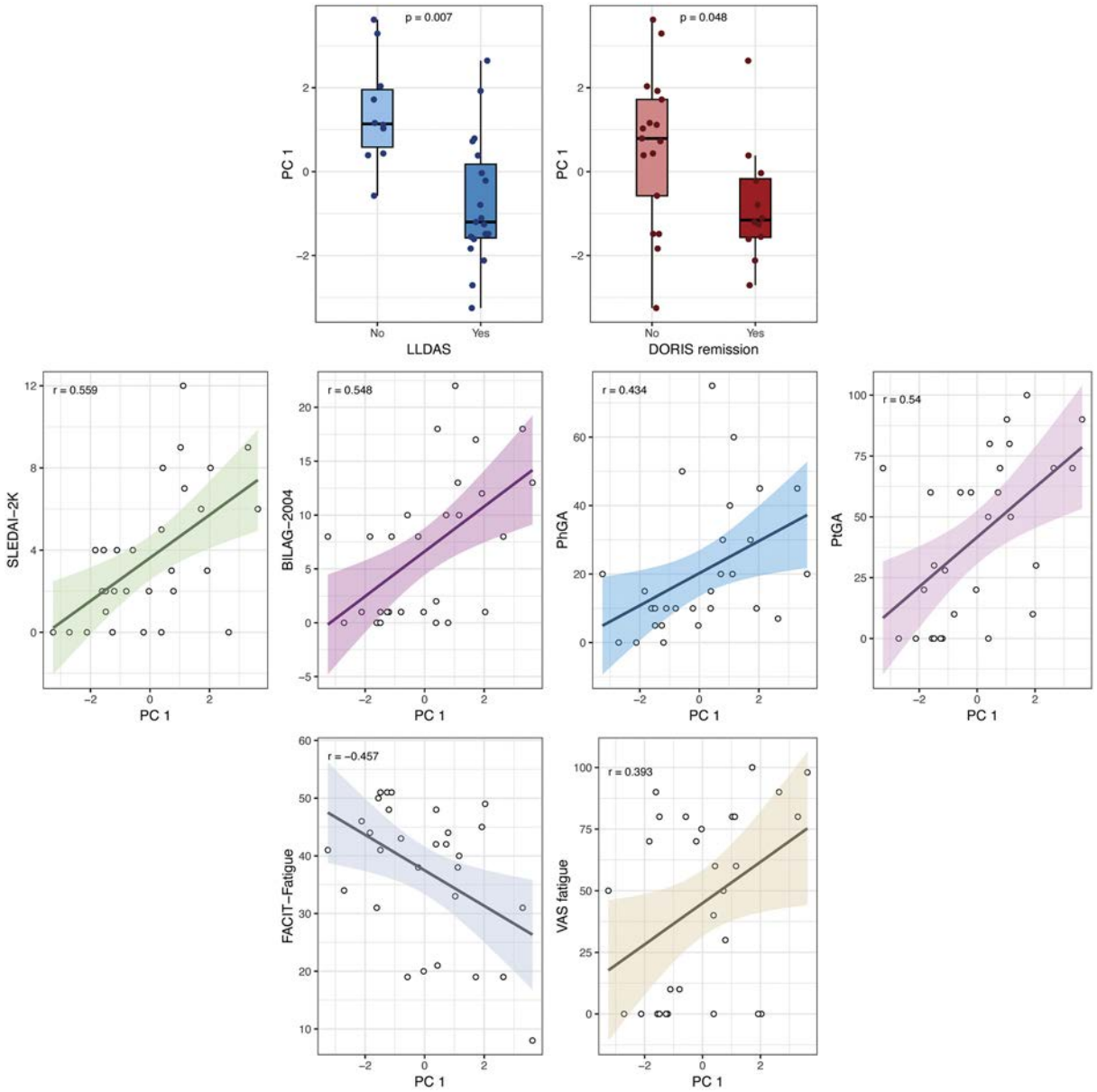

Figure 3. Principal component analysis of the branched alkene cluster (cluster 2). Plots of the first principal component analysis (PCA1) derived from PCA on covariate-adjusted residuals of 4 VOCs: 3-methyl-2-pentene, 2-methyl-1-butene, dipropenyl, and 3-pentanol. PCA1 summarises the main variance in this cluster and is significantly associated with clinical disease activity (SLEDAI-2K, BILAG-2004, PhGA, PtGA), DORIS remission/LLDAS, and fatigue (FACIT-F and VAS). No significant association with LupusQoL fatigue was observed. BILAG-2004, British Isles Lupus Assessment Group 2004; DORIS, Definition Of Remission In Systemic lupus erythematosus; FACIT-F, Functional Assessment of Chronic Illness Therapy-Fatigue; LLDAS, Lupus Low Disease Activity State; LupusQoL, Lupus Quality of Life; PhGA, physician's global assessment; PtGA, patient's global assessment; SLEDAI-2K, Systemic Lupus Erythematosus Disease Activity Index 2000; VAS, visual analogue scale.

reflect increased oxidative stress and/or exposure to electrophilic compounds known to modulate immune responses [48].

The final cluster, which included glycerol and 3-hydroxypropionitrile, showed associations limited to SLEDAI-2K and an inverse relationship with LLDAS. This pattern suggests that these compounds may reflect general metabolic stress rather than SLE-specific pathophysiological mechanisms.

This was a single-centre study conducted in a relatively small and predominantly quiescent SLE cohort, which may limit generalisability to broader SLE populations, especially to populations enrolled in clinical trials or those eligible for targeted interventions. Moreover, the sensitivity of VOC profiles to changes in treatment remains unknown and warrants dedicated investigation. On the other hand, the prevalence of LLDAS in our cohort is comparable to that in large real-world cohorts [49–52], enhancing the clinical relevance of our findings. Future work will require validation of the breathomic signatures documented in the present study in independent and, ideally, multicentre cohorts, as well as longitudinal assessments to determine responsiveness to treatment and fluctuating disease activity.

A key challenge in breathomics, shared by all such studies, lies in differentiating endogenous from exogenous VOCs. Despite rigorous sampling and analysis protocols, environmental and dietary influences may confound interpretation. Future studies should combine breath analysis with other biospecimens (eg, blood, urine, stools) to confirm VOC origin and metabolic fate. Since we restricted inclusion to nonsmokers to minimise exogenous VOC interference, further studies are needed to define how smoking and other airway exposures modify breathomic profiles in SLE.

Lastly, our data—including models adjusting fatigue scores for SLEDAI-2K—indicate that VOC alterations related to fatigue are not entirely dependent on disease activity. This is consistent with previous reports showing only partial concordance between inflammatory control and patient-reported fatigue in SLE [53,54] and with the notion that oxidative stress can contribute to fatigue independently of clinical activity [55,56]. Moreover, oxidative stress has been implicated in fibromyalgia [57,58], a condition that is not uncommon in patients with SLE and may amplify fatigue, suggesting an additional non-inflammatory pathway to persistent symptoms [59]. To this ends, it is important to note that fibromyalgia was not adjudicated in our cohort; nonetheless, its potential contribution to fatigue underscores the value of multidimensional assessment beyond inflammatory activity [60,61]. While our observations may support the use of breathomics to investigate mechanisms contributing to fatigue, larger and longitudinal studies are needed to determine whether these VOCs are responsive to treatment and whether they can track residual fatigue or predict flare risk.

In conclusion, this study demonstrates the potential of breathomics to noninvasively reflect systemic processes relevant to SLE pathogenesis, including inflammation, immune regulation, and gut barrier integrity. It also offers a novel window into the biological underpinnings of fatigue, a symptom often inadequately captured by traditional disease activity metrics. Breathomics may represent a promising tool for precision monitoring and a deeper understanding of SLE heterogeneity.

Competing interests

IP has received research funding and/or honoraria from Amgen, AstraZeneca, Aurinia, BMS, Elli Lilly, Gilead, GSK, Janssen, Novartis, Otsuka, and Roche. MAR has received funding and/or honoraria from AstraZeneca, BMS, and GSK. LG and MK are employees of Owlstone Medical Ltd., a company specialising in the development and application of breath-based diagnostic technologies. The other authors declare no conflicts of interest. The funders had no role in the design of the study, in the collection, analyses, or interpretation of data, in the writing of the manuscript, or in the decision to publish the results.

Contributors

IP, GB, AV, MAR, and LB were involved in the conceptualisation of the study. IP, MI, LR, DN, LP, LG, MK, CB, BV, and LB were involved in data curation. LG, MK, and LB were involved in the visualisation of the findings. IP, LM, MK, MAR, and LB were involved in the interpretation of results. IP, LP, and LB were involved in the manuscript drafting. All authors were involved in data analysis, critical review of manuscript drafts, and approval of the final draft prior to submission. IP and LB act as the guarantors of the study.

Funding

IP has received grants from the Swedish Rheumatism Association (R-995882), King Gustaf V's 80-year Foundation (FAI-2023-1055), Swedish Society of Medicine (SLS-974449), Nyckelfonden (OLL-1000881), Professor Nanna Svartz Foundation (2021-00436), Ulla and Roland Gustafsson Foundation (2024-43), Region Stockholm (FoUI-1004114), and Karolinska Institutet. DN has received grants from the Swedish Rheumatism Association (R-995557), King Gustaf V's 80-year Foundation (FAI-2023-1006), Ulla and Roland Gustafsson Foundation (2024-49), Ulla and Gustaf af Uggla Foundation (2023-025029), and Karolinska Institutet. We acknowledge scientific support from the Exploring Inflammation in Health and Disease (X-HiDE) Consortium, a research profile at Örebro University funded by the Knowledge Foundation (grant 20200017). This work has received funding from the Innovative Medicines Initiative (IMI) 2 Joint Undertaking (JU) for the Taxonomy, Treatment, Targets and Remission (3TR) project (grant 831434). The JU receives support from the European Union's Horizon 2020 research and innovation programme and European Federation of Pharmaceutical Industries and Associations (EFPIA).

Disclaimer

The content of this publication reflects only the authors' view, and the JU is not responsible for any use that may be made of the information it contains.

Patient consent for publication

Not applicable.

Ethics approval

This study involves human participants. It was reviewed and approved by the local ethics committee: Comitato Etico Area 2, Fondazione IRCCS Ca Granda Ospedale Maggiore Policlinico di Milano and University of Milan (approval no. 425 bis 19 November 2014 and no. 671_2018 19 September 2018).

Provenance and peer review

Not commissioned; externally peer reviewed.

Data availability statement

Data are available upon reasonable request. Raw data remain the property of the Taxonomy, Treatment, Targets and Remission (3TR) consortium and are protected under the European General Data Protection Regulation (GDPR). Metadata and aggregated processed data are available upon reasonable request from the corresponding author.

Supplementary materials

Supplementary material associated with this article can be found in the online version at doi:10.1016/j.ard.2025.12.005.

Orcid

Ioannis Parodis: http://orcid.org/0000-0002-4875-5395

REFERENCES

[1] Tselios K, Gladman DD, Touma Z, Su J, Anderson N, Urowitz MB. Disease course patterns in systemic lupus erythematosus. Lupus 2019;28(1):114–22.
[2] Kostopoulou M, Mukhtyar CB, Bertsias G, Boumpas DT, Fanouriakis A. Management of systemic lupus erythematosus: a systematic literature review informing the 2023 update of the EULAR recommendations. Ann Rheum Dis 2024;83(11):1489–501.
[3] Yu H, Nagafuchi Y, Fujio K. Clinical and immunological biomarkers for systemic lupus erythematosus. Biomolecules 2021;11(7):928.
[4] Zhang SJ, Xu RY, Kang LL. Biomarkers for systemic lupus erythematosus: a scoping review. Immun Inflamm Dis 2024;12(10):e70022.
[5] Idle JR, Gonzalez FJ. Metabolomics. Cell Metab. 2007;6(5):348–51.
[6] Clish CB. Metabolomics: an emerging but powerful tool for precision medicine. Cold Spring Harb Mol Case Stud 2015;1(1):a000588.

[7] Liu Y, Yang X. A review on the novel biomarkers of systemic lupus erythematosus discovered via metabolomic profiling. Front Immunol 2024;15:1443440.
[8] Lawal O, Ahmed WM, Nijsen TME, Goodacre R, Fowler SJ. Exhaled breath analysis: a review of 'breath-taking' methods for off-line analysis. Metabolomics 2017;13(10):110.
[9] Chou H, Godbeer L, Allsworth M, Boyle B, Ball ML. Progress and challenges of developing volatile metabolites from exhaled breath as a biomarker platform. Metabolomics 2024;20(4):72.
[10] Marzoog BA, Chomakhidze P, Gognieva D, Parunova AY, Demchuk SN, Silantyev A, et al. Updates in breathomics behavior in ischemic heart disease and heart failure, mass-spectrometry. World J Cardiol 2025;17(2):102851.
[11] Zanella D, Guiot J, Stefanuto PH, Giltay L, Henket M, Guissard F, et al. Breathomics to diagnose systemic sclerosis using thermal desorption and comprehensive two-dimensional gas chromatography high-resolution time-of-flight mass spectrometry. Anal Bioanal Chem 2021;413(14):3813–22.
[12] Massenet T, Potjewijd J, Tobal R, Gester F, Zanella D, Henket M, et al. Breathomics to monitor interstitial lung disease associated with systemic sclerosis. ERJ Open Res 2024;10(4):00175–2024.
[13] Chou H, Godbeer L, Ball ML. Establishing breath as a biomarker platform-take home messages from the Breath Biopsy Conference 2023. J Breath Res 2024;18(3).
[14] Arulvasan W, Chou H, Greenwood J, Ball ML, Birch O, Coplowe S, et al. High-quality identification of volatile organic compounds (VOCs) originating from breath. Metabolomics 2024;20(5):102.
[15] Arulvasan W, Greenwood J, Ball ML, Chou H, Coplowe S, Birch O, et al. Optimized breath analysis: customized analytical methods and enhanced workflow for broader detection of VOCs. Metabolomics 2025;21(1):17.
[16] Elefante E, Gualtieri L, Schilirò D, Stagnaro C, Signorini V, Zucchi D, et al. Impact of disease activity patterns on health-related quality of life (HRQoL) in patients with systemic lupus erythematosus (SLE). Lupus Sci Med 2024;11(2):e001202.
[17] Aringer M, Costenbader K, Daikh D, Brinks R, Mosca M, Ramsey-Goldman R, et al. 2019 European League Against Rheumatism/American College of Rheumatology classification criteria for systemic lupus erythematosus. Arthritis Rheumatol 2019;71(9):1400–12.
[18] Gladman DD, Ibañez D, Urowitz MB. Systemic lupus erythematosus disease activity index 2000. J Rheumatol 2002;29(2):288–91.
[19] Romero-Diaz J, Isenberg D, Ramsey-Goldman R. Measures of adult systemic lupus erythematosus: updated version of British Isles Lupus Assessment Group (BILAG 2004), European Consensus Lupus Activity Measurements (ECLAM), Systemic Lupus Activity Measure, Revised (SLAM-R), Systemic Lupus Activity Questionnaire for Population Studies (SLAQ), Systemic Lupus Erythematosus Disease Activity Index 2000 (SLEDAI-2K), and Systemic Lupus International Collaborating Clinics/American College of Rheumatology Damage Index (SDI). Arthritis Care Res (Hoboken) 2011;63(suppl 11):S37–46 (11).
[20] Franklyn K, Lau CS, Navarra SV, Louthrenoo W, Lateef A, Hamijoyo L, et al. Definition and initial validation of a Lupus Low Disease Activity State (LLDAS). Ann Rheum Dis 2016;75(9):1615–21.
[21] van Vollenhoven R, Voskuyl A, Bertsias G, Aranow C, Aringer M, Arnaud L, et al. A framework for remission in SLE: consensus findings from a large international task force on definitions of remission in SLE (DORIS). Ann Rheum Dis 2017;76(3):554–61.
[22] Carter LM, Gordon C, Yee CS, Bruce I, Isenberg D, Skeoch S, et al. Easy-BILAG: a new tool for simplified recording of SLE disease activity using BILAG-2004 index. Rheumatology (Oxford) 2022;61(10):4006–15.
[23] Cella D, Lai JS, Stone A. Self-reported fatigue: one dimension or more? Lessons from the Functional Assessment of Chronic Illness Therapy—Fatigue (FACIT-F) questionnaire. Support Care Cancer 2011;19(9):1441–50.
[24] McElhone K, Abbott J, Shelmerdine J, Bruce IN, Ahmad Y, Gordon C, et al. Development and validation of a disease-specific health-related quality of life measure, the LupusQol, for adults with systemic lupus erythematosus. Arthritis Rheum 2007;57(6):972–9.
[25] Leys C, Ley C, Klein O, Bernard P, Licata L. Detecting outliers: do not use standard deviation around the mean, use absolute deviation around the median. J Exp Soc Psychol 2013;49(4):764–6.
[26] Tuğran E, Kocak M, Mirtagioğlu H, Yiğit S, Mendes M. A simulation based comparison of correlation coefficients with regard to type I error rate and power. J Data Anal Inf Process 2015;3(3):87–101.
[27] Li JC. Effect size measures in a two-independent-samples case with non-normal and nonhomogeneous data. Behav Res Methods 2016;48(4):1560–74.
[28] Xie L, Saimaier K, Wang C, Yang J, Han M, Lv J, et al. Methyl acetate arrests Th1 in peripheral immune system and alleviates CNS inflammation in EAE. Int Immunopharmacol 2021;101(Pt B):108291.
[29] Hosmer J, McEwan AG. Kappler U. Bacterial acetate metabolism and its influence on human epithelia. Emerg Top Life Sci 2024;8(1):1–13.
[30] Ratcliffe N, Wieczorek T, Drabińska N, Gould O, Osborne A, De Lacy, Costello B. A mechanistic study and review of volatile products from peroxidation of unsaturated fatty acids: an aid to understanding the origins of volatile organic compounds from the human body. J Breath Res 2020;14(3):034001.
[31] Zhang T, Mohan C. Caution in studying and interpreting the lupus metabolome. Arthritis Res Ther 2020;22(1):172.
[32] Yan Y, Yu F, Li Q, Feng X, Geng L, Sun L. Metabolic alterations in vitamin D deficient systemic lupus erythematosus patients. Sci Rep 2024;14(1):18879.
[33] Scavuzzi BM, Simão ANC, Iriyoda TMV, Lozovoy MAB, Stadtlober NP, Franchi Santos LFDR, et al. Increased lipid and protein oxidation and lowered anti-oxidant defenses in systemic lupus erythematosus are associated with severity of illness, autoimmunity, increased adhesion molecules, and Th1 and Th17 immune shift. Immunol Res 2018;66(1):158–71.
[34] Sam NB, Tabiri S, Amofa E. Plasma/serum oxidant parameters in systemic lupus erythematosus patients: a systematic review and meta-analysis. Autoimmune Dis 2024;2024:9948612.
[35] Ogbodo JO, Arazu AV, Iguh TC, Onwodi NJ, Ezike TC. Volatile organic compounds: a proinflammatory activator in autoimmune diseases. Front Immunol 2022;13:928379.
[36] Morris G, Maes M. Oxidative and nitrosative stress and immune-inflammatory pathways in patients with myalgic encephalomyelitis (ME)/chronic fatigue syndrome (CFS). Curr Neuropharmacol 2014;12(2):168–85.
[37] Brkic S, Tomic S, Maric D, Novakov Mikic A, Turkulov V. Lipid peroxidation is elevated in female patients with chronic fatigue syndrome. Med Sci Monit 2010;16(12):CR628–32.
[38] Avalos I, Chung CP, Oeser A, Milne GL, Morrow JD, Gebretsadik T, et al. Oxidative stress in systemic lupus erythematosus: relationship to disease activity and symptoms. Lupus 2007;16(3):195–200.
[39] Segal BM, Thomas W, Zhu X, Diebes A, McElvain G, Baechler E, et al. Oxidative stress and fatigue in systemic lupus erythematosus. Lupus 2012;21(9):984–92.
[40] González-Regueiro JA, Cruz-Contreras M, Merayo-Chalico J, Barrera-Vargas A, Ruiz-Margáin A, Campos-Murguía A, et al. Hepatic manifestations in systemic lupus erythematosus. Lupus 2020;29(8):813–24.
[41] Martínez-Martínez MU, Borjas-García JA, Magaña-Aquino M, Cuevas-Orta E, Llamazares-Azuara L, Abud-Mendoza C. Renal function assessment in patients with systemic lupus erythematosus. Rheumatol Int 2012;32(8):2293–9.
[42] Frittoli RB, Vivaldo JF, Costallat LTL, Appenzeller S. Gastrointestinal involvement in systemic lupus erythematosus: a systematic review. J Transl Autoimmun 2021;4:100106.
[43] Azzouz D, Omarbekova A, Heguy A, Schwudke D, Gisch N, Rovin BH, et al. Lupus nephritis is linked to disease-activity associated expansions and immunity to a gut commensal. Ann Rheum Dis 2019;78(7):947–56.
[44] Pan Q, Guo F, Huang Y, Li A, Chen S, Chen J, et al. Gut microbiota dysbiosis in systemic lupus erythematosus: novel insights into mechanisms and promising therapeutic strategies. Front Immunol 2021;12:799788.
[45] Ma L, Morel L. Loss of gut barrier integrity in lupus. Front Immunol 2022;13:919792.
[46] Sevcíková Z, Pour M, Novák D, Ulrichová J, Vacek J. Chemical properties and biological activities of cyclopentenediones: a review. Mini Rev Med Chem 2014;14(4):322–31.
[47] Li J, Guo C, Wu J. 15-Deoxy-Δ-12,14-prostaglandin J2 (15d-PGJ2), an endogenous ligand of PPAR-γ: function and mechanism. PPAR Res 2019;2019:7242030.
[48] Pollard KM, Pearson DL, Hultman P, Deane TN, Lindh U, Kono DH. Xenobiotic acceleration of idiopathic systemic autoimmunity in lupus-prone bxsb mice. Environ Health Perspect 2001;109(1):27–33.
[49] Tanaka Y, Miyazaki Y, Hirata S, Kusaka K, Kosaka S, Nakatsuka K, et al. Impact of quality of life on overall work productivity impairment and activity impairment of patients with systemic lupus erythematosus: the PEONY study. Lupus Sci Med 2025;12(1):e001291.
[50] Golder V, Kandane-Rathnayake R, Li N, Louthrenoo W, Chen YH, Cho J, et al. Association of sustained lupus low disease activity state with improved outcomes in systemic lupus erythematosus: a multinational prospective cohort study. Lancet Rheumatol 2024;6(8):e528–e36.
[51] Signorini V, Tani C, Elefante E, Carli L, Stagnaro C, Zucchi D, et al. How do systemic lupus erythematosus patients with very-long disease duration present? Analysis of a monocentric cohort. Lupus 2021;30(3):439–47.
[52] Cho J, Shen L, Huq M, Kandane-Rathnayake R, Golder V, Louthrenoo W, et al. Impact of low disease activity, remission, and complete remission on flares following tapering of corticosteroids and immunosuppressive therapy in patients with systemic lupus erythematous: a multinational cohort study. Lancet Rheumatol 2023;5(10):e584–e93.
[53] Parodis I, Haugli-Stephens T, Dominicus A, Eek D, Sjöwall C. Lupus Low Disease Activity State and organ damage in relation to quality of life in systemic lupus erythematosus: a cohort study with up to 11 years of follow-up. Rheumatology (Oxford) 2025;64(2):639–47.

[54] Gomez A, Qiu V, Cederlund A, Borg A, Lindblom J, Emamikia S, et al. Adverse health-related quality of life outcome despite adequate clinical response to treatment in systemic lupus erythematosus. Front Med (Lausanne) 2021;8:651249.
[55] Lee JS, Kim HG, Lee DS, Son CG. Oxidative stress is a convincing contributor to idiopathic chronic fatigue. Sci Rep 2018;8(1):12890.
[56] Fukuda S, Nojima J, Motoki Y, Yamaguti K, Nakatomi Y, Okawa N, et al. A potential biomarker for fatigue: oxidative stress and anti-oxidative activity. Biol Psychol 2016;118:88–93.
[57] Otlu Ö, Kıran TR, Baykara RA, Erdem M, İnceoğlu F. Endoplasmic reticulum stress and oxidative imbalance is the missing link in fibromyalgia pathophysiology. Sci Rep 2025;15(1):36729.
[58] Assavarittirong C, Samborski W, Grygiel-Górniak B. Oxidative stress in fibromyalgia: from pathology to treatment. Oxid Med Cell Longev 2022;2022:1582432.
[59] Escoda T, Jourde-Chiche N, Granel B, Cornec D, Chiche L. Complex relationships between inflammatory manifestations/type 1 and type 2 symptoms in systemic lupus erythematosus: a narrative literature review. Lupus 2023;32(8):942–51.
[60] Parodis I, Studenic P. Patient-reported outcomes in systemic lupus erythematosus. Can lupus patients take the driver's seat in their disease monitoring? J Clin Med 2022;11(2).
[61] Parodis I, Lanata C, Nikolopoulos D, Blazer A, Yazdany J. Reframing health disparities in SLE: a critical reassessment of racial and ethnic differences in lupus disease outcomes. Best Pract Res Clin Rheumatol 2023;37(4):101894.

Ann Rheum Dis 85 (2026) 858–872

Contents lists available at ScienceDirect

Annals of the Rheumatic Diseases

journal homepage: https://www.sciencedirect.com/journal/annals-of-the-rheumatic-diseases

Antiphospholipid syndrome

CD40-CD40L inhibition attenuates platelet-neutrophil interaction and neutrophil extracellular trap release in primary antiphospholipid syndrome

Stavros Naoum[1,2], Charilaos Spyropoulos[2], Andriani Angelopoulou[3], Harikleia Gakiopoulou[4], Michalis Katsimpoulas[5], Vassilis G. Gorgoulis[3,5,6,7], Petros P. Sfikakis[1], Konstantinos Ritis[8], Ioanna-Evdokia Galani[5], Konstantinos Kambas[2], Maria G. Tektonidou[1,*]

[1] *First Department of Propaedeutic Internal Medicine, School of Medicine, National and Kapodistrian University of Athens, Joint Academic Rheumatology program, Athens, Greece*
[2] *Laboratory of Molecular Genetics, Department of Immunology, Hellenic Pasteur Institute, Athens, Greece*
[3] *Molecular Carcinogenesis Group, Department of Histology and Embryology, Medical School, National and Kapodistrian University of Athens, Athens, Greece*
[4] *First Department of Pathology, School of Medicine, National and Kapodistrian University of Athens, Athens, Greece*
[5] *Biomedical Research Foundation Academy of Athens, Athens, Greece*
[6] *Ninewells Hospital and Medical School, University of Dundee, Dundee, UK*
[7] *Molecular and Clinical Cancer Sciences, Manchester Cancer Research Centre, Manchester Academic Health Sciences Centre, University of Manchester, Manchester, UK*
[8] *First Department of Internal Medicine and Laboratory of Molecular Hematology, Department of Medicine, Democritus University of Thrace, Alexandroupolis, Greece*

ARTICLE INFO

Article history:
Received 19 September 2025
Received in revised form 19 December 2025
Accepted 20 December 2025

ABSTRACT

Objectives: Neutrophil extracellular traps (NETs) are increasingly recognised for their role in primary antiphospholipid syndrome (PAPS) pathogenesis. Herein, we examined underlying mechanisms driving NET formation and the thrombogenic effects of NETs in patients with PAPS, along with potential inhibitors.

Methods: We examined NET release in PAPS, asymptomatic antiphospholipid autoantibodies (aPLs) carriers, and healthy controls (HCs) as well as NET-bound proteins by immunofluorescence, immunoblotting, quantitative polymerase chain reaction (PCR), and enzyme-linked immunosorbent assay (ELISA). We assessed platelet-neutrophil aggregates by flow cytometry (CD61/CD66b staining) and autophagy using LC3B immunofluorescence and immunoblotting. Immunofluorescence was performed in paraffin-embedded kidney, skin ulcer, and endoarterial thrombus tissues from patients with PAPS. Suppression of NET release via CD40-CD40L inhibition was tested in *in vitro* and venous thrombosis mouse models.

Results: Neutrophils from patients with PAPS exhibited increased NET release compared with asymptomatic aPL carriers and HCs. NETs from patients with PAPS expressed tissue factor (TF) that induced thrombin generation in platelet-poor plasma from HCs. aPL induced *in vitro*

*Correspondence to Dr. Maria G. Tektonidou, First Department of Propaedeutic Internal Medicine, School of Medicine, National and Kapodistrian University of Athens, Laiko Hospital, Athens, Greece.

E-mail addresses: mtektonidou@gmail.com, mtektonidou@med.uoa.gr (M.G. Tektonidou).

Konstantinos Kambas and Maria G. Tektonidou are senior authors.

Handling editor Josef S. Smolen.

https://doi.org/10.1016/j.ard.2025.12.012

intracellular TF expression in HC neutrophils. TF-expressing NETs were abundant in the kidney, skin ulcer, and endoarterial thrombus tissues from patients with PAPS, and colocalised with fibrinogen. NET release in PAPS neutrophils was driven by aPL-mediated platelet activation, subsequent platelet-neutrophil interaction, and autophagy induction. CD40-CD40L blockade reduced platelet activation, autophagy, and NET formation in patients with PAPS. In a mouse model, inhibition of CD40-CD40L reduced neutrophil-platelet aggregates and myeloperoxidase (MPO)-DNA complexes in mouse peripheral blood, and the presence of NETs in the formed thrombi.

Conclusions: Targeting the platelet-neutrophil/autophagy/TF-expressing NETs axis by CD40-CD40L inhibition attenuates thromboinflammation in PAPS and should be explored as a potential therapeutic target.

WHAT IS ALREADY KNOWN ON THIS TOPIC

- The involvement of neutrophil extracellular traps (NETs) in thromboinflammation pathways in primary antiphospholipid syndrome (PAPS) is gaining increased attention, but there are still unanswered questions concerning the mechanisms driving NET release and thrombogenic effects of NETs, as well as potential inhibitors.

WHAT THIS STUDY ADDS

- NETs from patients with PAPS are decorated with bioactive tissue factor and induce thrombin generation.
- Tissue factor (TF)-expressing NETs are abundant in kidney, skin ulcer, and endoarterial thrombus tissues from patients with PAPS, and colocalised with fibrinogen.
- NET release in neutrophils from patients with PAPS is driven by antiphospholipid antibody-mediated platelet activation, subsequent platelet-neutrophil interaction, and autophagy induction.
- CD40-CD40L blockade in *in vitro* cultures reduces platelet activation, autophagy, and NET formation in patients with PAPS. In a mouse model, inhibition of CD40-CD40L reduces neutrophil-platelet aggregates and MPO-DNA complexes in mouse peripheral blood and the presence of NETs in the formed thrombi.

HOW THIS STUDY MIGHT AFFECT RESEARCH, PRACTICE OR POLICY

- These findings provide compelling proof-of-concept data that targeting the CD40-CD40L pathway can disrupt platelet-neutrophil interactions and mitigate thromboinflammation in PAPS.
- CD40-CD40L inhibition can represent a promising therapeutic target in PAPS. Its role should also be explored in other thromboinflammation-associated conditions.

INTRODUCTION

Antiphospholipid syndrome (APS) is a complex, systemic autoimmune disorder with a poorly understood pathophysiology. APS is characterised by recurrent arterial and venous thrombosis, microvascular manifestations, and pregnancy morbidity in the presence of antiphospholipid autoantibodies (aPLs), namely lupus anticoagulant (LA), anticardiolipin (aCL), and anti-β2 glycoprotein I (anti-β2GPI) antibodies [1]. Although earlier studies of APS pathogenesis were mainly focused on coagulation and fibrinolysis disruption processes, an interplay between thrombotic mechanisms and innate immune responses is increasingly recognised [2–9]. The involvement of neutrophil extracellular traps (NETs) in thromboinflammation pathways in primary APS (PAPS) is gaining increased attention [2], but there are still unanswered questions concerning the mechanisms driving NET release and thrombogenic effects of NETs, as well as potential inhibitors.

NETs decorated with bioactive tissue factor (TF), a main initiator of the extrinsic blood coagulation cascade, have been demonstrated in inflammatory conditions [eg, sepsis, acute myocardial infarction, and antineutrophil cytoplasmic antibody (ANCA) vasculitis] [10–12] and in systemic lupus erythematosus (SLE), a systemic autoimmune disorder often co-occurring with APS [13]. However, the expression of bioactive TF on NETs from patients with PAPS needs to be further elucidated.

A key intracellular mechanism in the regulation of NET generation is autophagy [11,14], a homeostatic mechanism for the elimination of harmful or damaged intracellular components. NET release has been shown to be mediated by increased levels of basal autophagy in SLE [13], but its role in the release of NETs in PAPS remains unexplored. Platelet-neutrophil complexes (PNCs), resulting from the interaction between neutrophils and activated platelets, have been shown to induce neutrophil autophagy and NET formation [15].

Interactions between platelets and neutrophils are mediated by P-selectin ligand and P-selectin, CD40 ligand (CD40L) and CD40, intracellular adhesion molecule 2 (ICAM-2) and integrin $\alpha L\beta 2$, and triggering receptor expressed on myeloid cells 1 (TREM-1) ligand (TREM-1L) and TREM-1 on platelets and neutrophils, respectively. It has been recently reported that PNCs might enhance the APS IgG-mediated NET release in a P-selectin-dependent manner [16]. CD40L enhances P-selectin activity on platelets and Mac-1 expression on neutrophils [17]. CD40-CD40L pathway acts as an amplifier of thromboinflammation pathways [18–20], and its inhibition has been examined as a targeted therapy in cardiovascular disease [21,22].

Herein, we aimed to examine: (1) NET release in patients with PAPS and asymptomatic aPL-positive individuals, (2) thrombogenicity of NETs through TF expression on NETs in both circulating neutrophils and organ tissues of patients with PAPS, (3) the role of aPL in platelet activation and subsequent platelet-neutrophil interaction for the generation of NETs, (4) autophagy as a potential mediator of NET release, and (5) the effect of inhibition of the CD40-CD40L axis as a mediator of the platelet-neutrophil cross-talk, both *in vitro* and in an APS murine model.

METHODS

In total, 30 patients fulfilling the classification criteria for thrombotic PAPS [1,23], 11 age- and sex-matched healthy controls (HCs), and 5 asymptomatic aPL individuals with positive aPL but without clinical criteria for APS (median duration of aPL positivity: 7 [6-9] years) were included in this study. None fulfilled the European Alliance of Associations of

Rheumatology/American College of Rheumatology (EULAR/ACR) classification criteria for SLE [24]. Additionally, sera from a disease control group that did not have underlying autoimmune disorders or aPL positivity were collected: 7 patients with acute arterial thrombosis (3 with acute stroke and 5 with ST-segment elevation acute myocardial infarction [STEMI]) and 8 patients with acute venous thrombosis; 1 patient had simultaneous arterial (stroke) and venous thrombosis. Participant characteristics and inclusion/exclusion criteria are presented in the Supplementary Table S1. None was on glucocorticoid or immunosuppressive treatment. The study was approved by the Ethics Committee of Laiko General Hospital (protocol number 398/31-05-2021) in compliance with the Declaration of Helsinki. All participants provided written informed consent. aPL quantification and aPL profile were determined as described in Supplementary Methods.

Venous blood samples were collected in EDTA and heparin-containing tubes for the study of neutrophils and NETs, in sodium citrate tubes for the study of platelets and isolation of platelet-poor plasma (PPP), and in serum-separating tubes for serum isolation. Polymorphonuclear neutrophils (PMNs) were isolated using Percoll for stimulation and inhibition studies. To investigate the bioactivity of NET-bound TF, thrombin ELISA was carried out on isolated NET structures from patients with PAPS. To inhibit the formation of NETs, isolated neutrophils were pretreated with the early-stage autophagy inhibitor SC79, whereas for the inhibition of CD40-CD40L interaction the inhibitor DRI-C21045 (at C = 10 μM) was used. Total IgG fractions were isolated and purified from 6 patients with triple aPL +ve PAPS and 2 HCs for the *in vitro* stimulation of neutrophils and platelets. NETs were visualised by confocal microscopy using immunofluorescence. MPO/DNA complex ELISA was carried out on isolated NET structures for the quantification of NET release. *TF* mRNA expression was assessed by quantitative real-time PCR. Neutrophil lysates and NET proteins were isolated for the study of TF and microtubule-associated protein 1 light chain 3B (LC3B) expression, using western blotting. Peripheral blood samples in heparin were used for the study of platelet-activated neutrophil aggregates, using flow cytometry. For *in vivo* CD40-CD40L inhibition, we utilised a thrombotic APS murine model, through inferior vena cava (IVC) ligation, as previously described [25]. More details on these methods are provided in Supplementary Methods.

Moreover, archival formalin-fixed, paraffin-embedded kidney (n = 5), skin ulcer (n = 4), and endoarterial thrombus (n = 2) tissues from patients with PAPS, along with kidney samples from the healthy parenchyma from 2 individuals who underwent nephrectomy for renal masses diagnosed as oncocytomas (used as 'healthy' controls) and a skin biopsy from 1 HC were examined by immunofluorescence microscopy to detect neutrophils, NETs and NET-bound TF, or fibrinogen. We also examined as disease controls, formalin-fixed paraffin-embedded kidney biopsies from 4 patients with acute renal thrombotic microangiopathy (2 patients with haemolytic uremic syndrome, 1 with thrombotic thrombocytopenic purpura, and 1 with Hemolysis, Elevated Liver enzymes and Low Platelets syndrome), a skin ulcer biopsy from a patient with diabetes mellitus, and endoarterial thrombus tissues retrieved during thrombectomy from 2 patients with acute femoral artery atherothrombosis. None of these patients fulfilled criteria for APS or any other autoimmune disorder, nor did they have positive aPL.

A more detailed description of the Methods is presented in Supplementary Methods.

Statistical analysis

For continuous variables, Wilcoxon (paired t-test) and Mann-Whitney (unpaired t-test) were used, after implementing the Shapiro-Wilk normality test. For comparison of more than 2 groups, 1-way analysis of variance (ANOVA, Tukey's multiple comparison test) with Bonferroni post hoc or Kruskal-Wallis was applied. Data analysis was performed using GraphPad Prism v9.0 software (www.graphpad.com). Data are presented as mean ± SD. Statistical significance was considered at $P < .05$.

RESULTS

Higher NET release in patients with PAPS compared with HCs and asymptomatic aPL individuals

Neutrophils from patients with PAPS demonstrated higher spontaneous NET release than neutrophils from age- and sex-matched HCs and asymptomatic aPL carriers, as assessed by immunofluorescence staining in *ex vivo* neutrophils (Fig 1A,B) and MPO-DNA complex ELISA in isolated NET structures (Fig 1C). In a 3-month follow-up, no significant difference was observed in the *ex vivo* generation of NETs in patients with PAPS (Fig 1D).

No correlation was demonstrated between NET release and any specific aPL type, isotype, or titres, or venous or arterial thrombosis history in patients with PAPS (Supplementary Fig Sl). Given that phosphatidylserine/prothrombin (aPS/PT) autoantibodies have been associated with elevated thrombotic risk and their presence can help identify individuals at higher risk [26] beyond the criteria aPL (aCL, anti-β2GPI, and LA), we measured aPS/PT IgG and IgM titres in isolated sera from all patients with PAPS included in the study (n = 30). aPS/PT antibodies did not correlate with NET release (Supplementary Figure S1K).

Overall, these findings suggest that patients with PAPS have persistently higher spontaneous NET release than HCs and asymptomatic aPL individuals.

NETs from patients with PAPS are decorated with bioactive TF

Using immunofluorescence staining, we observed that NETs from 9 of 30 patients with PAPS expressed TF (Fig 1E). These findings were verified by immunoblotting on isolated NET proteins. TF expression in immunoblotting was significantly higher in patients who also demonstrated TF expression by immunofluorescence staining (Fig 1F).

We further assessed the ability of NET-bound TF from patients with PAPS to generate thrombin, using *in vitro* stimulations of PPP from HCs with isolated NET structures. We found that NET structures isolated from PAPS neutrophils induced thrombin generation in PPP from HCs, as assessed by thrombin ELISA assay. This effect was dependent on NET-bound TF, since TF inhibition with an anti-TF neutralising antibody abrogated the generation of thrombin. Interestingly, NETs from patients with PAPS with no prominent TF expression did not induce thrombin generation (Fig 1G).

TF-bearing NETs and fibrinogen are present in arterial thrombi, skin ulcer, and kidney tissues from patients with PAPS

To gain further insight into the role of NETs in thrombus development and organ injury in PAPS, we examined the presence of neutrophils and NETs in acute arterial thrombi, skin ulcer, and kidney biopsies from patients with PAPS, in

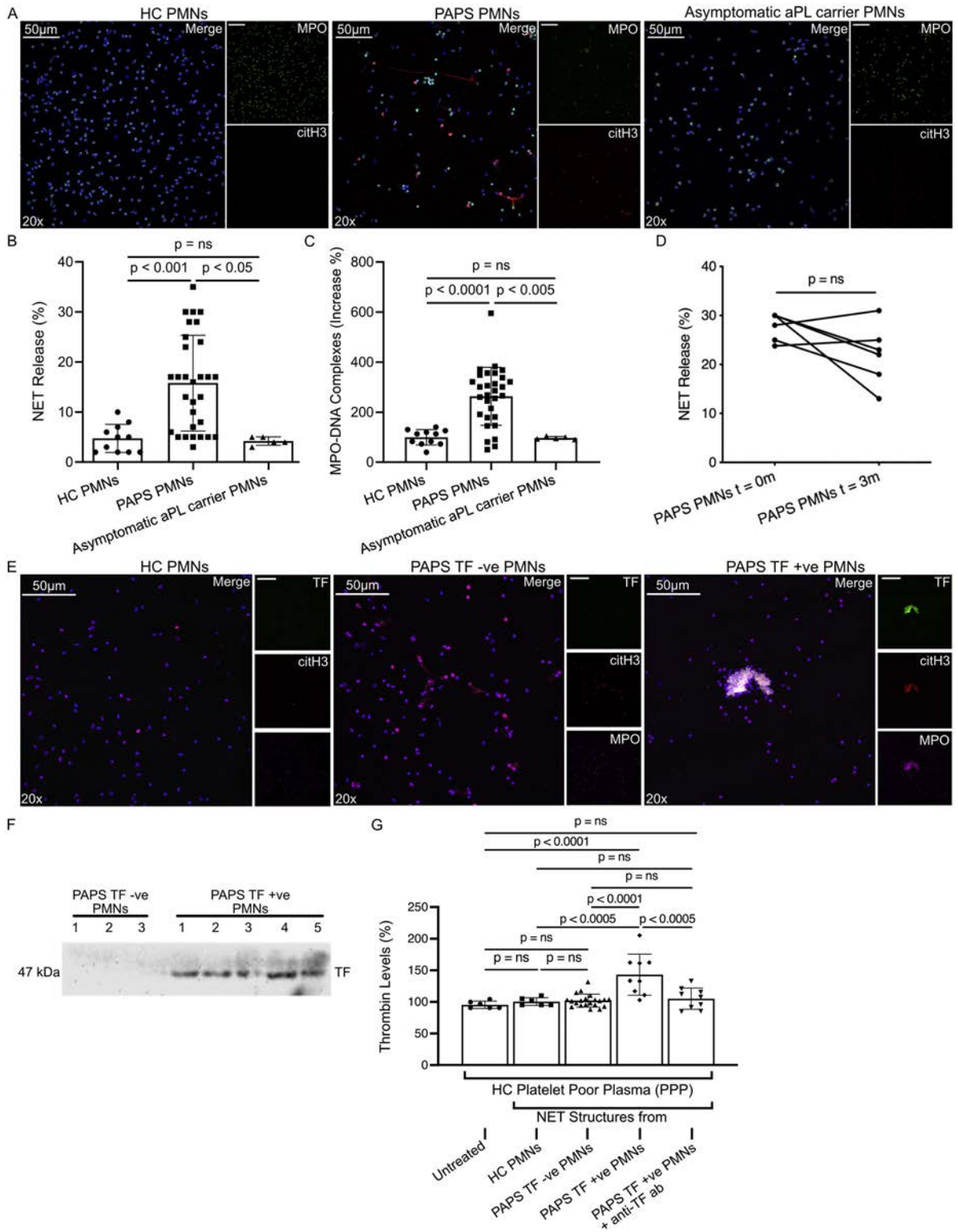

Figure 1. Increased spontaneous NET release is observed in neutrophils from patients with PAPS. (A) NET release by isolated peripheral neutrophils from patients with PAPS (n = 30) compared with HCs (n = 11) and asymptomatic aPL carriers (n = 5). Representative data from 1 of 30 patients with PAPS, 1 of 11 HCs, and 1 of 5 asymptomatic aPL carriers are shown. (B) Quantification of NET release in (A). (C) MPO-DNA complex enzyme-linked immunosorbent assay (ELISA) in isolated NET structures from neutrophils in (A). (D) NET release in neutrophils from patients with PAPS at t = 0 and 3 months later. (E) Expression of TF on NETs released by isolated peripheral neutrophils from patients with PAPS compared with HCs. Representative data from 2 out of 30 patients with PAPS are shown. (F) TF expression in purified NET proteins from isolated peripheral neutrophils from patients with PAPS (n = 8). (G) Thrombin generation levels in HC platelet-poor plasma treated with NET structures from patients with PAPS (n = 30) and HCs (n = 6). Representative data from 1 of 4 independent experiments. Green: (A) MPO, (E) TF, red: (A, E) citH3, magenta: (E) MPO, blue: (A, E) DAPI/DNA. For (B, C, G), statistical analysis was performed using ordinary 1-way analysis of variance (ANOVA) followed by Tukey's multiple comparisons test. For (D), statistical analysis was performed using the Wilcoxon signed-rank test for paired samples. For (B, C, G), bars represent mean values ± SD, and each dot represents a patient. ANOVA, analysis of variance; citH3, citrullinated histone H3; DAPI, 4′,6-diamidino-2-phenylindole; ELISA, enzyme-linked immunosorbent assay; HC, healthy controls; MPO, myeloperoxidase; NET, neutrophil extracellular trap; PAPS, primary antiphospholipid syndrome; TF, tissue factor.

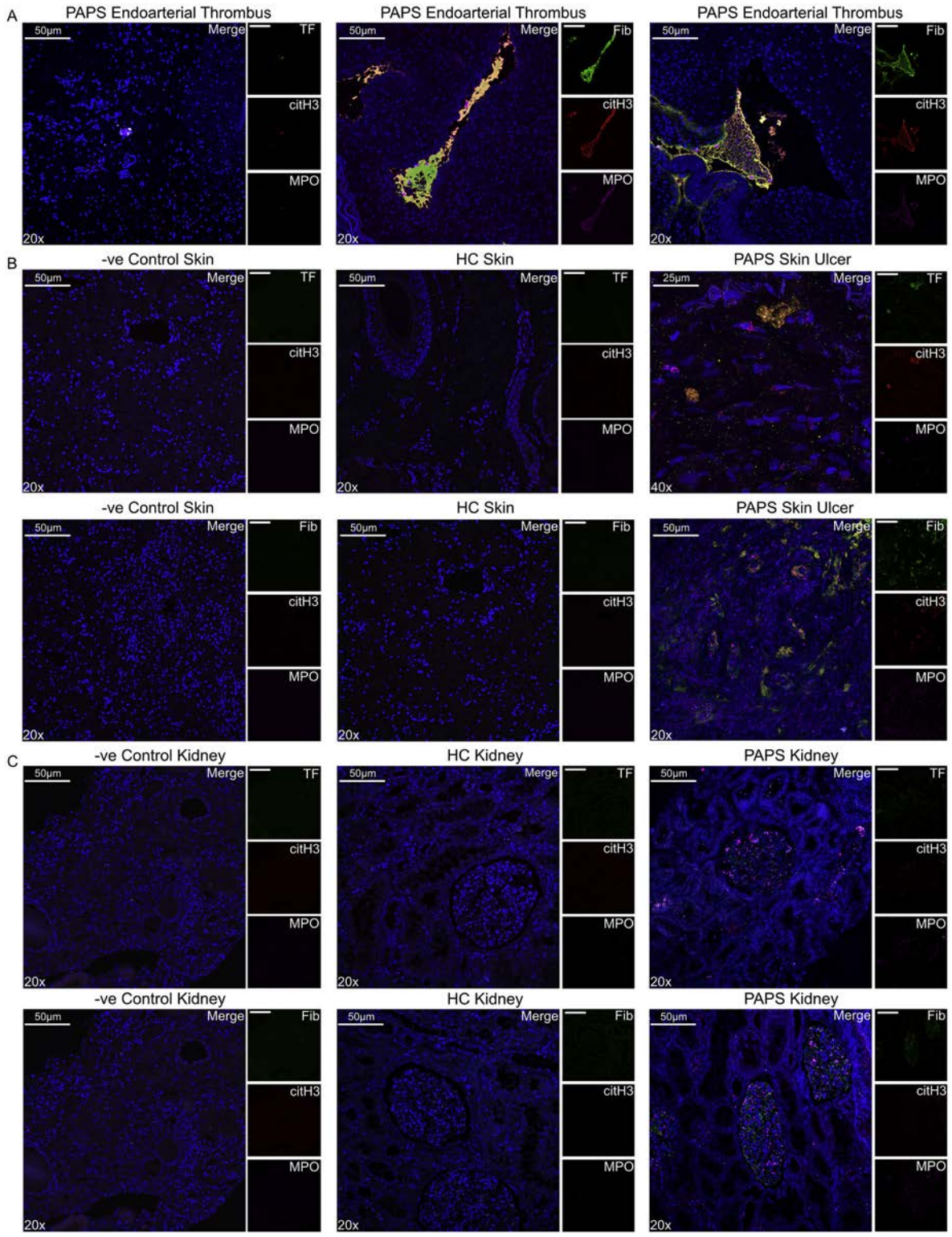

Figure 2. TF-bearing NETs and fibrinogen are identified in organised endoarterial thrombi, skin ulcer tissues, and kidney biopsies from patients with PAPS. (A) TF-bearing NETs and fibrinogen in an organised arterial thrombus from a patient with PAPS. Representative data from 1 of 2 patients. (B) TF-bearing NETs and fibrinogen in skin ulcer biopsies from patients with PAPS compared with skin biopsies from HCs. −ve control: secondary antibody control. Representative data from 1 of 4 patients. (C) TF-bearing NETs and fibrinogen in renal biopsies from patients with PAPS with renal involvement compared with kidney biopsies from apparently HCs (without autoimmune disorders). −ve control: secondary antibody control. Representative data from 1 of 5 patients. Green: TF/fibrinogen (Fib), red: citH3, magenta: MPO, blue: DAPI/DNA. ANOVA, analysis of variance; citH3, citrullinated histone H3; DAPI, 4′,6-diamidino-2-phenylindole; ELISA, enzyme-linked immunosorbent assay; HC, healthy controls; MPO, myeloperoxidase; NET, neutrophil extracellular trap; PAPS, primary antiphospholipid syndrome; TF, tissue factor.

comparison with skin and renal biopsies from individuals without a diagnosis of autoimmune disorder, serving as controls. Neutrophils and NETs were present in the arterial thrombi (Fig 2A) and skin ulcer biopsies from patients with PAPS (Fig 2B). NETs were often colocalised with TF and fibrinogen in all patients (Fig 2A,B). In the case of arterial thrombi, NETs were found within the organised thrombus in the arterial lumen, but also in the thrombi of the recanalised lumen (Fig 2A). In biopsies from skin ulcers, NETs and neutrophils were present, both inside the thrombotic vessels and in the perivascular space. However, they were also present in the reticular dermis, to a lesser extent. Skin biopsies obtained from HCs did not demonstrate any presence of neutrophils or NETs (Fig 2B).

Neutrophils and NETs were also observed in kidney biopsy tissues from patients with PAPS with renal involvement. Specifically, NETs colocalised with TF or fibrinogen were detected in the glomerular capillaries, in the peritubular capillaries, the tubulointerstitial tissue close to the Bowman's capsule, and within thrombosed arterioles, even when intact neutrophils were not visible (Fig 2C). Conversely, neutrophils and NETs were not detected in kidney biopsies from the healthy parenchyma of nephrectomy tissues (used as HC tissues) (Fig 2C).

Moreover, we used endoarterial thrombus tissues from patients with peripheral artery atherothrombosis (n = 2), kidney biopsies from patients with renal thrombotic microangiopathy (TMA, n = 4), and 1 skin ulcer biopsy from a patient with diabetes as disease control biopsies. We identified TF-expressing NETs (Supplementary Fig S2A) colocalised with fibrinogen (Supplementary Fig S2B) in endoarterial thrombus and renal TMA biopsies. NETs were also present in the skin biopsy of the patient with diabetes but were not colocalised with TF or fibrinogen (Supplementary Fig S2A,B).

Taken together, these findings indicate the presence of TF-bearing NETs, colocalised with fibrinogen, in endoarterial thrombi, skin, and kidney biopsy specimens, suggesting their involvement in the thromboinflammation process in target tissues/organs among patients with PAPS.

aPL are required for the intracellular expression of TF in neutrophils, activation of platelets, and subsequent NET release in PAPS

To test whether the observed difference in the presence of NET-bound TF in neutrophils of patients with PAPS is attributed to the capacity of aPL to induce the expression of intracellular TF in neutrophils, we treated HC neutrophils with isolated IgGs, which were isolated from 6 patients with triple-positive PAPS. We observed that IgGs from patients with PAPS with prominent expression of TF on their *ex vivo* NETs induced higher TF mRNA expression and TF protein levels, than IgGs from patients without prominent TF expression on their NETs (Fig 3A-C).

Neither IgGs isolated from patients with PAPS, nor PAPS sera were able to induce NET release directly in HC neutrophils, as assessed by immunofluorescence staining and MPO-DNA complex ELISA (Fig 3D,E). We further examined a disease control group of aPL-negative patients with acute arterial and/or venous thrombosis (n = 16). *In vitro* treatment of HC neutrophils with sera from the above patients has been shown to induce intracellular upregulation of TF expression (in 5 of 8 patients with arterial thrombosis and 4 of 8 patients with venous thrombosis) (Supplementary Figure S3A), but not NET formation as assessed by both immunofluorescence staining and MPO-DNA complex ELISA (Supplementary Fig S3A-C).

Studies have shown that activated platelets are involved in NET formation in infections and cardiovascular disease [10,27–30]. To assess the ability of PAPS platelets to induce NET release, we treated neutrophils from HCs with *ex vivo*-isolated platelets from patients with PAPS or heterologous HC platelets. We observed significantly increased NET release in HC neutrophils treated with platelets from patients with PAPS, compared with HC neutrophils treated with heterologous HC platelets or PAPS sera (Fig 3F-H). PAPS platelets did not induce TF expression in HC neutrophils (Fig 3I).

Considering that the presence of platelet-neutrophil aggregates is one of the most accurate markers of platelet activation, we investigated their levels in our patients. We observed increased platelet-neutrophil aggregates in the peripheral blood of patients with PAPS, compared with HCs, expressed as CD61/CD66b double-positive (+ve) events by flow cytometry (Fig 3J, K). The spontaneous NET release observed in neutrophils from patients with PAPS was strongly correlated with CD61/CD66b double +ve events (Fig 3L). Checking for correlations between CD61/CD66b double +ve events and PAPS clinical characteristics, the only association found was with the presence of venous thrombosis (Fig 3M, Supplementary Fig S4). CD61/CD66b double +ve events did not correlate with aPS/PT autoantibodies either (Supplementary Fig 4I). Moreover, we verified the presence of platelets on *ex vivo*-isolated neutrophils from patients with PAPS by immunofluorescence confocal microscopy (Fig 3N).

Prompted by these findings, we investigated whether aPL are involved in platelet-neutrophil interactions. To reproduce this hypothesis *in vitro*, we examined platelet-neutrophil aggregates in HC neutrophils treated with PAPS IgG-pretreated platelets. Increased CD61/CD66b double +ve events were observed in HC neutrophils treated with PAPS IgGs-pretreated platelets, compared with HC neutrophils treated with control IgG-pretreated platelets or untreated HC neutrophils (Fig 4A,B).

Furthermore, we treated HC platelets with either isolated IgGs from patients with PAPS, demonstrating TF-expressing NETs or not. Subsequently, these platelets were introduced to HC neutrophils, pretreated with the same PAPS IgGs. Pretreatment of platelets with either IgGs from patients with PAPS expressing or not TF on NETs induced NET release in HC neutrophils, compared with controls (Fig 4C,D). However, NET-bound TF was observed only when HC neutrophils were pretreated with IgGs from patients with NET-bound TF-expressing PAPS, but not with IgGs from patients with TF-negative PAPS or HCs (Fig 4C,D). Importantly, TF presence in these *in vitro* stimulated HC neutrophils was functional, since isolated NET structures were able to induce thrombin generation in PPP from HCs in a TF-dependent manner (Fig 4E).

Overall, aPL play a dual role by inducing TF expression in neutrophils and activating platelets with subsequent NET release in PAPS.

Autophagy in PAPS neutrophils is induced by their interaction with activated platelets and mediates NET release

Autophagy is a key mechanism in the regulation of NET generation and release [14]. Autophagy-mediated release of NETs has been described in patients with SLE with active disease [13]. Herein, we investigated autophagy in neutrophils from patients with PAPS and its association with NET release. We observed that neutrophils from patients with PAPS demonstrated higher basal autophagy levels than HCs, as assessed by

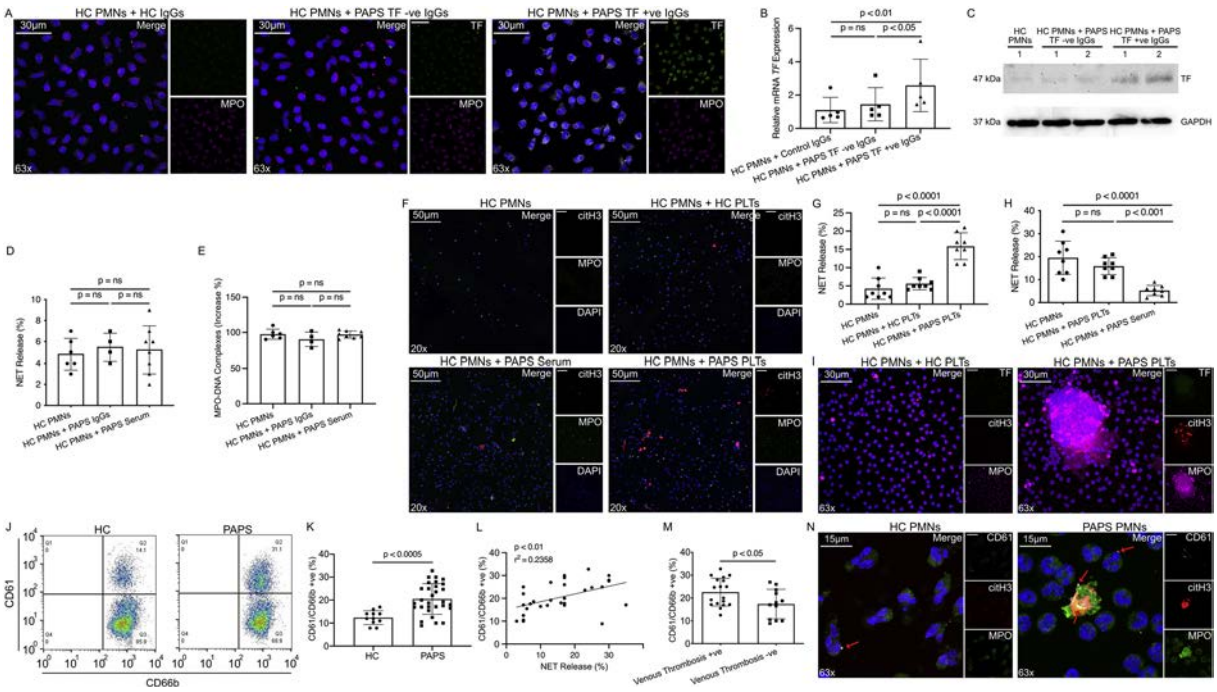

Figure 3. Platelets from patients with PAPS induce NET release in neutrophils. (A) Intracellular expression of TF in isolated peripheral neutrophils from HCs treated with HC IgGs (n = 2), IgGs from TF −ve (n = 3) or TF patients with +ve PAPS (n = 3). Representative data from 1 of 4 experiments. (B) Relative mRNA *TF* expression by neutrophils in (A). (C) TF expression in isolated peripheral neutrophils incubated with purified PAPS IgGs from TF −ve (n = 2) and TF +ve (n = 2) patients. (D) Quantification of NET release in isolated peripheral neutrophils from HCs (n = 6) treated *in vitro* with purified IgGs (n = 4) or sera (n = 8) from patients with PAPS. (E) MPO-DNA complex enzyme-linked immunosorbent assay (ELISA) in isolated NET structures from neutrophils in (D). (F) NETs released by isolated peripheral neutrophils from HCs treated with PAPS platelets (n = 8) or heterologous HC platelets (n = 8). Representative data from 1 of 4 experiments. (G) Quantification of NET release in (F). (H) Quantification of NET release by *ex vivo*-isolated peripheral neutrophils from patients with PAPS (n = 8) compared with *in vitro* treatment of HC neutrophils with the corresponding platelets or sera from these patients. Representative data from 1 of 4 experiments. (I) TF −ve NETs released by isolated peripheral neutrophils from HCs treated with PAPS platelets (n = 8) or heterologous platelets from HCs (n = 8). Representative data from 1 of 4 experiments. (J) CD61/CD66b flow cytometry dot plots in whole blood from patients with PAPS (n = 30) and HCs (n = 11). Representative data from 1 of 30 patients with PAPS. (K) Quantification of CD61/CD66b double +ve events in (I). (L) Correlation of NET formation in patients with PAPS (Fig 1B) with CD61/CD66b double +ve events. (M) CD61/CD66b double +ve events in patients with PAPS with venous thrombosis (n = 18) compared with patients without (n = 12). (N) Representative immunofluorescence images of *ex vivo*-isolated peripheral neutrophils from HC (n = 6) and PAPS (n = 6) patients, stained for the platelet marker CD61. Green: (A,I) TF, (F,N) MPO, red: (F,I) citH3, magenta: (A,I) MPO, white: (N) CD61, blue: (A,F,I,N) DAPI/DNA. For (B), statistical analysis was performed using repeated-measures 1-way analysis of variance (ANOVA) with Bonferroni's post hoc test. For (D,E,G,H), statistical analysis was performed using ordinary 1-way ANOVA followed by Tukey's multiple comparisons test. For (K,M), statistical analysis was performed using the Mann-Whitney U test. For (L), statistical analysis was performed using the Pearson (r) correlation test. For (B,D,E,G,H,K,M), bars represent mean values ± SD, and each dot represents a patient. ANOVA, analysis of variance; citH3, citrullinated histone H3; DAPI, 4′,6-diamidino-2-phenylindole; ELISA, enzyme-linked immunosorbent assay; HC, healthy controls; MPO, myeloperoxidase; NET, neutrophil extracellular trap; PAPS, primary antiphospholipid syndrome; TF, tissue factor.

immunofluorescence staining using LC3B, a major autophagy protein demonstrated in punctuated structures (puncta) (Fig 5A). These findings were quantified by immunoblotting for the lipidated form of LC3B (LC3B-II) and further verified by calculating the integrated optical density (IOD) ratio of LC3B-II to glyceraldehyde 3-phosphate dehydrogenase (GAPDH) (Fig 5B, C).

To further elucidate the involvement of autophagy in the formation of NETs, we pretreated isolated *ex vivo* PAPS neutrophils with SC79, a pan-AKT phosphorylator molecule, which acts as an early-stage autophagy inhibitor. Pretreatment of PAPS neutrophils with SC79 significantly attenuated basal autophagy levels (Fig 5D upper) and the subsequent release of NETs (Fig 5D lower, E, F), as assessed by immunofluorescence staining and MPO-DNA complex ELISA in isolated NET structures.

To investigate whether the increased autophagy levels observed in PAPS neutrophils are induced by their interaction with activated platelets, we treated HC neutrophils with HC platelets that had been pretreated with isolated PAPS IgGs. We observed that platelets pretreated with PAPS IgGs induced autophagy, in contrast to platelets pretreated with IgGs isolated from HC serum, as shown using immunofluorescence staining and immunoblotting of LC3B (Fig 5G,H).

These findings suggest that NET release in patients with PAPS is correlated with increased basal autophagy in neutrophils, which is mediated by aPL-activated platelets.

CD40-CD40L axis inhibition attenuates NET release and thrombin generation in PAPS

Evidence has shown that several neutrophil and platelet receptor pairs drive platelet-neutrophil interactions, including the P-selectin and P-selectin glycoprotein ligand-1 (PSGL-1), the adhesion molecule ICAM2 and integrin $\alpha L\beta 2$, known as lymphocyte function-associated antigen 1 (LFA-1), the TREM-1L and TREM-1, and the CD40 ligand (CD40L/CD154) and CD40 [21]. We performed *in vitro* studies using inhibitors for LFA-1 − ICAM-2 (Lifitegrast), TREM-1 − TREM-1L (VJDT), and CD40-

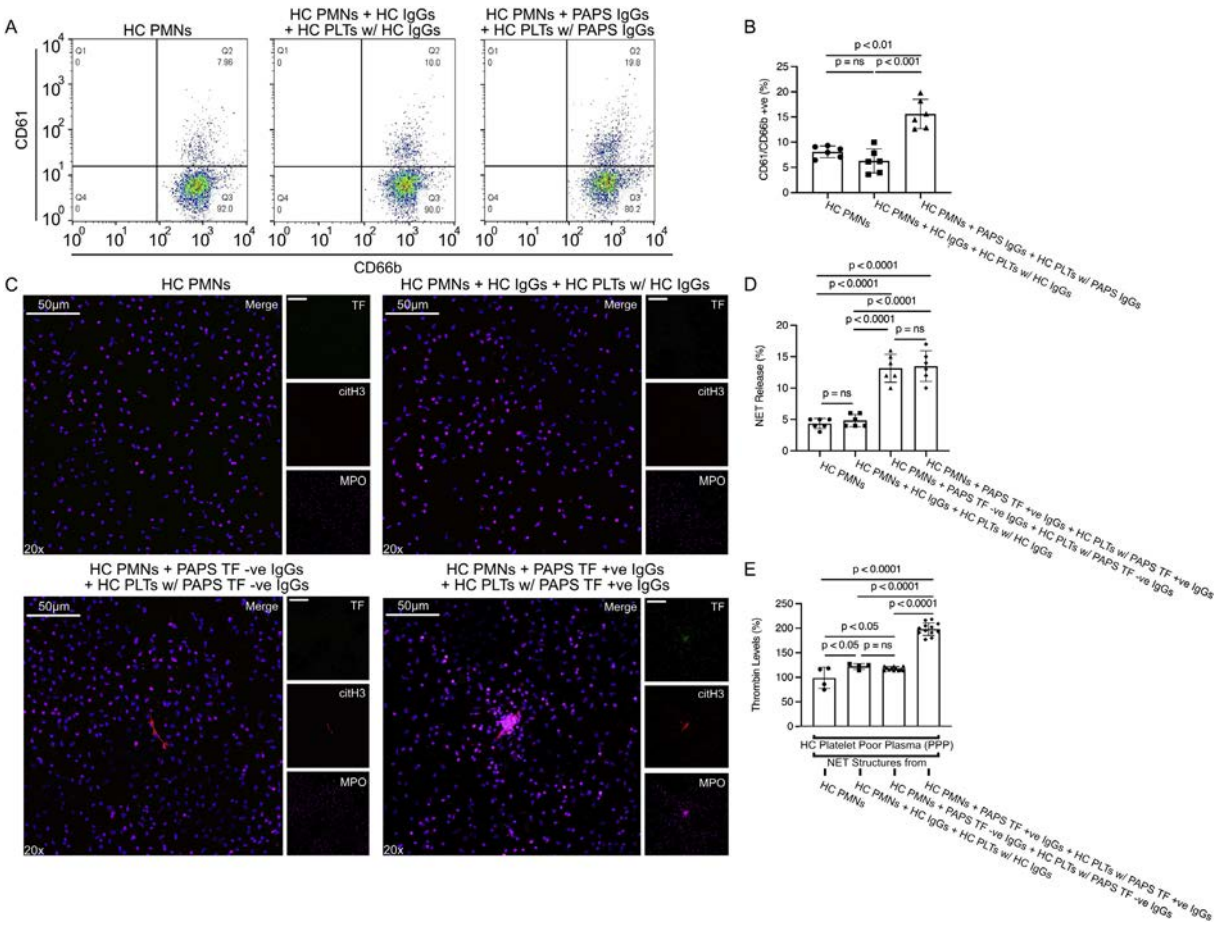

Figure 4. aPL require platelets to induce NET release. (A) CD61/CD66b flow cytometry dot plots in isolated peripheral neutrophils from HCs, stimulated with isolated HC platelets pretreated with purified HC or PAPS IgGs (n = 6). Representative data from 1 of 6 experiments. (B) Quantification of CD61/CD66b double +ve events in (A). (C) NETs released by isolated peripheral neutrophils from HCs pretreated with purified IgGs from TF −ve (n = 3) and +ve (n = 3) patients with PAPS, followed by stimulation with isolated HC platelets pretreated with IgGs from the same patients. Representative data from 1 of 3 experiments. (D) Quantification of NET release in (C). (E) Thrombin generation levels in HC platelet-poor plasma treated with NET structures from neutrophils in (C). Green: CD61, red: citH3, magenta: MPO, blue: DAPI/DNA. For (B,D,E), statistical analysis was performed using ordinary 1-way analysis of variance (ANOVA) followed by Tukey's multiple comparisons test. For (B,D,E), bars represent as mean values ± SD, and each dot represents a patient. ANOVA, analysis of variance; citH3, citrullinated histone H3; DAPI, 4′,6-diamidino-2-phenylindole; ELISA, enzyme-linked immunosorbent assay; HC, healthy controls; MPO, myeloperoxidase; NET, neutrophil extracellular trap; PAPS, primary antiphospholipid syndrome; TF, tissue factor.

CD40L (DRI-C21045); we did not examine the P-selectin and PSGL-1 interaction inhibition, since it has been previously examined in APS [16]. Among the above, only the CD40-CD40L inhibition could reduce NET release in HC neutrophils treated with PAPS IgG-activated platelets (Supplementary Fig S5A). Thus, we decided to extend our study of CD40-CD40L inhibition in PAPS.

Pretreatment of HC neutrophils with the CD40-CD40L inhibitor significantly reduced NET release induced by PAPS IgG-activated platelets, as assessed by immunofluorescence staining and MPO-DNA complex ELISA in isolated NET structures (Fig 6A-C). Moreover, pretreatment of HC neutrophils with DRI-C21045 resulted in a significant decrease in CD61/CD66b double +ve events, compared with neutrophils stimulated with PAPS IgG-activated platelets in the absence of pretreatment (Fig 6D). Importantly, inhibition of the CD40-CD40L interaction reduced the generation of thrombin in PPP from HCs, following stimulation with isolated NET structures from these cultures, as assessed by thrombin ELISA (Fig 6E).

To verify these findings, we repeated these experiments with platelets isolated from patients with PAPS. CD40-CD40L interaction blockade significantly reduced NET release in HC neutrophils induced by *ex vivo*-isolated PAPS platelets, as assessed by immunofluorescence staining and MPO-DNA complex ELISA in isolated NET structures (Fig 6F-H). Moreover, pretreatment of HC neutrophils with DRI-C21045 resulted in decreased CD61/CD66b double +ve events (Fig 6I).

Furthermore, we investigated the role of the CD40-CD40L axis in the process of autophagy. Pretreatment of HC neutrophils with DRI-C21045 significantly attenuated basal autophagy levels induced by PAPS IgG-stimulated platelets, as assessed by immunofluorescence staining and immunoblotting of LC3B (Supplementary Fig S5B,C).

CD40-CD40L axis inhibition alters thrombus composition in an in vivo venous thrombosis model

To validate our findings *in vivo*, we employed a murine model of venous thrombosis by performing flow restriction of the IVC in wild type (WT) mice, in combination with administration of PAPS IgGs (Fig 7A). CD40-CD40L inhibition in this model was mediated by a specific anti-CD40L antibody bearing LALA mutations similar to the second-generation anti-CD40L antibodies used in clinical practice [31]. CD40-CD40L inhibition significantly reduced platelet-neutrophil aggregates and

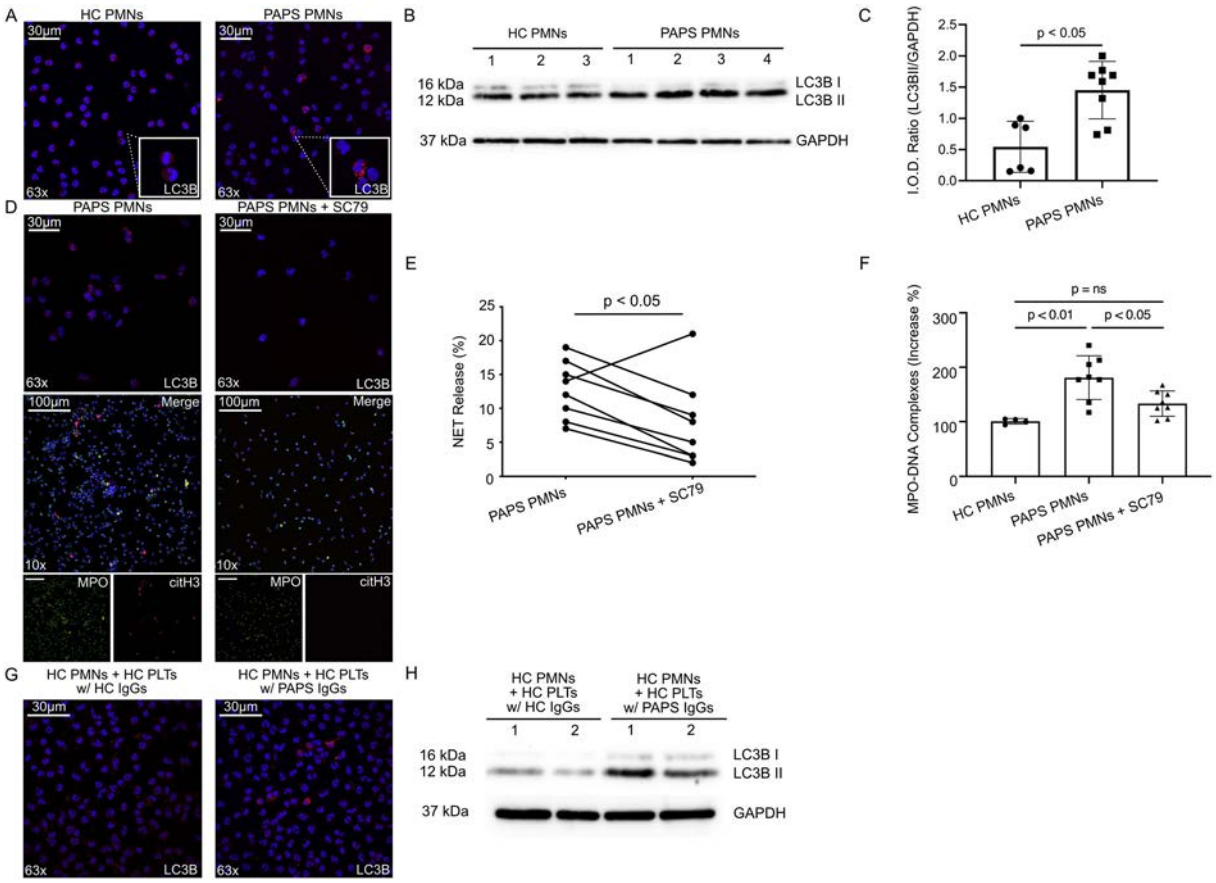

Figure 5. Increased basal autophagy levels observed in PAPS neutrophils are induced by their interaction with activated platelets and mediate NET release. (A) Detection of LC3B-positive puncta on autophagosomes in isolated peripheral neutrophils from patients with PAPS compared with HCs. Representative data from 1 of 30 patients. (B) Quantification of the nonlipidated and lipidated forms of LC3B, LC3B-I and LC3B-II, in isolated total proteins from patients with PAPS (n = 4) compared with HCs (n = 3). (C) Integrated optical density (IOD) in isolated total proteins from (B). Representative data from 1 of 2 independent experiments. (D) Basal autophagy levels (upper) and NET release (lower) in *ex vivo* PAPS patient neutrophils compared with neutrophils pretreated with SC79 inhibitor (n = 8). (E) Quantification of NET release in (D). (F) MPO-DNA complex enzyme-linked immunosorbent assay (ELISA) in isolated NET structures from neutrophils in (D). (G) Detection of LC3B-positive puncta on autophagosomes in isolated peripheral neutrophils from HCs treated *in vitro* with purified PAPS IgG-pretreated platelets. (H) Quantification of the non-lipidated and lipidated forms of LC3B, LC3B-I, and LC3B-II in isolated total proteins from neutrophils in (G). Green: (C—lower) MPO, red: (A, C—upper, F) LC3B, (C—lower) citH3, blue: (A,C,F) DAPI/DNA. For (E), statistical analysis was performed using the Wilcoxon signed-rank test for paired samples. For (F), statistical analysis was performed using ordinary 1-way analysis of variance (ANOVA) followed by Tukey's multiple comparisons test. For (C and F), bars represent mean values ± SD, and each dot represents a patient. ANOVA, analysis of variance; citH3, citrullinated histone H3; DAPI, 4′,6-diamidino-2-phenylindole; ELISA, enzyme-linked immunosorbent assay; HC, healthy controls; MPO, myeloperoxidase; NET, neutrophil extracellular trap; PAPS, primary antiphospholipid syndrome; TF, tissue factor.

the subsequent NET release in anti-CD40L-treated animals compared with saline or isotype IgG-treated mice, as assessed by flow cytometry in whole blood (Supplementary Fig S6A and Fig 7B) and MPO-DNA complex ELISA in mouse sera (Fig 7C), respectively. Accuracy of MPO-DNA complex ELISA for murine samples was verified on isolated PMA/ionomycin-induced NETs from murine neutrophils (Supplementary Figure S6B). Interestingly, CD40-CD40L inhibition significantly reduced NET presence in murine thrombi, as assessed by immunofluorescence staining (Fig 7D,E). Thrombus size and weight were not statistically different (Supplementary Fig S6C,D), whereas mouse weight was similar in all study groups (Supplementary Fig S6E).

Overall, the CD40-CD40L axis is implicated in the platelet-neutrophil interactions, as CD40-CD40L blockade inhibits platelet-neutrophil interaction, the subsequent autophagy-mediated release of NETs, and finally the generation of thrombin. Additionally, inhibition of the CD40-CD40L axis *in vivo* altered thrombus composition in an APS murine model by significantly reducing NET presence.

DISCUSSION

In this study, to our knowledge, we describe that *ex vivo* neutrophils from patients with PAPS can release TF-decorated NETs, which are able to generate thrombin in a TF-dependent manner, and that aPL play a dual role by inducing intracellular TF expression in neutrophils, and activating platelets, with subsequent platelet-neutrophil interaction, autophagy induction, and NET release. Most importantly, we demonstrate for the first time that CD40-CD40L blockade inhibits this platelet-neutrophil interaction and attenuates NET release both *in vitro* and *in vivo*.

More specifically, we observed that *ex vivo* peripheral blood neutrophils from patients with PAPS exhibit increased spontaneous release of NETs, compared with HCs and asymptomatic aPL-positive individuals, which was persistent in a 3-month follow-up. Studies have shown TF expression on NETs in some inflammatory conditions [10,12,13] and TF expression and procoagulant activity on monocytes from patients with PAPS [32]. A previous study showed that aPL-induced complement activation led to TF expression in neutrophils [33]; however, to our

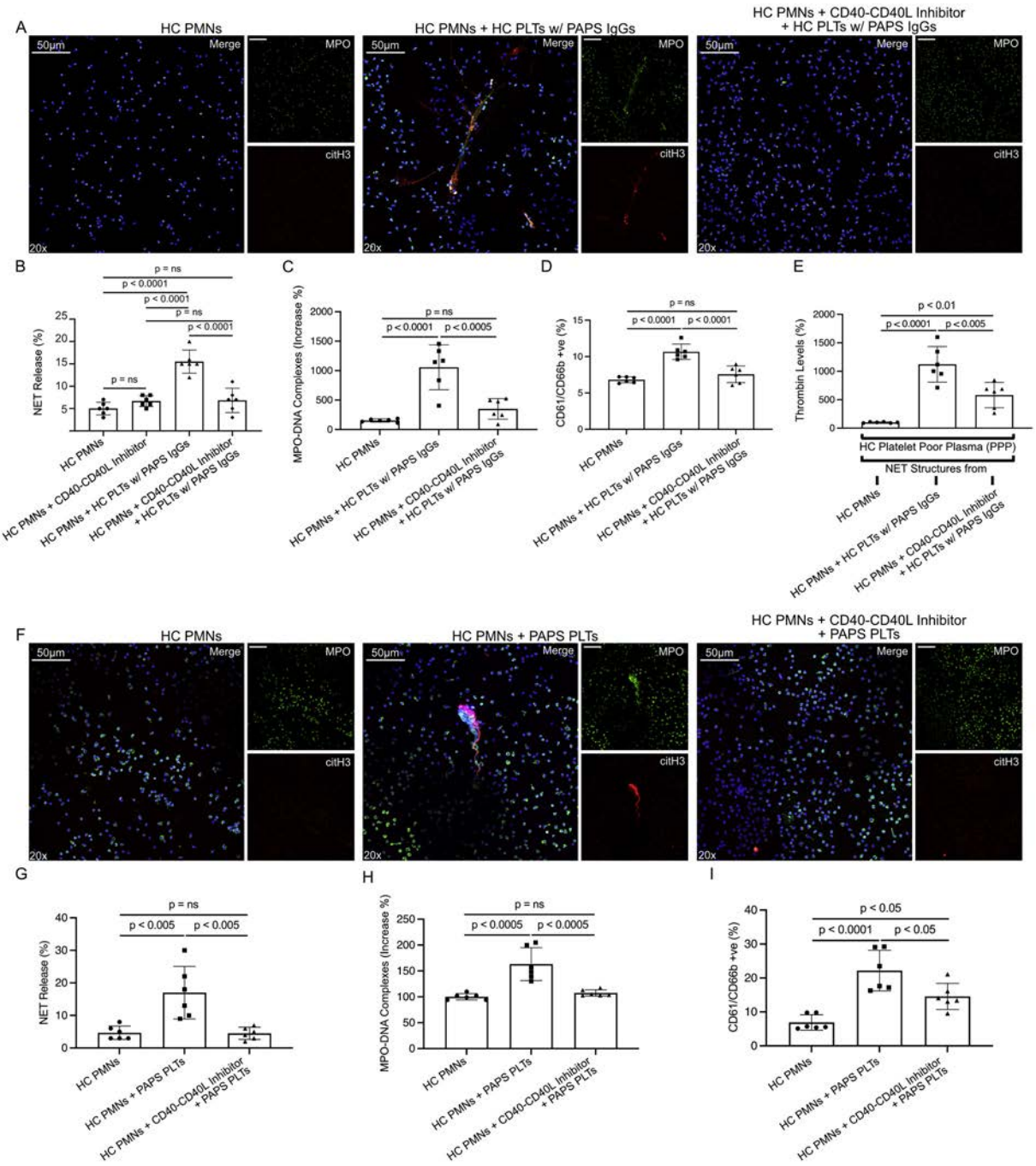

Figure 6. CD40-CD40L blockade attenuates NET formation in PAPS. (A) NETs released by isolated peripheral neutrophils from HCs stimulated with HC platelets pretreated with PAPS IgGs, with or without pretreatment with the CD40-CD40L interaction inhibitor DRI-C21045. Representative data from 1 of 6 experiments. (B) Quantification of NET release in (A). (C) MPO-DNA complex enzyme-linked immunosorbent assay (ELISA) in isolated NET structures from neutrophils in (A). (D) Quantification of CD61/CD66b double + ve events in (A). (E) Thrombin generation levels in HC platelet-poor plasma treated with NET structures from neutrophils in (A). (F) NETs released by isolated peripheral neutrophils from HCs treated with PAPS platelets (n = 6), compared with neutrophils pretreated with the CD40-CD40L interaction inhibitor DRI-C21045, prior to the addition of PAPS platelets. Representative data from 1 of 6 experiments. (G) Quantification of NET release in (F). (H) MPO-DNA complex enzyme-linked immunosorbent assay (ELISA) in isolated NET structures from neutrophils in (F). (I) Quantification of CD61/CD66b double + ve events in (F). Green: MPO, red: citH3, blue: DAPI/DNA. For (B-E,G-I), statistical analysis was performed using ordinary 1-way analysis of variance (ANOVA) followed by Tukey's multiple comparisons test. For (B-E,G-I), bars represent mean values ± SD, and each dot represents a patient. ANOVA, analysis of variance; citH3, citrullinated histone H3; DAPI, 4′,6-diamidino-2-phenylindole; ELISA, enzyme-linked immunosorbent assay; HC, healthy controls; MPO, myeloperoxidase; NET, neutrophil extracellular trap; PAPS, primary antiphospholipid syndrome; TF, tissue factor.

knowledge, no studies reported on the externalisation of TF in APS. Here, to our knowledge, we showed for the first time that *ex vivo* neutrophils from patients with PAPS externalise bioactive TF on released NETs.

Although NET release was observed in all patients with PAPS, not all patients demonstrated TF-decorated NETs. However, the thrombogenicity of NETs was TF-dependent. In previous studies, thrombin generation was enhanced by isolated neutrophils and cell supernatants from patients with PAPS [33,34], but not from isolated NETs. We also found that intracellular TF expression in neutrophils is induced by aPL. Notably, not all aPL from patients with PAPS were able to induce TF expression in neutrophils *in*

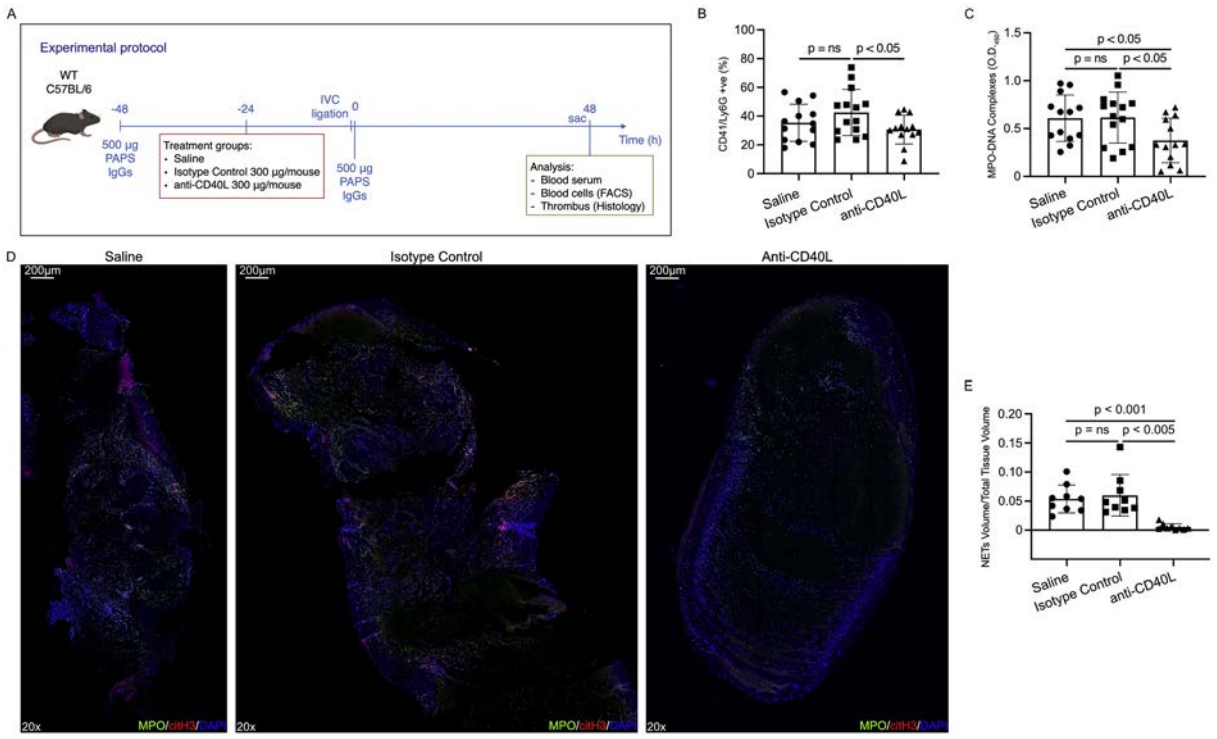

Figure 7. CD40-CD40L blockade alters thrombus composition in an experimental mouse model of PAPS. (A) Schematic representation of the experimental induction of PAPS in mice. C57BL/6 mice received 2 intraperitoneal (i.p.) doses of 500 μg isolated PAPS IgGs at a 48-hour interval. Treatment [saline (vehicle control), isotype control antibody (300 µg/mouse), or anti-CD40L antibody (300 µg/mouse)] was administered i.p. between the 2 PAPS IgG injections. Prior to the second PAPS IgG administration, mice underwent IVC ligation, and were humanely euthanised 48 hours later. (B) Quantification of platelet-neutrophil aggregates from mice in (A), determined as the % of CD41/Ly6G +ve cells by flow cytometry. (C) MPO-DNA complex enzyme-linked immunosorbent assay (ELISA) in isolated serum samples from mice in (A). (D) Presence of NETs, defined as MPO/citH3 +ve structures, in isolated thrombi from mice in (A). (E) Quantification of NET presence in thrombi from (D). Green: MPO, red: citH3, blue: DAPI/DNA. For (B,C,E), statistical analysis was performed using ordinary 1-way analysis of variance (ANOVA) followed by Tukey's multiple comparisons test. For (B,C,E), bars represent mean values ± SD. For (E), NET quantification was defined as the ratio NET volume/total tissue volume. IVC, inferior vena cava; ANOVA, analysis of variance; citH3, citrullinated histone H3; DAPI, 4′,6-diamidino-2-phenylindole; ELISA, enzyme-linked immunosorbent assay; HC, healthy controls; MPO, myeloperoxidase; NET, neutrophil extracellular trap; PAPS, primary antiphospholipid syndrome; TF, tissue factor.

vitro. Only aPL from patients who demonstrated TF expression in *ex vivo* neutrophils and NETs were able to induce *in vitro* TF expression. Moreover, sera from other thrombotic disorders (deep vein thrombosis, acute myocardial infarction, and stroke patients) were able to induce TF expression intracellularly in HC PMNs but were not able to induce NET release and externalisation of TF. These findings are in agreement with previous studies, which demonstrated that sera from patients with STEMI induce TF expression but do not induce NET release directly in PMNs [10].

The role of TF and NETs in thromboinflammation at the tissue level (eg, kidneys) has been demonstrated in an aPL-induced renal thrombotic microangiopathy mouse model [35]. However, their presence *in situ* was not previously investigated in tissue biopsies from patients with PAPS. Cutaneous manifestations in patients with APS may vary, from livedo reticularis to skin ulcers or necrosis, whereas kidney involvement in the form of APS nephropathy has been well-recognised in the context of both PAPS and SLE/APS [36]. We have shown here, for the first time, the presence of TF-decorated NETs and deposited fibrinogen in the proximity of NETs, in organ tissues from patients with PAPS, such as arterial thrombi and thrombosed vessels from skin ulcer biopsies. In kidney biopsies, TF-decorated NETs and fibrinogen were found in the glomerular capillaries and peritubular capillaries, but also in the tubulointerstitial compartment close to the Bowman's capsule, suggesting a possible involvement in the ongoing periglomerular scarring and tubular atrophy, in addition to TMA lesions [35]. Interestingly, a recent RNA-sequencing study on archival kidney biopsies from patients with PAPS showed higher expression of NET-related genes in PAPS vs control kidney samples [37]. We also found the presence of TF-decorated NETs and deposited fibrinogen in kidney biopsies of patients with renal TMA and in thrombus tissue from patients with peripheral artery atherothrombosis. These findings further support the importance of NETs as a mechanism in thromboinflammation and atherothrombosis [38].

We further investigated the intracellular pathways underlying NET release. Neutrophils and platelets interact minimally in the circulation in normal conditions, while the platelet-neutrophil cross-talk is important in the process of haemostasis and thrombosis, and is even implicated in the clearance of pathogens [39–44]. Circulating PNCs have been associated with thrombosis in individuals with acute coronary syndromes, and activated platelets were the main inducers of NET release in these patients [10]. In the context of APS, anti-β2GPI aPL interact with Fcγ-receptor IIa on the platelet surface and activate them [45]. Moreover, the release of platelet factor 4 (PF4) has been shown to promote the formation of highly antigenic PF4-complexed β2GPI, and subsequent platelet activation [46]. A previous study has demonstrated that platelets from patients with APS display a proinflammatory and procoagulant profile, including enhanced TF expression and participation in platelet-leukocyte aggregates

[47]. Platelet TF expression has been further characterised in APS, with TF-positive platelets and TF-positive platelet-leukocyte aggregates reinforcing the idea that platelet-driven thromboinflammation is itself a key contributor to APS thrombosis [48]. Additionally, a recent publication reported that platelets enhance the capacity of aPL to induce NET formation in neutrophils [16]. In the present study, we showed that patients with PAPS exhibit increased PNCs compared with HCs, and they are significantly correlated with the *ex vivo* NET release observed in neutrophils; PNCs also associate with the presence of venous thrombosis. We found for the first time that isolated *ex vivo* platelets alone from patients with PAPS can activate neutrophils and promote the formation of NETs.

Moreover, we showed that neutrophils in PAPS have increased basal autophagy levels, compared with HCs, and that increased autophagy was responsible for NET release. The use of a pan-AKT phosphorylator (autophagy inhibitor) halted this process, even in *ex vivo* PAPS neutrophils. We also observed that activated platelets that trigger NET release in patients with PAPS, induce autophagy in neutrophils of HCs.

Considering the role of platelets and their interaction with neutrophils in inducing thrombogenic NET release, targeting platelets or the platelet-neutrophil interaction can be a potential treatment strategy in APS. Platelet activation can be eliminated via platelet cyclooxygenase activity inhibition with aspirin, or via Toll-like receptor 7 inhibition with hydroxychloroquine [49]. Aspirin, in combination with vitamin K antagonists (with an INR 2-3), is one of the management options for thrombotic APS (with low level of evidence) [50], but it may increase the risk of bleeding. The platelet-neutrophil interaction in the blood and endothelium involves several receptor–ligand pairs, including P–selectin–P–selectin glycoprotein ligand, GPIbα–macrophage 1 antigen (MAC–1 and αMβ2), GPIIbIIIa–MAC–1 through fibrinogen, TREM-1 ligand and TREM-1, and CD40–CD40L [21]. CD40-CD40L interaction enhances neutrophil recruitment through upregulation of Mac-1, while CD40 has been shown to stimulate autophagy [51,52]. Performing functional validation assays using a CD40-CD40L interaction inhibitor, we found that CD40-CD40L blockade *in vitro* could eliminate platelet activation, autophagy, and NET formation in PAPS.

Most importantly, in our murine APS model, administration of a neutralising anti-CD40L antibody, inhibited platelet-neutrophil aggregation and subsequent NET release and significantly altered thrombus composition by significantly diminishing NET presence. It has already been established in several high-impact studies [53,54] that NETs are critical for the formation of arterial and venous thrombi in mice. A potential explanation for the lack of thrombus size reduction in our experiments might be that, as NET presence enhances thrombus stability through fibrin structure alterations and inhibits thrombus resolution [55], the chosen time point of analysis (48 hours after IVC ligation) was short to observe thrombus resolution, and we might be able to document thrombus size differences at a later experimental time point.

Treatments targeting CD40-CD40L pathway have been examined in systemic autoimmune diseases, mainly SLE [56–58]. First-generation anti-CD40L antibodies have been associated with increased thromboembolic risk, resulting from platelet activation triggered by FcγRIIa stimulation. However, the antibody used in our study has modifications in the Fc region, similar to the new anti-CD40L antibodies containing a modified Fc with low FcγRIIa binding. Trials of second-generation anti-CD40-CD40L antibodies have been recently completed, and others are currently taking place in patients with SLE and lupus nephritis [31,56–58].

A prior pioneering study demonstrated increased NET release in *ex vivo* neutrophils from patients with PAPS [34]. This study found an association between NET release and anti-β2GPI IgG positivity [34], a finding not observed in our study, which could be possibly due to a lack of power to detect possible associations. The study above showed that IgG purified from patients with APS stimulated the release of NETs from control neutrophils. In our experimental setting, we observed that serum or purified IgGs from patients with PAPS alone cannot induce NET release in neutrophils isolated from HCs, which could be due to different experimental settings, such as the neutrophil isolation method (presence/absence of platelets). In addition, our study group (patients with PAPS, asymptomatic aPL carriers, and HCs) consisted solely of White Europeans, limiting the generalisability of our findings to other ethnic groups. A multiethnic study with a larger sample size can lead to greater precision and higher power to detect true associations. Most patients with PAPS in our study were high-risk patients, with 63% experiencing recurrent thrombotic events, and 83% having LA positivity, 63% triple aPL positivity, and about 50% high IgG antiβ2GPI and aCL titres. These characteristics confirm a well-characterised APS population, and also help to better understand the pathophysiology of patients with high recurrence rates, who can benefit from potential new treatment targets.

In summary, our results showed a TF-dependent thrombogenicity of NETs and identified platelets as indispensable components of NET release in PAPS, while this process was mediated intracellularly by autophagy. Our data support a dual role of aPL, involving the intracellular TF expression in neutrophils and the activation of platelets for the generation of thrombogenic NETs. Inhibition of the platelet-neutrophil interaction through CD40-CD40L attenuated APS thrombogenicity both *in vitro* and *in vivo*. We also demonstrated the presence of TF-expressing NETs in endoarterial thrombi and microthrombi in skin ulcer and kidney biopsies. These findings provide additional evidence for intercepting NET-induced thromboinflammation in tissue damage in microvascular APS, a newly classified entity by the 2023 ACR/EULAR classification criteria for APS, including APS nephropathy, livedoid vasculopathy/skin ulcers, and alveolar haemorrhage [1]. These data may help in identifying potentially new therapeutic targets but also support repositioning of existing drugs, such as anti-CD40L antibodies in patients with refractory thrombotic APS, anticoagulation-resistant microvascular APS manifestations, or even other thrombotic disorders with prominent platelet-neutrophil interaction.

Competing interests

MT reports funding provided by National and Kapodistrian University of Athens and a relationship with National and Kapodistrian University of Athens. The other authors declare no competing interests.

CRediT authorship contribution statement

Stavros Naoum: Writing – review & editing, Writing – original draft, Methodology, Investigation, Data curation. **Charilaos Spyropoulos:** Writing – review & editing, Formal analysis. **Andriani Angelopoulou:** Writing – review & editing, Formal analysis. **Harikleia Gakiopoulou:** Writing – review & editing, Formal analysis. **Michalis Katsimpoulas:** Writing – review & editing, Formal analysis, Methodology. **Vassilis G. Gorgoulis:**

Writing – review & editing, Formal analysis. **Petros P. Sfikakis:** Writing – review & editing, Resources. **Konstantinos Ritis:** Writing – review & editing, Investigation, Conceptualization. **Ioanna-Evdokia Galani:** Writing – review & editing, Writing – original draft, Investigation, Formal analysis. **Konstantinos Kambas:** Writing – review & editing, Writing – original draft, Methodology, Investigation, Formal analysis, Conceptualization. **Maria G. Tektonidou:** Writing – review & editing, Writing – original draft, Supervision, Resources, Methodology, Investigation, Funding acquisition, Conceptualization.

Acknowledgements

We would like to thank the Light Microscopy Unit of Hellenic Pasteur Institute for providing the facilities for confocal microscopy. Additionally, we would like to thank Konstantinos Lazaridis for providing isolated and purified IgGs from serum samples, Evangelos Balafas for assisting in mouse surgery procedures, and Mrs. Anna Agapaki for preparing murine biopsies.

Contributors

SN conducted experiments, analysed the data and drafted the manuscript. CS and AA conducted experiments and analysed the data. HG contributed to biopsy samples acquisition and data interpretation. MK contributed to animal study design and conducted animal surgery experiments. VGG contributed to the design of experiments and data interpretation. PPS contributed to data acquisition and data interpretation. KR contributed to study design, design of experiments, and data interpretation. I-EG contributed to animal study design, conducted experiments, data analysis, data interpretation, and drafted the manuscript. KK conceived and supervised the project, contributed to study design, design of experiments, experiments supervision, data analysis, data interpretation, and drafted the manuscript. MGT conceived and supervised the project, contributed to study design, study funding, recruitment, sample collection, and clinical data extraction from patients and healthy individuals, data analysis, data interpretation, and drafted the manuscript. KK and MGT act as guarantors for the overall content. All authors critically revised the manuscript and approved its final version.

Funding

This work was supported by Special Account for Research Funding (E.L.K.E., grant number 11123), Medical School, National and Kapodistrian University of Athens, Athens, Greece.

Patient consent for publication

Not applicable.

Ethics approval

The study was approved by the Ethics Committee of Laiko General Hospital (protocol number 398/31-05-2021) and was conducted according to Declaration of Helsinki principles. All participants provided written informed consent.

Provenance and peer review

Not commissioned; externally peer reviewed.

Data availability statement

The data that support the findings of this study are available from the corresponding author, MGT, upon reasonable request.

Supplementary materials

Supplementary material associated with this article can be found in the online version at doi:10.1016/j.ard.2025.12.012.

Orcid

Maria G. Tektonidou: http://orcid.org/0000-0003-2238-0975

REFERENCES

[1] Barbhaiya M, Zuily S, Naden R, Hendry A, Manneville F, Amigo MC, et al. The 2023 ACR/EULAR antiphospholipid syndrome classification criteria. Arthritis Rheumatol 2023;75(10):1687–702. doi: 10.1002/art.42624.
[2] Knight JS, Branch W, Ortel TL. Antiphospholipid syndrome: advances in diagnosis, pathogenesis, and management. BMJ 2023;380:e069717. doi: 10.1136/bmj-2021-069717.
[3] Giannakopoulos B, Krilis SA. The pathogenesis of the antiphospholipid syndrome. N Engl J Med 2013;368(11):1033–44. doi: 10.1056/NEJMra1112830.
[4] De Groot PG, de Laat B. Mechanisms of thrombosis in systemic lupus erythematosus and antiphospholipid syndrome. Best Pract Res Clin Rheumatol 2017;31(3):334–41. doi: 10.1016/j.berh.2017.09.008.
[5] Corban MT, Duarte-Garcia A, McBane RD, Matteson EL, Lerman LO, Lerman A. Antiphospholipid syndrome: role of vascular endothelial cells and implications for risk stratification and targeted therapeutics. J Am Coll Cardiol 2017;69(18):2317–30. doi: 10.1016/j.jacc.2017.02.058.
[6] Tektonidou MG. Cardiovascular disease risk in antiphospholipid syndrome: thrombo-inflammation and atherothrombosis. J Autoimmun 2022;128:102813. doi: 10.1016/j.jaut.2022.102813.
[7] Salet DM, Bekkering S, Middeldorp S, van den Hoogen LL. Targeting thromboinflammation in antiphospholipid syndrome. J Thromb Haemost 2023;21(4):744–57.
[8] Raschi E, Borghi MO, Tedesco F, Meroni PL. Antiphospholipid syndrome pathogenesis in 2023: an update of new mechanisms or just a reconsideration of the old ones? Rheumatology (Oxford) 2024;63(Suppl I):SI4–SI13.
[9] López-Pedrera C, Pérez-Sánchez C, Tektonidou MG. Towards precision medicine in antiphospholipid syndrome. Lancet Rheumatol 2025;7(8):e576–89.
[10] Stakos DA, Kambas K, Konstantinidis T, Mitroulis I, Apostolidou E, Arelaki S, et al. Expression of functional tissue factor by neutrophil extracellular traps in culprit artery of acute myocardial infarction. Eur Heart J 2015;36(22):1405–14. doi: 10.1093/eurheartj/ehv007.
[11] Kambas K, Mitroulis I, Apostolidou E, Girod A, Chrysanthopoulou A, Pneumatikos I, et al. Autophagy mediates the delivery of thrombogenic tissue factor to neutrophil extracellular traps in human sepsis. PLOS ONE 2012;7(9):e45427. doi: 10.1371/journal.pone.0045427.
[12] Kambas K, Chrysanthopoulou A, Vassilopoulos D, Apostolidou E, Skendros P, Girod A, et al. Tissue factor expression in neutrophil extracellular traps and neutrophil derived microparticles in antineutrophil cytoplasmic antibody associated vasculitis may promote thromboinflammation and the thrombophilic state associated with the disease. Ann Rheum Dis 2014;73(10):1854–63. doi: 10.1136/annrheumdis-2013-203430.
[13] Frangou E, Chrysanthopoulou A, Mitsios A, Kambas K, Arelaki S, Angelidou I, et al. REDD1/autophagy pathway promotes thromboinflammation and fibrosis in human systemic lupus erythematosus (SLE) through NETs decorated with tissue factor (TF) and interleukin-17A (IL-17A). Ann Rheum Dis 2019;78(2):238–48. doi: 10.1136/annrheumdis-2018-213181.
[14] Remijsen Q, Kuijpers KW, Wirawan E, Lippens S, Vandenabeele P, Vanden Berghe T. Dying for a cause: NETosis, mechanisms behind an antimicrobial cell death modality. Cell Death Differ 2011;18(4):581–8. doi: 10.1038/cdd.2011.1.
[15] Sennett C, Pula G. Trapped in the NETs: multiple roles of platelets in the vascular complications associated with neutrophil extracellular traps. Cells 2025;14(5):335. doi: 10.3390/cells14050335.
[16] NaveenKumar SK, Tambralli A, Fonseca BM, Yalavarthi S, Liang W, Hoy CK, et al. Low ectonucleotidase activity and increased neutrophil-platelet

aggregates in patients with antiphospholipid syndrome. Blood 2024;143 (12):1193–7. doi: 10.1182/blood.2023022097.
[17] Liu Q, Zhu W, Wen X, Da Y. The role of platelet–neutrophil interactions in driving autoimmune diseases. Immunology 2025;175(1):1–15.
[18] Henn V, Slupsky JR, Gräfe M, Anagnostopoulos I, Förster R, Müller-Berghaus G, et al. CD40 ligand on activated platelets triggers an inflammatory reaction of endothelial cells. Nature 1998;391(6667):591–4. doi: 10.1038/35393.
[19] Cognasse F, Duchez AC, Audoux E, Ebermeyer T, Arthaud CA, Prier A, et al. Platelets as key factors in inflammation: focus on CD40L/CD40. Front Immunol 2022;13:825892. doi: 10.3389/fimmu.2022.825892.
[20] Barbar S, Noventa F, Rossetto V, Ferrari A, Brandolin B, Perlati M, et al. A risk assessment model for the identification of hospitalized medical patients at risk for venous thromboembolism: the Padua Prediction Score. J Thromb Haemost 2010;8(11):2450–7. doi: 10.1111/j.1538-7836.2010.04044.x.
[21] Kaiser R, Escaig R, Erber J, Nicolai L. Neutrophil-platelet interactions as novel treatment targets in cardiovascular disease. Front Cardiovasc Med 2022;8:824112. doi: 10.3389/fcvm.2021.824112.
[22] Daub S, Lutgens E, Münzel T, Daiber A. CD40/CD40L and related signaling pathways in cardiovascular health and disease-the pros and cons for cardioprotection. Int J Mol Sci 2020;21(22):8533. doi: 10.3390/ijms21228533.
[23] Miyakis S, Lockshin MD, Atsumi T, Branch DW, Brey RL, Cervera R, et al. International consensus statement on an update of the classification criteria for definite antiphospholipid syndrome (APS). J Thromb Haemost 2006;4 (2):295–306. doi: 10.1111/j.1538-7836.2006.01753.x.
[24] Aringer M, Costenbader K, Daikh D, Brinks R, Mosca M, Ramsey-Goldman R, et al. 2019 European League Against Rheumatism/American College of Rheumatology classification criteria for systemic lupus erythematosus. Arthritis Rheumatol 2019;71(9):1400–12. doi: 10.1002/art.40930.
[25] Payne H, Brill A. Stenosis of the inferior vena cava: a murine model of deep vein thrombosis. J Vis Exp 2017;130:56697. doi: 10.3791/56697.
[26] Vandevelde A, Chayoua W, de Laat B, Moore GW, Musiał J, Zuily S, et al. Added value of antiphosphatidylserine/prothrombin antibodies in the workup of thrombotic antiphospholipid syndrome: communication from the ISTH SSC Subcommittee on Lupus Anticoagulant/Antiphospholipid Antibodies. J Thromb Haemost 2022;20(9):2136–50. doi: 10.1111/jth.15785.
[27] Ott I, Neumann FJ, Gawaz M, Schmitt M, Schömig A. Increased neutrophil-platelet adhesion in patients with unstable angina. Circulation 1996;94 (6):1239–46. doi: 10.1161/01.cir.94.6.1239.
[28] Tuttle HA, Davis-Gorman G, Goldman S, Copeland JG, McDonagh PF. Platelet-neutrophil conjugate formation is increased in diabetic women with cardiovascular disease. Cardiovasc Diabetol 2003;2:12. doi: 10.1186/1475-2840-2-12.
[29] Petzold T, Zhang Z, Ballesteros I, Saleh I, Polzin A, Thienel M, et al. Neutrophil "plucking" on megakaryocytes drives platelet production and boosts cardiovascular disease. Immunity 2022;55(12):2285–2299.e7. doi: 10.1016/j.immuni.2022.10.001.
[30] Clark SR, Ma AC, Tavener SA, McDonald B, Goodarzi Z, Kelly MM, et al. Platelet TLR4 activates neutrophil extracellular traps to ensnare bacteria in septic blood. Nat Med 2007;13(4):463–9. doi: 10.1038/nm1565.
[31] Ramanujam M, Steffgen J, Visvanathan S, Mohan C, Fine JS, Putterman C. Phoenix from the flames: Rediscovering the role of the CD40-CD40L pathway in systemic lupus erythematosus and lupus nephritis. Autoimmun Rev 2020;19(11):102668. doi: 10.1016/j.autrev.2020.102668.
[32] Cuadrado MJ, López-Pedrera C, Khamashta MA, Camps MT, Tinahones F, Torres A, et al. Thrombosis in primary antiphospholipid syndrome: a pivotal role for monocyte tissue factor expression. Arthritis Rheum 1997;40(5):834–41. doi: 10.1002/art.1780400509.
[33] Ritis K, Doumas M, Mastellos D, Micheli A, Giaglis S, Magotti P, et al. A novel C5a receptor-tissue factor cross-talk in neutrophils links innate immunity to coagulation pathways. J Immunol 2006;177(7):4794–802. doi: 10.4049/jimmunol.177.7.4794.
[34] Yalavarthi S, Gould TJ, Rao AN, Mazza LF, Morris AE, Núñez-Álvarez C, et al. Release of neutrophil extracellular traps by neutrophils stimulated with antiphospholipid antibodies: a newly identified mechanism of thrombosis in the antiphospholipid syndrome. Arthritis Rheumatol 2015;67(11):2990–3003. doi: 10.1002/art.39247.
[35] Seshan SV, Franzke CW, Redecha P, Monestier M, Mackman N, Girardi G. Role of tissue factor in a mouse model of thrombotic microangiopathy induced by antiphospholipid antibodies. Blood 2009;114(8):1675–83. doi: 10.1182/blood-2009-01-199117.
[36] Tektonidou MG. Antiphospholipid syndrome nephropathy: from pathogenesis to treatment. Front Immunol 2018;9:1181. doi: 10.3389/fimmu.2018.01181.
[37] Tektonidou MG, Verrou KM, Gakiopoulou H, Manoloukos M, Lembessis P, Hatzis P, et al. Kidney whole-transcriptome profiling in primary antiphospholipid syndrome reveals complement, interferons and NETs-related gene expression. Rheumatology (Oxford) 2024;63(11):3184–90. doi: 10.1093/rheumatology/keae397.
[38] d'Alessandro E, Becker C, Bergmeier W, Bode C, Bourne JH, Brown H, et al. Thrombo-inflammation in cardiovascular disease: an expert consensus document from the third Maastricht Consensus Conference on Thrombosis. Thromb Haemost 2020;120(4):538–64. doi: 10.1055/s-0040-1708035.
[39] Lisman T. Platelet–neutrophil interactions as drivers of inflammatory and thrombotic disease. Cell Tissue Res 2018;371(3):567–76. doi: 10.1007/s00441-017-2727-4.
[40] Darbousset R, Thomas GM, Mezouar S, Frère C, Bonier R, Mackman N, et al. Tissue factor-positive neutrophils bind to injured endothelial wall and initiate thrombus formation. Blood 2012;120(10):2133–43. doi: 10.1182/blood-2012-06-437772.
[41] Deppermann C, Kubes P. Platelets and infection. Semin Immunol 2016;28 (6):536–45. doi: 10.1016/j.smim.2016.10.005.
[42] Jenne CN, Kubes P. Platelets in inflammation and infection. Platelets 2015;26 (4):286–92. doi: 10.3109/09537104.2015.1010441.
[43] Ed Rainger G, Chimen M, Harrison MJ, Yates CM, Harrison P, Watson SP, et al. The role of platelets in the recruitment of leukocytes during vascular disease. Platelets 2015;26(6):507–20. doi: 10.3109/09537104.2015.1064881.
[44] Pircher J, Engelmann B, Massberg S, Schulz C. Platelet-neutrophil crosstalk in atherothrombosis. Thromb Haemost 2019;119(8):1274–82. doi: 10.1055/s-0039-1692983.
[45] Hollerbach A, Müller-Calleja N, Ritter S, Häuser F, Canisius A, Orning C, et al. Platelet activation by antiphospholipid antibodies depends on epitope specificity and is prevented by mTOR inhibitors. Thromb Haemost 2019;119 (7):1147–53. doi: 10.1055/s-0039-1685453.
[46] Sikara MP, Routsias JG, Samiotaki M, Panayotou G, Moutsopoulos HM, Vlachoyiannopoulos PG. {beta}2 Glycoprotein I ({beta}2GPI) binds platelet factor 4 (PF4): implications for the pathogenesis of antiphospholipid syndrome. Blood 2010;115(3):713–23. doi: 10.1182/blood-2009-03-206367.
[47] Capozzi A, Manganelli V, Riitano G, Recalchi S, Truglia S, Alessandri C, et al. Tissue factor over-expression in platelets of patients with anti-phospholipid syndrome: induction role of anti-β2-GPI antibodies. Clin Exp Immunol 2019;196(1):59–66. doi: 10.1111/cei.13248.
[48] Camera M, Brambilla M, Lonati PA, Becchetti A, Grossi C, Nallio K, et al. Mechanisms sensitive to different drugs mediate a pro-adhesive and prothrombotic platelet phenotype in anti-phospholipid syndrome. Haematologica 2026;111(1):219–29. doi: 10.3324/haematol.2024.287133.
[49] Scherlinger M, Richez C, Tsokos GC, Boilard E, Blanco P. The role of platelets in immune-mediated inflammatory diseases. Nat Rev Immunol 2023;23 (8):495–510. doi: 10.1038/s41577-023-00834-4.
[50] Tektonidou MG, Andreoli L, Limper M, Amoura Z, Cervera R, Costedoat-Chalumeau N, et al. EULAR recommendations for the management of antiphospholipid syndrome in adults. Ann Rheum Dis 2019;78(10):1296–304. doi: 10.1136/annrheumdis-2019-215213.
[51] Jin R, Yu S, Song Z, Zhu X, Wang C, Yan J, et al. Soluble CD40 ligand stimulates CD40-dependent activation of the β2 integrin Mac-1 and protein kinase C zeda (PKCζ) in neutrophils: implications for neutrophil-platelet interactions and neutrophil oxidative burst. PLOS ONE 2013;8(6):e64631. doi: 10.1371/journal.pone.0064631.
[52] Portillo JA, Okenka G, Reed E, Subauste A, Van Grol J, Gentil K, et al. The CD40-autophagy pathway is needed for host protection despite IFN-Γ-dependent immunity and CD40 induces autophagy via control of P21 levels. PLOS ONE 2010;5(12):e14472. doi: 10.1371/journal.pone.0014472.
[53] Jiménez-Alcázar M, Rangaswamy C, Panda R, Bitterling J, Simsek YJ, Long AT, et al. Host DNases prevent vascular occlusion by neutrophil extracellular traps. Science 2017;358(6367):1202–6. doi: 10.1126/science.aam8897.
[54] von Brühl ML, Stark K, Steinhart A, Chandraratne S, Konrad I, Lorenz M, et al. Monocytes, neutrophils, and platelets cooperate to initiate and propagate venous thrombosis in mice in vivo. J Exp Med 2012;209(4):819–35. doi: 10.1084/jem.20112322.
[55] Thålin C, Hisada Y, Lundström S, Mackman N, Wallén H. Neutrophil extracellular traps: villains and targets in arterial, venous, and cancer-associated thrombosis. Arterioscler Thromb Vasc Biol 2019;39(9):1724–38. doi: 10.1161/ATVBAHA.119.312463.
[56] Shock A, Burkly L, Wakefield I, Peters C, Garber E, Ferrant J, et al. CDP7657, an anti-CD40L antibody lacking an Fc domain, inhibits CD40L-dependent

immune responses without thrombotic complications: an *in vivo* study. Arthritis Res Ther 2015;17(1):234. doi: 10.1186/s13075-015-0757-4.

[57] Furie RA, Bruce IN, Dörner T, Leon MG, Leszczyński P, Urowitz M, et al. Phase 2, randomized, placebo-controlled trial of dapirolizumab pegol in patients with moderate-to-severe active systemic lupus erythematosus. Rheumatology (Oxford) 2021;60(11):5397–407. doi: 10.1093/rheumatology/keab381.

[58] Chamberlain C, Colman PJ, Ranger AM, Burkly LC, Johnston GI, Otoul C, et al. Repeated administration of dapirolizumab pegol in a randomised phase I study is well tolerated and accompanied by improvements in several composite measures of systemic lupus erythematosus disease activity and changes in whole blood transcriptomic profiles. Ann Rheum Dis 2017;76 (11):1837–44. doi: 10.1136/annrheumdis-2017-211388.

Ann Rheum Dis 85 (2026) 873–879

Contents lists available at ScienceDirect

Annals of the Rheumatic Diseases

journal homepage: https://www.sciencedirect.com/journal/annals-of-the-rheumatic-diseases

Sjögren's syndrome

Transcriptomic stratification predicts response to rituximab, abatacept, or the association of hydroxychloroquine and leflunomide in 3 randomised controlled clinical trials of Sjögren's disease

Baptiste Chevet[1,2], Valérie Devauchelle-Pensec[1,2], Elena Pontarini[3], Valentin Baloche[4], Michele Bombardieri[3], Simon J. Bowman[5,6,7,8], Michael Barnes[9], Antoine G. Sreih[10,11,12], Jinqi Liu[11], Sheila Kelly[11], Antonia Christodoulou[11], Philippe Moingeon[13], Laurence Laigle[13], Perrine Soret[13], Christelle Le Dantec[2], Jacques-Olivier Pers[2], Marta E. Alarcon-Riquelme[14], Guillermo Barturen[14], Xavier Mariette[15], Joel van Roon[4], Raphaèle Seror[15], Gaetane Nocturne[15], Divi Cornec[1,2,*], Nathan Foulquier[2,16], PRECISEADS Clinical Consortium, NECESSITY consortium

[1] *Rheumatology Department, CHU Brest, Brest, France*
[2] *LBAI, UMR1227, INSERM, University of Brest, Brest, France*
[3] *Centre for Experimental Medicine and Rheumatology, William Harvey Research Institute, London, UK*
[4] *Department of Rheumatology and Clinical Immunology, University Medical Center Utrecht, Utrecht, The Netherlands*
[5] *Department of Rheumatology, University Hospitals Birmingham, Birmingham, UK*
[6] *School of Infection, Inflammation & Immunology, University of Birmingham, Birmingham, UK*
[7] *National Institute for Health and Care Research (NIHR) Birmingham Biomedical Research Centre, Birmingham, UK*
[8] *Milton Keynes University Hospital, Milton Keynes, UK*
[9] *Centre for Translational Bioinformatics, Queen Mary, University of London (QMUL), London, UK*
[10] *Division of Rheumatology, University of Pennsylvania, Philadelphia, PA, USA*
[11] *Bristol-Myers Squibb, Lawrenceville, NJ, USA*
[12] *Cullinan Therapeutics, Boston, MA, USA*
[13] *Institut de recherche Servier, Université Paris-Saclay, Gif-sur-Yvette, France*
[14] *Center for Genomics and Oncological Research (GENYO), Granada, Spain*
[15] *Department of Rheumatology, Université Paris-Saclay, INSERM UMR1184, IMVA, CEA, AP-HP, Hôpital Bicêtre, Le Kremlin Bicêtre, France*
[16] *Rheumatology, and Clinical Data Center, pôle PHARES, Inserm 1227, lymphocytes B et autoimmunité, CHU de Brest, University Brest, Brest, France*

ARTICLE INFO

Article history:
Received 24 September 2025
Received in revised form 17 November 2025
Accepted 18 November 2025

ABSTRACT

Objectives: Sjögren's disease (SjD) is clinically and biologically heterogeneous, and no immunomodulatory drug has yet demonstrated efficacy in phase 3 trials. We previously identified 4 transcriptomic endotypes in SjD patients using whole-blood RNA sequencing. We hypothesised that these endotypes may predict differential therapeutic responses.

*Correspondence to Prof. Divi Cornec, Rheumatology Department, CHU Brest, Brest, France.
E-mail address: divi.cornec@chu-brest.fr (D. Cornec).
Handling editor Josef S. Smolen.

https://doi.org/10.1016/j.ard.2025.11.017

Methods: We analysed clinical, biological, and transcriptomic data from 3 randomised controlled trials evaluating hydroxychloroquine-leflunomide (HCQ-LEF; n = 18; RepurpSS-I trial), rituximab (RTX; n = 56; TRACTISS trial), and abatacept (n = 117). Patients were assigned to the 4 endotypes using semisupervised uniform manifold approximation and projection combined with a support vector machine model. Demographics, disease activity, and therapeutic response, as defined by the Sjögren Tool for Assessing Response index, were compared across clusters in both pooled and individual trial analyses.

Results: Of 170 patients, 81, 24, 80, and 6 were classified into clusters 1 to 4, respectively. European Alliance of Associations for Rheumatology (EULAR) Sjögren's Syndrome Patient Reported Index scores were comparable across clusters, while the EULAR Sjögren's Syndrome Disease Activity Index was significantly higher in clusters 3 and 4 vs clusters 1 and 2 (P = .003). In pooled analyses, patients in cluster 1 had significantly greater response rates with active treatment vs placebo (61.5% vs 32.6%: P = .016), with a similar trend in the RTX trial. In contrast, patients in cluster 3 benefitted from HCQ-LEF, whereas cluster 2 (healthy-like patients) showed no significant response to any therapy.

Conclusions: Transcriptomic stratification of SjD patients revealed differential responses to HCQ-LEF and RTX. Notably, healthy-like patients exhibited minimal treatment response, suggesting they may be unsuitable candidates for future therapeutic trials.

WHAT IS ALREADY KNOWN ON THIS TOPIC

- Sjögren's patients are heterogeneous and can be clustered into transcriptomic-based endotypes.

WHAT THIS STUDY ADDS

- Rituximab is more effective than placebo in patients with a type I interferon signature. Those with a B-cell profile respond better to hydroxychloroquine-leflunomide. In contrast, healthy-like Sjögren's patients do not demonstrate a differential response to immunomodulatory treatment compared with placebo.

HOW THIS STUDY MIGHT AFFECT RESEARCH, PRACTICE OR POLICY

- Stratifying Sjögren's patients based on transcriptomic signatures may help identify those more likely to benefit from treatment.

INTRODUCTION

Sjögren's disease (SjD) [1] is a highly heterogeneous autoimmune disease characterised by eye and mouth dryness and systemic involvement, exhibiting both clinical [2,3] and biological [4,5] variability. Despite numerous randomised controlled trials (RCTs) conducted over the last 2 decades [6], no systemic drug has demonstrated significant efficacy in improving systemic manifestations or sicca symptoms in SjD patients in a phase 3 trial. Mainly used as the primary outcome by Seror et al [7], the European Alliance of Associations for Rheumatology (EULAR) Sjögren's Syndrome Disease Activity Index (ESSDAI) [8] is a disease activity score that evaluates systemic involvement. The lack of demonstrated drug efficacy in previous controlled trials may be attributed to several factors. First, most of the drugs tested so far were repurposed for rheumatoid arthritis, such as tumour necrosis factor blockers [9,10], hydroxychloroquine (HCQ) [11], rituximab (RTX) [12,13], and abatacept (ABA) [14–16], which may have no or low efficacy in SjD, as different immunopathological pathways may be involved. Second, the response rate in placebo arms [7] is high in most RCTs, which could mask the efficacy of the drugs tested. In response to this, the Sjögren Tool for Assessing Response (STAR) index has recently been developed to improve the discriminant capacity between drug and placebo responses, incorporating objective disease measures and broader clinical response [7]. This 5-item score includes systemic manifestations assessed by the clinical items of the ESSDAI (clinESSDAI), patient-reported outcomes assessed by the EULAR Sjögren's Syndrome Patient Reported Index (ESSPRI), lachrymal and salivary gland function, and biological markers of disease activity, including rheumatoid factor and gamma globulin levels. Third, the heterogeneity in SjD patients is likely to influence treatment responses. The absence of efficacy in some patients could undermine the drug's efficacy in other patient subgroups, resulting in unnecessary treatment exposure for some patients. Stratifying SjD patients into more homogeneous groups may reveal the efficacy of specific drugs in some subgroups.

We previously showed, using whole-blood RNA sequencing (RNAseq), that SjD patients can be clustered into 4 distinct groups (endotypes), characterised by differential interferon (IFN) and inflammatory signatures and displaying different clinical and biological features [4]. The first endotype includes SjD patients with a strong type I IFN transcriptomic signature. These patients have the highest levels of rheumatoid factor, hypergammaglobulinemia, and anti-SSA positivity in up to 99% of patients. The third endotype is characterised by B-cell transcriptomic and serological signatures, and an intermediate type I IFN signature. Patients from the fourth endotype show a mild type I IFN signature, but strong type II IFN and neutrophil signatures, and have the highest systemic disease activity, as defined by ESSDAI and the physician global assessment. Finally, patients with the second endotype show healthy-like transcriptomic features and are characterised by the absence of an IFN signature, the lowest inflammatory blood biomarkers, a lower prevalence of anti-SSA positivity, and the lowest ESSDAI score compared with other patients.

We hypothesised that different drugs may have different efficacy across these 4 different endotypes. Using whole-blood transcriptomic and clinical data from 3 previously published RCTs evaluating the efficacy of RTX [13], ABA [14], and combination therapy with HCQ and leflunomide (HCQ-LEF) [17], we aimed to compare the response rates of these drugs with placebo across the 4 defined endotypes.

METHODS

Design and population

In this post hoc study, we retrieved data from SjD patients included in 3 RCTs assessing HCQ-LEF in the RepurpSS-I trial

[17], RTX in the TRACTISS trial [13], and ABA [14]. All patients with available whole-blood RNAseq and clinical data necessary to calculate STAR were included in our analysis. The trials were approved by the appropriate ethics committees, as described in the original publications [13,14,17].

Stratification of the patients based on their transcriptomic profile

Patients in each clinical trial were stratified into 4 endotypes according to their whole-blood RNAseq profile at baseline [4]. We employed a 3–step, cluster–guided embedding and clustering pipeline. First, transcriptomic data from the PRECISESADS cohort were used to train a supervised uniform manifold approximation and projection (UMAP) embedding, explicitly incorporating the 4 molecular clusters defined by Soret et al [4] to shape the low-dimensional manifold and enhance the separation of known clusters. This was implemented via the label-aware extension in the UMAP-learn Python package, which integrates prior cluster labels during optimisation to produce a stable and interpretable representation [18]. Second, independent samples from the TRACTISS, RepurpSS-I, and ABA trial cohorts were projected into this learned UMAP space using its transform function, ensuring that all cohorts share a common coordinate system for downstream comparison. Finally, we applied hierarchical density-based spatial clustering of applications with noise to the embedded points using the algorithm's stability–based flat–cluster extraction method to identify density–defined clusters in each external dataset. We then mapped each resulting cluster to its nearest PRECISESADS centroid, as defined by Soret et al [4], thereby preserving consistency of cluster annotation across all cohorts.

Outcomes

The STAR criteria [7] were used to assess treatment response. This outcome is achieved when patients complete at least 5 points across 5 items, including a decrease ≥3 in clinical items of clinESSDAI (3 points), a decreases ≥1 or ≥15% in ESSPRI (3 points), an increase ≥5 mm in the Schirmer's test (1 point), an increase ≥25% in unstimulated salivary flow (1 point), and a decrease ≥10% in immunoglobulin G level or a decrease >25% in rheumatoid factor level (1 point).

The timing of assessment varied according to the studies. The response was assessed at the primary endpoint visit in each trial. In the ABA and the RepurpSS-I trials, STAR was assessed at week 24. In the TRACTISS trial, the primary endpoint was at week 48.

Statistics

Statistical differences in categorical clinical characteristics across clusters and cohorts were assessed using the chi-square test of independence, with Yates' correction for continuity applied to all 2 × 2 contingency tables to account for small sample sizes. Analyses were conducted in Python using the scipy.stats.chi2_contingency function.

RESULTS

Of the 349 patients included in the 3 RCTs, both baseline RNAseq data and the STAR index were retrieved for 210 (60.2%) patients (18/29 from the HCQ-LEF trial, 117/187 from the ABA trial, 75/133 from the RTX trial).

Overall, the mean age (SD) was 53.7 (12.8), and women represented 95.2% of the cohort (Table 1). Unstimulated salivary flow was <0.1 mL/min in 137/191 (72.1%) patients, while the Schirmer test was <5 mm/5 min in 137/189 (72.5%) patients.

The prevalence of anti-SSA antibodies ranged from 94% to 100% across the 3 cohorts. The differences in the serological profiles were driven by the inclusion criteria of the different studies, as the TRACTISS and ABA trials included anti-SSA positivity. Activity scores at baseline differed across the different cohorts. The mean (SD) ESSPRI was 6.0 (2.2) for the whole cohort, and 6.3 (2.0), 5.3 (2.1), and 5.6 (2.4) in the ABA, HCQ-LEF, and RTX trials, respectively (P = .79). The mean (SD) ESSDAI was 7.3 (4.8) overall and 9.4 (4.1), 7.3 (4.4), and 4.0 (4.0) in patients in the ABA, HCQ-LEF, and RTX trials, respectively (P = .44).

Comparison of patients' clinical features across the 4 different endotypes

Among the 210 patients, 82 (39.0%), 25 (11.9%), 95 (45.2%), and 8 (3.8%) were assigned to clusters 1 to 4, respectively. Of the 75 patients included in the TRACTISS trial, 37 (49.3%), 12 (16.0%), 23 (30.6%), and 3 (4.0%) were assigned to endotypes 1 to 4, respectively, whereas 5 (27.8%) and 13 (72.2%) patients in the RepurpSS-I trial were assigned to the endotypes 1 and 3, respectively. Among the 117 patients in the ABA trial, 40 (34.2%), 13 (11.1%), 59 (50.4%), and 5 (4.3%) were assigned to clusters 1 to 4, respectively (Supplementary Fig S1). Cluster 1

Table 1
Sjögren patients from the TRACTISS, RepurpSS-I, and abatacept trials retrieved for transcriptomic-based post hoc analysis

Features	TRACTISS n = 75	RepurpSS-I n = 18	Abatacept n = 117	Total N = 210	*P* value
Demographics					
Age (y), mean (SD)	55.0 (12.3)	55.8 (13.3)	52.6 (13.11)	53.7 (12.8)	.458
Sex female, n (%)	70 (93.3)	18 (100)	112 (95.7)	200 (95.2)	.343
Sjögren features					
Anti-SSA positivity, n/N (%)	75/75 (100)	17/18 (94.4)	117/117 (100)	209/210 (99.5)	.0857
Anormal unstimulated salivary flow, n/N (%)	42/56 (75.0)	15/18 (83.3)	80/117 (68.4)	137/191 (72.1)	.343
Anormal Schirmer test, n/N (%)	40/54 (74.1)	12/18 (66.7)	85/117 (72.6)	137/189 (72.5)	.820
ESSPRI, mean (SD)	5.59 (2.44)	5.32 (2.12)	6.32 (1.95)	5.97 (2.17)	.097
ESSPRI dryness, mean (SD)	5.91 (2.55)	5.56 (2.68)	6.85 (2.34)	6.46 (2.47)	.057
ESSPRI fatigue, mean (SD)	5.76 (2.97)	6.06 (2.53)	6.56 (2.36)	6.28 (2.58)	.387
ESSPRI pain, mean (SD)	4.7 (3.13)	4.33 (2.72)	5.54 (2.55)	5.18 (2.77)	.030
ESSDAI, mean (SD)	4.04 (4.06)	7.33 (4.37)	9.36 (4.09)	7.29 (4.78)	$<10^{-13}$

EULAR, European Alliance of Associations for Rheumatology; ESSDAI, EULAR Sjögren's Syndrome Disease Activity Index; ESSPRI, EULAR Sjögren's Syndrome Patient Reported Index.

Table 2
Sjögren patients from the TRACTISS, RepurpSS-I, and abatacept trials classified by transcriptomic-based clusters

Features	Cluster 1 n = 82	Cluster 2 n = 25	Cluster 3 n = 95	Cluster 4 n = 8	*P* value
Demographics					
Age (y), mean (SD)	52.84 (12.98)	57.28 (14.84)	53.02 (12.09)	59.5 (12.64)	.349
Sex female, n (%)	75 (91.46)	24 (96.00)	94 (98.95)	7 (87.50)	.088
Sjögren features					
Anti-SSA positivity, n/N (%)	82/82 (100)	25/25 (100)	94/95 (98.9)	8/8 (100)	1.0
Anormal unstimulated salivary flow, n/N (%)	55/71 (77.46)	16/24 (66.67)	62/90 (68.89)	4/6 (66.67)	.479
Anormal Schirmer test, n/N (%)	55/71 (77.46)	17/23 (73.91)	61/89 (67.78)	4/6 (66.67)	.595
ESSPRI, mean (SD)	6.02 (2.15)	5.80 (2.52)	5.92 (2.14)	6.67 (1.90)	.793
ESSPRI dryness, mean (SD)	6.65 (2.41)	6.48 (2.62)	6.07 (2.47)	7.00 (2.62)	.448
ESSPRI fatigue, mean (SD)	6.54 (2.44)	5.6 (2.81)	6.34 (2.55)	6.88 (2.42)	.517
ESSPRI pain, mean (SD)	4.87 (2.93)	5.32 (2.94)	5.35 (2.66)	6.12 (1.96)	.459
ESSDAI, mean (SD)	6.98 (5.01)	6.44 (4.80)	7.63 (4.59)	9.00 (4.66)	.440

EULAR, European Alliance of Associations for Rheumatology; ESSDAI, EULAR Sjögren's Syndrome Disease Activity Index; ESSPRI, EULAR Sjögren's Syndrome Patient Reported Index.

mainly comprised patients from the RTX trial, and cluster 3 mainly included patients from both the RTX and ABA trials (Supplementary Fig S2). No significant differences were found across all clusters regarding SjD features and activity scores (Table 2).

Drug efficacy across transcriptomic-based stratification

A total of 109 patients were treated by ABA, HCQ-LEF, and RTX. One hundred one patients received the placebo in the 3 RCTs. Considering all studies together, more treated patients achieved a significant improvement in the STAR score than those receiving a placebo in cluster 1 (characterised by a strong type I IFN signature) (61.5% vs 32.6%; $P = .016$) (Table 3, Figure). No difference between the active drug and placebo was found in the other clusters.

In the TRACTISS trial assessing RTX, SjD patients in cluster 1 were significantly more likely to achieve a STAR score compared with placebo (61.1% vs 15.8%; $P = .012$) (Table 3).

In the RepurpSS-I trial, patients stratified in cluster 3 (characterised by IFN and B-cell signatures) were more likely to achieve a STAR score than placebo patients (77.8% vs 0%; $P = .046$) (Table 3).

After transcriptomic-based stratification, ABA was not more efficient than placebo, according to the STAR index, in any of the endotypes (Table 3).

DISCUSSION

The current study demonstrated that whole-blood transcriptomic-based clustering may be relevant for stratifying SjD patients enrolled in RCTs. We showed that drugs exhibit different efficacies across the different endotypes. Interestingly, patients belonging to cluster 2, with healthy-like characteristics, did not respond to any of the drugs tested compared with placebo.

The present findings strengthen the importance of stratifying SjD patients, specifically the therapeutic relevance of transcriptomic-based clustering. In the original clustering analysis from the PRECISESADS cohort, which included >300 consecutive SjD patients seen at several referral centres across Europe [4], clusters 1 and 3 accounted for the majority of patients, while clusters 2 and 4 included fewer patients (33.2%, 28.9%, 25.3%, and 12.5% of the patients, respectively). In the present study, including patients enrolled in clinical trials, the proportions of clusters 1 to 4 were 39.0%, 45.2%, 11.9%, and 3.8%, respectively. Importantly, cluster 2, including healthy-like patients, was also present in this population, albeit at a lower proportion, likely due to the inclusion criteria of the clinical trials, specifically anti-SSA positivity and/or ESSDAI >5. Additionally, the ESSDAI score was the lowest among patients in cluster 2, consistent with the original findings.

Other methods of stratifying SjD patients have been proposed. Based on the United Kingdom Primary Sjögren's Syndrome Registry, Tarn et al [2] proposed a 5–symptom-based

Table 3
STAR score response in Sjögren patients after transcriptomic stratification in 3 previous controlled trials

A. STAR score response gathering all 3 trials, assessing rituximab, abatacept or the association of hydroxychloroquine and leflunomide vs placebo

Cluster	Treated n = 109	Placebo n = 101	*P* value
1	24/39 (61.5)	14/43 (32.6)	**.016**
2	6/16 (37.5)	4/9 (44.4)	1.0
3	31/50 (62.0)	22/45 (48.9)	.281
4	2/4 (50.0)	1/4 (25.0)	-

B. STAR score response in the TRACTISS trial, assessing rituximab vs placebo

Cluster	Treated n = 38	Placebo n = 37	*P* value
1	11/18 (61.1)	3/19 (15.8)	**.012**
2	3/8 (37.5)	1/4 (25/0)	1.0
3	7/11 (63.6)	4/12 (33.3)	.300
4	0/1	0/2	-

C. STAR score response in the RepurpSS-I trial, assessing the association of hydroxychloroquine and leflunomide vs placebo

Cluster	Treated n = 13	Placebo n = 5	*P* value
1	2/4	0/1	-
2	0/0	0/0	-
3	7/9 (77.8)	0/4	**.046**
4	0/0	0/0	-

D. STAR score response in the abatacept trial

Cluster	Treated n = 58	Placebo n = 59	*P* value
1	11/17 (64.7)	11/23 (47.8)	.46
2	3/8 (37.5)	3/5 (60.0)	.83
3	17/30 (56.7)	18/29 (62.1)	.88
4	2/3 (66.7)	1/2 (50.0)	1.0

STAR, Sjögren Tool for Assessing Response.
Data are presented as n/N (%).

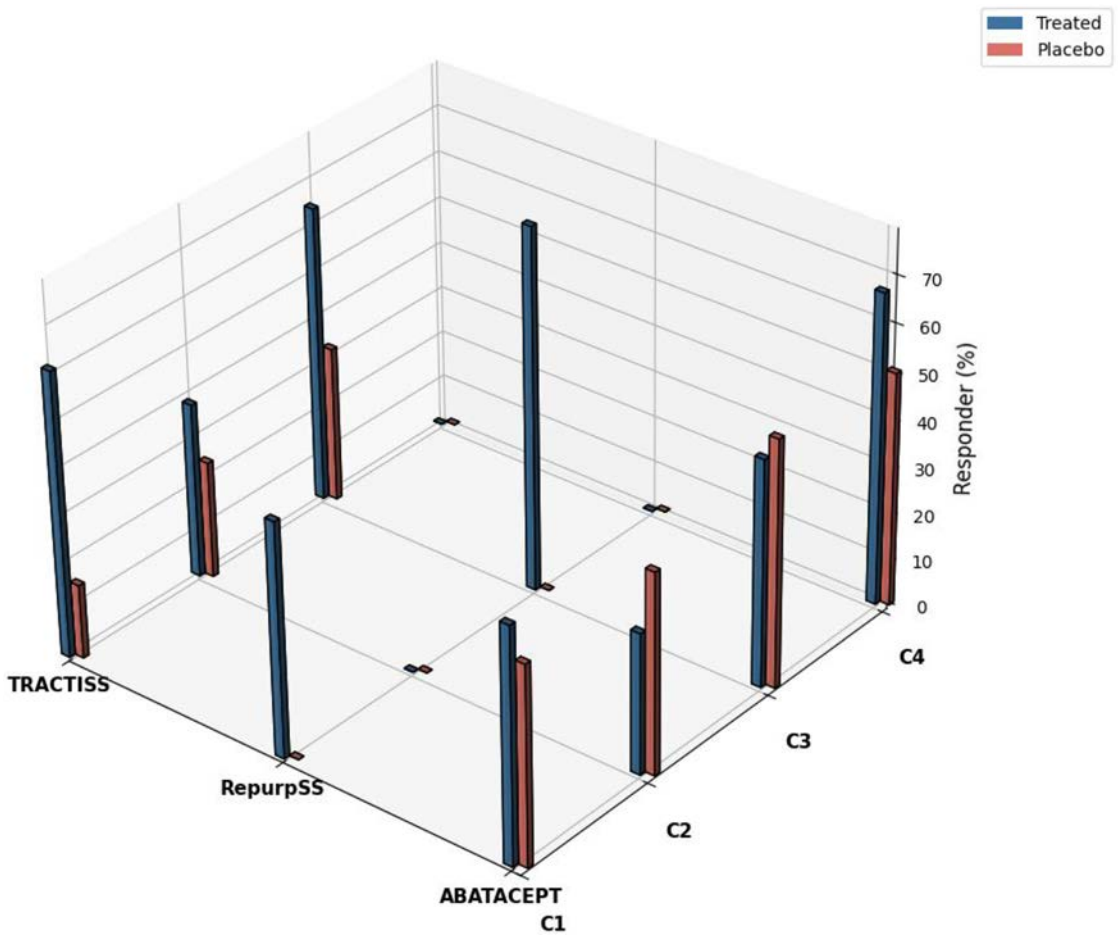

Figure. Sjögren Tool for Assessing Response (STAR) score rates across the different trials, stratified by cluster (C). Results are displayed as percentages. The first endotype includes Sjögren's patients with a strong type I interferon (IFN) transcriptomic signature. Patients from the second endotype present healthy-like transcriptomic features. The third endotype is characterised by B-cell transcriptomic and serological signatures, and an intermediate type I IFN signature. Patients from the fourth endotype show a mild type I IFN signature, but strong type II IFN and neutrophil signatures. C1 to C4, cluster 1 to cluster 4.

stratification: pain, fatigue, dryness, anxiety, and depression. Patients were classified into 1 of 4 clusters. Two subsequent post hoc studies stratified previous controlled trials according to this classification. Collins et al [19] revisited the JOQUER study, which evaluated HCQ vs placebo. The patients identified as 'high symptom burden' showed a relative improvement in ESSPRI (−1.49 points; $P = .002$) at 12 weeks with HCQ compared with placebo, with no further change between weeks 12 and 24. Among patients in the 'pain dominant with fatigue' and 'dryness dominant with fatigue' groups, significant reductions in overall IFN score at 24 weeks were observed, with no change in ESSPRI or ESSDAI. Berry et al [20] conducted a post hoc analysis of the ETAP trial, assessing tocilizumab vs placebo in SjD patients. No difference was shown in ESSPRI and ESSDAI after symptom-based stratification. Only a decrease in the Functional Assessment of Chronic Illness Therapy (FACIT)-Fatigue score was observed in the 'high symptom burden' patients treated with tocilizumab compared with those treated with placebo.

Recently, Nguyen et al [3] presented a clustering approach based on symptoms, systemic complications, and simple biological data routinely collected, built from 2 different French SjD cohorts. As of today, no analysis of RCTs has been conducted based on this stratification. Further studies are awaited to evaluate the degree of overlap between the different stratifications.

Given SjD heterogeneity, it is likely that different drugs targeting distinct biological pathways may exhibit different efficacy across various patient endotypes. Therefore, while a subset of SjD patients may respond to treatment, the heterogeneity in therapeutic response could reduce the observed global efficacy.

Interestingly, the efficacy of RTX in the TRACTISS trial was observed in cluster 1 (defined by a high IFN signature) but not in cluster 3 (defined by an IFN and B-cell signature). While it may seem counterintuitive that RTX (targeting B cells) has no clear efficacy in the cluster of patients defined by a B-cell signature, it has previously been reported that high B-cell activity driven by the B-cell activating factor (BAFF) cytokine was associated with nonresponse to RTX in patients with SjD [21]. ABA, which disrupts CD80/CD86-CD28–induced T-cell activation, did not show efficacy in any of the clusters, confirming that this therapeutic target is not relevant in patients with SjD. Finally, the association of HCQ (dampening the IFN pathway through its effect on lysosomal activity [22]) and leflunomide (decreasing lymphocyte activation [23]) showed clinical efficacy in clusters 1 and 3 (even though the small number of patients included in this study limited the power of the statistical comparison for cluster 1).

To our knowledge, no prior study has proposed efficient stratification, demonstrating that healthy-like SjD patients, characterised by RNAseq, flow cytometry, and clinical-serological features in our seminal work [4], do not respond to immunomodulatory treatment strategies, in contrast to other SjD

endotypes. Our study supports the rationale for designing dedicated clinical trials specifically for healthy-like SjD patients, distinct from those with type I or type II IFN signatures corresponding to endotypes 1, 3, and 4 [4].

Our study has multiple strengths. First, this study appropriately replicated the transcriptomic-based clusters described in the PRECISEADS cohort. The identified clusters were shown to predict response to treatment. RTX and HCQ-LEF might be effective for transcriptomic-based endotypes 1 and 3, respectively. Importantly, our study preserved the original randomisation design across patients receiving either active treatment or placebo. Additionally, a key strength of this study lies in the identification of a well-defined cluster of patients who did not respond to any of the 3 treatments. These healthy-like individuals present clinical and transcriptomic characteristics distinct from those of other endotypes, yet of similar therapeutic importance.

However, our study has some limitations. First, this post hoc analysis cannot substitute for an RCT, and additional controlled studies are warranted to validate our findings. Moreover, RNA-seq data were not available for all patients across the 3 trials, limiting the sample size relative to the original studies. Around 60% of the patients who originally participated in the 3 RCTs were included in these analyses due to data availability. This should not induce an attrition bias, as data availability was not dependent on treatment arm randomisation or transcriptomic-based classification. Although no selection criteria were applied for patient inclusion in the present study, we cannot rule out the possibility that excluded patients shared common characteristics (eg, being enrolled from the same country), which could introduce selection bias. Also, despite its current inapplicability in routine care due to the complexity of large-scale transcriptomic algorithms and the risk of misclassification of smaller gene sets, clustering may be useful in future trials to ensure balanced patient distribution across molecular subgroups, thereby avoiding skewed results due to cluster overrepresentation.

Thus, this study demonstrates that stratifying SjD patients based on transcriptomic signatures may help identify those more likely to benefit from treatment. This approach could support clinicians in anticipating therapeutic efficacy and making more informed treatment decisions. Notably, our findings may encourage reconsideration of excluding patients with molecular healthy-like profiles in future clinical trials.

Competing interests

BC received support for attending meetings from Sandoz, Sanofi, Novartis, Lilly, Amgen, AbbVie, and UCB. VD-P declares no competing interests. EP declares no competing interests. VB declares no competing interests. MB declares no competing interests. SJB provided consultancy on Sjögren's disease for AbbVie, Aera, Amgen, Argenx, Aurinia, Bain, BMS, EcoR1, Galapagos, IQVIA, J&J, Kiniksa, Novartis, and Scitaris. SJB's salary is partly funded by the Birmingham NIHR Biomedical Research Centre, UK. MB declares no competing interests. JvR declares no competing interests. AGS is an employee of Cullinan Therapeutics and a shareholder of BMS and AZ. JL is an employee of BMS. SK is an employee of BMS. AC is an employee of BMS. PM was an employee of Servier. LL was an employee of Servier. PS declares no competing interests. CLD declares no competing interests. J-OP declares no competing interests. MEA-R declares consulting fees from GSK. GB declares no competing interests. XM received consulting fees from BMS, GSK, Janssen, Novartis, and Otsuka, and support for attending meetings from Novartis. RS declares consulting fees from GSK, Boehringer, Novartis, Janssen, and AbbVie; support for attending meetings from GSK and Amgen; implication in trials with GSK, Servier, USB, Novartis, and Medimmune. GN received honorarium from Biogen, AbbVie, Novartis, Lilly, and Amgen, and support for attending meetings from Amgen and AbbVie. DC declares no personal financial competing interests and received research funding from Novartis and GSK. NF declares no competing interests.

Acknowledgements

We thank Vincent Bouget from ScientaLab for the discussion we shared regarding the Results and Discussion sections.

Contributors

BC: Conceptualisation, Methodology, Writing—original draft, Writing—review and editing. VD-P: Data curation, Investigation, Resources, Writing—review and editing. EP: Data curation, Investigation, Resources, Writing—review and editing. VB: Data curation, Investigation, Resources, Writing—review and editing. MB: Data curation, Investigation, Resources, Writing—review and editing. SJB: Data curation, Investigation, Resources, Writing—review and editing. MB: Data curation, Investigation, Resources, Writing—review and editing. JvR: Data curation, Investigation, Resources, Writing—review and editing. AGS: Data curation, Investigation, Resources, Writing—review and editing. JL: Data curation, Investigation, Resources, Writing—review and editing. SK: Data curation, Investigation, Resources, Writing—review and editing. AC: Data curation, Investigation, Resources, Writing—review and editing. PM: Data curation, Investigation, Resources, Writing—review and editing. LL: Data curation, Investigation, Resources, Writing—review and editing. PS: Data curation, Investigation, Resources, Writing—review and editing. CLD: Data curation, Investigation, Resources, Writing—review and editing. J-OP: Data curation, Investigation, Resources, Writing—review and editing. MEA-R: Data curation, Investigation, Resources, Writing—review and editing. GB: Data curation, Investigation, Resources, Writing—review and editing. XM: Data curation, Investigation, Resources, Writing—review and editing. RS: Data curation, Investigation, Resources, Writing—review and editing. GN: Data curation, Investigation, Resources, Writing—review and editing. DC: Conceptualisation, Methodology, Writing—original draft, Writing—review and editing, Validation, Supervision, Project administration. NF: Conceptualisation, Methodology, Writing—original draft, Writing—review and editing, Validation, Supervision, Project administration, Software.

Funding

This project has received funding from the Innovative Medicines Initiative 2 Joint Undertaking (JU) NECESSITY under grant agreement number 806975. The JU receives support from the European Union's Horizon 2020 research and innovation program and EFPIA. The present article reflects only the author's view, and the JU is not responsible for any use that may be made of the information it contains.

Patient consent for publication

Not applicable.

Ethics approval

Not applicable.

Provenance and peer review

Not commissioned; externally peer reviewed.

Supplementary materials

Supplementary material associated with this article can be found in the online version at doi:10.1016/j.ard.2025.11.017.

Orcid

Baptiste Chevet: http://orcid.org/0000-0002-9646-7603
Elena Pontarini: http://orcid.org/0000-0003-0439-0344
Valentin Baloche: http://orcid.org/0000-0001-9471-0043
Simon J. Bowman: http://orcid.org/0000-0001-9880-9948
Antoine G. Sreih: http://orcid.org/0000-0002-7864-0185
Philippe Moingeon: http://orcid.org/0000-0002-2380-9983
Marta E. Alarcon-Riquelme: http://orcid.org/0000-0002-7632-4154
Xavier Mariette: http://orcid.org/0000-0002-4244-5417
Joel van Roon: http://orcid.org/0009-0009-5571-2324
Raphaèle Seror: http://orcid.org/0000-0002-5523-1856
Gaetane Nocturne: http://orcid.org/0000-0001-6809-0733
Divi Cornec: http://orcid.org/0000-0002-9159-702X
Nathan Foulquier: http://orcid.org/0000-0003-4620-2794

REFERENCES

[1] Ramos-Casals M, Baer AN, Brito-Zerón MDP, Hammitt KM, Bouillot C, Retamozo S, et al. 2023 International Rome consensus for the nomenclature of Sjögren disease. Nat Rev Rheumatol 2025;21:426–37.
[2] Tarn JR, Howard-Tripp N, Lendrem DW, Mariette X, Saraux A, Devauchelle-Pensec V, et al. Symptom-based stratification of patients with primary Sjögren's syndrome: multi-dimensional characterisation of international observational cohorts and reanalyses of randomised clinical trials. Lancet Rheumatol 2019;1:e85–94.
[3] Nguyen Y, Nocturne G, Henry J, Ng WF, Belkhir R, Desmoulins F, et al. Identification of distinct subgroups of Sjögren's disease by cluster analysis based on clinical and biological manifestations: data from the cross-sectional Paris-Saclay and the prospective ASSESS cohorts. Lancet Rheumatol 2024;6:e216–25. doi: 10.1016/S2665-9913(23)00340-5.
[4] Soret P, Le Dantec C, Desvaux E, Foulquier N, Chassagnol B, Hubert S, et al. A new molecular classification to drive precision treatment strategies in primary Sjögren's syndrome. Nat Commun 2021;12:3523.
[5] Trutschel D, Bost P, Mariette X, Bondet V, Llibre A, Posseme C, et al. Variability of primary Sjögren's syndrome is driven by interferon-α and interferon-α blood levels are associated with the class II HLA-DQ locus. Arthritis Rheumatol 2022;74:1991–2002.
[6] Baldini C, Fulvio G, La Rocca G, Ferro F. Update on the pathophysiology and treatment of primary Sjögren syndrome. Nat Rev Rheumatol 2024;20:473–91.
[7] Seror R, Baron G, Camus M, Cornec D, Perrodeau E, Bowman SJ, et al. Development and preliminary validation of the Sjögren's Tool for Assessing Response (STAR): a consensual composite score for assessing treatment effect in primary Sjögren's syndrome. Ann Rheum Dis 2022;81:979–89.
[8] Seror R, Bowman SJ, Brito-Zeron P, Theander E, Bootsma H, Tzioufas A, et al. EULAR Sjögren's syndrome disease activity index (ESSDAI): a user guide. RMD Open 2015;1:e000022.
[9] Mariette X, Ravaud P, Steinfeld S, Baron G, Goetz J, Hachulla E, et al. Inefficacy of infliximab in primary Sjögren's syndrome: results of the randomized, controlled Trial of Remicade in Primary Sjögren's Syndrome (TRIPSS). Arthritis Rheum 2004;50:1270–6.
[10] Sankar V, Brennan MT, Kok MR, Leakan RA, Smith JA, Manny J, et al. Etanercept in Sjögren's syndrome: a twelve-week randomized, double-blind, placebo-controlled pilot clinical trial. Arthritis Rheum 2004;50:2240–5.
[11] Gottenberg JE, Ravaud P, Puéchal X, Le Guern V, Sibilia J, Goeb V, et al. Effects of hydroxychloroquine on symptomatic improvement in primary Sjögren syndrome: the JOQUER randomized clinical trial. JAMA 2014;312:249–58.
[12] Devauchelle-Pensec V, Mariette X, Jousse-Joulin S, Berthelot JM, Perdriger A, Puéchal X, et al. Treatment of primary Sjögren syndrome with rituximab: a randomized trial. Ann Intern Med 2014;160:233–42.
[13] Bowman SJ, Everett CC, O'Dwyer JL, Emery P, Pitzalis C, Ng WF, et al. Randomized controlled trial of rituximab and cost-effectiveness analysis in treating fatigue and oral dryness in primary Sjögren's syndrome. Arthritis Rheumatol 2017;69:1440–50.
[14] Baer AN, Gottenberg JE, St Clair EW, Sumida T, Takeuchi T, Seror R, et al. Efficacy and safety of abatacept in active primary Sjögren's syndrome: results of a phase III, randomised, placebo-controlled trial. Ann Rheum Dis 2021;80:339–48.
[15] van Nimwegen JF, Mossel E, van Zuiden GS, Wijnsma RF, Delli K, Stel AJ, et al. Abatacept treatment for patients with early active primary Sjögren's syndrome: a single-centre, randomised, double-blind, placebo-controlled, phase 3 trial (ASAP-III study). Lancet Rheumatol 2020;2:e153–63.
[16] de Wolff L, van Nimwegen JF, Mossel E, van Zuiden GS, Stel AJ, Majoor KI, et al. Long-term abatacept treatment for 48 weeks in patients with primary Sjögren's syndrome: the open-label extension phase of the ASAP-III trial. Semin Arthritis Rheum 2022;53:151955.
[17] van der Heijden EHM, Blokland SLM, Hillen MR, Lopes APP, van Vliet-Moret FM, Rosenberg AJWP, et al. Leflunomide–hydroxychloroquine combination therapy in patients with primary Sjögren's syndrome (RepurpSS-I): a placebo-controlled, double-blinded, randomised clinical trial. Lancet Rheumatol 2020;2:e260–9.
[18] McInnes L, Healy J, Melville J. UMAP: Uniform manifold approximation and projection for dimension reduction. arXiv:1802.03426 [Preprint]. 2020 [cited 2025 May 8]: [63 p.] Available from: https://doi.org/10.48550/arXiv.1802.03426
[19] Collins A, Lendrem D, Wason J, Tarn J, Howard-Tripp N, Bodewes I, et al. Revisiting the JOQUER trial: stratification of primary Sjögren's syndrome and the clinical and interferon response to hydroxychloroquine. Rheumatol Int 2021;41:1593–600.
[20] Berry JS, Tarn J, Casement J, Duret PM, Scott L, Wood K, et al. Examining the biological pathways underlying clinical heterogeneity in Sjögren's syndrome: proteomic and network analysis. Ann Rheum Dis 2024;83:88–95. doi: 10.1136/ard-2023-224503.
[21] Cornec D, Costa S, Devauchelle-Pensec V, Jousse-Joulin S, Marcorelles P, Berthelot JM, et al. Blood and salivary-gland BAFF-driven B-cell hyperactivity is associated to rituximab inefficacy in primary Sjögren's syndrome. J Autoimmun 2016;67:102–10.
[22] Schrezenmeier E, Dörner T. Mechanisms of action of hydroxychloroquine and chloroquine: implications for rheumatology. Nat Rev Rheumatol 2020;16:155–66.
[23] Fox RI, Herrmann ML, Frangou CG, Wahl GM, Morris RE, Strand V, et al. Mechanism of action for leflunomide in rheumatoid arthritis. Clin Immunol 1999;93:198–208.

Ann Rheum Dis 85 (2026) 880–898

Contents lists available at ScienceDirect

Annals of the Rheumatic Diseases

journal homepage: https://www.sciencedirect.com/journal/annals-of-the-rheumatic-diseases

Sjögren's syndrome

GZMK$^+$CD8$^+$ T cells target a specific acinar cell type in Sjögren's disease

Thomas J.F. Pranzatelli[1,2], Paola Perez[3], Anson Ku[4], Bruno Matuck[5], Khoa Huynh[6], Shunsuke Sakai[7], Mehdi Abed[3], Shyh-Ing Jang[3], Eiko Yamada[3], Kalie Dominick[3], Zara Ahmed[3], Amanda J. Oliver[8], Rachael Bogle[9], Quinn T. Easter[5], Alan N. Baer[10], Eileen Pelayo[10], Zohreh Khavandgar[3,10], David E. Kleiner[11], M. Teresa Magone[12], Sarthak Gupta[3,13], Christopher Lessard[14], A. Darise Farris[15], Peter D. Burbelo[1], Daniel Martin[16], Robert J. Morell[16], Changyu Zheng[16], Nicholas Rachmaninoff[2], Jose Maldonado-Ortiz[1,3,10], Katarzyna M. Tyc[6], Xufeng Qu[17], Marit Aure[18], Mohammad H. Dezfulian[19], Ross Lake[20], Sarah A. Teichmann[21,22,23,24,25], Daniel L. Barber[7], Lam C. Tsoi[9], Adam G. Sowalsky[4], Jinze Liu[6], Johann Gudjonsson[9], Kevin M. Byrd[3,5,26,27], Philip L.F. Johnson[2], John A. Chiorini[1], Blake M. Warner[3,10,*]

[1] *Adeno-Associated Virus Biology Section, National Institute of Dental and Craniofacial Research, National Institutes of Health, Bethesda, Maryland, USA*
[2] *Department of Biology, University of Maryland, College Park, Maryland, USA*
[3] *Salivary Disorders Unit, National Institute of Dental and Craniofacial Research, National Institutes of Health, Bethesda, Maryland, USA*
[4] *Laboratory of Genitourinary Cancer Pathogenesis, Center for Cancer Research, National Cancer Institute, National Institutes of Health, Bethesda, Maryland, USA*
[5] *Lab of Oral & Craniofacial Innovation, Department of Innovation & Technology Research, ADA Science & Research Institute, Gaithersburg, Maryland, USA*
[6] *Department of Biostatistics, Virginia Commonwealth University, Richmond, Virginia, USA*
[7] *T-lymphocyte Biology Section, National Institute of Allergy and Infectious Diseases, National Institutes of Health, Bethesda, Maryland, USA*
[8] *Wellcome Sanger Institute, Wellcome Genome Campus, Hinxton, Cambridge, UK*
[9] *Department of Dermatology, Michigan Medicine, University of Michigan, Ann Arbor, Michigan, USA*
[10] *Sjögren's Clinical Investigations Team, National Institute of Dental and Craniofacial Research, National Institutes of Health, Bethesda, Maryland, USA*
[11] *Laboratory of Pathology, Center for Cancer Research, National Cancer Institute, National Institutes of Health, Bethesda, Maryland, USA*
[12] *Consult Services Section, National Eye Institute, National Institutes of Health, Bethesda, Maryland, USA*
[13] *Lupus Clinical Trials Unit, National Institute of Arthritis and Musculoskeletal and Skin Diseases, National Institutes of Health, Bethesda, Maryland, USA*
[14] *Genes & Human Disease Research Program, Oklahoma Medical Research Foundation, Oklahoma City, Oklahoma, USA*
[15] *Arthritis & Clinical Immunology Research Program, Oklahoma Medical Research Foundation, Oklahoma City, Oklahoma, USA*

*Correspondence to Dr. Blake M. Warner, Stadtman Tenure Track Clinical Investigator, Salivary Disorders Unit, Sjögren's Disease Clinical Investigations Team, Bethesda, MD, USA.
E-mail address: blake.warner@nih.gov (B.M. Warner).
Handling editor Josef S. Smolen.

https://doi.org/10.1016/j.ard.2025.08.014

[16] *Genomics and Computational Biology Core, National Institute on Deafness and Other Communication Disorders, National Institutes of Health, Bethesda, Maryland, USA*
[17] *Massey Cancer Center, Virginia Commonwealth University, Richmond, Virginia, USA*
[18] *Matrix and Morphogenesis Section, National Institute of Dental and Craniofacial Research, National Institutes of Health, Bethesda, Maryland, USA*
[19] *Department of Genetics, Harvard Medical School, Boston, Massachusetts, USA*
[20] *Laboratory of Genitourinary Cancer Pathogenesis (LCGP) Microscopy Core Facility, Center for Cancer Research, National Cancer Institute, National Institutes of Health, Bethesda, Maryland, USA*
[21] *Cambridge Stem Cell Institute, University of Cambridge, Cambridge, UK*
[22] *Ensocell Therapeutics, BioData Innovation Centre, Wellcome Genome Campus, Cambridge, UK*
[23] *Theory of Condensed Matter, Cavendish Laboratory/Department of Physics, University of Cambridge, Cambridge, UK*
[24] *Department of Medicine, University of Cambridge, Cambridge, UK*
[25] *CIFAR Macmillan Multi-scale Human Program, CIFAR, Toronto, Ontario, Canada*
[26] *Department of Oral and Craniofacial Molecular Biology, Philips Institute for Oral Health Research, Virginia Commonwealth University, Richmond, Virginia, USA*
[27] *VCU Massey Comprehensive Cancer Center, Bioinformatics Shared Resource Core, Virginia Commonwealth University, Richmond, Virginia, USA*

ARTICLE INFO

Article history:
Received 19 March 2025
Received in revised form 28 July 2025
Accepted 12 August 2025

ABSTRACT

Objectives: Sjögren's disease (SjD) is a systemic autoimmune disorder characterized by dysfunction of exocrine glands, particularly the salivary and lacrimal glands, with no clear etiology or effective therapy. This study explores the complex interplay of varied cell types in the salivary glands and their role in the pathology of Sjögren's disease.
Methods: Utilizing single-cell and spatial transcriptomics alongside spatial immunophenotyping to analyze human minor salivary glands, we developed a comprehensive understanding of the cellular landscape of non-SjD salivary glands and how that landscape changes in SjD patients. In vitro cellular assays and novel patient-derived primary epithelial cells were co-cultured with autologous T cells to confirm effector states and the delivery and effect of disease-associated granzymes.
Results: We identified previously unrecognized heterogeneity among acinar cells, including a *PRR4*$^+$*CST3*$^+$*WFDC2*$^-$ seromucous acinar population that is selectively lost in Sjögren's disease. Expression and organizational changes were linked to clinical features: (i) T cells in the glands of SSA$^+$, high–focus score patients showed increased transcriptional signatures of activation, antigen presentation, and apoptosis resistance compared with patients with mild or moderate disease, and (ii) patients with low immune infiltration exhibited distinct epithelial organization. Notably, *GZMK*$^+$*CD8*$^+$ T cells, which accumulate with disease severity, displayed a cytotoxic transcriptional program, degranulated upon stimulation *ex vivo*, and localized spatially with immune-engaged epithelial cells. Functional assays demonstrated that GZMK activates interferon signaling *in vitro*, and autologous co-cultures of patient-derived T cells and epithelial cells validated these findings.
Conclusions: Using single-cell and spatial transcriptomics and proteomics, this study identifies a selective loss of *PRR4*$^+$*CST3*$^+$*WFDC2*$^-$ seromucous acinar cells and a rise in *GZMK*$^+$*CD8*$^+$ T cells in Sjögren's disease, revealing distinct immune-mediated epithelial remodeling and interferon-driven dysfunction across diverse clinical presentations. These findings uncover a novel sub-cytolytic effector mechanism by which *GZMK*$^+$*CD8*$^+$ T cells impair mitochondrial integrity and activate innate immune signaling, linking epithelial injury to type I interferon responses and offering new therapeutic targets.

INTRODUCTION

Sjögren's disease (SjD) is the second most common systemic autoimmune disease (0.1%-4% prevalence across studies in different countries) with a striking 9:1 female to male preponderance [1] and all patients with SjD are afflicted with an increased lifetime risk of lymphomagenesis [2,3]. Despite important advances in understanding the pathogenesis of SjD, neither a unifying aetiology nor an efficacious medication that meaningfully improves quality of life or preserves organ function has been established. The inherent clinical and biological heterogeneity of SjD is cited as the main factor that has limited the clinical success of identified targets and developed agents [4]. SjD is characterised by chronic lymphocytic infiltration of the exocrine organs and reduced secretory function. There are no effective and approved therapies for SjD and management remains suboptimal but includes palliative and supportive care for symptoms and immunosuppressants for more severe and systemic symptoms.

The aetiologic basis of SjD suggests a complex interaction between genetics, environmental insults, and hormonal factors. Genome-wide association studies [5,6] have now identified 22 single-nucleotide polymorphisms (SNPs) associated with SjD. Using polygenic risk scores, the genetic risk of SjD divides the SjD population into anti-Sjögren's syndrome-related antigen A (SSA) autoantibody-positive patients, with genetic association dominated by human leukocyte antigen (HLA) SNPs, and anti-SSA

WHAT IS ALREADY KNOWN ON THIS TOPIC

- Sjögren's disease (SjD) is an autoimmune condition of the salivary glands characterized by acinar cell loss and lymphocytic infiltration. While systemic immune alterations have been described using single-cell analyses of peripheral blood mononuclear cells and minor salivary glands, the specific glandular cell types targeted in disease and the mechanisms by which diverse immune infiltrates drive dysfunction remain unclear. Only recently have spatially-resolved single-cell studies begun to interrogate compositional, transcriptional, and organizational changes within the glands themselves, and these studies have not interrogated the affected epithelia.

WHAT THIS STUDY ADDS

- This study identifies a specific subset of saliva-producing cells that is selectively lost in the minor salivary glands of patients with Sjögren's disease. It implicates $GZMK^+CD8^+$ T cells of a T_{ex} phenotype, rather than conventional cytotoxic T_c cells, as drivers of this damage. These cells mediate a previously unrecognized mechanism of tissue injury in which mitochondrial disruption and sub-cytolytic reprogramming occur without overt cell killing. Using spatial phenotyping, the study shows that these immune and epithelial cell types colocalize even in mild to moderate disease, preceding overt histopathological changes, and drive alterations in cellular organization and signaling that may underlie glandular dysfunction.

HOW THIS STUDY MIGHT AFFECT RESEARCH, PRACTICE OR POLICY

- This work identifies a previously unrecognized immune mechanism driving sub-cytolytic tissue damage in SjD, highlighting a new cellular target for therapy. By clarifying how specific immune cells disrupt saliva-producing cells without killing them, it opens avenues for drug development, may refine diagnostic criteria, and could influence clinical strategies for SjD and other systemic autoimmune conditions.

autoantibody-negative patients, whose SNPs are limited in number, have a more muted effect size, and are unrelated to HLA SNPs [5]. Using polygenic risk scores alone is insufficient to distinguish SSA^- patients with SjD from controls [7]. How these risk haplotypes translate to cellular function and autoimmune pathogenesis in targeted organs is not entirely clear.

The salivary glands are composed primarily of acinar cells and ducts, with associated stromal tissues and tissue-resident inflammatory cells. Fluid and the majority of protein secretion in the salivary glands initiates in the acinar cells [8]. In humans, there are 3 sets of major salivary glands: parotid, composed purely of serous acinar cells; submandibular, a mixture of serous/seromucous cells and mucous acinar cells; and sublingual, predominantly mucous cells. In addition to these 3 pairs of major glands, hundreds to thousands of minor (submucosal) glands are distributed throughout the oral cavity and upper aerodigestive tract. Minor salivary gland salivary glands biopsies are used to evaluate the histopathological component of SjD classification criteria and serve as biological surrogates for major gland involvement [9,10]. Immune cells infiltrating the salivary gland in disease include T lymphocytes (CD4 > CD8), B-lymphocytes, and plasma cells; other immune cells are also found, although in fewer numbers including natural killer (NK) cells, macrophages, and dendritic cells [10–12]. In some patients, tertiary lymphoid-like structures and benign lymphoepithelial lesions can also be found [13]. Advances in genetic, epigenetic, transcriptomic, and proteomic technologies have advanced our understanding of the pathogenesis of SjD. These studies have shown that multiple inflammatory cytokines are involved including type I and type II interferons (IFNs) [14,15], interleukins (ILs) [14,16], and chemokines [17–20]. Emerging technologies (e.g., single-cell and spatial transcriptomics) are unravelling disease-specific cellular networks and signalling pathways, and spotlight effector cells and therapeutic pathways.

To date, most attention in SjD has been towards understanding the B cell and CD4 T cell involvement in SjD. The direct involvement of CD8 T cells in SjD requires further study. CD8 T cells, also known as cytotoxic T cells, are a subset of T cells involved in the immune response to viral infections, cancer, and autoimmune diseases. In SjD, CD8 T cells are thought to target the ductal and/or acinar epithelial cells in the salivary gland, leading to tissue damage and glandular dysfunction. However, direct evidence of CD8 T cells exerting cytotoxic effects on epithelial cells is lacking, their phenotypic profile is unknown, and the specific targeted epithelial cells (e.g., a specific type of acinar or ductal cell, or another cell type) or the antigens initiating or driving disease have not been reported.

Most of what is understood about the pathogenesis of SjD in the salivary glands is based on unbiased bulk approaches (e.g., microarray, RNAseq) or on low-throughput methods using focused panels of target genes or proteins. There is a critical need for an unbiased understanding of the molecular changes in the salivary glands at the cell level within the tissue context. Herein, we employed a multifaceted approach, combining the strengths of scRNAseq and spatial transcriptomics, *ex vivo* cellular assays, and high-throughput microscopy methods to achieve a comprehensive map of the cellular composition and cell-state changes in human salivary glands in patients with SjD. We then determine the disease-specific cellular interactions involved in the immune insult in the gland and uncover novel pathways driving the loss of gland function and parenchymal maintenance. This evidence further supports and also sheds light on the pivotal role of T cells in the pathogenesis of SjD, including direct effects on specific exocrine epithelia.

RESULTS

Single-cell and spatial transcriptomics of the minor salivary glands in SjD

We collected research biopsies for single-cell RNA sequencing from 11 patients with SjD and 14 without SjD (Supplementary Table S1). After quality control, 94,000 single cells were collected and sequenced (Fig 1a). Six thousand spots of spatial RNA-sequencing were collected from 38 patients: 19 with a diagnosis of SjD, 14 with sicca but without a diagnosis of SjD (non-SjD), and 5 healthy volunteers (Supplementary Table S2). These patients included clinical presentations with variation in age, sex, severity of disease, and positivity for autoantibodies (Fig 1c). Using the single-cell data to define cell types, 31 unique clusters were identified by Leiden clustering followed by manual annotation based on defined cell populations (Fig 1d). These included 6 unique types of seromucous acinar cells (SMAC/SMACs), 2 sets of mucous cells, and 5 groups of T cells (Fig 1d and Supplementary Fig S1a). Some cell types were enriched in disease (Supplementary Fig S1b) or in patients that were SSA^+ (e.g., $CD8^+$ exhausted T cells, $CD4^+$ T cells, B cells, and NK cells; Supplementary Fig S1c). These unique and complementary datasets were helpful to establish an unbiased portfolio of alterations in the SjD-affected salivary glands and a foundation for discovering and testing important cell types, cell states, and cell interactions in SjD.

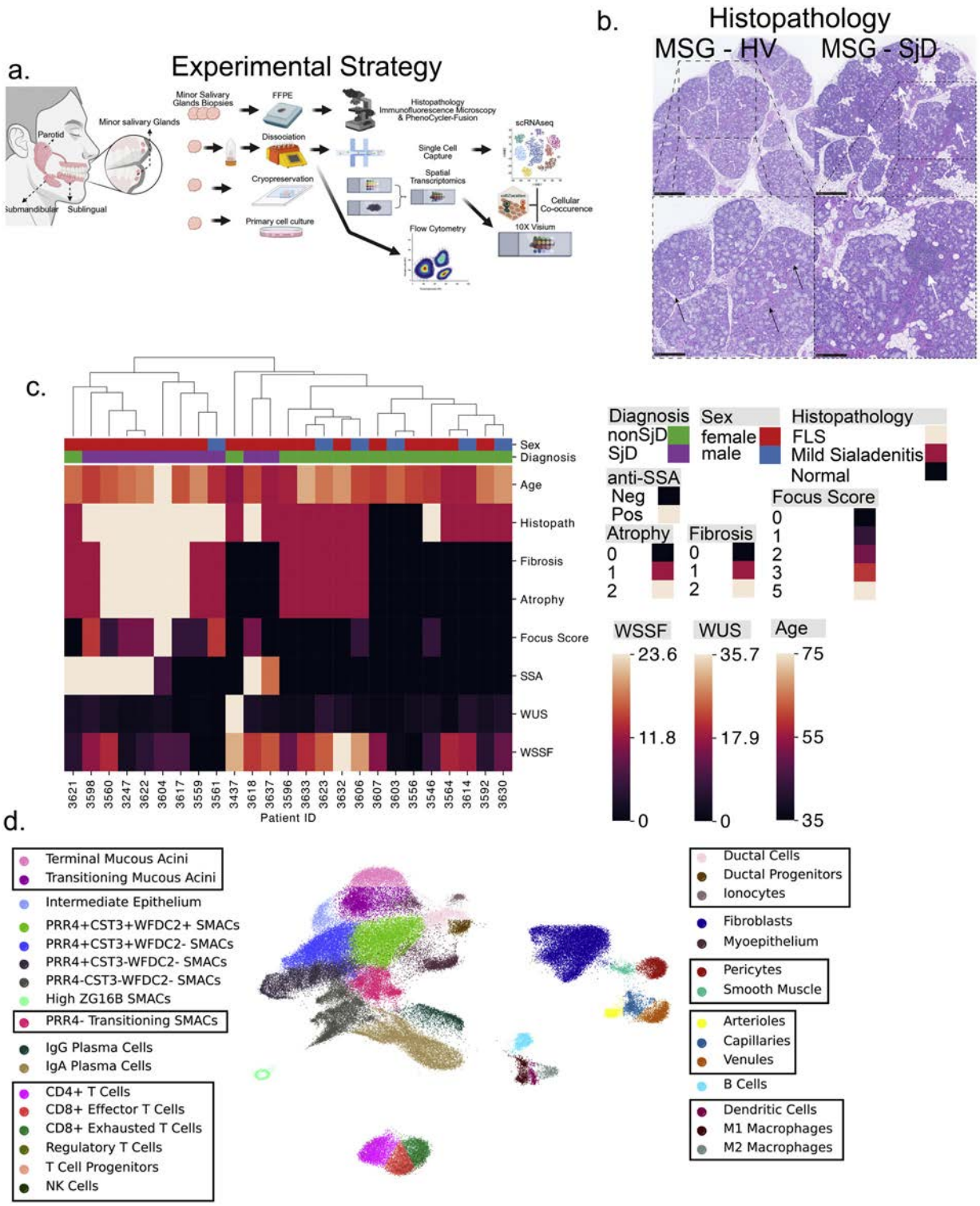

Figure 1. Clinical research investigations for 25 subjects included comprehensive oral, rheumatologic, and ophthalmologic investigations applying American College of Rheumatology 2016 Sjögren's Disease Classification Criteria including salivary gland biopsies on all subjects. Single-cell RNA-sequencing data from 94,227 cells were gathered across 25 patients with and without SjD. (a) A cartoon depicting the sample collection from subjects and the creation of scRNAseq and spRNAseq libraries. Histologic interpretations were primarily rendered on all participants' glands by the same board-certified anatomical pathologist trained in minor salivary gland evaluation (DEK) and confirmed by a board-certified oral and maxillofacial pathologist (BMW). Additional subjects, not included in the scRNAseq analyses, were used for flow cytometry, 10X Visium spatial transcriptomics, multiplex fluorescent *in situ* hybridisation (PhenoCycler-Fusion), and multiplex immunofluorescence microscopy. (b) The microscopic appearance of minor salivary glands from patients without SjD and with SjD is shown at 5× and insets at 10× digital magnification. In non-SjD, nonspecific sialadenitis is commonly found in healthy volunteers (black arrows); in SjD, multiple scattered lymphocytic foci (white arrows), periductal fibrosis, and atrophy characteristic of SjD. (c) A clustered heatmap of clinical features for the scRNAseq patients exhibiting the clinical heterogeneity of subject phenotypes (e.g., SjD, non-SjD sicca). Patient columns are coloured by sex and diagnosis, which were not included in the clustering. Patients clustered into 2 groups: a group enriched for patients with disease and a group of patients enriched for those without a diagnosis. Patients with disease were further divided into a high-focus score and autoantibody-positive group and an autoantibody-negative group. (d) Leiden clustering followed by manual annotation based on gene expression and UMAP embeddings enables granular distinctions between cell types. Cells clustered with Leiden clustering in scanpy are labelled along with manual annotations based on cell expression and boundaries in UMAP embeddings in boxes. In total, 31 unique cell

SjD is defined by loss of a SMAC population

The principal target cells and antigens have yet to be elucidated in SjD, yet unbiased efforts are ongoing [21]. To study the SjD-specific effects on epithelial cells, we used our single-cell analyses and spatial transcriptomics (Fig 1a,d) to study the composition and architectural changes in the context of SjD. Six distinct cell populations expressing key SMAC markers were identified (Fig 2a). When examining the differences in proportions of cells in the salivary glands of patients with SjD, the *PRR4*$^{+}$*CST3*$^{+}$ acinar cell cluster, which constitutes the largest single population of cells in non-SjD glands, is significantly reduced in SjD (Fig 2b) whereas the other acinar cell populations remain unaffected (Supplementary Fig S1a). Because the 5 other SMAC clusters remain unaffected, we do not believe that lower counts of the *PRR4*$^{+}$*CST3*$^{+}$ population in patients with SjD is due to an increased sampling of immune cells in affected glands. *MUC7*, a seromucous acinar protein, is highest in that *PRR4*$^{+}$*CST3*$^{+}$ SMACs cell population. The most 'stem-like' epithelial cells identified were a subpopulation of cells clustering within the ductal cell cluster subsequently named 'Ductal Progenitors' (*KRT5* and *MKI67*) [22]. Starting from this cell, Wishbone was used to calculate a trajectory score across all ductal and seromucous epithelial cells (Fig 2c). The gradient in trajectory score from ducts to more terminally differentiated acinar cells is consonant with developmental tubulogenesis [23] of the exocrine glands and the ability of ductal progenitor cells to regenerate acinar tissue [24]. Exploring the seromucous cells across this trajectory score, genes of ductal differentiation fall in expression (*WFDC2* and *ODAM*) and genes associated with seromucous cell function increase in expression (*ZG16B* and *PRR4*; Fig 2d). The cells seem to follow two differentiation trajectories terminating in *PRR4*-negative and *ZG16B*-high SMAC clusters. scRNAseq uncovers unexpected heterogeneity in the acinar compartment of salivary glands and identifies a selective vulnerability of one SMAC population in SjD (Fig 2b; Supplementary Fig S1a). To confirm changes in the heterogeneity and composition from scRNAseq among the salivary gland cell populations, we used hybrid fluorescent 12-plex *in situ* hybridization (ISH)/2-plex immunofluorescent spatial phenotyping. We applied markers that discriminate SMAC clusters (*MUC7, ZG16B, WFDC2, CST3*, and *PRR4*); and applied canonical markers of salivary differentiation (*MUC5B, BPIFB2, PIP, AMY1A,* and *CFTR*), markers of response to type I IFN (*ISG15* and *B2M*), a marker of contractile cells (e.g., myoepithelial cells, pericytes, and fibroblasts; *ACTA2*), and two protein markers (pan-cytokeratin [pCTK], CD45) to discriminate epithelial and immune cells (Fig 2e). Following recursive fluorescent whole slide imaging and registration, cells were segmented and phenotyped. Fluorescent ISH confirmed SMAC heterogeneity and population shifts demonstrated by scRNAseq (Fig 2f). Distribution of ISH quantifications separated cells from patients with and without SjD (Fig 2f,g and Supplementary Fig S3a,b,e). Finer-grained clustering separated patients on the severity of disease presentation as measured by focus score (Supplementary Fig S3c,d,f). Acinar cells from patients with SjD were uniformly higher in quantification of type I IFN response genes (ie, *ISG15* and *B2M*), indicative of their response to the inflamed microenvironment. Expression of markers for unaffected acinar cell types was unchanged in their expression of identity markers (*MUC5B* for mucous acini and *ZG16B* for terminally differentiated seromucous acini). In contrast, expression of *PRR4, CST3*, and other markers of differentiating acinar subsets was markedly reduced, consistent with the selective loss of these cells in disease (Fig 2f,g), and reinforcing our scRNAseq results, and confirming the heterogeneity of the SMAC compartment.

Cells grouped by index expression suggest T cell dysfunction in SSA^{+} *patients is distinct from dysfunction in SSA*$^{-}$ *patients*

To understand disease- and cell-type-specific annotated pathway utilisation, we hypothesised that scRNAseq data could be clustered based on indices of gene expression. Expression data were converted from log-normalised counts to *Z*-scores to make contributions between genes equivalent and summed across annotated indices to form *S*-scores. These *S*-scores were then log-normalised to conform to algorithmic expectations of data shape in single-cell data. As clusters were generated in the gene expression and gene index spaces, clusters based on gene indices represent a composite of previously named cell types (Fig 3a-d; Supplementary Fig S4a,b). These clusters encompassed multiple cell types and were characterised by a regulatory programme or shared function, or a cell identity consistent with previous annotation (Fig 3d). Myoepithelium, pericytes, and endothelium that were undergoing active contraction ('Response to metal ions', 'muscle contraction, SRF targets', 'GO: MUSCLE SYSTEM PROCESS') made up cluster 10, in contrast to the same types of cells performing other functions (cluster 11: 'enriched in antigen presentation (III)' or cluster 13: 'Alternative complement activation' and 'GO: COMPLEMENT ACTIVATION ALTERNATIVE PATHWAY'). Similarly, epithelium and a minority of secretory plasma cells expressed similar patterns of indices associated variously with homeostasis (cluster 2: 'GO: HOMEOSTATIC PROCESS'), the cell cycle (cluster 5: 'GO: CELL CYCLE', 'GO: MITOTIC CELL CYCLE', 'GO: CELL CYCLE PROCESS'), transcription elongation (cluster 1: 'GO: DNA TEMPLATED TRANSCRIPTION ELONGATION' and 'GO: TRANSCRIPTION ELONGATION FROM RNA POLYMERASE II PROMOTER') or nuclear export (cluster 12: 'NEP/NSR Interacts with the Cellular Export Machinery') and were so named. By contrast, one cluster (in red) was made up exclusively of cells annotated previously as fibroblasts, and was named 'Fibroblasts'.

Like the clusters based on expression (Fig 1e, Supplementary Fig S1a), clusters based on index scores were enriched for clinical features of interest in SjD (Supplementary Fig S4a-d). Cells from non-SjD and SSA^{-} patients' cells shared expression of indices, including sensory taste perception and pathological glycosylation, indicating their similarity (Supplementary Fig S5a-c). Conversely, cells from SSA^{+} patients

types, including 7 types of seromucous acinar cells, were identified. Two *PRR4*$^{-}$ SMAC populations were combined into 1 'transitioning' population. SjD, Sjögren's disease; SMACs, seromucous acinar cells; MSG, minor salivary gland; FFPE, formalin-fixed paraffin-embedded; WUS, whole unstimulated salivary flow; WSSF, whole stimulated salivary flow; UMAP, uniform manifold approximation and projection.

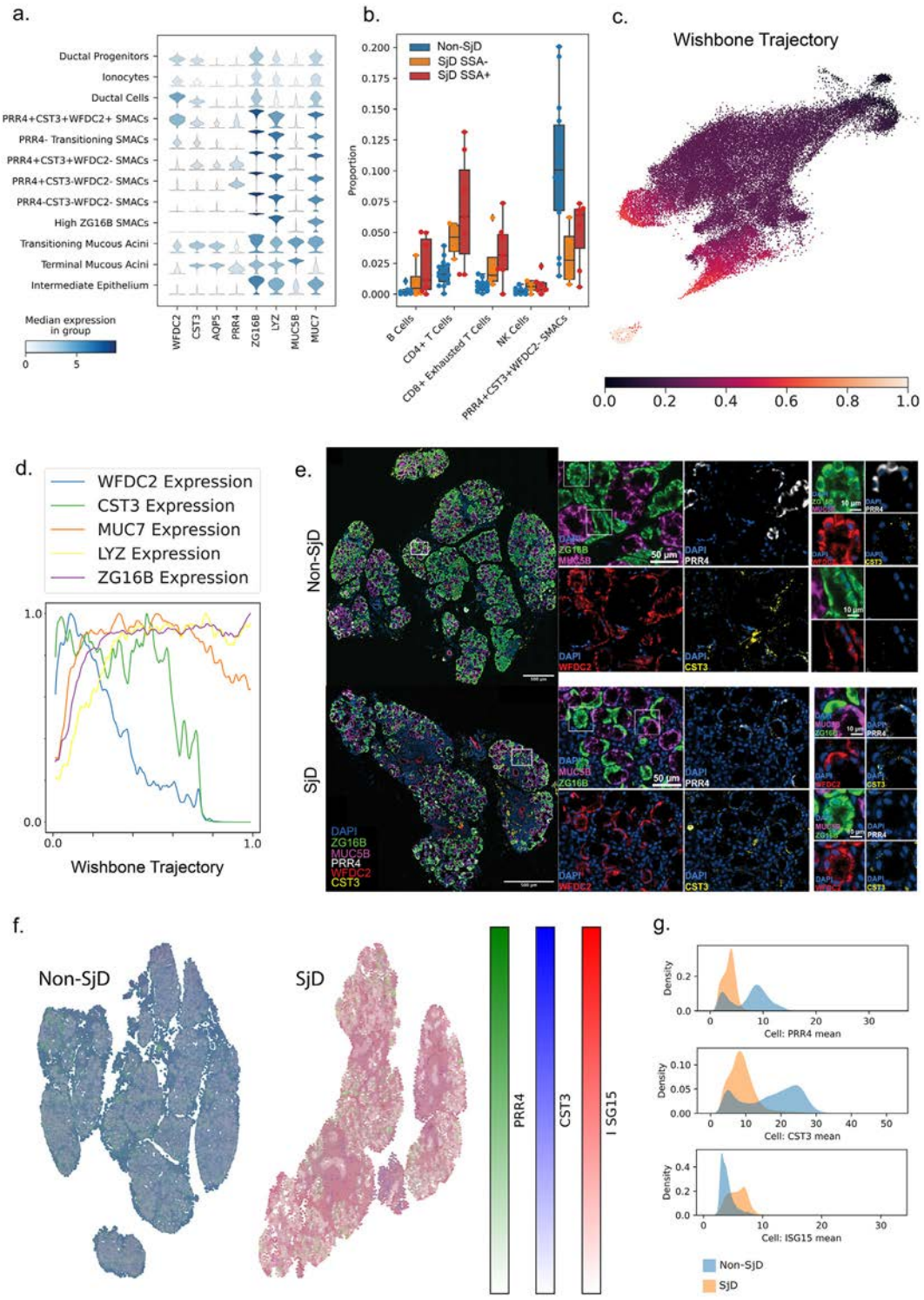

Figure 2. Among epithelial populations, one seromucous acinar cell population decreases in proportion in the glands of patients with disease. (a) Expression of acinar cell type markers in the scRNAseq data including in the 6 distinct populations of seromucous acinar cell types and 2 populations of mucous acinar cells. (b) Statistically significant changes in cell proportions between SjD and non-SjD. PRR4$^+$CST3$^+$WFDC2$^-$ SMACs were the most abundant population in patients without SjD and presented the greatest loss in SjD. (c) Cell trajectory for ductal and seromucous acinar cells using Wishbone, starting with the cell most positive for *MKI67*, a marker of progenitor state. The cell trajectory starts with a small population of ductal progenitors and proceeds along the ducts to the seromucous acinar cells, ending in the *CST3*$^-$ populations. (d) Gene expression (after log-transformation) for marker genes along the wishbone trajectory as a fraction of maximum expression. *WFDC2* expression is lost first, followed by *CST3*. *MUC7* expression peaks in the centre and *LYZ* and *ZG16B* are highest in the most differentiated SMACs. (e) ISH images of glands taken from patients with and without SjD (n = 18). Patients with SjD have fewer seromucous acinar cells in their gland and very few totally-seromucous acini (green in white box), but retain their ducts (in red). Very few acini in affected glands are *PRR4*$^+$ or *CST3*$^+$. (f) Representative images showing multiplex *in situ* RNA hybridisation of acinar and disease marker genes in salivary glands. (g) Distribution of quantified ISH fluorescence for 2 markers of acinar cell type and one marker of type I IFN signalling with a clear difference in distribution between patients with and without SjD. IFN, interferon; SjD, Sjögren's disease; SMACs, seromucous acinar cells; ISH, in situ hybridization.

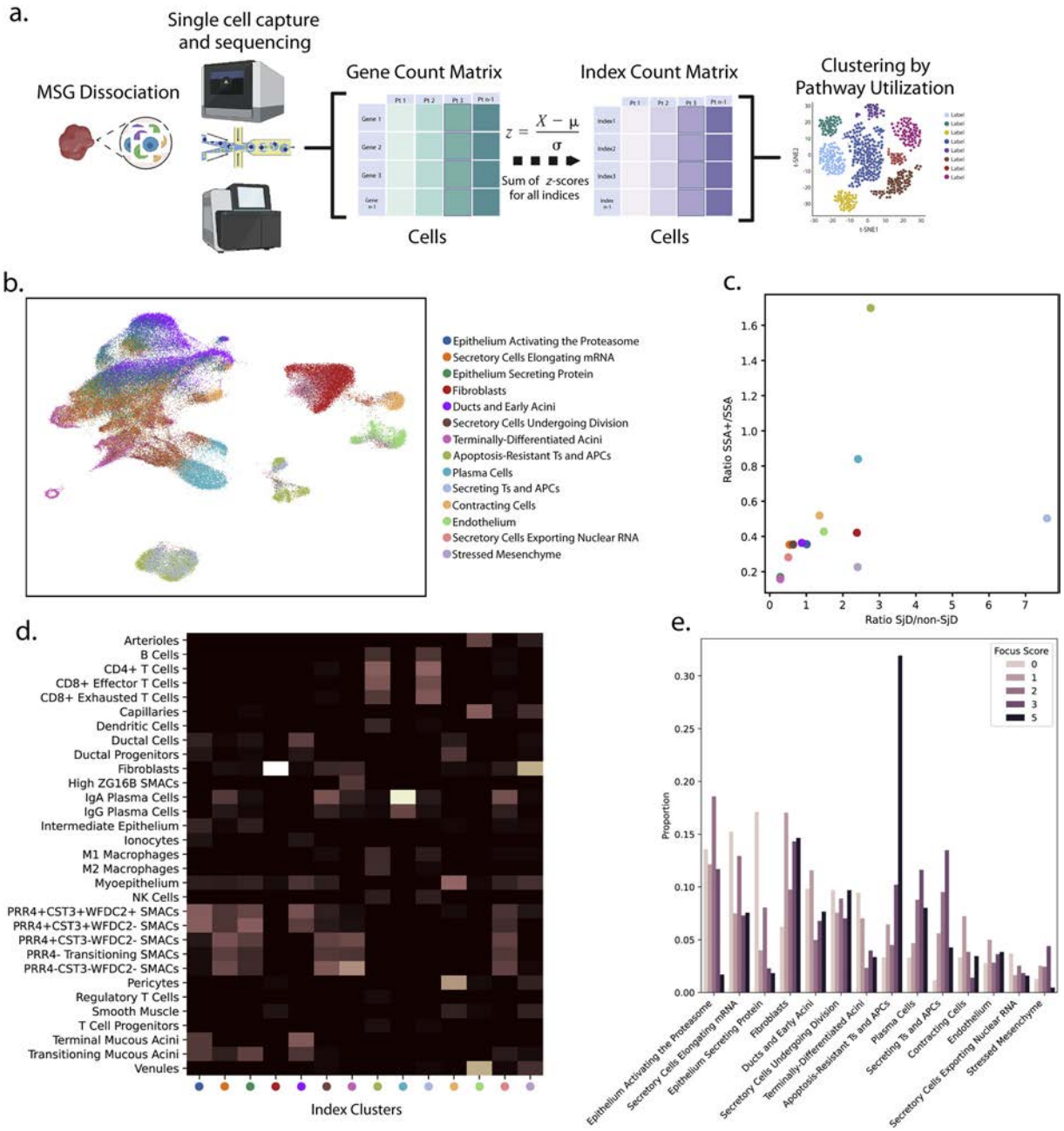

Figure 3. Transforming scRNAseq data from gene expression to indices reveals new organisations of cells and clinical feature-specific clusters. (a) The experimental analytic design of the index analysis. After dissociation and sequencing, a dot product of the gene expression matrix and a one-hot-encoded map of gene indices produced an S-score matrix of expression across indices. (b) The original scRNAseq UMAP overlaid with the index clusters. (c) Ratios of Sjögren's to non-Sjögren's and anti-SSA positive to negative patients in each of the index clusters. Two index clusters are found at the extreme of the plot: one with high SjD specificity and the other with high anti-SSA positive specificity. (d) Proportions of index clusters that represent annotations in the original single-cell space. Some clusters are close to a single-cell type; others contain a variety of cell types. There are no one-to-one mappings between index clusters and original annotations. Index clusters specific to patients with SjD and SSA^+ patients are composed of T cells, B cells, dendritic cells, and macrophages. (e) Barplot of each index-cluster as an average proportion of samples with a specific focus score. Patients with high-focus score have a high proportion of 'Apoptosis-Resistant Ts and APCs' and a low proportion of 'Epithelium Activating the Proteasome' whereas low-focus score patients with SjD have high 'Secreting Ts and APCs' and all patients with SjD have low 'Epithelium Secreting Protein'. SSA, Sjögren's syndrome-related antigen A; APCs, antigen-presenting cells; Ts, T cells; UMAP, uniform manifold approximation and projection.

were associated with many enriched pathways involving effector immune cell function, antigen processing, and IFN signaling (Supplementary Fig S5b). To illustrate this more clearly, a 21-gene type I IFN-stimulated genes score was constructed and found to be higher in every annotated cell type in SSA^+ patients, irrespective of SjD status (Supplementary Fig S4e-g). This index was highest in endothelial cells, macrophages, dendritic cells, and ducts. Calculating a ratio of cells in each clinical feature, two index clusters have notable enrichments with disease or SSA^+ (Fig 3c). These cells were almost exclusively identified previously as either T-lymphocytes or antigen-presenting cells (namely, B-lymphocytes, dendritic cells, or macrophages; Fig 3b,d). Comparing the indices directly, indices associated with T cell activation scored higher in the SSA^+ cluster, whereas no indices were significantly enriched in the SjD-diagnosed cluster, further underscoring disease heterogeneity between SSA^+ and SSA^- patients.

A uniform manifold approximation and projection (UMAP) built on gene indices split cells by an index of recombination linked to mitosis (Supplementary Fig S5c,d). Genes involved in mitosis are more highly expressed in epithelial populations in SjD, including in the seromucous acinar population lost in disease (Supplementary Fig S5c). To investigate these changes in chromatin accessibility upstream of gene expression, 10X multiomics data were generated on a limited set of available samples (n = 6, Supplementary Tables 1 and 2). The most differentially open chromatin in *PRR4*$^+$*CST3*$^+$*WFDC2*$^-$ SMACs was found at chr5:56860655-56861551 and linked to higher expression in *MAPK1*, a gene associated with cell division, and the most differentially closed chromatin was at chr2:178450424-178451508 and linked to higher expression of *PRKRA*, a gene involved in the IFN response pathway (Supplementary Fig S5e). Because open chromatin at this locus was associated with lower expression of *PRKRA*, we hypothesise that this region represents a cis-regulatory silencing element. Expression of both genes was higher in seromucous cells in SjD.

CD8$^+$*GZMK*$^+$ *T cells are enriched in SjD and exhibit effector functionality*

The data above highlight important immune cell populations involved in SjD pathogenesis. Most of these cells are located within dense periductal infiltrates, termed 'foci', which are characteristic of focal lymphocytic sialadenitis (Fig 1b). These immune foci are predominantly composed of T and B-lymphocytes. To understand the spatial organisation, function, and interactions of T cells within affected glands, we integrated spatial RNA sequencing (spRNAseq), single-cell RNA sequencing (scRNAseq), flow cytometry, and immunofluorescence microscopy (Fig 1a).

In scRNAseq, T cell subclusters were annotated based on gene expression markers: CD4$^+$ T cells (*CD40LG*), regulatory T cells (*FOXP3*), proliferating progenitor T cells (*MKI67* and *IL2RA*), exhausted CD8$^+$ T cells (T_{ex}; *CD8A, GZMK*, and *PDCD1*), cytotoxic CD8$^+$ T cells (T_c; *CD8A*, and *GZMB*), and NK cells (*NKG7* and *GNLY*) (Fig 4a). Among these, T_{ex} were the most enriched immune cell type in SjD salivary glands, with a 4.75-fold increase and a highly significant enrichment ($q = 0.0009$).

To understand the role of these T_{ex} cells, we assessed their distribution and transcriptional profiles. Clustering T cells by disease feature revealed T_{ex} enrichment in both SSA$^-$ and SSA$^+$ SjD samples, with these cells showing distinct clustering patterns along the periphery of the T cell subclusters (Fig 4a). Compared with controls, T_{ex} in SjD glands expressed higher levels of *GZMA* and *GZMK*, whereas expression of *GNLY* and *GZMB* was reduced—indicating a shift from cytotoxic to *GZMK*$^+$ effector/exhausted phenotypes (Fig 4b). Although *GZMB*$^+$ T_c cells were numerically increased in SjD glands, they were less abundant than T_{ex} and not significantly enriched. Pathway analysis showed similar activation profiles between T_c and T_{ex} subsets (Fig 4c), with greater activation in SSA$^+$ samples (Fig 3f, Supplementary S4e), further supporting the effector phenotype of T_{ex} cells in driving tissue-specific inflammation in SjD.

To corroborate these findings, 35-plex immunophenotyping was used to characterise immune infiltrates in patient's salivary gland biopsies. These results demonstrate immune foci composed primarily of CD4 T, CD8 T, and B cells cluster around ducts and interdigitating at the periphery of foci through acinar clusters in SjD (Fig 4d; Supplementary S4a-g). To corroborate T cell-mediated interactions in SjD, we analysed scRNAseq data using CellChat. Anti-SSA$^+$ SjD salivary glands showed enrichment of 'major histocompatibility complex 1' (MHC-I) signalling, consistent with elevated antigen presentation, and 'CD22' interactions, implicating altered B cell regulation (Fig 4e). Additional ligand-receptor pairs enriched in anti-SSA$^+$ SjD included 'NCAM', 'SELL', 'THY1', 'complement', and 'TIGIT' (Supplementary Data), reflecting enhanced immune adhesion (NCAM, THY1), aberrant lymphocyte trafficking (SELL), checkpoint engagement between T_{ex} and epithelial cells (TIGIT), and local activation of innate immunity (complement). These disease-specific pathways highlight coordinated immune-epithelial interactions that underlie SjD pathology. These data also underscore the prominence and uniqueness of SSA$^+$ signalling, involving T cell/B cell interactions for B cell costimulation and maturation (CD22), and coordinated lymphocyte infiltration into peripheral tissues (SELL and NCAM) (Fig 4e, Supplementary S6a-g). Collectively, this highlights the critical role of effector T cells in engaging target salivary gland cells (ducts and acini) and reinforces the immunological distinction between SSA$^+$ and SSA$^-$ SjD. However, the effector functions of T_{ex}, which are markedly enriched in SSA$^+$ glands, remain an open and important question.

To directly assess the cytotoxic potential of T cells infiltrating the salivary glands, we performed an *ex vivo* T-lymphocyte functional assay using lymphocytes isolated from minor salivary glands of patients with SjD (n = 6) and non-SjD controls (n = 5) (Fig 4f). Immune cells were stimulated with PMA/ionomycin and assessed for intracellular cytokine production and surface CD107a expression, a surrogate marker for T cell degranulation. SjD samples exhibited a trend towards increased T cell infiltration ($P = .08$), with significantly higher proportions of CD4$^+$ T cells (1.6-fold, $P < .05$) and decreased CD8$^+$ T cells (0.8-fold, $P < .01$) relative to controls. Despite their reduced proportion relative to CD4$^+$ T cells, CD8$^+$ T cells from SjD glands showed enhanced effector function, as evidenced by a significantly greater fraction of CD107a$^+$ cells following stimulation (2.1-fold, $P < .001$), indicating elevated cytotoxic potential. A substantial proportion of these CD8$^+$ T cells also produced IFNγ, supporting their functional activation *in situ*. Although T_{ex} and T_c subsets could not be separated in this assay, these data suggest that CD8$^+$ T cells in SjD glands—regardless of exhaustion state—retain robust effector function, consistent with our earlier findings of T cell–epithelial engagement via TIGIT and MHC-I signalling pathways.

Spatial phenotyping demonstrates SjD-specific cellular interactions

Multiplex spatial proteomics is a powerful tool for mapping cellular positions and interactions in salivary glands of SjD and healthy patients. Formalin-fixed, paraffin-embedded (FFPE) sections from patients with SjD (n = 5) and without SjD (n = 7) were analysed using a 35-plex spatial phenotyping platform. A total of 678,343 cells were segmented and classified into 16 cell types using TACIT [25]: T-helper (T_h), regulatory T cells (T_{reg}), cytotoxic T cells (T_c), NK cells, dendritic cells (DCs)/macrophages (macs), neutrophils, lymphatic endothelial cells (LECs) and vascular endothelial cells (VECs), progenitor VECs, fibroblasts, myofibroblasts/pericytes, myoepithelial cells, ductal cells, and acinar cells (Supplementary Fig S6a, Supplementary Methods). This panel did not reliably distinguish all scRNAseq-resolved cell types, such as seromucous versus mucous acinar cells (Fig 5a,b; Supplementary Fig S6a).

After segmentation, TACIT phenotyping [25] generally corroborated altered cellular compositions in SjD, including

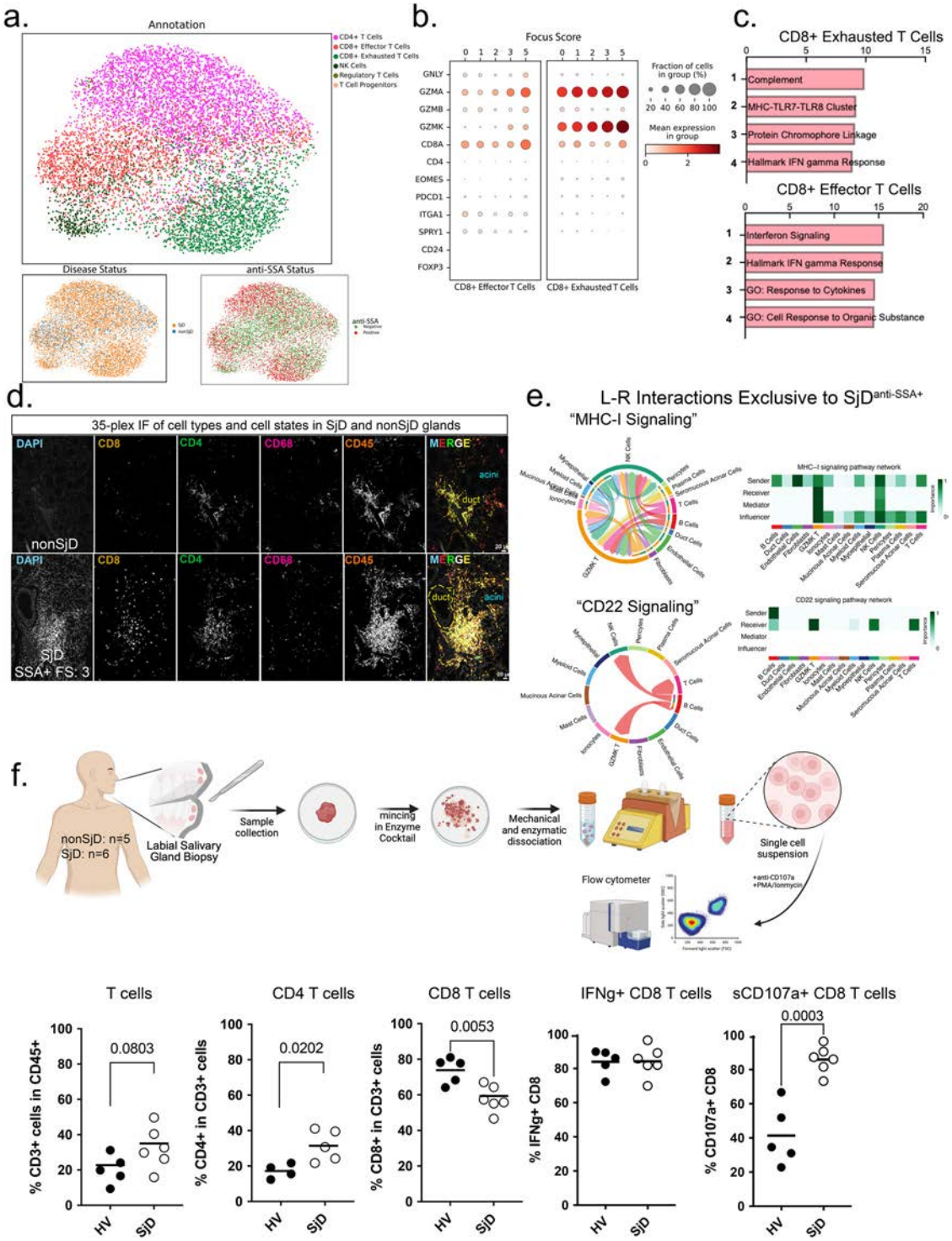

Figure 4. CD8$^+$ exhausted T cells are enriched in the immune infiltrates of SjD and exhibit an effector phenotype. (a) Highly multiplexed (4/35-plex shown) immunofluorescence microscopy shows distribution of CD4$^+$ and CD8$^+$ T cells, as well as CD68$^+$ macrophages in the glands of SjD and non-SjD. (b,c) scRNAseq UMAPs of expression using only T cells, with disease diagnosis and anti-SSA positivity visualised. T cells from SSA$^+$ individuals cluster on the periphery whereas SjD T cells are distributed throughout. (d) Expression of key T cell genes in exhausted and effector *CD8*$^+$ T cells across disease severity. (e) Single-cell pathway enrichment analysis shows similar activated profiles between *GZMK*$^+$*CD8*$^+$ exhausted T cells and *CD8*$^+$ effector T cells in SjD. (f) The potential for degranulation and cytotoxicity of T cells was measured *ex vivo* using a flow cytometry-based T-lymphocyte cytotoxicity assay. CD45$^+$ immune cells were dissociated from patients' salivary glands (non-SjD: n = 5 patients; SjD: n = 6 patients). IFN, interferon; SjD, Sjögren's disease; MHC, major histocompatibility complex; SSA, Sjogren's syndrome-related antigen A; GO, gene ontology; DAPI, 4′,6-diamidino-2-phenylindole; FS, focus score; HV, healthy volunteer; UMAP, uniform manifold approximation and projection.

reduced myoepithelial cells, fibroblasts, and myofibroblasts/pericytes, alongside increased ductal and immune cell proportions. Notably, T_{reg} cells and VEC progenitors were significantly enriched in SjD glands (2-fold; t-test, $P < .05$; Fig 5c,d). T cells in SjD showed higher activation (HLA-DR, CD38, CD107a, GZMB, and ICOS) and checkpoint marker expression (IDO1 and PD-1), whereas T_{reg} cells exhibited reduced FOXP3 and increased GZMB levels (Supplementary Fig S6f). B cells showed

plasma cell differentiation markers (CD38). Epithelial cells in SjD displayed elevated HLA-A and HLA-DR but lower PD-L1, differentiation markers (PHH3 and GATA3), and proliferation markers (Ki67).

Spatial proteomics demonstrated the expected compositional and cellular architectural changes of the glands: reduced acinar density and dense immune foci surrounding ducts and interdigitating acini in SjD glands (Figs 1b, 4d, and 5f). T cells aggregated near epithelial structures, correlating with increased HLA-A expression at the immune interface, as predicted by ligand-receptor analysis (Figs 4e and 5f). Fibroblast cell collections were found penetrating into the centres of acinar-rich areas in SjD, and myoepithelial cells were found in closer proximity to ducts, unlike in non-SjD glands. Modelling epithelial marker expression relative to immune cell proximity revealed disrupted spatial relationships in SjD. For instance, pan-cytokeratin expression typically decreased with immune cell proximity but was unchanged in SjD and reduced overall; conversely, CD66 (elevated in mucous acini) directly correlated with T cell proximity, illustrating spatial and functional gland remodelling (e.g., loss of seromucous cells in areas of T cell infiltration giving way to mucous cell predominance; Fig 5g).

Neighbourhood analysis highlighted significantly increased interactions between immune cells (e.g., B, DC, NK, T_{reg}, and T_c) and epithelial targets (acini, ducts, and myoepithelial cells) in SjD (Fig 5h). Enhanced interactions were observed at the immune-epithelial interface: acini with T_{reg}, T_h, DC, and T_c; ducts with B, T_{reg}, T_h, DC, and T_c; and myoepithelial cells with DC, T_c, and T_h but with reduced interactions with stromal and endothelial cells (Fig 5h). These findings illustrate the complexity of immune-epithelial crosstalk in SjD and align with scRNAseq results showing differential preservation of mucous versus seromucous cells.

To contextualise these compositional and architectural changes, we enumerated the 10 nearest neighbouring cell types for all cells and summarised the results using heatmap matrices (Fig 5i, and Supplementary Fig SF6b). Spatial distances between cell types reveal specific colocation trends across disease phenotypes. In non-SjD salivary glands, colocation clustering reveals discrete compartment differences in non-SjD and SjD. Examining the differential colocations shows increased interactions between immune cells that compose lymphocytic foci including T_c with T_{reg}, T_{reg} with acini, T_c and T_{reg} with myoepithelial cells, and increased colocations within epithelial cell types (acini to ducts and myoepithelial cells), indicative of shifts in composition and architecture.

GZMK drives type I IFN signalling in salivary epithelial cells

Very little is known about how $GZMK^+$ $CD8^+$ T cells exert effector functions or contribute to SjD pathology. Recent evidence in rheumatoid arthritis shows that lymphocyte-derived GZMK can function extracellularly to cleave and activate components of the complement cascade, thereby promoting chronic tissue inflammation [26]. In addition to the potential extracellular role, it is possible that GZMK may also function as an intracellular effector protease.

Classically, cytotoxic T cells engage target cells at the immunologic synapse, releasing granules containing perforin and granzymes to induce apoptosis. However, unlike granzyme B, GZMK does not trigger apoptosis via caspase activation. Instead, it may act intracellularly by cleaving BID at the mitochondrial membrane, promoting mitochondrial dysfunction and reactive oxygen species (ROS) generation. Thus, GZMK may contribute to tissue pathology through both extracellular complement activation and intracellular disruption of epithelial cell metabolic integrity.

We hypothesise that in addition to the potential generation of ROS, cytosolic granzyme K may affect mitochondrial membrane permeability, promoting the relocalisation of mitochondrial nucleic acids to the cytosol and the initiation of the pathogen recognition response (PRR) [27,28]. Epithelial cells in patients with SjD produce higher levels of MHC-I (Figs 4e and 5g,h) regardless of autoantibody positivity. Cells presenting autoantigenic peptides on their MHC-I may initiate effector cell engagement of T_{ex} cells to drive subacute effects on inflammatory signalling, thereby explaining (1) minimally increased apoptosis in the glands [29], and (2) the canonical increased type I IFN signature in SjD-affected ducts and acini, in all patients and in particular in SSA^+ patients. These observations raised new and important questions regarding the arrangement of $GZMK^+CD8^+$ T_{ex} cells in the gland and their role in SjD pathogenesis.

We next confirmed the location and proportions of $GZMK^+CD8^+$ T_{ex} and $GZMB^+CD8^+$ T_c cells in the peri-epithelial immune infiltrates using immunofluorescence microscopy followed by automated segmentation and phenotyping. $GZMB^+CD8^+$ T_c cells were fewer in number in the infiltrates and more distant from epithelial structures in SjD (Figs 5 and 6a). $GZMK^+CD8^+$ T_{ex} cells were more numerous and resided in close proximity to, or within, involved ducts and acini (Wilcoxon, $P = .0175$; Fig 6a).

To model the effector activity of cytotoxic granules containing GZMK from Tex on targeted epithelia in SjD, we transfected recombinant GZMB and recombinant GZMK into the cytosol of human acinar cells (AC cells; Fig 6b, Supplementary Fig S7a) or primary salivary gland epithelial cells (Fig 6c). Transfection of GZMK did not induce apoptosis by staining with Annexin V/PI flow cytometry (Supplementary Fig S7b); transfection of GZMB mildly increased apoptosis in transfected cells in a 24-hour assay. Western immunoblot analysis of GZMK shows the dose-dependent differences in GZMK protein levels in primary salivary gland epithelial cells (pSGECs) (Supplementary Fig S7c), and shows the time-dependent presence of cytosolic GMZK and GZMB protein in NS-SV-TT-AC cells out to 48 hours (Supplementary Methods). Using immunofluorescence microscopy, GZMK transfection, but not GZMB, results in mitochondrial DNA and RNA relocalisation (Supplementary Data) to the cytosol (2.6-fold, $P < .0001$; analysis of variance [ANOVA]; Fig 6b) in acinar cells. Correlation analysis of protein within the cell, labelled by His tag, shows that GZMK, but not GZMB, correlates with the presence of measurable cytosolic DNA. Cytosolic GZMK results in an increase in pIRF3/IRF3 ratio, suggesting IRF pathway activation and type I IFN signalling (Supplementary Fig S7d). The ability for GZMK to drive cytosolic mtDNA in reporter cells was confirmed using fluorescent microscopy of THP1-macrophages (Supplementary Fig S7e). To show that GZMK-induced cytosolic mtDNA drives type I IFN through PRR [27,28], we used reporter cell lines to show IRF pathway activation (1.6-fold, $P < .0001$; ANOVA; Supplementary Fig S7e) and type I IFN response (1.3-fold, $P = .023$; ANOVA; Supplementary Fig S7f), respectively. To further confirm this effect, we transfected GZMK into the cytosol of human pSGECs; GZMK-induced nuclear translocation of pIRF3 (1.2-fold, $P < .0001$; 2-sided *t*-test; Fig 6c, Supplementary Fig S6g) in pSGECs, and drives ISG expression (CXCL10, IL6, and tumour necrosis factor alpha [TNFa]).

To prove that the GZMK protein transfected into cells drives PRR, we devised an experiment to isolate the effects of granzymes on target cells. Dual fluorescence GZMK and GZMB sensor plasmids [21] were constructed and transfected into NS-SV-TT-AC

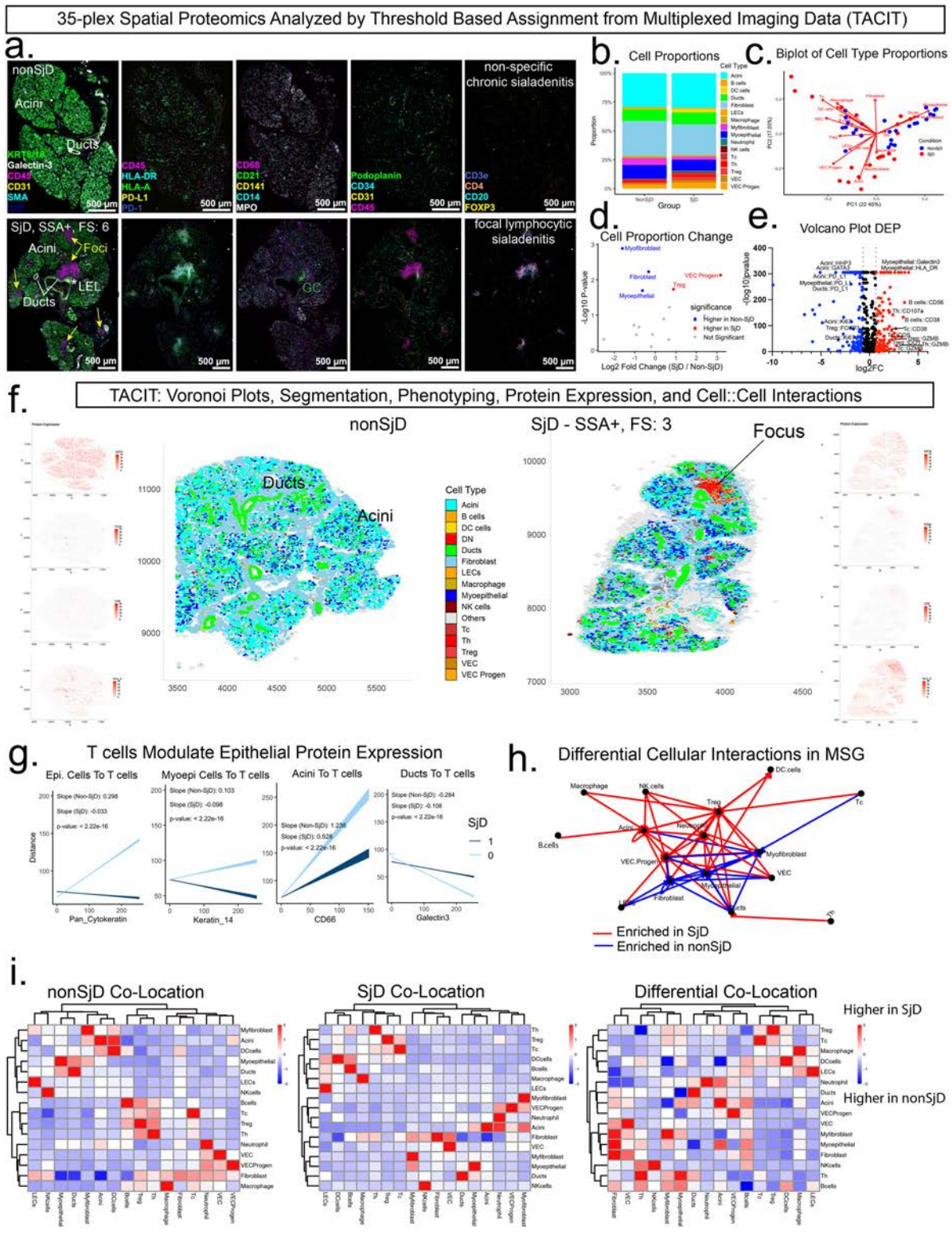

Figure 5. PhenoCycler-Fusion 35-plex spatial proteomics confirms changes in glandular composition and cellular interactions. (a) Representative PhenoCycler-Fusion immunofluorescent images from a lymphocytic focus showing infiltration with T- and B-lymphocytes around ducts and acini. (b) Cellular proportion changes in SjD compared with non-SjD. (c) Biplot of changes in cell proportion with samples coloured by diagnosis. (d) Per-cell $\log_2$ fold changes in protein expression in SjD compared with non-SjD were calculated for all phenotypes and segmented cells. (e) Volcano plots of per-cell-type protein expression changes in disease. (f) Cell segmentations produced by TACIT and coloured by cell type. The patient with SjD has increased inflammation and fibrosis and reduced acini. (g) Changes in protein expression in epithelial cells are driven by the distance between that epithelial cell and the nearest T cell. (h) Cellular neighbourhoods in SjD compared with non-SjD. (i) Colocalisation of cell types in SjD glands compared with the glands of patients without SjD. SjD, Sjögren's disease. MSG, minor salivary gland.

cells. Separately, HEK cells were transfected with plasmids engineered to express GZMK, GZMK' (catalytically dead), GZMA, and GZMB (Supplementary Methods). Crude cellular lysates from HEK cells were transfected into target cells expressing matched sensors (i.e., piGZMA + GZMA) and incubated for 24 hours (Supplementary Fig S8a,b). Using confocal fluorescence microscopy,

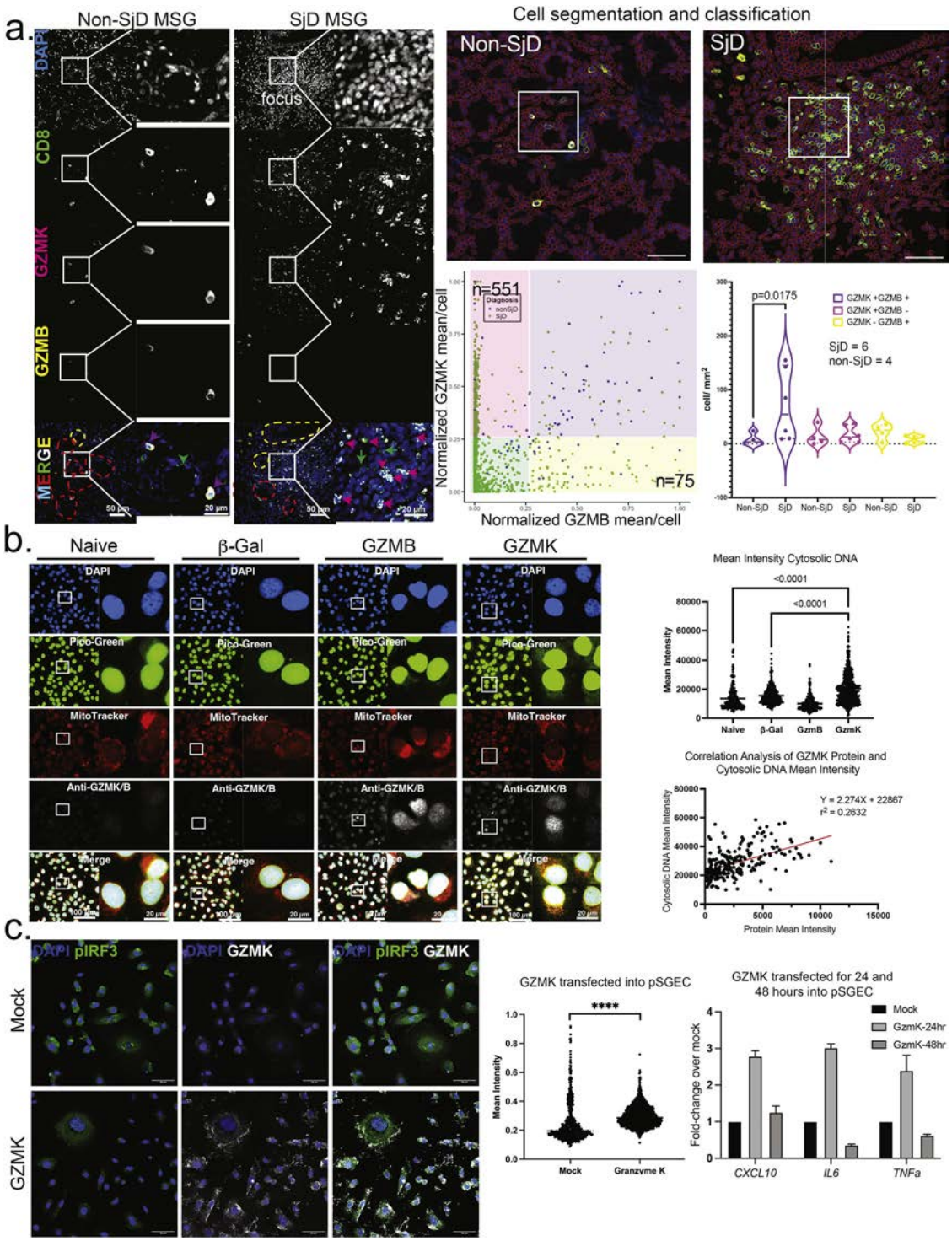

Figure 6. GZMK drives cellular innate immune signalling in SjD. (a) Multiplex immunofluorescence of salivary gland sections from patients with and without SjD hybridised with anti-GZMK, -GZMB, and -CD8. Immune infiltrates enriched with GZMK$^+$CD8$^+$ T cells in close proximity to acinar structures and ducts are shown. (b) Fluorescent confocal microscopy was used to measure cytosolic mitochondrial DNA after GZMK protein transfection. The transfection of recombinant GZMK and GZMB was monitored by their His tag. Image analysis demonstrates increased mtDNA in the cytoplasm. (c) Multiplex immunofluorescence microscopy shows cytosolic transfection of GZMK drives phosphorylated IRF3 (pIRF3) and nuclear translocation in pSGEC. SjD, Sjögren's disease.

NS-SV-TT-AC transfected with a sensor (green) and sensitive to granzyme cleavage (red) were evaluated for the presence of nuclear pIRF3. GZMK, but not GZMK', were able to activate the sensor, and these cells exhibited enhanced nuclear pIRF3 (2-sided *t*-test adj. *P* value < .0001; Supplementary Fig S8c). GZMB also induced nuclear pIRF3, but to a lesser degree (2-sided *t*-test, q < .0001; Supplementary Fig S8c).

In furtherance of these results, we wanted to understand if effector proteins can be delivered to the cytosol of target salivary epithelial cells (Fig 7a) in a disease-dependent manner. To answer this question, we devised a novel coculture method to directly assess effector and target cells using autologous patient-derived SGEC and peripheral blood mononuclear cells (PBMCs). Although CD8$^+$ T cells were successfully isolated from salivary

gland tissue for prior assays, the number of cells recovered was insufficient to allow for their predictable expansion and subsequent use in coculture (*data not shown*). Alternatively, $CD8^+$ T cells expanded from peripheral blood samples yielded sufficient cell numbers to evaluate their effector function in autologous coculture experiments. With this setup, we were able to measure the cell viability, proliferation (CellTrace), degranulation (sCD107a), activation (HLA-DR/CD38), expression of effector proteins granzymes (GZMB and GZMK), and perforin expression in $CD8^+$ T cells, and cell viability, granzymes, and perforin in epithelial cells using flow cytometry and immunofluorescence microscopy. Using cells of healthy and SSA^+ patients with SjD, we performed autologous coculture with expanded $CD8^+$ T cells at an experimentally-derived target:effector ratio of (1:5).

Even after 3 days of rest, expanded $CD8^+$ T cells maintain a highly cytotoxic state, characterised by elevated expression of granzyme B and perforin, as well as increased basal degranulation, which is similar between SjD and healthy tissues. In our coculture assay, compared with healthy patient-derived $CD8^+$ T cells, SjD-derived $CD8^+$ T cells exhibit more population doublings (greater fraction of $F3^+$ populations), more activation (increased fraction of $HLA\text{-}DR^+/CD38^+$ $CD8^+$ T cells) and exhibit greater degranulation after coculture (Fig 7c-e, Supplementary Fig S8d,e). Examining the subsequent generations of $CD8^+$ T cells after coculture, the fraction of cells positive for granzyme K increases modestly (Fig 7a-e). Using both flow cytometry and immunofluorescence microscopy, granzymes, both granzyme B and granzyme K, and perforin, secreted from CD8 T-lymphocytes, are delivered to target epithelial cells (Fig 7f-g and Supplementary Fig S8f,g) and induce nuclear translocation of pIRF3 (Supplementary Fig S8e). Based on this and our data above, we show that T_{ex}, similar to T_c, can form the immunological synapse and exert effector function upon the SjD salivary gland epithelium. Yet unlike granzyme B, granzyme K activates cellular innate immune signalling through PRR/nucleic acid sensing pathways, as predicted by our scRNAseq data, without inducing cell death.

$GZMK^+$ T_{ex}-like cells have been reported to be involved in multiple target organs (e.g., kidneys, synovium) in autoimmune diseases [30,31]. Contemporaneous to our analyses, $GZMK^+$ T_{ex}-like cells were found to be gland-enriched and clonally expanded in glands of patients with SjD, possibly suggesting a salivary-specific autoantigen [32,33]. Our coculture results support this finding and suggest that autoreactive $CD8^+$ T cells may be present in circulation in SjD, and expand when cultured with autologous salivary epithelial cells. Adding upon this foundation, our results explain a unique effector function of these cells by demonstrating the potential for autoreactive $GZMK^+$ T_{ex} cells to secrete GZMK on target cells to drive type I IFN immune signalling in the salivary gland epithelia. This may partially explain type I IFN signalling characteristic of SjD, including in duct and acinar cells, and implicate these cells in modulating immune signalling in foci with sustained antigen engagement. In our data, this effect is enhanced in the SSA^+ and high-focus score SjD subjects. However, the real-time direct observation of these events *in situ* has not yet been possible.

Spatial transcriptomics identifies cell interactions and architectural alterations in SjD

Important disease and tissue-specific changes in cellular composition and gene expression state changes can be gleaned from single-cell approaches in autoimmune diseases. Although high resolution at the single-cell level, this comes at the expense of losing important cell interactions in the tissue context, which can only be inferred bioinformatically. To determine cell interactions, spatially encoded RNA-sequencing (spRNAseq) was performed (Supplementary Fig S9a). Within-spot cell proportions were estimated using Cell2Location and expression patterns from scRNAseq (Supplementary Fig S9b). Structural characteristics of the gland, at a resolution of 55 μm, were compared between disease and health and recapitulate the typical architecture of the glands. The differences in within-spot cell proportions reveal important disease-specific changes in cellular interactions, such as increased association between immune cell types within lymphocytic foci, periductal fibrosis, and heightened contact between SMAC types distinct in glands of patients with SjD (Supplementary Fig S9c,d). Scoring co-occurrence for all cell types, and comparing SjD to non-SjD, supported these differences, highlighting a notable increase in within-spot co-occurrence of $CD8^+$ exhausted T cells and $PRR4^+CST3^+$ $WFDC2^-$ SMACs (Fig 8a, and Supplementary Figs S9a-d and S10a). Colocalisations also tracked changes in the architecture of the gland, such as the loss of contacts between fibroblasts and striated ducts and the increased contacts between myoepithelium and intercalated duct cells (Supplementary Fig S10a).

To investigate gene expression differences with disease at a higher resolution than is possible with spRNAseq, cells identified via ISH (Fig 2e-g) were segmented, phenotyped, and clustered based on expression (Supplementary Fig S10b). This clustering distinguished mucous cells from SMACs but was limited in its ability to distinguish immune cell types or identify endothelium. Neighbourhood analysis was performed for each cell type using each other cell type as the anchor. As expected, seromucous cells were found in lower numbers around other cell types (Fig 8b) and fibroblasts and immune cells were found in greater numbers around other cell types as the focus score increased (Fig 8c). Focus score was found to discriminate patients with SjD with a focus score of 3 or greater (moderate-to-severe sialadenitis) from patients with a focus score of 2 or less (mild sialadenitis). Patients were subdivided into those 3 groups, and neighbourhoods were compared. The greatest number of significant changes in colocalisations were found in patients with mild (FS < 3) sialadenitis, and these specific colocalisations were found in a diversity of cell types (Fig 8d,e; Supplementary Fig S9c,d). The number of cells identifiably acinar was much lower in patients with SjD, and the gland in mild SjD was dominated instead by other epithelial species, phenotyped as ducts, myoepithelium, and mucous acinar types (Fig 8f). These changes reflect true changes in composition (e.g., loss of SMACs) and altered expression states of acinar cells taking on more duct-like phenotypes (ie, expression of *WFDC2*). Fibroblasts could be found in and between acinar structures in mild SjD and immune cells, though not as numerous as in severe sialadenitis, were found near a greater diversity of cell types than in patients without SjD.

Similar to the spatial transcriptomic phenotyping data, the spatial proteomics data revealed clusters of cells based on spatial proximity and the non-random co-occurrence of specific cell types. These spatially organised niches reflect higher-order tissue structures, such as normal glandular parenchyma, immune-rich foci, or epithelial-mesenchymal units. Rather than clustering individual cells in isolation, the TACIT Cyto-community method identifies biologically important regions defined by their composite cellular composition and local spatial context (Fig 8g-i). Clusters containing normal acini (Clusters: 3, 7) and ducts (Clusters: 4, 9) were reduced in fold in patients with SjD (Fig 8h,i). Four clusters were increased in prevalence in patients

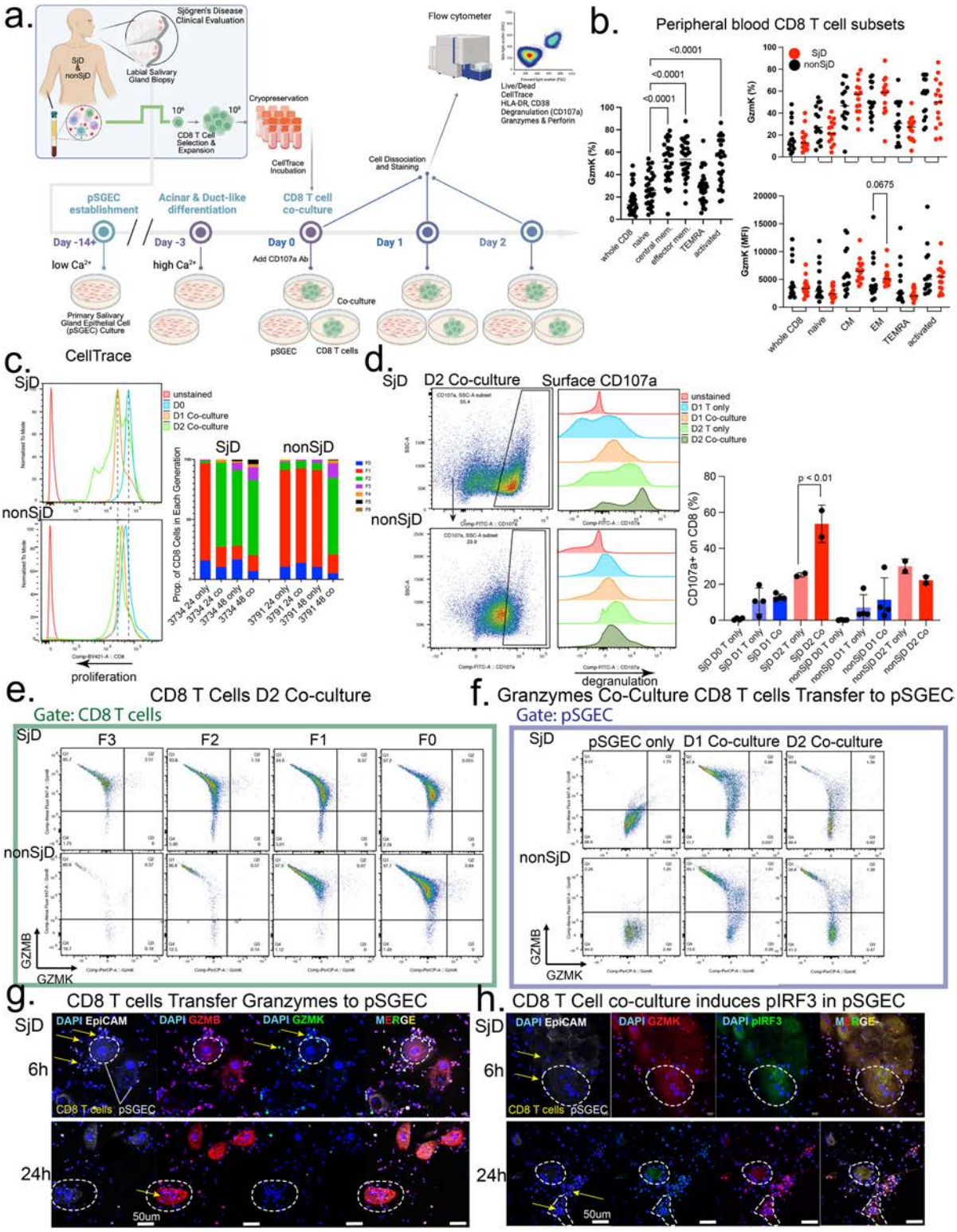

Figure 7. When cocultured with primary epithelium, T cells from patients with SjD deliver granzymes into epithelial cytosol and drive phosphorylation of interferon-stimulated response factors. (a) A cartoon depicting the culture of cells isolated from patients with and without SjD. Primary cells are cultured from labial salivary gland biopsies and differentiate into a quiescent acinar-like epithelium upon culture in a calcium-rich medium. CD8 T cells are selected and expanded from PBMC samples from patients and cocultured with differentiated epithelial cells from the same patient (*autologous coculture*). Cells are cocultured for up to 2 days. (b) CD8 T cells from patients' blood were typed, and GZMK expression compared between diagnostic conditions using flow cytometry. (c) CellTrace dye was used to monitor T cell proliferation and estimate division number in cultures with or without paired epithelium. The parental population (F0) and subsequent generations (F1-F6) were identified based on progressive halving of fluorescence intensity with each cell division. In patients with and without SjD, coculture increased the generation number of T cells in the same time window; however, SjD coculture showed a greater proportion of subsequent population doublings (F4-F6; see also Supplementary Methods figures for gating strategy). (d) CD107a positivity on T cells cultured with and without paired epithelium. T cells from patients with SjD have a higher level of CD107a than patients without SjD and, unlike T cells of patients without SjD, have greater surface CD107a if cocultured with paired epithelium. (e) FACS of GZMB and GZMK in T cells from patients with and without SjD. The proportion of T cells positive for either GZMB or GZMK remains high with a generation time in patients with SjD and a population of GZMK cells emerges in the same patients. (f) FACS of primary epithelium in patients with and without SjD, with and without T cell coculture. In both diagnostic conditions, primary epithelial cells incorporate T-cell-produced granzymes when cocultured

with SjD including clusters enriched by T cells and B cells (Clusters: 1, 5, 16), VECs, acini, and ducts (Clusters: 1, 8) (Fig 8h,i); the latter representing immune-engaged niches. In patients with moderate-to-severe sialadenitis, the gland is dominated by niches enriched with T cells and, separately, B cells (Fig 8h,i). Despite patients with mild disease retaining a gland mainly composed primarily of epithelial cell types, the structure of the gland is compositionally different from non-SjD, with expansion of a ductal/acinar-immune-vascular niches like cluster 1 surrounding a ductal-myoepithelial niche like cluster 4 (Fig 8i). This aligns both with the results in the ISH and with the histology of the glands, where in mild disease the acinar populations seem to be replaced in the branching gland structure with visibly smaller cells producing lower levels of gene products associated with acinar function while supporting tissues such as myoepithelium and fibroblasts are located in between and near niches unusual to those cell types in patients without disease.

DISCUSSION

Building on our prior works [21,34–36], in this study, we have applied data gained from single-cell RNAseq and spatial RNAseq to identify the changes in cell proportion, expression and organisation in the gland that define SjD in a patient cohort with great clinical diversity. We identified unique clusters of cells not previously found in the salivary gland, including 6 unique SMAC types not previously annotated and 5 different T cell types. One key difference that defines disease in both SSA^+ and SSA^- patients with SjD is a loss of $PRR4^+CST3^+WFDC2^-$ SMACs characterised by the highest levels of expression of *MUC7*, which falls from the largest single-cell population in patients without SjD to represent less than half that level in SjD. The proportions of other SMAC populations remain statistically unchanged by disease. This change was visible in ISH data as well, with statistically significant decreases in $PRR4^+$ and, in particular, $CST3^+$ cells.

The other key cell proportion difference in disease is the increase in specific immune populations in disease, most notably a previously unreported $GZMK^+$ population of exhausted T cells with effector functionality. Unsurprisingly for this autoimmune disease, invasive T lymphocytes replaced $PRR4^+CST3^+WFDC2^-$ SMACs nearly one-to-one on average. Why these particular SMACs are lost in disease remains an unanswered question, but open possibilities include acinar cells experiencing stress with a concomitant reduction in replacement alongside recruitment of immune cells, and immune-mediated reprogramming of epithelial function.

In addition to understanding disease as a change in the proportions of cells in the gland, disease can also be understood in terms of cells adopting a different functional program than in health. To this end, a manifold was built on sums-of-Z-scores for indices of annotated gene function. That manifold revealed two distinct paths to T cell dysfunction in SjD: one associated with autoantibody positivity, and one with negativity. Changes characteristic of SSA^+ included increased T cell activation, antigen presentation accompanied by changes in *MHC* expression and an upregulation across the gland of genes inducible by IFN signalling; these changes were absent in SSA^- disease, confirming the distinct biological heterogeneity between autoantibody-positive and autoantibody-negative disease [4]. Autoantibody-positive patients also transcribed higher levels of IFN-stimulated genes in every cell type in the gland. A finding of higher levels of IFN-stimulated genes in the salivary gland corresponds with our previous work showing an association between levels of IFN signalling and downstream gene expression in the PBMCs of patients and the severity of SjD presentation [34].

The clusters identified in single-cell were applied to spatial RNA-sequencing data to quantify the per cent of cell type in each spot, providing unbiased evidence of cell-cell colocalisation changes in disease and health. Looking at cell-cell type correlations within spots in the spRNAseq, negative correlations between unrelated cell types in the individuals without SjD gave way to zero or low positive correlations in SjD, suggesting a higher prevalence of interactions between previously spatially distinct cell types. Neighbourhood analysis on the spatial phenotyping data and cluster analysis on the spatial proteomic data supports these data: although cell-cell colocalisations in more severe disease and with higher focus scores followed the well-understood increases in immune cells and fibroblasts in those glands, the largest number and most diverse set of changes were seen in the glands of patients with the so-called "mild sialadenitis" or low focus score pathology. These patients lost SMACs and gained immune cells similar to patients with 'severe' disease, but retained an intact epithelium with higher proportions of mucous and myoepithelial cells in a branching pattern around a core of cells with expression patterns in between the canonical ductal and acinar expression sets. Cells with high and moderate levels of acinar cell expression can be found on the outside of these niches. The distribution of supporting tissue is also different from a gland of patient without SjD, with myoepithelial cells found near ductal cells and fibroblasts interdigitating with acini. The loss of a specific acinar population accompanying these organisational shifts in the salivary glands may partially explain how a patient can experience reduced salivary function whilst retaining a histologically-preserved epithelium.

Surviving members of the $PRR4^+CST3^+WFDC2^-$ seromucous cluster in SjD exhibit changes in developmental and proliferative indices that may sensitise them to immune dysregulation. This aligns with lymphoepithelial lesion pathology, where salivary ducts and acini paradoxically proliferate in response to infiltrating lymphocytes and the secretion of cytokines like IL-6, TNF-α, and IFN-α; among these, IL-6 is a key driver of epithelial proliferation, linking immune activity to glandular remodelling [37]. This pathology is most commonly associated with parotid glands in SjD and may describe the distinct glandular organisation seen in patients with higher focus scores and the presence of germinal centres.

With such a wide variety of clinical presentations, this patient set enabled us to track glandular disease severity and the cellular changes that accompany it. Patients with SjD had higher levels of surface CD107a, suggesting higher cytotoxic potential of CD8 T cells. Among the T cell populations present in the gland, the population of CD8 T cells positive for granzyme K (GZMK)

with T cells. (g) Immunofluorescent images of granzymes in epithelial-T cell coculture. When cultured together, T cells from patients with SjD form synapses with epithelial cells and transfer granzymes B and K into the cytosol of epithelial cells. (h) Immunofluorescence of a downstream target of GZMK, the phosphorylation of IRF3. The level of GZMK found in epithelial cytosol decreases from 6 to 24 hours and at both time points IRF3 is phosphorylated where GZMK is found. SjD, Sjögren's disease. PBMC, peripheral blood mononuclear cells; GZMK, granzyme K; FACS, flow-assisted cell sorting; FLS, focal lymphocytic sialadenitis.

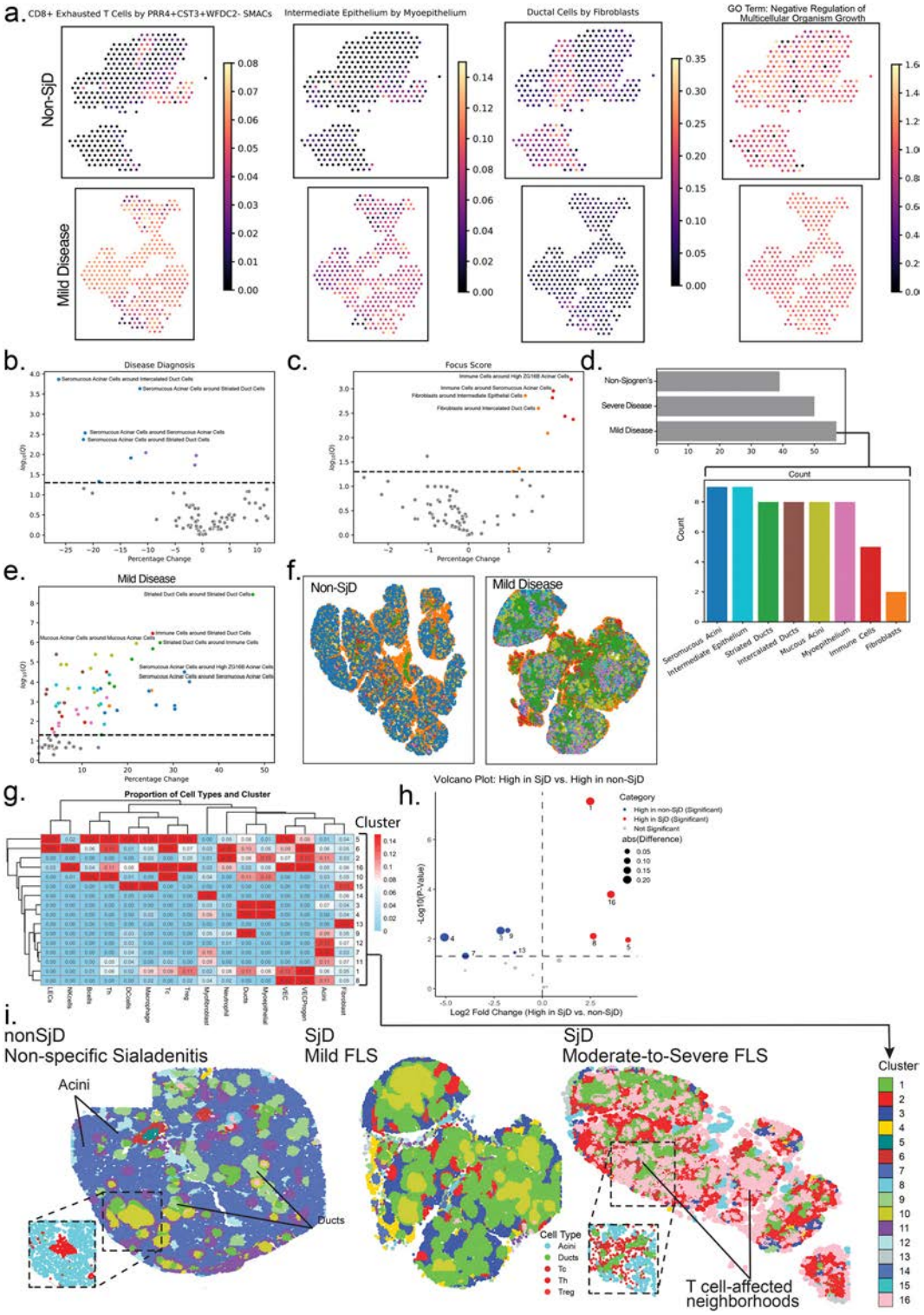

Figure 8. Patients with mild disease retain epithelium, which is extensively restructured. (a) Co-occurrence score spatial plots depict the altered co-occurrences between cell types including loss of co-occurrence of ductal cells with fibroblasts and increased co-occurrence of ductal cells with ductal progenitors, *CD8*$^{+}$ exhausted T cells with *PRR4*$^{+}$*CST3*$^{+}$*WFDC2*$^{-}$ SMACS, and high *ZG16B* SMACS with *PRR4*$^{+}$*CST3*$^{-}$*WFDC2*$^{-}$ SMACS. (b) Anchored neighbourhood analysis of cell localisation changes associated with disease diagnosis. Patients with disease have fewer seromucous acinar cells near other epithelial cell types. (c) Anchored neighbourhood analysis changes with increasing focus score. Patients suffering from immune infiltration have a higher chance of immune cells and fibroblasts localised near epithelial cells. Percentage change is per point of focus score. (d) The greatest number of statistically significant cell-cell colocalisations is found in patients with a low focus score. These colocalisations include new organisations of epithelial cell types, not included in disease diagnosis. (e) The anchored neighbourhood changes in moderate disease. Changes in ductal structure and acinar cell organisation predominate. (f) Quantified ISH images with cells labelled by ISH clustering. The majority species of the glands of patients without SjD are seromucous acini, whereas the glands of patients with moderate disease have very few identifiably seromucous acini and with the remaining duct-like and myoepithelium in an architecture not found in patients without SjD. (g) Proportion of cell types identified via spatial proteomics found in each proteomics cell type cluster. Cell clusters are organised in a phylogeny of cell type similarity. (h) Fold changes of cell type clusters in the proteomics space when patients with and without SjD are compared. Four clusters are significantly increased in SjD (1, 5, 8, and 16), whereas 5 clusters are diminished in SjD (3, 4, 7, 9, and 13). For example, cluster 5, a SjD-enriched cluster, represents a B-, T-, and DC-rich niche. Clusters 7, 9, and 3 represent clusters lost in disease and include high proportions of acinar cells. (i) Voronoi plots of cell type clusters from TACIT Cyto-community analysis of

increased significantly with focus score, and per-cell expression of *GZMK* in the *GZMK*$^+$ population increased as well. Other immune markers of disease, including the proportion of IgG plasma cells and the per-cell level of MHC-II expression in APCs, did not increase with disease severity. To test what effect GZMK might have on disease progression, primary salivary epithelia were derived from patient minor salivary glands and cocultured with T cells taken from patient blood. These circulating T cells may not be identical to the T cells found resident in patient glands, but do produce both GZMB and GZMK and degranulate successfully. Looking back at the gland, both granzymes can be confirmed in the cytosol of patient epithelia. Unlike GZMB, GZMK did not directly cause epithelial cells to apoptose; instead, the mitochondria in affected epithelia disgorged their nucleic acids (DNA and RNA) into the cytosol, leading to nucleic acid sensing and the phosphorylation of IRF3 and the putative activation of the IFN response. An assay for granzyme activity confirmed that GZMK and GZMB (albeit less than GZMK), but not GZMA, lead to higher levels of IRF3 phosphorylation. All three of these changes: an increase in GZMK T cells, mitochondrial DNA found in the cytosol, and IRF3 phosphorylation, were confirmed in the glands of patients with disease. These findings provide a mechanism linking the IFN signalling pathway found so highly expressed in patients with severe disease with the cell proportion changes found in those patients' glands.

Additionally, differential colocalisation scores revealed *GZMK*$^+$CD8$^+$ T cells adjacent to *PRR4*$^+$*CST3*$^+$*WFDC2*$^-$ SMACs in SSA$^+$ but not SSA$^-$ patients, suggesting effector cell targeting of putatively antigen-expressing epithelial cells as a mechanism of autoantibody-positive, higher focus score disease. Spatial phenotyping and *ex vivo* cellular assays further confirm that SjD-enriched *GZMK*$^+$CD8$^+$ T_{ex} cells are enriched in the glands, colocate with ducts and acini, and exhibit cytotoxic potential.

To our knowledge, for the first time, we provide both direct and indirect evidence that GZMK$^+$CD8$^+$ (effector-like T_{ex}) cells exert a potent and specific immune response against salivary epithelial cells that express acinar differentiation markers (e.g., *PRR4, CST3, MUC7,* and *PIGR*), yet are transcriptionally proximate to a duct-like progenitor cell type. This targeted immune activity leads to a selective reduction of terminally differentiated SMACs, whereas mucous acinar and ductal cells remain comparatively spared. Microscopically, this manifests as a shift in histopathology: mucous acinar cells and ducts predominate, and SMACs appear reduced in size and frequency in SjD minor salivary glands (MSGs). These findings are recapitulated in our spatial transcriptomic and ISH data. This cell type-specific immune targeting may underlie the selective vulnerability of serous acinar cells in the parotid and submandibular glands, helping to explain both the reduced saliva production and altered salivary composition commonly observed in patients with SjD. Leveraging multiple new transcriptomic and proteomic datasets, we identify not only the epithelial cell types most susceptible to immune attack in SjD-affected MSG, but also characterise a key effector T cell population, GZMK$^+$CD8$^+$ T cells, which we show to possess a previously unrecognised effector mechanism: disrupting mitochondrial membrane integrity and activating epithelial innate immune signalling (e.g., cGAS-STING pathway). These results provide a mechanistic link between epithelial injury and type I IFN responses in SjD, highlighting new therapeutic avenues to mitigate tissue damage and disease severity. Importantly, they also reveal a sub-cytolytic effector mechanism by which GZMK$^+$CD8$^+$ T cells disrupt mitochondrial integrity in target epithelial cells, impairing metabolic fitness and triggering innate immune activation without inducing apoptosis. This mode of immune attack represents a critical pathogenic axis in SjD and related chronic autoimmune or viral conditions, where tissue dysfunction arises independently of overt cytolysis.

Competing interests

BMW reports a relationship with Pfizer Inc that includes nonfinancial support. BMW reports a relationship with Mitobridge Inc that includes nonfinancial support. SAT reports a relationship with Sanofi that includes board membership and consulting or advisory. SAT reports a relationship with GlaxoSmithKline Inc that includes board membership, consulting or advisory, and employment. SAT reports a relationship with Foresight Labs that includes board membership and consulting or advisory. SAT reports a relationship with QIAGEN GmbH that includes board membership and consulting or advisory. SAT reports a relationship with Xaira Therapeutics that includes board membership and consulting or advisory. SAT reports a relationship with Ensocell that includes equity or stocks. SAT reports a relationship with Transition Bio, Inc. that includes equity or stocks. SAT, KMB, QTE, BFM, and BMW, are all active members of the Human Cell Atlas. NIAMS has CRADAs with AstraZeneca and Bristol Myers Squibb. The other authors declare that they have no known competing financial interests or personal relationships that could have appeared to influence the work reported in this paper.

CRediT authorship contribution statement

Thomas J.F. Pranzatelli: Writing – review & editing, Writing – original draft, Visualization, Validation, Software, Resources, Project administration, Methodology, Formal analysis, Data curation. **Paola Perez:** Writing – review & editing, Writing – original draft, Visualization, Validation, Software, Resources, Methodology, Formal analysis, Data curation. **Anson Ku:** Writing – review & editing, Visualization, Validation, Software, Resources, Methodology, Formal analysis, Data curation. **Bruno Matuck:** Writing – review & editing, Visualization, Validation, Methodology, Formal analysis. **Khoa Huynh:** Writing – review & editing, Visualization, Software, Resources, Methodology, Formal analysis, Data curation. **Shunsuke Sakai:** Writing – review & editing, Resources, Methodology, Formal analysis, Data curation. **Mehdi Abed:** Writing – review & editing, Writing – original draft, Visualization, Resources, Methodology. **Shyh-Ing Jang:** Writing – review & editing, Visualization, Validation, Supervision, Resources, Methodology, Formal analysis. **Eiko Yamada:** Writing – review & editing, Visualization, Validation, Resources, Methodology, Formal analysis, Data curation. **Kalie Dominick:** Writing – review & editing, Visualization,

spatial proteomics data. Clusters enriched for acini are lost in disease, and clusters enriched for ducts and myoepithelial cells are extensive across the gland. Fibroblasts are also found in a different pattern in patients with mild disease compared with health. To illustrate these changes in this example, lines are drawn from cluster numbers to corresponding clusters on the Voronoi plots. SjD, Sjögren's disease; SMACs, seromucous acinar cells; ISH, in situ hybridization.

Resources, Methodology, Data curation. **Zara Ahmed:** Writing – review & editing, Validation, Resources, Methodology, Formal analysis. **Amanda J. Oliver:** Writing – review & editing, Software, Methodology, Formal analysis, Data curation. **Rachael Bogle:** Writing – review & editing, Resources, Methodology, Data curation. **Quinn T. Easter:** Writing – review & editing, Resources, Methodology, Formal analysis. **Alan N. Baer:** Writing – review & editing, Supervision, Resources, Project administration. **Eileen Pelayo:** Writing – review & editing, Resources, Methodology, Data curation. **Zohreh Khavandgar:** Writing – review & editing, Resources, Methodology, Data curation. **David E. Kleiner:** Writing – review & editing, Resources. **M. Teresa Magone:** Writing – review & editing, Supervision, Resources. **Sarthak Gupta:** Writing – review & editing, Supervision, Resources, Methodology, Formal analysis. **Christopher Lessard:** Writing – review & editing, Supervision, Resources, Methodology. **A. Darise Farris:** Writing – review & editing, Supervision, Resources. **Peter D. Burbelo:** Writing – review & editing, Supervision, Resources. **Daniel Martin:** Writing – review & editing, Validation, Software, Resources, Methodology, Formal analysis, Data curation. **Robert J. Morell:** Writing – review & editing, Supervision, Software, Resources, Methodology, Formal analysis, Data curation. **Changyu Zheng:** Writing – review & editing, Supervision, Resources. **Nicholas Rachmaninoff:** Writing – review & editing, Validation, Software, Methodology. **Jose Maldonado-Ortiz:** Writing – review & editing, Resources, Methodology. **Katarzyna M. Tyc:** Writing – review & editing, Visualization, Supervision, Software, Resources, Formal analysis. **Xufeng Qu:** Writing – review & editing, Software, Resources, Formal analysis. **Marit Aure:** Writing – review & editing, Supervision, Resources. **Mohammad H. Dezfulian:** Writing – review & editing, Validation, Supervision, Software, Resources, Data curation. **Ross Lake:** Writing – review & editing, Supervision, Resources. **Sarah A. Teichmann:** Writing – review & editing, Supervision, Software, Resources, Methodology, Formal analysis. **Daniel L. Barber:** Writing – review & editing, Supervision, Resources. **Lam C. Tsoi:** Writing – review & editing, Resources, Data curation. **Adam G. Sowalsky:** Writing – review & editing, Validation, Supervision, Resources, Methodology, Formal analysis. **Jinze Liu:** Writing – review & editing, Visualization, Supervision, Software, Resources, Methodology, Formal analysis, Data curation. **Johann Gudjonsson:** Writing – review & editing, Supervision, Resources, Formal analysis. **Kevin M. Byrd:** Writing – review & editing, Supervision, Resources. **Philip L.F. Johnson:** Writing – review & editing, Writing – original draft, Validation, Supervision, Software, Resources, Project administration, Methodology, Investigation, Formal analysis, Data curation. **John A. Chiorini:** Writing – review & editing, Writing – original draft, Validation, Supervision, Software, Resources, Project administration, Methodology, Investigation, Funding acquisition, Formal analysis, Data curation. **Blake M. Warner:** Writing – review & editing, Writing – original draft, Visualization, Validation, Supervision, Software, Resources, Project administration, Methodology, Investigation, Funding acquisition, Formal analysis, Data curation, Conceptualization.

Acknowledgements

We owe our gratitude to the research participants and patient advocacy groups (Sjögren's Foundation) who provide their support of our clinical studies through their volunteerism. We would also like to thank the support and the staff of the NIDCR Office of the Clinical Director, NIDCR Dental Clinic, the National Eye Institute Ophthalmology Clinic, and the NCI Center for Cancer Research Anatomic Pathology. This work utilised the computational resources of the NIH HPC Biowulf cluster (http://hpc.nih.gov). We would like to thank the following NIH core facilities, which enabled this study: NIDCR/NICHD Computational Biology and Genomics Core, the NIDCR Microscopy Core, the NIDCR Combined Technical Research Core, and the Laboratory of Genitourinary Cancer Pathogenesis (LCGP) Microscopy Core Facility. We would also like to thank the generous support of the NIH/UMD Graduate Partnership Program for TJFP.

Funding

This research was supported by the Intramural Research Program of the National Institutes of Health (NIH). The contributions of the NIH authors were made as part of their official duties as NIH federal employees, are in compliance with agency policy requirements, and are considered Works of the United States Government. However, the findings and conclusions presented in this paper are those of the authors and do not necessarily reflect the views of the NIH or the U.S. Department of Health and Human Services. This publication is part of the Human Cell Atlas – www.humancellatlas.org/publications. This research was principally supported through research awards to BMW from the Division of Intramural Research (DIR) Program of the National Institute of Dental and Craniofacial Research of the National Institutes of Health (NIH/NIDCR ZIA: DE000704) with additional support from (Z01-DE00695, PI-Chiorini). A portion of these studies was supported by the NIH Office of Autoimmune Disease Research in the Office of Research on Women's Health (OADR-ORWH), situated within the NIH Office of the Director (OD), to BMW. Additional support was provided by the DIR Program of the National Institute of Arthritis and Musculoskeletal and Skin Diseases of the NIH (NIH/NIAMS ZIA: AR041199). TFJP is supported through the NIH Graduate Partnership Program. This work also received support from the VCU Massey Comprehensive Cancer Center Bioinformatics Shared Resource, funded, in part, by NIH-NCI Cancer Center Support Grant P30 CA016059.

Patient consent for publication

All patients seen at the author's (B.M.W.) institute (NIH/NIDCR) reported herein provided informed consent before participation in any IRB-approved research protocols (NIH IRB: 15-D-0051, NCT02327884).

Ethics approval

The NIH single institutional review board (IRB) conducts regular ethical reviews for human research studies as required by Department of Health and Human Services regulations for the Protection of Human Subjects.

Provenance and peer review

This manuscript was not commissioned. It was independently submitted to the journal by the authors and underwent external peer reviewer and editorial review.

Data availability statement

10X Single Cell and Visium spatial transcriptomic data have been uploaded to CZ CELLxGENE Discover (https://cellxgene.cziscience.com) and will be available at https://cellxgene.cziscience.com/collections/21bbfaec-6958-46bc-b1cd-1535752f6304. Spatial phenotyping (PhenoCycler-Fusion) and spatial transcriptomic (HiPlex ISH) data are available at Mendeley Data: DOI: 10.17632/b5j9dhgyp4.1 https://data.mendeley.com/preview/b5j9dhgyp4?a=3eb748ca-8f09-4e2b-8b09-2281350a5c94. Code used for the analyses is available at the following websites: https://github.com/pranzatelli/scRNAseqNM2023, https://github.com/huynhkl953/Sjogren_paper, and CellProfiler pipelines are available at https://cellprofiler.org/published-pipelines. All other data are available upon request.

Supplementary materials

Supplementary material associated with this article can be found in the online version at doi:10.1016/j.ard.2025.08.014.

Orcid

Thomas J.F. Pranzatelli: http://orcid.org/0000-0002-5763-1036
Blake M. Warner: http://orcid.org/0000-0002-4961-018X

REFERENCES

[1] Chatzis L, Pezoulas VC, Ferro F, Gandolfo S, Donati V, Binutti M, et al. Sjögren's syndrome: the clinical spectrum of male patients. J Clin Med 2020;9:2620.
[2] Mavragani CP, Moutsopoulos HM. Sjögren syndrome. CMAJ 2014;186:E579–86.
[3] Mavragani CP, Moutsopoulos HM. Sjögren's syndrome: old and new therapeutic targets. J Autoimmun 2020:110.
[4] Hall JC, Baer AN, Shah AA, Criswell LA, Shiboski CH, Rosen A, et al. Molecular subsetting of interferon pathways in Sjögren's syndrome. Arthritis Rheumatol 2015;67:2437–46.
[5] Khatri B, Tessneer KL, Rasmussen A, Aghakhanian F, Reksten TR, Adler A, et al. Genome-wide association study identifies Sjögren's risk loci with functional implications in immune and glandular cells. Nat Commun 2022;13:4287.
[6] Taylor KE, Wong Q, Levine DM, McHugh C, Laurie C, Doheny K, et al. Genome-wide association analysis reveals genetic heterogeneity of Sjögren's syndrome according to ancestry. Arthritis Rheumatol 2017;69:1294–305.
[7] Fugmann C, Wong Q, Levine DM, McHugh C, Laurie C, Doheny K, et al. A high polygenic risk score is associated with SSA/SSB antibody positivity and early onset in primary Sjögren's disease. Rheumatology (Oxford) 2025;64(7):4341–6. doi: 10.1093/rheumatology/keae693.
[8] Chibly AM, Aure MH, Patel VN, Hoffman MP. Salivary gland function, development, and regeneration. Physiol Rev 2022;102:1495–552.
[9] Shiboski CH, Shiboski SC, Seror R, Criswell LA, Labetoulle M, Lietman TM, et al. 2016 American College of Rheumatology/European league against rheumatism classification criteria for primary Sjögren's syndrome: a consensus and data-driven methodology involving three international patient cohorts. Arthritis Rheumatol. 2027;69:35-45.
[10] Verstappen GM, Pringle S, Bootsma H, Kroese FGM. Epithelial–immune cell interplay in primary Sjögren syndrome salivary gland pathogenesis. Nat Rev Rheumatol 2021;17:333–48.
[11] Christodoulou MI, Kapsogeorgou EK, Moutsopoulos HM. Characteristics of the minor salivary gland infiltrates in Sjögren's syndrome. J Autommun 2010;34:400–7.
[12] Gottenberg J-E, Cagnard N, Lucchesi C, Letourneur F, Mistou S, Lazure T, et al. Activation of IFN pathways and plasmacytoid dendritic cell recruitment in target organs of primary Sjögren's syndrome. Proc Natl Acad Sci USA 2006;103:2770–5.
[13] Pipi E, Nayar S, Gardner DH, Colafrancesco S, Smith C, Barone F. Tertiary lymphoid structures: autoimmunity goes local. Front Immunol 2018;9:1952.
[14] Gandolfo S, Ciccia F. JAK/STAT pathway targeting in primary Sjögren syndrome. Rheumatol Immunol Res 2022;3:95–102.
[15] Nezos A, Gravani F, Tassidou A, Kapsogeorgou EK, Voulgarelis M, Koutsilieris M, et al. Type I and II interferon signatures in Sjögren's syndrome pathogenesis: contributions in distinct clinical phenotypes and Sjögren's related lymphomagenesis. J Autoimmun 2015;63:47–58.
[16] Nguyen CQ, Hu MH, Li Y, Stewart C, Peck AB. Salivary gland tissue expression of interleukin-23 and interleukin-17 in Sjögren's syndrome: findings in humans and mice. Arthritis Rheum 2008;58:734–43.
[17] Lee YJ, Scofield RH, Hyon JY, Yun PY, Lee HJ, Lee EY, et al. Salivary chemokine levels in patients with primary Sjögren's syndrome. Rheumatology (Oxford) 2010;49:1747–52.
[18] Hernandez-Molina G, Michel-Peregrina M, Hernandez-Ramirez DF, Sanchez-Guerrero J, Llorente L. Chemokine saliva levels in patients with primary Sjögren's syndrome, associated Sjögren's syndrome, pre-clinical Sjögren's syndrome and systemic autoimmune diseases. Rheumatology (Oxford) 2011;50:1288–92.
[19] McCoy SS, Parker M, Gurevic I, Das R, Pennati A, Galipeau J. Ruxolitinib inhibits IFNγ-stimulated Sjögren's salivary gland MSC HLA-DR expression and chemokine-dependent T cell migration. Rheumatology (Oxford) 2022;61:4207–18.
[20] Barone F, Bombardieri M, Rosado MM, Morgan PR, Challacombe SJ, De Vita S, et al. CXCL13, CCL21, and CXCL12 expression in salivary glands of patients with Sjögren's syndrome and MALT lymphoma: association with reactive and malignant areas of lymphoid organization. J Immunol 2008;180:5130–40.
[21] Dezfulian MH, Kula T, Pranzatelli T, Kamitaki N, Meng Q, Khatri B, et al. TScan-II: a genome-scale platform for the de novo identification of CD4+ T cell epitopes. Cell 2023;186:5569–5586.e21.
[22] Setty M, Tadmor MD, Reich-Zeliger S, Angel O, Salame TM, Kathail P, et al. Wishbone identifies bifurcating developmental trajectories from single-cell data. Nat Biotechnol 2016;34:637–45.
[23] Mattingly A, Finley JK, Knox SM. Salivary gland development and disease. Wiley Interdiscip Rev Dev Biol 2015;4:573–90.
[24] Weng P-L, Aure MH, Maruyama T, Ovitt CE. Limited regeneration of adult salivary glands after severe injury involves cellular plasticity. Cell Rep 2018;24:1464–1470.e3.
[25] Huynh KLA, Tyc KM, Matuck BF, Easter QT, Pratapa A, Kumar NV, et al. Deconvolution of cell types and states in spatial multiomics utilizing TACIT. Nat Commun 2025;16:3747.
[26] Donado CA, Theisen E, Zhang F, Nathan A, Fairfield ML, Rupani KV, et al. Granzyme K activates the entire complement cascade. Nature 2025;641:211–21.
[27] Bouwman AC, Van Daalen KR, Crnko S, Ten Broeke T, Bovenschen N. Intracellular and extracellular roles of Granzyme K. Front Immunol 2021;12:677707.
[28] Riley JS, Tait SW. Mitochondrial DNA in inflammation and immunity. EMBO Rep 2020;21:e49799.
[29] Ohlsson M, Skarstein K, Bolstad AI, Johannessen AC, Jonsson R. Fas-induced apoptosis is a rare event in Sjögren's syndrome. Lab Invest 2001;81:95–105.
[30] Jonsson AH, Zhang F, Dunlap G, Gomez-Rivas E, Watts GFM, Faust HJ, et al. Granzyme K $^{+}$ CD8 T cells form a core population in inflamed human tissue. Sci Transl Med 2022;14:eabo0686.
[31] Shi M, Wang Y, Zhang H, Ling Z, Chen X, Wang C, et al. Single-cell RNA sequencing shows the immune cell landscape in the kidneys of patients with idiopathic membranous nephropathy. Front Immunol 2023;14:1203062.
[32] Xu T, Zhu HX, You X, Ma JF, Li X, Luo PY, et al. Single-cell profiling reveals pathogenic role and differentiation trajectory of granzyme K +CD8+ T cells in primary Sjögren's syndrome. JCI Insight 2023;8:e167490.
[33] Donado CA, Jonsson AH, Theisen E, Zhang F, Nathan A, Rupani KV, et al. Granzyme K drives a newly-intentified pathway of complement activation. 2024; doi:10.1101/2024.05.22.595315
[34] Gupta S, Yamada E, Nakamura H, Perez P, Pranzatelli TJ, Dominick K, et al. Inhibition of JAK-STAT pathway corrects salivary gland inflammation and interferon driven immune activation in Sjögren's disease. Ann Rheum Dis 2024;83:1034–47.
[35] Warner BM, Baer AN, Lipson EJ, Allen C, Hinrichs C, Rajan A, et al. Sicca syndrome associated with immune checkpoint inhibitor therapy. Oncologist 2019;24:1259–69.
[36] Yin H, Pranzatelli TJF, French BN, Zhang N, Warner BM, Chiorini JA, et al. Sclerosing sialadenitis is associated with salivary gland hypofunction and a unique gene expression profile in Sjögren's syndrome. Front Immunol 2021;12:699722.
[37] Pringle S, Verstappen GM, van Ginkel MS, Nakshbandi U, Girigoria Z, Bootsma H, et al. Lymphoepithelial lesions in the salivary glands of primary Sjögren's syndrome patients: the perfect storm? Clin Exp Rheumatol 2022;40(12):2434–42. doi: 10.55563/clinexprheumatol/06an99.

Ann Rheum Dis 85 (2026) 899–910

Contents lists available at ScienceDirect

Annals of the Rheumatic Diseases

journal homepage: https://www.sciencedirect.com/journal/annals-of-the-rheumatic-diseases

Systemic sclerosis

Shared and unique molecular signatures across different autoantibody groups in systemic sclerosis: a multiomics analysis

Wanyi Lin[1,#], Zhangyi Zhao[1,#], Chenhan Jia[1,#], Ruru Guo[1], Fenglin Wu[1], Chaoyu Gu[1], Rui Li[1], Yuankai Sun[1], Zhe Ding[1], Xuesong Liu[2], Aiting Wang[3,4], Xianting Ding[3,4,**], Liangjing Lu[1,*], Hanlin Yin[1,*]

[1] *Department of Rheumatology, Renji Hospital, Shanghai Jiao Tong University School of Medicine, Shanghai, China*
[2] *Department of Ultrasound, Renji Hospital, Shanghai Jiao Tong University School of Medicine, Shanghai, China*
[3] *Department of Anesthesiology and Surgical Intensive Care Unit, Xinhua Hospital, School of Medicine and School of Biomedical Engineering, Shanghai Jiao Tong University, Shanghai, China*
[4] *State Key Laboratory of Oncogenes and Related Genes, Institute for Personalized Medicine, Shanghai Jiao Tong University, Shanghai, China*

ARTICLE INFO

Article history:
Received 8 July 2025
Received in revised form 27 October 2025
Accepted 22 November 2025

ABSTRACT

Objectives: Each autoantibody associated with systemic sclerosis (SSc) is linked to distinct clinical features, suggesting underlying molecular heterogeneity. Although studies have characterised molecular signatures in anticentromere (ACA), antitopoisomerase I (ATA), and anti-RNA polymerase III (ARA) antibodies in patients who are SSc-positive, less frequent autoantibody groups remain unexplored. Our study employed multiomics analysis to identify shared and unique molecular profiles across SSc-associated autoantibody subgroups.

Methods: We enrolled 166 patients with SSc stratified by antibody status (ACA = 55, ATA = 58, ARA = 24, anti-U1 ribonucleoprotein [U1RNP] = 12, anti-U3 ribonucleoprotein [U3RNP] = 8, anti-Ku [Ku] = 4, and anti-Th/To [Th/To] = 5). We performed multiomics profiling, including plasma proteomics, peripheral blood mononuclear cells (PBMCs) transcriptomics, immune cell phenotyping, and plasma metabolomics to identify shared and distinct features across groups.

Results: All SSc subsets demonstrated common pathogenic features, including endothelial injury, extracellular matrix deposition identified by plasma proteomics, upregulated type I interferon (IFN) signalling revealed by transcriptomic analysis, and decreased regulatory B cells observed by immune cell profiling. Meanwhile, each autoantibody subgroup exhibited unique disease mechanisms, such as calcinosis in ACA-positive patients, metabolic oxidative stress in ATA-positive patients, activation of oncogenic signalling in ARA-positive patients, enhanced chromatin remodelling activity in U1RNP-positive patients, muscle involvement in U3RNP/Ku groups, and unique metabolic signalling related to pulmonary hypertension in Th/To-positive cases.

Conclusions: Our study addresses a critical gap by providing a comprehensive multiomics characterisation of both common and rare SSc-associated autoantibody groups, revealing shared and distinct molecular signatures that correlate with clinical features. Our findings highlight the

*Correspondence to: Prof. Liangjing Lu and Dr. Hanlin Yin, Department of Rheumatology, Renji Hospital, Shanghai Jiao Tong University School of Medicine, 145 Middle Shandong Rd, Shanghai 200001, China. **Correspondence to: Prof. Xianting Ding, State Key Laboratory of Oncogenes and Related Genes, Institute for Personalized Medicine, Shanghai Jiao Tong University, 1954 Huashan Road, Shanghai, 200030, China.

E-mail addresses: dingxianting@sjtu.edu.cn (X. Ding), lu_liangjing@163.com (L. Lu), hanlinyin123@163.com (H. Yin).

Handling editor Josef S. Smolen.

# Wanyi Lin, Zhangyi Zhao and Chenhan Jia contributed equally and should be regarded as co-first authors.

https://doi.org/10.1016/j.ard.2025.11.020

potential for autoantibody-based stratification to guide precision management of SSc, paving the way for biomarker-driven approaches in SSc care.

WHAT IS ALREADY KNOWN ON THIS TOPIC

- Systemic sclerosis (SSc) is a clinically heterogeneous disease. Each autoantibody associated with SSc is linked to distinct clinical features.
- Previous studies have established that anticentromere (ACA), antitopoisomerase I (ATA), and anti-RNA polymerase III (ARA) antibody-positive patients exhibit unique molecular signatures.

WHAT THIS STUDY ADDS

- We provide a multiomics characterisation of biological signatures and immune cell dysfunction in SSc patients with less common autoantibodies (anti-Th/To, anti-U3 ribonucleoprotein [U3RNP], anti-U1 ribonucleoprotein [U1RNP], and anti-Ku), expanding understanding of SSc heterogeneity.
- Despite antibody-specific differences, all SSc subsets share core pathogenic pathways, including endothelial injury, dysregulated extracellular matrix deposition, and chronic immune activation.

HOW THIS STUDY MIGHT AFFECT RESEARCH, PRACTICE OR POLICY

- Our findings underscore the clinical relevance of autoantibody-based stratification in SSc, supporting its integration into precision management strategies.

INTRODUCTION

Systemic sclerosis (SSc) is an orphan and complex connective tissue disease characterised by widespread fibrosis of the skin and internal organs, vasculopathy, and dysregulated autoimmunity. Clinically, SSc is notable for its heterogeneity. Patients can present with a wide spectrum of features, including Raynaud's phenomenon, skin involvement, digital ulcers (DUs), telangiectasia, abnormal nailfold capillaries, pulmonary arterial hypertension (PAH), interstitial lung disease (ILD), musculoskeletal inflammation, gastrointestinal complications, and renal crisis [1,2].

The pathogenesis of SSc remains incompletely understood, but an autoimmune basis is well established. Antinuclear antibodies (ANAs) are detected in 90% to 95% of patients with SSc [3]. Autoantibodies in SSc are not only highly prevalent but also highly disease-specific, with profound clinical significance. The most frequent of these include antitopoisomerase I (ATA; also known as anti-Scl-70), anticentromere (ACA), and anti-RNA polymerase III (ARA) antibodies, whereas others, such as anti-Th/To, antifibrillarin (also known as anti-U3 ribonucleoprotein [U3RNP]), anti-U1 ribonucleoprotein (U1RNP), and anti-Ku, are less common. These autoantibodies are generally mutually exclusive and tend to emerge early in the disease course, remaining relatively stable over time [4]. Importantly, the presence of a given SSc-specific autoantibody correlates strongly with particular clinical manifestations and outcomes. For example, ATA antibodies are classically associated with diffuse cutaneous SSc (dcSSc) and confer a high risk of severe ILD, whereas ACA antibodies are predominantly seen in limited cutaneous SSc (lcSSc), often with a milder course and persistent Raynaud's phenomenon, and in late-onset PAH [5]. ARA antibodies identify patients prone to rapid skin thickening, renal crisis, and cancer [6]. Other antibodies define additional subphenotypes. For instance, patients with SSc who test positive for anti-U1RNP antibodies are at higher risk of pulmonary fibrosis and SSc-associated myopathy [7]. Anti-U3RNP antibodies are associated with a higher incidence of skeletal muscle involvement and intrinsic PAH [8]. Anti-Th/To antibody-positive patients typically present with limited cutaneous sclerosis, but they have a higher incidence of pulmonary involvement than other lcSSc patients [9]. Anti-Ku antibodies are associated with an overlap syndrome combined with myositis [10].

The traditional framework for classifying SSc has been based on the pattern of cutaneous involvement. Patients are conventionally divided into lcSSc and dcSSc subsets, depending on whether skin fibrosis is restricted to the distal extremities or extends proximally to the limbs and trunk [11]. However, significant heterogeneity exists within these subsets, and an intermediate patient group exhibiting distinct clinical features has been misclassified [12]. The limitations of skin-based classification have become increasingly apparent, prompting a shift toward immunologically defined stratification. In particular, subclassifying SSc by autoantibody profile offers a more nuanced approach that aligns with the disease's molecular diversity [13]. This has spurred efforts to redefine SSc subsets based on serologic and molecular features rather than focusing solely on clinical phenotypes [14].

In line with this paradigm, recent studies have begun to explore the molecular distinctions among SSc patients across different autoantibody groups. For example, transcriptomic analyses of SSc skin have identified both shared and subset-specific pathways across different autoantibody-defined groups [15]. A recent study utilised multiomics techniques to compare the biological features of patients with ATA- and ACA-positive SSc. Their findings showed that peripheral blood cells from patients who were ATA-positive exhibited transcriptional characteristics related to inflammation and fibrosis, associated with tissue repair. In contrast, patients who were ACA-positive showed transcriptional features related to immune regulation and tissue homeostasis [16]. Single-cell RNA sequencing (RNA-seq) of skin biopsy samples from patients with SSc revealed significant differences in immune clusters between the ATA-positive and ARA-positive subsets of dcSSc [17]. Nevertheless, such molecular studies to date have largely focused on the predominant autoantibody subsets, such as ACA, ATA, and ARA, owing to their higher frequency in patient cohorts. Patients with less common SSc-associated autoantibodies (including anti-Th/To, anti-U3RNP, anti-U1RNP, and anti-Ku) have been underrepresented in prior research, leaving their molecular and cellular disease drivers relatively unexplored. Importantly, these less common autoantibodies characterise unique clinical subtypes, emphasising the need to investigate their disease mechanisms and discover potential treatments.

Here, we address this gap by presenting a multiomics analysis of SSc that encompasses both the common and rare autoantibody-defined subgroups. In this study, we integrated unbiased plasma proteomics, transcriptomic profiling of peripheral blood mononuclear cells (PBMCs), detailed immune cell phenotyping, and plasma metabolomics to compare molecular profiles across multiple SSc autoantibody clusters. By applying this comprehensive approach, we aimed to identify subset-specific molecular signatures underlying the divergent clinical phenotypes of SSc, as well as shared molecular mechanisms.

METHODS

Study design and population

This was a single-centre, cross-sectional observational study conducted at the Department of Rheumatology, Shanghai Jiao Tong University School of Medicine, Affiliated Renji Hospital, Shanghai, China. A total of 166 patients with SSc who met the 2013 American College of Rheumatology and European League Against Rheumatism (ACR/EULAR) classification criteria were included in this study. All samples were collected in the morning under fasting conditions. The exclusion criteria were as follows: (1) patients who had received corticosteroids at doses >10 mg/d, or any immunosuppressive therapy, or intravenous immunoglobulins within 3 months, or rituximab within 6 months prior to inclusion; (2) patients presenting with an ongoing infectious event; (3) patients with severe cardiovascular or metabolic conditions, such as coronary artery disease, obesity (body mass index [BMI] > 30 kg/m^2), uncontrolled diabetes, or hypertension or dyslipidaemia.

Healthy control (HC, n = 48) samples were obtained from individuals undergoing routine health examinations at our hospital, who consented to the use of residual blood samples for research. Individuals with malignancies, severe cardiovascular or metabolic diseases, or active infections were excluded.

Anti-U1RNP antibodies were detected using a line immunoassay (EUROLINE ANA Profile, Euroimmun). ACA antibodies, ATA antibodies, ARA antibodies, U3RNP antibodies, anti-Th/To antibodies, and anti-Ku antibodies were detected using the EUROLINE Systemic sclerosis (Nucleoli) profile (IgG). A result of "+ +" or "+ + +" was considered positive and qualified the patient for inclusion in the study. Patients were classified into 7 groups based on their antibody profiles: ACA, ATA, ARA, U1RNP, U3RNP, Ku, and Th/To. Patients who tested positive for 2 or more of the SSc-related antibodies were excluded from this study, as were those who were ANA-positive but extractable nuclear antigen (ENA)-negative, and those who were entirely antibody-negative.

For each individual, blood samples and demographic and clinical data were collected at the time of their first consultation with the department. Autoantibody profiling was performed using serum samples. Proteomic and metabolomic analyses were conducted on plasma samples. Peripheral blood was collected in EDTA tubes, and PBMCs were isolated via Ficoll (Lymphoprep) density gradient centrifugation. A portion of the PBMCs was used for flow cytometric analysis of immune cell subsets, while the remaining cells were lysed with TRIzol Reagent (Invitrogen) for RNA-seq (Fig 1). Multiomics analyses, including detailed statistical methodologies, are presented in the Supplementary Methods.

RESULTS

Patient characteristics

Our study population comprised 166 patients with SSc, all enrolled in the Renji Scleroderma Longitudinal Cohort (Renji-SLOC). The demographics and clinical characteristics are summarised in the Table. Among these patients, 55 tested positive

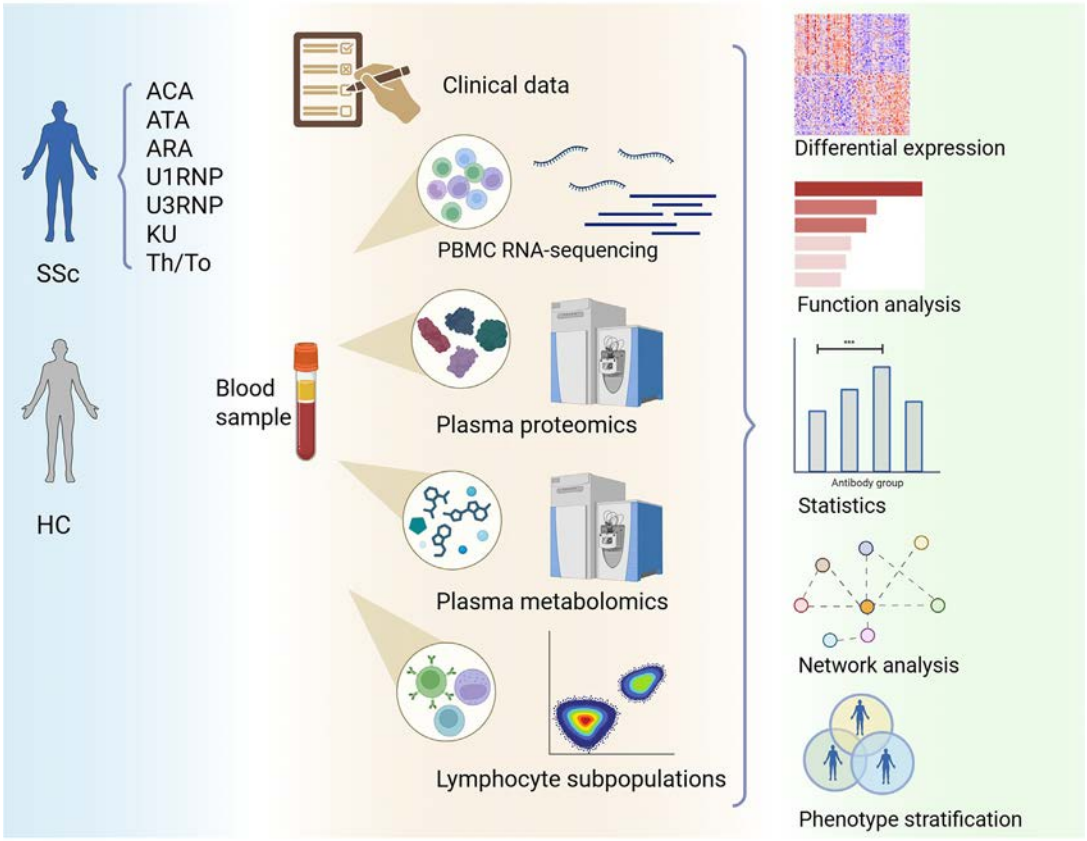

Figure 1. Schematic of the study design. Patients with systemic sclerosis (SSc) were stratified based on their autoantibody profiles. At the time of their initial consultation in the department, blood samples were collected along with demographic and clinical data. Plasma samples were subsequently subjected to proteomic and metabolomic profiling. Peripheral blood mononuclear cells (PBMCs) were isolated from the collected blood; a portion of these cells was analysed by flow cytometry to characterise immune cell subsets, while the remaining cells were processed for RNA sequencing. ACA, anticentromere antibody; ARA, anti-RNA polymerase III antibody; ATA, antitopoisomerase I antibody; KU, anti-Ku antibody; Th/To, anti-Th/To antibody; U1RNP, anti-U1 ribonucleoprotein antibody; U3RNP, anti-U3 ribonucleoprotein antibody.

Table

Demographic and clinical characteristics of systemic sclerosis patients

Variables	Total N = 166	ACA n = 55	ATA n = 58	ARA n = 24	U1RNP n = 12	U3RNP n = 8	Ku n = 4	Th/To n = 5
Age, mean ± SD, y	55.2 ± 13.4	57.7 ± 11.1	51.1 ± 15.3	57.9 ± 13.6	53.8 ± 8.3	53.8 ± 14.3	66.5 ± 16.6	58.8 ± 10.3
Sex, female	81.9	89.1	81.0	83.3	66.6	75.0	25	100
Disease duration, median (IQR), y	1.5 (0.3, 3.6)	2.0 (1.0, 4.5)	1.0 (0.3, 3.0)	1.0 (0.7, 2.9)	2.5 (1.0, 5.0)	1.75 (0.6, 3.0)	2.0 (1.3, 2.0)	3.0 (0.3, 7.0)
Raynaud phenomenon	94.0	94.5	89.7	95.8	100	100	100	100
Digital ulcers	21.7	14.5	31.3	8.3	33.3	12.5	0.0	60.0
dcSSc	34.9	7.3	50.0	50.0	50.0	62.5	0.0	40.0
mRSS, median (IQR)	6.0 (3.0, 14.0)	4.0 (2.0, 6.0)	11.0 (4.0, 19.0)	16.0 (6.5, 23.5)	10.5 (5.0, 15.5)	12.0 (6.0, 15.5)	6.0 (3.0, 11.0)	5.0 (3.0, 10.5)
ILD	62.0	49.1	69.0	62.5	83.3	50.0	100.0	60.0
FVC (%), mean ± SD	81.0 ± 16.4	89.1 ± 10.7	76.1 ± 18.0	79.5 ± 15.8	77.3 ± 11.6	77.7 ± 25.5	75.3 ± 12.0	73.6 ± 21.0
DLCO (%), mean ± SD	75.1 ± 19.6	86.3 ± 11.9	68.0 ± 22.1	75.1 ± 18.3	72.7 ± 13.8	69.9 ± 24.3	68.3 ± 10.9	54.8 ± 17.1
PH	12.0	10.9	8.6	4.2	33.3	25.0	0.0	40.0
Gastro-oesophageal reflux	47.6	45.5	48.3	50.0	33.3	75.0	25.0	60.0
Myopathy	11.4	1.8	13.8	4.2	33.3	37.5	50.0	0.0
Treatment								
Corticosteroids	34.9	25.5	39.7	33.3	41.7	62.5	0.0	60.0
Average dose, median (IQR), mg	0 (0, 5.0)	0 (0, 2.5)	0 (0, 5.0)	0 (0, 4.4)	0 (0, 5.0)	5 (0, 7.5)	0 (0, 0)	5 (0, 10.0)
Vasodilators	14.5	14.5	17.2	4.2	16.7	12.5	0.0	40.0

Categorical variables are expressed as percentages (%). Continuous parameters that follow a normal distribution are expressed as mean ± SD; other parameters are expressed as median (IQR). All patients underwent HRCT and echocardiography at the time of inclusion to evaluate for ILD and PH. Only 15 patients (9.0%) received right heart catheterisation.

ACA, anticentromere antibodies; ARA: anti-RNA polymerase III antibodies; ATA, antitopoisomerase I antibodies; dcSSc, diffuse cutaneous systemic sclerosis; DLCO, diffusing capacity of the lungs for carbon monoxide; FVC, forced vital capacity; HRCT, high-resolution computed tomography; ILD, interstitial lung disease; Ku, anti-Ku antibody; mRSS, modified Rodnan Skin Score; PH, pulmonary hypertension; Th/To, anti-Th/To antibody; U1RNP, anti-U1 ribonucleoprotein antibodies; U3RNP, anti-U3 ribonucleoprotein antibody.

for ACA, 58 for ATA, 24 for ARA, 12 for anti-U1RNP, 8 for anti-U3RNP, 4 for anti-Ku, and 5 for anti-Th/To antibodies.

Of the total cohort, 136 (81.9%) patients with SSc were female, compared with 38 (79.2%) in the HC group (P = .666). The mean age ± SD was 55.2 ± 13.4 years in SSc patients and 53.5 ± 10.8 years in HC (P = .413). The patients with SSc had relatively short disease durations, with a median of 1.5 years (IQR, 0.3-3.6 years). Raynaud's phenomenon was reported in 94% of patients, and 33.7% had a history of DUs. DcSSc was diagnosed in 58 patients (34.9%), with notably lower proportions observed in the ACA and Ku groups than in the other groups.

The overall prevalence of ILD was 62.0%, and pulmonary hypertension (PH) was present in 12.0% of patients. Gastroesophageal reflux affected nearly half of the cohort (47.6%). SSc-associated myopathy was observed in 11.4% of patients, with markedly higher prevalence in the U1RNP, U3RNP, and Ku subgroups.

Plasma proteomics identifies shared and distinct expression profiles of different antibody groups

Plasma proteomics revealed 1159 proteins, of which 846 valid proteins were retrieved after stringent filtering. Differential expression analysis of the proteomics data revealed 86 shared upregulated proteins across the antibody spectrum compared with HC (Fig 2A, Supplementary Fig S1A-F, and Supplementary Table S1). These proteins were functionally enriched in extracellular matrix (ECM) formation, cell adhesion, and growth factor binding (Fig 2B). Contributors to these enrichments included molecules associated with vascular injury (von Willebrand factor [VWF]) and matrix accumulation (spondin 1 [SPON1], tissue inhibitor of metalloproteinase 1 [TIMP1], and collagen type VI α2 chain [COL6A2]).

Notably, "collagen-containing ECM" was also the most enriched pathway among upregulated differentially expressed proteins (DEPs) across all antibody groups (Supplementary Fig S1G-M).

To further examine the molecular characteristics of shared upregulated proteins, protein–protein interactions were analysed using STRING (Fig 2C). Unsupervised Louvain clustering of the interaction graph revealed 2 clusters. Cluster 1 included VWF, vascular cell adhesion protein 1 (VCAM1), intercellular adhesion molecule 1 (ICAM1), TIMP1, insulin-like growth factor 2 receptor (IGF2R), and insulin-like growth factor (IGF)-binding proteins, which are markers of biological processes such as endothelial dysfunction [18,19], cell–cell adhesion [20,21], and regulators of ECM deposition [22,23]. Cluster 2 mainly consisted of ECM components (laminin subunit β1 [LAMB1], laminin subunit α2 [LAMA2], laminin subunit γ1 [LAMC1], COL6A2, versican [VCAN], tenascin C [TNC], chondroitin sulphate proteoglycan 4 [CSPG4], and heparan sulphate proteoglycan 2 [HSPG2]), suggesting general pathogenic mechanisms of SSc despite the presence of different antibodies, and also supported by gene ontology (GO) analysis (Fig 2B).

Shared downregulated proteins included reversion-inducing cysteine-rich protein with Kazal motifs (RECK). It is worth noting that RECK was reported to negatively regulate the matrix-degrading matrix metalloproteinases (MMPs) MMP-1, MMP-2,

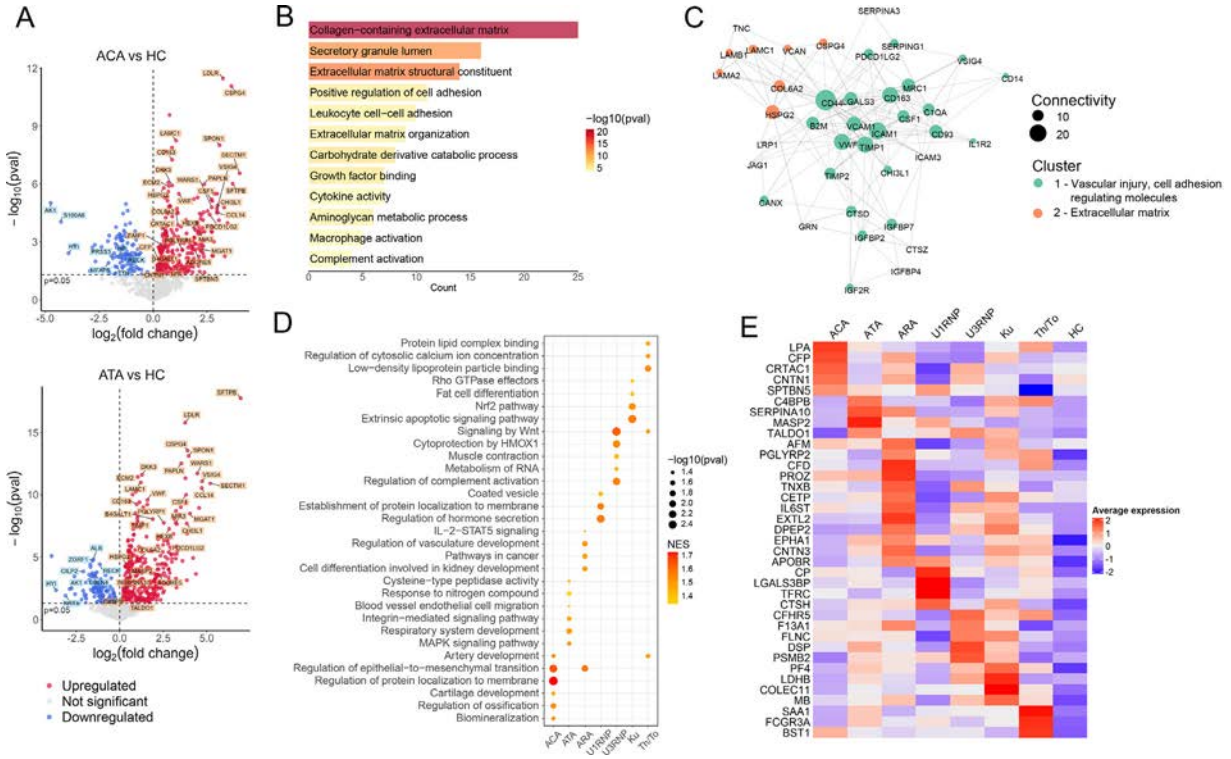

Figure 2. Plasma proteomic profiles of different antibody groups compared with the healthy control (HC) group. A, Volcano plots showing significantly differentially expressed proteins (DEPs) for comparisons of anticentromere (ACA) and antitopoisomerase I (ATA) antibodies vs HC. B, Gene ontology (GO) enrichment analysis of shared upregulated proteins across antibody groups. C, Interaction network of shared upregulated proteins with a connectivity ≥ 4. The size of the circle represents the degree of each node, and the colour represents different Louvain clusters. D, Bubble plot showing uniquely upregulated pathways across the different antibody groups identified using Gene Set Enrichment Analysis (GSEA). Pathways with P < .05 and normalized enrichment score (NES) > 1 are visualised. The size and colour of the dot denote the log-transformed P value and the NES of the corresponding pathways, respectively. E, Heatmap displaying scaled expression of uniquely upregulated proteins across the different antibody groups. ARA, anti-RNA polymerase III antibody; KU, anti-Ku antibody; Th/To, anti-Th/To antibody; U1RNP, anti-U1 ribonucleoprotein antibody; U3RNP, anti-U3 ribonucleoprotein antibody.

and MMP-9 [24,25], suggesting possible regulations of ECM accumulation.

Gene Set Enrichment Analysis (GSEA) of different antibody groups was performed to decipher the distinct features of each antibody group (Fig 2D). Pathways unique to the ACA group included ossification and biomineralisation, consistent with a higher tendency toward calcinosis in this group [26,27]. The presence of kidney- and cancer-associated pathways in ARA group aligned with elevated renal crisis and cancer tendency in this disease subset [4,28,29]. The term "muscle contraction" was enriched in the U3RNP group. Interestingly, filamin-C (FLNC), a protein with established associations with myopathy and cardiomyopathy [30], was found to be the most upregulated in the U3RNP and Ku groups, which are known to have a higher risk of developing myopathies [4,8,31]. The Th/To group was enriched in pathways related to low-density lipoprotein particle binding, protein-lipid complex binding, and regulation of cytosolic calcium ion concentration. The proteins of statistical significance and biological relevance in each subgroup are presented in Figure 2E (Supplementary Table S2). In the ACA group, cartilage acidic protein 1 (CRTAC1), which is associated with cartilage formation, was upregulated. ATA group showed a higher level of transaldolase 1 (TALDO1), an important enzyme involved in NADPH and lipid synthesis. Cholesteryl ester transfer protein (CETP), which mediates cholesterol transfer, was found to be upregulated in the ARA group. Ceruloplasmin (CP) and transferrin receptor (TFRC) were uniquely upregulated in the U1RNP group, which are both associated with iron metabolism. These findings suggest altered biological processes in the disease, consistent with the unique pathways enriched in each group.

RNA-seq of PBMCs identifies shared and distinct transcriptomic profiles among different antibody groups

Differential expression analysis identified 44 shared upregulated differentially expressed genes (DEGs) across the antibody spectrum compared with HC (Fig 3A, Supplementary Fig S2A-F, and Supplementary Table S1). DEGs were functionally enriched in pathways associated with immune response and interferon (IFN) production (Fig 3B and Supplementary Fig S2B). These pathways were also consistently enriched across subgroups (Supplementary Fig S2G-M). Among the shared upregulated genes, several were associated with type I IFN signalling, including *STAT1, GBP1, GBP4, IFIT3, IFITM3, PLSCR1, PARP9, OAS1, OAS2, OASL, TLR7*, and *TLR8*. In interaction network analysis of the shared upregulated genes, STAT1 exhibited the highest number of interactions, underscoring its pivotal role in IFN signalling (Fig 3C). These genes also formed a highly interconnected module for immune activation and chemotaxis.

Distinct signatures of the antibody groups were identified using GSEA and analysis of significantly upregulated genes

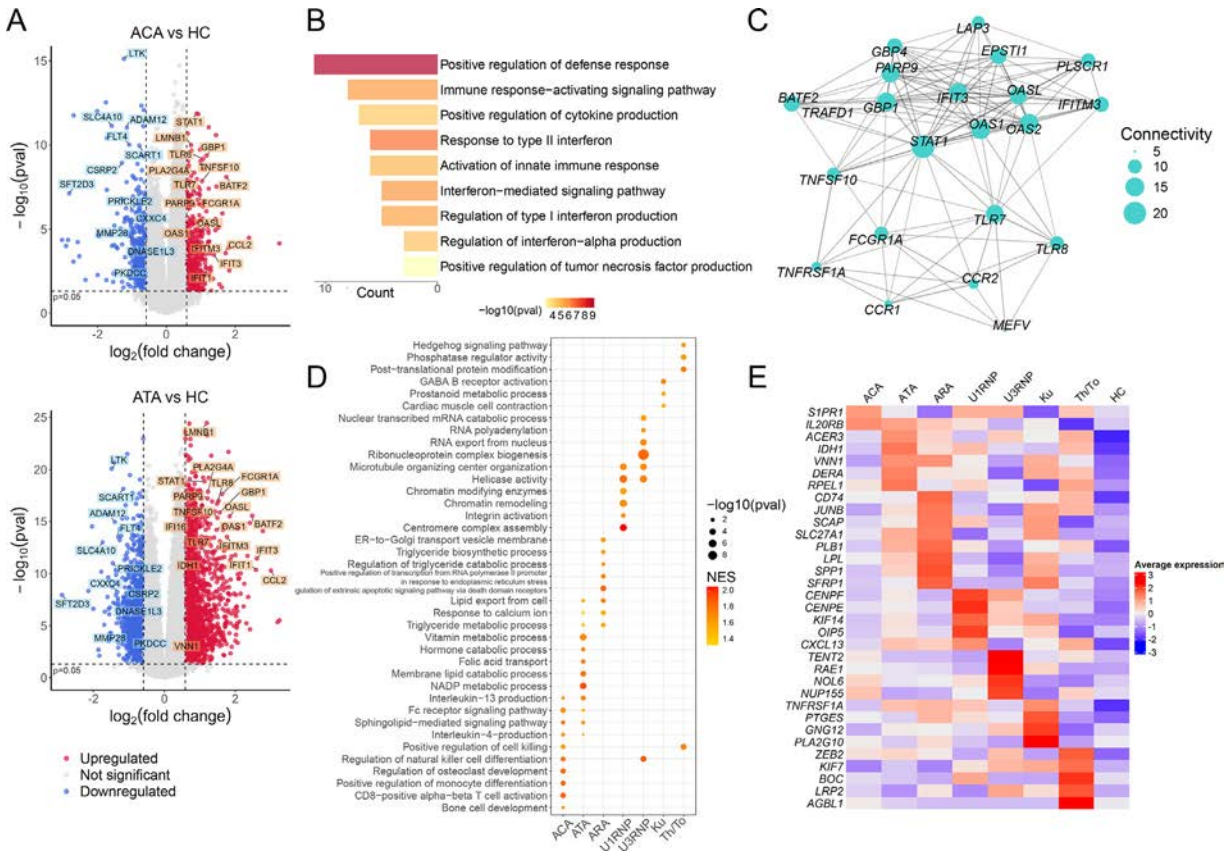

Figure 3. Transcriptomic profiles of different antibody groups compared with the healthy control (HC) group. A, Volcano plots showing significantly differentially expressed genes (DEGs) for comparisons of anticentromere (ACA) and antitopoisomerase I (ATA) antibodies vs HC. B, GO enrichment analysis of shared upregulated genes across antibody groups. C, Interaction network of shared upregulated genes with a connectivity ≥ 4. The size of the circle represents the degree of each node. D, Gene Set Enrichment Analysis (GSEA) identified distinct upregulated pathways across the different antibody groups. Pathways with $P < .05$ and NES > 1 are visualised. The size and colour of the dot denote the log-transformed P value and the NES of the corresponding pathways, respectively. E, Heatmap displaying scaled expression of uniquely upregulated genes across the different antibody groups. ARA, anti-RNA polymerase III antibody; KU, anti-Ku antibody; Th/To, anti-Th/To antibody; U1RNP, anti-U1 ribonucleoprotein antibody; U3RNP, anti-U3 ribonucleoprotein antibody.

(Fig 3D, E, and Supplementary Table S3). In the ACA group, pathways associated with bone cells were uniquely enriched, which was consistent with findings from proteomics analysis. NADP metabolic process was uniquely enriched in ATA group, matching the upregulation of TALDO1 in plasma proteomics. Among uniquely upregulated genes in the ATA group, deoxyribose-phosphate aldolase (*DERA*) encodes a key enzyme involved in pentose phosphate pathway, which generates NADPH and pentoses. ATA and ARA groups were both enriched in lipid metabolic processes, suggesting potential impairment specific to these groups. Lipoprotein lipase (*LPL*) and SREBP cleavage-activating protein (*SCAP*), which are functionally important genes in lipid and cholesterol metabolism, respectively, were significantly upregulated in the ARA group. Another significantly upregulated gene specific to the ARA group, *JUNB*, contributes to dermal fibrosis [32] and has been included in the inflammatory gene module of CD16$^+$ monocytes in SSc [33]. U1RNP group was characterised by processes and genes associated with cell cycle, which were also enriched in GO analysis (Supplementary Fig S2K). U3RNP group was mostly enriched in RNA metabolic processes, including RNA polyadenylation and nuclear export, indicating the presence of active transcription. It has been shown that alternative polyadenylation may be a mechanism of dermal fibrosis in SSc [34]. Ku group showed enrichment in cardiac muscle cell contraction, GABA B receptor activation, and prostanoid metabolic process. Th/To group was enriched in posttranslational protein modification, phosphatase regulator activity, and the hedgehog signalling pathway. Overall, these findings suggest distinct mechanisms of pathogenesis despite harbouring shared features.

Immunophenotyping of different antibody groups

Immune cells play a crucial role in the pathogenesis of SSc and have been associated with specific clinical outcomes. Previous studies have shown that a higher baseline neutrophil count is predictive of lower forced vital capacity percentage (FVC%) and higher modified Rodnan Skin Score (mRSS) [35]. Additionally, the ATA group has been reported to exhibit a higher frequency of neutrophils than the ACA group [16]. In our study, both the ATA and Th/To subgroups showed significantly elevated neutrophil counts and percentages compared with the HC group, whereas no significant differences were observed in the other subgroups (Fig 4A, B, and Supplementary Fig S3A). We also observed increased monocyte counts in nearly all SSc subgroups, with statistically significant elevations in the ATA, ARA, and U3RNP subgroups (Fig 4A, B, and Supplementary Fig S3A).

All SSc patient groups showed lower absolute lymphocyte counts and percentages than HC. Total T lymphocyte counts, along with T helper (Th; CD4$^+$ T cells and Th cells) and Tc cell (CD8$^+$ T cells and T cytotoxic cells) counts, also exhibited downward trends (Fig 4A, C), in line with prior research [16,36]. Notably, the decrease in Th cell numbers reached statistical significance only in the U1RNP and Th/To subgroups, whereas the reduction in Tc cells was particularly prominent in the ACA, ATA, U1RNP, and Th/To groups (Fig 4C). For B-cell analysis, nearly all patient groups exhibited a trend toward an increased proportion of B cells within total lymphocytes (Fig 4A and Supplementary Fig S3B), reflecting similar patterns described in earlier research [37]. Patients in the ACA, ATA, ARA, and U1RNP subgroups demonstrated significantly

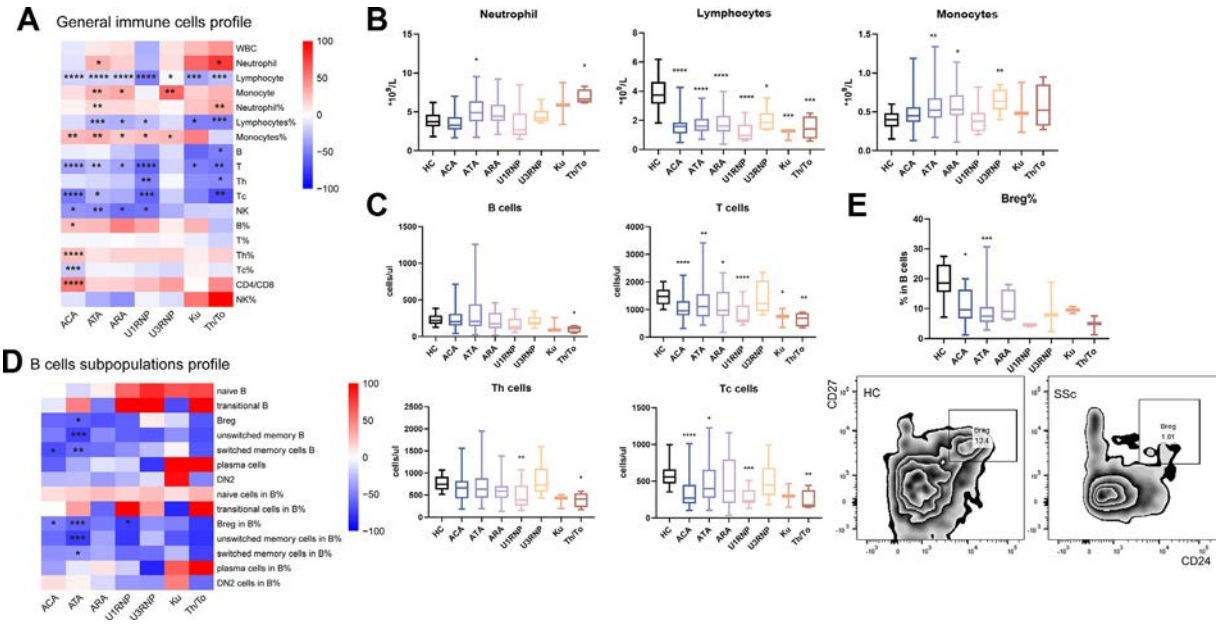

Figure 4. Cytometry profile according to antibody group. A, Heatmap showing differences in the counts and proportions of neutrophils, lymphocytes, monocytes, B cells, T cells, T helper (Th) cells, Tc cells, and natural killer (NK) cells across the autoantibody-defined subgroups compared with the healthy control (HC) group. The proportions of B cells (B%), T cells (T%), and NK cells (NK%) represent their percentages within total lymphocytes, while Th (Th%) and Tc cell (Tc%) proportions are calculated within total T cells. B, Box plots illustrating the absolute counts and statistical differences of neutrophils, lymphocytes, and monocytes across the autoantibody subgroups and the HC group. C, Box plots showing the absolute counts and differences in B cells, T cells, Th cells, and Tc cells across the autoantibody subgroups and the HC group. D, Heatmap depicting changes in B-cell subpopulations across systemic sclerosis (SSc) autoantibody subgroups compared with the HC group. E, Box plots showing the relative proportions of regulatory B cells (Bregs; CD19$^+$CD24^{hi}CD27^{hi} cells) across the autoantibody subgroups and the HC group, along with representative gating plots of the HC and SSc groups. Box plots display the median, IQR, and minimum/maximum values. Statistical significance was determined using the Kruskal-Wallis test followed by Dunn's multiple comparisons to compare each subgroup with the HC group. *P < .05; **P < .01; ***P < .001; ****P < .0001. ACA, anticentromere antibody; ARA, anti-RNA polymerase III antibody; ATA, antitopoisomerase I antibody; KU, anti-Ku antibody; Th/To, anti-Th/To antibody; U1RNP, anti-U1 ribonucleoprotein antibody; U3RNP, anti-U3 ribonucleoprotein antibody; WBC, white blood cell.

decreased natural killer (NK) cell counts in peripheral blood (Fig 4A).

A proportion of enrolled patients underwent advanced immunophenotyping for comprehensive B- and T-cell subset characterisation. B-cell homeostasis is known to be disrupted in SSc, characterised by a reduction in memory B cells and an increase in naïve B cells [38]. In our B-lymphocyte subpopulation analysis, we observed that, compared with HC, all SSc subgroups exhibited a trend toward increased naive B-cell proportions. Both percentages and absolute counts of memory B cells, including unswitched and switched memory B cells, showed decreasing trends, with the ATA subgroup demonstrating statistically significant differences vs HC (Fig 4D and Supplementary Fig S3C). Regulatory B cells (Bregs), a subset of B cells that produce interleukin (IL)-10, play a crucial role in suppressing autoimmune responses. Previous studies have reported both numerical reductions and functional impairments in Bregs in patients with SSc [39]. In our study, Bregs exhibited a downward trend, with significantly reduced proportions in the ACA, ATA, and U1RNP subgroups and notably decreased absolute concentrations, specifically in the ATA subgroup (Fig 4D, E).

As for T-cell subset characterisation, the proportions of naive and memory T cells showed no significant alterations compared with HC. However, the ACA and ATA subgroups exhibited elevated percentages of activated $CD8^+$ T cells ($HLA\text{-}DR^+CD8^+$) (Supplementary Fig S3D), supporting earlier observations in SSc patients [40].

Overall, although all SSc patient subgroups exhibited similar trends in immune cell alterations, such as increased neutrophils and monocytes, decreased lymphocytes and Breg cells, and elevated activated T cells, there were still differences in the extent of these changes among the different autoantibody-defined subgroups.

Metabolic profile of different antibody groups

A total of 2908 metabolites were initially identified. Following data preprocessing and filtering, 2028 metabolites were retained, comprising 1392 in positive ion mode and 636 in negative ion mode. A total of 271 metabolites were significantly upregulated in the ACA group compared with HC, with a variable importance in projection (VIP) > 1, while 255 were identified in the ATA group, 346 in the ARA group, 277 in the U1RNP group, 279 in the U3RNP group, 163 in the Ku group, and 278 in the Th/To group. Each antibody was associated with a distinct upregulated metabolic profile, although there was some overlap between them. Among these upregulated metabolites, 80 were commonly upregulated across all antibody groups (Supplementary Fig S4). The top 30 metabolites, ranked by their VIP scores, are shown in Figure 5A (Supplementary Table S4). Kyoto Encyclopedia of Genes and Genomes (KEGG) enrichment analysis revealed that all these commonly upregulated metabolites were significantly enriched in several pathways, including phenylalanine, tyrosine, and tryptophan biosynthesis; phenylalanine metabolism; taurine and hypotaurine metabolism; and ascorbate and aldarate metabolism (Fig 5B). Notably, taurine and hypotaurine metabolism, which is implicated in oxidative stress and inflammation, was found to be upregulated in both patients with SSc and fibrotic mouse models [41].

To investigate the distinct metabolic profiles of each group, enrichment analyses were performed using upregulated metabolites in each group relative to HC (Fig 5C), with representative metabolites identified in each group (Fig 5D and Supplementary Table S5). ACA-positive patients exhibited elevated adenosine-related metabolites, including N6-phenylisopropyladenosine and inosine, which are linked to enhanced vascular impairment [42]. In contrast, ATA-positive patients showed increased levels of apigenin 7-sulphate, a metabolite associated with antioxidant and antifibrotic pathways, suggesting a compensatory response to their pronounced fibrotic and inflammatory phenotype [43]. Meanwhile, ARA-positive patients demonstrated elevated phosphatidylethanolamine levels, indicative of active membrane remodelling. Notably, U1RNP-positive patients displayed higher levels of L-NIL, a selective inducible nitric oxide synthase (iNOS) inhibitor, reflecting immune activation and inflammatory regulation [44]. U3RNP-positive patients underwent broad metabolic remodelling, characterised by altered lipid oxidation (hexadecenoylcarnitine), dysregulated bile acid metabolism (murocholic acid), and disrupted prostaglandin signalling (tetranor-PGFM). In the Ku group, the arginine and proline metabolism pathway was more prominently enriched, with a notable increase in creatine levels associated with this pathway, which has been reported to be elevated in the serum of patients with idiopathic inflammatory myopathies (IIM) in prior metabolomic analyses [45]. In the Th/To group, the tryptophan metabolism pathway was enriched. The accumulation of 5-hydroxytryptophan suggests enhanced activity of tryptophan hydroxylase, an enzyme known to contribute to pulmonary artery smooth muscle cell hyperplasia in idiopathic PH [46].

These findings indicate that although common metabolic traits exist among all patients with SSc, specific metabolic profiles closely linked to the clinical features of different antibody groups may contribute to the development of organ involvement in SSc.

DISCUSSION

We employed a comprehensive multiomics approach, including plasma proteomics, transcriptomic profiling of PBMCs, immune cell phenotyping, and metabonomic analysis to systematically compare molecular signatures across diverse SSc autoantibody clusters.

Despite the significant clinical heterogeneity of SSc, our multiomics analysis revealed a set of shared mechanistic threads across all 7 autoantibody-defined subgroups. Endothelial injury is widely recognised as an early and critical event in the pathogenesis of SSc. Our proteomics data showed that markers of vascular endothelial injury and activation, such as VWF, VCAM1, and ICAM1, were universally upregulated across all SSc subgroups.

This finding is consistent with the idea that microvascular damage is an initiating event in SSc pathogenesis, leading to overexpression of adhesion molecules and inflammatory recruitment. Parallel to vascular injury is pan-fibrotic ECM dysregulation. Proteomics analysis revealed that all subgroups shared a signalling signature of ECM deposition. Our study supports the 4-protein plasma biomarker panel (COL4A1, COMP, SPON1, and TNC) for skin severity, as validated by Clark et al [47]. We independently confirmed the universal upregulation of TNC and SPON1 across all SSc subgroups, reinforcing their central role in the fibrotic microenvironment. Furthermore, a prominent common feature was the universal activation of type I IFN signalling. We observed that a series of IFN-inducible genes (such as STAT1, GBP1, OAS1, and IFIT3) were significantly upregulated in the PBMCs from all 7 subgroups. This not only reaffirms that SSc possesses an intrinsic IFN-dominated inflammatory microenvironment [48,49] but also suggests that this IFN signature is a

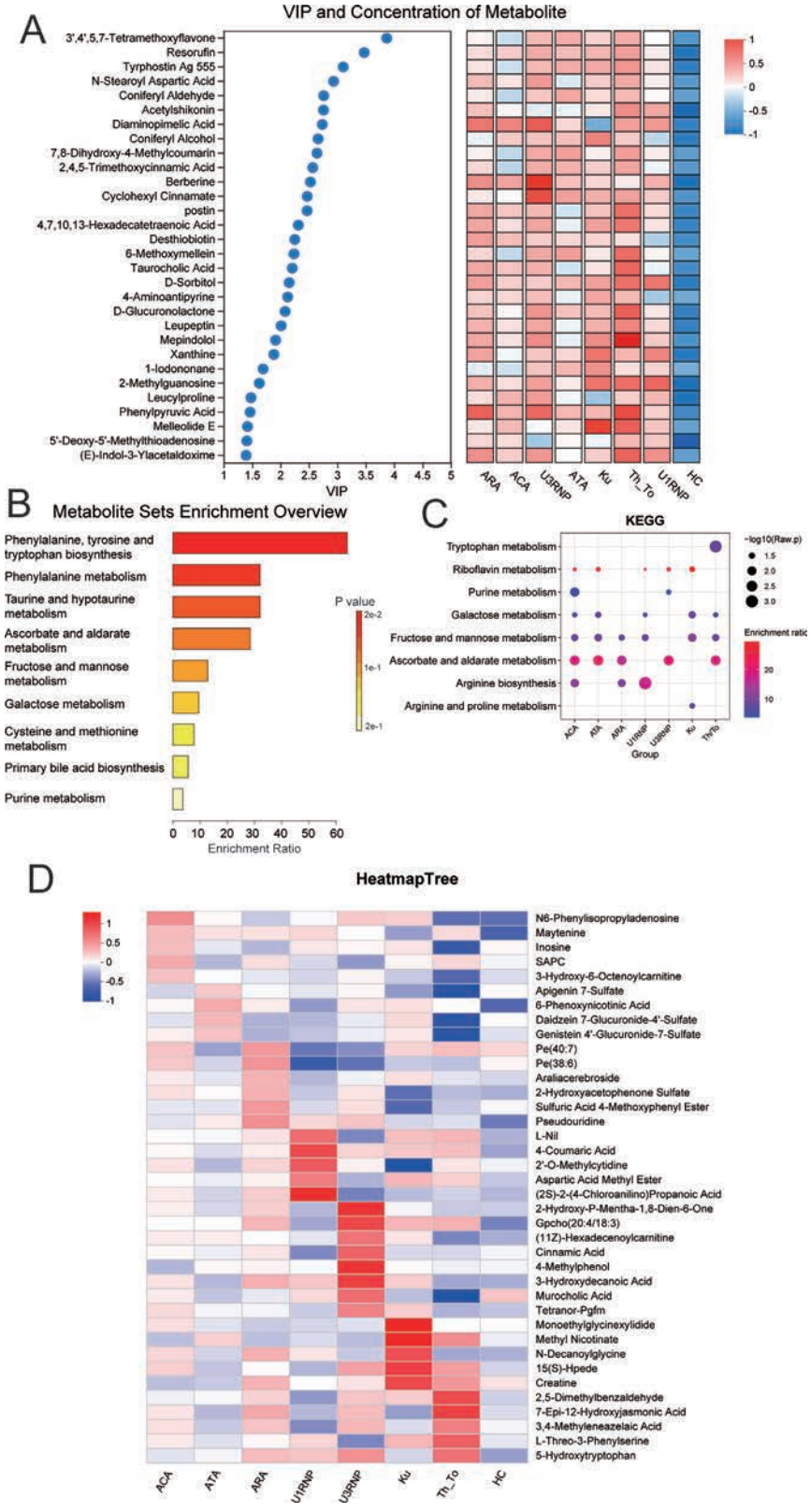

Figure 5. Plasma metabolomic profiles of different antibody groups compared with the healthy control (HC) group. A, Heatmap displaying the top 30 commonly upregulated metabolite ions ($P < .05$) across all antibody groups, ranked by variable importance in projection (VIP) values. B, Overview of metabolite set enrichment analysis of the commonly upregulated metabolites, based on the Kyoto Encyclopedia of Genes and Genomes (KEGG) database and performed using MetaboAnalyst 6.0. C, Bubble plot illustrating the upregulated metabolic pathways in each antibody group, identified through KEGG-based metabolite set enrichment analysis using MetaboAnalyst 6.0. Only pathways with $P < .05$ are shown. Dot size represents the log-transformed P value, and colour indicates the hits-to-expected ratio. D, Heatmap showing scaled concentration levels of uniquely upregulated metabolites specific to each antibody group. ACA, anticentromere antibody; ARA, anti-RNA polymerase III antibody; ATA, antitopoisomerase I antibody; KU, anti-Ku antibody; Th/To, anti-Th/To antibody; U1RNP, anti-U1 ribonucleoprotein antibody; U3RNP, anti-U3 ribonucleoprotein antibody.

fundamental component of SSc immune dysregulation, independent of the specific autoantibody profile.

At the level of immune regulation, we found a relative paucity of Bregs ($CD19^{+}CD24^{hi}CD27^{hi}$ B cells) across all subgroups. This aligns with multiple studies reporting that SSc patients have an imbalance of B-cell subsets, with diminished Breg numbers and function contributing to unchecked inflammation [39]. The loss of B-cell regulation, alongside hyperactive effector B cells, is a unifying immunologic abnormality that can promote autoimmunity and fibrosis in all forms of SSc. It should be noted, however, that in our study, Bregs were defined solely by surface markers, and we did not directly verify their IL-10-producing capacity. This functional aspect requires further investigation. Previous studies have shown that patients with SSc exhibit an increased frequency of Th17 cells and a Th1/Th2 cytokine balance that is significantly shifted toward the Th2 subtype [50]. Further studies are needed to determine whether this

pattern of immune dysregulation is consistent across different autoantibody subsets in patients with SSc.

In summary, regardless of autoantibody status, patients with SSc share a core pathogenetic framework of microvascular injury, profibrotic remodelling, IFN-dominated inflammation, and immune dysregulation. These common pathways likely underlie the convergent fibrotic and immune features observed across this heterogeneous disease.

Building on a shared core pathology, each autoantibody-defined SSc subgroup exhibited unique pathway activation patterns. One clinical hallmark of the ACA subgroup is calcinosis cutis, the deposition of calcium hydroxyapatite in skin and subcutaneous tissues. Interestingly, our multiomics findings of pro-calcification signalling in patients with ACA provide a molecular basis for this phenotype and suggest underlying bone remodelling processes. As for ATA subgroup, a key feature was the enhancement of NADPH-generating pathways and NADPH oxidase components, suggesting increased reactive oxygen species (ROS) production. This aligns with evidence that NADPH oxidases are essential sources of oxidative stress in SSc fibroblasts [51]. The ARA subgroup was known to be associated with a higher prevalence of cancer and renal crisis. In our study, the ARA subgroup revealed unique activation of oncogenic signalling cascades and kidney-related pathways. Both anti-U3RNP and anti-Ku subsets showed unexpected enrichment of pathways related to muscle fibre function, cytoskeletal organisation, and cardiac muscle contractility. Proteomic analysis revealed elevated levels of muscle structural proteins, most notably FLNC, a protein crucial for myofibrillar integrity [30], in the plasma of these patients. Transcriptomic data likewise indicated activation of genes associated with muscle contraction and development. This molecular pattern provides a clear rationale for the well-documented clinical observation that both anti-U3RNP and anti-Ku autoantibodies are associated with inflammatory myopathy and cardiac involvement in SSc overlap syndromes. Previous studies have demonstrated that U1RNP broadly facilitates the tethering and mobilisation of lncRNAs to chromatin in a transcription-dependent manner [52] and plays a role in cell proliferation [53]. Consistent with these findings, our transcriptomic analysis revealed that the U1RNP subgroup exhibited distinct upregulation of chromatin-modifying enzymes and enhanced chromatin remodelling activity. Additionally, we observed significant enrichment in cell-cycle phase transition, further supporting its involvement in proliferation-related processes. In the Th/To subgroup, a unique enrichment of the tryptophan metabolism pathway was observed, marked by an accumulation of 5-hydroxytryptophan, a metabolite implicated in pulmonary artery smooth muscle cell hyperplasia in idiopathic PH [46]. This finding may partially explain the higher prevalence of PH in this patient subset. These outcomes underscore the heterogeneity of immune dysregulation in SSc and suggest that future omics studies should stratify patients by autoantibody status to gain more precise, biologically meaningful insights.

Through comparisons with previous multiomics studies of SSc, we can construct a more complete, multidimensional model of SSc pathogenesis. Rouvière et al [16] summarised the molecular characteristics of patients who are ATA-positive as "proinflammatory and profibrotic features," while defining patients who are ACA-positive as those with "immunomodulation and tissue homeostasis features." Our results provide more specific mechanistic details of this functional classification. For example, we found that the ATA subgroup is centred on oxidative stress and NADPH metabolism, which are key upstream mechanisms driving inflammation and fibrosis, whereas changes in adenosine-related metabolites in the ACA subgroup are directly linked to the regulation of vascular function and tissue homeostasis [54]. At the cellular level, we observed elevated neutrophil counts in the ATA subgroup, which aligns with the dominant neutrophil signature reported by Rouvière et al [16] in patients who are ATA-positive. Metabolically, our data on NADPH pathway activation in ATA patients complement their findings of dysregulated carnitine metabolism and fatty acid oxidation (FAO), together painting a picture of a "hypermetabolic, pro-oxidative" state that fuels sustained inflammation and fibrosis.

By integrating our findings with those of Clark et al [17,55], we can better understand the divergent skin fibrosis trajectories in patients with ATA and ARA. Although our bulk transcriptomics data show shared immune activation pathways, the single-cell data of Clark et al [17] reveal a critical distinction: transforming growth factor (TGF)-β signalling is driven primarily by fibroblasts in patients with ATA but by endothelial cells in patients with ARA. This difference in the cellular driver may explain why fibroblast-autonomous fibrosis (in ATA) is more persistent, whereas endothelial-driven fibrosis (in ARA) may be more reversible. Furthermore, our cross-sectional proteomics data align with the longitudinal findings of Clark et al [55], who showed that serum fibrosis markers (eg, PIIINP) tend to decrease over time in ATA patients but increase in patients with ARA. This suggests that the unique oncogenic signalling we identified in the ARA subgroup may reflect a more proliferative, albeit ultimately more resolvable, fibrotic process.

Our findings refine the understanding of SSc as a pathobiologically diverse yet convergent fibrotic disease. Historically, SSc has been considered a spectrum of syndromes due to its varied autoantibody profiles and organ manifestations [56]. Indeed, our data confirm that each autoantibody subgroup engages unique biological pathways, underscoring the multiple, distinct pathogenic routes that exist within SSc. This heterogeneity likely reflects different inciting antigens or immune triggers that set off specialised cellular responses. However, a crucial insight from our multiomics analysis is that these disparate pathways converge into a final common pathway: microvascular injury, immune activation, and progressive fibrosis of the skin and internal organs. Regardless of the autoantibody, patients with SSc ultimately show uncontrolled fibroblast activation and immune-mediated damage. Thus, SSc can be viewed as a unified fibrotic disorder with diverse immunologic initiators. This convergent evolution of the disease explains why therapies that broadly suppress immunity or fibrosis have general efficacy across SSc subsets, yet the existence of subset-specific pathways could account for the variable responses to certain treatments.

This study has several limitations. First, as a single-centre investigation with a restricted sample size, the statistical power, particularly for rare autoantibody subgroups (eg, Th/To and U3RNP), was inherently limited due to their low prevalence. This inevitably limits the statistical power and robustness of our conclusions. Second, we did not include patients with autoantibody overlap or those who were seronegative (ANA-positive but SSc-associated antibody-negative or fully antibody-negative), which may serve as important anchors for exploring shared pathogenic mechanisms of SSc or represent distinct clinical or molecular subsets. Third, although we excluded individuals with severe cardiovascular and metabolic diseases to reduce potential confounding, dietary habits were not included as a variable in our analysis. Given that nutrition and food intake can substantially influence metabolomic profiles [57], the absence of dietary information may have introduced residual

confounding effects. Fourth, it should be noted that although patients who had received immunosuppressive therapy within 3 months prior to inclusion were excluded, a proportion of patients (34.9%) were treated with low-dose corticosteroids, and vasodilator use (14.6%) was also reported. These treatments may have influenced the transcriptomic, proteomic, cytometric, and metabolic profiles [16,41] and, therefore, could act as potential confounders in the interpretation of our findings. Fifth, apart from including rare autoantibody subgroups, our findings largely confirm previous reports; therefore, the incremental novelty of this study is limited. Finally, although our multiomics approach identified potential biomarkers and pathways, mechanistic validation and larger-scale, multicentre studies are needed to confirm these findings and elucidate their biological relevance in SSc pathogenesis.

To the best of our knowledge, our study is the first to explore the biological signature of rare autoantibody subgroups (Th/To, U3RNP, U1RNP, and Ku) in patients with SSc. By delineating the shared and unique molecular features of each autoantibody cluster, we explored common pathogenic mechanisms in SSc while elucidating the biological heterogeneity underlying this complex disease.

CONCLUSION

In conclusion, by stratifying SSc patients by autoantibody status and applying multiomics analysis, we illuminated how different immunologic triggers converge on a common fibrotic highway. All SSc subsets share a foundation of endothelial injury, immune dysregulation, and fibrosis, yet each autoantibody imparts a distinct twist on the disease's mechanistic theme, from calcinosis in ACA-positive patients to metabolic oxidative stress in ATA-positive patients, cancer-related pathways in ARA-positive patients, nucleic acid sensing and cell cycling in U1RNP-positive subsets, muscle involvement in U3RNP-positive or Ku-positive patients, and unique metabolic signalling in Th/To-positive cases. These findings support the idea that SSc develops through distinct biological pathways in different patients, yet ultimately leads to the same set of problems: immune system dysfunction, vessel damage, and fibrosis. This encourages precision medicine in SSc, treating the patient's specific pathway abnormalities, while also reinforcing therapies that address the final common fibrotic and vascular pathways. Our findings, therefore, not only enhance the understanding of SSc's complex biology but also lay the groundwork for more targeted, pathway-informed interventions that could improve outcomes in this challenging disease.

Acknowledgements

We would like to thank all the patients participating in the study. We thank Dr. Bisheng Shi from the Department of Laboratory Medicine, Renji Hospital, School of Medicine, Shanghai Jiao Tong University, for her assistance.

Contributors

WL: Formal analysis, Writing – original draft; ZZ: Formal analysis, Writing – original draft; CJ: Resources, Data Curation; RG: Resources; FW: Validation; CG: Visualisation; RLi: Validation; YS: Validation; ZD: Validation; ZL: Software; AW: Methodology; XD: Project administration, Supervision; LL: Supervision, Writing – review & editing; HY: Conceptualisation, Writing – review & editing.

Funding

This work was supported by Fundamental Research Funds for the Central Universities (YG2023ZD09), National Natural Science Foundation of China (82502197), Natural Science Foundation of Shanghai (25ZR1402327), Shanghai Municipal Health Commission (202540185), China Postdoctoral Science Foundation (2025M772362), Renji Hospital Clinical Research Incubation Fund (LYPYQN-06), and the Renji program (RJTJ25-QN-132).

Competing interests

The authors declare they have no conflict of interest.

Patient consent for publication

The patients included in this study gave written informed consent.

Ethics approval

Approval of this study was obtained by the Local Ethics Committee of Renji Hospital, Shanghai Jiao Tong University School of Medicine (number 2024-330-C).

Provenance and peer review

Not commissioned; externally peer reviewed.

Data availability statement

Data will be made available on reasonable request from the corresponding author.

Supplementary materials

Supplementary material associated with this article can be found in the online version at doi:10.1016/j.ard.2025.11.020.

Orcid

Wanyi Lin: http://orcid.org/0009-0009-2992-1456
Zhangyi Zhao: http://orcid.org/0009-0001-6185-6174
Chenhan Jia: http://orcid.org/0009-0009-5487-9843
Xianting Ding: http://orcid.org/0000-0002-1549-3499
Liangjing Lu: http://orcid.org/0000-0001-9116-6038
Hanlin Yin: http://orcid.org/0000-0003-0706-3998

REFERENCES

[1] Denton CP, Khanna D. Systemic sclerosis. Lancet 2017;390(10103):1685–99.
[2] Yin H, Li R, Lu L, Yan Q. Understanding fibrosis in systemic sclerosis: novel and emerging treatment approaches. Curr Rheumatol Rep 2020;22(11):77.
[3] Stochmal A, Czuwara J, Trojanowska M, Rudnicka L. Antinuclear antibodies in systemic sclerosis: an update. Clin Rev Allergy Immunol 2020;58(1):40–51.
[4] Cavazzana I, Vojinovic T, Airo' P, Fredi M, Ceribelli A, Pedretti E, et al. Systemic sclerosis-specific antibodies: novel and classical biomarkers. Clin Rev Allergy Immunol 2023;64(3):412–30.
[5] Walker UA, Tyndall A, Czirják L, Denton C, Farge-Bancel D, Kowal-Bielecka O, et al. Clinical risk assessment of organ manifestations in systemic sclerosis: a report from the EULAR Scleroderma Trials and Research group database. Ann Rheum Dis 2007;66(6):754–63.

[6] Lepri G, Catalano M, Bellando-Randone S, Pillozzi S, Giommoni E, Giorgione R, et al. Systemic sclerosis association with malignancy. Clin Rev Allergy Immunol 2022;63(3):398–416.
[7] Chevalier K, Chassagnon G, Leonard-Louis S, Cohen P, Dunogue B, Regent A, et al. Anti-U1RNP antibodies are associated with a distinct clinical phenotype and a worse survival in patients with systemic sclerosis. J Autoimmun 2024;146:103220.
[8] Aggarwal R, Lucas M, Fertig N, Oddis CV, Medsger Jr. TA. Anti-U3 RNP autoantibodies in systemic sclerosis. Arthritis Rheum 2009;60(4):1112–8.
[9] Mitri GM, Lucas M, Fertig N, Steen VD, Medsger Jr. TA. A comparison between anti-Th/To- and anticentromere antibody-positive systemic sclerosis patients with limited cutaneous involvement. Arthritis Rheum 2003;48(1):203–9.
[10] Rozman B, Cucnik S, Sodin-Semrl S, Czirják L, Varjú C, Distler O, et al. Prevalence and clinical associations of anti-Ku antibodies in patients with systemic sclerosis: a European EUSTAR-initiated multi-centre case-control study. Ann Rheum Dis 2008;67(9):1282–6.
[11] LeRoy EC, Black C, Fleischmajer R, Jablonska S, Krieg T, Medsger Jr TA, et al. Scleroderma (systemic sclerosis): classification, subsets and pathogenesis. J Rheumatol 1988;15(2):202–5.
[12] Cottrell TR, Wise RA, Wigley FM, Boin F. The degree of skin involvement identifies distinct lung disease outcomes and survival in systemic sclerosis. Ann Rheum Dis 2014;73(6):1060–6.
[13] Elhai M, Sritharan N, Boubaya M, Balbir-Gurman A, Siegert E, Hachulla E. Stratification in systemic sclerosis according to autoantibody status versus skin involvement: a study of the prospective EUSTAR cohort. Lancet Rheumatol 2022;4(11):e785–94.
[14] Yin H, Lin W, Jia C, Gu C, Zhao Z, Wu F, et al. Dual positivity for Anti-Ro52 and Anti-Ro60 antibodies is linked to greater organ involvement and disease progression in systemic sclerosis. Semin Arthritis Rheum 2025;74:152810.
[15] Inamo J. Association of differentially expressed genes and autoantibody type in patients with systemic sclerosis. Rheumatology (Oxford) 2021;60(2):929–39.
[16] Rouvière B, Le Dantec C, Bettacchioli E, Beretta L, Foulquier N, Cao C, et al. Stratification according to autoantibody status in systemic sclerosis reveals distinct molecular signatures. Ann Rheum Dis 2025;84(3):480–90.
[17] Clark KEN, Xu S, Attah M, Ong VH, Buckley CD, Denton CP. Single-cell analysis reveals key differences between early-stage and late-stage systemic sclerosis skin across autoantibody subgroups. Ann Rheum Dis 2023;82(12):1568–79.
[18] Vischer UM. von Willebrand factor, endothelial dysfunction, and cardiovascular disease. J Thromb Haemost 2006;4(6):1186–93.
[19] Patnaik E, Lyons M, Tran K, Pattanaik D. Endothelial dysfunction in systemic sclerosis. Int J Mol Sci 2023;24(18):14385.
[20] Springer TA. Traffic signals for lymphocyte recirculation and leukocyte emigration: the multistep paradigm. Cell 1994;76(2):301–14.
[21] Singh V, Kaur R, Kumari P, Pasricha C, Singh R. ICAM-1 and VCAM-1: gatekeepers in various inflammatory and cardiovascular disorders. Clin Chim Acta 2023;548:117487.
[22] Gomis-Rüth FX, Maskos K, Betz M, Bergner A, Huber R, Suzuki K, et al. Mechanism of inhibition of the human matrix metalloproteinase stromelysin-1 by TIMP-1. Nature 1997;389(6646):77–81.
[23] LeRoith D, Holly JMP, Forbes BE. Insulin-like growth factors: ligands, binding proteins, and receptors. Mol Metab 2021;52:101245.
[24] Takahashi C, Sheng Z, Horan TP, Kitayama H, Maki M, Hitomi K, et al. Regulation of matrix metalloproteinase-9 and inhibition of tumor invasion by the membrane-anchored glycoprotein RECK. Proc Natl Acad Sci U S A. 1998;95(22):13221–6.
[25] Oh J, Takahashi R, Kondo S, Mizoguchi A, Adachi E, Sasahara RM, et al. The membrane-anchored MMP inhibitor RECK is a key regulator of extracellular matrix integrity and angiogenesis. Cell 2001;107(6):789–800.
[26] Avanoglu-Guler A, Campochiaro C, De Luca G, Hughes M, Tufan A, Green L, et al. Calcinosis in systemic sclerosis: an update on pathogenesis, related complications, and management: a heavy burden still waiting to be lifted off patients' hands. Semin Arthritis Rheum 2024;66:152431.
[27] Valenzuela A, Pérez G, Chung L, Sánchez F, Iturriaga C, Montalva R, et al. Osteoclastogenesis in patients with systemic sclerosis with and without calcinosis cutis. ACR Open Rheumatol 2025;7(4):e70029.
[28] Cole A, Ong VH, Denton CP. Renal disease and systemic sclerosis: an update on scleroderma renal crisis. Clin Rev Allergy Immunol 2023;64(3):378–91.
[29] Nemes-Tömöri D, Jász DK, Tari D, Bói B, Ágoston-Szabó Á, Szűcs G, et al. Malignancy in systemic sclerosis: a multicenter retrospective study. Biomedicines 2025;13(4):993.
[30] Goli R, Li J, Brandimarto J, Levine LD, Riis V, McAfee Q, et al. Genetic and phenotypic landscape of peripartum cardiomyopathy. Circulation 2021;143(19):1852–62.
[31] Tall F, Dechomet M, Riviere S, Cottin V, Ballot E, Tiev KP, et al. The clinical relevance of antifibrillarin (anti-U3-RNP) autoantibodies in systemic sclerosis. Scand J Immunol 2017;85(1):73–9.
[32] Ponticos M, Papaioannou I, Xu S, Holmes AM, Khan K, Denton CP, et al. Failed degradation of JunB contributes to overproduction of type I collagen and development of dermal fibrosis in patients with systemic sclerosis. Arthritis Rheumatol 2015;67(1):243–53.
[33] Kobayashi S, Nagafuchi Y, Okubo M, Sugimori Y, Shirai H, Hatano H, et al. Integrated bulk and single-cell RNA-sequencing identified disease-relevant monocytes and a gene network module underlying systemic sclerosis. J Autoimmun 2021;116:102547.
[34] Weng T, Huang J, Wagner EJ, Ko J, Wu M, Wareing NE, et al. Downregulation of CFIm25 amplifies dermal fibrosis through alternative polyadenylation. J Exp Med 2020;217(2):e20181384.
[35] Wareing N, Mohan V, Taherian R, Volkmann ER, Lyons MA, Wilhalme H, et al. Blood neutrophil count and neutrophil-to-lymphocyte ratio for prediction of disease progression and mortality in two independent systemic sclerosis cohorts. Arthritis Care Res (Hoboken) 2023;75(3):648–56.
[36] Almeida I, Silva SV, Fonseca AR, Silva I, Vasconcelos C, Lima M. T and NK cell phenotypic abnormalities in systemic sclerosis: a cohort study and a comprehensive literature review. Clin Rev Allergy Immunol 2015;49(3):347–69.
[37] Sato S, Fujimoto M, Hasegawa M, Takehara K. Altered blood B lymphocyte homeostasis in systemic sclerosis: expanded naive B cells and diminished but activated memory B cells. Arthritis Rheum 2004;50(6):1918–27.
[38] Forestier A, Guerrier T, Jouvray M, Giovannelli J, Lefèvre G, Sobanski V, et al. Altered B lymphocyte homeostasis and functions in systemic sclerosis. Autoimmun Rev 2018;17(3):244–55.
[39] Mavropoulos A, Simopoulou T, Varna A, Liaskos C, Katsiari CG, Bogdanos DP, et al. Breg cells are numerically decreased and functionally impaired in patients with systemic sclerosis. Arthritis Rheumatol 2016;68(2):494–504.
[40] Gustafsson R, Tötterman TH, Klareskog L, Hällgren R. Increase in activated T cells and reduction in suppressor inducer T cells in systemic sclerosis. Ann Rheum Dis 1990;49(1):40–5.
[41] Guo M, Liu D, Jiang Y, Chen W, Zhao L, Bao D, et al. Serum metabolomic profiling reveals potential biomarkers in systemic sclerosis. Metabolism 2023;144:155587.
[42] Johnston-Cox HA, Koupenova M, Ravid K. A2 adenosine receptors and vascular pathologies. Arterioscler Thromb Vasc Biol 2012;32(4):870–8.
[43] Jiao R, Chen H, Wan Q, Zhang X, Dai J, Li X, et al. Apigenin inhibits fibroblast proliferation and reduces epidural fibrosis by regulating Wnt3a/β-catenin signaling pathway. J Orthop Surg Res 2019;14(1):258.
[44] Song W, Li D, Tao L, Luo Q, Chen L. Solute carrier transporters: the metabolic gatekeepers of immune cells. Acta Pharm Sin B 2020;10(1):61–78.
[45] Guleria A, Kumar U, Kumar D, Naveen R, Anuja AK, Singh MK, et al. NMR-based serum and muscle metabolomics for diagnosis and activity assessment in idiopathic inflammatory myopathies. Anal Sci Adv 2021;2(11-12):515–26.
[46] Eddahibi S, Guignabert C, Barlier-Mur AM, Dewachter L, Fadel E, Dartevelle P, et al. Cross talk between endothelial and smooth muscle cells in pulmonary hypertension: critical role for serotonin-induced smooth muscle hyperplasia. Circulation 2006;113(15):1857–64.
[47] Clark KEN, Csomor E, Campochiaro C, Galwey N, Nevin K, Morse MA, et al. Integrated analysis of dermal blister fluid proteomics and genome-wide skin gene expression in systemic sclerosis: an observational study. Lancet Rheumatol 2022;4(7):e507–16.
[48] Londe AC, Fernandez-Ruiz R, Julio PR, Appenzeller S, Niewold TB. Type I interferons in autoimmunity: implications in clinical phenotypes and treatment response. J Rheumatol 2023;50(9):1103–13.
[49] Yin H, Distler O, Shen L, Xu X, Yuan Y, Li R, et al. Endothelial response to type I interferon contributes to vasculopathy and fibrosis and predicts disease progression of systemic sclerosis. Arthritis Rheumatol 2024;76(1):78–91.
[50] Jin W, Zheng Y, Zhu P. T cell abnormalities in systemic sclerosis. Autoimmun Rev 2022;21(11):103185.
[51] Svegliati S, Spadoni T, Moroncini G, Gabrielli A. NADPH oxidase, oxidative stress and fibrosis in systemic sclerosis. Free Radic Biol Med 2018;125:90–7.
[52] Yin Y, Lu JY, Zhang X, Shao W, Xu Y, Li P, et al. U1 snRNP regulates chromatin retention of noncoding RNAs. Nature 2020;580(7801):147–50.
[53] Li S, Zhang S, Huang M, Hu H, Xie Y. U1RNP/lncRNA/transcription cycle axis promotes tumorigenesis of hepatocellular carcinoma. Diagnostics (Basel) 2022;12(5):1133.
[54] Karmouty-Quintana H, Xia Y, Blackburn MR. Adenosine signaling during acute and chronic disease states. J Mol Med (Berl) 2013;91(2):173–81.
[55] Clark KEN, Campochiaro C, Csomor E, Taylor A, Nevin K, Galwey N, et al. Molecular basis for clinical diversity between autoantibody subsets in diffuse cutaneous systemic sclerosis. Ann Rheum Dis 2021;80(12):1584–93.
[56] Abraham DJ, Black CM, Denton CP, Distler JHW, Domsic R, Feghali-Bostwick C, et al. An international perspective on the future of systemic sclerosis research. Nat Rev Rheumatol 2025;21(3):174–87.
[57] Low DY, Mina TH, Sadhu N, Wong KE, Jain PR, Dalan R, et al. Metabolic variation reflects dietary exposure in a multi-ethnic Asian population. Nat Metab 2025;7(9):1939–54.

Ann Rheum Dis 85 (2026) 911–920

Contents lists available at ScienceDirect

Annals of the Rheumatic Diseases

journal homepage: https://www.sciencedirect.com/journal/annals-of-the-rheumatic-diseases

Vasculitis

A phase 2, randomised, placebo-controlled study of guselkumab in adults with new-onset or relapsing giant cell arteritis

Jean-Paul Makhzoum[1,*], Maria C. Cid[2], Maxime Samson[3], Joerg Henes[4], Verena Schönau[5,6], Georgina Espigol-Frigole[2], Carolyn Ross[1], Mark A. Ahlman[7], Ming-Chun Hsu[8], Shu Li[8], Pauline Verdijk[9], Linda Okonkwo[8], Peter C. Grayson[10], Daniel Blockmans[11,12]

[1] *Division of Internal Medicine, Vasculitis Clinic, Hopital Sacré-Coeur de Montréal, University of Montreal, Montreal, QC, Canada*
[2] *Department of Autoimmune Diseases, Hospital Clinic, University of Barcelona, Institut d'Investigacions Biomèdiques August Pi i Sunyer (IDIBAPS), Barcelona, Spain*
[3] *Department of Internal Medicine and Clinical Immunology, Referral Center for Rare Systemic Autoimmune and Autoinflammatory Diseases, Dijon-Bourgogne University Hospital, University EPE Bourgogne Europe, Dijon, France*
[4] *Department of Internal Medicine II (Hematology, Oncology, Clinical Immunology, and Rheumatology), University Hospital Tuebingen, Tuebingen, Germany*
[5] *Department of Medicine 3, Rheumatology and Immunology, Friedrich-Alexander Universität Erlangen-Nürnberg and Uniklinikum Erlangen, Erlangen, Germany*
[6] *Deutsches Zentrum fur Immuntherapie (DZI) Freidrich-Alexander-Universitat Erlangen-Nurnberg and Uniklinikum Erlangen, Erlangen, Germany*
[7] *Department of Radiology and Imaging, Medical College of Georgia, Augusta, GA, USA*
[8] *Johnson & Johnson, Spring House, PA, USA*
[9] *Johnson & Johnson, Leiden, The Netherlands*
[10] *National Institute of Arthritis and Musculoskeletal and Skin Diseases, NIH, Bethesda, MD, USA*
[11] *Department of General Internal Medicine, University Hospital of Leuven, Leuven, Belgium*
[12] *Department of Microbiology, Immunology, and Transplantation, KU Leuven, Leuven, Belgium*

ARTICLE INFO

Article history:
Received 15 September 2025
Received in revised form 9 January 2026
Accepted 10 January 2026

ABSTRACT

Objectives: Guselkumab, a monoclonal antibody, selectively targets the p19 subunit of interleukin-23. This randomised, double-blind, placebo-controlled, phase 2 study evaluated guselkumab vs placebo for the treatment of giant cell arteritis (GCA).

Methods: Patients ≥50 years of age with new-onset or relapsing GCA were randomised 2:1 to guselkumab or placebo. Both arms received background glucocorticoid (GC) therapy, with a protocol-defined taper through week 26. The primary endpoint was the proportion of patients achieving GC-free remission at week 28.

Results: Thirty-five patients were randomised to receive guselkumab and 18 to receive placebo. All patients were White, 70% were female, and the mean age was 71.5 years; 60% had new-onset and 40% had relapsing GCA. At week 28, 40% (14/35) and 33% (6/18) of patients in the guselkumab and placebo groups, respectively, achieved GC-free remission (P = .64), whereas 31% (11/35) and 39% (7/18) had experienced a GCA flare or discontinued due to worsening GCA. Median time to first GCA flare through week 28 was not estimable (NE) in the guselkumab group

*Correspondence to Dr. Jean-Paul Makhzoum, Vasculitis Clinic, Montreal, QC, Canada.
E-mail address: jean-paul.makhzoum@umontreal.ca (J.-P. Makhzoum).
Handling editor Josef S. Smolen.

https://doi.org/10.1016/j.ard.2026.01.009

(90% CI: 27.7-NE) and 29.7 weeks (90% CI: 20.1-NE) in the placebo group (P = .64). Through week 60, 97% (34/35) and 94% (17/18) of patients in the guselkumab and placebo groups, respectively, had adverse events (AEs); the most common AEs, aside from worsening of GCA (49% and 56%, respectively), were COVID-19 infection (23% and 28%) and headache (17% and 39%).

Conclusions: The study's primary endpoint (GC-free remission) was not met; results do not support the use of guselkumab in the treatment of GCA.

WHAT IS ALREADY KNOWN ON THIS TOPIC

- Giant cell arteritis (GCA) causes vessel wall inflammation resulting in arterial damage and systemic inflammatory response; it is difficult to treat due to its variable presentation, risk of irreversible complication, and frequent relapses.
- Evidence suggests that the interleukin (IL)-23/IL-17 axis contributes to GCA pathogenesis.

WHAT THIS STUDY ADDS

- Guselkumab, a fully human monoclonal antibody that selectively targets the p19 subunit of IL-23, was compared with placebo in a phase 2 clinical study in patients with new-onset or relapsing GCA.
- There was no significant improvement in the primary study endpoint of glucocorticoid-free remission in guselkumab-treated patients at week 28 or other endpoints.

HOW THIS STUDY MIGHT AFFECT RESEARCH, PRACTICE OR POLICY

- Alternative mechanisms to target the pathology of GCA should be investigated.

INTRODUCTION

Giant cell arteritis (GCA), a granulomatous vasculitis involving medium- and large-sized arteries [1], typically affects individuals aged ≥50 years [2,3]. GCA produces vessel wall inflammation that can cause significant arterial damage and elicits a prominent systemic inflammatory response [1,4]. Despite advances in diagnostics and therapy, GCA remains difficult to treat due to its variable presentation, risk of irreversible complication, and frequent relapses [5–7]. Glucocorticoid (GC; prednisone 40-60 mg/d or equivalent, with tapered dosing) treatment is the current standard of care for GCA [8,9]. However, ≈50% of patients relapse with GC treatment alone; long-term GC use has significant risks, including diabetes, hypertension, osteoporosis, cataracts, infection, and psychosis [8,10,11]. Novel efficacious treatments with favourable long-term safety are needed. Tocilizumab, an interleukin (IL)-6 receptor inhibitor, is approved for patients with GCA [12]; however, disease recurs in about one-quarter of treated patients, and tocilizumab impairs the ability to monitor disease activity via C-reactive protein (CRP) or erythrocyte sedimentation rate (ESR) [13–15]. A phase 3 study of sarilumab, another IL-6 receptor inhibitor, was terminated due to slow recruitment, preventing clear conclusions [16]. Ustekinumab, a monoclonal antibody that blocks IL-12 and IL-23, showed potential efficacy in GC-refractory patients with GCA [17]; however, a subsequent prospective, open-label study was unsuccessful [18]. Phase 2 studies of GC with secukinumab (an IL-17A antagonist) or mavrilimumab (a granulocyte-macrophage colony-stimulating factor receptor antagonist) in GCA showed higher rates of remission vs GC with placebo [19,20]. However, a phase 3 trial of secukinumab failed to meet its primary endpoint [21]; another phase 3 trial evaluating secukinumab for GCA is ongoing [22]. A recent phase 3 study reported that upadacitinib, a Janus kinase (JAK) inhibitor, combined with GC demonstrated superior efficacy and reduced GC use compared with placebo plus GC in patients with GCA [23]. Upadacitinib is approved for the treatment of GCA, but includes a black box warning about association with higher risks of cancer and major cardiovascular events based on data from patients with other autoimmune conditions, warranting caution when used to treat GCA [24].

Several lines of evidence suggest that the IL-23/IL-17 axis contributes to GCA pathogenesis. Lesional tissue from affected vessels demonstrates infiltration by IL-23-maintained Th17 cells [25], and circulating levels of IL-17$^+$ T cells are higher in patients with GCA than in controls [26]. Single-nucleotide polymorphisms in IL-17 pathway genes were identified in patients with GCA, and changes in epigenetic markers suggest upregulation of genes that promote T cell activation [27–29]. Serum and biopsies from patients with GCA contain elevated levels of proinflammatory cytokines (eg, IL-17) that are responsive to GC exposure, and IL-23 is highly expressed in GCA tissues, with IL-23p19 expression exceeding that of IL-23p40 [27,30,31]. Finally, IL-23 transgenic mice develop aortic root inflammation [32]. Guselkumab, a fully human monoclonal antibody that selectively targets the p19 subunit of IL-23, is approved to treat adults with moderate-to-severe plaque psoriasis, active psoriatic arthritis, ulcerative colitis, and Crohn's disease [33]. Here, the efficacy of guselkumab vs placebo, in combination with a 26-week GC taper regimen, was evaluated in patients with new-onset or relapsing GCA.

METHODS

Patients

Patients with a confirmed diagnosis of active GCA (within 6 weeks of the first study dose) that was either new-onset or relapsing (diagnosis >6 weeks before first study intervention and, in the interim, achieved remission) were eligible (see detailed inclusion and exclusion criteria in Supplementary Methods). All patients were aged ≥50 years and fulfilled revised American College of Rheumatology criteria for GCA [2]. Patients with a history of severe/uncontrolled complications of GCA; chronic/recurrent infectious disease; another rheumatic disease; arterial thrombosis/venous thromboembolism; malignancy (within 5 years of screening); lymphoproliferative disease; or active tuberculosis were excluded. Patients who had failed treatment with investigational/approved biologic agents, including, but not limited to, IL-23, IL-12/23, or IL-17 inhibitors, tocilizumab, sirukumab, sarilumab, mavrilimumab, abatacept, belimumab, a tumour necrosis factor α-inhibitor or a JAK inhibitor within 90 days or 5 half-lives; received natalizumab or visilizumab within 6 months/5 half-lives; received rituximab or alemtuzumab within 12 months/5 half-lives; received

intramuscular, intra-articular, intrabursal, epidural, intralesional, or intravenous (IV) GCs within 6 weeks; newly started or were not on a stable dose of methotrexate for ≥4 weeks before first study treatment; or used systemic GCs for >4 years or were unable to withdraw from GC treatment through the protocol-defined taper were excluded.

Study design

Patients in this double-blind, multicentre, phase 2 study (THEIA; NCT04633447, EudraCT 2020-000622-26) were randomised 2:1 to receive guselkumab or placebo. Both arms received background GC therapy (20-60 mg/d prednisone or equivalent), with a protocol-defined taper through week 26 (Supplementary Fig S1 and Supplementary Methods). Initially, patients randomised to guselkumab received an induction dose of 400 mg IV at weeks 0, 4, and 8, and then maintenance dosing of 200-mg subcutaneous (SC) injection every 4 weeks from weeks 12 to 48. A change to a fully SC dosing regimen (200-mg SC every 4 weeks from weeks 0 to 48) occurred after 23 participants enrolled because of emergent data from studies of guselkumab in inflammatory bowel disease, suggesting that IV induction would not add incremental response compared with SC-only dosing [34,35].

Randomisation was balanced using permuted blocks and stratified by new-onset vs relapsing GCA and baseline GC dose (≤30 vs >30 mg/d). An interactive web response system assigned unique codes matching randomised patients to the study intervention. Patients who completed the week 52 visit in sustained remission could enrol in the long-term extension, continuing to receive study intervention from weeks 52 to 100, until a GCA flare or study discontinuation, whichever occurred first (GCA flares were recorded as adverse events [AEs] due to worsening GCA). For patients in GCA remission, flare was defined as the recurrence of signs and symptoms of GCA, with or without elevation of inflammatory markers, and the necessity for an increase in GC dose for GCA. Having CRP/ESR elevations in isolation without clinical signs and symptoms attributable to GCA did not qualify as flare unless the investigator increased GC dose.

Blinding

Investigators and patients were blinded to study intervention; containers were labelled with a reference number to maintain the blinding. Unblinding by investigators was possible for safety reasons. Investigators were not blinded to patients' ESR or CRP.

Assessments

Serum CRP and ESR were assessed using a validated CRP assay and the Westergren method, respectively; ESR testing was performed locally. Whole-body fluorodeoxyglucose (FDG) positron emission tomography (PET) (FDG-PET)/computerised tomography (CT) utilised a low-dose radiation protocol. All patients underwent imaging during the screening period, except those who had PET imaging before screening as standard of care (active disease not required); all patients imaged at screening were receiving GC. If FDG-PET/CT scans were obtained 0 to 3 months before randomisation, a protocol-defined PET/CT scan was not required to reduce radiation exposure, and pre-study images were used as baseline scans; the same parameters were used during follow-up. Imaging was repeated at the time of disease flare (preferably within 2 weeks) or at week 52 for those achieving sustained remission. Each image was qualitatively evaluated by 2 central readers blinded to clinical information using the PET Vascular Activity Score (PETVAS), described previously [36]. Semiquantitative analysis was also performed by the central readers, as previously described [37]. Briefly, FDG uptake was quantified in the large arteries, liver, and blood pool by manually drawing regions of interest, with attention to CT anatomic location and coregistered PET activity. Region-specific quantification aligned with territories defined for PETVAS measurement. The maximum standardised uptake value (SUV) averaged across each arterial region was then averaged into a global metric ($SUV_{LARGE\ VESSEL}$) for the aorta and branch arteries of interest. Target-to-background ratios (TBRs) were calculated by dividing the $SUV_{LARGE\ VESSEL}$ by the mean SUV of the mediastinal blood pool and liver (TBR_{BLOOD} and TBR_{LIVER}, respectively).

Endpoints

The primary endpoint was the proportion of patients achieving GC-free remission (no signs/symptoms of GCA and adherence to 26-week taper without GCA flare) at week 28. Secondary endpoints included the proportion of patients achieving GC-free remission from week 28 through week 52, GC-free remission and normalisation of ESR at week 28 and through week 52, GC-free remission and normalisation of CRP at week 28 and through week 52, and GC-free remission and normalisation of both ESR and CRP (ESR + CRP) at week 28 and through week 52. Other secondary endpoints included cumulative GC dose through weeks 28 and 52, the number of GCA disease flares/discontinuations due to an AE of worsening GCA through weeks 28 and 52, and time to these events. FDG-PET/CT imaging was an exploratory endpoint. Safety endpoints included frequency and types of treatment-emergent and serious AEs, coded using the Medical Dictionary for Regulatory Activities version 26.

Statistical analyses

In a phase 3 study of tocilizumab in GCA, GC-free remission rates at week 28 were 74% and 38% for active-treatment and placebo arms, respectively [14]. Assuming similar response rates for placebo and guselkumab, 51 patients randomised 2:1 (guselkumab:placebo) were estimated to provide 82% power to detect a difference between treatment arms at a 2-sided significance level of 0.10. Patients who discontinued study drug due to lack of efficacy or an AE of worsening GCA, or who initiated a prohibited medication that could improve GCA/GC rescue therapy before week 28, were considered nonresponders for primary and binary secondary endpoints. Observed data were used for patients who discontinued study treatment for other reasons before week 28. After accounting for these intercurrent events prior to week 28, patients with missing data at week 28 were considered nonresponders. The primary endpoint was assessed using the Cochran-Mantel-Haenszel chi-square statistic stratified by new-onset vs relapsing GCA and baseline prednisone dose (≤30 vs >30 mg/d); a 2-sided significance level of 0.10 was used, and the difference in response rates between treatment arms, and corresponding 90% CIs, were calculated. We used Type 1 error of 0.1 instead of 0.05 because this was a proof-of-concept study, not a confirmatory study. Subgroup analyses by baseline characteristics, new-onset vs relapsing disease, and GC dose at baseline were performed. For imaging data, change in PETVAS and semiquantitative metrics of arterial FDG uptake

were compared between the baseline and follow-up visits at week 52 or time of GCA flare, using Wilcoxon signed rank tests, stratified by treatment group. Multivariable linear regression was used to compare the change in PETVAS between treatment groups, adjusting for differences in GC use at the time of imaging.

Ethics

THEIA was conducted in accordance with Good Clinical Practice guidelines of the International Council for Harmonisation and the principles of the Declaration of Helsinki. All investigators received approval from an ethics committee, and written informed consent was obtained from all patients.

RESULTS

Patients

From January 11, 2021 to May 22, 2024, THEIA enrolled 53 patients. Thirty-five (66%) were randomised to guselkumab (400 mg IV induction, n = 16 [30%]; 200 mg SC only, n = 19 [36%]) and 18 (34%) to placebo; 13 (37%) and 6 (33%) patients in the guselkumab and placebo groups, respectively, discontinued the study before week 60 (Fig 1). Demographic and baseline disease characteristics were generally balanced across treatment groups (Table 1). All patients were White, 37 (70%) were female, and the mean age was 71.5 years. Most patients had new-onset disease (n = 32 [60%]). GCA diagnosis was confirmed by biopsy in a higher proportion of patients in the guselkumab group than the placebo group (13 [37%] vs 2 [11%], respectively). Three patients were receiving background methotrexate at baseline.

Despite numerically higher remission rates in the guselkumab group vs the placebo group (see the *Efficacy* section), the difference was not statistically significant; the study was discontinued by the sponsor to allow patients to receive alternative treatments. At the time of study discontinuation, 20 of 35 guselkumab-treated (57%) and 12 of 18 placebo-treated patients (67%) had completed week-52 efficacy assessment; therefore, week 52 endpoints were reported. Reasons for discontinuation among guselkumab- and placebo-treated patients, respectively, included AE (8/35 [23%] and 2/18 [11%], most commonly GCA flare in 5/35 [14%] and 2/18 [11%]), study terminated by sponsor (3/35 [9%] and 3/18 [17%]), withdrawal by patient (2/35 [6%] and 0/18 [0%]), and physician decision (0/35 [0%] and 1/18 [6%]).

Table 1
Demographics and baseline characteristics

Characteristic, n (%) or mean (SD)	GUS (N = 35)	PBO (N = 18)	Total (N = 53)
Age, y	71.9 (7.65)	70.8 (7.14)	71.5 (7.43)
Female sex	25 (71)	12 (67)	37 (70)
Race			
White	35 (100)	18 (100)	53 (100)
Ethnicity			
Hispanic or Latino	8 (23)	3 (17)	11 (21)
Not Hispanic or Latino	27 (77)	15 (83)	42 (79)
GCA disease duration, wk	47.44 (85.35)	34.93 (63.80)	43.19 (78.29)
Diagnostic confirmation of GCA by			
Doppler ultrasound	15 (43)	10 (56)	25 (47)
Temporal artery biopsy	13 (37)	2 (11)	15 (28)
Cranial MRI	1 (3)	1 (6)	2 (4)
Other[a]	6 (17)	5 (28)	11 (21)
GCA diagnosis at screening			
New-onset	22 (63)	10 (56)	32 (60)
Relapsing	13 (37)	8 (44)	21 (40)
Acute-phase reactants at baseline			
ESR ≥30 mm/h	11 (31)	3 (17)	14 (26)
CRP ≥10 mg/L	3 (9)	1 (6)	4 (8)
Baseline glucocorticoid use			
≤30 mg/d	18 (51)	10 (56)	28 (53)
>30 mg/d	17 (49)	8 (44)	25 (47)
Baseline methotrexate use	2 (6)	1 (6)	3 (6)
15 mg/wk	1 (3)	1 (6)	2 (4)
20 mg/wk	1 (3)	0	1 (2)
In remission at baseline (no signs or symptoms of GCA)[b]	18 (51)	10 (56)	28 (53)

CRP, C-reactive protein; CT, computed tomography; ESR, erythrocyte sedimentation rate; FDG, fluorodeoxyglucose; GCA, giant cell arteritis; GUS, guselkumab; MRA, magnetic resonance angiography; MRI, magnetic resonance imaging; PBO, placebo; PET, positron emission tomography.

[a] 'Other' methods of confirming GCA diagnosis included FDG-PET/CT, CT scan, and PET-MRI MRA.

[b] Active disease was not required at baseline but was required within 6 weeks of the first study dose.

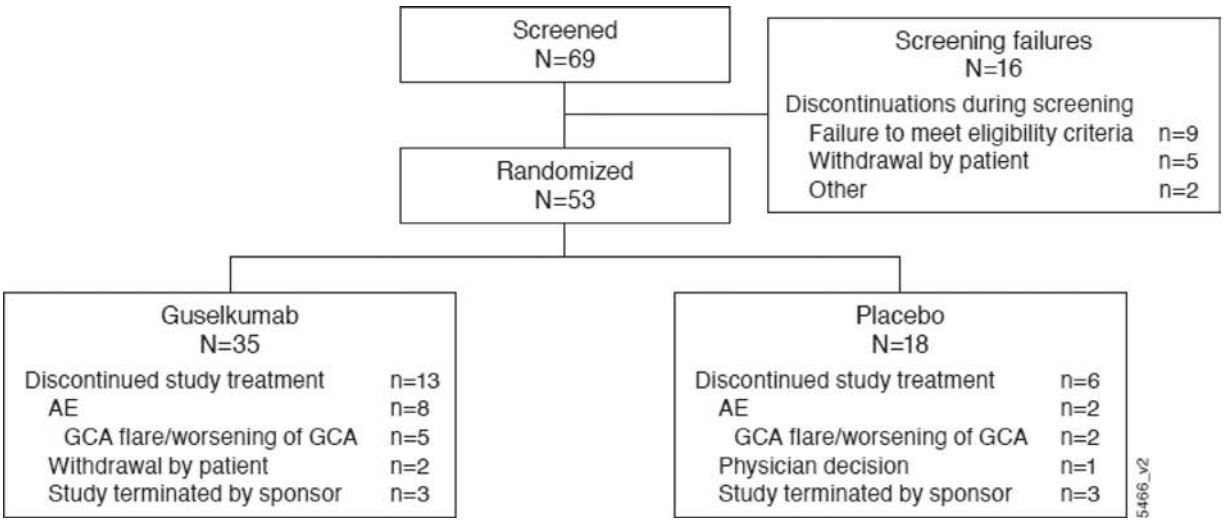

Figure 1. Treatment disposition through up to week 60. AE, adverse event; GCA, giant cell arteritis.

Pharmacokinetics and immunogenicity

Regardless of whether guselkumab was administered by IV or SC through the first 8 weeks, after initiating SC dosing of 200 mg every 4 weeks at week 12, median serum guselkumab concentrations at week 28 were similar across guselkumab-treated patients (Supplementary Fig S2). These findings supported combining data from both guselkumab dosing groups to evaluate efficacy. Overall, the median trough serum guselkumab concentration was 12.04 μg/mL (range: 4.8-22.9) at week 28. Of 34 patients evaluated for antidrug antibodies (ADAs) to guselkumab through week 52, 2 (4%) developed guselkumab ADAs from first guselkumab exposure; neither developed neutralising antibodies to guselkumab.

Efficacy

The study did not meet the primary endpoint: GC-free remission at week 28 was achieved in 14 of 35 [40%] and 6 of 18 [33%] patients in the guselkumab and placebo groups, respectively (treatment difference [90% CI]: 7% [−15%, 28%]; P = .64; Fig 2). Numerically higher proportions of guselkumab- vs placebo-treated patients achieved GC-free remission and normalisation of ESR (8/35 [23%] vs 1/18 [6%]; treatment difference: 17% [3%, 31%]; nominal P = .11), GC-free remission and normalisation of CRP (8/35 [23%] vs 3/18 [17%]; treatment difference: 6% [−12%, 24%]; nominal P = .60), and GC-free remission and normalisation of ESR + CRP (5/35 [14%] vs 1/18 [6%]; treatment difference: 9% [−4%, 22%]; nominal P = .34) at week 28. There were no notable differences in the proportions of patients achieving GC-free remission in post-hoc subgroup analyses (Supplementary Fig S3). By week 52, 9/35 [26%] guselkumab-treated and 5/18 [28%] placebo-treated patients achieved GC-free remission (Fig 2); 8/35 [23%], 6/35 [17%], and 6/35 [17%] guselkumab-treated patients reached GC-free remission and normalisation of ESR, CRP, and ESR + CRP, respectively (vs 3/18 [17%], 4/18 [22%], and 3/18 [17%] of placebo-treated patients, respectively).

Through week 28, 11/35 [31%] and 7/18 [39%] patients in the guselkumab and placebo groups, respectively, had a GCA disease flare/discontinued the study due to worsening GCA (all were considered major relapses, per protocol definition of flare), based on Kaplan-Meier estimates (Fig 3). Through week 52, 13/35 [37%] and 7/18 [39%] patients in the guselkumab and placebo groups, respectively, experienced 1 event (GCA flare/discontinuation due to worsening GCA); 3/35 [9%] and 3/18 [17%] had 2 events. Median time to first GCA disease flare, or discontinuation due to worsening GCA, through week 28 was not estimable (NE) in the guselkumab group (90% CI: 27.7, NE) and 29.7 weeks (90% CI: 20.1, NE) in the placebo group (hazard ratio = 0.79 [0.34, 1.84]; nominal P = .64); corresponding values through week 52 were NE (27.1, NE) and 30.1 (20.1, NE) weeks, respectively.

Median (range) total cumulative GC dose was similar between guselkumab and placebo groups through week 28 (2231.0 [1315-4146] vs 2205.0 [1736-6010] mg, respectively) and numerically lower for the guselkumab group through week 52 (2418.5 [1315-4319] vs 2902.1 [1736-7345] mg; Supplementary Table S1). Among patients with new-onset GCA at baseline, median cumulative GC dose through week 52 was 2418.5 (1315-4319) and 2494.4 (2086-6047) mg in the guselkumab and placebo groups, respectively; corresponding values among patients with relapsing GCA at baseline were 2237.0 (1838-4146) and 3385.0 (1736-7345) mg.

In post-hoc analyses, the proportions of patients achieving GC-free remission at week 28 were comparable between those who initially received guselkumab by IV induction and those who received guselkumab by SC administration only (Supplementary Table S2).

Imaging

Forty-one patients (77%) completed baseline and follow-up FDG-PET/CT imaging: 21 (40%) did not achieve GC-free

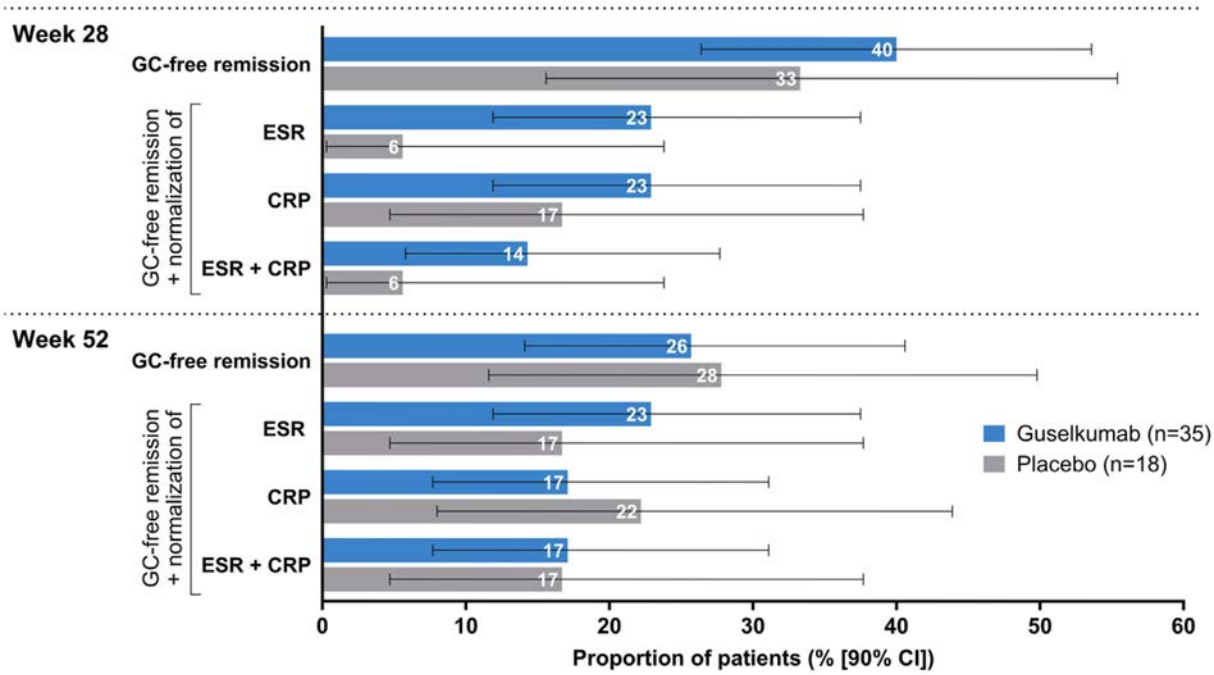

Figure 2. Proportion of patients achieving GC-free remission. CRP, C-reactive protein; ESR, erythrocyte sedimentation rate; GC, glucocorticoid.

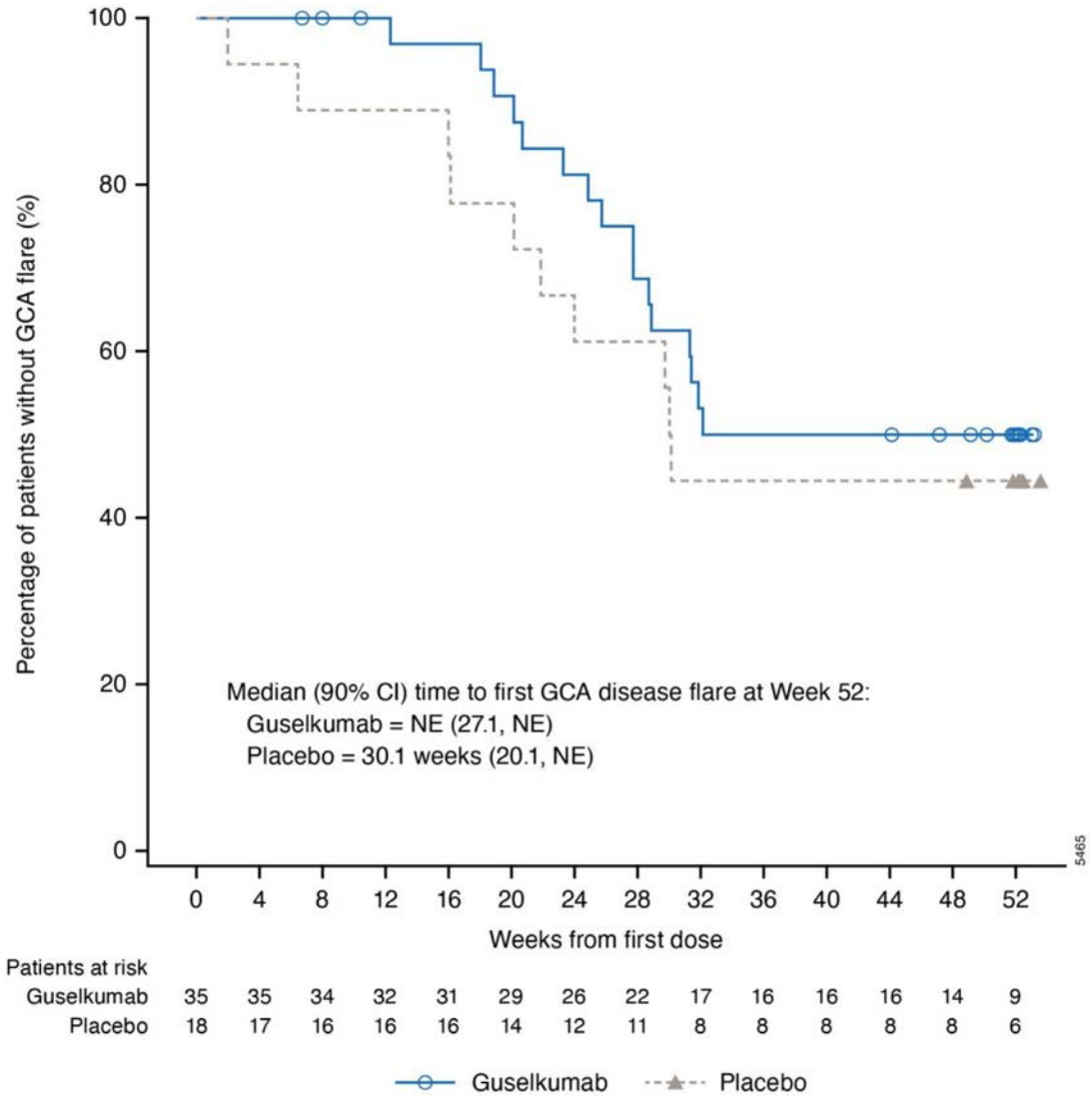

Figure 3. Time to first GCA disease flare. GCA flares were also considered AEs due to worsening of GCA; GCA flares were always considered to precede discontinuation due to an AE of worsening GCA. AE, adverse event; GCA, giant cell arteritis; NE, not estimable.

remission and were imaged at baseline and subsequent flare visit (guselkumab = 13 [37%]; placebo = 8 [44%]), and 20 achieved GC-free remission and were imaged at baseline and week 52 visits (guselkumab = 13 [37%]; placebo = 7 [39%]). No difference in median PETVAS score was observed between baseline and follow-up visits among patients who received guselkumab (17 vs 21; P = .13) or placebo (24 vs 25; P = .18; Fig 4A). After adjusting for differences in GC dose at baseline imaging, there was still no difference in change in median PETVAS score from baseline to follow-up among patients who received guselkumab vs placebo (ß estimate = −0.10, P = .91). Further, there was no difference between median PETVAS scores between groups when comparing baseline to week 52 in patients who achieved sustained GC-free remission (median difference: guselkumab, +1 [P = .40]; placebo, +3.0 [P = .13]) or to disease flare in patients who did not (+2 [P = .30] vs −0.5 [P = .72], respectively; Supplementary Fig S4A).

$SUV_{LARGE\ VESSEL}$ values did not differ significantly between baseline and follow-up visits for guselkumab-treated patients (3.29 vs 3.38; P = .24) but significantly worsened in placebo-treated patients (3.11 vs 3.48; P = .02; Fig 4B), specifically at week 52 rather than at flare visits (Supplementary Fig S4B). No significant differences between baseline and follow-up visits were detected for either group using median TBR_{LIVER} (guselkumab: 1.60 vs 1.43, P = .54; placebo: 1.80 vs 1.70; P = .20). However, there was a significant, albeit modest, reduction in median TBR_{BLOOD} between baseline and follow-up in the guselkumab-treated group, but not the placebo-treated group (guselkumab: 2.67 vs 2.47, P = .04; placebo: 2.93 vs 2.92, P = .45; Supplementary Fig S5). Significantly greater FDG uptake at follow-up imaging was observed in patients treated with guselkumab vs placebo for both blood pool (1.54 vs 1.16; P = .01) and liver (2.28 vs 2.03; P = .01) compartments.

Safety

The mean number of guselkumab or placebo administrations was similar through week 48 (10.5 vs 11.2, respectively). Through week 60, most patients experienced AEs (guselkumab group, 34/35 [97%]; placebo group, 17/18 [94%]). The most common AEs (>20% in either group; Table 2), aside from worsening GCA (17/35 [49%] and 10/18 [56%], respectively), were COVID-19 infection (8/35 [23%] and 5/18 [28%]), and headache (6/35 [17%] and 7/18 [39%]).

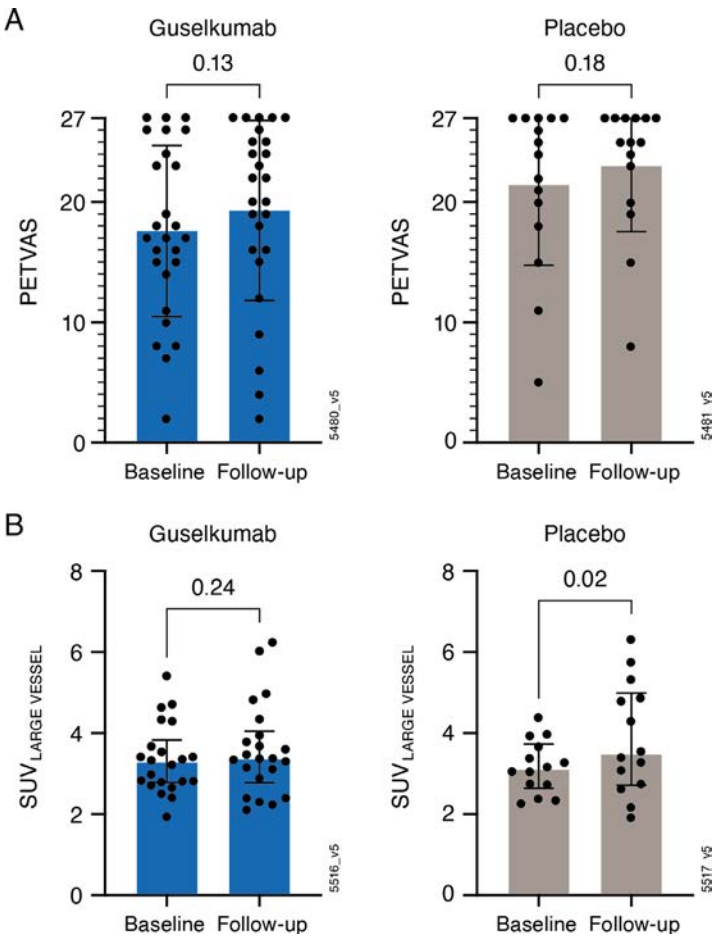

Figure 4. Median PETVAS (A) and $SUV_{LARGE\ VESSEL}$ (B) scores from baseline to follow-up by treatment group. Comparisons made using the Wilcoxon signed rank test. Error bars indicate IQRs. PETVAS, Positron Emission Tomography Vascular Activity Score; SUV, standardised uptake value; $SUV_{LARGE\ VESSEL}$, SUV average across each arterial region and subsequently averaged into a global metric for the entire aorta and branch arteries of interest.

Two (of 23) patients in the guselkumab 400 mg IV-induction group (9%) experienced venous thromboembolic events (VTE; pulmonary embolism [serious AE] and deep vein thrombosis [not serious AE], n = 1 patient each; Supplementary Table S3), both considered unrelated to treatment by the investigator. One GCA-related event of transient vision loss (amaurosis fugax) was reported in a guselkumab-treated patient and occurred in the context of a GCA flare. One death due to an AE (urosepsis at day 68, considered unrelated to treatment by the investigator) occurred in a guselkumab-treated patient.

Through week 60, serious AEs occurred in 17% (6/35) of guselkumab-treated and 0% (0/18) of placebo-treated patients; 1 serious AE (increase in alanine and aspartate transferase after a single IV dose; Supplementary Table S3) was considered related to study treatment.

Across a mean of 19.8 and 21.6 injections through week 60 in the guselkumab and placebo groups, respectively, no injection site reactions occurred.

DISCUSSION

The THEIA study did not meet its primary endpoint; overall, the results did not support the use of guselkumab for treating GCA, and the study was discontinued. Although there was a trend towards higher proportions of guselkumab-treated vs placebo-treated patients achieving GC-free remission at week 28, no statistically significant difference was observed. Measures of GC-free remission that incorporated ESR and/or CRP normalisation were also numerically higher in the guselkumab group at week 28, but differences were limited and generally not maintained at week 52. Early study termination led to missing (but imputed) data that could have affected week 52 results. Additionally, the proportions of patients experiencing a GCA flare/discontinuation due to worsening GCA were similar between groups over time. Consistent with the clinical findings, FDG-PET/CT imaging did not reveal any changes in arterial wall inflammation that might indicate a tissue-level response to guselkumab.

Although the occurrence of overall AEs was comparable between guselkumab- and placebo-treated patients, serious AEs incidence was higher in the guselkumab group. However, no patterns were observed across serious AEs, and all were considered unrelated to study treatment by investigators, with 1 exception (increase in alanine and aspartate transferases after a single dose). Two cases of VTE occurred in the guselkumab group, but a comprehensive review of each case concluded that these were not adverse drug reactions to guselkumab.

Data from phase 2 dose-ranging studies of guselkumab in Crohn's disease and ulcerative colitis indicated that lower doses of guselkumab than those studied in this trial were sufficient to achieve clinical endpoints, and reductions in CRP were not dose dependent [34,35]. Based on these data, the dosing regimen in THEIA was revised to SC administration only. In THEIA, the guselkumab pharmacokinetics were similar in patients who received 400-mg IV induction dosing vs SC-only dosing. These data supported the decision to revise the protocol to SC administration only and to combine efficacy data from patients who received guselkumab by IV induction and SC delivery only. There was no change to planned therapy for the initial 23 patients, and all subsequent patients received only SC-administered therapy.

Table 2
Common treatment-emergent AEs through up to week 60

Treatment-emergent AEs	GUS (N = 35)	PBO (N = 18)
Average duration of follow-up, wk	49.0	54.1
Average number of administrations	10.1	11.2
≥1 AE, n (%)	34 (97)	17 (94)
Common (>10% of any treatment group) AEs, n (%)		
Infections and infestations	21 (60)	11 (61)
COVID-19	8 (23)	5 (28)
Nasopharyngitis	4 (11)	1 (6)
Upper respiratory tract infection	4 (11)	1 (6)
Urinary tract infection	4 (11)	2 (11)
Bronchitis	3 (9)	2 (11)
Acute sinusitis	0	2 (11)
Gastroenteritis	0	2 (11)
Pharyngitis	0	2 (11)
Musculoskeletal and connective tissue disorders	19 (54)	5 (28)
Arthralgia	6 (17)	0
Osteoarthritis	5 (14)	0
Back pain	4 (11)	1 (6)
Vascular disorders	18 (51)	11 (61)
Giant cell arteritis	17 (49)	10 (56)
General disorders and administration site conditions	10 (29)	6 (33)
Malaise	1 (3)	2 (11)
Nervous system disorders	9 (26)	9 (50)
Headache	6 (17)	7 (39)
≥1 serious AE, n (%)	5 (14)	0
Abdominal sepsis	1 (3)	0
Urosepsis	1 (3)	0
Fractured sacrum	1 (3)	0
Alanine aminotransferase increased	1 (3)	0
Aspartate aminotransferase increased	1 (3)	0
Acute kidney injury	1 (3)	0
Pulmonary embolism	1 (3)	0
AEs leading to discontinuation, n (%)	9 (26)	2 (11)
Vascular disorders[a]	6 (17)	2 (11)
GCA	6 (17)	2 (11)

AE, adverse event; GCA, giant cell arteritis; GUS, guselkumab; MedDRA, Medical Dictionary for Regulatory Activities; PBO, placebo.
Patients are counted only once for any given event, regardless of the number of times they actually experienced the event. AEs were coded using MedDRA Version 26.
[a] All vascular disorders leading to discontinuation were attributed to GCA.

The limited efficacy of guselkumab in GCA may reflect poor translation of preclinical studies into clinical efficacy. Prior studies suggest that the IL-12 and IL-23 pathways are activated in GCA [27]. Guselkumab selectively targets the p19 subunit of IL-23 [33] and shows benefit in other diseases, but blocking IL-23 signalling alone may be insufficient to impact disease mechanisms driving GCA. Ustekinumab, which inhibits both the IL-12 *and* IL-23 pathways by targeting their shared p40 subunit, yielded promising initial results in GCA [17] that contributed to our study rationale; however, a subsequent study showed a high rate of treatment failure [18]. Because IL-23 functions upstream of IL-17, targeting IL-23 with guselkumab was expected to demonstrate efficacy in GCA. However, discordant results have been observed in other diseases when targeting this pathway. Despite the efficacy of IL-17–targeting therapies in axial spondyloarthritis and ankylosing spondylitis, treatments blocking IL-23 were ineffective in these diseases. A more comprehensive understanding of GCA-specific mechanisms of pathogenesis is needed [38]; successful therapies for GCA may require a multifaceted approach or combination of therapies.

Similarly, recent studies suggest that the intracellular IL-23p19 subunit can act as an endogenous activator of endothelial inflammation, promoting leukocyte adhesion to endothelial cells and transendothelial migration [39]. This proinflammatory function of the p19 subunit is independent of IL-12/IL-23p40 and may contribute to the pathogenesis of GCA, as the p19 subunit is broadly expressed in adventitial capillaries in GCA [39]. This could potentially limit the efficacy of guselkumab in GCA, since guselkumab is a large monoclonal antibody that may be unable to access the intracellular endothelial p19 subunit. However, it is unclear whether the activity of IL-23p19 as an independent subunit has a role in GCA and, if so, how much its endothelial localisation might limit the effect of guselkumab, as it is also widely expressed by infiltrating leukocytes.

Alternatively, effective treatment for GCA may require targeting different pathways in patients with new-onset vs relapsing disease. Although mRNA analyses showed no significant difference between IL-23p19 subunit levels in tissues from patients who did vs did not achieve remission, temporal artery sections from patients with GCA suggest that expression of inflammatory proteins may change with disease progression [25,31]. For example, more pronounced IL-23 expression was observed in tissue from patients with multiple relapses [25,31], including patients with both new-onset and relapsing GCA, which may have masked a possible treatment effect in relapsing participants treated with guselkumab vs placebo, but not in those with new-onset disease at baseline. Regardless, the study was not powered to compare outcomes in new-onset vs relapsing GCA.

THEIA is the first randomised, controlled, interventional study in GCA to incorporate advanced molecular imaging as an exploratory outcome. Although the utility of vascular imaging for GCA diagnosis is more established, using FDG-PET to monitor disease activity and response to treatment is less common. Observational cohort studies demonstrate that vascular FDG activity may improve with clinical response to treatment, but frequently may not normalise, even in patients achieving clinical remission [40]. Whether persistent vascular PET activity in the later phase of disease represents subclinical disease, vascular remodelling, or another nonspecific process presents an interpretive limitation for PET scans obtained after treatment initiation. In this study, no significant improvement in vascular inflammation (assessed by arterial FDG uptake by visual or semiquantitative approaches) occurred in either treatment arm, with the exception of a significant but modest reduction in TBR_{BLOOD} for guselkumab-treated vs placebo-treated patients. Although a reduction in TBR_{BLOOD} may indicate a partial vascular response to guselkumab, improvement confined to the TBR_{BLOOD} metric could reflect a drug effect on background blood pool FDG activity, which was significantly greater in guselkumab-treated than placebo-treated patients at follow-up. In clinical trials incorporating PET imaging, variability in background FDG activity across treatment arms is a recognised confounder of changes in vascular inflammation, even with the use of simple mathematical compensatory mechanisms, such as TBR [41]. In our study, no significant improvement in vascular inflammation was seen among patients who achieved clinical remission by week 52 or after adjusting for concomitant GC use during imaging. Consistent with prior studies, evaluations by PETVAS or semiquantitative assessment provided similar results, with the latter offering additional precision to detect subtle differences in response between the treatment groups [37]. Future studies may provide further insights by assessing multiple imaging parameters of FDG uptake in parallel. In-depth additional exploration of FDG-PET imaging from this trial will be reported as a future ancillary study.

THEIA used multiple tools to thoroughly assess the effects of guselkumab on GCA, including GC-free remission, incidence of disease flares, known pharmacodynamic markers of disease, and imaging data. Because GCA is a rare disease, recruiting patients can be challenging. By randomising 2:1 and evaluating a variety of endpoints, THEIA maximised the data derived from >50 enrolled patients. However, the relatively small number of included patients represents a study limitation. In addition, patients who experienced ≥1 GCA flare could continue to participate, which may have contributed to the variability in outcomes observed in THEIA.

In conclusion, the lack of significant improvements in GC-free remission in guselkumab-treated patients at week 28, as well as the lack of efficacy across other endpoints, suggests limited benefit of guselkumab for the treatment of GCA.

Competing interests

J-PM has received consultation and presentation fees from Amgen, AstraZeneca, GlaxoSmithKline, KabiCare, Otsuka, Roche, and Sanofi, and is an investigator in studies funded by AbbVie, AstraZeneca, Johnson & Johnson, and Novartis. MCC has received consulting fees from AbbVie, Alexion, AstraZeneca, Boehringer-Ingelheim, CSL Vifor, GSK, Novartis, and Royalty Pharma and a research grant from Kiniksa Pharmaceuticals. MCC was supported by Ministerio de Ciencia, Innovación y Universidades (Agencia Estatal de Investigación): PID2023-152265OB-I00, and Agencia de Gestió d'Ajuts Universitaris i de Recerca (AGAUR): 2021 SGR 01561. MS has received consultation fees from AbbVie, Argenx, AstraZeneca, Boerhinger-Ingelheim, Chugai, CSL Vifor, GSK, Novartis, and Fresenius and a research grant from Novartis. JH has received speaker fees or honoraria from AbbVie, AstraZeneca, Boehringer-Ingelheim, BMS, Johnson & Johnson, Lilly, Novartis, Pfizer, Roche, SOBI, Otsuka, EUSA, and UCB. VS has received consultation and presentation fees or honoraria from Lilly, Novartis, Pfizer, Roche, AbbVie, and Chugai and is an investigator in studies funded by Chugai, Roche, Novartis, and Johnson & Johnson. GE-F has received consultation and presentation fees from GSK and CSL Vifor and a research grant from GSK. CR has received consultation and presentation fees from Otsuka and is an investigator in studies funded by Johnson & Johnson and Novartis. MAA has volunteered for the NIH and has performed official government work for NIH, which ended in December 2022. M-CH, SL, PV, and LO are employees of Johnson & Johnson; employees may own stock/stock options in Johnson & Johnson. PCG was supported by the Intramural Research Program of the National Institutes of Health (NIH). The contributions of PCG are considered Works of the United States Government. The findings and conclusions presented in this paper are those of the authors and do not necessarily reflect the views of the NIH or the U.S. Department of Health and Human Services. DB reports no conflicts of interest.

CRediT authorship contribution statement

Formal analysis, methodology: M-CH and SL, MAA and PG (imaging); **writing (original draft) and visualization:** PV, M-CH, SL, and LO; **visualization:** MAA, PG (imaging); **data curation, validation, supervision:** PV and LO; **investigation:** J-PM, MCC, MS, JH, VS, GF, CR, and DB; **writing, review and editing:** all authors.

Acknowledgements

The authors thank the study patients and all the investigators and their staff who made the clinical trial possible. The authors also thank Kaitlin Quinn and Sovira Tan for their contributions to imaging data and Jie Shao for her contributions to the pharmacokinetic data. We would like to express our heartfelt gratitude to Augustine Obirieze, Christine Kothe, Bart van Hartingsveldt, and all sponsor team members whose contributions were invaluable to the success of this study. Valuable advice was provided by Eomonn Molloy, Peter Merkel, Susan Mollan, Sri Sharma, Justin Mason, Christian Pagnoux, and Sebastian Unizony. Medical writing support was provided by Erica Chevalier-Larsen, PhD, of Johnson & Johnson, under the direction of the authors and in accordance with Good Publication Practice guidelines (Ann Intern Med. 2002;175(9):1298-304).

Funding

This study was funded by Johnson & Johnson.

Patient consent for publication

Not applicable.

Ethics approval

This study (THEIA) was conducted in accordance with Good Clinical Practice guidelines of the International Council for Harmonisation and the principles of the Declaration of Helsinki. All investigators received approval from an ethics committee, and written informed consent was obtained from all patients.

Provenance and peer review

Not commissioned; externally peer reviewed.

Patient and public involvement

A patient advisory board gave feedback on the proposed clinical trial and shared relevant experiences on their journey to diagnosis and treatment.

Data availability statement

The data sharing policy of Johnson & Johnson is available at https://www.jnj.com/about-jnj/policies-and-positions/our-position-on-clinical-trial-data-transparency. As noted on this site, request for access to the study data can be submitted through the Yale Open Data Access Project site at https://yoda.yale.edu.

Supplementary materials

Supplementary material associated with this article can be found in the online version at doi:10.1016/j.ard.2026.01.009.

Orcid

Jean-Paul Makhzoum: http://orcid.org/0000-0003-4523-8525

REFERENCES

[1] Pugh D, Karabayas M, Basu N, Cid MC, Goel R, Goodyear CS, et al. Large-vessel vasculitis. Nat Rev Dis Primers 2022;7(1):93.

[2] Salehi-Abari I. 2016 ACR revised criteria for early diagnosis of giant cell (temporal) arteritis. Autoimmune Dis Ther Approaches Open Access 2016;3 (1):119.

[3] Salvarani C, Pipitone N, Versari A, Hunder GG. Clinical features of polymyalgia rheumatica and giant cell arteritis. Nat Rev Rheumatol 2012;8 (9):509–21.

[4] Koster MJ, Matteson EL, Warrington KJ. Large-vessel giant cell arteritis: diagnosis, monitoring and management. Rheumatology (Oxford) 2018;57(Suppl 2):ii32–42.

[5] Gonzalez-Gay MA, Lopez-Diaz MJ, Barros S, Garcia-Porrua C, Sanchez-Andrade A, Paz-Carreira J, et al. Giant cell arteritis: laboratory tests at the time of diagnosis in a series of 240 patients. Medicine (Baltimore) 2005;84 (5):277–90.

[6] González-Gay MÁ, Ortego-Jurado M, Ercole L, Ortego-Centeno N. Giant cell arteritis: is the clinical spectrum of the disease changing? BMC Geriatr 2019;19(1):200.

[7] Waldman CW, Waldman SD, Waldman RA. Giant cell arteritis. Med Clin North Am 2013;97(2):329–35.

[8] Mainbourg S, Tabary A, Cucherat M, Gueyffier F, Lobbes H, Aussedat M, et al. Indirect comparison of glucocorticoid-sparing agents for remission maintenance in giant cell arteritis: a network meta-analysis. Mayo Clin Proc 2022;97(10):1824–35.

[9] Hellmich B, Agueda A, Monti S, Buttgereit F, de Boysson H, Brouwer E, et al. 2018 Update of the EULAR recommendations for the management of large vessel vasculitis. Ann Rheum Dis 2020;79(1):19–30.

[10] Baig IF, Pascoe AR, Kini A, Lee AG. Giant cell arteritis: early diagnosis is key. Eye Brain 2019;11:1–12.

[11] Proven A, Gabriel SE, Orces C, O'Fallon WM, Hunder GG. Glucocorticoid therapy in giant cell arteritis: duration and adverse outcomes. Arthritis Rheum 2003;49(5):703–8.

[12] Genentech Inc. ACTEMRA (tocilizumab) injection, for intravenous or subcutaneous use. 2025. [cited February 5, 2026]. Available from: www.gene.com/download/pdf/actemra_prescribing.pdf.

[13] Prieto-González S, Terrades-García N, Corbera-Bellalta M, Planas-Rigol E, Miyabe C, Alba MA, et al. Serum osteopontin: a biomarker of disease activity and predictor of relapsing course in patients with giant cell arteritis. Potential clinical usefulness in tocilizumab-treated patients. RMD Open 2017;3(2): e000570.

[14] Stone JH, Klearman M, Collinson N. Trial of tocilizumab in giant-cell arteritis. N Engl J Med 2017;377(4):317–28.

[15] Stone JH, Tuckwell K, Dimonaco S, Klearman M, Aringer M, Blockmans D, et al. Glucocorticoid dosages and acute-phase reactant levels at giant cell arteritis flare in a randomized trial of tocilizumab. Arthritis Rheumatol 2019;71(8):1329–38.

[16] Schmidt WA, Dasgupta B, Sloane J, Giannelou A, Xu Y, Unizony SH, et al. A phase 3 randomized, double-blind, placebo-controlled study to evaluate the efficacy and safety of sarilumab in patients with giant cell arteritis. Arthritis Res Ther 2023;25(1):199.

[17] Conway R, O'Neill L, Gallagher P, McCarthy GM, Murphy CC, Veale DJ, et al. Ustekinumab for refractory giant cell arteritis: a prospective 52-week trial. Semin Arthritis Rheum 2018;48(3):523–8.

[18] Matza MA, Fernandes AD, Stone JH, Unizony SH. Ustekinumab for the treatment of giant cell arteritis. Arthritis Care Res (Hoboken) 2021;73(6):893–7.

[19] Cid MC, Unizony SH, Blockmans D, Brouwer E, Dagna L, Dasgupta B, et al. Efficacy and safety of mavrilimumab in giant cell arteritis: a phase 2, randomised, double-blind, placebo-controlled trial. Ann Rheum Dis 2022;81 (5):653–61.

[20] Venhoff N, Schmidt WA, Bergner R, Rech J, Unger L, Tony HP, et al. Safety and efficacy of secukinumab in patients with giant cell arteritis (TitAIN): a randomised, double-blind, placebo-controlled, phase 2 trial. Lancet Rheumatol 2023;5(6):e341–50.

[21] Novartis Pharmaceuticals. Novartis provides update on Phase III GCAptAIN study of Cosentyx in giant cell arteritis (GCA). [updated July 3, 2025; cited February 5, 2026]. Available from: https://www.novartis.com/news/media-releases/novartis-provides-update-phase-iii-gcaptain-study-cosentyx-giant-cell-arteritis-gca.

[22] Novartis Pharmaceuticals. Efficacy and safety of secukinumab in patients with new onset of giant cell arteritis who are in clinical resmission (GigAINt). [updated December 22, 2025; cited February 5, 2026]. Available from: https://clinicaltrials.gov/study/NCT05380453

[23] Blockmans D, Penn SK, Setty AR, Schmidt WA, Rubbert-Roth A, Hauge EM, et al. A phase 3 trial of upadacitinib for giant-cell arteritis. N Engl J Med 2025;392(20):2013–24.

[24] Ytterberg SR, Bhatt DL, Mikuls TR, Koch GG, Fleischmann R, Rivas JL, et al. Cardiovascular and cancer risk with tofacitinib in rheumatoid arthritis. N Engl J Med 2022;386(4):316–26.

[25] Conway R, O'Neill L, McCarthy GM, Murphy CC, Fabre A, Kennedy S, et al. Interleukin 12 and interleukin 23 play key pathogenic roles in inflammatory and proliferative pathways in giant cell arteritis. Ann Rheum Dis 2018;77 (12):1815–24.

[26] Samson M, Audia S, Fraszczak J, Trad M, Ornetti P, Lakomy D, et al. Th1 and Th17 lymphocytes expressing CD161 are implicated in giant cell arteritis and polymyalgia rheumatica pathogenesis. Arthritis Rheum 2012;64(11):3788–98.

[27] Paroli M, Caccavale R, Accapezzato D. Giant cell arteritis: advances in understanding pathogenesis and implications for clinical practice. Cells 2024;13 (3):267.

[28] Coit P, De Lott LB, Nan B, Elner VM, Sawalha AH. DNA methylation analysis of the temporal artery microenvironment in giant cell arteritis. Ann Rheum Dis 2016;75(6):1196–202.

[29] Márquez A, Hernández-Rodríguez J, Cid MC, Solans R, Castañeda S, Fernández-Contreras ME, et al. Influence of the IL17A locus in giant cell arteritis susceptibility. Ann Rheum Dis 2014;73(9):1742–5.

[30] Deng J, Younge BR, Olshen RA, Goronzy JJ, Weyand CM. Th17 and Th1 T-cell responses in giant cell arteritis. Circulation 2010;121(7):906–15.

[31] Espígol-Frigolé G, Planas-Rigol E, Lozano E, Corbera-Bellalta M, Terrades-García N, Prieto-González S, et al. Expression and function of IL12/23 related cytokine subunits (p35, p40, and p19) in giant-cell arteritis lesions: contribution of p40 to Th1- and Th17-mediated inflammatory pathways. Front Immunol 2018;9:809.

[32] Sherlock JP, Joyce-Shaikh B, Turner SP, Chao CC, Sathe M, Grein J, et al. IL-23 induces spondyloarthropathy by acting on ROR-γt+ CD3+CD4-CD8-entheseal resident T cells. Nat Med 2012;18(7):1069–76.

[33] Janssen Biotech Inc. TREMFYA (guselkumab) injection, for subcutaneous use. 2025. [cited February 5, 2026]. Available from: www.janssenlabels.com/package-insert/product-monograph/prescribing-information/TREMFYA-pi.pdf.

[34] Dignass A, Rubin D, Bressler B, Huang KH, Shipitofsky N, Germinaro M, et al. OP23 The efficacy and safety of guselkumab induction therapy in patients with moderately to severely active ulcerative colitis: phase 2b QUASAR study results through week 12. J Crohns Colitis 2022;16(Suppl 1):i025–6.

[35] Sandborn WJ, D'Haens GR, Reinisch W, Panés J, Chan D, Gonzalez S, et al. Guselkumab for the treatment of Crohn's disease: induction results from the phase 2 GALAXI-1 study. Gastroenterology 2022;162(6):1650–1664.e8.

[36] Grayson PC, Alehashemi S, Bagheri AA, Civelek AC, Cupps TR, Kaplan MJ, et al. ^{18}F-fluorodeoxyglucose-positron emission tomography as an imaging biomarker in a prospective, longitudinal cohort of patients with large vessel vasculitis. Arthritis Rheumatol 2018;70(3):439–49.

[37] Dashora HR, Rosenblum JS, Quinn KA, Alessi H, Novakovich E, Saboury B, et al. Comparing semiquantitative and qualitative methods of vascular ^{18}F-FDG PET activity measurement in large-vessel vasculitis. J Nucl Med 2022;63(2):280–6.

[38] Zhang H, Jiang HL, Dai SM. No significant effects of IL-23 on initiating and perpetuating the axial spondyloarthritis: the reasons for the failure of IL-23 inhibitors. Front Immunol 2022;13:818413.

[39] Espígol-Frigolé G, Planas-Rigol E, Ohnuki H, Salvucci O, Kwak H, Ravichandran S, et al. Identification of IL-23p19 as an endothelial proinflammatory peptide that promotes gp130-STAT3 signaling. Sci Signal 2016;9 (419):ra28.

[40] Schönau V, Roth J, Tascilar K, Corte G, Manger B, Rech J, et al. Resolution of vascular inflammation in patients with new-onset giant cell arteritis: data from the RIGA study. Rheumatology (Oxford) 2021;60(8):3851–61.

[41] Ahlman MA, Vigneault DM, Sandfort V, Maass-Moreno R, Dave J, Sadek A, et al. Internal tissue references for ^{18}Fluorodeoxyglucose vascular inflammation imaging: implications for cardiovascular risk stratification and clinical trials. PLoS One 2017;12(11):e0187995.

Ann Rheum Dis 85 (2026) 921–931

Contents lists available at ScienceDirect

Annals of the Rheumatic Diseases

journal homepage: https://www.sciencedirect.com/journal/annals-of-the-rheumatic-diseases

Polymyalgia Rheumatic

Effects of clofutriben, a selective 11β-hydroxysteroid dehydrogenase type 1 inhibitor, on the efficacy and toxicity of prednisolone in patients with polymyalgia rheumatica: a single-blind controlled trial with sequential cohorts

Frank Buttgereit[1], Andrea Everding[2], Ioana Andreica[3,4], Herbert L Kellner[5], Florian Schuch[6], Cornelia Weyand[7], Paul M. Stewart[8], Peter A. Merkel[9], Christian Dejaco[10,11], Frank S. Czerwiec[12], Ketan Desai[12], David A. Katz[12,*]

[1] *Department of Rheumatology and Clinical Immunology, Charité Universitätsmedizin Berlin, Berlin, Germany*
[2] *Hamburger Rheuma Forschungszentrum II, Hamburg, Germany*
[3] *Ruhr-Universität Bochum, Bochum, Germany*
[4] *Rheumazentrum Ruhrgebiet, Herne, Germany*
[5] *Schwerpunktpraxis für Rheumatologie und Gastroenterologie München, München, Germany*
[6] *Internistische Praxisgemeinschaft Rheumatologie Nephrologie Erlangen, Erlangen, Germany*
[7] *Department of Immunology, Mayo Clinic, Rochester, Minnesota, USA*
[8] *Department of Medicine, University of Leeds, Leeds, UK*
[9] *Departments of Medicine (Rheumatology) and Epidemiology, University of Pennsylvania, Philadelphia, Pennsylvania, USA*
[10] *Department of Rheumatology, Teaching Hospital of the Paracelsus Medical University, Brunico, BZ, Italy*
[11] *Department of Rheumatology, Medical University of Graz, Graz, Austria*
[12] *Sparrow Pharmaceuticals, Portland, Oregon, USA*

ARTICLE INFO

Article history:
Received 2 August 2025
Received in revised form 10 October 2025
Accepted 14 October 2025

ABSTRACT

Objectives: Glucocorticoids effectively treat many diseases, but toxicity limits their utility. We aimed to learn whether, by reducing active intracellular glucocorticoid exposures, the 11β-hydroxysteroid dehydrogenase type 1 inhibitor clofutriben could selectively reduce glucocorticoid efficacy but reduce toxicity more strongly. We hypothesised that by increasing the prednisolone dose, it might be possible to restore efficacy back to the original level, thereby improving the benefit-risk profile.

Methods: In sequential cohorts, adults with polymyalgia rheumatica received (single blind) prednisolone 10 mg/d with placebo for 2 weeks, then clofutriben with either prednisolone 10, 15, 20, or 30 mg/d for 2 weeks.

Results: Forty-nine and 47 participants completed each trial period with evaluable data. Five who received prednisolone 10 mg/d with clofutriben experienced clinical relapse. No clinical relapses occurred during other treatments. Participants reported more severe symptoms and physical disability when prednisolone 10 mg/d or 15 mg/d, but not 20 mg/d or 30 mg/d, was given with clofutriben. Inflammatory biomarkers followed a similar pattern. Across all prednisolone doses, clofutriben coadministration mitigated glucocorticoid-related adverse effects on

*Correspondence to Dr. David A. Katz, Sparrow Pharmaceuticals, Portland, OR, USA.
E-mail address: david@sparrowpharma.com (D.A. Katz).
Handling editor Josef S. Smolen.

https://doi.org/10.1016/j.ard.2025.10.015

biomarkers of bone turnover, lipid metabolism, hypercoagulability, and cardiovascular and adrenal function.
Conclusions: Further trials to assess clofutriben's potential to improve the benefit-risk profile of prednisolone are warranted.

WHAT IS ALREADY KNOWN ON THIS TOPIC

- 11β-Hydroxysteroid dehydrogenase type 1 (HSD-1) is a tissue-specific regulator of intracellular active glucocorticoids, which have biological activity. Patients with tumour-associated hypercortisolism, but deficient in HSD-1, did not show signs/symptoms of Cushing's syndrome, leading to the hypothesis that HSD-1 inhibitors could prevent or reverse morbidity associated with glucocorticoid excess. In a clinical trial in healthy adults who received prednisolone 20 mg/d for 7 days and randomised to a HSD-1 inhibitor or placebo, the inhibitor prevented the appearance of insulin resistance, changes on markers of lipid metabolism and bone turnover, and nocturnal blood pressure increase, with limited impact on prednisolone's anti-inflammatory activity.

WHAT THIS STUDY ADDS

- This placebo-controlled proof-of-concept and dose range finding clinical trial reports for the first time in patients with a rheumatic disease (polymyalgia rheumatica [PMR]) that a HSD-1 inhibitor (clofutriben) not only prevented, but also reversed, changes on markers of prednisolone toxicity, while combinations of prednisolone 20 or 30 mg/d with clofutriben 6 mg/d had similar clinical efficacy as prednisolone 10 mg/d alone. The results suggest that HSD-1 inhibition alters the dose-response relationships for both the efficacy and toxicity of glucocorticoids in a favourable manner, with larger impacts on toxicity. Therefore, by adjusting the glucocorticoid and clofutriben doses, the clinical benefit-risk profile of this combination could be favourably modified.

HOW THIS STUDY MIGHT AFFECT RESEARCH, PRACTICE, OR POLICY

- These findings could be generalisable to the >1% of our ageing population who rely on chronic use of drugs such as prednisolone across rheumatology, oncology, gastroenterology, and additional disciplines of medicine, and suffer >10% of all drug-associated adverse effects. This trial represents a major leap towards the goal of a treatment that retains the broad, often unparalleled, efficacy of glucocorticoids, exposing patients only to an acceptable level of harm. If noninferior efficacy and superior safety compared to prednisolone are confirmed in definitive trials in PMR and other diseases, fixed-dose combinations of prednisolone and clofutriben could be substituted directly for all current prednisolone strengths to provide overall better outcomes for patients.

INTRODUCTION

Glucocorticoids (GCs) effectively treat many inflammatory, autoimmune, and other diseases, but toxicity limits these drugs' utility. Despite the availability of targeted immunomodulators and other agents, many such patients are treated chronically with GCs to maintain disease control. For example, GCs are the standard treatment for polymyalgia rheumatica (PMR), a common immune-mediated disease of older adults for whom the toxicity of GCs is particularly pernicious. There remains an unmet need to develop regimens through which GCs can retain their anti-inflammatory properties while avoiding their common toxicities.

11β-Hydroxysteroid dehydrogenases (HSDs) regulate the intracellular biological activity of endogenous and exogenous GCs. In mineralocorticoid-sensitive cells, such as in the kidney distal tubule, HSD type 2 (HSD-2) inactivates active GCs (eg, prednisolone to prednisone). The inactive GCs so formed re-enter circulation, from which they can enter GC-sensitive cells. There, HSD type 1 (HSD-1) reactivates, eg, prednisone to prednisolone. HSD-1 is a tissue-specific activator of GCs [1] and a major contributor to whole-body GC exposures [2,3]. HSD-1 activity is highest in tissues impacted by GC-related toxicity (eg, liver, adipose, brain, and bone) and low in immune cells where GCs exert anti-inflammatory efficacy. Several sets of evidence suggest that HSD-1 tissue specificity contributes to differential inhibitor modulation on GC efficacy and toxicity [4–13].

Clofutriben (C; previously ASP3662, SPI-62), a selective inhibitor of HSD-1 in humans [14], prevented several corticosterone toxicities in mice [15]. We hypothesised that clofutriben would shift the dose-response relationships for prednisolone efficacy and toxicity, with larger shifts on toxicity, in patients with rheumatic disease. Then, it should be possible to increase the prednisolone dose administered with clofutriben to achieve similar efficacy as, yet retain a safety advantage over, prednisolone monotherapy.

We report a proof-of-concept and dose range finding trial of prednisolone with clofutriben in patients with PMR. Objectives of the trial were to learn whether prednisolone with clofutriben shows similar disease control, and less toxicity, compared to prednisolone monotherapy, and which combinations of prednisolone and clofutriben most improve prednisolone's benefit-risk profile through differential modulation of efficacy and toxicity.

METHODS

Participants and design

Adults with established PMR per European Alliance of Associations for Rheumatology/ American College of Rheumatology criteria [16] who received prednisolone 10 mg/d for at least 1 week before enrolment, and not in relapse based on symptoms or acute phase markers, were recruited from September 2022 to May 2024. All but 1 were recruited at 5 centres in Germany (Berlin, Hamburg, Herne, München, and Erlangen). They entered a 4-week treatment period during which they continued prescribed prednisolone 10 mg/d without dose reduction (Fig 1). Exclusion criteria included prednisolone contraindication, giant cell arteritis diagnosis or clinical features, autoimmune disease other than PMR, and PMR prior treatment for protocol-specified periods other than with prednisolone. Four sequential cohorts with 12 participants each were planned. Treatment order could not be randomised due to clofutriben's long pharmacodynamic half-life, which is more than 4 weeks in the liver. Participants were not aware that the design was sequential rather than crossover, but that information was known by investigators. During the first 2 weeks, participants received a single-blinded placebo for clofutriben with prednisolone 10 mg/d (P10). During the second 2 weeks, participants received single-blinded clofutriben 6 mg/d (modelled to achieve continuous, maximal HSD-1 inhibition at steady state in the liver [17], brain [18], and adipose [Clinical and Translational Science]) with

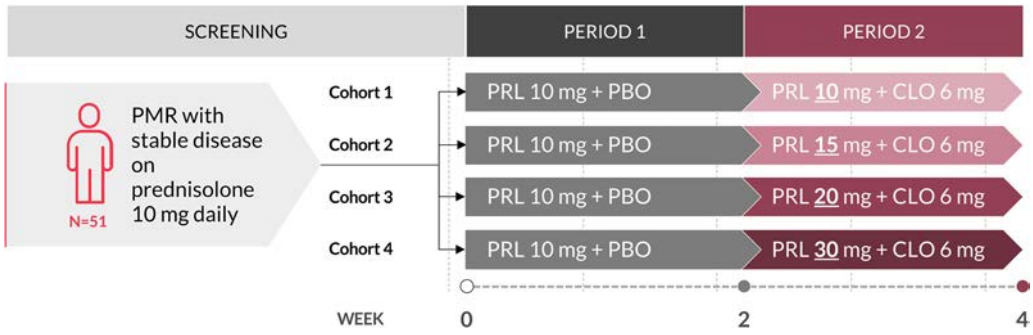

Figure 1. Clinical trial schematic. Eligible patients were enrolled in sequential cohorts with the aim that 12 in each cohort would complete the trial. Trial participants received 2 treatment regimens sequentially for 2 wk each. Prednisolone 10 mg with a blinded placebo for clofutriben served as a run-in period during which the stability of each participant's condition was assessed. Then, participants received prednisolone (at the doses indicated) with blinded clofutriben. Except during the first cohort, participants also received overencapsulated prednisolone during the second period, and dummy capsules during the first period. Participants continued their prescribed prednisolone 10 mg throughout the trial. CLO, clofutriben; PBO, placebo; PRL, prednisolone; PMR, polymyalgia rheumatica.

a cohort-specific prednisolone dose. Additional single-blinded prednisolone 0, 5, 10, or 20 mg/d was administered in successive cohorts. The total prednisolone dose coadministered with clofutriben was 10 (P10C), 15 (P15C), 20 (P20C), or 30 (P30C) mg/d. Participants were aware of the total prednisolone dose that they were to receive during the clofutriben period. The total prednisolone dose coadministered with clofutriben for each cohort after the first was determined by 2 authors (FSC, DAK) based on analysis of data from the completed cohort(s). In particular, a higher prednisolone dose (coadministered with clofutriben) compared to the prior cohort was selected if the accumulated data had not yet indicated that the prior regimen's efficacy was similar in all aspects to that of prednisolone 10 mg alone. Except in the first cohort, placebo for the additional prednisolone was administered during the first 2 weeks. Prednisolone efficacy and toxicity, and clofutriben safety and pharmacology, were monitored at weeks 0, 2, and 4. Safety was assessed for 4 weeks after the treatment period.

The protocol was approved by Bundesinstitut für Arzneimittel und Medizinprodukte (#4045419) and Ethik-Kommission des Landes Berlin (#22/076-IV-E). All patients provided written informed consent before any trial procedures. The trial was conducted in accordance with the World Medical Association Declaration of Helsinki: ethical principles for medical research involving human subjects. The trial is registered on clinicaltrials.gov (NCT05436652).

Assessments

Core efficacy assessments were clinical relapse (investigator's judgement that PMR activity justified a prednisolone dose increase), symptoms of PMR (numeric rating scales [NRS] for pain, stiffness, and fatigue intensity [range 0 (no symptom)-10 (very severe symptom)], and pain chronicity [range 0 (none of the time)-4 (all of the time)]), physical function (Health Assessment Questionnaire-Disability Index [HAQ-DI]) [19], inflammation (erythrocyte sedimentation rate [ESR; conducted at the clinical sites using materials provided by the central laboratory], C-reactive protein [CRP], fibrinogen), and Patient Global Impression (PGI; state range 1 [not present]-4 [severe], change range 1 [much improved]-5 [much worse]) (Supplementary material). Participants completed NRS daily at home with 24-hour look-back, and during trial visits with a 7-day look-back. Daily NRS data were summarised as the maximum value of each week for analysis. Exploratory efficacy assessments were inflammatory cytokines (B-cell activating factor [BAFF], C-X-C motif chemokine ligand 10 [CXCL10], granulocyte colony stimulating factor [G-CSF], granulocyte macrophage colony stimulating factor [GM-CSF], interferon gamma [IFNγ], interleukin [IL]-1β, IL-1 receptor antagonist [IL-1RA], IL-2, IL-2 receptor subunit alpha [IL-2RA], IL-6, IL-10, IL-17, tumor necrosis factor alpha [TNFα]), complete blood count components (basophils, eosinophils, lymphocytes, monocytes, neutrophils, platelets), lymphocyte subsets by quantitative polymerase chain reaction (PCR) (total B, IL-6R+, memory B, CD3+ T, IL-17A+, regulatory T), and gamma prime fibrinogen.

Prednisolone-related toxicity domains included bone turnover (osteocalcin, procollagen type I N-terminal propeptide [PINP], C-terminal telopeptide of type 1 collagen [CTX], bone alkaline phosphatase), lipid metabolism (triglycerides, cholesterol), hypercoagulability (activated partial thromboplastin time [APTT], prothrombin time, international normalised ratio), glucose metabolism (oral glucose tolerance test, homeostatic assessment of insulin resistance, glycated haemoglobin A1c), blood pressure (diurnal amplitude from daily at-home midday and prior-to-bed measurements), heart rate, and adrenal function (adrenocorticotrophic hormone [ACTH], morning serum cortisol). Blood pressure diurnal amplitude data were summarised as the weekly means for analysis.

Safety assessments included clinical laboratory tests, electrocardiograms, and orthostatic vital signs. Adverse events of PMR are reported as a prednisolone efficacy parameter, rather than as clofutriben safety. Electrocardiogram-measured heart rate is reported as a parameter of prednisolone toxicity. As increases in ACTH have been associated with clofutriben and other HSD-1 inhibitors, dehydroepiandrosterone sulfate (DHEA-S), testosterone, and aldosterone were measured.

Urinary biomarkers for hepatic HSD-1 ([tetrahydrocortisol + allotetrahydrocortisol]/tetrahydrocortisone) and renal HSD-2 (cortisone/cortisol) activity were calculated, and serum cortisone measured, as pharmacodynamic parameters. Clofutriben and prednisolone plasma levels were measured before dosing and at 1/2, 1, 2, and 3 hours postdose.

Trial operations were overseen by FGK. Laboratory tests were performed by SGS except urinary biomarkers and plasma drug levels (IQVIA Laboratories) and quantitative PCR (Precision for Medicine).

Statistical analysis

No sample size calculations were performed. Twelve participants per cohort were selected based on a prior trial's results in patients with PMR with analogous objectives [20]. Analyses

were conducted based on the regimen(s) actually received by each participant. Clofutriben safety was reported for all participants, including those who did not adhere to protocol-specified prednisolone regimens. When a participant received a prednisolone dose increase pursuant to an increase of PMR symptoms, the clinical relapse, associated treatment-emergent adverse event (TEAE), and data before the dose change were attributed to the lower prednisolone dose, while data after the dose increase were analysed as the higher prednisolone dose. As trial objectives were inductive, the use of deductive methods was not appropriate. For prednisolone efficacy and toxicity parameters, change during the placebo period (P10) was compared to change during the clofutriben period separately for each regimen (P10C, P15C, P20C, P30C). For clofutriben safety and pharmacology parameters, end-of-treatment values were compared between placebo and clofutriben periods. Descriptive statistics, including CIs, are presented (derived using JMP Clinical 18.0.1 [SAS Institute]).

Data Statement

These data were presented at EULAR 2025 [39].

RESULTS

Participants

Participant flow is shown in Supplementary Figure S1. Subsequent visit data from participants who discontinued dosing were included for analysis. Those who discontinued placebo continued active prednisolone therapy. Those who discontinued clofutriben still had active clofutriben at the next visit due to its long pharmacodynamic half-life [14].

Actual treatment assignments differ from those planned (48 in P10, 12 in each PnnC group) for the following reasons.

- One P10C participant withdrew before receiving clofutriben but provided P10 data.
- Two P10C participants' prednisolone dose increased on clinical relapse (see Core outcomes below) and were evaluated as P15C for parameters measured subsequently.
- Two P10C participants were found to have been prescribed prednisone rather than prednisolone. As prednisone and prednisolone are equivalent (in the absence of a HSD-1 inhibitor), their P10 and safety results are reported, but they could not be evaluated within any of the protocol-specified treatment groups with clofutriben.
- One P20C participant was found to have been prescribed prednisone rather than prednisolone. Prednisolone plasma levels were consistent with their being evaluated as P10C.
- One P30C participant withdrew before receiving clofutriben but provided P10 data.
- Two participants were noncompliant with prednisolone. Their safety results are reported, but they could not be evaluated within any of the protocol-specified treatment groups.

Participant demographics (Table 1) were as expected for German patients with PMR [21]. Nine patients had onset of PMR more than 1 year, and 4 less than 1 month, before trial entry. Nine patients had been at a stable prednisolone 10 mg dose for less than 2 weeks before trial entry. At week 0, mean scores were 2.4, 2.4, and 2.9 of 10 for pain, stiffness,

Table 1
Participant demographics at week 0

	Safety		P10		P10C		P15C		P20C		P30C	
N	53		49		11		14		11		11	
Prescribed prednisolone (mg)			10		10		10		10		10	
Additional prednisolone (mg)			0		0		5		10		20	
Clofutriben (mg)			0		6		6		6		6	
Self-reported sex (% M/F/N)	43/57/0		45/55/0		45/55/0		50/50/0		45/55/0		36/64/0	
Mean (range) age (y)	68 (49-88)		68 (49-88)		67 (58-78)		68 (56-82)		65 (49-81)		72 (54-88)	
Race (% white/not reported)	96/4		98/2		100/0		100/0		91/9		100/0	
Ethnicity (% Hispanic/Latino)	2		0		0		0		0		0	
Median (range) duration of PMR from diagnosis (d)	110 (18-3269)		110 (18-3269)		135 (18-3269)		111 (22-1284)		105 (18-1237)		71 (21-1689)	
Median (range) cumulative dose of prednisolone (mg)	1679 (230-77,337)		1675 (230-77,337)		1725 (760-32,415)		1930 (230-10,160)		1679 (570-77,337)		852.5 (465-29,052)	
Medical history	n	%	n	%	n	%	n	%	n	%	n	%
Hypertension	30	57	28	57	9	82	9	64	4	36	6	55
Arthritis	23	43	20	41	5	45	7	50	5	45	3	27
Dyslipidaemia	18	34	17	35	4	36	6	43	2	18	3	27
Hypothyroidism	8	15	8	16	2	18	1	7	1	9	3	27
Osteopenia/osteonecrosis	7	13	7	14	4	36	1	7	1	9	1	9
Concomitant medications	n	%	n	%	n	%	n	%	n	%	n	%
Antihypertensives	36	68	34	69	8	73	10	71	8	73	7	64
Vitamin D	35	66	33	67	6	56	11	79	10	91	5	45
Proton pump inhibitors	22	42	21	43	5	45	9	64	5	45	2	18
Cholesterol lowering	14	26	13	27	3	27	5	36	1	9	3	27
Antiplatelet/antithrombotic	10	19	10	20	3	27	3	21	3	27	1	9
Levothyroxine	8	15	8	15	1	9	1	7	1	9	4	36
Analgesics	6	11	5	10	0	0	2	14	2	18	1	9

PMR, polymyalgia rheumatica.
Relevant medical history and concomitant medications prevalent in at least 10% of participants are shown. Additional medical history and prior medication data are in Supplementary Tables S19 and S20.

Table 2
Evidence for loss of efficacy in patients with polymyalgia rheumatica treated with prednisolone without or with clofutriben

	P10		P10C		P15C		P20C		P30C	
N	49		13		12		11		11	
	n	%	n	%	n	%	n	%	n	%
Clinical relapse	–	–	5	38	–	–	–	–	–	–
Increased activity	–	–	7	54	1	8	2	18	1	9

PMR, polymyalgia rheumatica.
Clinical relapse was defined as activity of PMR that justified a prednisolone dose increase. Investigator judgement that a participant's PMR activity had increased, including to a lesser degree that did not justify a dose increase, was also recorded. P10 = prednisolone 10 mg. C = clofutriben. Clinical relapse was experienced by 1 of 2 participants during coadministration of prednisone with clofutriben. Increased activity of PMR was experienced by 1 of 2 participants who were non-compliant with prednisolone.

and fatigue intensity NRS, 1.3 of 4 for pain chronicity NRS, and 0.6 of 3 for HAQ-DI total score (Supplementary Tables S1 and S2). On PGI 15, 57, or 28% of participants endorsed no, mild, or moderate PMR severity (Supplementary Table S3). Participants who received P20C reported the highest, and those who received P30C the lowest, baseline disease activity.

Efficacy of prednisolone

Core outcomes

Clinical relapse was experienced by 5 of 13 participants after switch to clofutriben without prednisolone dose adjustment (P10C). Of those, the prednisolone dose was increased for 3 participants only after they completed all week 4 assessments. No

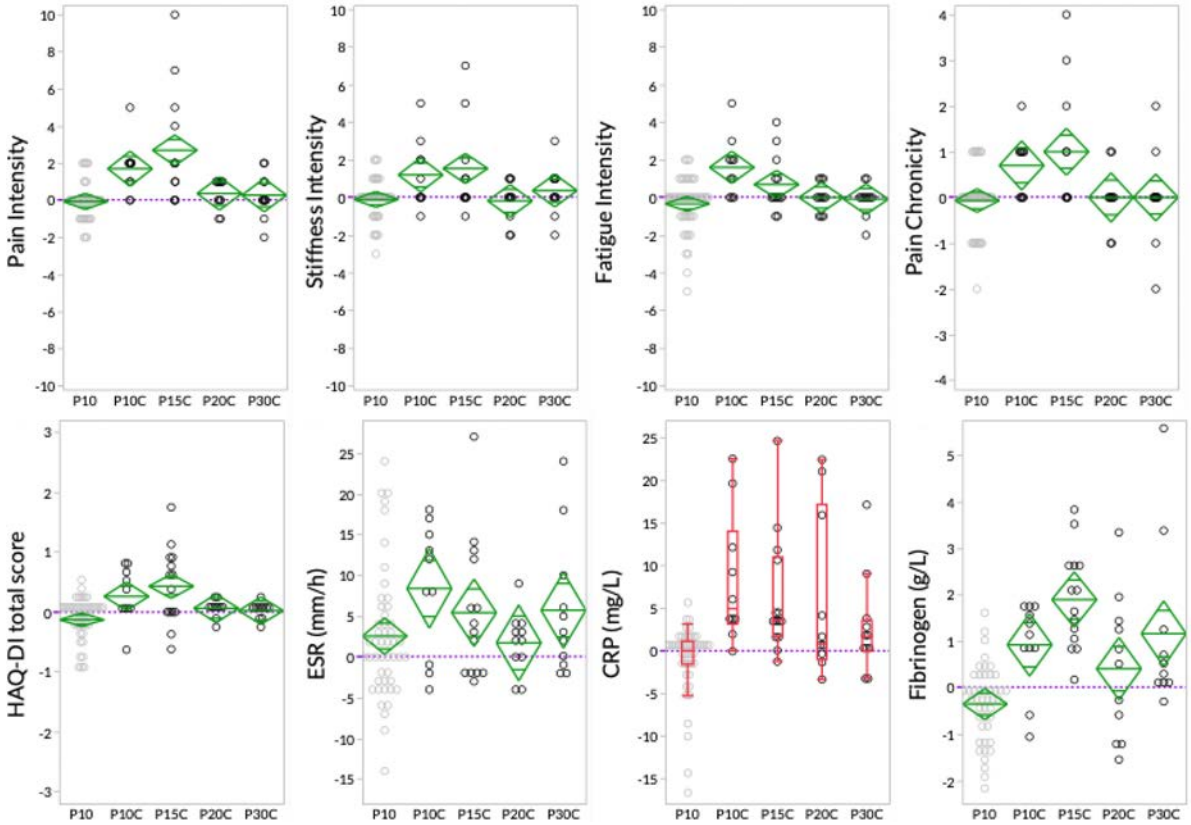

Figure 2. Efficacy outcomes in patients with polymyalgia rheumatica treated with prednisolone without or with clofutriben. Participants completed symptom numeric rating scales (NRS; range: intensity 0-10, chronicity 0-4) with 24 hours look-back at-home daily throughout the trial. Data were summarised as the weekly maximum reported value for the change from baseline calculation. Disability on instrumental activities of daily living was assessed using the Health Assessment Questionnaire-Disability Index (HAQ-DI; total score range: 0-3), and erythrocyte sedimentation rate (ESR), C-reactive protein (CRP), and fibrinogen, were measured during trial visits. Clofutriben (C)-containing regimen data are changes from week 2 to week 4. Prednisolone 10 mg (P10) data are changes from week 1 (NRS) or week 0 (HAQ-DI, inflammatory biomarkers) to week 2. Diamond midlines and vertices indicate the mean and 95% CI of the mean. The top and bottom horizontal lines are overlap lines. If the top overlap line of 1 diamond is below the bottom overlap line of another diamond, the treatments would have been statistically significantly different by pairwise comparison had the data been analysed in an analysis of variance framework. Boxes indicate median and interquartile range. Whiskers extend to the most extreme datum that is within 1.5 times the interquartile range of the quartile. Boxes-and-whiskers are presented when the parameter was not normally distributed.

participants experienced clinical relapse during P10 (N = 49), or after switch to P15C, P20C, or P30C (total N = 34). Increased PMR activity that did not require a dose increase was experienced by 7 additional participants (2, 1, 2, and 1 during P10C, P15C, P20C, and P30C, and one who was noncompliant with P) (Table 2).

Change in daily NRS in the second week of each treatment period was the main symptom evaluation. Group means and CIs were consistent with no or clinically irrelevant change from baseline for P10, P20C, and P30C (Fig 2, Supplementary Table S4, Supplementary Fig S2). P10C and P15C means and CIs suggest an increase in symptoms. Results of the first week of daily NRS entries during clofutriben-containing regimens (Supplementary Table S4, Supplementary Fig S3) and NRS completed during trial visits (Supplementary Table S1, Supplementary Fig S4) were similar.

Patient-reported physical function followed a similar pattern (Fig 2, Supplementary Table S2, Supplementary Fig S2). HAQ-DI means and CIs were consistent with no or clinically irrelevant change from baseline for P10, P20C, and P30C. P10C or P15C means and CIs suggest an increase in disability.

Most participants on P10 or P20C, and the largest number of those on P30C, reported no change in overall health on PGI (Supplementary Table S3). Half or more on P10C or P15C reported worse overall health.

Acute phase biomarkers (Fig 2, Supplementary Table S5) were consistent with observations made for symptoms and physical function. Mean ESR increased during all treatments, least with P10 and P20C; both CIs of change overlapped 0. ESR increased most during P10C. The median CRP change during P10 was 0. The median increased most during P10C and least during P20C treatment. CIs of change for P10 and P20C overlapped 0. Fibrinogen changed little with P10 and after switch to P20C; both CIs overlapped zero. Fibrinogen increased most after switch to P15C.

Exploratory outcomes

Inflammatory cytokines showed distinct patterns (Supplementary Fig S5). BAFF, CXCL10, IL-2RA, and IL-6 baseline levels were either above or in the upper portion of assay reference ranges. They were stable during P10, increased substantially with P10C and P15C, and less so with P20C and P30C (Supplementary Table S6). Baseline G-CSF, IFNγ, IL-1RA, and TNFα values were not elevated and remained within assay reference ranges during treatment. Baseline IFNγ values were elevated and, on average, did not show large percentage change with treatment, although some individuals with high baseline values showed further increases during the trial (Supplementary Table S7). All or most GM-CSF, IL-1β, IL-2, IL-10, and IL-17 values were below the assay limits of quantitation.

Complete blood count components showed increases of basophils and platelets with P10C that were not clinically significant (Supplementary Table S8, Supplementary Figs S6 and S7). Clofutriben-containing regimens were associated with decreased lymphocyte counts that abated as the prednisolone dose increased. Each lymphocyte subset followed the same pattern (Supplementary Tables S9 and S10, Supplementary Fig S8).

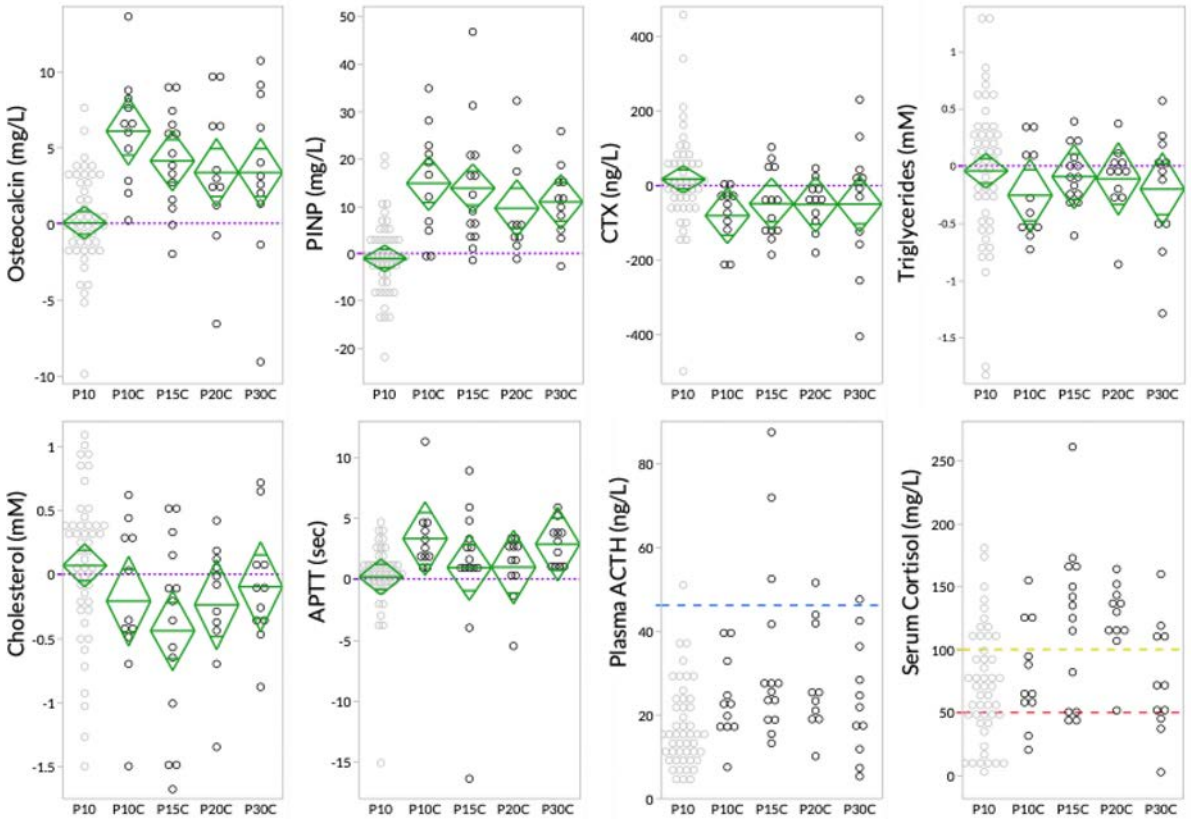

Figure 3. Glucocorticoid-related toxicity outcomes in patients with polymyalgia rheumatica treated with prednisolone without or with clofutriben. Osteocalcin, procollagen type I N-terminal propeptide (PINP), C-terminal telopeptide of type 1 collagen (CTX), triglycerides, cholesterol, and activated partial thromboplastin time (APTT) were measured during trial visits. Clofutriben (C)-containing regimen data are changes from week 2 to week 4. Prednisolone 10 mg (P10) data are changes from week 0 to week 2. See Figure 2 legend for description of visual conventions. Plasma adrenocorticotropic hormone (ACTH) and serum cortisol were measured during trial visits in the morning prior to administration of prednisolone or clofutriben. C-containing regimen data are values at week 4. P10 data are values at week 2. Red and gold dashed lines represent Endocrine Society/European Society of Endocrinology upper thresholds for high and intermediate risk of glucocorticoid-associated adrenal insufficiency [22].

Gamma prime fibrinogen means were within the reference range and did not change with treatment (Supplementary Table S5, Supplementary Fig S9).

Toxicity of prednisolone

Favourable bone biomarker changes were observed with clofutriben, even with a prednisolone dose increase (Fig 3, Supplementary Table S11, Supplementary Figs S10 and S11). Osteocalcin was suppressed during P10, with half of the participants' values below the reference range. Almost half of those, counted across all prednisolone doses, shifted into the reference range with clofutriben. PINP values increased with clofutriben, with all except one in the lower portion of the reference range shifting to midrange or higher. CTX values decreased with clofutriben, with all those that were above the reference range normalising. There was no difference between treatments on bone-specific alkaline phosphatase.

Serum lipid decreases were observed with clofutriben (Fig 3, Supplementary Table S12, Supplementary Figs S11 and S12). Half of the participants with elevated triglycerides with P10 had values in the reference range with clofutriben. Cholesterol changes were attributable to lowered high-density lipoprotein (HDL). Low-density lipoprotein did not differ between treatment groups.

Increased values of APTT were seen with clofutriben (Fig 3, Supplementary Table S13, Supplementary Fig S13). All values below the reference range with P10 normalised with clofutriben. Other coagulation biomarkers (Supplementary Table S13, Supplementary Figs S11 and S13) showed no differences between treatments.

No differences between treatments were observed on parameters of glycaemic control (Supplementary Table S14, Fig S14) or blood pressure (Supplementary Table S15, Fig S15).

Heart rate increases were observed with clofutriben (Supplementary Table S16, Fig S16).

P10 repressed the hypothalamic-pituitary-adrenal axis (Fig 3, Supplementary Table S17, Fig S17). Most morning ACTH values were in the lower portion of the reference range. Morning serum cortisol levels were below 50 ng/L (high risk for adrenal insufficiency) [22] in 18, 50–100 ng/L (reduced risk) in 19, and above 100 ng/L (low risk) in 12 of 49 participants. After 2 weeks' clofutriben treatment (across all doses), morning ACTH increased, and morning serum cortisol levels indicated high, reduced, and low risk for 10, 11, and 26 of 47 participants.

Table 3
Treatment-emergent adverse events

	Placebo		Clofutriben		Follow-up	
N	51		51		51	
	n	%	n	%	n	%
Any event	13	25	17	33	6	12
Any infection	2	4	5	10	4	8
Nasopharyngitis	1	2	3	6	1	2
Arthralgia	1	2	2	4	1	2
Headache	3	6	1	2	–	–
Dizziness	2	4	1	2	–	–
Insomnia	2	4	–	–	–	–
Abdominal pain	1	2	1	2	–	–
Constipation	1	2	1	2	–	–
Anxiety	1	2	–	–	–	–
Bronchitis	1	2	–	–	–	–
Dental caries	1	2	–	–	–	–
Diarrhoea	1	2	–	–	–	–
Dizziness postural	1	2	–	–	–	–
Eye irritation	1	2	–	–	–	–
Hyperglycaemia	1	2	–	–	–	–
Hyperkalaemia	1	2	–	–	–	–
Neck pain	1	2	–	–	–	–
Penile operation	1	2	–	–	–	–
Sinusitis	1	2	–	–	–	–
Skin wound	1	2	–	–	–	–
Tinnitus	1/	2	–	–	–	–
Bacteruria	–		1	2	–	–
Cough	–	–	1	2	–	–
Dry skin	–	–	1	2	–	–
Gastro-oesophageal reflux disease	–	–	1	2	–	–
Hypertension	–	–	1	2	–	–
Hypertensive crisis	–	–	1	2	–	–
Influenza	–	–	1	2	–	–
Inguinal hernia	–	–	1	2	–	–
Migraine	–	–	1	2	–	–
Peripheral swelling	–	–	1	2	–	–
Pyrexia	–	–	1	2	–	–
Sciatica	–	–	1	2	–	–
Skin irritation	–	–	1	2	–	–
Vertigo	–	–	1	2	–	–
Cervical radiculopathy	–	–	–	–	1	2
Cystitis	–	–	–	–	1	2
Epistaxis	–	–	–	–	1	2
Pulpitis dental	–	–	–	–	1	2
Urinary tract infection	–	–	–	–	1	2

Adverse events of polymyalgia rheumatica are reported separately as loss of efficacy. Data are the number/percent of participants who experienced an event or type of event.

Safety of clofutriben

TEAEs (Table 3) were mild or moderate in severity. There were no serious TEAEs. The investigational drug was withdrawn due to TEAEs from 2 participants who received P10C, two who received P10, and one who was noncompliant with prednisolone (before receiving clofutriben). Numerically, more mild, nonserious infections occurred with clofutriben, even when higher prednisolone doses were given. Androgens increased with clofutriben (Supplementary Table S18, Supplementary Fig S18) with testosterone levels above the reference range in 5 of 26 females. No TEAEs suggestive of hyperandrogenism were reported.

Clofutriben pharmacology

In hepatocytes, sequential actions of 5- and 3-steroid dehydrogenases form metabolites from cortisol and cortisone that are rapidly excreted in urine. The ratio cortisol metabolites: cortisone metabolites in urine is a biomarker of the cortisol:cortisone ratio in the liver. An HSD-1 inhibitor should substantially reduce that ratio. Urinary HSD-1 ratios in participants who received P10 were elevated compared to observations in adults who received no GC [14] (Supplementary Fig S19), unsurprisingly as GCs are understood to induce HSD-1 [1]. Pooled results for clofutriben-containing regimens showed a decrease of about 90%, consistent with full HSD-1 inhibition, in most participants. In renal tubule epithelium, HSD-2 regulates the ratio cortisone: cortisol, both of which can diffuse into urine. A selective HSD-1 inhibitor should not alter that ratio much. The urinary HSD-2 ratio decreased by about 20% with clofutriben. Serum levels of the HSD-1 substrate cortisone increased with clofutriben (Supplementary Fig S17).

Without prednisolone formation by fully inhibited HSD-1, increased clearance of prednisolone was observed with clofutriben (Supplementary Fig S20). No effect on the absorption of

prednisolone was apparent. Prednisone (HSD-1 substrate) levels increased with clofutriben. Levels of clofutriben and its metabolite AS2570469 showed some cohort-to-cohort variability, but without an apparent relationship to prednisolone dose.

DISCUSSION

GCs are a mainstay of treatment across multiple areas of medicine. While effective without question, they have the potential to induce severe side effects. Clinical practice is to minimise GC dose and duration. Many patients with rheumatic disease require chronic GC to achieve disease control despite the availability of targeted therapies [23–25]. Among multiple attempts to develop GC with a better safety profile, only topical administration (including modified-release budesonide for selective gastrointestinal delivery) that limits systemic exposure has been successful. Locally administered GCs show reduced, yet significant, morbidity and cannot benefit patients with PMR or other systemic diseases.

HSD-1 inhibitors can prevent GC-related toxicity. Patients with tumour-associated hypercortisolism, but deficient in HSD-1, did not show signs/symptoms of Cushing's syndrome [4–6]. HSD-1 knockout mouse did not develop corticosterone-induced osteopenia, hyperlipidaemia, hyperglycaemia, hypertension, skeletal myopathy, dermal atrophy, or trabecular bone loss [7,26]. HSD-1 inhibitors (including clofutriben) prevented corticosterone-induced hyperphagia, weight gain, increased adiposity, hyperglycaemia, skeletal myopathy, impaired wound healing, epidermal atrophy, and ocular hypertension [9–11]. An open-label trial of an HSD-1 inhibitor in patients with mild endogenous hypercortisolism showed modest clinical benefits [12]. In a placebo-controlled 7-day trial of an HSD-1 inhibitor with prednisolone 20 mg/d in healthy adults, adverse effects on bone, blood glucose, blood lipids, and blood pressure were observed only in participants randomised to placebo [13].

We build on this foundation for HSD-1 inhibitors with this report that clofutriben not only prevented but also reversed several toxicity biomarkers in patients treated with prednisolone. At trial entry, participants had abnormalities on biomarkers of bone mineralisation (osteocalcin), bone deposition (PINP), bone resorption (CTX), lipid metabolism (triglycerides), hypercoagulability (APTT), and hypothalamic-pituitary-adrenal axis suppression (morning serum cortisol) plausibly related to prior GC exposure. None worsened with prednisolone 10 mg for 2 additional weeks. That no effect was observed on some parameters of prednisolone toxicity was not surprising. For example, prothrombin time and international normalised ratio was expected to be less sensitive for GC-associated hypercoagulability [27]. Notable biomarker improvements were observed with coadministration of prednisolone with clofutriben for 2 further weeks, including individual clinically relevant shifts such as from elevated to normal triglyceride levels. About one-third of participants at baseline and the end of prednisolone 10 mg were at high risk for adrenal insufficiency. GC-associated adrenal insufficiency can lead to, rarely, adrenal crisis and, very rarely, sudden death. It often resolves only over months or longer. Cortisol improvement with clofutriben occurred in only 2 weeks. Longer-term outcomes, e.g., bone mineral density, should be evaluated in larger trials.

HSD-1 inhibitors showed no impact of GC-induced suppression of neutrophil maturation [28] or T cell inflammatory cytokine release [29] *in vitro*. Knockout mouse clinical outcomes in challenge models have been mostly similar to control (thioglycollate-induced peritonitis, carrageenan-induced pleurisy, standard-dose K/BxN serum transfer arthritis) [30] or superior (coronary artery ligation [31], lipopolysaccharide-induced sickness behaviour [32]), despite apparently adverse molecular/cellular phenotypes, in a knockout mouse. Dose-response relationship shifts have been reported. Reduced-dose K/BxN serum transfer was associated with worse clinical outcomes in knockout mouse [30]. Corticosterone 100 μg/mL prevented synovitis and joint destruction in tumour necrosis factor transgenic mouse, but not when crossed with HSD-1 knockout. Corticosterone 50 μg/mL in the transgenic (non-HSD-1-knockout) also did not prevent damage [8]. HSD-1 knockout showed a similar effect as a 50% corticosterone dose reduction. Most prednisolone effects on inflammatory biomarkers in healthy adults were maintained under HSD-1 inhibition [13].

Results of this trial show that HSD-1 inhibition shifts the prednisolone dose-response relationship for PMR disease control. Participants for this trial were required to have stable disease activity while taking prednisolone 10 mg (P10), confirmed by no or limited mean changes during 2 additional weeks on symptoms, physical function, and inflammation biomarkers. When clofutriben was added without a prednisolone dose increase (P10C), there was a clear loss of efficacy. Five participants experienced relapse requiring a prednisolone dose increase. Participants reported more intense symptoms and additional physical disability. Inflammation biomarker levels rose. Dose increases in prednisolone resolved loss of clinical efficacy. With P20C and P30C, mean changes in symptoms and physical function were indistinguishable from those of P10.

Changes in inflammation biomarkers partially resolved with prednisolone dose increase, but clear molecular/cellular differences of the immune system state compared to P10 were apparent. Whether observed differences of cytokines (BAFF, CXCL10, IL-2RA, IL-6) and lymphocytes between P10 and P20C/P30C groups are clinically significant is unknown. Those differences had no relevant clinical impact in this short-term trial, as in animal studies. Longer, larger trials are needed to learn what happens to molecular/cellular immune biomarkers with longer prednisolone/clofutriben coadministration and whether the combination of prednisolone and clofutriben is appropriate for chronic use.

Some results can be understood as a reversal of the known effects of prednisolone by clofutriben and suggest that HSD-1 mediates additional effects of GC. Dexamethasone has a bradycardic effect in healthy adults [33]. Heart rate increases observed with clofutriben were similar in magnitude to the decrease observed with dexamethasone; clofutriben might have fully reversed heart rate suppression by prednisolone. The cholesterol decrease associated with clofutriben was of HDL. GCs have been associated with HDL increase [33]. The GC receptor antagonist mifepristone was associated with similar HDL decreases, which were interpreted as not clinically detrimental [34]. GCs suppress lymphocyte extravasation via diverse mechanisms [35]. Relative lymphopenia associated with clofutriben could represent reversal of one or more of those GC effects. Speculatively, more lymphocytes might reach tissue inflammation sites as, mostly without adverse outcomes, in animal models. Whether these effects of clofutriben are beneficial, neutral, or detrimental should be studied in longer, larger trials.

Combinations of clofutriben with prednisolone were generally well tolerated in patients with PMR. More infections, mainly mild upper respiratory, were reported by participants during clofutriben treatment. Clofutriben [14] and other HSD-1 inhibitors [36] cause ACTH increases and, consequently, androgen increases. In this trial, some female participants had testosterone

levels above the reference range, but not to a level that in isolation would cause endocrine concern. No related clinical effects were reported. Both aspects of clofutriben safety should continue to be monitored in longer, larger trials.

Notable strengths of this trial include its design for its specific purposes—to learn whether combinations of prednisolone with clofutriben could achieve similar efficacy and less toxicity compared to prednisolone alone and, if so, estimate how the prednisolone dose should be adjusted to achieve a favourable benefit-risk profile. Those learning objectives were achieved through iterative experimentation with inductive protocol-driven treatment decisions. That participants received both treatments in sequence enabled such inference in a smaller trial, compared to a parallel group design. The core disease-related outcomes were aligned with a domain framework derived from patient and clinician input [37]. Clinically relevant outcomes related to multiple domains of GC-associated toxicity and general drug safety were collected, as were comprehensive physiologic outcomes related to clofutriben's mechanism of action.

This trial has some limitations to consider. Order of treatments could not be randomised due to clofutriben's long pharmacological half-life [14]. A washout of months is needed to follow clofutriben treatment with a placebo. Investigators could not be blinded as the order of treatments could not be masked in the protocol. As designed, the first treatment period served as a placebo run-in to confirm participants' clinical stability. While it is not possible to prove that unblinded investigators had no subconscious impact on the symptoms and physical function responses of blinded participants, at least for symptoms, this potential risk was mitigated by primary reliance on daily at-home surveys, which would be less subject to such confounding. The trial's limited duration and size might have influenced results on domains for which clofutriben did not show benefit. Morning oral glucose tolerance test is not sensitive to P10 [38]; hence, no toxicity to reverse/prevent could be expected. Twice-daily blood pressure measurements over multiple days were tried to detect changes in diurnal amplitude instead of 24-hour ambulatory monitoring, which is burdensome to participants. That some participants took prior-to-bed measurements within 2 hours of typical dinner time might have confounded the results with postprandial blood pressure increases. The decision to continue prednisolone as prescribed medication rather than as trial medication led to loss of usable data (except for clofutriben safety) from 4 participants: 2 who had prescriptions for prednisone (a prodrug that requires HSD-1 for activation to prednisolone) and 2 who, on their own, took regimens other than prednisolone 10 mg daily.

We demonstrated proof-of-concept for the hypothesis that clofutriben favourably shifts the dose-response curves for safety of prednisolone further than those for efficacy, such that dose increases in prednisolone could restore disease control similarly to P10 alone, yet with a possible safety advantage. Dose range finding for prednisolone showed an improved benefit-risk profile for a fixed-dose combination of clofutriben with double the dose of prednisolone compared to prednisolone when dosed alone, at least for prednisolone 10 mg. Our results support additional trials of that combination, across a wider dose range for patients with systemic rheumatic and other inflammatory diseases. Perhaps paradoxically after 75 years of clinical practice to limit glucocorticoid dose, such trials would compare prednisolone alone to a combination of clofutriben and a higher prednisolone dose.

Competing interests

FB, PMS, and KD were consultants in Sparrow Pharmaceuticals. AE and HLK had no competing interest. IA was consultant in Amgen, BI, Chugai Pharma, Galapagos, Lilly, Novartis, Pfizer, SOBI, Takeda, UCB; speaker in AbbVie, Chugai, Gilead, Lilly, MSD, Novartis, Pfizer, SOBI, UCB. FS was consultant in AbbVie, Galapagos, Lilly, Novartis, Sanofi; speaker in AbbVie, Galapagos, Lilly, Novartis, Sanofi; and received research support from AbbVie, Galapagos, Lilly, Novartis, Sanofi. CW was consultant in AbbVie, Bristol-Myers Squibb, Novartis, Ono Pharmaceutical, Boehringer-Ingelheim, Sparrow Pharmaceuticals. PAM was consultant in AbbVie, Alpine, Amgen, ArGenx, AstraZeneca, Boehringer-Ingelheim, Bristol-Myers Squibb, CSL Behring, GlaxoSmithKline, iCell, Interius, Kinevant, Kyverna, Metagenomia, Neutrolis, Novartis, NS Pharma, Q32, Quell, Regeneron, Sanofi, Sparrow, Takeda, Vistera; received research support from AbbVie, Amgen, AstraZeneca, Boehringer-Ingelheim, Bristol-Myers Squibb, Eicos, Electra, GlaxoSmithKline, Neutrolis, Takeda; Stock options: Kyverna, Q32, Lifordi, Neutrolis, Sparrow Pharmaceuticals; Royalties: UpToDate. CD was consultant in AbbVie, Novartis, Sparrow Pharmaceuticals, Roche, Sanofi, Janssen, Boehringer; speaker: AbbVie, Pfizer, Lilly, AlfaSigma, Novartis, Roche, Sanofi; and received research support from AbbVie. FSC and DAK were employees in Sparrow Pharmaceuticals; stock from Sparrow Pharmaceuticals. Sparrow Pharmaceuticals' roles included funding, trial design, safety monitoring, data collection, analysis, and interpretation, the decision to publish, and manuscript preparation.

Acknowledgements

The authors are grateful to the patients who volunteered based only on the hope that they might help future patients like themselves, and to our colleagues at Sparrow Pharmaceuticals, trial sites, and partner organisations who made trial operations possible. Eva Fernandez generated figures and tables. Claire Hodgkinson provided word processing support.

Contributors

PMS and DAK were responsible for conceptualisation. CW, PMS, PAM, CD, FSC, and DAK were responsible for methodology. FB, AE, IA, HLK, FS, FSC, KD, and DAK were responsible for investigation. FB, KD, and DAK were responsible for formal analysis. FB, CW, PMS, PAM, CJ, FSC, KD, and DAK were responsible for interpretation. FB and DAK were responsible for writing – original draft. All authors had access to the data and participated in the development, review, approval, and decision to submit this manuscript for publication. No honoraria or payments were made for authorship.

Funding

Sparrow Pharmaceuticals Inc. provided financial support, administrative support, article publishing charges, and statistical analysis. DAK reports a relationship with Sparrow Pharmaceuticals Inc that includes: employment, equity or stocks, and nonfinancial support. FSC reports a relationship with Sparrow Pharmaceuticals Inc that includes: employment, equity or stocks, and nonfinancial support. PAM reports a relationship with Sparrow Pharmaceuticals Inc that includes: equity or stocks. DAK has patent issued to Sparrow Pharmaceuticals.

Patient consent for publication

All patients consented to scientific publications and presentations that do not permit them to be directly identified.

Ethics approval

The protocol was approved by Bundesinstitut für Arzneimittel und Medizinprodukte (#4045419) and Ethik-Kommission des Landes Berlin (#22/076-IV-E).

Provenance and peer review

Not commissioned; externally peer reviewed.

Data availability statement

Participants did not consent for deposit of the underlying data in a public repository.

Supplementary materials

Supplementary material associated with this article can be found in the online version at doi:10.1016/j.ard.2025.10.015.

Orcid

David A. Katz: http://orcid.org/0000-0002-4400-5669

REFERENCES

[1] Tomlinson JW, Walker EA, Bujalska IJ, Draper N, Lavery GG, Cooper MS, et al. 11b-hydroxysteroid dehydrogenase type 1: a tissue-specific regulator of glucocorticoid response. Endocr Rev 2004;25:831–66.
[2] Basu R, Singh RJ, Basu A, Chittilapilly EG, Johnson CM, Toffolo G, et al. Splanchnic cortisol production occurs in humans: evidence for conversion of cortisone to cortisol via the 11b-hydroxysteroid Dehydrogenase (11 -HSD) type 1 pathway. Diabetes 2004;53:2051–9.
[3] Andrew R, Westerbacka J, Wahren J, Yki-Järvinen H, Walker BR. The contribution of visceral adipose tissue to splanchnic cortisol production in healthy humans. Diabetes 2005;54:1364–70.
[4] Tomlinson JW, Draper N, Mackie J, Johnson AP, Holder G, Wood P, et al. Absence of cushingoid phenotype in a patient with Cushing's disease due to defective cortisone to cortisol conversion. J Clin Endocrinol Metab 2002;87:57–62.
[5] Arai H, Kobayashi N, Nakatsuru Y, Masuzaki H, Nambu T, Takaya K, et al. A case of cortisol producing adrenal adenoma without phenotype of cushing's syndrome due to impaired 11β-hydroxysteroid dehydrogenase 1 activity. Endocr J 2008;55:709–15.
[6] Weber RJ, Kawaja C, Wallerstein R, Kunwar SM, Liu C. Impaired 11β-HSD1 activity in a male patient with cushing disease resulting in lack of the full cushingoid phenotype. JCEM Case Rep 2024;2:luae158.
[7] Morgan SA, McCabe EL, Gathercole LL, Hassan-Smith ZK, Larner DP, Bujalska IJ, et al. 11β-HSD1 is the major regulator of the tissue-specific effects of circulating glucocorticoid excess. Proc Natl Acad Sci USA 2014;111:E2482–91.
[8] Fenton C, Martin C, Jones R, Croft A, Campos J, Naylor AJ, et al. Local steroid activation is a critical mediator of the anti-inflammatory actions of therapeutic glucocorticoids. Ann Rheum Dis 2021;80:250–60.
[9] Song Z, Gong Y, Liu H, Ren Q, Sun X. Glycyrrhizin could reduce ocular hypertension induced by triamcinolone acetonide in rabbits. Mol Vis 2011;17:2056–64.
[10] Morgan SA, Hassan-Smith ZK, Doig CL, Sherlock M, Stewart PM, Lavery GG. Glucocorticoids and 11β-HSD1 are major regulators of intramyocellular protein metabolism. J Endocrinol 2016;229:277–86.
[11] Tiganescu A, Hupe M, Uchida Y, Mauro T, Elias PM, Holleran WM. Topical 11β-hydroxysteroid dehydrogenase type 1 inhibition corrects cutaneous features of systemic glucocorticoid excess in female mice. Endocrinology 2018;159:547–56.
[12] Oda S, Ashida K, Uchiyama M, Sakamoto S, Hasuzawa N, Nagayama A, et al. An open-label phase I/IIa clinical trial of 11β-HSD1 inhibitor for Cushing's syndrome and autonomous cortisol secretion. J Clin Endocrinol Metab 2021;106:e3865–80.
[13] Othonos N, Pofi R, Arvaniti A, White S, Bonaventura I, Nikolaou N, et al. 11β-HSD1 inhibition in men mitigates prednisolone-induced adverse effects in a proof-of-concept randomised double-blind placebo-controlled trial. Nat Commun 2023;14:1025.
[14] Bellaire S, Walzer M, Wang T, Krauwinkel W, Yuan N, Marek GJ. Safety, pharmacokinetics, and pharmacodynamics of ASP3662, a novel 11β-hydroxysteroid dehydrogenase type 1 inhibitor, in healthy young and elderly subjects. Clin Transl Sci 2019;12:291–301.
[15] Pan X, Hou Q, Su J, Xu J, Li M, Li J, et al. The 11β-hydroxysteroid dehydrogenase type 1 inhibitor SPI-62 prevents morbidity in a mouse model of Cushing's syndrome. bioRxiv 2024. https://www.biorxiv.org/content/10.1101/2024.05.27.596076v1.
[16] Dasgupta B, Cimmino MA, Maradit-Kremers H, Schmidt WA, Schirmer M, Salvarani C, et al. 2012 provisional classification criteria for polymyalgia rheumatica: a European League Against Rheumatism/American College of Rheumatology collaborative initiative. Ann Rheum Dis 2012;71:484–92.
[17] Wu N, Katz DA, An G. Population target-mediated pharmacokinetic/pharmacodynamic modeling to evaluate SPI-62 exposure and hepatic 11β-hydroxysteroid dehydrogenase type 1 (HSD-1) inhibition in healthy adults. Clin Pharmacokinet 2023;62:1275–88.
[18] Katz DA, Methods for administering corticosteroids. US Patent 12, 220, 412 https://patents.google.com/patent/US12220412B2/en?oq=us12220412.
[19] Fries JF, Spitz P, Kraines RG, Holman HR. Measurement of patient outcome in arthritis. Arthritis Rheum 1980;23:137–45.
[20] Lund B, Egsmose C, Jørgensen S, Krogsgaard MR. Establishment of the relative antiinflammatory potency of deflazacort and prednisone in polymyalgia rheumatica. Calcif Tissue Int 1987;41:316–20.
[21] Thiele K, Albrecht K, Alexander T, Aringer M, Eidner T, Henes J, et al. National database of the German Collaborative Arthritis Centres—Trends in health care provision 2024. German Rheumatism Research Centre Berlin. https://refubium.fu-berlin.de/bitstream/handle/fub188/45498/National_-Database_Trends_2024.pdf
[22] Beuschlein F, Else T, Bancos I, Hahner S, Hamidi O, van Hulsteijn L, et al. European Society of Endocrinology and Endocrine Society Joint Clinical Guideline: Diagnosis and therapy of glucocorticoid-induced adrenal insufficiency. Eur J Endocrinol 2024;190:G25–51.
[23] Floris A, Piga M, Chessa E, Congia M, Erre GL, Angioni MM, et al. Long-term glucocorticoid treatment and high relapse rate remain unresolved issues in the real-life management of polymyalgia rheumatica: a systematic literature review and meta-analysis. Clin Rheumatol 2022;41:19–31.
[24] Palmowski A, Nielsen SM, Boyadzhieva Z, Schneider A, Pankow A, Hartman L, et al. Safety and efficacy associated with long-term low-dose glucocorticoids in rheumatoid arthritis: a systematic review and meta-analysis. Rheumatology 2023;62:2652–60.
[25] Palmowski A, Pankow A, Terziyska K, Nielsen SM, Christensen R, Bliddal H, et al. Continuing versus tapering low-dose glucocorticoids in patients with rheumatoid arthritis and systemic lupus erythematosus in states of low disease activity or remission: a systematic review and meta-analysis of randomised trials. Semin Arthritis Rheum 2024;64:152349.
[26] Fenton CG, Doig CL, Fareed S, Naylor A, Morrell AP, Addison O, et al. 11β-HSD1 plays a critical role in trabecular bone loss associated with systemic glucocorticoid therapy. Arthritis Res Ther 2019;21:188.
[27] van Zaane B, Nur E, Squizzato A, Gerdes VE, Büller HR, Dekkers OM, et al. Systematic review on the effect of glucocorticoid use on procoagulant, anti-coagulant and fibrinolytic factors. J Thromb Haemost 2010;8:2483–93.
[28] Freeman L, Hewison M, Hughes SV, Evans KN, Hardie D, Means TK, et al. Expression of 11β-hydroxysteroid dehydrogenase type 1 permits regulation of glucocorticoid bioavailability by human dendritic cells. Blood 2005;106:2042–9.
[29] Zhang TY, Ding X, Daynes RA. The expression of 11β-hydroxysteroid dehydrogenase type I by lymphocytes provides a novel means for intracrine regulation of glucocorticoid activities. J Immunol 2005;174:879–89.
[30] Coutinho AE, Gray M, Brownstein DG, Salter DM, Sawatzky DA, Clay S, et al. 11β-hydroxysteroid dehydrogenase type 1, but not type 2, deficiency worsens acute inflammation and experimental arthritis in mice. Endocrinology 2012;153:234–40.
[31] McSweeney SJ, Hadoke PW, Kozak AM, Small GR, Khaled H, Walker BR, et al. Improved heart function follows enhanced inflammatory cell recruitment and angiogenesis in 11bHSD1-deficient mice post-MI. Cardiovasc Res 2010;88:159–67.
[32] Verma M, Kipari TMJ, Zhang Z, Man TY, Forster T, Homer NZM. 11β-hydroxysteroid dehydrogenase-1 deficiency alters brain energy metabolism in acute systemic inflammation. Brain Behav Immun 2018;69:223–34.

[33] Brotman DJ, Girod JP, Garcia MJ, Patel JV, Gupta M, Posch A, et al. Effects of short-term glucocorticoids on cardiovascular biomarkers. J Clin Endocrinol Metab 2005;90:3202–8.
[34] Zemskova M. FDA Clinical Review of NDA. 202107:2012. https://www.accessdata.fda.gov/drugsatfda_docs/nda/2012/202107Orig1s000MedR.pdf
[35] Cain DW, Cidlowski JA. Immune regulation by glucocorticoids. Nat. Rev. Immunol. 2017;17:233–47.
[36] Liu W, Katz DA, Locke C, Daszkowski D, Wang Y, Rieser MJ, et al. Clinical safety, pharmacokinetics, and pharmacodynamics of the 11β-hydroxysteroid dehydrogenase type 1 inhibitor ABT-384 in healthy volunteers and elderly adults. Clin Pharmacol Drug Dev 2013;2:133–51.
[37] Mackie SL, Twohig H, Neill LM, Harrison E, Shea B, Black RJ, et al. The OMERACT core domain set for outcome measures for clinical trials in polymyalgia rheumatica. J Rheumatol 2017;44:1515–21.
[38] Kauh E, Mixson L, Malice MP, Mesens S, Ramael S, Burke J, et al. Prednisone affects inflammation, glucose tolerance, and bone turnover within hours of treatment in healthy individuals. Eur J Endocrinol 2012;166:459–67.
[39] Buttgereit F, Everding A, Andreica I, Kellner HL, Schuch F, Weyand C, et al. OP0058 Effects of clofutriben, a selective 11ß-hydroxysteroid dehydrogenase type 1 inhibitor, on efficacy and toxicity of prednisolone in patients with polymyalgia rheumatica. Ann Rheum Dis 2025;84(Suppl 1):51.

Ann Rheum Dis 85 (2026) 932–941

Contents lists available at ScienceDirect

Annals of the Rheumatic Diseases

journal homepage: https://www.sciencedirect.com/journal/annals-of-the-rheumatic-diseases

Autoinflammatory disorders

A germline IκBα mutation outside the signal reception domain blocks nuclear translocation of NFκB1 and associates with autoinflammation-like features

Abdulwahab Elsayed[1,2,a], Ignatius Ryan Adriawan[1,2,a], Faranaz Atschekzei[1,2], Natalia Dubrowinskaja[1,2], Manfred Anim[1], Fabian Hauck[3], Ulrich Baumann[4], Torsten Witte[1,2], Georgios Sogkas[1,2,*]

[1] *Department of Rheumatology and Immunology, Hannover Medical School, Hannover, Germany*
[2] *Hannover Medical School, Cluster of Excellence RESIST (EXC 2155), Hannover, Germany*
[3] *Division of Pediatric Immunology and Rheumatology, Department of Pediatrics, Dr. von Hauner Children's Hospital, Ludwig-Maximillians-Universität München, Munich, Germany*
[4] *Department of Pediatric Pneumology, Allergy and Neonatology, Hannover Medical School, Hannover, Germany*

ARTICLE INFO

Article history:
Received 24 April 2025
Received in revised form 8 August 2025
Accepted 8 August 2025

ABSTRACT

Objectives: IκBα controls the canonical activation of NFκB. IκBα gain-of-function due to *NFKBIA* variants affecting the N-terminus of IκBα—especially residues 32 and 36—manifests with combined immunodeficiency. The role of *NFKBIA* variants affecting other IκBα domains has not been described.

Methods: Variants in *NFKBIA* were identified using whole-exome sequencing. IκBα expression has been quantified by flow cytometry and Western blotting. Activation-induced IκBα degradation, NFκB1 activation, and nuclear translocation as well as inflammasome activity were evaluated.

Results: The p.Gln228* variant in *NFKBIA*, identified in a family with a history of arthritis and psoriasis, did not affect induced degradation of IκBα. Its expression in HEK293T cells confirmed its truncating effect and revealed reduced NFκB activation. Similar to transfected HEK293T cells, peripheral blood mononuclear cells from patients harbouring the p.Gln228* variant displayed substantially reduced nuclear levels of NFκB1 p50. The latter findings suggest that the p.Gln228* variant causes a functional insufficiency of NFκB1. Similar to patients with NFκB1 haploinsufficiency, high serum levels of interleukin (IL)-18, as well as enhanced induced apoptosis-associated speck-like protein containing a caspase recruitment domain speck formation and IL-1β secretion *in vitro*, suggest enhanced inflammasome activation.

Conclusions: *NFKBIA* variants not localising to the signal reception domain can affect IκBα function and consequently restrict the canonical activation of NFκB. In contrast to the phenotype of N-terminal variants, which is dominated by combined immunodeficiency, the here-reported C-terminal deletion of IκBα was identified in patients with autoinflammatory arthritis and psoriasis.

*Correspondence to Dr. Georgios Sogkas, Department of Rheumatology and Immunology, Hannover Medical School, Hannover, Germany.
E-mail address: sogkas.georgios@mh-hannover.de (G. Sogkas).
Handling editor Josef S. Smolen.
[a] Abdulwahab Elsayed and Ignatius Ryan Adriawan contributed equally to this work.

https://doi.org/10.1016/j.ard.2025.08.010

WHAT IS ALREADY KNOWN ON THIS TOPIC

- Germline monoallelic variants in *NFKBIA* affecting the signal response domain of IκBα cause severe immunodeficiency.

WHAT THIS STUDY ADDS

- *NFKBIA* variants affecting the C-terminus of IκBα can cause inflammatory arthritis, mimicking psoriatic arthritis, by affecting NFκB activation and enhancing inflammasome activation.

HOW THIS STUDY MIGHT AFFECT RESEARCH, PRACTICE OR POLICY

- Patients with well-classifiable rheumatic disorders might have an underlying inborn error of immunity leading to enhanced inflammasome activation.
- Identification of inflammasomopathies in patients with rheumatic disorders can lead to personalised treatment targeting interleukin (IL)-1 or IL-6.

INTRODUCTION

In resting cells, the inhibitor of NFκB α (IκBα), encoded by the NFκB inhibitor alpha gene (*NFKBIA*), inhibits canonical NFκB activation by physical sequestration of p65 (RelA) and NFκB1-p50 in the cytosol [1]. On cell activation, the signal response domain of IκBα gets phosphorylated following the activation of the IκB kinases, resulting in its ubiquitin-dependent proteasomal degradation, which in turn enables the translocation of activated NFκB to the nucleus, enabling NFκB to modulate gene expression in the context of various biological functions, including processes related to inflammation and immunity. Polymorphisms in *NFKBIA* have been identified in genome-wide association studies to confer risk for rheumatic disorders, including rheumatoid arthritis and psoriatic arthritis [2,3]. Rare germline monoallelic variants in *NFKBIA* have been reported in the literature to have a gain-of-function effect by hampering ubiquitin-dependent degradation of IκBα, which consequently results in sequestration of NFκB in the cytosol [4]. Patients with IκBα gain-of-function display variable combined immunodeficiency as a consequence of compromised innate, cellular and humoral immunity. In addition, the majority of patients with IκBα gain-of-function have been reported to display ectodermal dysplasia [4,5]. Of the 25 described cases, 13 harboured variants localised at serine 32 or serine 36 of IκBα, while 5 additional gain-of-function variants were identified adjacent to the aforementioned serine residues (Gly33Val, Asp31Asn, Met37Lys, Met37Arg, Leu34Pro) [5–9]. Another subset of previously reported variants (Trp11*, Gln9*, and Glu14*) results in N-proximal truncation of IκBα, thereby skipping phosphorylable residues and causing IκBα gain-of-function. Immune dysregulation in IκBα gain-of-function includes eczema, psoriasis, arthritis, inflammatory bowel disease, and autoimmune endocrinopathies. While *NFKBIA* variants located at the signal reception domain have been well studied, the role and the possible functional consequences of variants located outside the N-terminus have not been investigated.

METHODS

Patient samples

Whole blood was collected in EDTA tubes (Sarstedt), and peripheral blood mononuclear cells (PBMCs) were isolated by diluting the blood 1:3 with Roswell Park Memorial Institute Medium (RPMI) 1640 (PAN-Biotech), layering it over a density gradient medium BioColl (Bio&SELL), and centrifuging at room temperature for 20 minutes without a break. Subsequently, PBMCs were collected, washed in complete RPMI medium (supplemented with 10% [v/v] fetal bovine serum [FBS] [Merck], 1% penicillin-streptomycin [Gibco], 1% L-glutamine [Gibco], and 1% sodium pyruvate 100 mM [Gibco]), and cryopreserved in FBS 10% (v/v) dimethyl sulfoxide (Santa Cruz) until further use. For serum samples, whole blood was collected in serum-gel tubes (Sarstedt). Serum was collected by centrifugation at 4°C for 10 minutes and stored at −80°C.

Genetic analysis

Blood samples were collected in the outpatient clinic for Rheumatology at the Hannover Medical School. Sample preparation, whole-exome sequencing (WES) analysis and the assessment of rare single-nucleotide variants (SNVs) were performed as described previously [10]. Briefly, for WES, genomic DNA was extracted from peripheral blood samples and sequenced on Illumina NextSeq 500 Sequencer using the IDT Exome (xGen, IDT). 150-bp paired-end reads were generated, aligned to the human reference genome (UCSC Genome Browser build GRCh37/hg19) and analysed with the next-generation sequencing (NGS) data analysis pipeline medical genetics Sequence Analysis Pipeline (megSAP v.0.2-8-ga9d80c2). Sample verification was performed by comparing NGS data to 14 single-nucleotide polymorphisms independently analysed by competitive allele-specific polymerase chain reaction. SNVs were filtered for genes associated with inborn errors of immunity (IEIs) according to the International Union of Immunological Societies Classification and classified following American College of Medical Genetics Standards and Guidelines [11,12]. Follow-up of SNVs was performed using databases Exome Aggregation Consortium 19, the 1000 Genomes Project and the genome Aggregation Database (gnomAD) for filtering for rare variants (≤1% minor allele frequency). For evaluation of pathogenicity, databases Leiden Open Variation Database and ClinVar and prediction tools including phyloP, SIFT, PolyPhen2, FATHMM, and CADD were used.

Plasmid construction, cloning, and transfection

Mutant *NFKBIA* plasmids were constructed through site-directed mutagenesis and conventional molecular cloning methods, using the wild-type *NFKBIA* sequence inserted into the pcDNA3.1(+) expression vector (GenScript) as the backbone. Human embryonic kidney 293 T (HEK293T) cells (ATCC) were cultured in high-glucose Dulbecco's Modified Eagle Medium (Merck) supplemented with 10% FBS, 1% penicillin-streptomycin (Gibco), 1% L-glutamine (Gibco), and 1% sodium pyruvate 100 mM (Gibco), at 37°C with 5% CO_2. For transfection, cells were plated in 6-well plates at a density of 5×10^5 cells per well and allowed to adhere overnight. The *NFKBIA* expressing plasmids were then transfected as Lipofectamine Transfection Reagent (Roche Diagnostics) according to the manufacturer's protocol. Plasmid DNA was mixed with Lipofectamine reagent in OptiMEM medium and incubated for 30 minutes at room temperature before adding it to the cells. After 24 hours, the transfected cells were washed and prepared for downstream assays or analyses. Transfection efficiency was evaluated using an enhanced green fluorescent protein (EGFP)-expressing control plasmid and confirmed through fluorescence microscopy. Cells were harvested 24 hours post-transfection for Western blot (WB) analysis.

Western blotting

PBMCs were thawed and plated in 6-well plates at a density of 1×10^6 cells per well and subsequently stimulated with phorbol 12-myristate (PMA) (50 ng/mL) and ionomycin (500 ng/mL) for 60 minutes. Proteins were isolated from lymphocytes of healthy volunteers and patients, as well as from transfected HEK293T cells, using NE-PER Nuclear and Cytoplasmic Extraction Reagents (Thermo Scientific). Protein concentration was determined for each sample/condition and protein samples were loaded onto 12% sodium dodecyl sulfate (SDS)-polyacrylamide gels (FastGene) in a 12-well format for electrophoretic separation. The separated proteins were transferred onto polyvinylidene difluoride membranes (Thermo Scientific) using blotting at 100 mA (constant current) for 90 minutes. The membranes were then blocked with 5% milk prepared in phosphate-buffered saline (PBS) with Tween detergent containing 0.1% Tween-20 for 60 minutes at room temperature and subsequently incubated with primary polyclonal rabbit antibody NFKBIA (Abcam), primary polyclonal rabbit antibody NFKB1 (Cell Signaling) or primary monoclonal rabbit antibody phospho NFKB (Cell Signaling) overnight at 4°C with gentle agitation. Afterwards, the membrane was washed 3 times with Tris-buffered saline (TBS) and incubated with a horseradish peroxidase (HRP)-conjugated goat anti-rabbit secondary antibody (Abcam) for 1 hour at room temperature. After incubation with the secondary antibody, the membranes were washed with TBS, and protein bands were visualised using enhanced chemiluminescence (Thermo Scientific SuperSignal West Dura Extended Duration Substrate) for 5 minutes. Images were captured using the Azure c300 imaging system with ROTI Lumin (Carl Roth). Beta-actin rabbit mAb HRP Conjugate (Cell Signaling) was used as a loading control, and densitometric analysis was conducted using ImageJ software.

IκBα degradation assay

Thawed PBMCs were rested for 2 hours in a 5% CO_2, 37°C incubator, plated in a 96-well plate at 200,000 cells/well density, and then stimulated with PMA and ionomycin (50 ng/mL and 500 ng/mL, respectively, both from Sigma-Aldrich), lipopolysaccharide (LPS) (from *Escherichia coli* O127:B1, 1 μg/mL, Sigma-Aldrich), or anti-IgM antibody (25 μg/mL, Sigma-Aldrich), as described previously [6]. After 30 minutes, cells were collected in fluorescence-activated cell sorting (FACS) tubes and washed with ice-cold FACS buffer (PBS + 2% FCS) at 4°C to stop the stimulation. After washing, Fc receptor blocking was performed with human immunoglobulin Octagam (Octapharma) at 4°C for 5 minutes, followed by surface staining with CD3/APC-Cy7, CD19/BV421, and eF506 fixable viability dye at 4°C for 30 minutes. Then, the cells were washed with FACS buffer and fixed with formaldehyde at 37°C for 10 minutes. Cells were once again washed with FACS buffer and permeabilised with Perm/Wash Buffer I (BD Biosciences). Cells were then stained with anti-IκBα/PE at room temperature for 1 hour, and then washed with FACS buffer. Data were acquired with FACSCanto II (Becton-Dickinson).

Phenotypic analyses of lymphocytes

PBMC were isolated from peripheral whole blood collected in sterile lithium heparin tubes. Phenotypic analyses were performed as multicolour immunofluorescence of PBMCs, using directly labelled monoclonal antibodies as described previously [13]. Briefly, 1×10^5 to 2×10^6 cells/well were incubated with murine monoclonal antibodies against the appropriate antigens at an optimal dilution for 20 minutes at 4°C. Nonspecific binding was eliminated by mixing the samples with a 1:5 solution of a commercial human IgG (Octagam, Octapharma). Samples were washed 3 times in PBS/bovine serum albumin (BSA), and at least 10^4 cells per appropriate gate were analysed. The following antibodies (all purchased from Biolegend, if not otherwise stated) were used for this study: CD3 PerCP (BD Pharmingen), CD3 PE-Cy7, CD3 BUV563 (BD Biosciences), abTCR BU711, abTCR APC, gdTCR BUV395 (BD Biosciences), CD4 APC-Cy7, CD4 PerCP, CD8 PE, CD8a Spark Blue 550, CD8b APC, CD16 FITC, CD19 BV510, CD21 PE, CD24 FITC, CD27 BUV661 (BD Biosciences), CD27 FITC, CD28 PE-Cy5, CD28 APC, CD31 FITC, CD38 PECy7, CD45 APC-Cy7, CD45RO PE-Dazzle 594, CD45RO BV421, CD45 BV785, CD45RA V500, CD56 BV421, CCR7 PE, HLA-DR APC, PD1 V500, IgD PE, IgM Alexa Fluor 647. Each flow cytometric analysis was controlled with appropriate isotype-matched antibodies. CD19+ cells in the lymphocyte gate were subdivided into the following subsets: naive B cells (IgD+, IgM+, CD27−), IgM+ memory B cells (CD27+, IgD+, IgM+), class-switched B cells (CD27+, IgD−, IgM−), plasmablasts (CD19+dim, CD27++, CD38++), transitional B cells (IgM++, CD38++,CD24+), CD21 low B cells (CD38 low, CD21 low). CD3+ cells in the lymphocyte gate were subdivided into the following subsets: naive CD4+ T cells (CD4+, CD45RA+), recent thymic emigrants (CD4+, CD45RA+, CD31+), $CD4^+$ memory T cells (CD4+, CD45RO+), follicular like CD4+ T cells (CD4+, CD45RO+, CCR5+), CD8+ early effector memory T cells (CD8+, CD27+, CD28-) and CD8+ late effector memory T cells (CD8+, CD27−, CD28−).

Secreted interleukin-1β and TNF-α ELISA for monocytes

PBMCs were obtained from the blood of healthy donors or patients. Monocytes were enriched by EasySep Magnet (STEMCELL) using EasySep Direct Human Monocyte Isolation Kit (STEMCELL) according to the manufacturer's protocol. Purified monocytes were seeded in 96-well plates at a density of 8×10^5 cells per well in RPMI 1640 medium (PAN-Biotech) supplemented with 10% FBS, 1% penicillin-streptomycin (Gibco), 1% Sodium pyruvate 100 mM (100 ×) (Gibco), and 1% L-glutamine (Gibco), as described previously [14]. Afterwards, monocytes were stimulated with LPS-SM (Invivogen) (500 ng/mL) for 18 hours followed by adenosine triphosphate (ATP) (Invivogen) stimulation (1 mM) for 1 hour, or only with LPS or ATP, or unstimulated. The supernatant was then carefully collected from each well, centrifuged at 4°C at 13,000 × g for 30 minutes, and then the supernatant was recollected and stored at −80°C until use. Enzyme-linked immunosorbent assay (ELISA) was performed with interleukin (IL)-1β (Bio-Techne) and tumor necrosis factor (TNF-α) (Bio-Techne) kits as per the manufacturer's instruction.

Apoptosis-associated speck-like protein containing a caspase recruitment domain speck visualisation by confocal microscope

Monocytes were enriched and stimulated as described for ELISA above. At the end of the stimulation, monocytes were collected in FACS tubes (by scrapping 3 times with ice-cold PBS), washed with FACS buffer at 4°C, fixed with paraformaldehyde 4%, permeabilised (BD Biosciences) with Perm/Wash-Triton (Bio-Rad) BSA (PBS-Triton 0.05%, Perm-Wash buffer 1 × [BD Biosciences], supplemented with 0.001% [w/v] bovine serum albumin), and stained with an antibody against the apoptosis-

associated speck-like protein containing a caspase recruitment domain (ASC) (Biomol) overnight at 4°C. After washing, the cells were stained with the secondary antibody (AlexaFluor 594 goat anti-rabbit IgG [Thermo Fisher Scientific]), and counterstained with 4,6-diamidino-2-phenylindole (DAPI) (Carl Roth). Cells were then immobilised on slides using Cytospin (1800 rpm for 6 minutes), air-dried, and mounted with Dako fluorescence mounting medium. ASC specks were visualised and images were captured using a Zeiss 980 Airyscan. Subsequently, ASC specks were counted with the ImageJ software.

Measurement of serum levels of IL-18

Serum samples, collected as indicated above, were cryopreserved for up to 4 weeks, thawed and serially diluted up to 1 in 50 with substrate reagent (Bio-Techne). IL-18 levels were measured with a human IL-18 ELISA kit (Bio-Techne) according to the manufacturer's instruction.

Patient and public involvement

Patients and/or the public were not involved in the design, or conduct, or reporting, or dissemination plans of this research.

Statistical analysis

For statistical calculation, we used GraphPad prism 9 (GraphPad). To evaluate differences between HEK293T cells transfected with either a plasmid expressing the full-length or the mutant IκBα, we employed t-test.

RESULTS

Case reports

Seven individuals from 3 unrelated families were identified to harbour monoallelic *NFKBIA* variants (Fig 1A,B, Supplementary Tables S1 and S2). In the first family (FamA), a variant predicted to cause a C-terminal truncation of IκBα segregated with inflammatory disease. The index patient (P2) is a currently 58-year-old male with seronegative erosive chronic polyarthritis diagnosed at the age of 17 years (Fig 1C). Therapeutic regimens that he has received so far included oral corticosteroids, diverse conventional synthetic as well as biological (etanercept, adalimumab, tocilizumab) and targeted-synthetic (baricitinib, tofacitinib) disease-modifying antirheumatic drugs (DMARDs). Compared to all other DMARDs, tocilizumab was most effective in controlling arthritis, though synovial flares necessitated intermittent prednisolone pulses. At the age of 56 years, he was diagnosed with psoriasis vulgaris. Despite hypogammaglobulinaemia, which developed during treatment with antirheumatic drugs and steroids, his infection record has remained so far inconspicuous. His father (P1) had also a history of chronic polyarthritis and eczema. He was diagnosed at the age of 68 with laryngeal cancer and died at the age of 74 years of lung cancer. The daughter of P2 (P3) had intermittent arthralgia since her late childhood and was diagnosed with seronegative arthritis, enthesitis (Fig 1C) and plantar fasciitis at the age of 29 years, which in view of her father's psoriasis was classified as psoriatic arthritis. In both the 2 other families, *NFKBIA* variants affected the serine 36 residue. P4, a female infant, died at 148 days of age from severe encephalopathy that developed after haematopoietic stem cell transplantation. She was born to consanguineous parents of Southern Slavic ancestry and had severe recurrent infections since the first month of life, leading to the diagnosis of IκBα gain-of-function. P5 to P7 were previously reported [6]. Briefly, all 3 patients displayed recurrent pneumonias, bronchiectasis (Fig 1C), and warts. In addition, P5 had a treatment-refractory rheumatoid factor-positive polyarticular juvenile idiopathic arthritis.

Intact induced proteasomal degradation in case of the p.Gln228 variant*

To evaluate the impact of the c.682C>T, p.(Gln228*) variant in *NFKBIA* (NM_020529) on IκBα expression, we performed WB analysis with PBMC samples from P2 and P3. This revealed a truncated IκBα with a molecular mass of approximately 25 kDa, in accordance with the predicted premature stop codon (Fig 1D). The truncating effect of identified variant was also confirmed in HEK293T cells transfected with a plasmid expressing the EGFP-fused full-length or mutant IκBα (Fig 1E). In view of the fact that all so far reported deleterious variants in *NFKBIA* affected the activation-induced degradation [4–9], we employed an IκBα degradation assay to compare cells from the patients harbouring the Gln228* variant with cells from patients with variants replacing serine 36 (Fig 1F). As expected, the latter variants (p.Ser36Ala and p.Ser36Pro) almost abrogated IκBα degradation, as reflected by the unaffected IκBα expression in cells treated with different NFκB activating stimuli (PMA and ionomycin, anti-IgM, LPS). On the other hand, the truncation variant p.Gln228* had no effect on IκBα degradation in all 3 tested cell types (B cells, T cells, and monocytes).

The p.Gln228 variant causes a functional NFκB1 insufficiency*

To test the effect of the wild-type vs. truncated p.Gln228*-IκBα on NFκB1 activation, we evaluated cytoplasmic vs. nuclear expression of the NFκB1 p105/p50 subunits in HEK293T cells transfected to express either the wild-type or the p.Gln228*-IκBα (Fig 2A-D). P.Gln228*-IκBα expressing cells displayed significantly higher cytoplasmic expression of p50, while nuclear p50 expression was substantially reduced. This finding suggests a stronger inhibitory effect of the mutant p.Gln228*-IκBα on NFκB1 activation, that is, a functional NFκB1 insufficiency. HEK293T cells transfected to express the p.Ser36Ala-IκBα, which causes IκBα gain-of-function by abrogating its induced proteasomal degradation, displayed a similar reduction in nuclear p50 expression. However, in contrast to p.Gln228*-IκBα expressing cells, cytoplasmic levels of p50 were similar to the wild-type-IκBα transfected cells, suggesting the differential effect of the p.Gln228* variant vs. those that abrogate induced proteasomal degradation on NFκB1 activation. Given the latter effect of the p.Gln228*-IκBα in HEK293T cells, we tested PBMCs from patients harbouring the c.682C>T, p.Gln228* variant (ie, P2 and P3), patients with frameshift mutations in *NFKB1* causing haploinsufficiency of the NFκB1 subunit p50 (P9 to P11, Fig 3A and Supplementary Table S2) and healthy blood donors. Tested patients with NFκB1 haploinsufficiency harboured either the c.236_239del, p.(Lys79Serfs*47) (family D) or the c.1012delT, p.(Ser338Leufs*94) variant (family E) in *NFKB1* (NM_003998.4). The latter variant has been reported previously [15,16]. Similar to the previous finding in p.Gln228*-IκBα expressing HEK293T cells, this analysis revealed a substantial reduction in nuclear p50 levels in both patients with the c.682C>T, p.Gln228* variant in *NFKBIA* as well as in patients with NFκB1 haploinsufficiency, which was more prominent in

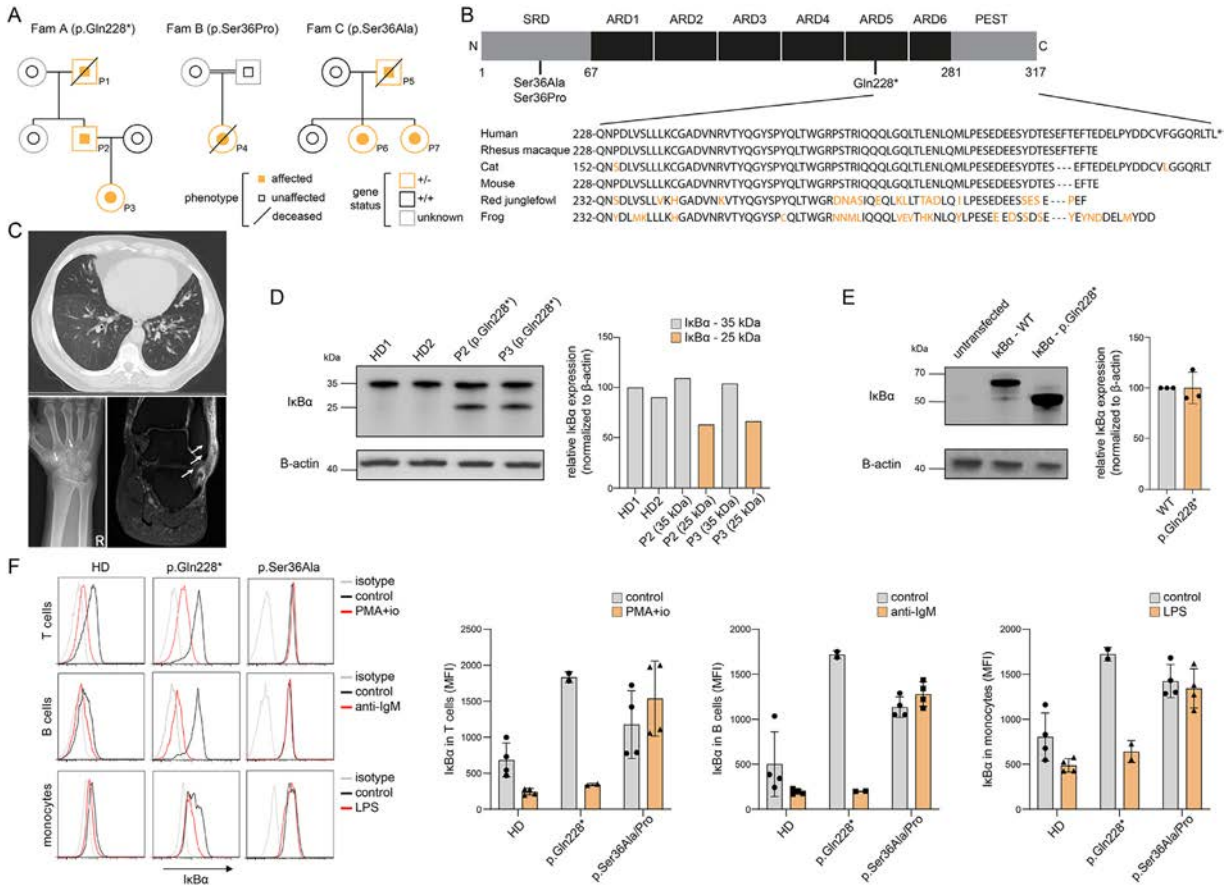

Figure 1. (A) Pedigrees highlighting patients or unaffected family members who were subjected to whole-exome sequencing and were identified with *NFKBIA* variants. Gene status refers to variant indicated in the header of each pedigree, '±' indicates heterozygosity for the indicated variant, while '+/+' indicates the absence of *NFKBIA* variants. (B) Localisation of identified *NFKBIA* variants across the diverse domains of IκBα (upper part). Further, residues missing as a consequence of the c.682C>T, p.Gln228* variant in *NFKBIA* and degree of their conservation across diverse species (lower part). (C) Computed tomography (CT) scan of the chest from P5 showing widespread cylindrical bronchiectasis with bronchial wall thickening (marked with '*'upper part). Wrist x-ray from P2 showing erosive arthritis affecting the carpal and carpometacarpal joints (lower left part) and magnetic resonance imaging (MRI) of the ankle and foot from P3 showing peroneal tenosynovitis (lower right part). (D) Expression of IκBα and β-actin in PBMCs from patients P2 and P3 as well as from 2 healthy blood donors (HD1 and HD2), Western blots (left) and densitometric analysis of relative expression of IκBα (right). (E) Expression of wild-type (WT) or p.Gln228*-IκBα as well as β-actin in HEK293T cells, transfected with a plasmid expressing either the full-length (WT) or the mutant (p.Gln228*) IκBα. Western blots (left) and densitometric analysis of relative expression of IκBα (right). Graph summarises findings from 3 experiments and indicates the mean ± SD. (F) IκBα degradation in response to phorbol 12-myristate (PMA), anti-IgM or lipopolysaccharide (LPS) in T cells, B cells or monocytes. Representative histograms of IκBα expression are shown (left, red histogram: stimulation with the each time indicated stimulus for 30 min, black colour: unstimulated sample) and summary of data on median fluorescence intensity from 4 healthy blood donors (HDs), P2 and P3 (p.Gln228*) and 4 patients with variants affecting serine 36 (ie, P4 to P7, p.Ser36Ala/Pro). Graphs summarise findings from different healthy blood donors or patients with indicated *NFKBIA* variants and indicate the mean ± SEM. ARD, ankyrin repeat domain; Fam, family; IκBα, inhibitor of NFκB α; PEST, sequence enriched in proline (P), glutamate (E), serine (S) and threonine (T); P1-P7, patient 1 to 7, as indicated in pedigrees (A); SRD, signal response domain.

activated PBMCs (Fig 3B-F). In addition, the expression levels of both the truncated (p.Gln228*) and full-length IκBα were found to be substantially reduced following stimulation with PMA and ionomycin. This finding is consistent with the above-presented flow cytometry data, showing that the activation-induced proteasomal degradation of p.Gln228*-IκBα remained unaffected. Altogether, aforementioned findings suggest that the p.Gln228*-IκBα exhibits a stronger inhibitory effect on NFκB1, as it reduces nuclear levels of NFκB1-p50 levels in a mode resembling NFκB1 haploinsufficiency [17].

Immunological findings in patients with the p.Gln228 variant in NFKBIA*

Between the 2 tested patients, only P2 had hypogammaglobulinaemia, diagnosed as secondary hypogammaglobulinaemia, as it developed after the diagnosis of rheumatic disease, during treatment with corticosteroids and DMARDs (Supplementary Table S1). However, analysis of peripheral lymphocyte subsets revealed reduced percentages of switched B cells ($IgD^{-}CD27^{+}$) in both patients harbouring the c.682C>T, p.Gln228* variant (ie, P2 and P3) (Fig 4A-C), suggesting a defect in the differentiation of B cells, which represents the immunophenotypic hallmark of common variable immunodeficiency (CVID) and a common finding in patients with NFκB1 haploinsufficiency [18,19]. The NFκB1 haploinsufficiency has been associated with autoinflammatory manifestations, including arthritis, eczema, adult Still disease, and pyoderma gangrenosum [16,19,20]. Recently, mutations causing NFκB1 haploinsufficiency have been shown to cause enhanced inflammasome activation, while the IL 1 receptor antagonist (anakinra) has been successfully employed to treat cutaneous autoinflammation in patients with

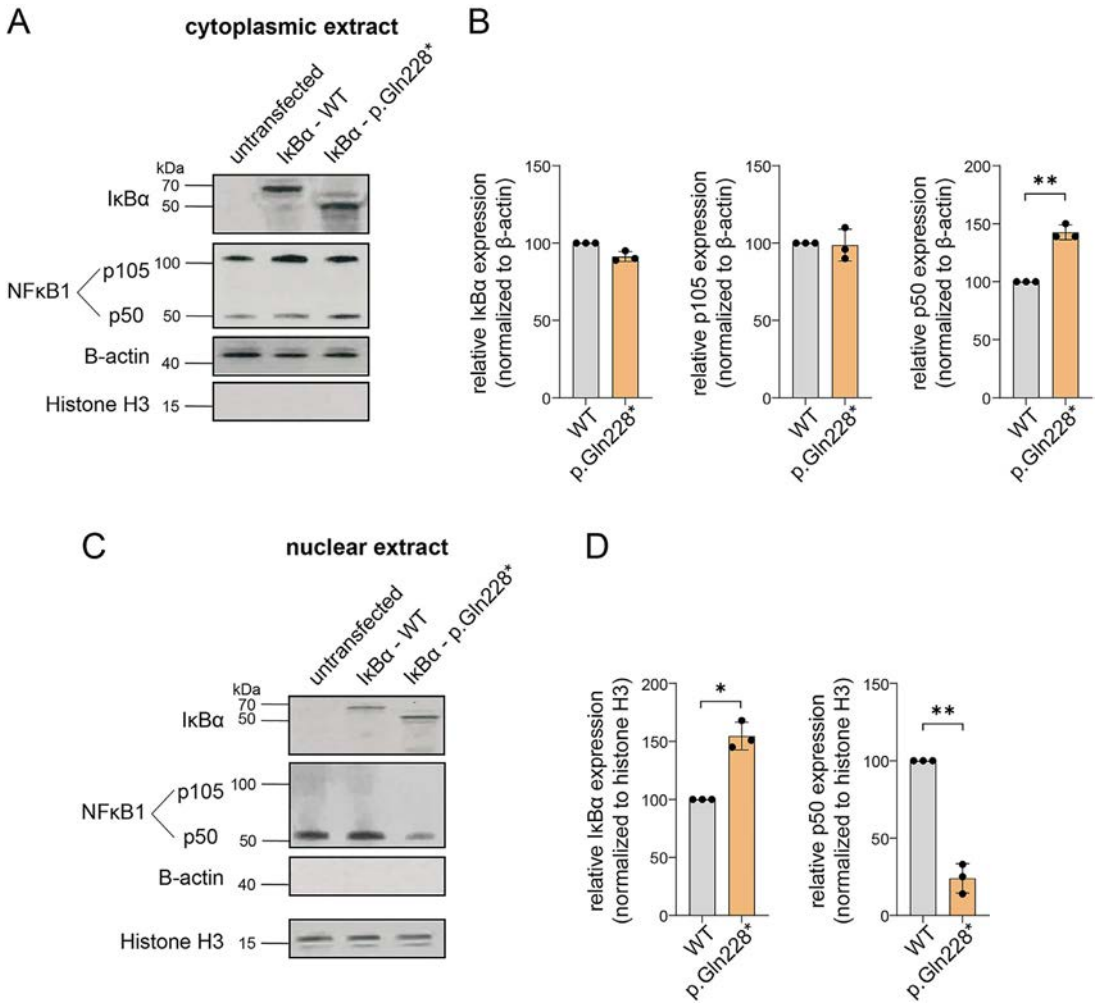

Figure 2. (A) Expression of wild-type (WT) or p.Gln228*-IκBα, NFκB1-p50 and p105 as well as β-actin and histone H3 in cytoplasmic extracts from transfected HEK293T cells, expressing either the full-length (WT) or the mutant (p.Gln228*) IκBα. Representative Western blots from cytoplasmic extracts. (B) Summary of densitometric analyses of relative expression of phospho-p105 (left), NFκB1-p105 (middle) and NFκB1-p50 (right) from Western blots from cytoplasmic extracts of transfected HEK293T cells. (C) Representative Western blots with nuclear extracts from HEK293T cells transfected the same way as in (A). (D) Summary of densitometric analyses of relative nuclear expression of IκBα (left) or NFκB1-p50 (right) from Western blots with nuclear extracts from transfected HEK293T cells. Graphs summarise findings from 3 experiments and indicate the mean ± SD (*$P < .05$; **$P < .01$). IκBα, inhibitor of NFκB α.

NFκB1 haploinsufficiency [21]. In view of the finding of a functional NFκB1 haploinsufficiency due to the p.Gln228*-IκBα mutant as well as the above discussed association of NFκB1 haploinsufficiency with enhanced activation of the NLRP3 inflammasome, we hypothesised that the c.682C>T, p.Gln228* variant in *NFKBIA* might also enhance inflammasome activation. We therefore assessed primary monocytes from P2 and P3 for inflammasome activation by evaluating LPS- and ATP-induced IL-1β secretion (Fig 4D). This revealed increased IL-1β secretion by monocytes from patients with the c.682C>T, p.Gln228* variant in *NFKBIA*. On the other hand, TNFα secretion was similar. To confirm that IL-1β secretion was due to higher inflammasome activity, we visualised ASC speck formation by immunofluorescence (Fig 4E,F). Indeed, monocytes expressing the p.Gln228*-IκBα displayed higher ASC speck frequency than monocytes from healthy blood donors. Elevated levels of IL-18 have been reported to represent a serological marker in inflammasome-mediated autoinflammatory diseases [22,23]. In accordance with these reports and the aforementioned *in vitro* findings, which suggested inflammasome-driven inflammation, both P2 and P3 displayed substantially elevated serum levels of IL-18 (Fig 4G).

DISCUSSION

Besides *NFKB1* and *NFKBIA*, several genes involved in the regulation of the canonical NFκB pathway have been implicated in autoinflammatory disease [24–27]. Similar to the NFκB1 haploinsufficiency and the IκBα gain-of-function [7,21], enhanced NLRP3 inflammasome activation has been reported to be involved in *TNFAIP3* and *OTULIN*-related autoinflammation [28,29]. As reported for NFκB1 haploinsufficiency-related autoinflammation, identification of an inflammasome-dominated aetiology of immune dysregulation can lead to effective anti-inflammatory treatment by means of an IL-1 inhibition [21,30]. Continuous inflammasome activation and IL-1β secretion in the context of Muckle-Wells syndrome have been reported to induce secretion of IL-6, which may further augment inflammation. The latter may account for the partial response to tocilizumab in case of P2, whom we offered an IL-1 inhibitor, which he however, so far denied, given the positive and sustained effect of tocilizumab in comparison to all other previously administered DMARDs [31].

Here we show that the p.Gln228* variant, a C-terminal truncation of IκBα, causes a strong reduction in the baseline as well

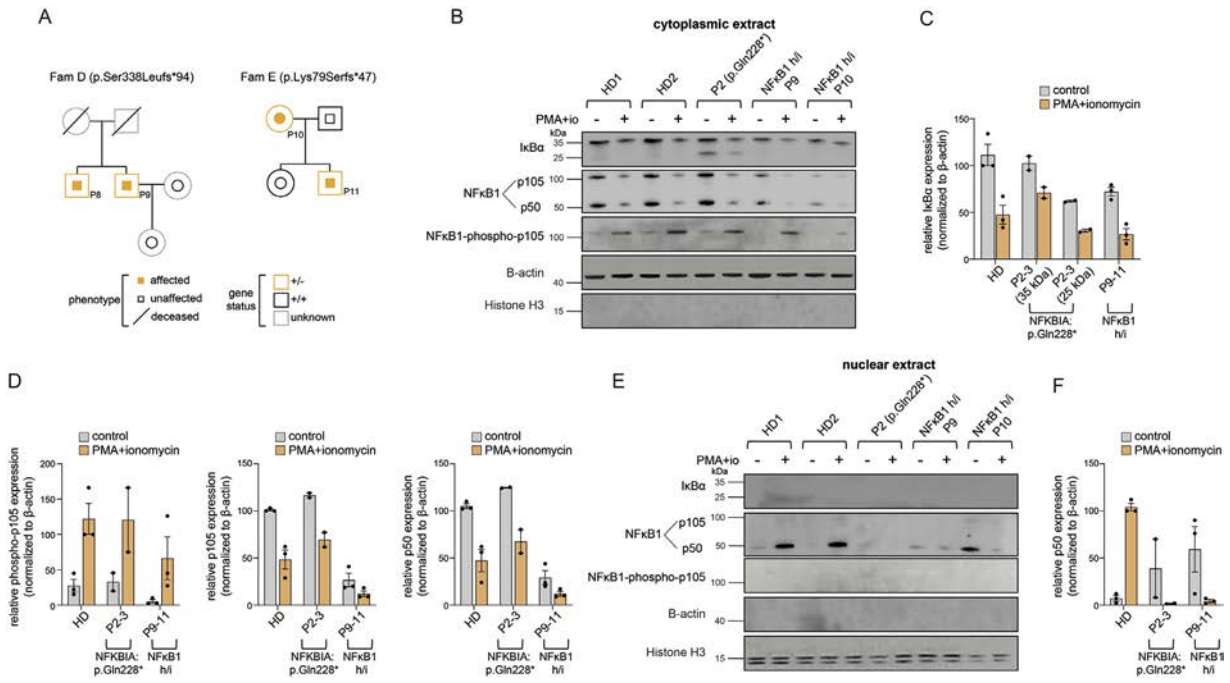

Figure 3. (A) Pedigrees of patients with NFκB1 haploinsufficiency due to the indicated variants in *NFKB1*. Gene status refers to variant indicated in the header of each pedigree, '±' indicates heterozygosity for the indicated variant, while '+/+' indicates the absence of *NFKB1* variants. (B) Expression of IκBα, NFκB1-p105, NFκB1-p50, and NFκB1-phospho-p105 as well as β-actin and histone H3 in cytoplasmic extracts from peripheral blood mononuclear cells (PBMCs) from patients with the c.682C>T, p.Gln228* variant in *NFKBIA* as well as from patients with NFκB1 haploinsufficiency (h/i). Cells were stimulated with phorbol 12-myristate (PMA) and ionomycin or left unstimulated, representative Western blots. (C) Summary of densitometric analyses of relative expression of IκBα from Western blots including P2 and P3 (p.Gln228*) as well as P9, P10 and P11 (NFκB1 haploinsufficiency). (D) Summary of densitometric analyses of relative expression of NFκB1-phospho-p105 (left), NFκB1-p105 (middle) and NFκB1-p50 (right) from previous Western blots with PBMCs from the same patients (see C). (E) Same analyses in (F) were performed with nuclear extracts from PBMCs from P2 and P3 (p.Gln228*) as well as P9, P10, and P11 (NFκB1 haploinsufficiency). Representative Western blots. (F) Summary of densitometric analyses of relative nuclear expression of NFκB1-p50 from Western blots including P2 and P3 (p.Gln228*) as well as P9, P10, and P11 (NFκB1 haploinsufficiency). In (C), (D), and (E), graphs summarise findings from different healthy blood donors (HDs) or patients with indicated variant in *NFKB1* or the p.Gln228* variant in *NFKBIA* and indicate the mean ± SEM. IκBα, inhibitor of NFκB α.

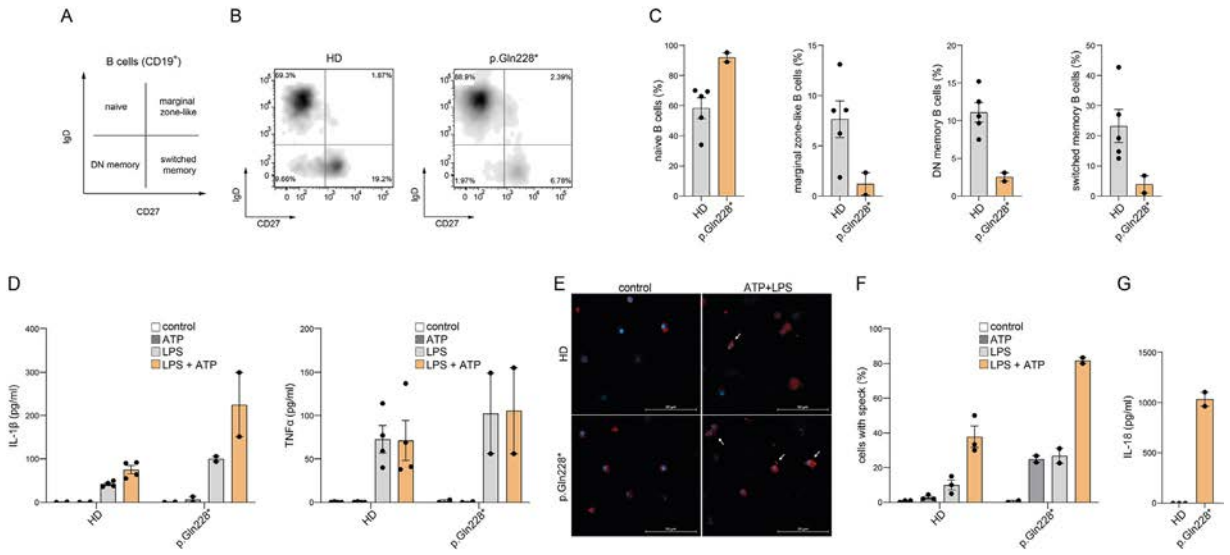

Figure 4. (A) Gating strategy for immunophenotyping of B cells. (B) Representative flow cytometry plots from a healthy blood donor (HD) and P2 (p.Gln228*). (C) Summary of immunophenotyping of B cells from P2 and P3 (p.Gln228*) and 4 HDs. (D) Secreted interleukin (IL)-1β and tumor necrosis factor (TNFα) levels after monocyte stimulation with lipopolysaccharide (LPS) + adenosine triphosphate (ATP), ATP or LPS. (E) Representative confocal microscopy images of apoptosis-associated speck-like protein containing a caspase recruitment domain (ASC) speck structure in the presence or absence of LPS + ATP stimulation. (F) Summary of cells with ASC specks in monocytes from healthy blood donors (HDs) vs. P2 and P3 (p.Gln228*) after stimulation with LPS + ATP. (G) Serum levels of IL-18 in healthy blood donors (HDs) vs. P2 and P3 (p.Gln228*). In (C), (D), and (F), graphs summarise findings as mean ± SEM.

as the activation-induced nuclear translocation of NFκB-p50, mimicking NFκB1 insufficiency. In line with these findings, C-terminal truncation mutants of IκBα have previously been shown to significantly reduce the nuclear activity of NFκB [32]. In cells expressing such IκBα-mutants, residual NFκB activation was slower as compared to cells expressing wild-type IκBα, which correlated with delayed phosphorylation and degradation of the C-terminal truncation variant of IκBα. However, the precise mechanism accounting for the substantially decreased NFκB activation in case of the C-terminal truncation of IκBα remains unknown and needs to be further investigated. In case of the p.Gln228*-IκBα, missing domains include the 2 C-terminal ankyrin-rich domains (ARDs) (ie, ARD5 and ARD6), which are involved in the interaction of IκBα with p50 and p65 [33,34]. Besides these 2 ARDs, the C-terminal sequence enriched in proline (P), glutamate (E), serine (S) and threonine (T) (PEST), that lies within the missing sequences of the p.Gln228*-IκBα, has been shown to be involved in NFκB binding [35]. Therefore, the p.Gln228* variant may be impairing binding to the NFκB subunits and consequently result in increased levels of free IκBα (not bound to NFκB) as well as free p50-p65 (Fig 5). The latter is in line with the finding of elevated cytoplasmic p50 levels, which we observed both in case of HEK293T cells expressing the Gln228*- IκBα as well as in primary cells from patients harbouring same variant. The loss of the PEST domain is expected to impair the steady-state degradation of free IκBα [32,36], which could also enhance expression of free IκBα. The crystal structure of IκBα reveals a more extensive interaction between the ARD5 and ARD6 domains and p65 as compared to p50 [34]. Consequently, the p.Gln228* variant may differentially modulate the interaction between IκBα and the individual subunits of NFκB complex, favouring activator NFκB dimers or proinflammatory gene expression enhancing inflammasome activation over repressor dimers or regulatory gene expression. Besides inhibiting NFκB in the cytoplasm, IκBα has been shown to bind NFκB in the nucleus, exporting it back in the cytoplasm [37,38]. While IκBα nuclear import depends largely on the ARD2, its nuclear export is contingent on N residues [39,40], which are all expected to be preserved in p.Gln228*-IκBα. Therefore, enhanced nucleocytoplasmic shuttling of the p.Gln228*-IκBα might be an alternative hypothesis for the substantially reduced nuclear levels of NFκB-p50 in HEK293T cells expressing the p.Gln228*-IκBα as well as in primary cells from patients harbouring the same variant. A genotype-matched cell model would enable in-depth investigation of the above proposed hypotheses (Fig 5) and facilitate identification of the specific molecular aberrations leading to nuclear p50 depletion in cells harbouring the p.Gln228* variant.

Previously, monoallelic *NFKBIA* variants affecting the N-terminus of IκBα and compromising its degradation have been associated with autoinflammation [4]. In case of the p.Leu34-Pro-IκBα variant, which was identified in a patient with hepatic autoinflammation [7], increased induced production of IL-1β by patient-derived cells and macrophages from a conditional knock-in mouse model harbouring the same variant, suggested enhanced inflammasome activation and provided a direct casual link between this variant and autoinflammation. The latter suggested that IκBα gain-of-function and the consequent cytoplasmic sequestration of NFκB can cause autoinflammation. In the present work, patients studied displayed early-onset,

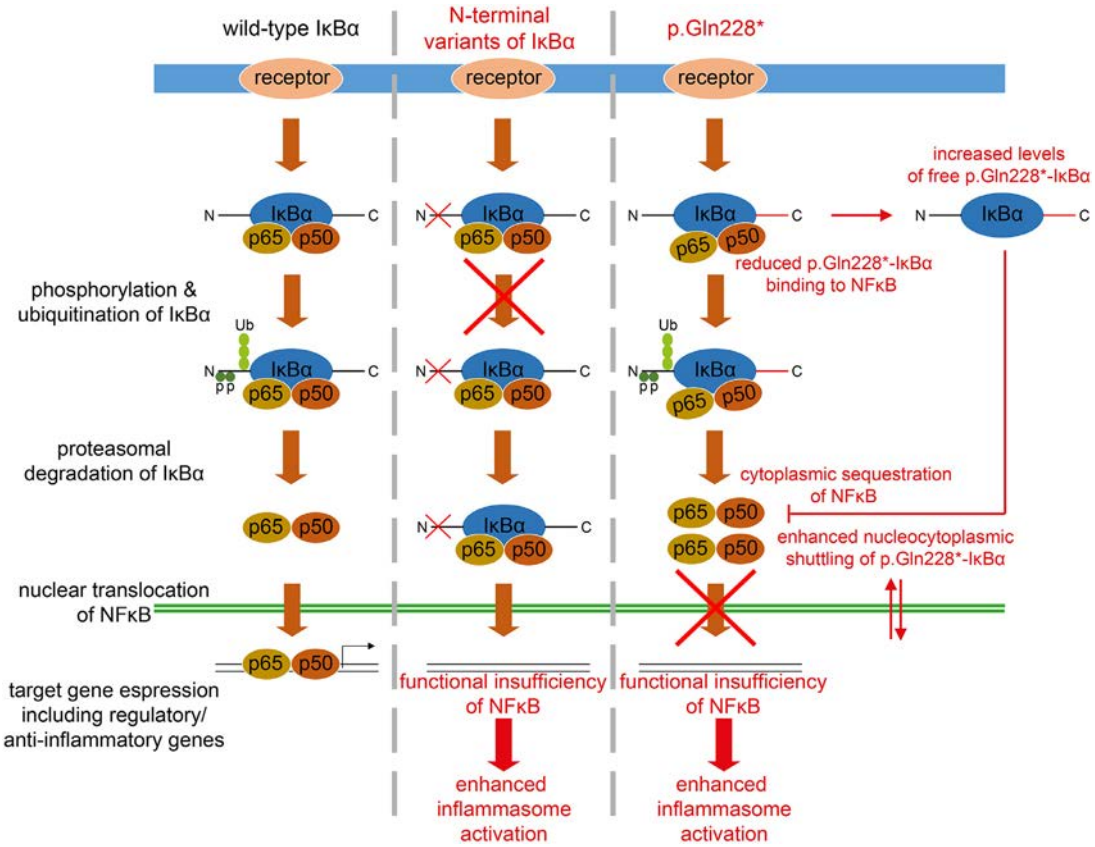

Figure 5. Schematic representation of the proposed molecular aberrations caused by the truncation variant of IκBα, leading to functional NF-κB insufficiency and enhanced inflammasome activation. These changes are depicted in comparison to the physiological canonical NF-κB activation pathway and to the effects of an N-terminal variants that affect serine 32 or 36 residues and abrogate induced proteasomal degradation. Proposed pathogenic alterations are highlighted with red symbols and red text. IκBα, inhibitor of NFκB α; pp, phosphorylation; Ub, ubiquitination.

episodic and seronegative arthritis, consistent with an autoinflammatory phenotype. The observed elevation of serum IL-18 levels, together with increased inflammasome activation in patient monocytes, is consistent with an autoinflammatory disease. The identification of the p.Gln228* variant, along with its impact on canonical NFκB activation, further supports its role in impairing innate immune regulation in a manner comparable to NFκB1 insufficiency [21], thereby contributing to autoinflammation. However, the lack of a genotype-matched myeloid cell model, which would provide a direct causative link between the p.Gln228* variant and autoinflammation, represents a limitation of the present work. In addition, the absence of data on treatment with an IL-1β inhibitor precluded direct clinical assessment of the inflammasome dependency of arthritis in the studied patients.

NFKBIA is one of the genes that were previously identified to confer risk for rheumatic disorders and simultaneously relate to IEIs [41]. Besides overlapping genetic backgrounds, well-classifiable rheumatic disorders represent a relatively common phenotypic trait of IEIs [42,43]. Reciprocally, IEIs have been identified in patients, initially diagnosed with rheumatic disorders. Early disease onset, extra-articular manifestations, such as pustular psoriasis and inflammatory bowel disease, the macrophage activation syndrome, persistent hypogammaglobulinaemia, even if induced by DMARDs, lymphocyte differentiation defects, such as reduced class-switch memory B cell and familial clustering of immune dysregulation represent red flags that could indicate an underlying IEI in patients with rheumatic disease [44–47]. Among IEIs, disease of immune dysregulation and autoinflammatory disorders commonly present with features of rheumatic disease, such as arthritis, vasculitis, and eczema [11]. Despite the commonly reported phenotypic complexity of autoinflammatory disorders and diseases of immune dysregulation, as in case of the present patients, articular inflammation can represent the dominant or sole clinical manifestation of an IEI.

In summary, we report a novel pathogenic *NFKBIA* variant, which in contrast to all previously reported variants lies outside the N-terminus of IκBα and results in C-terminal truncation. Despite intact induced degradation of IκBα, the p.Gln228* variant strongly restricts canonical NFκB activation. The latter together with the findings of affected B cell differentiation and enhanced inflammasome activation, which represent common immunological features in NFκB1 haploinsufficiency, suggest a functional NFκB1 insufficiency as the main pathomechanism in the case of the p.Gln228*-IκBα variant.

Competing interests

The authors declare that they have no known competing financial interests or personal relationships that could have appeared to influence the work reported in this paper.

Acknowledgements

We sincerely thank all patients and volunteers for participating in the study, and clinic nurses for their excellent help with blood sampling.

Contributors

GS, AE, and IRA were responsible for conception and design of the work. AE, IRA, FA, ND, MA, and GS were responsible for data acquisition, analysis, and interpretation. FH, UB, TW, and GS were responsible for patient recruitment. GS, AE, and IRA were responsible for first manuscript draft. GS, IRA, and TW were responsible for funding. All authors revised and approved the manuscript.

Funding

This project was funded by the Rosemarie-Germscheid Foundation. It was additionally supported by the Deutsche Forschungsgemeinschaft (DFG, German Research Foundation) under Germany's Excellence Strategy—EXC 2155 'RESIST'—Project ID 39087428 and the German network for multi-organ autoimmune diseases (GAIN_01GM2206B) and the German Center for Infection Research (DZIF TTU 01.801). AE was supported by the Hannover Biomedical Research School (HBRS) and the Center for Infection Biology (ZIB).

Patient consent for publication

All studied patients signed an informed consent form.

Ethics approval

This study was conducted in accordance with the Declaration of Helsinki and was also approved from the Ethical committee of the Hannover Medical School (approval number: 10794_BO_K_2023). All patients signed an informed consent form.

Provenance and peer review

Not commissioned; externally peer reviewed.

Data availability statement

Data are available for formal research purposes only upon request to the corresponding author.

Supplementary materials

Supplementary material associated with this article can be found in the online version at doi:10.1016/j.ard.2025.08.010.

Orcid

Georgios Sogkas: http://orcid.org/0000-0003-0855-2945

REFERENCES

[1] Liu T, Zhang L, Joo D, Sun S-C. NF-κB signaling in inflammation. Signal Transduct Target Ther 2017;2:17023. doi: 10.1038/sigtrans.2017.23.
[2] Kwon YC, Lim J, Bang SY, Ha E, Hwang MY, Yoon K, et al. Genome-wide association study in a Korean population identifies six novel susceptibility loci for rheumatoid arthritis. Ann Rheum Dis 2020;79:1438–45. doi: 10.1136/annrheumdis-2020-217663.
[3] Stuart PE, Nair RP, Tsoi LC, Tejasvi T, Das S, Kang HM, et al. Genome-wide association analysis of psoriatic arthritis and cutaneous psoriasis reveals differences in their genetic architecture. Am J Hum Genet 2015;97:816–36. doi: 10.1016/j.ajhg.2015.10.019.
[4] Boisson B, Puel A, Picard C, Casanova J-L. Human IκBα gain of function: a severe and syndromic immunodeficiency. J Clin Immunol 2017;37:397–412. doi: 10.1007/s10875-017-0400-z.
[5] Wu J, YY Jin, Mo X, Chen TX. T-cell defects in a patient with NFKBIA gene mutation. J Clin Immunol 2024;44:110. doi: 10.1007/s10875-024-01703-y.
[6] Sogkas G, Adriawan IR, Ringshausen FC, Baumann U, Schröder C, Klemann C, et al. A novel NFKBIA variant substituting serine 36 of IκBα causes immunodeficiency with warts, bronchiectasis and juvenile rheumatoid arthritis in

the absence of ectodermal dysplasia. Clin Immunol 2020;210:108269. doi: 10.1016/j.clim.2019.108269.
[7] Tan EE, Hopkins RA, Lim CK, Jamuar SS, Ong C, Thoon KC, et al. Dominant-negative NFKBIA mutation promotes IL-1β production causing hepatic disease with severe immunodeficiency. J Clin Invest 2020;130:5817–32. doi: 10.1172/JCI98882.
[8] Wen W, Wang L, Deng M, Li Y, Tang X, Mao H, et al. A heterozygous N-terminal truncation mutation of *NFKBIA* results in an impaired NF-κB dependent inflammatory response. Genes Dis 2021;9:176–86. doi: 10.1016/j.gendis.2021.03.005.
[9] Petersheim D, Massaad MJ, Lee S, Scarselli A, Cancrini C, Moriya K, et al. Mechanisms of genotype-phenotype correlation in autosomal dominant anhidrotic ectodermal dysplasia with immune deficiency. J Allergy Clin Immunol 2018;141:1060–1073.e3. doi: 10.1016/j.jaci.2017.05.030.
[10] Olfe L, von Hardenberg S, Hofmann W, Auber B, Baumann U, Beier R, et al. CTLA-4 insufficiency due to a novel CTLA-4 deletion, identified through copy number variation analysis. Int Arch Allergy Immunol 2023;184:76–84. doi: 10.1159/000527051.
[11] Poli MC, Aksentijevich I, Bousfiha AA, Cunningham-Rundles C, Hambleton S, Klein C, et al. Human inborn errors of immunity: 2024 update on the classification from the International Union of Immunological Societies expert committee. J Hum Immun 2025;1:e20250003. doi: 10.70962/jhi.20250003.
[12] Richards S, Aziz N, Bale S, Bick D, Das S, Gastier-Foster J, et al. Standards and guidelines for the interpretation of sequence variants: a joint consensus recommendation of the American College of Medical Genetics and Genomics and the Association for Molecular Pathology. Genet Med 2015;17:405–24. doi: 10.1038/gim.2015.30.
[13] Elsayed A, von Hardenberg S, Atschekzei F, Graalmann T, Jänke C, Witte T, et al. Phenotypic and pathomechanistic overlap between tapasin and TAP deficiencies. J Allergy Clin Immunol 2024;154:1069–75. doi: 10.1016/j.jaci.2024.06.003.
[14] Atschekzei F, Fedchenko M, Elsayed A, Dubrowinskaja N, Graalmann T, Ringshausen FC, et al. Rituximab to treat prolidase deficiency due to a novel pathogenic copy number variation in *PEPD*. RMD Open 2023;9:e003507. doi: 10.1136/rmdopen-2023-003507.
[15] Li J, Lei WT, Zhang P, Rapaport F, Seeleuthner Y, Lyu B, et al. Biochemically deleterious human NFKB1 variants underlie an autosomal dominant form of common variable immunodeficiency. J Exp Med 2021;218:e20210566. doi: 10.1084/jem.20210566.
[16] Schröder C, Sogkas G, Fliegauf M, Dörk T, Liu D, Hanitsch LG, et al. Late-onset antibody deficiency due to monoallelic alterations in *NFKB1*. Front Immunol 2019;10:2618. doi: 10.3389/fimmu.2019.02618.
[17] Tuijnenburg P, Lango Allen H, Burns SO, Greene D, Jansen MH, Staples E, et al. Loss-of-function nuclear factor κB subunit 1 (NFKB1) variants are the most common monogenic cause of common variable immunodeficiency in Europeans. J Allergy Clin Immunol 2018;142:1285–96. doi: 10.1016/j.jaci.2018.01.039.
[18] Jablonka A, Etemadi H, Adriawan IR, Ernst D, Jacobs R, Buyny S, et al. Peripheral blood lymphocyte phenotype differentiates secondary antibody deficiency in rheumatic disease from primary antibody deficiency. J Clin Med 2020;9:1049. doi: 10.3390/jcm9041049.
[19] Lorenzini T, Fliegauf M, Klammer N, Frede N, Proietti M, Bulashevska A, et al. Characterization of the clinical and immunologic phenotype and management of 157 individuals with 56 distinct heterozygous NFKB1 mutations. J Allergy Clin Immunol 2020;146:901–11. doi: 10.1016/j.jaci.2019.11.051.
[20] Kaustio M, Haapaniemi E, Göös H, Hautala T, Park G, Syrjänen J, et al. Damaging heterozygous mutations in NFKB1 lead to diverse immunologic phenotypes. J Allergy Clin Immunol 2017;140:782–96. doi: 10.1016/j.jaci.2016.10.054.
[21] Nurmi K, Silventoinen K, Keskitalo S, Rajamäki K, Kouri VP, Kinnunen M, et al. Truncating NFKB1 variants cause combined NLRP3 inflammasome activation and type I interferon signaling and predispose to necrotizing fasciitis. Cell Rep Med 2024;5:101503. doi: 10.1016/j.xcrm.2024.101503.
[22] Weiss ES, Girard-Guyonvarc'h C, Holzinger D, de Jesus AA, Tariq Z, Picarsic J, et al. Interleukin-18 diagnostically distinguishes and pathogenically promotes human and murine macrophage activation syndrome. Blood 2018;131:1442–55. doi: 10.1182/blood-2017-12-820852.
[23] Shimizu M, Takei S, Mori M, Yachie A. Pathogenic roles and diagnostic utility of interleukin-18 in autoinflammatory diseases. Front Immunol 2022;13:951535. doi: 10.3389/fimmu.2022.951535.
[24] Zhou Q, Yu X, Demirkaya E, Deuitch N, Stone D, Tsai WL, et al. Biallelic hypomorphic mutations in a linear deubiquitinase define otulipenia, an early-onset autoinflammatory disease. Proc Natl Acad Sci U S A 2016;113:10127–32. doi: 10.1073/pnas.1612594113.
[25] Zhou Q, Wang H, Schwartz DM, Stoffels M, Park YH, Zhang Y, et al. Loss-of-function mutations in TNFAIP3 leading to A20 haploinsufficiency cause an early-onset autoinflammatory disease. Nat Genet 2016;48:67–73. doi: 10.1038/ng.3459.
[26] Damgaard RB, Walker JA, Marco-Casanova P, Morgan NV, Titheradge HL, Elliott PR, et al. The deubiquitinase OTULIN is an essential negative regulator of inflammation and autoimmunity. Cell 2016;166:1215–1230.e20. doi: 10.1016/j.cell.2016.07.019.
[27] Aksentijevich I, Zhou Q. NF-κB pathway in autoinflammatory diseases: dysregulation of protein modifications by ubiquitin defines a new category of autoinflammatory diseases. Front Immunol 2017;8:399. doi: 10.3389/fimmu.2017.00399.
[28] Rajamäki K, Keskitalo S, Seppänen M, Kuismin O, Vähäsalo P, Trotta L, et al. Haploinsufficiency of A20 impairs protein-protein interactome and leads into caspase-8-dependent enhancement of NLRP3 inflammasome activation. RMD Open 2018;4:e000740. doi: 10.1136/rmdopen-2018-000740.
[29] Doglio MG, Verboom L, Ruilova Sosoranga E, Frising UC, Asaoka T, Gansemans Y, et al. Myeloid OTULIN deficiency couples RIPK3-dependent cell death to Nlrp3 inflammasome activation and IL-1β secretion. Sci Immunol 2023;8:eadf4404. doi: 10.1126/sciimmunol.adf4404.
[30] Sönmez HE, Özen S. A clinical update on inflammasomopathies. Int Immunol 2017;29:393–400. doi: 10.1093/intimm/dxx020.
[31] Yamazaki T, Masumoto J, Agematsu K, Sawai N, Kobayashi S, Shigemura T, et al. Anakinra improves sensory deafness in a Japanese patient with Muckle-Wells syndrome, possibly by inhibiting the cryopyrin inflammasome. Arthritis Rheum 2008;58:864–8. doi: 10.1002/art.23261.
[32] Mathes E, O'Dea EL, Hoffmann A, Ghosh G. NF-kappaB dictates the degradation pathway of IkappaBalpha. EMBO J 2008;27:1357–67. doi: 10.1038/emboj.2008.73.
[33] Jacobs MD, Harrison SC. Structure of an IkappaBalpha/NF-kappaB complex. Cell 1998;95:749–58. doi: 10.1016/s0092-8674(00)81698-0.
[34] Huxford T, Huang DB, Malek S, Ghosh G. The crystal structure of the IkappaBalpha/NF-kappaB complex reveals mechanisms of NF-kappaB inactivation. Cell 1998;95:759–70. doi: 10.1016/s0092-8674(00)81699-2.
[35] Bergqvist S, Ghosh G, Komives EA. The IkappaBalpha/NF-kappaB complex has two hot spots, one at either end of the interface. Protein Sci 2008;17:2051–8. doi: 10.1110/ps.037481.108.
[36] Beauparlant P, Lin R, Hiscott J. The role of the C-terminal domain of I kappa B alpha in protein degradation and stabilization. J Biol Chem 1996;271:10690–6. doi: 10.1074/jbc.271.18.10690.
[37] Saccani S, Pantano S, Natoli G. Modulation of NF-kappaB activity by exchange of dimers. Mol Cell 2003;11:1563–74. doi: 10.1016/s1097-2765(03)00227-2.
[38] Arenzana-Seisdedos F, Turpin P, Rodriguez M, Thomas D, Hay RT, Virelizier JL, et al. Nuclear localization of I kappa B alpha promotes active transport of NF-kappa B from the nucleus to the cytoplasm. J Cell Sci 1997;110:369–78. doi: 10.1242/jcs.110.3.369.
[39] Turpin P, Hay RT, Dargemont C. Characterization of IkappaBalpha nuclear import pathway. J Biol Chem 1999;274:6804–12. doi: 10.1074/jbc.274.10.6804.
[40] Huang TT, Kudo N, Yoshida M, Miyamoto S. A nuclear export signal in the N-terminal regulatory domain of IkappaBalpha controls cytoplasmic localization of inactive NF-kappaB/IkappaBalpha complexes. Proc Natl Acad Sci USA 2000;97:1014–9. doi: 10.1073/pnas.97.3.1014.
[41] Sogkas G, Atschekzei F, Adriawan IR, Dubrowinskaja N, Witte T, Schmidt RE. Cellular and molecular mechanisms breaking immune tolerance in inborn errors of immunity. Cell Mol Immunol 2021;18:1122–40. doi: 10.1038/s41423-020-00626-z.
[42] Pott NM, Atschekzei F, Pott CC, Ernst D, Witte T, Sogkas G. Primary antibody deficiency-associated arthritis shares features with spondyloarthritis and enteropathic arthritis. RMD Open 2022 Dec;8(2):e002664. doi: 10.1136/rmdopen-2022-002664.
[43] Sogkas G, Witte T. The link between rheumatic disorders and inborn errors of immunity. EBioMedicine 2023;90:104501. doi: 10.1016/j.ebiom.2023.104501.
[44] Spârchez M, Lupan I, Delean D, Bizo A, Damian L, Muntean L, et al. Primary complement and antibody deficiencies in autoimmune rheumatologic diseases with juvenile onset: a prospective study at two centers. Pediatr Rheumatol Online J 2015;13:51. doi: 10.1186/s12969-015-0050-8.
[45] Sogkas G, Dubrowinskaja N, Adriawan IR, Anim M, Witte T, Schmidt RE, et al. High frequency of variants in genes associated with primary immunodeficiencies in patients with rheumatic diseases with secondary hypogammaglobulinaemia. Ann Rheum Dis 2021;80:392–9. doi: 10.1136/annrheumdis-2020-218280.
[46] Atschekzei F, Dubrowinskaja N, Anim M, Thiele T, Witte T, Sogkas G. Identification of variants in genes associated with autoinflammatory disorders in a cohort of patients with psoriatic arthritis. RMD Open 2022;8:e002561. doi: 10.1136/rmdopen-2022-002561.
[47] Kaufman KM, Linghu B, Szustakowski JD, Husami A, Yang F, Zhang K, et al. Whole-exome sequencing reveals overlap between macrophage activation syndrome in systemic juvenile idiopathic arthritis and familial hemophagocytic lymphohistiocytosis. Arthritis Rheumatol 2014;66:3486–95. doi: 10.1002/art.38793.

Ann Rheum Dis 85 (2026) 942–952

Contents lists available at ScienceDirect

Annals of the Rheumatic Diseases

journal homepage: https://www.sciencedirect.com/journal/annals-of-the-rheumatic-diseases

Autoinflammatory disorders

A human-STING specific macrocyclic peptide suppresses cGAS-STING-induced inflammation

Jian Zheng[1], Junjie Wu[2], Hang Yin[1], Zhiyue Zhang[3], Qifeng Zhao[1], Xiaoshen Wang[4], Xuzichao Li[4], Yang Liu[3], Youming Zhang[2], Zhi Yao[1], Heng Zhang[1,4,*], Yizhen Yin[2,5,*], Long Li[1,6,*]

[1] *Department of Immunology and Department of Pharmacology, Tianjin Institute of Immunology, Key Laboratory of Immune Microenvironment and Disease (Ministry of Education), State Key Laboratory of Experimental Hematology, Tianjin Medical University, Tianjin, China*

[2] *State Key Laboratory of Microbial Technology, Institute of Microbial Technology, Shandong University, Qingdao, China*

[3] *NMPA Key Laboratory for Technology Research and Evaluation of Drug Products, Key Laboratory of Chemical Biology (Ministry of Education), Shandong Key Laboratory of Targeted Drug Delivery and Advanced Pharmaceutics, Department of Pharmaceutics, School of Pharmaceutical Sciences, Cheeloo College of Medicine, Shandong University, Jinan, China*

[4] *Department of Biochemistry and Molecular Biology, School of Basic Medical Sciences, Tianjin Medical University, Tianjin, China*

[5] *Shandong Research Institute of Industrial Technology, Jinan, China*

[6] *Hebei Key Laboratory of Autoimmune Disease Medicine Research, Shijiazhuang, China*

ARTICLE INFO

Article history:
Received 14 December 2024
Received in revised form 29 September 2025
Accepted 22 October 2025

ABSTRACT

Suppression of hyperactive stimulator of interferon genes (STING) may provide therapeutic benefits to treat inflammatory diseases. We identified a macrocyclic peptide, named P1, which binds to human STING (hSTING) by a new platform for the discovery of pseudonatural macrocyclic peptides. In cellular experiments, P1 effectively blocked the translocation of hSTING from endoplasmic reticulum (ER) to the trans-Golgi network, increasing the accumulation of hSTING on ER, and thus interrupted the downstream STING signalling transduction, which resulted in reduced production of interferon-β (IFN-β) and proinflammatory cytokines, the major effectors of the STING pathway. Mechanistically, the crystallographic structure of P1-bound hSTING reveals that P1 binds to the cyclic nucleotides binding domain of hSTING dimers, the same domain as 2′3′-cyclic guanosine monophosphate-adenosine monophosphate (GMP-AMP) (2′3′-cGAMP) binds, and that P1-bound hSTING dimers are trapped in an 'open' conformation due to 38°-rotated wings compared with the 'closed' conformation associated with 2′3′-cGAMP-mediated hSTING activation. Nano-P1, the nanoparticle form to increase its cellular membrane permeability, dampened the infectious inflammation induced by herpes simplex virus type 1 both in human cells and in humanised-*STING* (*hSTING*$^{+/+}$) mice. *Trex1*-deficient *hSTING*$^{+/+}$ mice, which develop uncontrolled type I interferon-driven inflammation with growth failure and early lethality, were used to assess the effects of STING inhibition. Treatment with Nano-P1 suppressed the systemic inflammation, restored the regular growth, and substantially extended the survival of the otherwise runt and short-lived mice. Furthermore, neither *in vitro* nor *in vivo* experiments showed toxicity of Nano-P1, proving its safety for potential clinical application. Therefore, the macrocyclic peptide-based Nano-P1, an hSTING inhibitor, has great potential for treating the inflammation resulting from hyperactive STING.

*Correspondence to Dr Heng Zhang, Dr Yizhen Yin, Dr Long Li.

E-mail addresses: zhangheng134@gmail.com (H. Zhang), yizhenyin.1987@sdu.edu.cn (Y. Yin), Long.Li@tmu.edu.cn (L. Li).

Jian Zheng, Junjie Wu, Hang Yin, and Zhiyue Zhang contributed equally to this work.

Handling editor Josef S. Smolen.

https://doi.org/10.1016/j.ard.2025.10.023

INTRODUCTION

The cGAS-STING pathway plays a crucial role in host defence against foreign pathogens or environmental stimuli. Its primary function is to sense cytoplasmic double-stranded (ds) DNA, triggering an innate immune response. cGAS recognises dsDNA and catalyses the synthesis of 2′3′-cyclic GMP-AMP (2′3′-cGAMP from adenosine triphosphate (ATP) and guanosine triphosphate (GTP)) [1]. As a second messenger, 2′3′-cGAMP binds to the groove in the cyclic nucleotide binding (CBD) domain of STING dimers on the endoplasmic reticulum (ER) membrane, inducing STING dimers to transform into an activated conformation. Activated STING dimers translocate from ER to the trans-Golgi networks (TGN) [2,3]. On reaching the TGN, the oligomerisation of STING dimers initiates the aggregation and autophosphorylation of TANK binding kinase 1 (TBK1) [4], subsequently triggering the phosphorylation of interferon regulatory factor 3 (IRF3) [5] or inhibitory kappa B kinase β (IKKβ) [6]. This cascade of events culminates in the production of type I interferon or the activation of the nuclear factor kappa B (NF-κB) pathway that facilitates the transcription of proinflammatory cytokines such as interleukin-1β (IL-1β), interleukin-6 (IL-6), etc.

Because dsDNA is one of the most important genetic materials, the response of the cGAS-STING pathway to dsDNA must be strictly regulated [7]. For example, the dsDNA that activates cGAS has to be greater than a certain length in the cytosol [3]; once STING gets activated, the cells initiate a set of degradation mechanisms to tightly calibrate the strength of STING signalling [8]. Many pieces of evidence have shown that aberrant activation of and/or prolonged cGAS-STING signalling is implicated in the pathogenesis of a diverse array of diseases, including autoimmune inflammation [9], neurodegenerative disorders [10], cancers [11], and accelerated ageing [12,13]. Therefore, inhibition of the cGAS-STING pathway holds promise as a therapeutic strategy for these conditions.

Currently, the reported STING inhibitors are predominantly small-molecule compounds like H-151 [14], cyclic peptide Astin C [15], linear peptide SN-011 [16], etc. Although these compounds are capable of interfering with the activation of STING in cellular experiments or in mouse models, their clinical application is impeded by the inherent limitations of small molecules, such as high off-target rates, short half-lives, and poor selectivity. Macrocyclic peptides serve as a bridge between small molecules and protein biomolecules. They are known for their significant advantages, including improved specificity, enhanced stability, and greater structural diversity [17,18]. Their cyclisation design allows for increased conformational restriction, which leads to reduced entropy costs when interacting with biological targets. Despite the discovery of several small cyclic peptides that bind and inhibit STING, there remains a compelling need to identify novel candidates in the macrocyclic peptide category as a safe and highly efficient medicine option for clinical inhibition of STING in conditions stemming from its overactivation [19].

In this study, we utilised the random nonstandard peptide integrated discovery (RaPID) system [17,20–24] and screened more than 10^{12} macrocyclic peptides for the ones that bind to human STING (hSTING). A macrocyclic peptide, named P1, with demonstrated inhibitory effects on hSTING was identified. The crystal structure of the P1-hSTING complex was solved, providing molecular insights into the inhibition mechanism of P1 on hSTING. To facilitate the entry of P1 into cells, we utilise both poly(β-amino ester) (PBAE, a cationic polymer) and pDMA-pEPEMA (poly [dimethylacrylamide]-poly [2-(N-ethyl-N-propyl amino] ethyl methacrylate) (an amphiphilic polymer), which are capable of enhancing drug permeability in cells, as well as promoting drug stability and distribution in the body [25,26], to formulate P1 into a nanoparticle, Nano-P1. Both *in vitro* and *in vivo* experiments demonstrated that Nano-P1 ameliorated inflammation caused by hyperactivity of STING, especially in *the 3′ repair exonuclease 1* (*Trex1*)-deficient mice that had systemic inflammation resulting from inappropriately high expression of IFN-β due to constant activation of cGAS-STING [27–29]. Therefore, Nano-P1 holds promise as a safe and potent therapeutic agent for addressing autoimmune inflammatory diseases resulting from aberrant activation of STING.

METHODS

Methods and materials are provided in the Supplementary Online Information file.

RESULTS

Identification of macrocyclic peptides capable of binding to hSTING

We first adopted the RaPID system to identify *de novo* macrocyclic peptide ligands to human STING. A mRNA library consisting of AUG-$(NNK)_{8\text{-}12}$-UGC-$(GGC\text{-}AGC)_3$-UAG [30] was devised and ligated to a puromycin-CC-polyethylene glycol (PEG)-linker-DNA fragment for the expression of displayed macrocyclic peptide libraries. The start codon AUG was reprogrammed to replace *N*-formylmethionine with *N*-chloroacetyl-*L*-tyrosine (L-library) or *N*-chloroacetyl-*D*-tyrosine (D-library), which could spontaneously react with the thiol side chain of a downstream cysteine residue to afford the thioether macrocyclic peptides. We employed $(NNK)_{8\text{-}12}$, where N and K, respectively, denote any of the 4 bases and U or G, for encoding 8 to 12 random sequences. The inclusion of $(GGC\text{-}AGC)_3$ repeat codons encoded a triple-repeat glycine-serine peptide linker, and the stop codon UAG arrests the progression of ribosomes in the release factor 1 omitted flexible *in vitro* translation system. It was anticipated that more than 10^{12} macrocyclic peptides would be expressed in each library, and the resulting libraries were individually panned against biotinylated hSTING immobilised on streptavidin beads (Fig 1A). On 4 rounds of screening and selection, the enriched cDNA pools were then sequenced (Supplementary Fig S1A,B). Based on hit frequency assessment and sequence consensus (Supplementary Fig S1C,D), we selected 2 macrocyclic peptides P1 (peptide L1 in Supplementary Fig S1C) and P2 (peptide D1 in Supplementary Fig S1D), and then successfully synthesised them using solid-phase peptide synthesis (Fig 1B, Supplementary Fig S1E-H) to validate their interactions with hSTING and to further determine the mode of actions.

Nano-P1 is an hSTING inhibitor

Macrocyclic peptides generally face challenges in targeting intracellular targets due to their difficulty in crossing the cellular membrane [17]. P1 and P2, as macrocyclic peptides, are no exceptions after our test. To enable both peptides to target hSTING in the cytosol, we developed a nanoparticle-based macrocyclic peptide delivery system to enhance the membrane permeability of peptides P1 and P2, facilitating their entry into cells. Briefly, a cationic polymer, PBAE, was synthesised to electrostatically interact with the peptides. Additionally, an

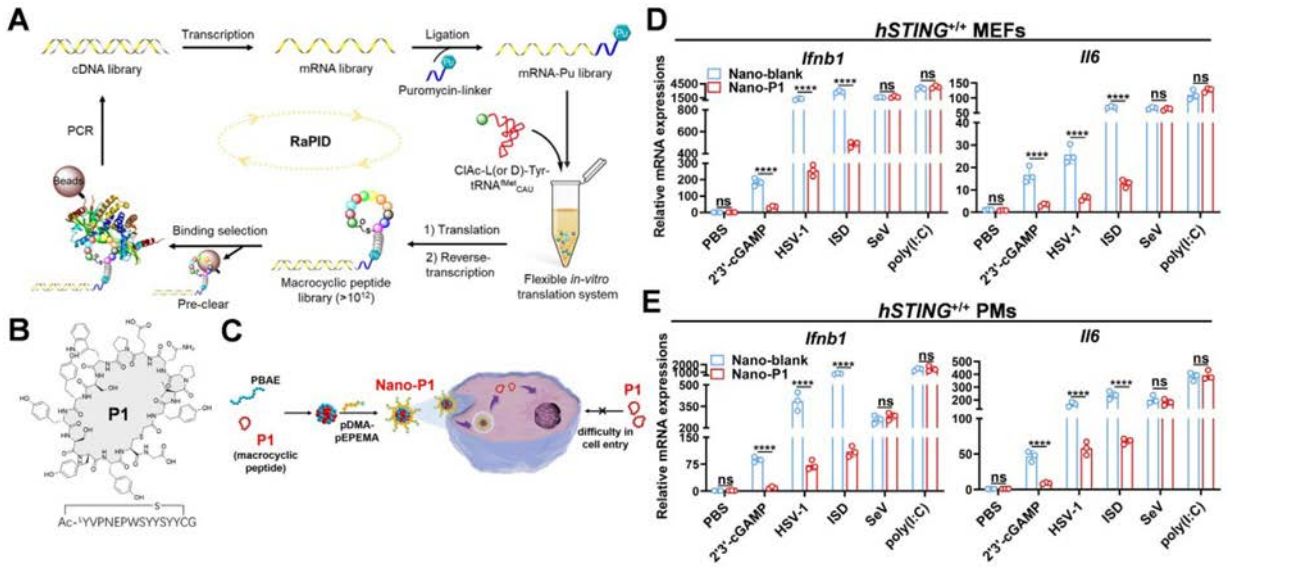

Figure 1. Nano-P1 is a human-STING inhibitor. (A) Schematic process flow of screening for macrocyclic peptides targeting hSTING with the RaPID system. (B) Chemical structure of the selected macrocyclic peptide P1. (C) Schematic design of nanoparticular macrocyclic peptides. (D and E) *hSTING*$^{+/+}$ MEFs or *hSTING*$^{+/+}$ PMs were treated with Nano-blank or Nano-P1 (30 μM) for 6 h and then stimulated with 2′3′-cGAMP for 3 h, or infected with HSV-1 or SeV for 6 h, or transfected with ISD or poly(I:C) for 6 h. The mRNA expressions of *Ifnb1* and *Il6* in *hSTING*$^{+/+}$ MEFs or *hSTING*$^{+/+}$ PMs were shown. The experiments in (D) and (E) were repeated 3 times, and data were presented as mean ± SD, with n = 3; ns: $P > .05$, ***$P < .001$, ****$P < .001$. 2′3′-cGAMP, 2′3′-cyclic GMP-AMP; hSTING, human STING; *hSTING*$^{+/+}$, humanised-*STING*; HSV-1, herpes simplex virus type 1; ISD, interferon stimulatory DNA; MEFs, mouse embryo fibroblasts; pDMA, poly (dimethylacrylamide); pEPEMA, poly (2-[N-ethyl-N-propyl amino] ethyl methacrylate); PMs, peritoneal macrophages; RaPID, random nonstandard peptide integrated discovery; SeV, Sendai Virus.

amphiphilic polymer, pDMA-pEPEMA, composed of a hydrophilic pDMA segment and an acid-sensitive pEPEMA chain, was synthesised through reversible addition fragmentation chain transfer (RAFT) polymerisation and chosen as the delivery vehicle for nanoparticle preparation (Fig 1C, Supplementary Fig S2A,B). The final products, P1 and P2 loaded with nanoparticles, were named Nano-P1 and Nano-P2, respectively.

To investigate the functional effects of Nano-P1 or Nano-P2 on hSTING, mouse embryo fibroblasts (MEFs) from humanised-*STING* (*hSTING*$^{+/+}$) mice were treated with Nano-P1 or Nano-P2 plus the canonical STING-activating ligand 2′3′-cGAMP. The results showed that both P1 and Nano-P1 were able to suppress 2′3′-cGAMP-induced *Ifnb1* expression, with Nano-P1 being more efficient than P1 alone (Supplementary Fig S2C) and acting in a dose-dependent manner. This indicates that the nanoparticle delivery system might effectively assist in the entry of P1 into cells. Although P2 binds to hSTING, neither P2 nor Nano-P2 had effect on the expression of *Ifnb1* induced by 2′3′-cGAMP (Supplementary Fig S2D). In addition, nanoparticle characteristic analysis revealed that Nano-P1 was a stable particle (Supplementary Fig S2E,F). Therefore, we decided to focus our efforts on Nano-P1 in the search for a potential hSTING inhibitor.

In *hSTING*$^{+/+}$ MEFs and *hSTING*$^{+/+}$ peritoneal macrophages, Nano-P1 significantly inhibited the expressions of *Ifnb1* and *Il6* triggered by 2′3′-cGAMP, herpes simplex virus type 1 (HSV-1, a dsDNA virus), or interferon stimulatory DNA (ISD) (Fig 1D,E), all of which are potent inducers of STING activity. In contrast, Nano-P1 did not inhibit the expressions of *Ifnb1* or *Il6* stimulated by poly(I:C) (dsRNA mimics) or Sendai Virus (a negative-sense single-stranded RNA virus) (Fig 1D,E), neither of which is the inducer of cGAS-STING, indicating the specificity of Nano-P1's inhibitory effect on STING. The RNA-seq analysis of *hSTING*$^{+/+}$ MEFs treated with Nano-P1 with or without 2′3′-cGAMP demonstrated that Nano-P1 decreased the expression of a set of genes induced by 2′3′-cGAMP (Supplementary Fig S3A), many of which are proven effector genes of the STING signalling transduction pathway, further proving the inhibition of hSTING by Nano-P1.

Insights into the molecular basis of the interaction between P1 and hSTING

To elucidate how P1, the active component of Nano-P1, inhibits the activation of hSTING, the crystal structure of the P1-hSTING complex was solved at 2.49 Å resolution (Supplementary Table S1). The structure analysis showed P1 binds to the V-shaped pocket of the hSTING C-terminal (hSTING^{CTD}) dimer through both polar and hydrophobic interactions (Fig 2A, Supplementary Fig S4A), with several residues (eg, Trp7, Tyr10 of P1, and Tyr163, Tyr167, Pro264 of hSTING) were being tested essential for the binding. In detail, Trp7 and Tyr10 from P1 insert directly into a hydrophobic pocket formed by residues from molecule A (Leu159, Ser162, Tyr163, Thr263, Pro264, and Thr267) and molecule A′ (Tyr163, Tyr167, and Thr263) (Fig 2B-D, Supplementary Fig S4B-F). The binding affinity of hSTING to P1 ($K_D \approx 5.4$ nM) (Fig 2C) is comparable with that of the natural ligand 2′3′-cGAMP ($K_D \approx 4$ nM) [31]. We then compared the structure of the P1-hSTING^{CTD} complex with that of 2′3′-cGAMP-hSTING^{CTD} (4KSY) (Fig 2E). Unlike 2′3′-cGAMP, which induces a closed conformation of hSTING, P1 stabilises an open state with rotated 'wings', preventing the conformational transition required for ligand-induced activation, which suggests that P1 acts as a competitive inhibitor of hSTING.

The *STING* locus transcribes transcripts with a diverse array of single-nucleotide polymorphisms (SNPs) that are variably distributed across global populations [32]. P1 was tested in the major hSTING variants found in global populations (HAQ, R232H, AQ, R293Q) [32,33] (Supplementary Fig S5A). We found P1 binds to R232H, AQ, and R293Q variants with K_D

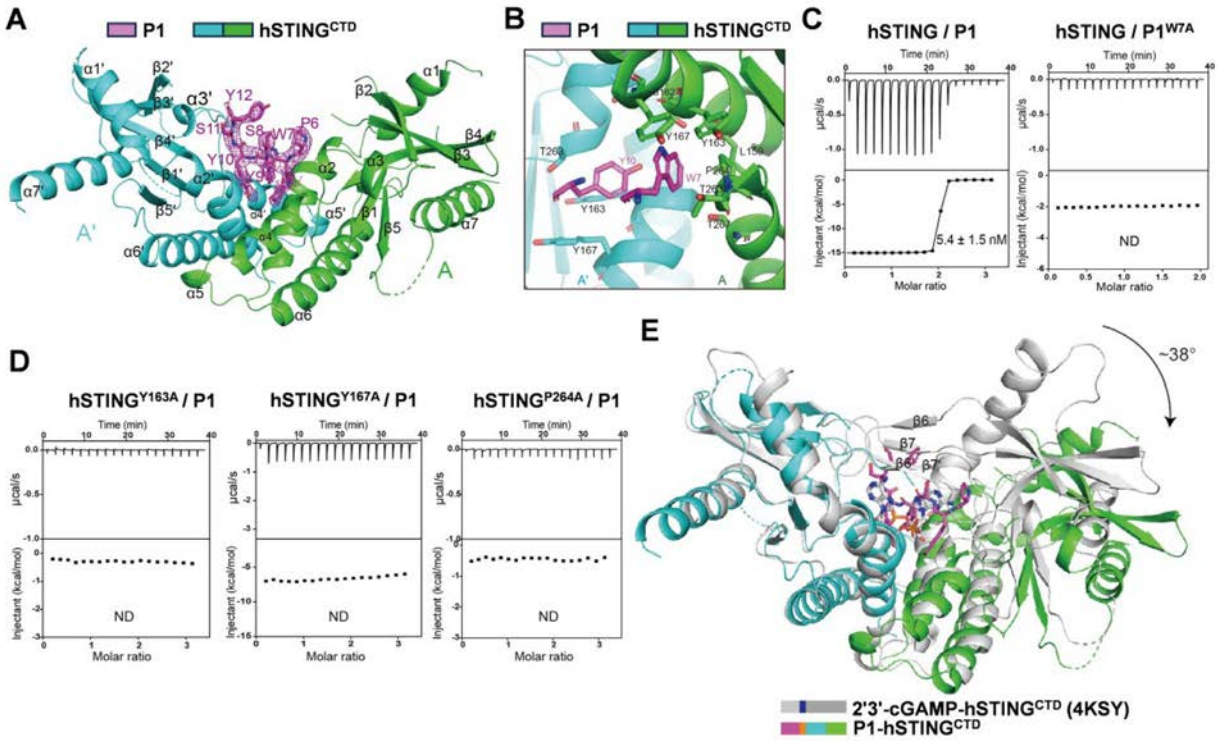

Figure 2. P1 binds to the cyclic nucleotide binding (CBD) domain of hSTING. (A) Overall structure of P1-hSTING^{CTD} (hSTING 153-343aa) complex. STING forms a dimer, and the 2 molecules are coloured in cyan and green, respectively. 2Fo-Fc electron-density map for P1, shown in purple mesh, is contoured at 1.6 σ; hSTING^{CTD} dimer exhibits a V-shaped pocket-like architecture, where P1 is located at the bottom of the pocket through extensive interactions. The V-shaped binding domain is primarily composed of 3 α-helices (α1, α2, and α3), a β-sheet (β4) and 2 loops (β2-β3 and β4-α4) from hSTING^{CTD} molecule A, and corresponding structures (α1′, α2′, α3′, β4′, β2′-β3′, and β4′-α4′) from the other molecule A′. (B) The interface between P1 and hSTING^{CTD}, with residues W7 and Y10 in P1 shown in purple sticks; Trp7 and Tyr10 from P1 insert directly into a hydrophobic pocket formed by residues from molecule A (Leu159, Ser162, Tyr163, Thr263, Pro264, and Thr267) and molecule A′ (Tyr163, Tyr167, and Thr263). (C) Binding affinity of hSTING^{CTD} with P1 and P1^{W7A} measured by isothermal titration calorimetry (ITC). (D) Binding affinity of hSTING^{CTD} mutants with P1 measured by ITC. (E) Structural comparison of 2′3′-cGAMP-hSTING (PDB: 4KSY) with P1-hSTING^{CTD}. The structure of 2′3′-cGAMP-hSTING is shown in grey. The arrow indicates the conformational change in hSTING on P1 binding. In detail, binding of P1 to the V-shaped pocket prompts the structure of hSTING^{CTD} dimer to adopt an 'open' state with 38°-rotated wings compared with 2′3′-cGAMP does. cGAMP, cyclic GMP-AMP; hSTING, human STING.

values between ~11.5 and ~23.0 nM (Supplementary Fig S5B), all of which were comparable with the prototype hSTING (K_D of ~5.4 nM). When HEK293T cells ectopically expressed the individual variants, Nano-P1 suppressed *IFNB1* expression on 2′3′-cGAMP stimulation in each variant (Supplementary Fig S5C). These results prove that Nano-P1 has broad inhibitory capabilities towards hSTING with major SNPs found in global populations.

Nano-P1 inhibits hSTING signalling transduction

The effectors of STING activation include both TBK1→IRF3→type I interferons and TBK1→NF-κB→proinflammatory cytokines pathways. In this study, we found that P1 binds to hSTING and suppresses the expression of *IFNB1* induced by 2′3′-cGAMP. We next aimed to confirm the suppression of both effector pathways by Nano-P1. The results revealed that Nano-P1 effectively inhibited the phosphorylation of both IRF3 and p65 as well as the phosphorylation of STING and TBK1 in *hSTING*$^{+/+}$ MEFs on HSV-1 infection (Fig 3A). Nano-P1^{W7A} did not suppress the phosphorylation of STING and its effectors, which was consistent with the fact that P1^{W7A} does not bind to hSTING (Fig 2C). Moreover, Nano-P1 reduced the amount of nuclear IRF3 and nuclear p65 in HSV-1-infected *hSTING*$^{+/+}$ MEFs (Fig 3A) and inhibited the translocation of IRF3 and p65 from cytoplasm to nucleus after hSTING activation by 2′3′-cGAMP (Fig 3B,C). Because phosphorylation and nuclear translocation of transcription factors IRF3 and p65 are key checkpoints of STING activation, these results collectively demonstrate that the inhibition of hSTING by Nano-P1 resulted in the suppression of the canonical hSTING signalling transduction pathways.

On binding with 2′3′-cGAMP, STING dimers translocate from the ER membrane to the TGN apparatus, during which process STING dimers aggregate and form oligomers to initiate downstream signal transductions [4,34]. Because P1 binds to the same V-shaped pocket domain on hSTING dimers as 2′3′-cGAMP, but hinders the formation of lids, we speculated that the lid-less state and the aberrant rotation of the wings of hSTING by P1 inhibited the oligomerisation and translocation of hSTING. The results from native-gel electrophoresis proved our hypothesis, as Nano-P1 effectively reduced the tetramerisation and oligomerisation of hSTING, whereas the dimers of hSTING accumulated (Fig 3D), with the protein levels of hSTING in treated cells remaining unchanged (Supplementary Fig S6A). This mode of action by Nano-P1 was comparable with H-151, a proven inhibitor of hSTING, which inhibits the activation of hSTING by suppression of the aggregation of hSTING [14]. Furthermore, Nano-P1 and H-151 exhibited similar inhibitory effects on the expression of *Ifnb1, Isg15, Cxcl10*, and *Il6* induced

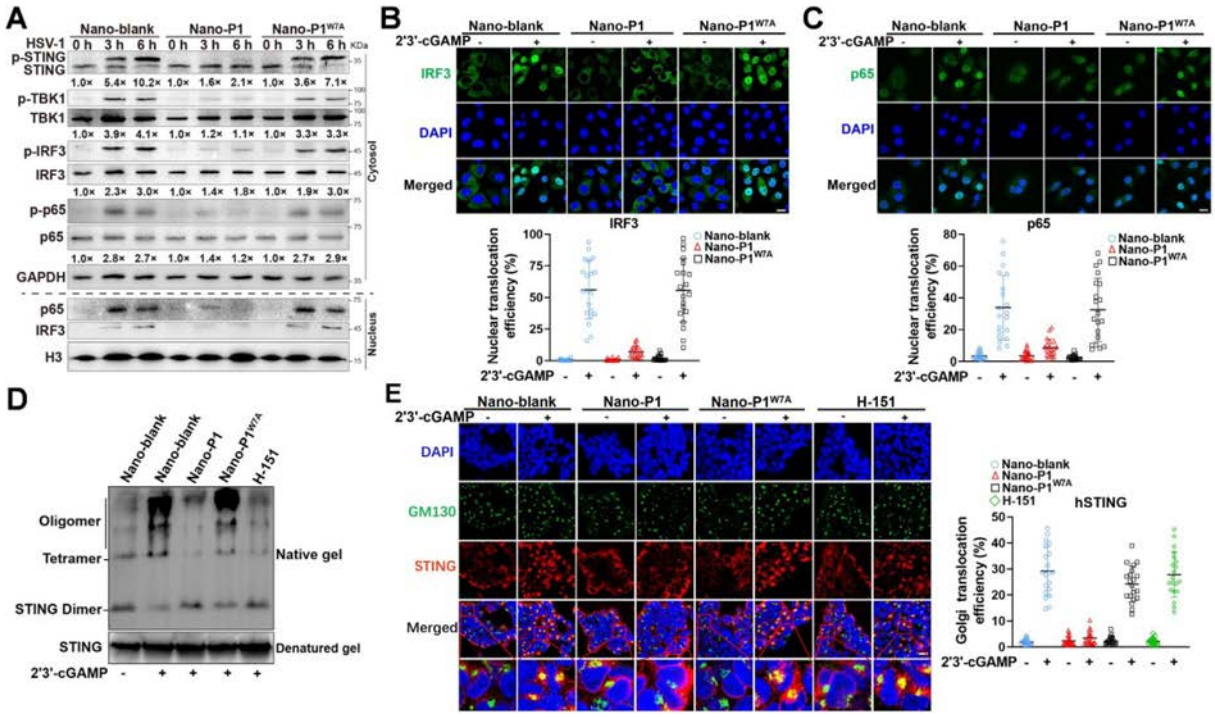

Figure 3. Nano-P1 inhibits hSTING signalling transduction. (A) *hSTING*$^{+/+}$ MEFs were infected with HSV-1 for indicated time following Nano-blank, Nano-P1 or Nano-P1^{W7A} treatment for 6 h. The phosphorylation of STING, TBK1, IRF3-S396, and p65 in cytosol and the presence of IRF3 and p65 in the nucleus were detected by Western blot. All blots were quantified by Image J. (B and C) Hela cells were treated with Nano-blank, Nano-P1, or Nano-P1^{W7A} (30 μM) for 6 h and then stimulated with 2′3′-cGAMP for 3 h. (B) Representative immunofluorescences of IRF3 (green) and DAPI (blue). (C) Representative immunofluorescences of p65 (green) and DAPI (blue). Scale bar = 20 μm. The efficiency of nuclear translocation of IRF3 and p65 in each cell was quantified as the percentage of merged cyan colour intensity within the DAPI-stained nuclear area. (D) HEK293T-*hSTING*^{OE} were treated with Nano-blank, Nano-P1, and Nano-P1^{W7A} (30 μM) for 6 h, or with H-151 (2 μM) for 2 h and then stimulated with 2′3′-cGAMP for 3 h. The oligomerisations of STING were detected by native PAGE and immunoblot. (E) HEK293T-*hSTING*^{OE} were treated with Nano-blank, Nano-P1, and Nano-P1^{W7A} (30 μM) for 6 h, or with H-151 (2 μM) for 2 h and then stimulated with 2′3′-cGAMP for 3 h. Scale bar = 20 μm. Left, representative immunofluorescences of GM130 (green), STING (red), and DAPI (blue). Right, statistics on the percentage of the number of STING-Golgi colocalised loci to the number of STING loci in each cell. The experiments in (A-E) were repeated 3 times. Data in (E) was presented as mean ± SD, with n = 20. cGAMP, cyclic GMP-AMP; hSTING, human STING; *hSTING*$^{+/+}$, humanised-*STING*; HSV-1, herpes simplex virus type 1; MEFs, mouse embryo fibroblasts.

by 2′3′-cGAMP in *hSTING*$^{+/+}$ MEFs (Supplementary Fig S6B). Therefore, Nano-P1 is as effective as H-151 in inhibiting STING. However, we observed a significant difference in Nano-P1 from H-151: hSTING did not translocate to the TGN following Nano-P1 treatment, indicating that Nano-P1 exerts its inhibitory function at the ER stage of hSTING activation, whereas H-151 did not block the translocation of hSTING from ER to the TGN (Fig 3F, Supplementary Fig S6C).

Nano-P1 attenuates HSV-1-induced host inflammation response

STING is an important effector of host anti-infection innate immunity, especially for the anti-DNA virus infections. Because Nano-P1 inhibits the activation of hSTING, we decided to investigate whether it would dampen the host anti-HSV-1 innate immune responses. Peripheral blood mononuclear cells (PBMCs) obtained from healthy human donors were pretreated with Nano-P1 and then infected with HSV-1. The serum levels of IFN-β and IL-6 in the PBMCs decreased in a Nano-P1 concentration-dependent manner (Fig 4A, Supplementary Fig S7A,B). Similar effects were observed in *hSTING*$^{+/+}$ mice when Nano-P1 was intravenously injected into the mice followed by HSV-1 infection. The serum levels of IFN-β and IL-6 (Fig 4B, Supplementary Fig S7C) in these mice were significantly lower than those in the mice treated with Nano-blank (nanoparticles alone). Because STING is the major effector of host anti-HSV-1 innate immunity, its inhibition by Nano-P1 in the HSV-1-infected *hSTING*$^{+/+}$ mice resulted in increased HSV-1 viral loads in brain and spleen, and thereafter, significantly lower survival rate (Fig 4C,D). Collectively, these findings demonstrate that Nano-P1 suppressed the inflammatory response triggered by HSV-1 infection and dampened host anti-HSV-1 immunity, further confirming the inhibitory effects of Nano-P1 on the STING pathway *in vivo*.

Nano-P1 suppresses systemic inflammation and autoimmune features in humanised-STING mice

Because Nano-P1, an hSTING inhibitor, has the capacity to suppress the production of inflammatory cytokines in HSV-1-infected *hSTING*$^{+/+}$ mice, it is reasonable to propose that it may constrain autoimmune inflammation as well, including the development of antinuclear autoantibodies (ANAs) that are a hallmark of lupus and other autoimmune diseases. Inactivation of TREX1, an enzyme responsible for degrading cytosolic DNA fragments, results in aberrant activation of cGAS-STING and subsequent systemic autoimmune inflammation. The *Trex1*$^{-/-}$ mice are reminiscent of autoimmune diseases, and lupus-like features in the mice include spontaneous development of high-titre ANAs, elevated type I interferon signalling, fatal inflammatory myocarditis, and splenomegaly. Therefore, we decided to

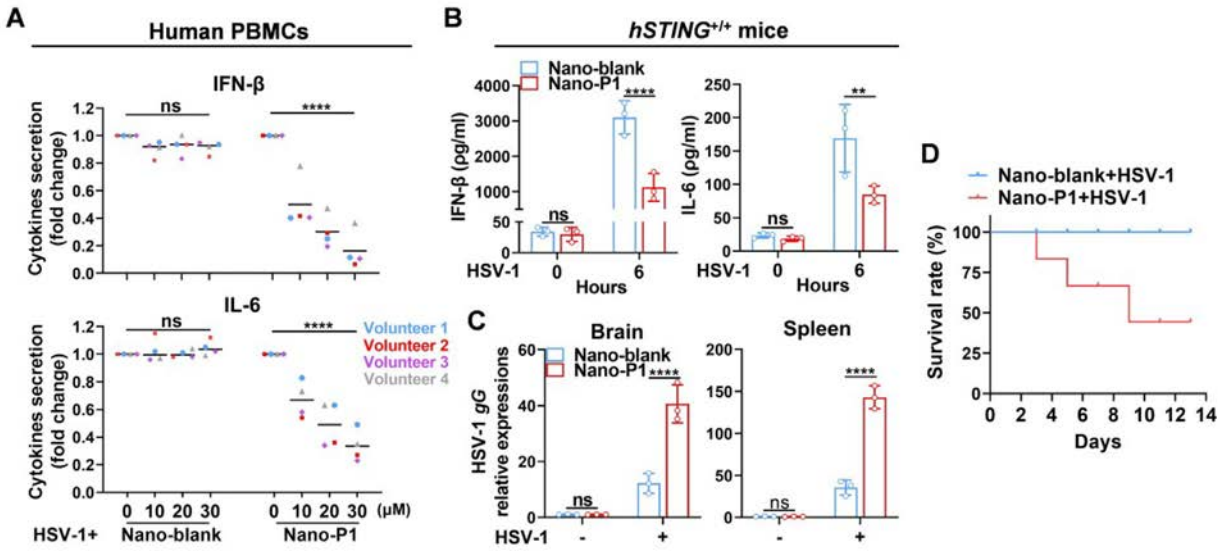

Figure 4. Nano-P1 attenuates HSV-1-induced inflammatory response. (A) PBMCs obtained from healthy volunteers were treated with nanoblank or Nano-P1 with indicated concentrations and then infected with HSV-1 for 6 h. The secretion of interferon-β (IFN-β) or interleukin-6 (IL-6) was detected by ELISA. The fold changes of the IFN-β (left) or IL-6 (right) concentrations were shown. (B) The *hSTING*$^{+/+}$ mice were treated with Nano-P1 for 12 h and then were infected with HSV-1 for 6 h. The concentrations of IFN-β (left) or IL-6 (right) in serum was detected by ELISA. (C) The *hSTING*$^{+/+}$ mice were treated with Nano-P1 for 12 h and then were infected with HSV-1 for 24 h. The expressions of HSV-1 structural gene *gG* in mouse brains were detected by qPCR; (D) The *hSTING*$^{+/+}$ mice were treated with Nano-P1 for 12 h and then were infected with HSV-1. Nano-P1 was administered every other day. The survival curve of HSV-1-infected mice with or without Nano-P1 treatment is shown. The experiments were repeated 3 times. Data in (A) were presented as median, data in (B) and (C) were presented as mean ± SD, with n = 4 (A), n = 3 (B and C), n = 4 (D); ns: $P > .05$, $^{**}P < .01$, $^{****}P < .0001$. *hSTING*$^{+/+}$, humanised-*STING*; HSV-1, herpes simplex virus type 1; PBMCs, peripheral blood mononuclear cells; ELISA, enzyme linked immunosorbent assay; qPCR, quantitative PCR.

use *hSTING*$^{+/+}$*Trex1*$^{-/-}$ mice to investigate whether Nano-P1 could suppress the systemic inflammation induced by hyperactivity of cGAS-STING in these transgenic mice (Fig 5A). The *hSTING*$^{+/+}$*Trex1*$^{-/-}$ mice were much smaller than wild-type controls (Fig 5B, Supplementary Fig S8A) at every age starting from birth, and they died within 7 weeks of age (Fig 5C). The runt *hSTING*$^{+/+}$*Trex1*$^{-/-}$ mice that received Nano-P1 treatment had body weights and survival rates comparable with those of *hSTING*$^{+/+}$*Trex1*$^{WT/WT}$ mice with or without Nano-P1 treatments (Fig 5B,C, Supplementary Fig S8A). Unsurprisingly, because Nano-P1^{W7A} does not bind to hSTING, it did not correct the low body weights of the runt *hSTING*$^{+/+}$*Trex1*$^{-/-}$ mice, nor did it substantially extend their lifespans. Consistent with these results, *hSTING*$^{+/+}$*Trex1*$^{-/-}$ mice had splenomegaly, while the Nano-P1-treated mice had spleens of normal size as controls; no such effects were observed in the spleens of Nano-P1^{W7A} treated *hSTING*$^{+/+}$*Trex1*$^{-/-}$ mice (Supplementary Fig S8B). These results indicate that Nano-P1 has significant therapeutic effects on systemic autoimmune inflammation in the *hSTING*$^{+/+}$*Trex1*$^{-/-}$ mice.

We next investigated Nano-P1's anti-inflammatory efficacy at both organ and molecular levels. Histological and morphological changes as well as lymphocyte infiltrations observed in the heart, liver, intestine, stomach, kidney, muscle, and tongue of the Nano-P1-treated *hSTING*$^{+/+}$*Trex1*$^{-/-}$ mice were all comparable with those in *Trex1*$^{WT/WT}$ mice (Fig 5D,E, Supplementary Fig S8C,D) following a 14-day treatment. Nano-P1 significantly reduced the mRNA expression of inflammatory cytokines, such as *Ifnb1, Isg15, Cxcl10,* and *Il6* in the heart, liver, and intestine of *hSTING*$^{+/+}$*Trex1*$^{-/-}$ mice, though not to the same levels as in the *hSTING*$^{+/+}$*Trex1*$^{WT/WT}$ mice (Fig 5F), whereas Nano-P1^{W7A} had no such effects. The presence of ANAs is a defining feature of lupus-like autoimmune inflammation. The test of ANAs in the serum of *hSTING*$^{+/+}$*Trex1*$^{-/-}$ mice showed strong positive signals, and Nano-P1 significantly reduced serum ANA levels (Fig 5G,H), a result that was consistent with the histopathological or gene expression of other lupus-like features like elevated type I interferon signalling, fatal inflammatory myocarditis, and splenomegaly. Collectively, Nano-P1 effectively suppressed the systemic autoimmune inflammation especially lupus-like features in *hSTING*$^{+/+}$*Trex1*$^{-/-}$ mice and extended their survival, proving that Nano-P1 may serve as a viable therapeutic option for such conditions.

Regarding the toxicity of Nano-P1, it was observed that Nano-P1 did not cause weight loss, alterations in spleen size, or histological changes of major organs of *hSTING*$^{+/+}$*Trex1*$^{WT/WT}$ mice (Fig 5B,D,E, Supplementary Fig S8A-D). *In vitro*, Nano-P1 had no effect on the proliferation of *hSTING*$^{+/+}$*Trex1*$^{WT/WT}$ MEFs (Supplementary Fig S9A), and RNA-seq results indicated a high correlation between the Nano-P1 treatment group and the phosphate-buffered saline (PBS) control group in terms of global gene expression in *hSTING*$^{+/+}$*Trex1*$^{WT/WT}$ MEFs (Supplementary Fig S9B). These results suggest that Nano-P1 is safe both *in vitro* and *in vivo*.

Characterising the *in vivo* distribution and retention of Nano-P1 is critical for its preclinical development. To track Nano-P1 in *hSTING*$^{+/+}$*Trex1*$^{WT/WT}$ mice, fluorescein isothiocyanate (FITC)-conjugated P1 (Fig 6A,B) was formulated to nanoparticles (Nano-P1-FITC). *In vivo* imaging was performed at 6- and 12-hour postintravenous injection, assessing whole-body fluorescent intensity and tissue-specific accumulation in brain, spinal cord, stomach, intestine, liver, heart, kidney, lung, tongue, muscle, spleen, and lymph nodes, totally 12 organs/tissues. The results showed that Nano-P1-FITC exhibited widespread systemic distribution by 6 hours, with fluorescence signals declining between 6 and 12 hours (Fig 6C-E). Notably, the signal intensity was particularly

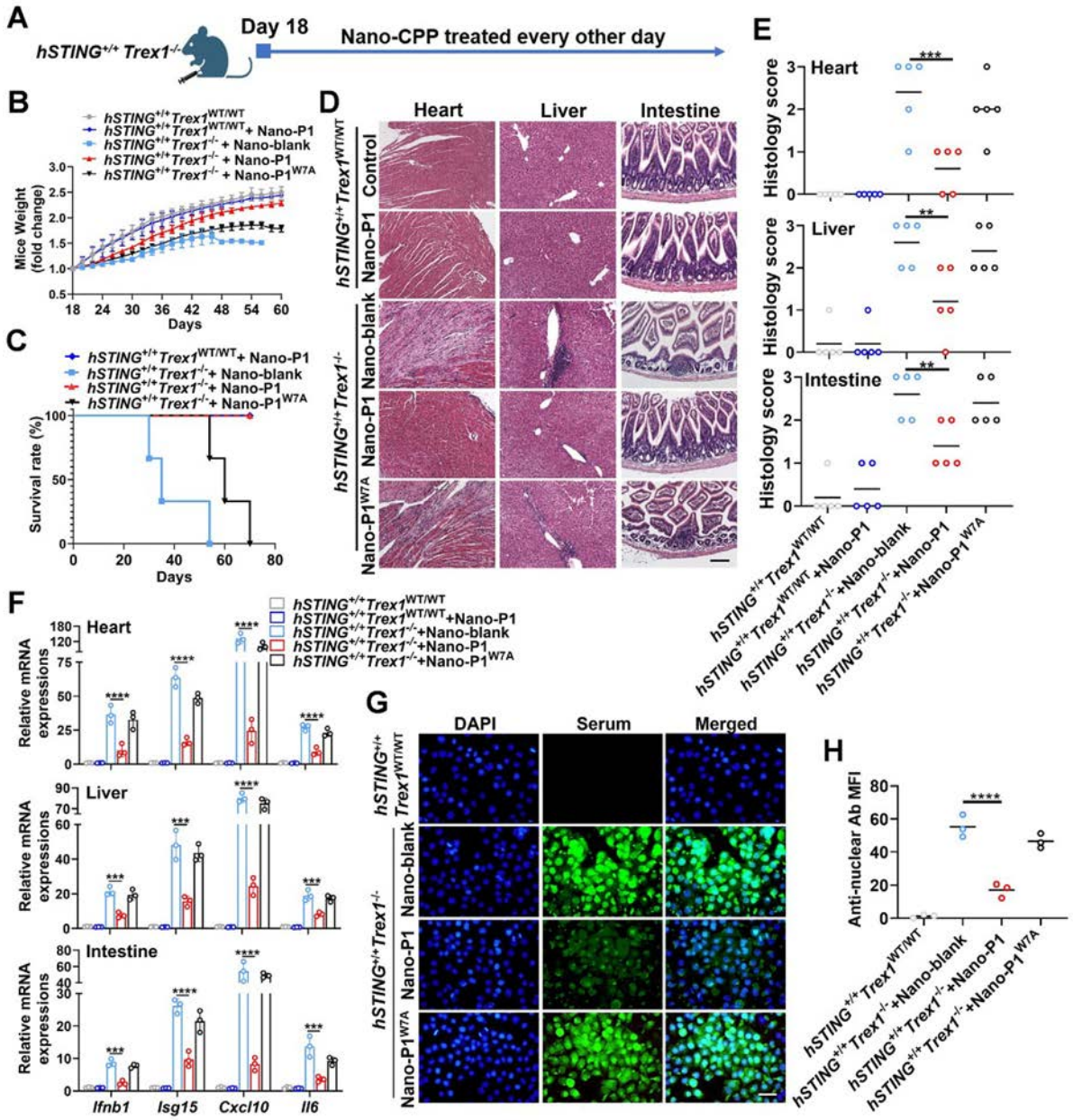

Figure 5. Nano-P1 suppresses the systemic autoimmune inflammation in *hSTING*$^{+/+}$*Trex1*$^{-/-}$ mice. (A) The schematic procedure for Nano-cyclic peptides (Nano-CPP) treatment in the mice. (B-F) *hSTING*$^{+/+}$*Trex1*$^{WT/WT}$ mice were treated with Nano-P1, and *hSTING*$^{+/+}$*Trex1*$^{-/-}$ mice were treated with Nano-blank, Nano-P1, or Nano-P1^{W7A} following the procedure in (A). (B) Body weights of the mice. (C) Survival rate of the mice. (D) Representative haematoxylin and eosin (H&E) staining of heart, liver, and intestine sections of the mice. Scale bar = 100 μm. (E) The histology score of tissues in (D). (F) The mRNA expression of *Ifnb1, Isg15, Cxcl10*, and *Il6* in the heart, liver, or intestine of the mice was detected by qPCR. (G and H) Antinuclear antibody testing. The serum from *hSTING*$^{+/+}$*Trex1*$^{WT/WT}$ mice and Nano-blank, Nano-P1, Nano-P1^{W7A}-treated *hSTING*$^{+/+}$*Trex1*$^{-/-}$ mice was tested. (G) Representative immunofluorescences of serum antinuclear IgG (green) staining were shown. (H) The mean fluorescence intensity (MFI) of serum antinuclear IgG. The experiments were repeated 3 times. Data were presented as mean ± SD, with n = 3 (B, C, F, H), n = 5 (E); $^{**}P$ <.01, $^{***}P$ <.001, $^{****}P$ <.0001. *hSTING*$^{+/+}$, humanised-*STING*.

strong in the intestine, brain, muscle, and lung, while there was no detectable signal in heart. The findings highlight Nano-P1's tissue-specific pharmacokinetic profile and support its further exploration as a promising therapeutic candidate for targeted modulation of STING-dependent systemic inflammation in clinical applications.

DISCUSSION

STING is a key component of the cGAS-STING pathway, which plays an essential role in innate immunity. Recent studies have extensively examined its activation and degradation, offering a theoretical foundation for the development of drugs targeting distinct mechanisms of its functions and life cycle. Aberrant hyperactivation and/or prolonged activity of STING have been considered as a causality in many pathologies, including but not limited to autoimmune inflammation. Therefore, searching for clinically useful STING inhibitors is of great interest. Although STING inhibitors in the form of linear peptides or cyclic peptides within small-molecule category have been documented, there remains a strong demand for other types of inhibitors, such as macrocyclic peptides. Unlike small-molecule chemicals or peptides, macrocyclic peptides offer enhanced safety and greater specificity for the targets. In this study,

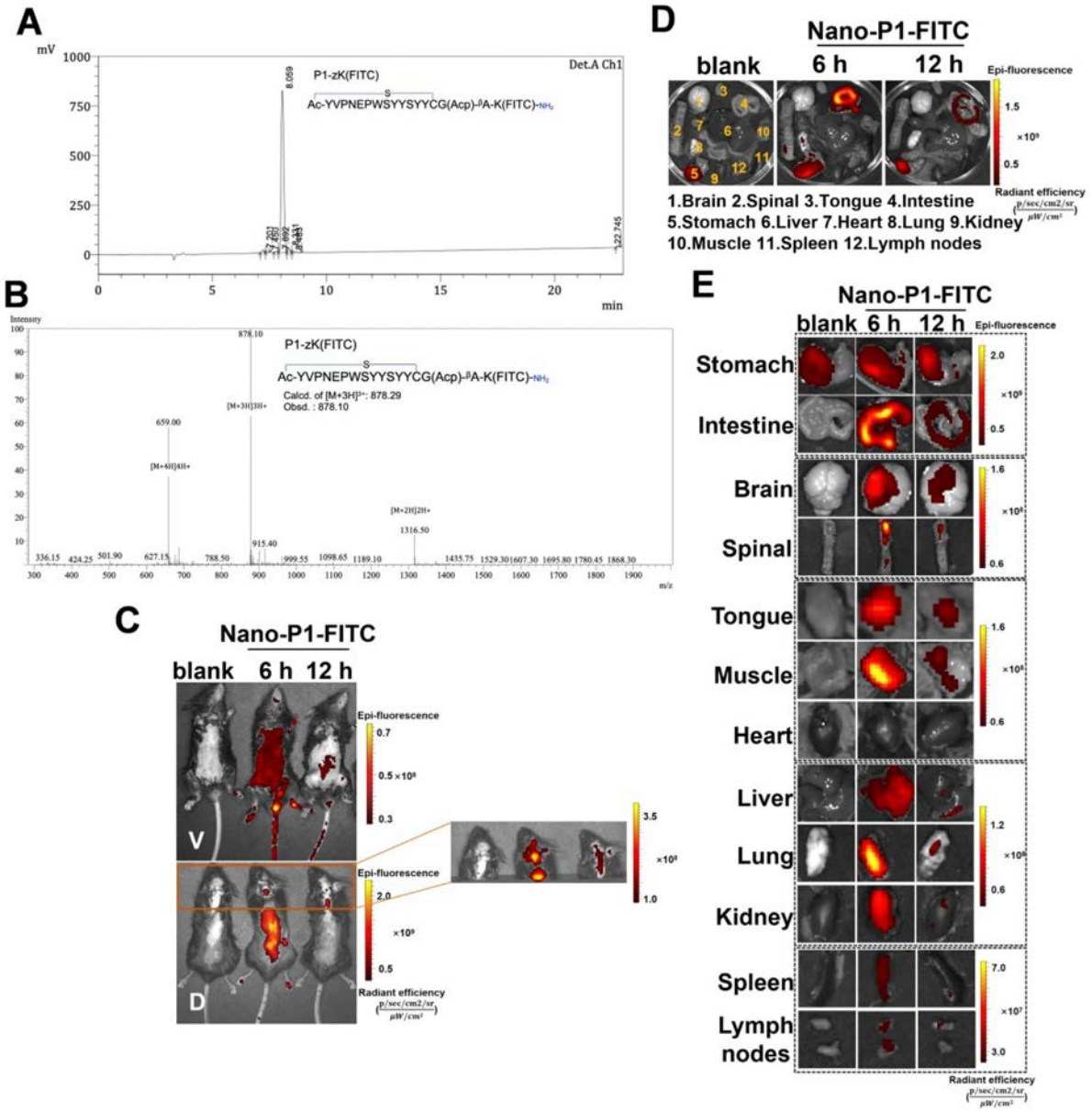

Figure 6. The distribution and retention of Nano-P1-FITC in mice. (A) High performance liquid chromatography (HPLC) spectra of synthesised P1-zk (FITC) (P1-FITC) peptides. (B) Electrospray ionization mass spectrometry (ESI-MS) spectra of the synthesised P1-FITC peptides after HPLC purification. (C) *In vivo* imaging system (IVIS) scanned the fluorescence of *hSTING*$^{+/+}$ mice 6 and 12 h after intravenous (i.v.) injection of Nano-P1-FITC. Left: Whole-body images of mice (V: ventral, D: dorsal). Right: long exposure of the brain of the mice shown in a dorsal section of C. (D and E) IVIS scanned the fluorescence of tissues from *hSTING*$^{+/+}$ mice 6 and 12 h after i.v. injection of Nano-P1-FITC. (D) All of the 12 tissues were exposed simultaneously by IVIS. (E) Each of the 12 tissues shown in (D) was exposed alone by IVIS. Tissues in each dashed box were exposed at the same time. *hSTING*$^{+/+}$, humanised-*STING*; FITC, fluorescein isothiocyanate.

macrocyclic peptides P1 and P2 were identified by RaPID to target hSTING. However, cell permeability represents a major challenge for macrocyclic peptides. To address this limitation, extensive chemical modifications, such as incorporation of non-natural amino acids, backbone *N*-methylation, or lipidation, have been explored to improve membrane penetration [17]. In addition, advanced delivery strategies, including nanoparticle encapsulation and conjugation to cell-penetrating moieties, offer promising tools to enhance both cellular uptake and tissue penetration [17,35–37]. To facilitate the ability of macrocyclic peptides to cross cellular membranes, PBAE and pDMA-pEPEMA modifications were employed to transform P1 and P2 into nanoparticles Nano-P1 and Nano-P2, respectively. Nano-P1 effectively suppresses the activation of hSTING, whereas Nano-P2 does not have such effects. The binding constant of P1 and hSTING ($K_D \approx 5.4$ nM) is comparable with that of 2′3′-cGAMP and hSTING ($K_D \approx 4$ nM) [38], and the structure of P1-hSTING complex indicates that P1 binds within the CBD pocket region of hSTING, akin to the binding position of 2′3′-cGAMP. Compared with the 'open' conformation structure of P1-hSTING, previous structural studies have shown that binding of 2′3′-cGAMP results in a closing of the STING dimer angle [39], but this 'closed' conformation does not appear to be necessary for activation. Notably, crystal structures of STING bound to other agonists, including cyclic-di-GMP [40] and diABZI [41], suggest that STING can still be active in the 'open' conformation. Considering the facts that nano-P1 suppresses hSTING activation, P1 binds hSTING with a K_D similar to that of the natural ligand 2′3′-cGAMP and the structure of P1-bound hSTING^{CTD}, we hypothesise that P1 may inhibit the binding of 2′3′-cGAMP to

hSTING by exerting steric hindrance through its interaction with the hSTING CBD, thereby interfering with the further activation of hSTING.

The activation of STING primarily involves the binding of 2′3′-cGAMP to STING dimer and translocation from the ER to the TGN, where STING forms oligomer and activates downstream pathways. H-151, the most studied and well-recognised gold-standard inhibitor for STING oligomerisation, covalently binds to STING at cysteine-91, blocking the palmitoylation and clustering of STINGs when STINGs are on the TGN, without inhibiting the translocation of STING from the ER to the TGN. Nano-P1, based on the analysis of the crystal structure of P1-hSTING^{CTD} complex, binds to hSTING in the same domain as 2′3′-cGAMP, with a K_D comparable with that of 2′3′-cGAMP. It prevents the regular conformational change of hSTING, and thus inhibits the clustering of hSTING and blocks the translocation of STING to the TGN. These observations prompted us to propose that Nano-P1 exerts its competitively inhibitory effects on STINGs anchored on the ER membrane, representing a different mode of action from H-151. It is worth noting that numerous studies have suggested that macrocyclic peptides possess the capability to interfere with protein-protein interactions. Hence, whether Nano-P1 may affect the binding of other proteins to hSTING warrants future exploration.

The mode of action of Nano-P1 requires wild-type CBD in the signalling pathway for its inhibitory function. The STING transcript variants that are common in the general populations have lower binding affinity and are less responsive to Nano-P1 (Supplementary Fig S5B,C) than the canonical transcript, suggesting that Nano-P1 may have to be dose adjusted to provide comparable results. In contrast, STING-associated vasculopathy with onset in infancy is caused by ligand-independent activation of STING due to gain-of-function (GOF) mutations in *STING1*, which would not be amenable to blockade with Nano-P1. Furthermore, in the subset of systemic lupus erythematosus where the production of type 1 interferon is dependent on GOF mutations in *TLR7* [42], we suspect that Nano-P1 would not block the mechanism.

To pave the way for possible clinic applications in the future, we tested the inhibitory effects of Nano-P1 in humanised-STING mice. The genetic manipulations replaced the codons from the sixth exon of mSTING with hSTING sequences, including the V-shaped domain of hSTING that binds P1, based on our structural analysis. We also introduced *Trex1*-knockout mutant alleles into the mice. As a 3′-to-5′ DNA exonuclease, *Trex1*-deficiency results in the cytoplasmic accumulation of DNA [43], thereby perpetually triggering the cGAS-STING pathway. Therefore, *hSTING*$^{+/+}$*Trex1*$^{-/-}$ mice provide a suitable model to study the functions of P1 on hSTING, both *in vitro* and *in vivo*. Compared with *hSTING*$^{+/+}$*Trex1*$^{WT/WT}$ mice, *hSTING*$^{+/+}$*Trex1*$^{-/-}$ mice exhibited lower body weights and persistent multiorgan autoinflammation, ultimately resulting in premature mortality. Nano-P1 demonstrated significant therapeutic effects on *hSTING*$^{+/+}$*Trex1*$^{-/-}$ mice, leading to enhanced growth, a substantial reduction in systemic inflammation, and improved survival. In addition, our findings showed that Nano-P1 was safe when administered intravenously or intraperitoneally in mice, without eliciting toxic side reactions.

Trex1$^{-/-}$ mice have been widely used for studying cGAS-STING. The mice model many aspects of immunopathology of systemic autoimmune inflammation, such as systemic lupus erythematosus (SLE) and Aicardi-Goutières Syndrome (AGS). In *Trex1*$^{-/-}$ mice, we observed lupus-like features, including high titre of ANAs, transient skin redness at 2-4 weeks of age, elevated type I interferon signalling, fatal inflammatory myocarditis, nephritis, splenomegaly, growth failure, and early lethality. However, the pathology of systemic inflammation in *Trex1*$^{-/-}$ mice is mainly driven by STING activation rather than by TLR7 (Supplementary Fig S10A). These mice do not develop antibody-mediated organ manifestations of SLE, nor do they develop anti-dsDNA antibodies. *Trex1*$^{-/-}$ mice do not develop central nerve system disease, which is the disease defining and often devastating feature of human AGS. Therefore, the interpretation of therapeutic potential of Nano-P1 on systemic inflammation in *Trex1*$^{-/-}$ mice should be careful, especially when SLE and AGS are considered.

Trex1$^{-/-}$ mice bearing wild-type allele of *mSting1* exhibited much weaker response to Nano-P1 than the mice with human allele of *STING1* (*hSTING*$^{+/+}$*Trex1*$^{-/-}$) in terms of *Ifnb1, Isg15, Cxcl10*, and *Il6* expression (Supplementary Fig S11A,B), which is a confirmation of species specificity from the initial high-throughput screening with human-STING as bait that yields Nano-P1 (Fig 1A, Supplementary Fig S1A,C). This specificity strongly favours to use humanised-STING mice for future studies on Nano-P1.

Besides systemic autoimmune inflammation, Nano-P1 suppressed the inflammatory responses induced by the DNA virus HSV-1 in *hSTING*$^{+/+}$ mice and thus enhanced HSV-1 replication in the mice, suggesting that the inhibitory effect of Nano-P1 on hSTING would dampen the antiviral innate immunity centred on STING *in vivo*. *In vitro* experiments with HSV-1-infected human PBMCs showed similar results, with levels of IFN-β as the readouts. The findings suggest that there might be a risk for uncontrollable infections when using Nano-P1 to treat systemic autoimmune inflammation, which we believe would be a general issue for STING inhibitors.

P1 is not the only STING inhibitor targeting the CBD. In comparison with published STING CBD-blocking compounds, P1 exhibits a comparable K_D value to the other compounds, and its nanoform Nano-P1 shows a competitive effective dose *in vivo* (Supplementary Fig S12), which is an advantage of Nano-P1 over the other STING CBD-blocking compounds analysed.

In conclusion, we identified a macrocyclic peptide, named P1, which binds to and inhibits hSTING, providing molecular insights into its inhibitory function (Supplementary Fig S13). Both *in vitro* and *in vivo* experiments demonstrated that the macrocyclic peptide inhibited systemic autoimmune inflammation as well as infectious inflammation, providing compelling evidence to support Nano-P1 as a potential therapeutic agent for the clinical management of systemic inflammatory diseases.

Competing interests

The authors have a patent application related to this work. The authors declare no other competing interests.

Contributors

LL, YY, HZ, and JZ designed the project. JZ and QZ performed the cellular and animal experiments. JW performed the macrocyclic peptide selection and designed synthesis strategy. ZZ performed the preparation of nanopeptide with the help from YL. HY and XW purified and crystallised the proteins. XL determined the crystal structure and analysed the SAXS data with the help from HY. LL, YY, HZ, and JZ analysed data and wrote the paper with input from all other authors.

Funding

This work was supported in part by fundings from National Key R&D Program of China (2024YFC3407100, YY), the National Natural Science Foundation of China (22277065, YY; 32270970, LL; 82241220, ZY), Tianjin Municipal Science and Technology Program (22JCYBJC00440, 23JCZXJC00360, 24ZXZSSS00030, LL), Taishan Scholar Program of Shandong Province (No. tsqn202103148, YY), Shandong Provincial Excellent Young Scholars Fund (ZR2024YQ024, YY), and State Key Laboratory of Microbial Technology Open Projects Fund (Project no. 20220904-17, YY).

Patient consent for publication

Not applicable.

Ethics approval

The animal study was approved by the Animal Ethics Committee of Tianjin Medical University. The research with human PBMCs was approved by the Ethics Committe of Tianjin Medical University.

Provenance and peer review

Not commissioned; externally peer reviewed.

Supplementary materials

Supplementary material associated with this article can be found in the online version at doi:10.1016/j.ard.2025.10.023.

Orcid

Long Li: http://orcid.org/0000-0002-4727-9307

REFERENCES

[1] Sun L, Wu J, Du F, Chen X, Chen ZJ. Cyclic GMP-AMP synthase is a cytosolic DNA sensor that activates the type I interferon pathway. Science 2013;339:786–91. doi: 10.1126/science.1232458.
[2] Hopfner K-P, Hornung V. Molecular mechanisms and cellular functions of cGAS-STING signalling. Nat Rev Mol Cell Biol 2020;21:501–21. doi: 10.1038/s41580-020-0244-x.
[3] Decout A, Katz JD, Venkatraman S, Ablasser A. The cGAS-STING pathway as a therapeutic target in inflammatory diseases. Nat Rev Immunol 2021;21:548–69. doi: 10.1038/s41577-021-00524-z.
[4] Zhang C, Shang G, Gui X, Zhang X, Bai XC, Chen ZJ. Structural basis of STING binding with and phosphorylation by TBK1. Nature 2019;567:394–8. doi: 10.1038/s41586-019-1000-2.
[5] Liu S, Cai X, Wu J, Cong Q, Chen X, Li T, et al. Phosphorylation of innate immune adaptor proteins MAVS, STING, and TRIF induces IRF3 activation. Science 2015;347:aaa2630. doi: 10.1126/science.aaa2630.
[6] de Oliveira Mann CC, Orzalli MH, King DS, Kagan JC, Lee ASY, Kranzusch PJ. Modular architecture of the STING C-Terminal tail allows interferon and NF-κB signaling adaptation. Cell Rep 2019;27 1165-75.e5. doi: 10.1016/j.celrep.2019.03.098.
[7] Ablasser A, Hur S. Regulation of cGAS- and RLR-mediated immunity to nucleic acids. Nat Immunol 2020;21:17–29. doi: 10.1038/s41590-019-0556-1.
[8] Liu Y, Xu P, Rivara S, Liu C, Ricci J, Ren X, et al. Clathrin-associated AP-1 controls termination of STING signalling. Nature 2022;610:761–7. doi: 10.1038/s41586-022-05354-0.
[9] An J, Durcan L, Karr RM, Briggs TA, Rice GI, Teal TH, et al. Expression of cyclic GMP-AMP synthase in patients with systemic lupus erythematosus. Arthritis Rheumatol 2017;69:800–7. doi: 10.1002/art.40002.
[10] Sliter DA, Martinez J, Hao L, Chen X, Sun N, Fischer TD, et al. Parkin and PINK1 mitigate STING-induced inflammation. Nature 2018;561:258–62. doi: 10.1038/s41586-018-0448-9.
[11] Liang H, Deng L, Hou Y, Meng X, Huang X, Rao E, et al. Host STING-dependent MDSC mobilization drives extrinsic radiation resistance. Nat Commun 2017;8:1736. doi: 10.1038/s41467-017-01566-5.
[12] Gulen MF, Samson N, Keller A, Schwabenland M, Liu C, Glück S, et al. cGAS-STING drives ageing-related inflammation and neurodegeneration. Nature 2023;620:374–80. doi: 10.1038/s41586-023-06373-1.
[13] Victorelli S, Salmonowicz H, Chapman J, Martini H, Vizioli MG, Riley JS, et al. Apoptotic stress causes mtDNA release during senescence and drives the SASP. Nature 2023;622:627–36. doi: 10.1038/s41586-023-06621-4.
[14] Haag SM, Gulen MF, Reymond L, Gibelin A, Abrami L, Decout A, et al. Targeting STING with covalent small-molecule inhibitors. Nature 2018;559:269–73. doi: 10.1038/s41586-018-0287-8.
[15] Li S, Hong Z, Wang Z, Li F, Mei J, Huang L, et al. The cyclopeptide Astin C specifically inhibits the innate immune CDN sensor STING. Cell Rep 2018;25 3405-21.e7. doi: 10.1016/j.celrep.2018.11.097.
[16] Hong Z, Mei J, Li C, Bai G, Maimaiti M, Hu H, et al. STING inhibitors target the cyclic dinucleotide binding pocket. Proc Natl Acad Sci U S A 2021;118: e2105465118. doi: 10.1073/pnas.2105465118.
[17] Vinogradov AA, Yin Y, Suga H. Macrocyclic peptides as drug candidates: recent progress and remaining challenges. J Am Chem Soc 2019;141:4167–81. doi: 10.1021/jacs.8b13178.
[18] Nielsen DS, Shepherd NE, Xu W, Lucke AJ, Stoermer MJ, Fairlie DP. Orally absorbed cyclic peptides. Chem Rev 2017;117:8094–128. doi: 10.1021/acs.chemrev.6b00838.
[19] Lin CW, Harner MJ, Douglas AE, Lafont V, Yu F, Lee VG, et al. A selection of macrocyclic peptides that bind STING from an mRNA-Display library with split degenerate codons. Angew Chem Int Ed Engl 2021;60:22640–5. doi: 10.1002/anie.202103043.
[20] Goto Y, Suga H. The RaPID platform for the discovery of pseudo-natural macrocyclic peptides. Acc Chem Res 2021;54:3604–17. doi: 10.1021/acs.accounts.1c00391.
[21] Huang Y, Wiedmann MM, Suga H. RNA display methods for the discovery of bioactive macrocycles. Chem Rev 2019;119:10360–91. doi: 10.1021/acs.chemrev.8b00430.
[22] Goto Y, Katoh T, Suga H. Flexizymes for genetic code reprogramming. Nat Protoc 2011;6:779–90. doi: 10.1038/nprot.2011.331.
[23] Yamagishi Y, Shoji I, Miyagawa S, Kawakami T, Katoh T, Goto Y, et al. Natural product-like macrocyclic N-methyl-peptide inhibitors against a ubiquitin ligase uncovered from a ribosome-expressed de novo library. Chem Biol 2011;18:1562–70. doi: 10.1016/j.chembiol.2011.09.013.
[24] Peacock H, Suga H. Discovery of de novo macrocyclic peptides by messenger RNA display. Trends Pharmacol Sci 2021;42:385–97. doi: 10.1016/j.tips.2021.02.004.
[25] Zhang X, Li H, Liu Y, Yu J, Zhang P, Yu P, et al. Acid-responsive CST@NPs enhanced diabetic wound healing through rescuing mitochondrial dysfunction. Bioact Mater 2025;44:269–82. doi: 10.1016/j.bioactmat.2024.10.004.
[26] Zhou D, Gao Y, Aied A, Cutlar L, Igoucheva O, Newland B, et al. Highly branched poly(β-amino ester)s for skin gene therapy. J Control Release 2016;244:336–46. doi: 10.1016/j.jconrel.2016.06.014.
[27] Ablasser A, Hemmerling I, Schmid-Burgk JL, Behrendt R, Roers A, Hornung V. TREX1 deficiency triggers cell-autonomous immunity in a cGAS-dependent manner. J Immunol 2014;192:5993–7. doi: 10.4049/jimmunol.1400737.
[28] Gray EE, Treuting PM, Woodward JJ, Stetson DB. Cutting Edge: cGAS is required for lethal autoimmune disease in the Trex1-deficient mouse model of Aicardi-Goutières syndrome. J Immunol 2015;195:1939–43. doi: 10.4049/jimmunol.1500969.
[29] Gao D, Li T, Li XD, Chen X, Li QZ, Wight-Carter M, et al. Activation of cyclic GMP-AMP synthase by self-DNA causes autoimmune diseases. Proc Natl Acad Sci U S A 2015;112:E5699–705. doi: 10.1073/pnas.1516465112.
[30] Wu J, Wang Y, Cai W, Chen D, Peng X, Dong H, et al. Ribosomal translation of fluorinated non-canonical amino acids for de novo biologically active fluorinated macrocyclic peptides. Chem Sci 2024;15:13889–98. doi: 10.1039/d4sc04061a.
[31] Zhang X, Shi H, Wu J, Zhang X, Sun L, Chen C, et al. Cyclic GMP-AMP containing mixed phosphodiester linkages is an endogenous high-affinity ligand for STING. Mol Cell 2013;51:226–35. doi: 10.1016/j.molcel.2013.05.022.
[32] Yi G, Brendel VP, Shu C, Li P, Palanathan S, Cheng, Kao C. Single nucleotide polymorphisms of human STING can affect innate immune response to cyclic dinucleotides. PLOS ONE 2013;8:e77846. doi: 10.1371/journal.pone.0077846.
[33] Patel S, Jin L. TMEM173 variants and potential importance to human biology and disease. Genes Immun 2019;20:82–9. doi: 10.1038/s41435-018-0029-9.
[34] Gui X, Yang H, Li T, Tan X, Shi P, Li M, et al. Autophagy induction via STING trafficking is a primordial function of the cGAS pathway. Nature 2019;567:262–6. doi: 10.1038/s41586-019-1006-9.

[35] Tao W, Wang J, Parak WJ, Farokhzad OC, Shi J. Nanobuffering of pH-Responsive polymers: a known but sometimes overlooked phenomenon and its biological applications. ACS Nano 2019;13:4876–82. doi: 10.1021/acsnano.9b01696.

[36] Eweje F, Ibrahim V, Shajii A, Walsh ML, Ahmad K, Alrefai A, et al. Self-assembling protein nanoparticles for cytosolic delivery of nucleic acids and proteins. Nat Biotechnol. 2025;1-14. doi: 10.1038/s41587-025-02664-2.

[37] Sun Y, Lau SY, Lim ZW, Chang SC, Ghadessy F, Partridge A, et al. Phase-separating peptides for direct cytosolic delivery and redox-activated release of macromolecular therapeutics. Nat Chem 2022;14:274–83. doi: 10.1038/s41557-021-00854-4.

[38] Cong X, Yuan Z, Du Y, Wu B, Lu D, Wu X, et al. Crystal structures of porcine STINGCBD-CDN complexes reveal the mechanism of ligand recognition and discrimination of STING proteins. J Biol Chem 2019;294:11420–32. doi: 10.1074/jbc.RA119.007367.

[39] Shang G, Zhang C, Chen ZJ, Bai XC, Zhang X. Cryo-EM structures of STING reveal its mechanism of activation by cyclic GMP–AMP. Nature 2019;567:389–93. doi: 10.1038/s41586-019-0998-5.

[40] Shu C, Yi G, Watts T, Kao CC, Li P. Structure of STING bound to cyclic di-GMP reveals the mechanism of cyclic dinucleotide recognition by the immune system. Nat Struct Mol Biol 2012;19:722–4. doi: 10.1038/nsmb.2331.

[41] Ramanjulu JM, Pesiridis GS, Yang J, Concha N, Singhaus R, Zhang SY, et al. Design of amidobenzimidazole STING receptor agonists with systemic activity. Nature 2018;564:439–43. doi: 10.1038/s41586-018-0705-y.

[42] Brown GJ, Cañete PF, Wang H, Medhavy A, Bones J, Roco JA, et al. TLR7 gain-of-function genetic variation causes human lupus. Nature 2022;605:349–56. doi: 10.1038/s41586-022-04642-z.

[43] Stetson DB, Ko JS, Heidmann T, Medzhitov R. Trex1 prevents cell-intrinsic initiation of autoimmunity. Cell 2008;134:587–98. doi: 10.1016/j.cell.2008.06.032.

Ann Rheum Dis 85 (2026) 953–954

Contents lists available at ScienceDirect

Annals of the Rheumatic Diseases

journal homepage: https://www.sciencedirect.com/journal/annals-of-the-rheumatic-diseases

Images in rheumatology

An unusual cause of lumbar back pain

Ying Cai[1], Fan Yang[2], Chong Chen[2], Xian-Zheng Tan[2,*]

[1] *Department of Spine Surgery, Loudi Central Hospital, Loudi, Hunan, China*
[2] *Department of Radiology, Hunan Provincial People's Hospital and the First Affiliated Hospital of Hunan Normal University, Changsha, Hunan, China*

A 19-year-old man presented with a chief complaint of atraumatic lumbar back pain for 4 months. He had a body mass index of 33.4 (weight: 112 kg; height: 183 cm) but no other metabolic comorbidities. His family history was unremarkable. He was afebrile with no symptoms of neurological deficits. On admission to hospital, physical examinations were unremarkable except for lower lumbar paraspinal tenderness. Laboratory examinations showed biochemical evidence of hyperuricemia and inflammation, with a serum uric acid level of 759 μmol/L, white cell count of 12,550 cells per mm^3, C-reactive protein of 101 mg/L, and erythrocyte sedimentation rate of 82 mm/h. Contrast-enhanced magnetic resonance imaging of the lumbar spine showed multiple intraspinal and extraspinal masses with obvious enhancement involving bilateral L3-L4 facet joints, leading to marked lumbar stenosis (Fig, A). Computed tomography (CT) revealed that the masses were heterogeneously hyperattenuating with bony erosion of bilateral L3-L4 facet joints (Fig, B-D). Spinal gout was suspected. Dual-energy CT subsequently confirmed the diagnosis by demonstrating extensive monosodium urate (MSU) crystal deposition in the masses (Fig, E,F). The patient was managed with anti-inflammatory treatment and urate-lowering therapy and discharged home with symptomatic relief.

Spinal gout is defined by the deposition of MSU crystals in the axial skeleton, with an estimated prevalence of 14% to 35% in patients with gout [1]. The differential diagnoses include septic or inflammatory arthritis, pseudogout, and neoplasms [2]. As clinical manifestations are usually nonspecific, discrimination between spinal gout and its mimics is often challenging. The European League Against Rheumatism recommends imaging, particularly ultrasonography and dual-energy CT, to noninvasively identify MSU deposition when crystal identification by invasive punctures is unavailable and a clinical diagnosis of gout is uncertain [3]. Dual-energy CT can explore 'deep-seated' anatomical structures where ultrasonography is not feasible, aiding in the correct diagnosis of spinal gout [3].

*Correspondence to Dr Xian-Zheng Tan, Department of Radiology, Hunan Provincial People's Hospital and the First Affiliated Hospital of Hunan Normal University, Changsha, Hunan, China.

E-mail address: xianzhengtan@163.com (X.-Z. Tan).

Handling editor Josef S. Smolen.

Ying Cai, Fan Yang, and Chong Chen share co-first authorship.

https://doi.org/10.1016/j.ard.2025.10.027
Received 13 September 2025; Revised 23 October 2025; Accepted 25 October 2025

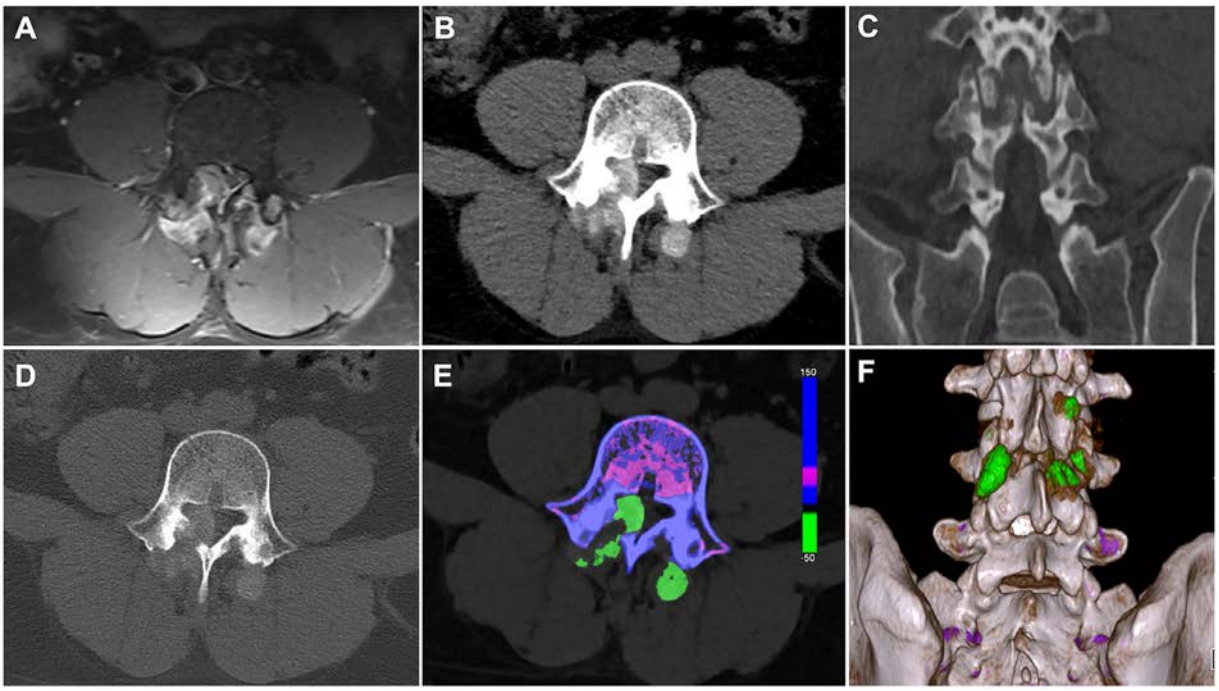

Figure. Spinal gout. (A) Contrast-enhanced magnetic resonance imaging showed multiple intraspinal and extraspinal mass lesions with obvious enhancement displacing the posterior spinal cord at the level of L3-L4, with narrowing of the spinal canal. (B-D) Conventional computed tomography (CT) depicted erosion of bilateral L3-L4 facet joints by multiple slightly hyperattenuating masses that encroached on the left neural foramen and caused marked canal stenosis. (E,F) Dual-energy CT demonstrated green colour-coded monosodium urate deposition in the intraspinal and extraspinal hyper-attenuated masses around the bilateral L3-L4 facet joints.

Contributors

YC, FY and CC (co-first authors)—design, acquisition, and interpretation of the work, drafting of the work, and approval of the final version. X-ZT (corresponding author)—interpretation of the work, revision and approval of the final version.

Funding

This study is supported by the National Natural Science Foundation for Young Scientists of China (82202266), Doctor Foundation of Hunan Provincial People's Hospital (BSJJ202109), Youth Medical Key Talents Foundation of Hunan Province (20230508-1034), Hunan Provincial Health High-Level Talent Scientific Research Project (R2023121), and General Program of Hunan Provincial Natural Science Foundation (2025JJ50695).

Competing interests

None declared.

Patient consent for publication

Consent obtained directly from the patient.

Ethics approval

Not applicable.

Provenance and peer review

Not commissioned; externally peer reviewed.

Orcid

Ying Cai: http://orcid.org/0009-0001-7574-4480
Xian-Zheng Tan: http://orcid.org/0000-0001-9319-1237

REFERENCES

[1] Jin HJ, Son ES, Kim DH. The frequency of axial deposition in Korean patients with gout at a tertiary spine center. Front Med (Lausanne) 2020;7:339.
[2] Si M, Cong M, Wang D, Ma H. Intraspinal gouty tophus. Ann Neurol. 2020 Nov;88(5):1048–9.
[3] Richette P, Doherty M, Pascual E, Barskova V, Becce F, Castaneda J, et al. 2018 updated European League Against Rheumatism evidence-based recommendations for the diagnosis of gout. Ann Rheum Dis 2020 Jan;79(1):31–8.

Ann Rheum Dis 85 (2026) 955–957

Contents lists available at ScienceDirect

Annals of the Rheumatic Diseases

journal homepage: https://www.sciencedirect.com/journal/annals-of-the-rheumatic-diseases

Letter

Ultrasound localisation microscopy reveals mural neovascularisation to diagnose and track giant cell arteritis

Giant cell arteritis (GCA) is a systemic, immune-mediated vasculitis that preferentially affects the extracranial branches of the carotid artery, most commonly the superficial temporal artery (STA), in patients older than 50 years [1]. Accurate phenotyping of arterial wall inflammation is essential to distinguish between active and quiescent disease states, thereby enabling precise risk stratification and individualised therapeutic strategies [2]. Although ultrasonography is recommended as a first-line imaging modality due to its cost-effectiveness, absence of ionising radiation, repeatability, and broad availability [3], conventional techniques lack the spatial resolution to visualise microvascular enrichment associated with inflammatory activity. Ultrasound localisation microscopy (ULM), an emerging superresolution approach, overcomes this limitation by integrating intravenous microbubble contrast, ultrafast plane-wave imaging, and spatiotemporal tracking algorithms to achieve unprecedented resolution (10-100 μm) for microvascular assessment [4].

A 74-year-old woman presented with a 4-week history of bilateral temporal headache, scalp tenderness, and transient visual blurring. Laboratory evaluation revealed markedly elevated C-reactive protein (CRP) (61.5 mg/L) and erythrocyte sedimentation rate (ESR) (>90 mm/h). B-mode ultrasound showed concentric, homogeneous, hypoechoic wall thickening of the frontal branch of the STA (Fig, A). The outcome measures in rheumatology (OMERACT) GCA ultrasonography score (OGUS) was calculated to be 2.84 [5]. Ultrasonographic imaging was performed using an ULTIMUS 9E ultrasound system (Vinno) equipped with a U5-15L linear array transducer (Vinno; bandwidth: 6-14 MHz) for ULM data acquisition. After intravenous injection of 1.5 mL sulfur hexafluoride microbubble contrast agent (SonoVue, Bracco, Milano, Italy), ULM revealed dense, tortuous neovascular networks within the thickened intima-media complex (Fig, B). Quantitative ULM parametric mapping indicated a vessel ratio of 11.32%, a mean density of 5.47, a mean velocity of 10.05 mm/s, and a perfusion index of 1.88 (Fig, C). The diagnosis of GCA was established based on the clinical manifestations, laboratory results, and imaging findings [6]. Treatment was initiated with intravenous methylprednisolone (40 mg/d for 5 days), followed by an oral regimen starting at 20 mg/d, which was tapered in 4 mg decrements at 1- to 2-week intervals down to 4 mg, with a final reduction to a maintenance dose of 2 mg/d. After 4 months, the patient's clinical symptoms resolved, with normalisation of inflammatory markers (CRP: 3.5 mg/L; ESR: 3 mm/h). Follow-up ultrasound showed a 40.92% reduction in the vessel outer diameter (from 3.91 mm to 2.31 mm; reduction: 1.60 mm) and a 72.60% decrease in wall thickness (from 1.46 mm to 0.40 mm; reduction: 1.06 mm) (Fig, D). The OGUS value at follow-up was 1.16. To evaluate measurement reproducibility, 2 experienced sonographers independently repeated measurements on ultrasound images. Excellent intra- and interobserver agreement was confirmed, with intraclass correlation coefficients exceeding 0.89. Concurrently, ULM disclosed a significant reduction in the actual values of key microvascular parameters relative to baseline, including vessel ratio (0.59%), mean density (2.45), mean velocity (5.68 mm/s), and perfusion index (0.09), consistent with resolved vascular inflammation (Fig, E and F). For comparison, ultrasonographic images of the frontal branch of the STA in a healthy person are also presented (Fig, G-I).

This study reports the first in-human application of ULM for delineating and quantifying pathological microvasculature within the STA wall. As an emerging technique, ULM shows promise in providing noninvasive, high-resolution evidence that may aid in the diagnosis of GCA and the evaluation of therapeutic response. By surpassing the resolution limits of conventional ultrasound, ULM enables detailed characterisation of contrast agent dynamics and mural neovascularisation associated with GCA-related inflammation. Preliminary applications in Takayasu's arteritis have further illustrated the ability of ULM to visualise microvessels within thickened arterial walls, with increased microbubble density observed during active disease [2]. These initial findings indicate that ULM may serve as a sensitive biomarker of inflammatory activity and could potentially inform future clinical decision-making. It should be noted, however, that current evidence is derived from a limited number of cases, including a representative case comparison. Large-scale prospective studies are required to validate ULM-derived metrics for diagnostic accuracy, disease activity monitoring, and treatment personalisation in GCA.

Funding

This work was supported by the Natural Science Foundation of Liaoning Province (2024-MSLH-554).

Competing interests

All authors declare they have no competing interests.

https://doi.org/10.1016/j.ard.2025.10.017
Received 1 August 2025; Revised 13 October 2025; Accepted 16 October 2025

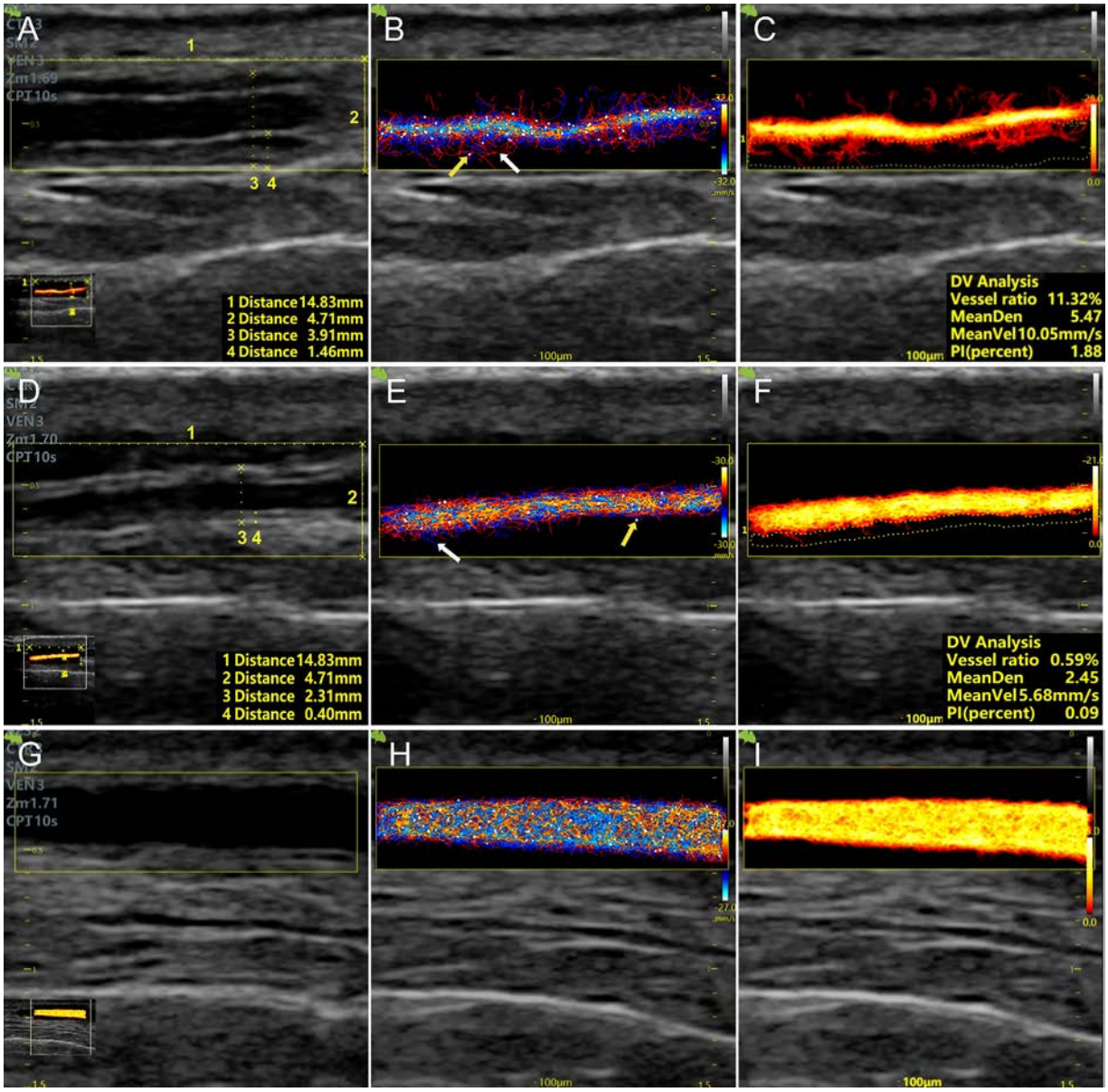

Figure. Ultrasonographic evaluation of the frontal branch of the superficial temporal artery (STA) in a patient with giant cell arteritis (GCA). A, Longitudinal B-mode image depicting pronounced, concentric intima-media thickening of the STA wall at baseline. B, Corresponding ultrasound localisation microscopy (ULM) map revealing dense intramural neovascular networks (white arrow) and individual tracked microbubbles (yellow arrow). The colour bar indicates flow direction relative to the transducer (red: towards; blue: away). C, ULM-derived vessel-density (VD) map quantifying the spatial distribution and fractional area of neovessels within the thickened arterial wall. Vessel ratio: proportion of the region of interest (ROI) occupied by tracked microbubbles; mean density (MeanDen): average number of microbubbles passing through a given vascular site during acquisition; mean velocity (MeanVel): average velocity of tracked microbubbles within the ROI; perfusion index (PI): product of the MeanVel and MeanDen, reflecting overall tissue perfusion. D, The follow-up B-mode image showing a marked reduction in wall thickness. E, Corresponding ULM map demonstrating obvious regression of intramural microvasculature (white arrow) and individual tracked microbubbles (yellow arrow). The colour bar indicates flow direction relative to the transducer (red: towards; blue: away). F, Quantitative ULM analysis suggests a significant decrease in mural microvessel density compared with baseline. Vessel ratio: proportion of the ROI occupied by tracked microbubbles; MeanDen: average number of microbubbles passing through a given vascular site during acquisition; MeanVel: average velocity of tracked microbubbles within the ROI; PI: product of the MeanVel and MeanDen, reflecting overall tissue perfusion. G-I, Ultrasonographic assessment of the STA frontal branch in a healthy control. G, Longitudinal B-mode image showing normal wall thickness. H, Corresponding ULM map and (I) ULM-derived VD map revealing absence of intramural microvascular signals.

CRediT authorship contribution statement

Tan Li: Writing – review & editing, Writing – original draft, Validation, Supervision, Methodology, Investigation, Funding acquisition, Conceptualization. **Yifei Gai:** Software, Resources, Investigation, Data curation. **Chunyan Ma:** Visualization, Validation, Supervision, Resources, Project administration, Methodology.

Patient consent for publication

Not applicable.

Ethics approval

Not applicable.

Provenance and peer review

Not commissioned; externally peer reviewed.

REFERENCES

[1] von der Emde L, Petzinna SM, Herwig-Carl MC, Adamson MS, Bauer CJ, Esser J, et al. Advances in diagnosing and treating giant cell arteritis: new hope for arteritic anterior ischemic optic neuropathy. Surv Ophthalmol 2025 in press. doi: 10.1016/j.survophthal.2025.06.009.

[2] Goudot G, Jimenez A, Mohamedi N, Sitruk J, Khider L, Mortelette H, et al. Assessment of Takayasu's arteritis activity by ultrasound localization microscopy. EBioMedicine 2023;90:104502. doi: 10.1016/j.ebiom.2023.104502.

[3] Dejaco C, Ramiro S, Bond M, Bosch P, Ponte C, Mackie SL, et al. EULAR recommendations for the use of imaging in large vessel vasculitis in clinical practice: 2023 update. Ann Rheum Dis 2024;83(6):741–51. doi: 10.1136/ard-2023-224543.

[4] Xia S, Zheng Y, Hua Q, Wen J, Luo X, Yan J, et al. Super-resolution ultrasound and microvasculomics: a consensus statement. Eur Radiol 2024;34(11):7503–13. doi: 10.1007/s00330-024-10796-3.

[5] Dejaco C, Ponte C, Monti S, Rozza D, Scirè CA, Terslev L, et al. The provisional OMERACT ultrasonography score for giant cell arteritis. Ann Rheum Dis 2023;82(4):556–64. doi: 10.1136/ard-2022-223367.

[6] van der Geest KSM, Sandovici M, Brouwer E, Mackie SL. Diagnostic accuracy of symptoms, physical signs, and laboratory tests for giant cell arteritis: a systematic review and meta-analysis. JAMA Intern Med 2020;180(10):1295–304. doi: 10.1001/jamainternmed.2020.3050.

Tan Li[1,2], Yifei Gai[1], Chunyan Ma[1,2,*]

[1] *Department of Cardiovascular Ultrasound, The First Hospital of China Medical University, Shenyang, China*

[2] *Clinical Medical Research Center of Imaging in Liaoning Province, The First Hospital of China Medical University, Shenyang, China*

*__Correspondence to__ Dr Chunyan Ma.
E-mail address: macy@cmu1h.com (C. Ma).

Ann Rheum Dis 85 (2026) 958–961

Contents lists available at ScienceDirect

Annals of the Rheumatic Diseases

journal homepage: https://www.sciencedirect.com/journal/annals-of-the-rheumatic-diseases

Letter

Mosunetuzumab, a CD20xCD3 bispecific T-cell engager, in granulomatosis with polyangiitis

B-cell depletion with the monoclonal anti-CD20 antibody rituximab (RTX) is effective in granulomatosis with polyangiitis (GPA) [1–4]. However, RTX-refractory cases and the fact that glucocorticoids are necessary for a sufficient RTX response in active GPA indicate that more efficient treatment strategies are needed.

We present the case of a 38-year-old female diagnosed with GPA according to American College of Rheumatology / European Alliance of Associations for Rheumatology classification criteria [5] in March 2023. She suffered from upper airway, skin and joint manifestations, and a large retro-orbital inflammatory pseudotumor. The kidneys were not affected. Retro-orbital biopsy confirmed a necrotising granuloma and vasculitis (Fig, A). Initial treatment with prednisolone, RTX, and avacopan was switched to cyclophosphamide (CYC) pulses due to progressive disease in June 2023. Symptoms and the pseudotumor significantly regressed, accompanied by normalisation of anti-proteinase 3 (anti-PR3) autoantibodies. After 6 CYC pulses, early clinical and serologic relapse prompted us to administer an additional 3 pulses (cumulative: 10.6 g) at extended intervals without effect.

Given the general efficacy of RTX in GPA but its limited efficacy in patients with large granulomas, as in our patient, we sought an alternative anti-CD20 agent with greater tissue cytotoxicity than that of RTX [6]. We rejected the idea of using another monoclonal anti-CD20 antibody, such as obinutuzumab [7–9], because its cytotoxicity depends, in part, on natural killer cells, which are absent in GPA granulomas [10], as we confirmed in our patient (Fig, A). As CD3+ cytotoxic T cells reside adjacent to $CD20^{+}$ B cells in the granuloma, we decided to use the off-label bispecific CD20xCD3 T-cell engager (TCE), mosunetuzumab, after shared decision-making and signed informed consent. Mosunetuzumab is approved for the treatment of lymphoma and has a favourable safety profile [11]. Two weeks before baseline, avacopan was discontinued. Prednisolone (5 mg/d) was initially maintained.

Dosing of mosunetuzumab was planned in analogy to the oncologic step-up protocol, with a reduced maximal dose (Fig, B,C). The third infusion was postponed for non-medical reasons and resumed with a repetition of the second step-up dose. Premedication of each infusion consisted of 20 mg dexamethasone, paracetamol, and clemastine. The initial and first maximum doses were given in the hospital; all other doses were given in an outpatient setting.

Mosunetuzumab induced B-cell depletion, serologic remission (Fig, D), and complete resolution of fatigue, night sweats, arthritis, skin lesions, diplopia, and sensations of retro-orbital pressure. For the first time since the GPA diagnosis, opiates were stopped and prednisolone fully tapered. The Birmingham Vasculitis Activity Score version 3 for new/worse or persistent symptoms regressed to 0 at days 90 and 200, respectively (Fig, E). Ophthalmologic exams and magnetic resonance imaging demonstrated reduced strabismus (Fig, F) and a trend towards further shrinkage of the pseudotumor (Fig, G). After 200 days from baseline (110 days after the last mosunetuzumab infusion), blood B cells remained depleted, and the patient was in stable clinical and serological remission without further immunosuppression. On a visual analogue scale, the patient reported a 75% increase in global health.

Mosunetuzumab was well-tolerated. No cytokine release syndrome occurred. Except for a prolonged mild seasonal cold, no infections occurred.

The superior efficacy of mosunetuzumab compared with RTX was highlighted by the serological response (Fig, H). While RTX led to a marginal decline in anti-PR3, the decay curve after mosunetuzumab treatment resembled the presumed half-life curve of immunoglobulin (Ig) G (~21 days, according to textbooks). Total Igs and postvaccination/postinfection IgGs remained stable (Fig, I, J). While future studies are needed to confirm these results, the selective decay observed here suggests that CD20-expressing cells or their short-lived plasma cell progenies are the main producers of anti-PR3, and that mosunetuzumab efficiently depletes them. As the clinical relapse during CYC treatment was associated with B-cell repopulation and the reemergence of anti-PR3 autoantibodies, we continue to regularly monitor peripheral blood B cells and anti-PR3 titres.

Together, this case report describes a histology-guided selection of a novel, highly effective CD20-targeting TCE in autoimmunity. We report the first application of mosunetuzumab outside oncology and the first application of TCE in autoimmune vasculitis. In our refractory GPA case, mosunetuzumab demonstrated safety and efficacy without concomitant glucocorticoids. The inherent limitations of a single-case report must be considered. Therefore, robust trials will be key to advancing this field.

Mosunetuzumab possesses several advantages over CD19-targeting Chimeric Antigen Receptor T cells or the TCEs blinatumomab (CD3xCD19) and teclistamab (CD3xBCMA), which have recently been tested in autoimmunity [12–18], including a favourable safety profile and its application in an outpatient setting. Mosunetuzumab, as a new CD20-targeting TCE, may thus be of broad interest in autoimmunity, particularly in GPA.

Funding

The study was financially supported by the John Grube Foundation and the German Society of Internal Medicine (DGIM) (to WM).

https://doi.org/10.1016/j.ard.2025.10.026
Received 3 September 2025; Revised 21 October 2025; Accepted 24 October 2025

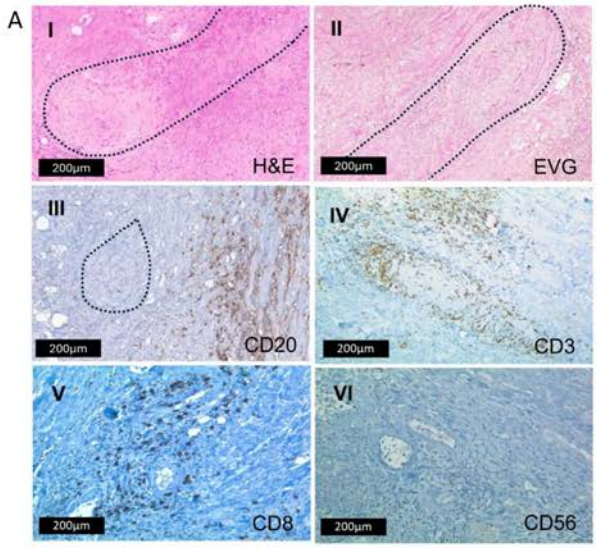

B

mosunetuzumab	planned		carried out	
Cycle 1	Day +0	1mg	Day +0	1mg
	Day +7	2mg	Day +7	2mg
			Day +56	2mg
	Day +14	30mg	Day +63	30mg
Cycle 2	Day + 21	30mg	Day +70	30mg
Cycle 3	Day +42	30mg	Day +91	30mg

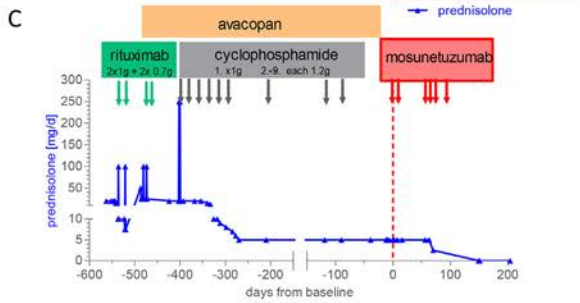

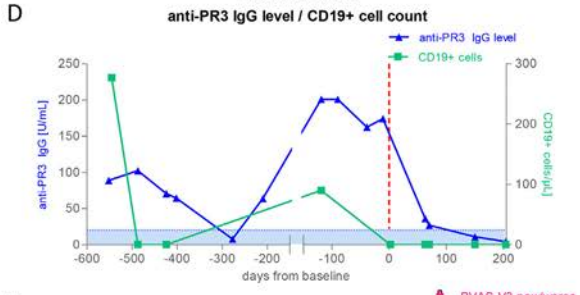

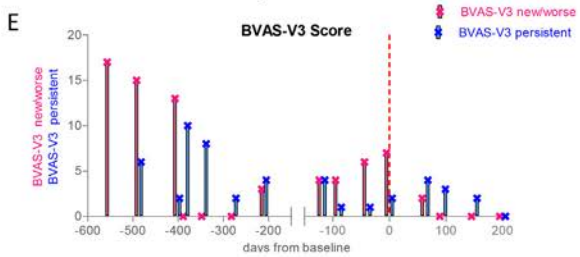

F

alternating prism cover test (right fixation)		pre mosunetuzumab (day -8)	5 months post mosunetuzumab (day +171)
angle of strabsimus	distance	1° exophoria	orthophoria (normal)
	near	3.5° exophoria	0.5° exophoria

G

	day -551	day -60	day +216
Coronal			
length	2,08	1,33	1,33
width	0,99	0,59	0,36
Axial			
length	2,65	1,37	1,05
width	1,16	0,5	0,48

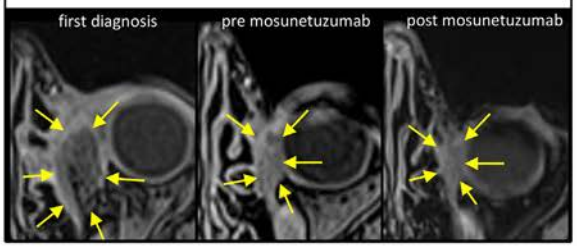

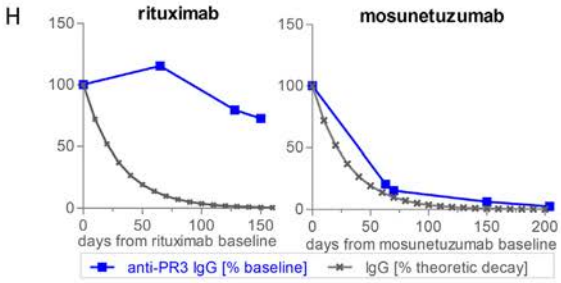

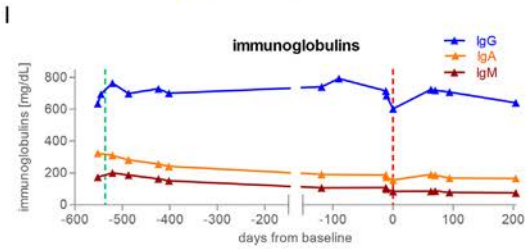

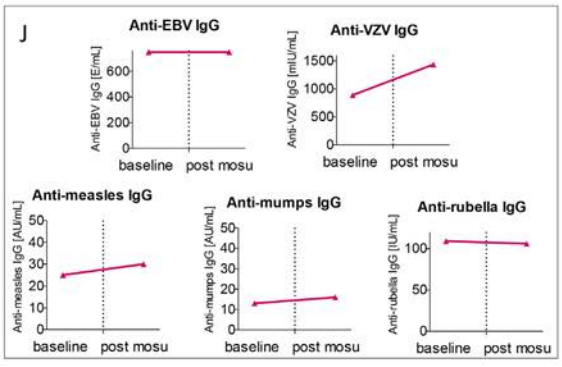

Figure. Mosunetuzumab, a CD20xCD3-targeting T-cell engager, in granulomatosis with polyangiitis. A, Histopathology of the initial biopsy of orbital granuloma. I, Hematoxylin and eosin (H&E) staining showing destroyed, completely obliterated vessels (dotted line) with endothelial proliferation, media necrosis, mixed inflammatory cells (mainly neutrophils and a few lymphocytes), and cellular/nuclear debris. II, Corresponding serial section by Elastica by van Gieson (EVG) staining; vessels are highlighted by a dotted line. III-VI, Immunohistochemistry (20× magnification) and (III) scattered aggregates of CD20-positive B cells (brown) in the outer areas of inflammation; vessels are highlighted by a dotted line. IV, Detection of CD8-positive and (V) CD3-positive T cells in the inflammatory infiltrates. VI, No detection of CD56-positive natural killer (NK) cells. B, Mosunetuzumab treatment protocol as planned and carried out. C, Overview of the treatment regimen since first diagnosis, including daily prednisolone intake (mg/d), counted in days from the first mosunetuzumab infusion. D, Levels of anti-proteinase 3 (anti-PR3) immunoglobulin (Ig) G (U/mL) autoantibodies (determined by immunosorbent assay, normal <20 U/mL) and CD19+ B cells in peripheral blood (cells/µL) over time. E, Birmingham Vasculitis Activity Score version 3 (BVAS-V3) (score range, 0-63 for new/worse symptoms and 0-33 for persistent symptoms). F, Angle of strabismus measured using the alternating prism cover test (right fixation). G, Cranial magnetic resonance imaging. Coronal T1-weighted contrast-enhanced imaging and axial T1-weighted contrast-enhanced imaging with fat saturation were used to measure the size of the orbital pseudotumor (results shown in the tabular display);

Competing interests

WM has received grants or contracts from the German Society of Internal Medicine (DGIM), argenx, Kyverna, Lilly, Galapagos, Boehringer Ingelheim, Evotec, and BMS; consulting fees and payment or honoraria for lectures and presentations from Lilly, Galapagos, and Boehringer Ingelheim; support for attending meetings and/or travel from Kyverna, Lilly, Galapagos, and Boehringer Ingelheim; patents planned for Evotec and BMS; participation on an Advisory Board for Lilly and Boehringer Ingelheim; receipt of equipment, materials, and drugs from argenx. JHWD has received grants or contracts from AbbVie, Anamar, argenx, ARXX, BMS, Bayer Pharma, Boehringer Ingelheim, Cantargia, Celgene, CSL Behring, ExoTherapeutics, Galapagos, GSK, Inventiva, Kiniksa, Lassen, Novartis, Sanofi-Aventis, RedX, and UCB; consulting fees from AbbVie, Active Biotech, Anamar, ARXX, AstraZeneca, Bayer Pharma, Boehringer Ingelheim, Celgene, Galapagos, Genentech, GSK, Inventiva, Janssen, Novartis, Pfizer, Roche, and UCB; payment or honoraria for lectures, presentations, speakers bureaus, manuscript writing or educational events from AbbVie, Active Biotech, Anamar, ARXX, AstraZeneca, Bayer Pharma, Boehringer Ingelheim, Celgene, Galapagos, Genentech, GSK, Inventiva, Janssen, Novartis, Pfizer, Roche, and UCB; payment for expert testimony from AbbVie, Anamar, ARXX, AstraZeneca, Bayer Pharma, Boehringer Ingelheim, Cantargia, Celgene, Galapagos, Genentech, GSK, Inventiva, Janssen, Novartis, Pfizer, Roche, and UCB; support for attending meetings and/or travel from AbbVie and Sobi; stock or stock options from 4D Science and FibroCure; receipt of medical writing from Boehringer Ingelheim. All other authors declared no conflict of interest.

CRediT authorship contribution statement

Ayla Nadja Stütz: Conceptualization, Formal analysis, Investigation, Methodology, Validation, Visualization, Writing – original draft, Writing – review & editing. **Laura-Marie Lahu:** Investigation, Writing – review & editing. **Sandra Jaschinski:** Investigation, Methodology, Visualization, Writing – review & editing. **Christina Düsing:** Investigation, Writing – review & editing. **Nebile Güzel:** Formal analysis, Investigation, Writing – review & editing. **Daniel Schwarz:** Formal analysis, Investigation, Software, Visualization. **Jörg H.W. Distler:** Resources, Supervision, Writing – review & editing. **Wolfgang Merkt:** Conceptualization, Funding acquisition, Investigation, Project administration, Resources, Supervision, Writing – original draft, Writing – review & editing.

Patient consent for publication

The patient provided written informed consent for the publication of this case report.

Ethics approval

Not applicable.

Provenance and peer review

Not commissioned; externally peer reviewed.

Orcid

Wolfgang Merkt: http://orcid.org/0000-0002-3108-154X

REFERENCES

[1] Hellmich B, Sanchez-Alamo B, Schirmer JH, Berti A, Blockmans D, Cid MC, et al. EULAR recommendations for the management of ANCA-associated vasculitis: 2022 update. Ann Rheum Dis 2024;83:30–47.
[2] Geetha D, Specks U, Stone JH, Merkel PA, Seo P, Spiera R, et al. Rituximab versus cyclophosphamide for ANCA-associated vasculitis with renal involvement. J Am Soc Nephrol 2015;26:976–85.
[3] Smith RM, Jones RB, Specks U, Bond S, Nodale M, Al-Jayyousi R, et al. Rituximab versus azathioprine for maintenance of remission for patients with ANCA-associated vasculitis and relapsing disease: an international randomised controlled trial. Ann Rheum Dis 2023;82:937–44.
[4] Guillevin L, Pagnoux C, Karras A, Khouatra C, Aumaître O, Cohen P, et al. Rituximab versus azathioprine for maintenance in ANCA-associated vasculitis. N Engl J Med 2014;371:1771–80.
[5] Robson JC, Grayson PC, Ponte C, Suppiah R, Craven A, Judge A, et al. 2022 American College of Rheumatology/European Alliance of Associations for Rheumatology classification criteria for granulomatosis with polyangiitis. Ann Rheum Dis 2022;81:315–20.
[6] Tur C, Eckstein M, Velden J, Rauber S, Bergmann C, Auth J, et al. CD19-CAR T-cell therapy induces deep tissue depletion of B cells. Ann Rheum Dis 2025;84:106–14.
[7] van Leeuwen JR, Bredewold OW, Rabelink TJ, Teng YKO. Obinutuzumab in rituximab-intolerant antineutrophil cytoplasmic antibody-associated vasculitis patients. Kidney Int Rep 2025;10:1288–91.
[8] Amudala NA, Boukhlal S, Sheridan B, Langford CA, Geara A, Merkel PA, et al. Obinutuzumab as treatment for ANCA-associated vasculitis. Rheumatology (Oxford) 2022;61:3814–7.
[9] McGovern DP, McClure ME, Coates M, Bond S, Martinez Del Pero M, Mynard K, et al. Study protocol for a randomised, phase II, double-blind, experimental medicine study of obinutuzumab versus rituximab in ANCA-associated vasculitis: ObiVas. BMJ Open 2024;14:e083277.
[10] Merkt W, Sturm P, Lasitschka F, Tretter T, Watzl C, Saure D, et al. Peripheral blood natural killer cell percentages in granulomatosis with polyangiitis correlate with disease inactivity and stage. Arthritis Res Ther 2015;17:337.
[11] Budde LE, Sehn LH, Matasar M, Schuster SJ, Assouline S, Giri P, et al. Safety and efficacy of mosunetuzumab, a bispecific antibody, in patients with relapsed or refractory follicular lymphoma: a single-arm, multicentre, phase 2 study. Lancet Oncol 2022;23:1055–65.
[12] Uhlmann L, Pierer M, Krasselt M, Franke G, Zeidler R, Sabri O, et al. Effective use of anti-CD19 chimeric antigen receptor T-cells in a case of treatment-resistant granulomatosis with polyangiitis. Ann Rheum Dis 2025;84:1280–3.
[13] Minopoulou I, Wilhelm A, Albach F, Kleyer A, Wiebe E, Schallenberg S, et al. Anti-CD19 CAR T cell therapy induces antibody seroconversion and complete B cell depletion in the bone marrow of a therapy-refractory patient with ANCA-associated vasculitis. Ann Rheum Dis 2025;84:e4–7.
[14] Hagen M, Bucci L, Böltz S, Nöthling DM, Rothe T, Anoshkin K, et al. BCMA-targeted T-cell-engager therapy for autoimmune disease. N Engl J Med 2024;391:867–9.
[15] Alexander T, Krönke J, Cheng Q, Keller U, Krönke G. Teclistamab-induced remission in refractory systemic lupus erythematosus. N Engl J Med 2024;391:864–6.
[16] Siegert E, Biesen R, Dzamukova M, Furth C, Probst M, Doellinger F, et al. Teclistamab in relapsed systemic sclerosis after autologous

representative axial images are shown at the bottom. H-J, Specific elimination of anti-PR3 autoantibodies after mosunetuzumab treatment. H, Anti-PR3 levels following initiation of rituximab on day −552 from baseline (left) and mosunetuzumab on day 0 from baseline (right). Measured values (blue) are compared with a theoretical IgG decay curve (grey) assuming an average IgG half-life of 21 days. $C(t) = C_0 \times (0.5)^{t/21}$, where C(t) is the antibody concentration at time t (in days); C_0 is the initial antibody concentration at time $t = 0$; and t is time in days postrituximab or mosunetuzumab baseline. I, Immunoglobulin levels in serum (mg/dL); left dashed line (green): start of rituximab treatment; right dashed line (red): start of mosunetuzumab treatment (day = +0). J, Protective IgG levels following vaccination or infection before baseline and +12 months after baseline (post mosu) remained stable. EBV, Epstein-Barr virus; VZV, Varizella-zoster virus.

haematopoietic stem cell transplantation. Ann Rheum Dis 2025;84:653–6.
[17] Subklewe M, Magno G, Gebhardt C, Bücklein V, Szelinski F, Arévalo HJR, et al. Application of blinatumomab, a bispecific anti-CD3/CD19 T-cell engager, in treating severe systemic sclerosis: a case study. Eur J Cancer 2024;204:114071.
[18] Bucci L, Hagen M, Rothe T, Raimondo MG, Fagni F, Tur C, et al. Bispecific T cell engager therapy for refractory rheumatoid arthritis. Nat Med 2024;30:1593–601. doi: 10.1038/s41591-024-02964-1.

Ayla Nadja Stütz[1,2], Laura-Marie Lahu[1,2], Sandra Jaschinski[3], Christina Düsing[1,2,4], Nebile Güzel[5], Daniel Schwarz[6], Jörg H.W. Distler[1,2,4], Wolfgang Merkt[1,2,7,*]
[1] *Department of Rheumatology, University Hospital Düsseldorf, Medical Faculty of Heinrich-Heine University, Düsseldorf, Germany*
[2] *Hiller Research Centre, University Hospital Düsseldorf, Medical Faculty of Heinrich-Heine University, Düsseldorf, Germany*
[3] *Department of Pathology, University Hospital Düsseldorf, Medical Faculty of Heinrich-Heine University, Düsseldorf, Germany*
[4] *Fraunhofer Institute for Translational Medicine and Pharmacology (ITMP) and Fraunhofer Cluster of Excellence for Immune Mediated Diseases (CIMD), Frankfurt am Main, Germany*
[5] *Department of Ophthalmology, University Hospital Düsseldorf, Medical Faculty of Heinrich-Heine University, Düsseldorf, Germany*
[6] *Department of Neuroradiology, University Hospital Heidelberg, Medical Faculty of University Heidelberg, Germany*
[7] *Department of Haematology, Oncology and Rheumatology, Internal Medicine V, University Hospital Heidelberg, Heidelberg, Germany*

*__Correspondence to__ Dr Wolfgang Merkt, Department of Rheumatology and Hiller Research Center, University Hospital Düsseldorf, Heinrich-Heine University, Düsseldorf, Germany.
E-mail address: Wolfgang.Merkt@med.uni-duesseldorf.de (W. Merkt).

Ann Rheum Dis 85 (2026) e47–e48

Contents lists available at ScienceDirect

Annals of the Rheumatic Diseases

journal homepage: https://www.sciencedirect.com/journal/annals-of-the-rheumatic-diseases

Correspondence

Correspondence on "ChatGPT vs rheumatologists: cross-sectional study on accuracy and patient perception of AI-generated information for psoriatic arthritis" by Forte et al.

Dear Editor,

We read with interest the cross-sectional study by Forte et al [1], which compared ChatGPT-4 with expert rheumatologists in answering patient-generated questions about psoriatic arthritis (PsA) and was complemented by blinded expert scoring and patient preference assessment. The authors should be commended for using real-world patient questions (32 unique items; 296 selections) and for implementing anonymisation and blinded scoring procedures across a broad panel of clinicians. The study also provides an important early indication that patients may prefer artificial intelligence (AI)-generated responses and that readability differs meaningfully across sources.

However, the central question is not whether an a large language model (LLM) can produce 'acceptable' text under constrained conditions, but whether we can reliably evaluate, safely deploy, and clinically govern LLM-based education in PsA. Several design features and result patterns in this study point to concrete next steps.

1. Rating reliability: the 'expert consensus' signal is fragile at the individual level.

The study explicitly reports very low interrater reliability for individual scores (accuracy: Fleiss' $\kappa = 0.079$; intraclass correlation coefficient, ICC = 0.12; completeness: $\kappa = 0.086$; ICC = 0.11), despite improved average-rater ICCs.

This matters because 'accuracy' and 'completeness' are not purely objective constructs in patient education; they combine factuality, framing, risk emphasis, and contextual tailoring. When single-rater agreement is this low, small-observed differences (or nondifferences) can be driven by scorer interpretation rather than by model performance.

Future evaluations should predefine a structured rubric and move beyond global Likert ratings towards itemised checklists: (i) guideline concordance, (ii) missing critical safety elements, (iii) presence/absence of contraindications and red flags, (iv) uncertainty calibration, and (v) harmful omission vs benign brevity. This would convert subjective impressions into reproducible endpoints and enable targeted model improvement.

2. Ecological validity: a 40-word cap and noninteractive design may systematically bias both completeness and preference.

To ensure a fair comparison, the authors constrained ChatGPT-4 to a standardised prompt with a maximum length of 40 words, used no system-level instructions, and did not allow interactive clarification. These are not trivial implementation details; they effectively redefine what 'good' looks like. A 40-word cap compresses safety caveats, patient-specific preconditions, and uncertainty signalling—mechanisms that typically increase clinical robustness—thereby privileging readability while mechanically penalising completeness. Consistent with this, AI responses were shorter, achieved more favourable readability metrics, and were preferred more frequently by patients. Thus, the current findings most directly support parity under a 'single-turn, short-answer, no-clarification' task, rather than under real-world patient LLM use.

From an ecological validity perspective, the defining affordance of LLMs in patient education is their ability to support multiturn interaction: patients iteratively disclose comorbidities, medication history, and pregnancy intentions, and refine their risk interpretation through follow-up questions [2]. The authors note that the study design could not evaluate interactive clarification. We therefore encourage an additional pragmatic evaluation arm using standardised multiturn scripts (eg, baseline question → patient reveals methotrexate use → asks about conception timing; or baseline question → patient reports prior uveitis/inflammatory bowel disease (IBD) → asks about biologic choice), with outcomes focused on whether the model (i) elicits missing critical context, (ii) signals uncertainty, and (iii) appropriately triggers clinician escalation for high-stakes topics. Such an approach would generate transportable evidence on real deployment boundaries and failure modes—particularly relevant given the observed lower accuracy in pregnancy/fertility.

3. The pregnancy/fertility signal should be treated as a 'high-risk domain' finding, not a footnote.

Theme-specific analysis showed the only statistically significant accuracy gap in pregnancy/fertility (odds ratio (OR) 0.42 vs clinicians).

This is precisely the domain where patient-facing misinformation can cause disproportionate harm (teratogenic medications, timing of conception, breastfeeding compatibility, or disease control vs foetal risk). Patient preference for this theme

Jiding Xie, Lei Shi, and Jie Cui contributed equally to this work.

https://doi.org/10.1016/j.ard.2025.12.016
Received 28 December 2025; Accepted 29 December 2025

numerically favoured ChatGPT-4, raising a safety paradox: users may prefer confident, readable text even when accuracy is lower [3].

Future tools should implement domain gating: for pregnancy/fertility, vaccination, infection risk on biologics/Janus kinase inhibitors, perioperative management, and acute red flag symptoms, the system should switch to (i) evidence-grounded retrieval, (ii) mandatory citation to up-to-date guidelines, and (iii) 'contact your clinician urgently if…' triage statements. These domains can be prospectively audited using 'never-event' criteria (eg, unsafe medication advice).

4. 'Preference' is not 'benefit': patient-centred endpoints must include comprehension, decisional quality, and behavioural outcomes.

Patients preferred ChatGPT-4 overall (491/998 choices) to clinicians (343/998). However, preference can reflect tone, fluency, or cognitive ease rather than correctness or actionability. The study already shows readability differences that plausibly explain preference.

For clinical translation, the more important outcomes are:

- Objective knowledge gain (pre/postquizzes)
- Decisional conflict and shared decision-making quality
- Anxiety or reassurance (including inappropriate reassurance)
- Adherence and self-management behaviours, and
- Downstream healthcare utilisation (unplanned visits, messages, or calls).

5. Generalisability and governance: a single-language, single-country evaluation is a start, but deployment requires auditable evidence and accountability.

This study involved Italian-speaking patients and Italian experts. Cohorts could not be linked due to anonymity. The work was conducted as an anonymised quality improvement initiative in accordance with the General Data Protection Regulation (GDPR), without formal ethics approval. These design decisions are understandable for feasibility reasons, but they also underscore a key point: once such systems move towards clinical integration, governance must evolve to include traceability of model versions, logging, audit trails, and oversight pathways.

The field needs a consensus 'minimum reporting set' for patient-facing LLM tools in rheumatology, including model version/date, prompting policy, retrieval sources, update frequency, safety guardrails, monitoring plans, and accountability for adverse events. Without this, 'accuracy' becomes a moving target as models and web knowledge drift.

In summary, Forte et al [1] provide an important feasibility demonstration that ChatGPT-4 can produce readable answers that patients often prefer and that experts rate as broadly comparable in accuracy under constrained conditions. The next step in the field is to shift from 'can it answer?' to 'can we measure and govern it well enough to safely deploy it?', especially in high-risk domains where a small accuracy gap can translate into outsized clinical harm.

Funding

This work was supported by the Beijing Natural Science Foundation (number 7232308) and the Special Fundamental Research Funds for Central Public Welfare Research Institutes (number XTCX2023002).

Competing interests

The authors declare no conflicts of interest relevant to this work.

CRediT authorship contribution statement

Jiding Xie: Conceptualization, Writing – original draft. **Lei Shi:** Writing – original draft, Writing – review & editing. **Jie Cui:** Writing – original draft. **Leiyong Wang:** Conceptualization, Methodology, Writing – original draft, Writing – review & editing. **Jingang Dai:** Conceptualization, Funding acquisition, Writing – original draft, Writing – review & editing.

Patient consent for publication

Not applicable.

Ethics approval

Not applicable (no human or animal experiments were conducted).

Provenance and peer review

Not applicable.

REFERENCES

[1] Forte G, Mauro D, Raimondi M, Pantano I, Gandolfo S, Cauli A, et al. ChatGPT vs rheumatologists: cross-sectional study on accuracy and patient perception of AI-generated information for psoriatic arthritis. Ann Rheum Dis 2025. doi: 10.1016/j.ard.2025.11.012.

[2] Mahajan A, Powell D. Transforming healthcare delivery with conversational AI platforms. NPJ Digit Med 2025;8(1):581. doi: 10.1038/s41746-025-01968-6.

[3] Cau FM, Hauptmann H, Spano LD, Tintarev N. Effects of AI and logic-style explanations on users' decisions under different levels of uncertainty. ACM Trans Interact Intell Syst 2023;13(4):1–42. doi: 10.1145/3588320.

Jiding Xie[1], Lei Shi[2], Jie Cui[3], Leiyong Wang[4,**], Jingang Dai[1,*]

[1] *Experimental Research Center, China Academy of Chinese Medical Sciences, Beijing, China*

[2] *College of Physical Education, Yangzhou University, Yangzhou, Jiangsu, China*

[3] *Department of Hernia and Abdominal Wall Surgery, Beijing Chao-Yang Hospital, Capital Medical University, Beijing, China*

[4] *Beijing Hospital of Traditional Chinese Medicine, Capital Medical University, Beijing, China*

*__Correspondence to__ Dr Jingang Dai, Experimental Research Center, China Academy of Chinese Medical Sciences, Beijing, China.

**__Correspondence to__ Dr Leiyong Wang, Beijing Hospital of Traditional Chinese Medicine, Capital Medical University, Beijing, China.

E-mail addresses: lywang@126.com (L. Wang), zhongyidai@outlook.com (J. Dai).

Ann Rheum Dis 85 (2026) e49–e50

Contents lists available at ScienceDirect

Annals of the Rheumatic Diseases

journal homepage: https://www.sciencedirect.com/journal/annals-of-the-rheumatic-diseases

Response

Response to correspondence on 'ChatGPT vs rheumatologists: cross-sectional study on accuracy and patient perception of AI-generated information for psoriatic arthritis' by Xie et al

Dear Editor,

We thank Xie and colleagues for their correspondence regarding our study comparing ChatGPT-4 with psoriatic arthritis specialists in answering patient-generated questions [1]. We agree that the field should now focus on evaluation frameworks that are reproducible, safety-oriented and deployable.

Regarding expert agreement, the limited single-rater reliability observed in our study reflects the intrinsic subjectivity of global Likert-type ratings, which inevitably capture multiple dimensions, including factual accuracy, framing, and risk communication. This consideration underpinned our use of a relatively large expert panel and our focus on aggregated reliability metrics while transparently reporting individual variability. Future studies would indeed benefit from structured, itemised rubrics incorporating checklist-based endpoints (eg, guideline concordance, presence of safety statements or harmful omissions), as previously suggested in methodological evaluations of clinical decision tools and artificial intelligence systems.

We also acknowledge that the 40-word, single-turn design defines a deliberately constrained evaluation task. As discussed in the Limitations section of our original manuscript, this format was chosen to maximise standardisation and comparability between AI- and clinician-generated responses by applying the same response-length and single-turn constraints to both groups, rather than to emulate real-world clinical counselling. Although brevity may favour readability and preference at the expense of completeness, our findings should therefore be interpreted within this defined setting. We agree that future research should prioritise multiturn, context-aware evaluations to assess whether large language models (LLMs) appropriately elicit missing information, calibrate uncertainty, and defer to clinician input in high-risk scenarios [2].

The theme-specific analysis identified pregnancy/fertility as the only domain with significantly lower ChatGPT accuracy. Although no explicit safety issues were flagged in expert scoring, this accuracy gap represents a clinically relevant signal in a high-risk area prone to misinformation. It aligns with reports of LLM limitations in reproductive health, underscoring needs for domain-specific safeguards and guideline linkage [3].

We further concur that patient preference should not be conflated with clinical benefit. Although preference represents a relevant patient-centred signal, meaningful evaluation of LLM-based education tools should incorporate outcomes such as knowledge acquisition, decisional quality, and potential unintended effects such as inappropriate reassurance or anxiety.

Finally, we agree that any move towards clinical deployment requires robust governance, including model traceability, version control, monitoring for performance drift, and clear accountability frameworks. As recently emphasised, responsible integration of conversational AI into health care must be accompanied by transparent reporting standards and continuous oversight to ensure patient safety and trust.

In summary, we view our study as an initial, controlled evaluation that highlights both the potential and the limitations of LLM-based patient education. We appreciate the contribution of Xie et al in underscoring the methodological and governance priorities necessary to guide future, more pragmatic investigations in this rapidly evolving field.

CRediT authorship contribution statement

Giulio Forte: Conceptualization, Writing – original draft. **Daniele Mauro:** Writing – original draft, Writing – review & editing. **Francesco Ciccia:** Conceptualization, Writing – review & editing.

Funding

This research did not receive any specific grant from funding agencies in the public, commercial, or not-for-profit sectors.

Competing interests

The authors declare that they have no competing interests.

Patient consent for publication

Not applicable.

DOI of original article: http://dx.doi.org/10.1016/j.ard.2025.12.016.

https://doi.org/10.1016/j.ard.2026.01.011
Received 12 January 2026; Accepted 15 January 2026

Ethics approval

Not applicable.

Provenance and peer review

Not commissioned; externally peer reviewed.

Declaration of generative AI and AI-assisted technologies in the writing process

During the preparation of this work, the authors used ChatGPT-4 (OpenAI) in order to assist with proofreading the manuscript text. After using this tool, the authors reviewed and edited the content as needed and take full responsibility for the content of the publication.

REFERENCES

[1] Forte G, Mauro D, Raimondi M, Pantano I, Gandolfo S, Cauli A, et al. ChatGPT vs rheumatologists: cross-sectional study on accuracy and patient perception of AI-generated information for psoriatic arthritis. Ann Rheum Dis 2025. doi: 10.1136/ard-2025-11-012.

[2] Mahajan A, Powell D. Transforming healthcare delivery with conversational AI platforms. NPJ Digit Med 2025;8:581. doi: 10.1038/s41746-025-01968-6.

[3] Penny-Dimri JC, Bachmann M, Cooke WR, Mathewlynn S, Dockree S, Tolladay J, et al. Show more et al. Measuring large language model uncertainty in women's health using semantic entropy and perplexity: a comparative study. Lancet Obstet Gynaecol Womens Health 2025;1(1):e47–56.

Giulio Forte, Daniele Mauro, Francesco Ciccia*
Department of Precision Medicine, University of Campania 'Luigi Vanvitelli', Naples, Italy

*Correspondence to Prof Francesco Ciccia, Department of Precision Medicine, University of Campania 'Luigi Vanvitelli', Naples, Italy.
E-mail address: francesco.ciccia@unicampania.it (F. Ciccia).

Ann Rheum Dis 85 (2026) e51–e52

Contents lists available at ScienceDirect

Annals of the Rheumatic Diseases

journal homepage: https://www.sciencedirect.com/journal/annals-of-the-rheumatic-diseases

Letter

Correspondence to: 'Post hoc comparison of the effectiveness of tocilizumab, rituximab, mycophenolate mofetil, and cyclophosphamide in patients with SSc-ILD from the EUSTAR database'

Dear Editor,

We read with great interest the article titled, 'Post hoc comparison of the efficacy of tocilizumab, rituximab, mycophenolate mofetil and cyclophosphamide in patients with SSc-ILD from the EUSTAR database' authored by Yan et al [1]. This article is a retrospective study using data from the European Scleroderma Trials and Research Group (EUSTAR) database to compare the effectiveness of tocilizumab (TCZ), rituximab (RTX), mycophenolate mofetil (MMF), and cyclophosphamide (CYC) in patients with systemic sclerosis-associated interstitial lung disease (SSc-ILD). The study found that there was no statistically significant difference in the effectiveness of these 4 treatments on forced vital capacity (FVC) change in SSc-ILD patients. While the findings are promising, we maintain reservations regarding certain aspects of the study and eagerly anticipate the authors' response or further discourse.

We want to raise several methodological concerns regarding the inclusion/exclusion criteria and study design: (1) potential selection bias: the requirement for ≥2 FVC records may exclude patients with severe disease or those unable to complete FVC assessments, potentially underestimating therapeutic efficacy or safety in advanced SSc-ILD populations. (2) Limited generalisability: the exclusion of patients with prior targeted immunosuppressants or stem cell transplantation may disproportionately enrol treatment-naïve or milder cases, restricting the extrapolation of findings to broader clinical populations. (3) Unaddressed cancer comorbidity: given the well-established association between systemic sclerosis (SSc) and malignancies—particularly lung cancer [2], which is linked to poorer treatment response, accelerated interstitial lung disease progression, and increased mortality in SSc-ILD [3]—the failure to report lung cancer prevalence in the cohort leaves open the possibility that observed FVC changes could be confounded by this critical comorbidity.

SSc-ILD exhibits marked clinical heterogeneity [4], with approximately 30% of newly diagnosed patients progressing within 1 year while others remain stable or progress slowly [5]. The median follow-up of 11 months (IQR, 8-14 months) appears insufficient to capture meaningful disease progression, as SSc-ILD typically requires 2 to 3 years of observation to evaluate therapeutic outcomes adequately. This short-term design may obscure both long-term efficacy differences and late-emerging safety signals among the compared immunosuppressants.

While we commend the authors for their diligent work in conducting this first real-world comparative study of 4 immunosuppressants in SSc-ILD, the observational design, limited follow-up duration, potential selection biases, and incomplete safety reporting constrain the robustness of conclusions. We strongly advocate for future prospective randomised controlled trials to validate these findings, supplemented by longitudinal imaging biomarkers, patient-reported outcomes, and comprehensive safety monitoring. We appreciate the authors' contributions to this critical area and look forward to their continued efforts to advance our understanding of SSc-ILD management.

Contributors

Y-LY contributed to conceptualisation, supervision, validation, visualisation, writing – original draft, writing – review & editing. R-HG contributed to writing – original draft, conceptualisation, writing – review & editing. JC-CW contributed to supervision, validation, writing – review & editing. L-YZ contributed to writing – review & editing, conceptualisation.

Funding

This research did not receive any specific grant from funding agencies in the public, commercial, or not-for-profit sectors.

Competing interests

All authors declare they have no competing interests.

Patient consent for publication

Not required.

Yan-li Yang, Rong-hong Guo and James Cheng-Chung Wei contributed equally to this work.

Handling editor Josef S. Smolen.

https://doi.org/10.1016/j.ard.2025.04.026

Ethics approval

Not required.

Provenance and peer review

Not commissioned; externally peer reviewed.

REFERENCES

[1] Yan Q, Bruni C, Garaiman A, Mihai C, Jordan S, Becker MO, et al. EUSTAR collaborators. Post hoc comparison of the effectiveness of tocilizumab, rituximab, mycophenolate mofetil, and cyclophosphamide in patients with SSc-ILD from the EUSTAR database. Ann Rheum Dis 2025;84(4):620–31.

[2] Lepri G, Catalano M, Bellando-Randone S, Pillozzi S, Giommoni E, Giorgione R, et al. Systemic sclerosis association with malignancy. Clin Rev Allergy Immunol 2022;63(3):398–416.

[3] Tyndall AJ, Bannert B, Vonk M, Airò P, Cozzi F, Carreira PE, et al. Causes and risk factors for death in systemic sclerosis: a study from the European Scleroderma Trials and Research Group (EUSTAR) database. Ann Rheum Dis 2010;69(10):1809–15.

[4] Hoffmann-Vold AM, Maher TM, Philpot EE, Ashrafzadeh A, Barake R, Barsotti S, et al. The identification and management of interstitial lung disease in systemic sclerosis: evidence-based European consensus statements. Lancet Rheumatol 2020;2(2):e71–83.

[5] Hoffmann-Vold AM, Allanore Y, Alves M, Brunborg C, Airió P, Ananieva LP, et al. Progressive interstitial lung disease in patients with systemic sclerosis-associated interstitial lung disease in the EUSTAR database. Ann Rheum Dis 2020;80(2):219–27.

Yan-li Yang[1], Rong-hong Guo[1], James Cheng-Chung Wei[1,2,3,4], Li-yun Zhang[1,*]

[1] *Department of Rheumatology, Third Hospital of Shanxi Medical University, Shanxi Bethune Hospital, Shanxi Academy of Medical Sciences; Tongji Shanxi Hospital, Taiyuan, China*

[2] *Institute of Medicine, Chung Shan Medical University, Taichung, Taiwan*

[3] *Department of Allergy, Immunology & Rheumatology, Chung Shan Medical University Hospital, Taichung, Taiwan*

[4] *Graduate Institute of Integrated Medicine, China Medical University, Taichung, Taiwan*

*__Correspondence to__ Dr Li-yun Zhang

E-mail address: zhangly@sxbqeh.com.cn (L.-y. Zhang).